RESEARCH

Field Validation of Intelligent Compaction Monitoring Technology for Unbound Materials

Take the steps...

Research...Knowledge...Innovative Solutions!

Transportation Research

Technical Report Documentation Page

1. Report No. MN/RC-2007-10	2.	3. Recipients Accession No.	
4. Title and Subtitle Field Validation of Intelligent Compaction Monitoring Technology for Unbound Materials		5. Report Date March 2007	
		6.	
7. Author(s) David White, Mark Thompson, and Pavana Vennapusa		8. Performing Organization Report No.	
9. Performing Organization Name and Address Center for Transportation Research and Education Iowa State University 2711 South Loop Drive, Suite 4700 Ames, IA 50010-8664		10. Project/Task/Work Unit No.	
		11. Contract (C) or Grant (G) No. (c) 82617 (wo) 9	
12. Sponsoring Organization Name and Address Minnesota Department of Transportation 395 John Ireland Boulevard Mail Stop 330 St. Paul, Minnesota 55155		13. Type of Report and Period Covered Final Report	
		14. Sponsoring Agency Code	
15. Supplementary Notes ttp://www.lrrb.org/PDF/200710.pdf			

16. Abstract

The successful implementation of intelligent compaction technology into earthwork construction practice requires knowledge of the roller-integrated compaction measurements and their relationships with the engineering and index properties of soil that may be used for pavement design (e.g. California bearing ratio, elastic modulus, resilient modulus). These relationships were studied at three earthwork construction projects in Minnesota. In these field studies, intelligent compaction and in-situ test data were collected to demonstrate use of the various technologies, characterize the variation associated with each measurement system, and ultimately aid performance of regression analyses.

For the pilot study at TH 64, a GIS database was created with roller data and parallel quality assurance data to demonstrate one method for managing large quantities of data. Spatial statistics were also determined using variogram modeling and discussed with regards to their potential for characterizing uniformity.

A laboratory compaction study using different compaction methods (e.g. static, impact, gyratory, and vibratory) was conducted to show different moisture-density-compaction energy relationships for granular and cohesive soils. Resilient modulus test results showed that vibratory and impact compaction methods produce higher-modulus samples than static compaction.

The findings from field studies of intelligent compaction systems provide the basis for developing QC/QA guidelines regarding effective and appropriate use of the technology. These recommendations, along with a brief summary of European specifications for continuous compaction control, are provided in the report.

17. Document Analysis/Descriptors		18. Availability Statement	
earthwork quality resilient modulus geostatistics	in-situ testing laboratory compaction testing intelligent compaction	No restrictions. Document available from: National Technical Information Services, Springfield, Virginia 22161	
19. Security Class (this report) Unclassified	20. Security Class (this page) Unclassified	21. No. of Pages 412	22. Price

Field Validation of Intelligent Compaction Monitoring Technology for Unbound Materials

Final Report

Prepared by:

David J. White

Mark J. Thompson

Pavana KR Vennapusa

Department of Civil, Construction and Environmental Engineering
Iowa State University

March 2007

Acknowledgements

Table of Contents

List of Tables

List of Figures

Executive Summary

Field Evaluation of Intelligent Compaction Technology

The successful implementation of intelligent compaction (IC) technology into earthwork construction practice requires knowledge of the IC measurement values and their relationships with the in-situ properties of earth materials that relate to performance (e.g. resilient modulus). This research project used experimental methods to investigate the relationships between in-situ and IC measurement values and also laboratory compaction techniques for cohesive and granular soils. Based on analysis results and a statistical framework for incorporating measurement variation, guidelines for QC/QA procedures are documented.

Three field studies were conducted with three IC rollers at two different project sites. *Compaction meter value* (CMV) and *machine drive power* (MDP) from Caterpillar rollers and Ammann k_B (stiffness) were compared with dry unit weight, soil strength, and modulus parameters obtained from in-situ test devices (e.g. nuclear gauge, DCP, LWD) for validation of the technologies. In Field Study 1, IC mapping trials were performed with in-situ testing at select locations of the mapped area verifying that the IC technologies are able to identify areas of weak or poorly-compacted soil. In Field Study 2, test strips were established for collecting compaction data and performing regression analysis to better describe the relationships between in-situ and IC measurement values. Statistically-significant correlation was observed between different measurements for data collected over a relatively wide range of soil characteristics. Ammann k_B was also related to rut depth measured after test rolling procedures. Field Study 3 was conducted on a grading project, in which IC technology was used as the principal method for quality control. The testing and analysis of this study, therefore, focused on evaluating the experience in terms of how the technology was used and how the technology performed. The calibration procedure and results are documented, and the relationships between in-situ and IC measurement values were investigated at the proof scale and at the project scale. The study findings show that IC technology is a feasible alternative for quality control, and potentially quality acceptance, but that some challenges in interpreting the measurements still remain.

Intelligent Compaction Data Management and Analysis

IC technology provides opportunity to collect and evaluate information for 100 percent of the project area, but it also produces large data files that create analysis, visualization, transfer, and archival challenges. An approach for managing large quantities of data is to create a "geodatabase" using ArcGIS modules. A geodatabase of the TH 64 project IC data and in-situ spot test measurements was created to demonstrate this application.

Applying geostatistical methods in the analysis of IC data has the advantage of quantifying spatial variability, which is not possible with classical statistical analysis. A "variogram" model can be used to characterize uniformity of the IC data. To demonstrate the application, IC data collected for two *control* and two *proof* sections of the TH 64 project was analyzed and compared with the Mn/DOT specified quality control criteria. Critical differences in spatial statistics relating to uniformity were observed between the two control sections, which were not observed with the univariate statistics. The two proof sections which "pass" the Mn/DOT

acceptance criteria failed to meet an alternatively proposed "sill" criterion that establishes a uniformity criterion at the 30 m spatial scale. The implication of such incremental spatial analysis is that it will aid the contractor in identifying localized poorly compacted areas or highly non-uniform conditions, which are often the route cause of pavement problems. Using "range" distance determined from a variogram model as the minimum window size for an area of evaluation, a 60 m long section was analyzed and found that several isolated locations failed to meet the Mn/DOT acceptance criteria. The scale at which the acceptance criterion is based is still a question that needs further discussion and analysis.

Laboratory Compaction Study

Laboratory compaction of soils should simulate the mechanics and energy delivery system that occurs in the field. This is particularly important as it relates to soil fabric/structure and measuring engineering properties (e.g. strength and stiffness) of materials compacted in the lab. Laboratory compaction tests were performed using impact, static, gyratory and vibratory compaction methods for one cohesive soil and one granular soil to examine the differences in moisture-density relationships between these methods. Results showed distinctly different moisture-density relationships for the different compaction methods. On an energy per unit volume basis, the static compaction method can be more efficient than impact compaction for the cohesive soil, but is found inadequate for the granular soil as it requires high application stresses. The vibratory compaction method is inadequate to characterize moisture-density relationships for the cohesive soil, while it works effectively for the granular soil.

In addition to compaction tests, laboratory resilient modulus (M_r) and unconsolidated-undrained (UU) strength tests were performed to evaluate the effects of compaction method on these soil properties. From limited testing, it is found that the vibratory and impact compaction samples produce higher M_r and shear strength (τ_{max}) than static compaction samples for both soils. The vibratory method generally resulted in lower τ_{max} than the impact method, while it produced similar or slightly higher τ_{max} than the impact method for granular soil. A profound influence of moisture content is realized for the cohesive soil with M_r and τ_{max} values decreasing with increasing moisture content. Moisture content did not have as significant an influence on the M_r and τ_{max} values for the granular soil.

Field Comparison Study of LWD Devices

Mn/DOT is in the process of evaluating and implementing LWD devices as a QC/QA tool on a state-wide basis. To successfully implement the use of these devices, it is important to understand the conditions for which they provide reliable measurements and also if differences exist between the calculated elastic modulus values between the various devices. Two LWD devices (ZFG 2000 manufactured by Zorn Stendal from Germany, and the Keros manufactured by Dynatest in Denmark) with different plate diameters were used side-by-side for testing pavement subgrade and base layers to observe the differences in E_{LWD} between the devices, and the influence of plate diameter on the E_{LWD} values. It was determined that the Keros E_{LWD} is on average 1.9 to 2.2 times greater than Zorn E_{LWD}. The primary contributor for differences in E_{LWD} values between these devices is the difference in measured deflections. The Zorn device measures approximately 1.5 times greater deflection than Keros for the same plate diameter,

drop height, and drop weight. A Zorn device with 200 mm plate results in E_{LWD} about 1.4 times greater than with 300 mm plate.

Limited data is available in the literature relating E_{LWD} to laboratory M_r. An effort was made in this research to build a database of this relationship by obtaining shelby tube samples from a compacted subgrade, at the locations of LWD tests. A linear relationship between E_{LWD} and M_r is observed at a selected stress condition, with R^2 values ranging from 0.85 to 0.97. E_{LWD} was also compared with the secant modulus estimated from the M_r test, which also showed strong linear relationships with R^2 values ranging from 0.75 to 0.88.

Implementation of Intelligent Compaction Technology

To facilitate implementation of IC technology, selected international specifications are summarized in this report. And, to improve upon the existing calibration guidelines, a detailed, conceptual process for on-site calibration and quality acceptance using IC technology is outlined with the option to incorporate one of three levels of sampling requirements. Specific recommendations relating to education and future research on the IC technology are provided.

During the course of this research, significant interaction between Mn/DOT personnel, contractors, industry representatives, and researchers occurred during field demonstrations, special seminars, and full-scale construction with execution of the first fully specified IC project in the U.S. These efforts contributed significantly to the results of this research report and to future implementation of IC technology in Minnesota.

Chapter 1
Introduction

1.1 Problem Statement

1.1.1 Industry Problem

Transportation agencies in Minnesota spend millions of dollars each year on the construction of pavement structures. Current methods used for quality control and acceptance (QC/QA) testing have only an indirect connection to the material properties used for pavement design, and the QC/QA testing requires substantial personnel resources. In addition, quality control testing is increasingly becoming the responsibility of contractors, such that the quality assurance testing performed by agency personnel needs to be made more efficient using available technology.

In order to more efficiently design and construct earth structures and pavement, the Minnesota Department of Transportation (Mn/DOT) has already invested significant resources to develop and advance the use of mechanistic pavement design and in-situ testing devices. A current barrier to greater implementation of mechanistic design and in-situ testing is the difficulty of collecting the field data necessary to provide confidence in the new design and field testing procedures. Fortunately, this barrier is being reduced, because construction equipment is becoming available that can measure the deformation characteristics of grading materials during the compaction process. Some of these rollers also adjust their compaction energy in real time during compaction through variable feedback control of vibration amplitude and/or frequency. This feature of roller-integrated compaction monitoring technology is referred to as "intelligent compaction." Intelligent compaction (IC) may optimize resources by allowing the specified stiffness to be achieved without overcompaction. The benefits of IC technology are many and they are measurable.

From the construction perspective, labor and equipment resources are more efficiently utilized by applying additional compaction effort only in areas that require it. From the agency perspective, an important outcome will be a more rapid implementation of continuous mechanistic property measurement during construction. Intelligent compaction may eventually provide an alternative to current acceptance testing procedures for grading and base and provide continuous quality control information. In an era of shrinking resources and limited budgets, this is an area of great importance.

1.1.2 Technical Problem

The successful implementation of IC technology into earthwork construction practice requires knowledge of the IC measurement values and their relationships with the engineering properties of earth materials that may be used for pavement design (e.g. resilient modulus). These relationships are influenced by the various factors affecting machine response during compaction

operations, including: (1) roller size and operational parameters (e.g. vibration amplitude and frequency), (2) soil type, (3) moisture content, (4) lift thickness and/or stiffness of underlying layers, and (5) type of data used for developing regressions (e.g. statistically averaged). If sufficiently understood, the parameters may be controlled during compaction operations or, at a minimum, monitored and recorded for post-processing of roller data to account for the variable conditions. This research project used experimental methods to investigate the relationships between in-situ and IC measurement values. Based on analysis results and a statistical framework for incorporating measurement variation, guidelines for QC/QA procedures are documented.

1.2 Project Objectives

To facilitate the implementation of IC technology into earthwork construction practice, the objectives of this research include:

- Evaluate IC technology under actual field conditions for a wide range of unbound materials.

- Develop relationships between in-situ and IC measurement values, including dry unit weight, dynamic cone penetration index, Clegg impact value, soil stiffness gauge modulus, light weight deflectometer modulus, and static plate load test modulus.

- Characterize the measurement variation observed for the various measurement systems.

- Identify the influences of compaction energy and method on laboratory moisture-density relationships.

- Characterize laboratory resilient modulus in terms of soil type, stress state conditions, moisture content, and dry unit weight.

- Investigate the relationships between modulus obtained from two light weight deflectometers, static plate loading tests, and laboratory resilient modulus.

- Develop QC/QA guidelines for incorporating roller-integrated compaction monitoring technology into soil compaction specifications.

1.3 Project Scope

The project report summarizes experimental testing programs, field and laboratory test results, and statistical analyses for evaluating recently-implemented IC technology. The field studies were conducted on two earthwork construction sites in Minnesota, namely the US 14 and TH 64 highway reconstruction projects at Janesville and Akeley, respectively. At both sites, in-situ and IC measurement values were collected and compared to assess the relationships between the various measurements and also to examine the variation observed for the measurement systems.

A geodatabase of the TH 64 project IC roller data and in-situ spot test measurements was created for demonstrating an approach for managing the large quantities of the IC data using ArcGIS modules.

Applying geostatistical methods in the analysis of IC data has the advantage of quantifying spatial variability, which is not possible with classical statistical analysis. IC data obtained from the TH 64 project is analyzed by comparing spatial statistics with current Mn/DOT acceptance criteria to demonstrate the advantages of geostatistical methods.

Different laboratory compaction techniques (static, impact, gyratory, and vibratory) were evaluated by developing moisture-density relationships as a function of compaction energy. Laboratory resilient modulus (M_r) and unconsolidated-undrained (UU) strength tests were performed on samples prepared using the abovementioned compaction methods to evaluate the affects of compaction methods on these soil properties.

Two LWD devices (ZFG 2000 manufactured by Zorn Stendal from Germany, and the Keros manufactured by Dynatest in Denmark) with different plate diameters were evaluated to investigate the influences of plate diameter and calculated LWD modulus (E_{LWD}) values. Relationships between E_{LWD} and laboratory resilient modulus are examined by obtaining shelby tube samples from a compacted subgrade.

The findings from field study of roller-integrated compaction monitoring systems provide the basis for developing QC/QA guidelines regarding effective and appropriate use of the technology. These recommendations, along with a brief summary of European specifications for continuous compaction control, are provided at the end of the report.

1.4 Report Organization

This report is comprised of eleven chapters. Chapter 2 describes the laboratory and field testing methods used throughout the research project with test procedures referencing test standards, when applicable. Chapters 3, 4, and 5 document field studies conducted at project sites in Minnesota for evaluating CMV and k_B technologies as applied to Caterpillar and Ammann rollers, respectively. In these chapters, field data are summarized and statistical analyses are presented with particular focus on defining the relationships between in-situ and IC measurement values and also the variation observed for the various measurements. In Chapters 6, a GIS database created for in-situ and IC measurement values from the TH 64 project is presented. Using data from Chapters 5 and 6, Chapter 7 documents geostatistical analysis of IC measurement values, and comparison to in-situ test measurements. Chapter 8 documents the moisture-density-compaction energy relationships for different compaction methods on two soil types — cohesive and granular. In addition, influence of compaction method on laboratory resilient modulus and UU shear strength results are presented in Chapter 8. Based on in-situ compaction measurements from the field studies, comparison of Zorn ZFG and Keros light weight deflectometers is made in Chapter 9. In this chapter, modulus values from the two portable devices are compared to each other, and to laboratory resilient modulus. Chapter 10 discusses the incorporation of IC measurement values into specifications. The key attributes of

European specifications regarding continuous compaction control are summarized, and further recommendations are provided. Chapter 11 summarizes the project and lists the key research findings.

Chapter 2
Research Methodology

Several laboratory and field testing methods were employed in this research. This chapter summarizes the standard procedures with any deviations or modifications implemented in performing these tests.

2.1 Laboratory Testing Methods

2.1.1 Soil Index Properties

Particle-size analysis was conducted in accordance with ASTM D422-63(2002) "*Standard Test Method for Particle-Size Analysis of Soils.*" Coarse grained particle-size analysis was performed by washing about 2000 grams of air-dried soil over a No. 10 sieve, oven drying the retained soil, and sieving through the 1 inch, 0.75 inch, 0.375 inch, and No. 4 sieve sizes. Fine-grained particle-size analysis was performed using the hydrometer method with an air dried sample of about 70 grams passing the No. 10 sieve. After completing the hydrometer test, the suspended material was washed through the No. 200 sieve. The material retained on the No. 200 sieve was then oven dried and sieved through the No. 40 and No. 100 sieve sizes.

Atterberg limits were determined in accordance with ASTM D4318-05, "*Liquid Limit, Plastic Limit, and Plasticity Index of Soils.*" Representative samples for the Liquid Limit and Plastic Limit tests were prepared using the "wet preparation" method by screening the sample through the No. 40 sieve using a spatula. Liquid limit tests were performed according to Method A (multi-point liquid limit method).

Based on the Atterberg limits and particle size analysis test results, the soils were classified according to AASHTO and Unified Soil Classification System (USCS).

Specific gravity was determined in accordance with ASTM D 854-06, "*Standard Test Methods for Specific Gravity of Soil Solids by Water Pyconometer*". Representative samples for the test were prepared and tested according to Method A – Procedure for oven-dried specimens.

2.1.2 Soil Compaction Characteristics

Several compaction test methods were employed in this research. A detailed study with testing of one cohesive and one granular soil using different compaction methods is presented in Chapter 8. An overview of these different test procedures is provided in this section.

Impact Compaction. Laboratory impact compaction tests were performed in accordance with the ASTM D 698–00 *"Standard Test Methods for Laboratory Compaction Characteristics of Soil Using Standard Effort"*, and the ASTM D 1557–02 *"Standard Test Methods for Laboratory Compaction Characteristics of Soil Using Modified Effort"* standard test procedures. The appropriate test method (i.e. mold size) was identified from particle size distribution criteria. In addition to standard compaction energy (591 kN-m/m^3) and modified compaction energy (2696 kN-m/m^3), compaction tests on some soils were performed at lower and intermediate compaction energy levels (358, 990, and 1670 kN-m/m^3). The impact compaction energy is determined using equation 2.1 (Proctor 1948). The purpose of performing tests at multiple energies is to derive relationships between moisture content, dry unit weight, and compaction energy. An automated, calibrated mechanical rammer (*see* Figure 2.1) was used to perform these tests.

$$\text{Energy}_{\text{impact}} = \frac{\left(\begin{array}{c}\text{number of blows}\\\text{per layer}\end{array}\right) \times \left(\begin{array}{c}\text{number of}\\\text{layers}\end{array}\right) \times \left(\begin{array}{c}\text{weight of}\\\text{hammer}\end{array}\right) \times \left(\begin{array}{c}\text{height of}\\\text{drop hammer}\end{array}\right)}{\text{Volume of mold}} \qquad (2.1)$$

Figure 2.1. Automated mechanical rammer for impact compaction test

Static Compaction. Currently, there is no standard procedure available for static compaction tests. Some test methods, for example, AASHTO T-307 suggest static compaction in sample preparation for resilient modulus testing that uses a five layer compaction method (described below under resilient modulus test). Bell (1977) and Zhang *et al.* (2005) report on static compaction procedures used in their research. The primary purpose of using static compaction in this study was to compare moisture-density relationships with other compaction methods. The procedure followed in this study is described in the following.

A compaction mold of size similar to the Proctor test mold (100 mm diameter x 116 mm height) was specially fabricated for this research. Specimens for testing were prepared by moisture conditioning based on pre-determined moisture requirements and mellowed in accordance with ASTM D-698. Moist soil of approximately 2500 grams was then placed in the mold in one lift and compacted using a manual hydraulic compression device by placing a spacer on the top of the soil and pushing it against a solid plate. Components of the setup are pictured in Figure 2.2. A load cell was placed between the hydraulic compression device and the bottom of the mold to measure the applied compaction force. Deformation of the sample was measured using two LVDT's mounted to the load frame during the compaction process. The load cell and the two LVDT's were connected to a data acquisition system and computer. The applied load and soil deformation information was automatically recorded during the test. A typical load versus deformation curve is presented in Figure 2.3. Static compaction energy was determined from the load-compaction curve using equation 2.2.

$$\text{Energy}_{\text{static}}\,(\text{kN - m/m}^3) = \frac{\text{area of load versus deformation curve}\,(\text{kN - m})}{\text{Volume of mold}\,(\text{m}^3)} \tag{2.2}$$
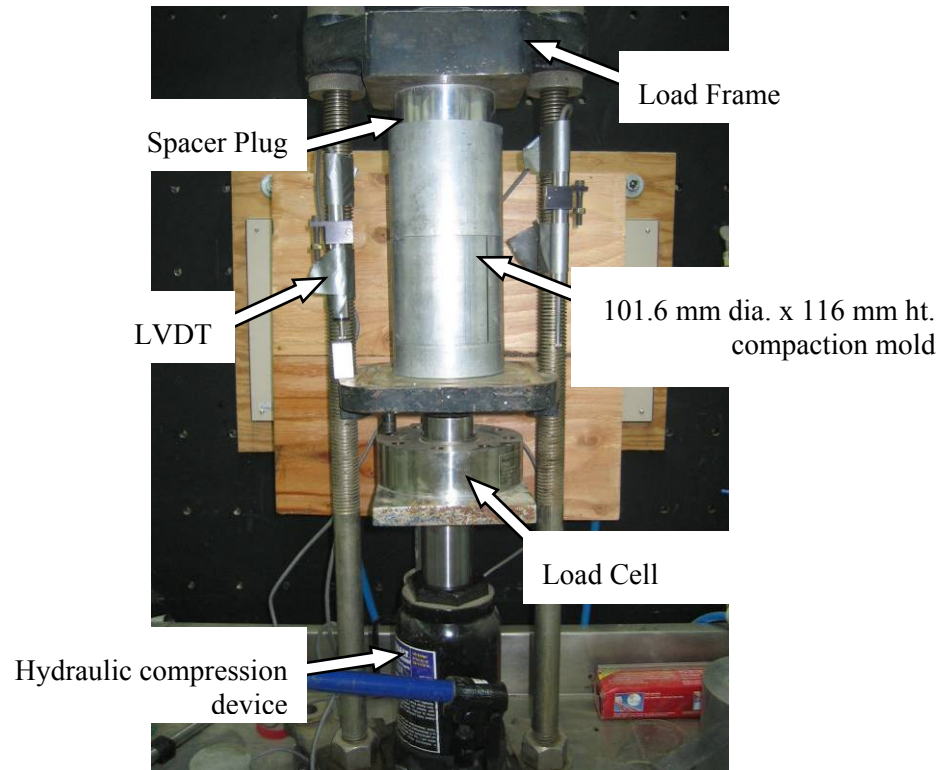
Figure 2.2. Static compaction mold assembly and components
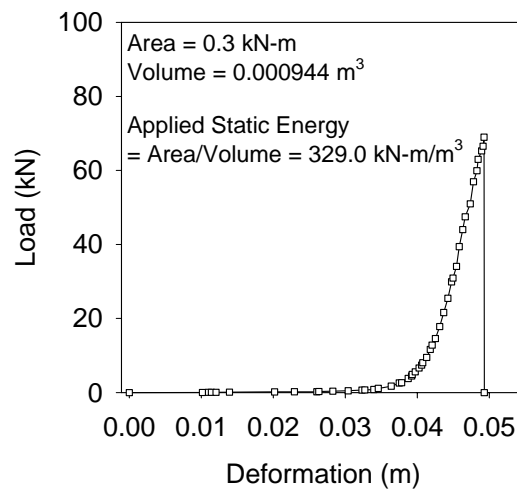
Figure 2.3. Typical load versus deformation curve from a static compaction test

Vibratory Compaction. Vibratory compaction tests were performed in accordance with ASTM D4253-00 (2006), *"Standard Test Method for Maximum Index Density and Unit Weight of Soils using a Vibratory Table"*. The minimum index density was determined in accordance with ASTM D4254-00 (2006), *"Standard Test Method for Minimum Index Density and Unit Weight of Soils and Calculation of Relative Density"*. Vibratory compaction energy is estimated using equation 2.3. The vibratory table and mold assembly is shown in Figure 2.4.

$$Energy_{vib} = \frac{W \times f \times A \times t}{V} \qquad (2.3)$$

where:
Energy$_{vib}$ = vibratory compaction energy (kN-m/m^3)
W = weight of surcharge (kN)
f = frequency of vibration (Hz)
A = amplitude (m)
t = time (sec)
V = volume of mold (m^3)

Figure 2.4. 152 mm (6 inch) diameter compaction mold and vibratory table

Gyratory Compaction. In generally, the method proposed by McRae (1965) for performing gyratory compaction tests on subgrade and base materials was followed. According to this procedure, a thoroughly mixed, loose, moist sample is placed in to the cylindrical mold, and then a controlled normal force is applied to both the top and bottom of the sample for several revolutions (gyrations) at a constant rate (gyrations per minute). The applied normal force is supplemented with a kneading action or gyratory motion at an angle (gyration angle) to compact the material.

There are no recommendations, however, available on gyratory variables (applied pressure, angle, number of gyrations, gyration rate) that are specific to soil type. Smith (2000) used 1380 kPa vertical stress, 1.0 degree gyration angle, and 30 – 40 gyrations in a study on well-graded crushed stone material to achieve field densities. For fine sand material, Ping (2003) indicated that tests conducted at 200 kPa vertical stress, 1.25 degree gyration angle, 90 gyrations, at 20 gyrations per minute showed promise in replicating field compaction. Recently, Kim and Labuz (2006) performed tests using 600 kPa vertical stress, 1.25 degree gyration angle, 50 gyrations, at 30 gyrations per minute on recycled granular materials and concluded that the results matched well with the field densities.

Figure 2.5 shows the AFGB1A Brovold gyratory compactor (manufactured by Pine Instrument Company) used in this study. Samples were prepared using an applied vertical pressure of 600 kPa, a constant gyration angle of 1.25 degrees, and 50 gyrations at a rate of 30 gyrations per minute.

Figure 2.5. Gyratory compactor

The gyratory compaction energy is determined using equation 2.4 (McRae 1965). The total energy is calculated as the sum of energy applied during compaction via vertical and shear forces on the sample.

$$\text{Energy}_{\text{gyratory}} = \frac{\left[p_{\text{vertical}} \times A_{\text{sample}} \times (H_{\text{before}} - H_{\text{after}})\right] + \left[4 \times s \times H \times \theta)\right]}{V} \qquad (2.4)$$

where:
$\text{Energy}_{\text{gyratory}}$ = Gyratory compaction energy (kN-m/m^3)
p_{vertical} = vertical applied pressure (kPa)
A_{sample} = area of sample (m^2)
H_{before} = height of sample before compaction (m)
H_{after} = height of sample after compaction (m)
s = applied shear stress (kPa)
H = height of sample at a given gyration cycle (m)
θ = gyration angle (radians)
V = volume of mold (m^3)

The shear stress, s, in equation 2.4 is a function of the applied gyratory shear force, which is the force required to maintain the imposed angle of gyration. The gyratory shear force varies with the state of compaction of the material and can be determined using a sensor attached to the mold. The machine used in this research is not setup to measure the gyratory shear force, and therefore, compaction energy calculations were not performed.

2.1.3 Resilient Modulus

Resilient modulus tests were performed in general accordance with AASHTO T-307 (1999), *"Standard Method of Test for Determining Resilient Modulus of Soils and Aggregate Materials"*. The Geocomp automated resilient modulus test setup (*see* Figure 2.6) was utilized in this study. The setup consists of a Load Trac-II load frame, a hydraulic pump, a servo value with a hydraulic cylinder, an external signal conditioning unit, and a computer with a network card for data acquisition. The system utilizes a high speed, precision micro stepper motor to apply the vertical load as well as constant rate of displacement. The servo value is coupled with hydraulic actuator driven by an air-cooled hydraulic pump for applying cyclic loads. The repeated axial deviator stress of a fixed magnitude, load duration, and cycle duration during a resilient modulus test are facilitated by a closed-loop electro-hydraulic system (Marr *et al.* 2003).

Figure 2.7 shows the triaxial chamber used in this study. This chamber is setup to perform resilient modulus tests on 71 mm (2.8 in.) and 101.6 mm (4 in) diameter samples. LVDT is mounted to the piston rod to measure resilient strains in the sample during the test. According to Marr *et al.* (2003), the use of one versus two LVDT's with this system (two LVDT's is suggested in AASHTO T-307) does not make a difference as the LVDT's rest on a rigid surface.

Tests were performed using AASHTO T-307 conditioning and loading sequences suggested for subgrade and base course materials. Each load cycle consisted of a 0.1 second harversine load pulse followed by a 0.9 second rest period. Summary results based on the average of the last five

cycles of a loading sequence are output by the Geocomp Resilient Modulus software. Regression coefficients are also shown in the summary chart provided by the software. Following the resilient modulus test, unconsolidated undrained (UU) strength testing, also referred to as the quick-shear test, was performed. The UU tests were performed up to a maximum of 5% axial, or failure, whichever occurs first.
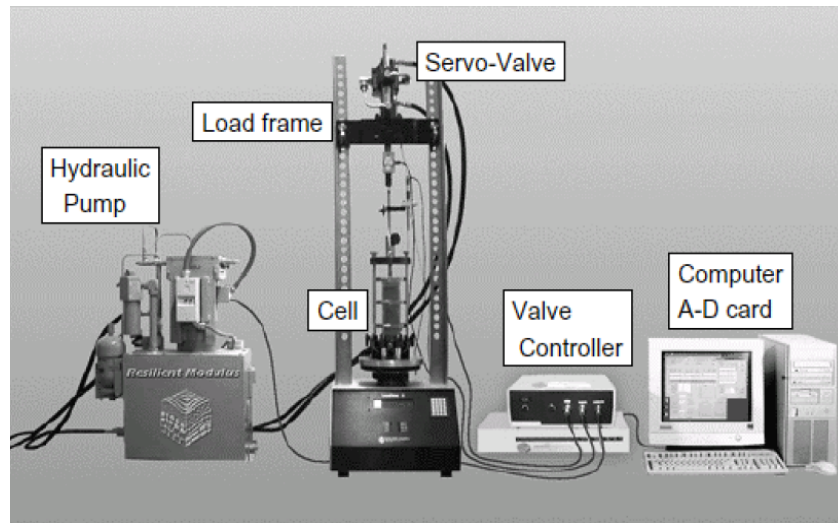
Figure 2.6. Geocomp automated resilient modulus system setup (Marr *et al*. 2003)

Figure 2.7. Resilient modulus triaxial chamber setup

For cohesive soils, 71.1 mm (2.8 inch) diameter by 142.2 mm (5.6 inch) height specimens were prepared, while for granular soils, 101.6 mm (4 inch) diameter by 203.2 mm (8 inch) height specimens were prepared. Soil samples were moisture conditioned before compaction. Cohesive soil samples were mellowed for about 24 hours, and granular samples were mellowed for about 1 hour. Three different compaction methods (static, impact, and vibratory) were used in preparing test specimens. Cohesive soils were compacted in a special compaction mold fabricated for this research (*see* Figure 2.8). Granular soils were compacted directly on top of the triaxial chamber platen with the aid of a split mold (*see* Figure 2.9).

Cohesive Soil Specimen Preparation

Static compaction was performed on cohesive soils in accordance with the procedure suggested in AASHTO T-307 for Type 2 soils. Specimens were compacted in five 14.2 mm thick layers statically using a hydraulic jack (*see* Figure 2.8a) with the aid of spacer plugs to achieve a target density at a given moisture content. Each layer consisted of an equal mass of material. The mold was inverted after compacting each layer, and the layer was scarified before placing a new layer.

For impact compaction, the specimens were also compacted in five layers of equal mass and thickness (14.2 mm). Each layer was compacted using a Marshall hammer with the aid of spacer plugs (*see* Figure 2.8b). Similar to the static compaction method, the mold was inverted after compacting each layer and the layer was scarified before placing a new layer. Impact blows were applied until the plug was level with the top of the sample mold.

Vibratory compaction was also performed in five layers of equal mass and thickness (14.2 mm). A new layer was placed directly on top of the previous layer without inverting the mold. Vibratory compaction was achieved using an electric rotary drill hammer. The compaction process was continued until reaching a predetermined target height. This process is shown in Figure 2.8c.

After compaction, the specimens were extruded into the extrusion mold and weighed. The specimens were then carefully placed in the triaxial chamber.

Granular Soil Specimen Preparation

For impact compaction, specimens were compacted in six layers of equal mass and thickness (33.9 mm). Each layer was compacted using the standard Proctor hammer until a target density was achieved (*see* Figure 2.9a). Vibratory compaction was also performed in six layers of equal mass and thickness. Vibratory compaction was achieved using an electric rotary drill hammer. The compaction process was continued until the predetermined density was reached. This process is shown in Figure 2.9b.

After compaction, a filter paper, porous stone and top platen were placed on the sample, and the rubber membrane was rolled off the split mold. Two O-rings were placed on the top platen to secure the membrane. A vacuum was applied to the specimen and the split mold was removed. The triaxial chamber was then assembled for testing.

(a) (b) (c)
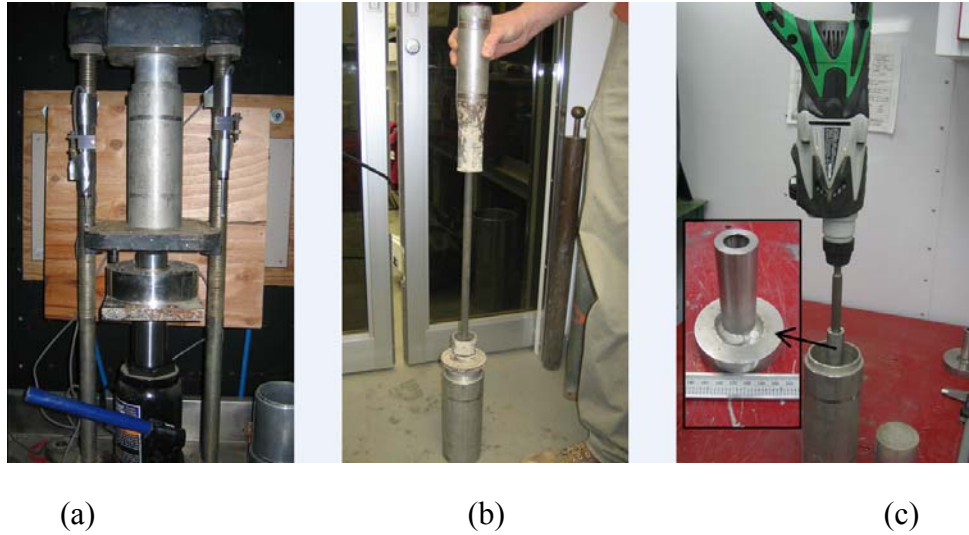
Figure 2.8. Compaction procedures for cohesive soil specimen preparation: (a) static, (b) impact, and (c) vibratory

(a) (b)
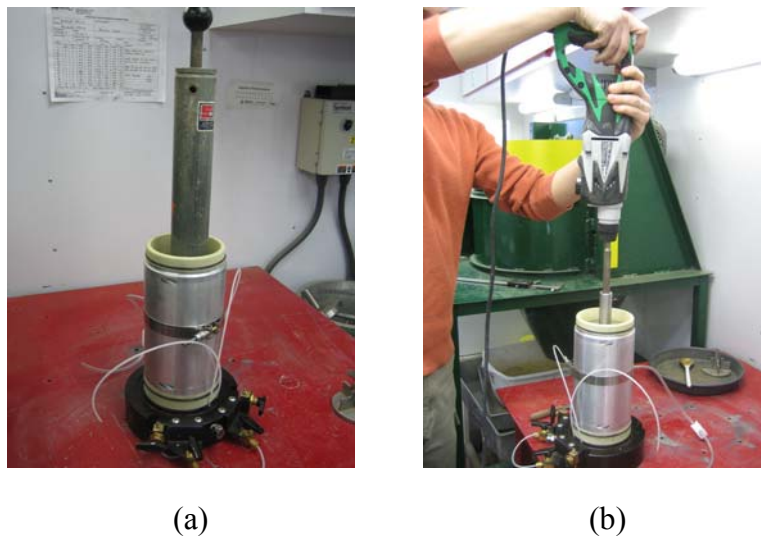
Figure 2.9. Compaction procedures for granular soil specimen preparation: (a) impact and (b) vibratory

2.2 Field Testing Methods

The calibrated nuclear moisture-density gauge provided a rapid measurement of soil dry unit weight and moisture content. The Humboldt HS-5001B122 device is shown in Figure 2.10. Following ASTM WK218, two measurements of moisture and dry unit weight at a particular location were averaged.

Figure 2.10. Nuclear moisture-density gauge

The dynamic cone penetrometer, shown in Figure 2.11, is a testing device that provides the stability characteristics of pavement layers. The test involves dropping an 8-kg hammer 575 mm (i.e. drop height) and measuring the penetration rate of a 20-mm-diameter cone. Penetration index, which typically has units of mm per blow, is inversely related to penetration resistance (i.e. soil strength). DCP testing is discussed in literature (Burnham and Johnson 1993; Gabr *et al*. 2000; Livneh *et al*. 2000; Siekmeier *et al*. 2000; Gabr *et al*. 2001; Konrad and Lachance 2001; Amini 2004; Ampadu and Arthur 2006) with a general focus of correlating DCP index to other measures of pavement performance (e.g. CBR, modulus). The following relationships have previously been proposed in ASTM D 6951-03:

$$CBR = \frac{292}{(DCPI)^{1.12}} \text{, all soils except for CH and CL soils with CBR < 10} \tag{2.5}$$

$$CBR = \frac{1}{(0.017019 \cdot DCPI)^2} \text{, CL soils with CBR < 10} \tag{2.6}$$

$$CBR = \frac{1}{(0.002871 \cdot DCPI)} \text{, CH soils} \tag{2.7}$$

Figure 2.11. Strength determination using dynamic cone penetrometer

Soil strength (DCPI) profiles were converted to single values for assessing roller-integrated compaction data. In some cases the initial penetration – DCP index at the soil surface, denoted as $DCPI_S$ – can be used for correlation with other roller-integrated or in-situ compaction measurements. Two other typical approaches are to calculate "average" and "weighted mean" DCP index values from the soil surface to a depth (z). The calculations for these parameters are provided in equation 2.4 and equation 2.5. A fourth method, which is sometimes used by Mn/DOT for quality acceptance of compacted materials, is described in equation 2.10. Two seating drops are followed by three additional drops from which the average DCP index (DPI in this case) is calculated. Example calculations for the second and third methods are provided in Appendix A.

$$DCPI_{A\text{-}z} = \frac{Penetration_z}{Cumulative\ blows\ to\ penetration} \tag{2.8}$$

$$DCPI_{M\text{-}z} = \frac{DCPI_1 \cdot z_1 + DCPI_2 \cdot z_2 + ... + DCPI_n \cdot z_n}{\sum z_n} \tag{2.9}$$

$$DPI = \frac{\sum_{i=3}^{5} Penetration_i}{3\ blows} \tag{2.10}$$

16

Clegg impact hammers, which were developed by Clegg during the late 1970's and later standardized as ASTM D 5874-02 for evaluating compacted fill and pavement materials, are shown in Figure 2.12. The Clegg impact value is derived from the peak deceleration of a 4.5-kg or 20-kg hammer free falling 450 mm in a guide sleeve for four consecutive drops. Clegg impact values ($CIV_{4.5-kg}$ or CIV_{20-kg}) have been correlated to CBR (Clegg 1986).

$$CBR = (0.24\,IV + 1)^2 \tag{2.11}$$

Figure 2.12. Strength determination using Clegg impact testers: 4.5-kg (left) and 20-kg (right)

The soil stiffness gauge (see Figure 2.13) may be the least destructive device for obtaining the in-situ deformation characteristics of soil. The device, which is also referred to as the GeoGauge, rests on the soil surface and vibrates at 25 frequencies ranging from 100 to 196 Hz. The vibrating device produces small dynamic forces and soil deflections, from which soil modulus can be calculated as (Humboldt Mfg. Co. 2000):

$$E_{SSG} = \frac{F}{\delta} \cdot \frac{(1-v^2)}{(1.77R)} \tag{2.12}$$

where F is a dynamic force caused by the vibrating device, δ is the deflection measured with a geophone, v is Poisson's ratio, and R is the radius of the annular ring. Only modulus from the soil stiffness gauge (E_{SSG}) was used for developing correlations with other soil properties, because stiffness and modulus from the SSG are related through a linear relationship, dependent on Poisson's ratio ($v = 0.40$) and the diameter of the annular ring of the device (Humboldt Mfg. Co. 2000).

Figure 2.13. Modulus determination using soil stiffness gauge

Two light weight deflectometers (LWDs) were used to determine elastic modulus. In performing the tests with the Keros model, a 10-kg weight is dropped to produce a dynamic load on a plate. A load sensor measures the load pulse, and a geophone at the center of the plate measures the corresponding soil deflection. For the Zorn ZFG model, a plate stress is assumed based on calibration of the falling weight, and plate deflection is obtained from an accelerometer. For both devices, soil modulus is then calculated as:

$$\mathrm{E_{LWD\text{-}K2(DH)}} \text{ or } \mathrm{E_{LWD\text{-}Z2(DH)}} = \frac{f\,(1 - v^2) \cdot \sigma_0 \cdot r}{h_0} \tag{2.13}$$

where $E_{LWD\text{-}K2}$ = elastic modulus from 200-mm Keros device, $E_{LWD\text{-}Z2}$ = elastic modulus from 200-mm Zorn device, DH = drop height in cm, v = Poisson's ratio ($v = 0.40$), σ_0 = peak applied stress at surface, r = plate radius, h_0 = peak plate deflection, and f is a factor that depends on the stress distribution (*see* Chapter 9).

Figure 2.14. 300-mm light weight deflectometers: Zorn ZFG (left) and Keros (right)

Displacement-controlled static plate load tests were performed for soil modulus (E_{V1}) using a 300-mm plate, a 90-kN load cell, and three 50-mm linear voltage displacement transducers (LVDT). Elastic modulus (E_{V1}) was calculated with equation 2.8, with the stiffness response taken from 0.2 to 0.4 MPa plate stress for granular soil and from 0.1 to 0.2 MPa for cohesive soil (see Figure 2.16).
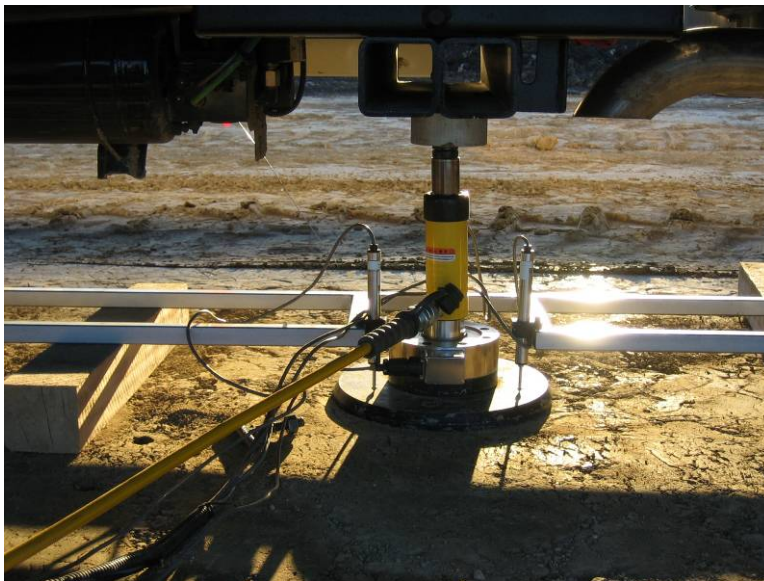
Figure 2.15. Static plate load test performed for modulus determination using 300-mm plate, load cell, and three displacement transducers

19
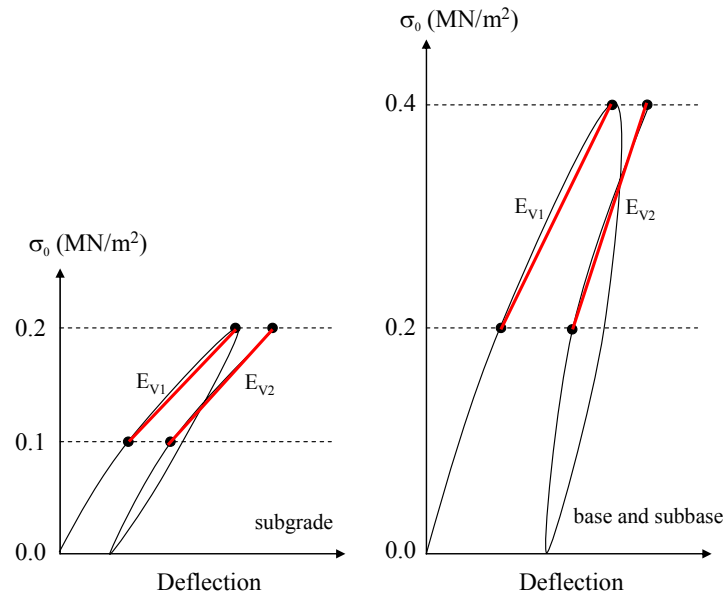
Figure 2.16. Static plate load test data modulus scheme for subgrade, subbase, and base materials

Chapter 3
Field Study 1: CMV and MDP Evaluation at US 14

3.1 Project Description

Field Study 1 is comprised of field measurements and intelligent compaction data collected during a demonstration project held from July 18 to 21, 2005 on US 14 near Janesville, MN. Field testing for dry unit weight, moisture content, soil strength and modulus were obtained to demonstrate the ability of the Caterpillar Inc. intelligent compaction technology to indicate the level of soil compaction achieved with the prototype roller and identify localized areas of an earthwork construction site that may be poorly compacted.

For this project, two Caterpillar rollers were on site. A CP-533 vibratory padfoot collected machine drive power (MDP) measurements, and a CS-563 vibratory smooth drum roller (see Figure 3.1) collected MDP and Compaction Meter Value (CMV) measurements.

Figure 3.1. Caterpillar CS-563 vibratory smooth drum roller

The specific objectives of the field study included:

- Demonstrating intelligent compaction technology for a transportation agency (Mn/DOT) and earthwork contractors, and discussing the role of such technology in construction and quality management.

- Demonstrating the use of in-situ testing devices (e.g. dynamic cone penetration, Clegg impact test, and light weight deflectometers) with emphasis placed on using soil properties from these compaction control tests to calibrate and evaluate intelligent compaction technology.

- Mapping select areas of the project with the intelligent compaction technology. Performing in-situ tests to verify soil properties of localized weak spots identified by the roller.

- Comparing the MDP and CMV intelligent compaction technologies.

3.2 Description of CMV and MDP Technologies

CMV technology uses accelerometers installed on the drum of a vibratory roller to measure roller drum accelerations in response to soil behavior during compaction operations. Previous studies have found that the ratio between the amplitude of the first harmonic (A_1) and the amplitude of the fundamental frequency (A_0) is a reliable indicator of soil compaction. Accordingly, CMV is defined as:

$$CMV = C \cdot \frac{A_1}{A_0}$$

$$(3.1)$$

where C is a constant equal to 300 to give a full scale reading of about 100. CMV technology is further described by Sandström and Pettersson (2004). CMV has been correlated to conventional in-situ field compaction measurements by White and Thompson (2006) for several soils.

The use of MDP as a measure of soil compaction is a concept originating from study of vehicle-terrain interaction. MDP, which relates to the soil properties controlling drum sinkage, uses the concepts of rolling resistance and sinkage to determine the stresses acting on the drum and the energy necessary to overcome the resistance to motion (White *et al*. 2005, Komandi 1999, Muro and O'Brien 2004). Using MDP for describing soil compaction, where higher power indicates soft or weak material and lower power indicates compact or stiff material, is documented by White *et al*. (2004) and White *et al*. (2005). The net MDP that is required to propel the machine over a layer of soil can be represented as:

$$MDP = P_g - WV\left(\sin\theta + \frac{a}{g}\right) - (mV + b)$$

$$(3.2)$$

where P_g is the gross power needed to move the machine, W is the roller weight, V is the roller velocity, θ is a slope angle, a is acceleration of the machine, g is acceleration of gravity, m and b are machine internal loss coefficients specific to a particular machine (White *et al*. 2005). The second and third terms of equation (2) account for the machine power associated with sloping grade and internal machine loss, respectively. Further details of the calibration process of machine internal loss coefficients are described in White and Thompson (2006).

3.3 Testing Methods and Material Properties

Testing methods for this field study followed procedures documented in Chapter 2.

Laboratory and in-situ compaction measurements were collected for existing subgrade and granular borrow materials at the US 14 highway reconstruction project. The borrow material classifies as SW-SM well graded sand with silt and as A-1-b. The classification properties of the soil are summarized in Table 3.1. The particle size distribution curve is provided in Figure 3.2.

Table 3.1. Schedule of testing material

Soil Property	Granular Borrow
USCS	SW-SM
AASHTO	A-1-b (0)
$F_{3/4}$ (%)	98
$F_{3/8}$ (%)	93
F_4(%)	88
F_{200} (%)	9
Percent gravel (>4.75 mm)	12
Percent sand (>0.075 mm)	79
Percent silt (>0.002 mm)	–
Percent clay (<0.002 mm)	–
C_u	8.8
C_c	1.0
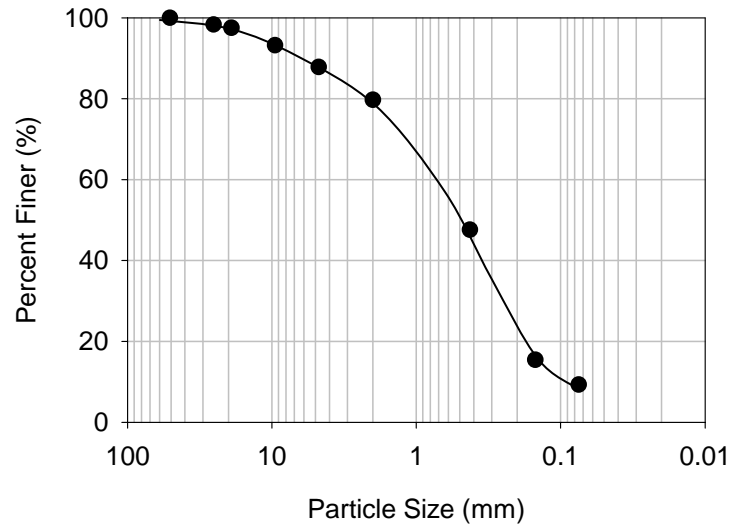
Figure 3.2. Particle size distribution curve for WB Mainline granular borrow material

3.4 Experimental Evaluation of Intelligent Compaction Technologies

This section provides details on the intelligent compaction mapping trials and the in-situ test results at select locations of the project site. The trials, which are comprised of paired roller and in-situ soil property measurements, are described in the following sections.

3.4.1 Testing Location No. 1: Westbound Mainline from STA 345 to 360

Intelligent compaction data (both MDP and CMV) were collected along westbound Mainline from Station 345 to 360 on July 20 using the CS-563 smooth drum roller. Dry unit weight, moisture content, strength, and modulus of the clean sand material were determined using in-situ testing devices at ten randomly-spaced test points within these limits. The compaction monitor view of the tested area is shown in Figure 3.3.
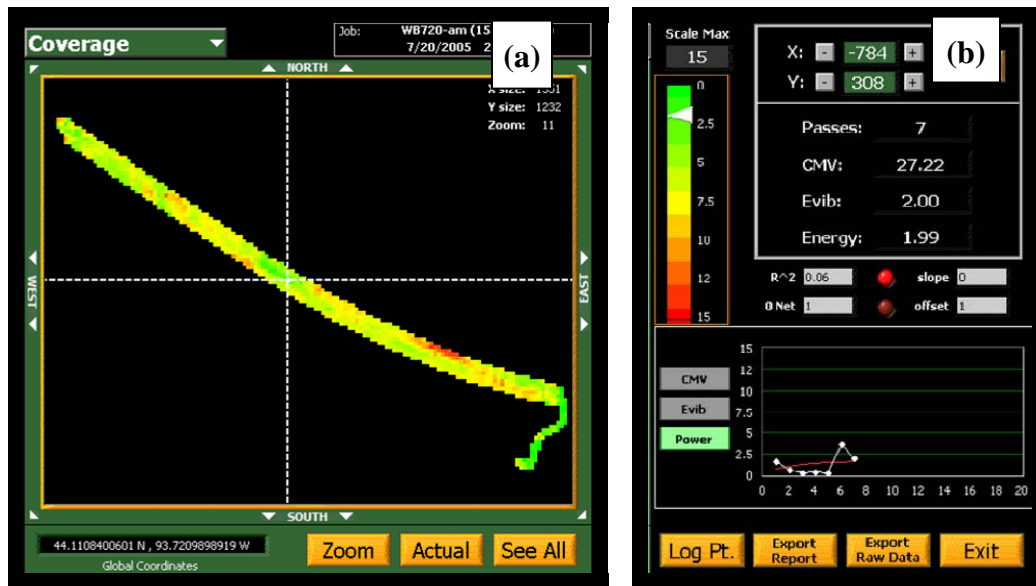
Figure 3.3. Compaction monitor view (viewing area 473 x 376 m) for WB Mainline: (a) MDP and (b) reference scale and compaction history

Variation in both roller-integrated and in-situ compaction measurements was observed over the test area. Both MDP and CMV are shown in Figure 3.4 for the ten test points, along with modulus, Clegg impact value, and dry unit weight measurements. The beginning and end of the test area (test points 1 and 10) exhibited considerably different soil deformation characteristics. Soil strength and modulus at these locations were determined using dynamic cone penetrometer and static plate load tests. DCP profiles and plate stress-deflection relationships at the two test points are provided in Figure 3.5. From these tests, both soil strength and modulus are observed to be higher at Point 10 than at Point 1. The unload-reload modulus values are comparable for tests performed at each location.
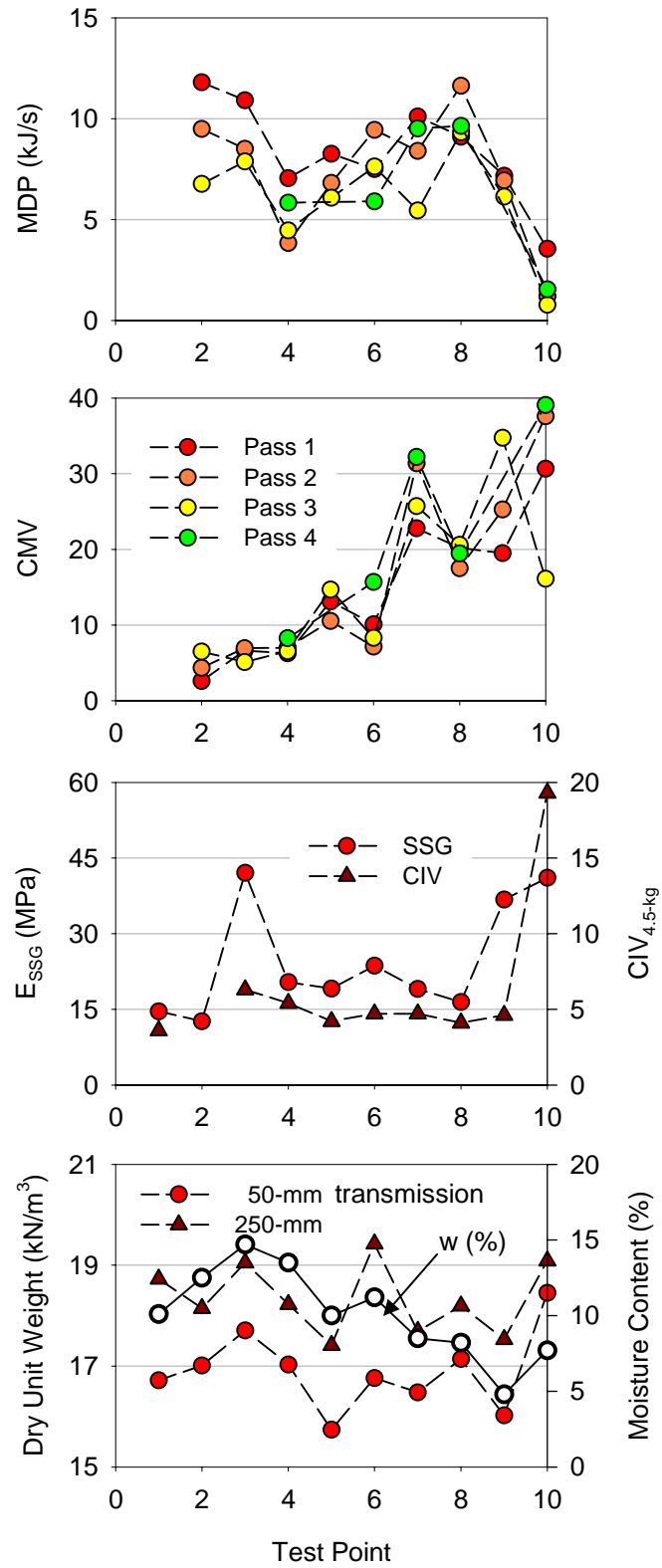
Figure 3.4. Roller-integrated and in-situ compaction measurements at test locations
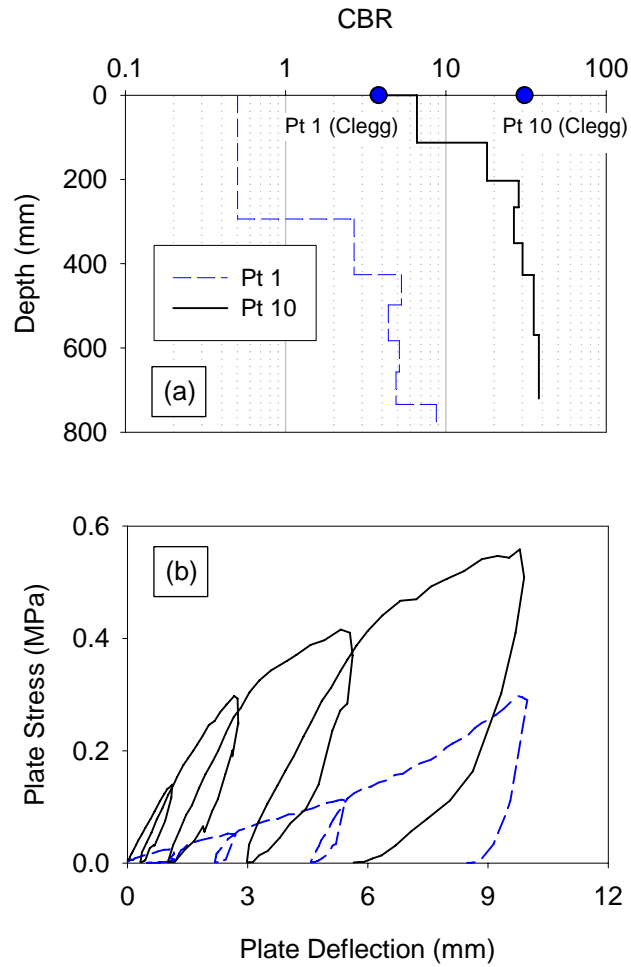
Figure 3.5. CBR profiles (calculated from DCP index) from WB STA 345 to 360 at static plate load test locations

Scatter plots that compare field measurements with intelligent compaction data are provided in Figure 3.6. The observed relationships are statistically weak and/or strongly influenced by one or two points. In some cases, the models were not significant (i.e. the linear model did not provide a better prediction of the field measurement than the overall mean). The models for dry unit weight, for example, are not provided. Insufficient data were available to apply averaging techniques for mitigating the effects of measurement variability (see White *et al.* 2006).
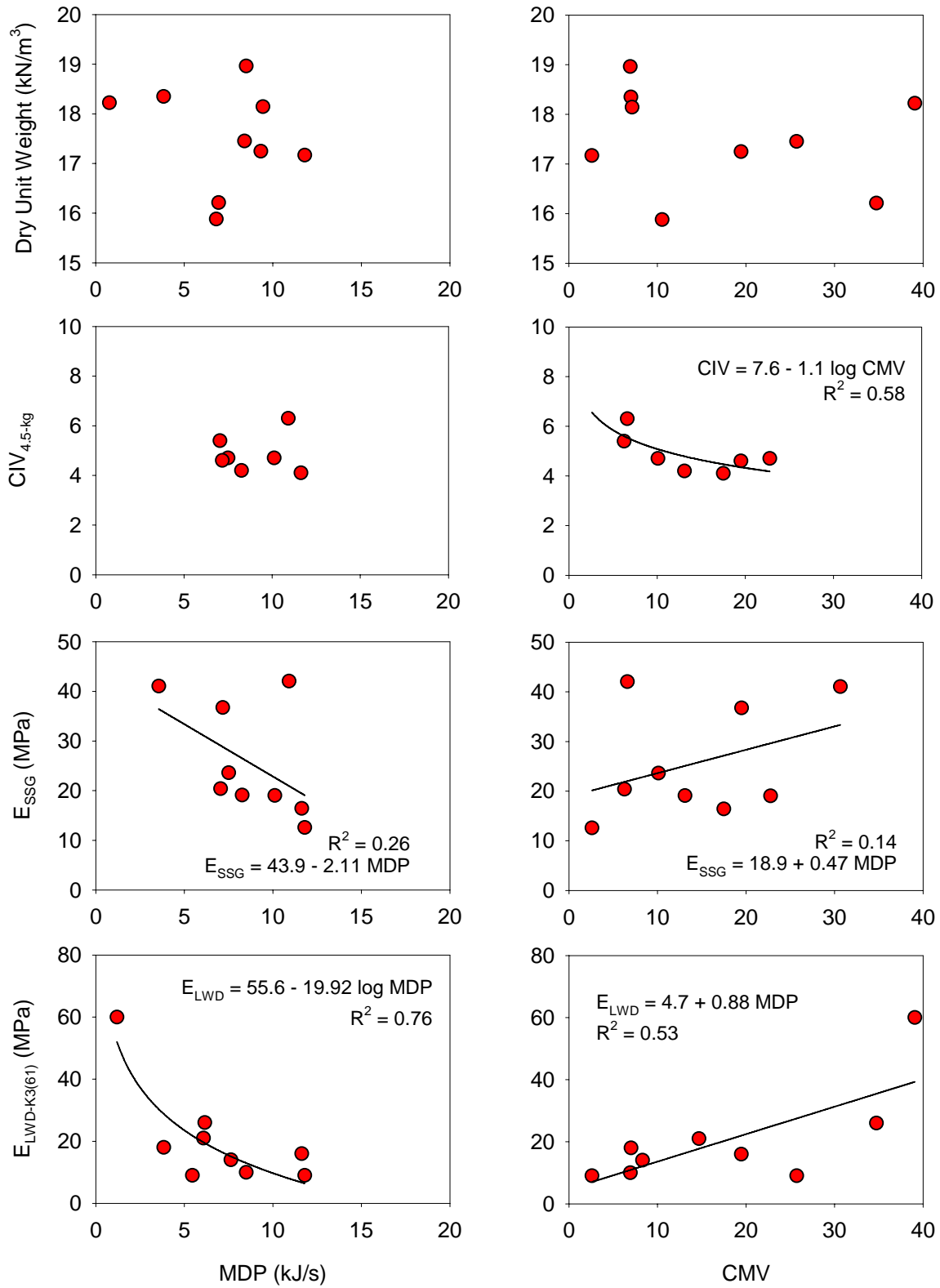
Figure 3.6. Scatter plots of roller-integrated and in-situ compaction measurements

MDP and CMV data from the test area were explored by sorting the data by pass number and producing frequency distribution plots. These plots are shown in Figure 3.7. Average MDP is observed to decrease with increasing roller passes. The more compact material offers less resistance to roller motion. Average CMV increases with roller pass to indicate increasing soil stiffness. Both roller-integrated compaction measurements were variable. The soil surface was comprised of fine sand and uniformly loose due to lack of confinement. And, considering that MDP is believed to be controlled largely by soil properties at the soil surface, MDP was less variable than CMV.

Raw (i.e. statistically untreated) MDP and CMV data were weakly correlated.
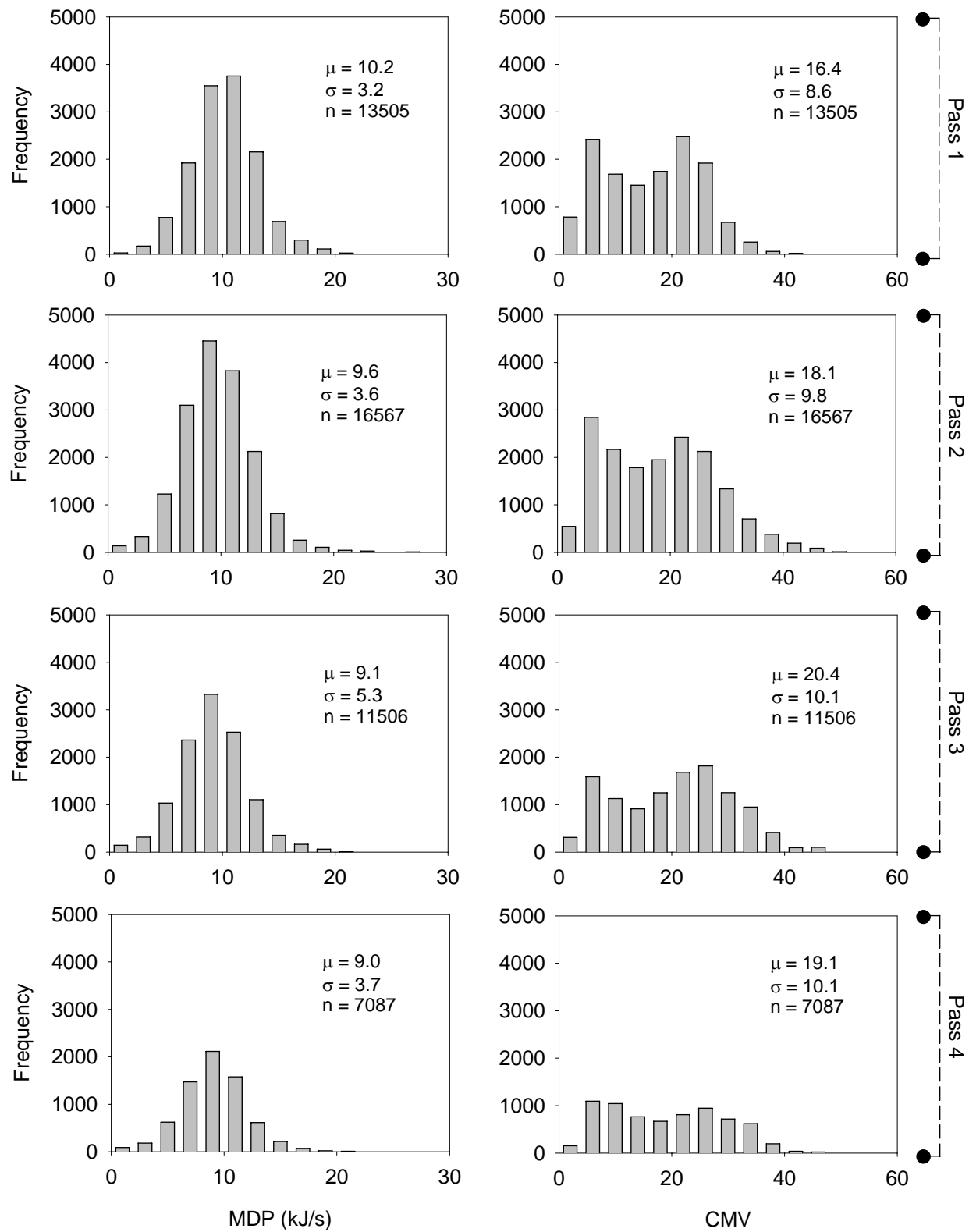
Figure 3.7. Distribution of MDP and CMV for westbound Mainline, STA 345 to 360

3.4.2 Testing Location No. 2: Eastbound Mainline from STA 345 to 360

MDP and CMV measurements were collected on eastbound Mainline from STA 362 to 385 on July 19. As the data were also collected for sand material, MDP showed distributions of data similar to those for westbound Mainline (Testing Location No. 1). The mean values were slightly lower than for westbound Mainline, but standard deviations of the data were higher.

Mean CMV was higher than for westbound Mainline, consistent with lower MDP (higher stiffness). The variation of the measurement was considerably higher with standard deviation ranging from about 13 to 20 (coefficient of variation from 53 to 74 percent). Compaction was achieved below the soil surface due to the aid of confinement. The loose material at the surface, however, may be responsible for producing variable CMV measurements.

Previous testing on granular materials with MDP and CMV showed MDP to be more locally variable (White and Thompson 2006). The data from US 14 demonstrates the need to better understand how surface and subsurface layers affect roller-generated measurements (taken at the surface), including the measurement influence depth and also the relative influence of soil properties at different depths on roller measurements.
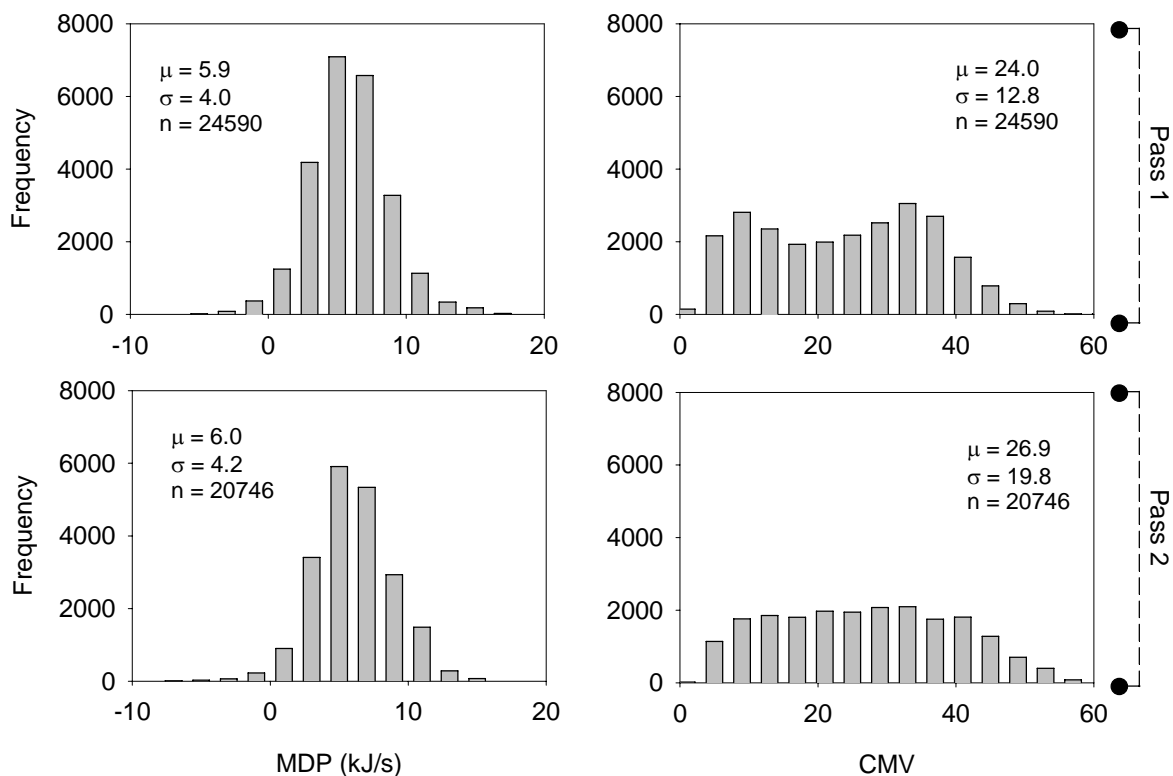
Figure 3.8. Distribution of MDP and CMV for eastbound Mainline, STA 345 to 360

3.4.3 Testing Location No. 3: Eastbound Mainline from STA 362 to 385

Test rolling (see Mn/DOT specification 2111) at the US 14 project serves as acceptance testing for the constructed subgrade. The test roller shown in Figure 3.9 is comprised of a 267-kN load pulled on a rubber-tired trailer to give a target contact pressure of 650 kPa. To ensure quality, rutting observed using the test roller is limited to about 1.9 cm (0.75 inch). To evaluate whether intelligent compaction technology might also identify weak subgrade susceptible to poor performance, several areas of the project were mapped using the prototype roller and then test rolled on July 19.

Figure 3.9. Test roller used for quality acceptance

The intelligent compaction data collected on the eastbound Mainline from STA 362 to 385 using the CP-533 is shown in Figure 3.10 (a) as a screen capture from the onboard monitor. The roller data indicate that a referenced level of soil stability corresponding to the calibration surface is achieved for most of the test area, evidenced by largely green cells observed over the compacted area. Several sections of the subgrade, however, are shown to have lower stability by yellow or red pixels in the compaction monitor view. This entire test area was then test rolled, and rutting was observed (see Figure 3.10 (b)). Five test points were established. Points 1, 2, and 3 showed considerable rutting. Point 5 showed minimal rutting (see Figure 3.11). These specific locations were tested with the dynamic cone penetrometer and moisture content with the field moisture oven (FMO). DCP profiles for the test points are shown in Figure 3.12. The moisture content was about 23 percent near Point 4 and about 12 percent near Point 5. The comparatively-wet moisture contents near Point 4 are likely responsible for low stability and the areas shown by MDP to require either additional compaction or alternative measures to dry the soil for increasing stability.

Figure 3.10. Eastbound STA 362 to 385: (a) compaction monitor view (viewing area 165 x 132 m) and (b) rutting at Point 4
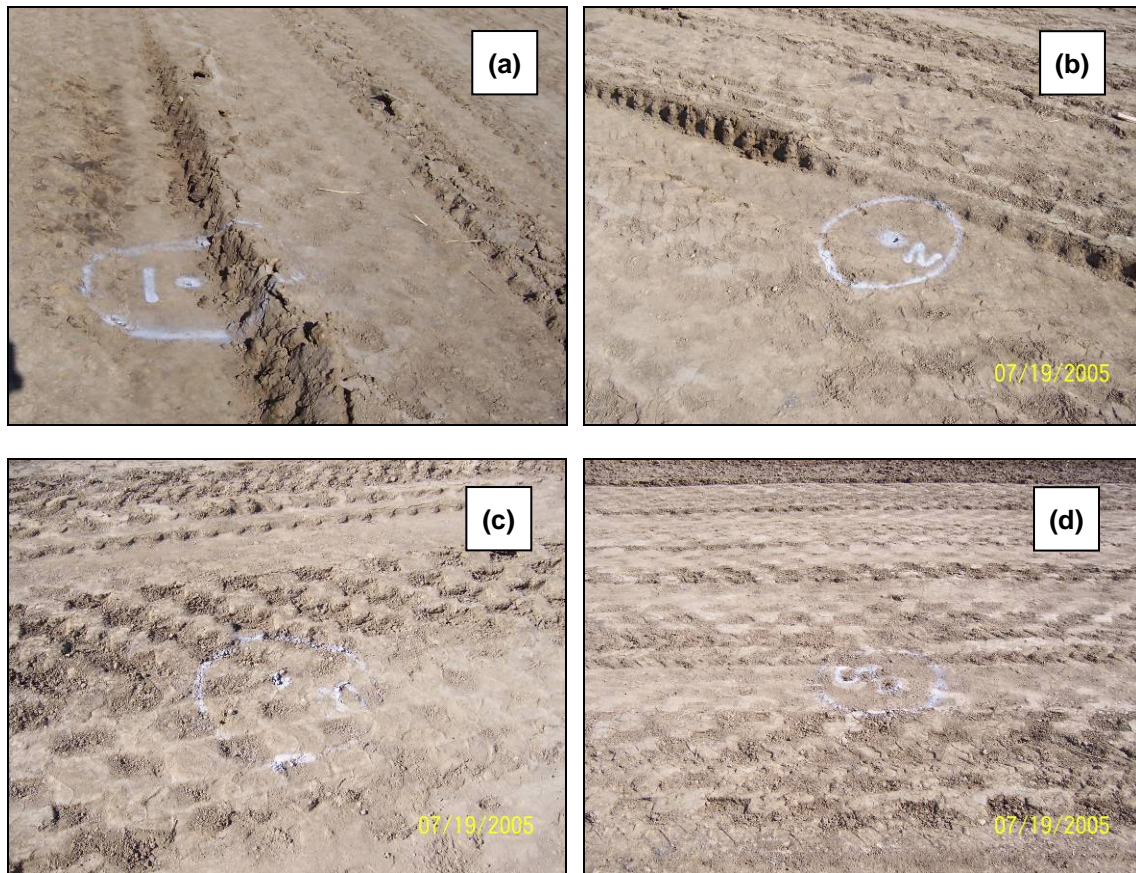
Figure 3.11. Test rolling results at EB STA 362 to 385: (a) Pt 1, (b) Pt 2, (c) Pt 3, and (d) Pt 5
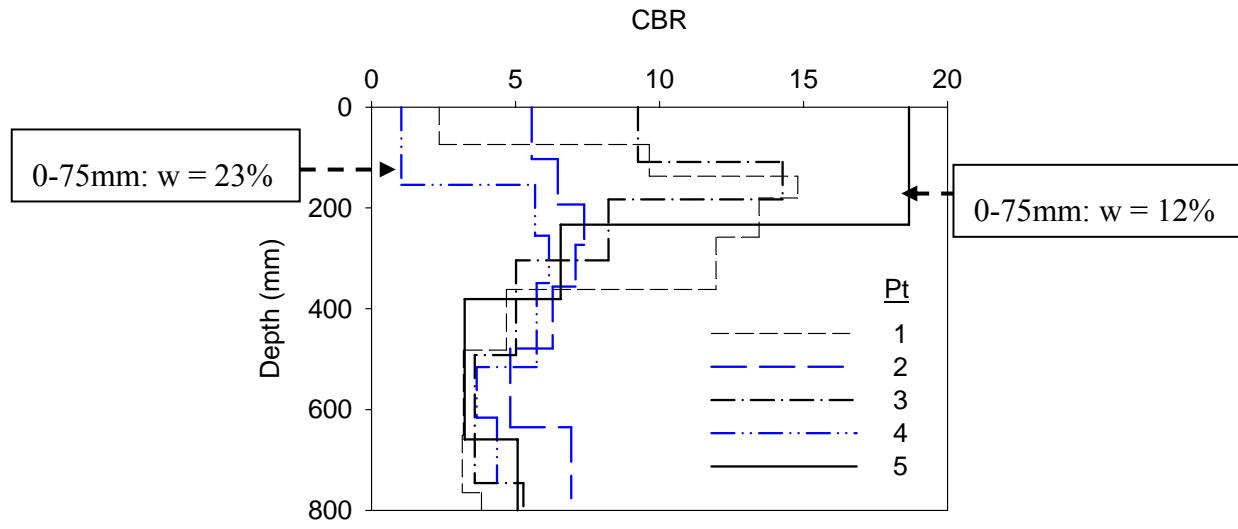
(a)

(b)

Figure 3.12. Field measurements: (a) DCP profiles and moisture contents and (b) Field Moisture Oven device

3.4.4 Testing Location No. 4: County 55

The ability of MDP and CMV to identify areas of low stability soil was also illustrated on County 55. As shown in Figure 3.13 through MDP data and also DCP profiles in Figure 3.14, weak (or poorly compacted) soil near Point 1 is indicated by yellow and red pixels in the viewer. Higher-stability measurements were collected near Point 3, based on green pixels in the compaction viewer and higher-CBR profiles. DCP testing confirmed the presence of localized areas of lower and higher stability that matched the MDP results.
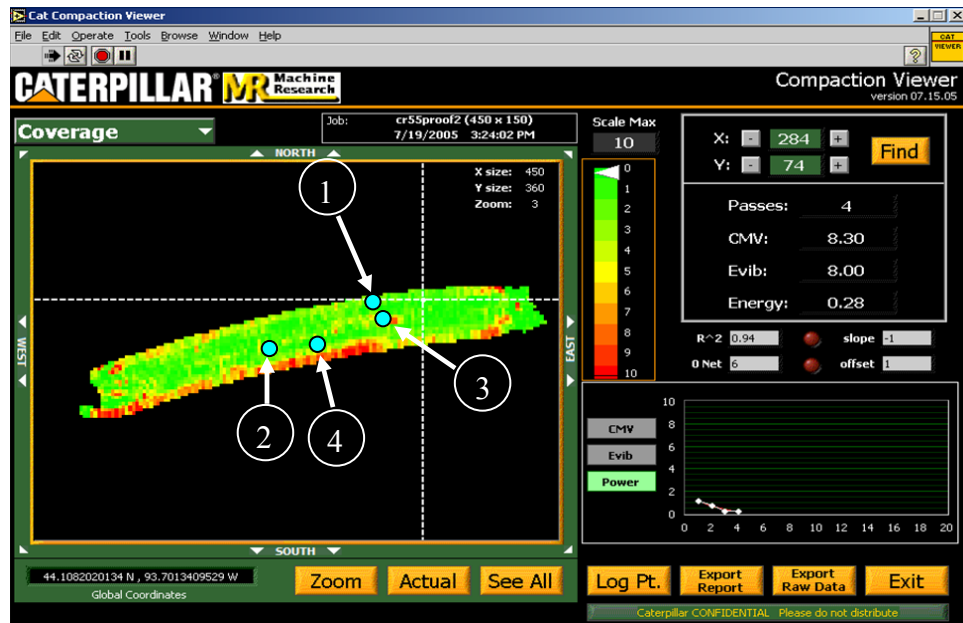
Figure 3.13. Compaction monitor view at County 55 (viewing area 137 x 110 m)
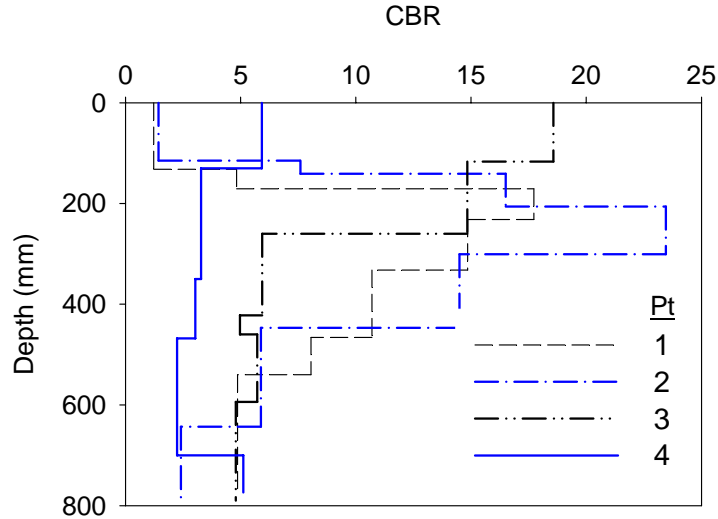
Figure 3.14. DCP profiles at County 55, subgrade

3.5 Project Observations

The following observations were made from experimental testing at US 14 near Janesville, MN.

- Bringing intelligent compaction technology to field projects of transportation agencies helps to transfer the technology to both agency and contractor personnel that will benefit in the future.

- Intelligent compaction technology may identify areas of weak or poorly-compacted soil with real-time readings and 100-percent coverage. Mapping trials were conducted using two instrumented rollers and in-situ testing devices to verify intelligent compaction output. Insufficient data were collected to quantify the reliability of spatial data.

- Monitoring MDP during soil compaction may provide an alternative to test rolling subgrade for assuring quality subgrade resistant to rutting.

- Intelligent compaction technology may not accurately indicate soil compaction (i.e. dry unit weight, strength, or modulus) for granular materials that do not compact at the soil surface, as shown at WB STA 345-360. Clean sands often lack sufficient confining pressure and base friction to achieve high density immediately under the roller.

- For this project, CMV measurements from the CS-563 vibratory smooth drum roller were weakly correlated with MDP for sand.

The following table summarizes intelligent compaction measurements from Field Study 1.

Table 3.2. Observed MDP, CMV and in-situ compaction measurements for sand material (mean, coefficient of variation (%))

Location	Soil	MDP (kJ/s) [a]	CMV [a]	Dry Unit Weight (kN/m^3) [b]	Moisture Content (%) [b]
WB STA 345 to 360	SW-SM	9.0, 41	19.1, 53	18.3, 4	10, 30
EB STA 345 to 360	SW-SM	6.0, 70	26.9, 74	–	–
a Last pass data b 250-mm transmission depth					

Chapter 4
Field Study 2: Ammann k_B Evaluation at US 14

4.1 Project Description

Field Study 2 is comprised of field measurements and data collected during a study conducted from October 28 through November 7, 2005 on US 14 near Janesville, Minnesota. Field testing for dry unit weight, moisture content, soil strength, and modulus was conducted. The measurements were compared with the output of the Ammann ACE (Ammann Compaction Expert) variable control smooth drum roller (see Figure 4.1) for a direct assessment of the intelligent compaction technology.

Figure 4.1. Ammann vibratory smooth drum roller

4.2 Description of Ammann k_B System

The dynamic characteristics of a vibratory roller drum on soil have been described analytically. The soil-drum interaction force is defined as:

$$F_B = -m_d\,\ddot{u}_d + m_u\,r_u\,\Omega^2 \cdot \cos(\Omega t) + (m_f + m_d) \cdot g \qquad (4.1)$$

where m_d = mass of the drum, u_d = vertical displacement of the drum, $\ddot{u}_d$ = acceleration of the drum, m_f = mass of the frame, m_u = unbalanced mass, r_u = radial distance at which m_u is

attached, $m_u r_u$ = static moment of the rotating shaft, $\Omega = 2\pi f$, t = time, g = acceleration due to gravity, and f = frequency of the rotating shaft (Anderegg 2000). Soil is described using spring-dashpot elements, where the soil-force is given by:

$$F_B = k_B u_d + d_B \mathring{u}_d \qquad\qquad (4.2)$$

By setting these two equations equal to each other, the Ammann system calculates k_B – soil stiffness – as a measure of stability and the level of compaction achieved with the roller. The roller-measured stiffness is reportedly independent of machine-related parameters such as the frequency and rotating eccentric shaft mass (Anderegg 2000).

Vibratory rollers may achieve different compaction results by adjusting the amplitude and/or frequency of drum vibration. Higher drum amplitude delivers greater energy to the soil, resulting in a more stable, compacted material. Lower drum amplitude produces a lesser compaction effect. The Ammann system combines soil stiffness measurement with automatic feedback control of both amplitude and frequency parameters based on existing soil characteristics. In using the variable control operation mode, the important factors to be considered include:

- High-amplitude and to some degree low-frequency vibration compacts deeper than low amplitude-high frequency vibration. To this end, high amplitude-low frequency vibration is used on thicker soil lifts and during initial passes of a freshly-placed lift.

- High-amplitude vibration has a tendency to loosen surface layer material and cause overcompaction and grain crushing during later passes. Therefore, low amplitude-high frequency vibration is more ideal for the finishing passes.

- The measurement depth (the depth influencing the k_B measurement), which can range up to 1.5 m (ISSMGE), may be influenced by vibration amplitude and frequency.

4.3 Material Properties

Laboratory and in-situ compaction measurements were collected for two soils from the US 14 highway reconstruction project, namely subgrade and Class 5 subbase materials. The subgrade soil classifies as CL sandy lean clay, while the Class 5 subbase material classifies as SP-SM poorly graded sand with silt and gravel. The classification and compaction properties of the soils are summarized in Table 4.1. Particle size distribution curves are provided in Figure 4.2. Standard Proctor moisture-density relationships are provided in Figure 4.3 and Figure 4.4 for subgrade and Class 5 subbase materials, respectively.

Table 4.1. Schedule of testing materials

Soil Property	Subgrade	Class 5
USCS	CL sandy lean clay	SP-SM poorly graded sand with silt and gravel
AASHTO	A-6 (9)	A-1-b(0)
$F_{3/4}$ (%)	100	97
$F_{3/8}$ (%)	100	82
F_4(%)	98	73
F_{200} (%)	62	9
Percent gravel (>4.75 mm)	2	27
Percent sand (>0.075 mm)	86	64
Percent silt (>0.002 mm)	37	6
Percent clay (<0.002 mm)	25	3
LL (PI)	39 (17)	NP
Standard Proctor:		
$\gamma_{d, max}$ (kN/m	16.16	19.58
w_{opt} (%)	18.1	8.1
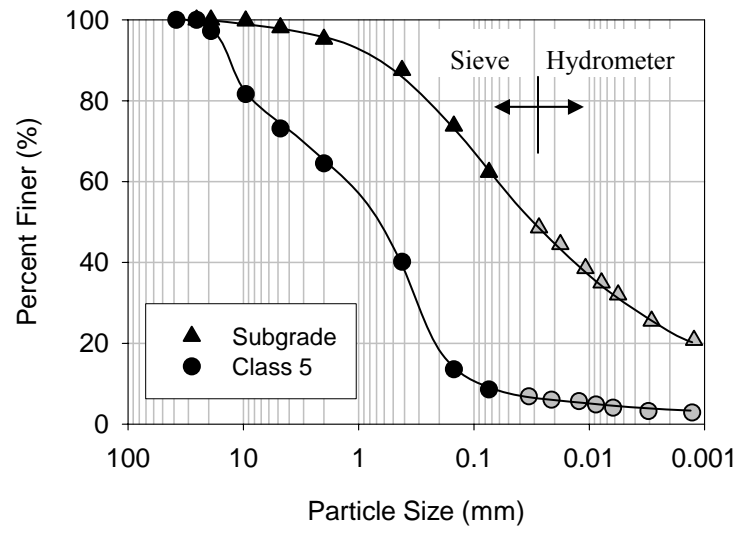
Figure 4.2. Particle size distribution curves for subgrade and Class 5 materials
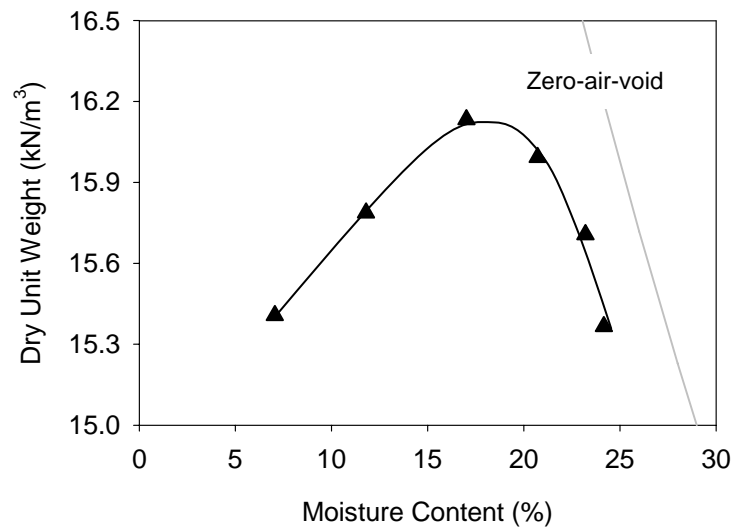
Figure 4.3. Standard Proctor moisture-density relationship for subgrade material
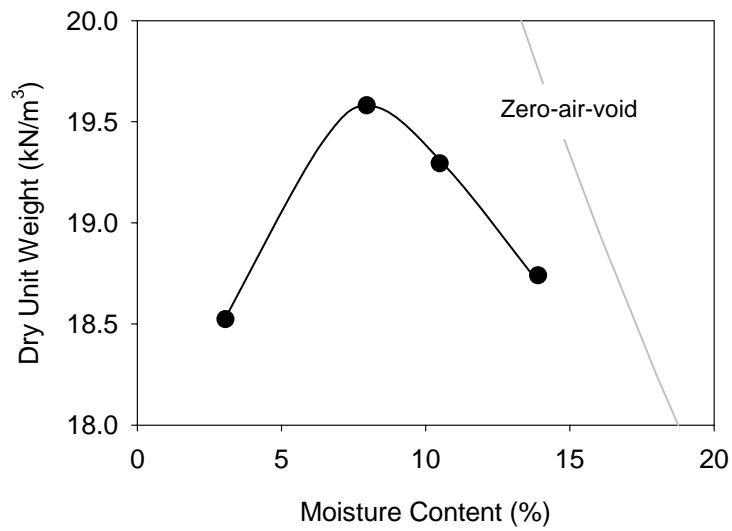
Figure 4.4. Standard Proctor moisture-density relationship for Class 5 subbase material

4.4 Experimental Testing Program

The test strips designed to evaluate the Ammann system are summarized in Table 4.2 and shown from Figure 4.5 to Figure 4.9. Test strips 1 and 4 were established perpendicular to the highway alignment. The roller was operated over both pavement subgrade sections, crossing the comparatively soft median. This arrangement resulted in a wide range of soil stiffness to be identified by the Ammann roller and the in-situ measurement devices. Strips 2, 3, 5, and 6 were prepared to test only one soil in the direction parallel to the highway alignment. In addition to testing subgrade material, several of these strips (Strips 2, 3, and 5) were comprised of Class 5 subbase material. Generally, these strips consisted of more uniform soil conditions, such that the sensitivity of the Ammann k_B measurement to small changes in soil stiffness was observed. In addition, the subbase material at several locations had been placed with variable lift thickness solely as a subgrade cover for the winter season. The material had not yet been compacted and thus gave low dry unit weight and base stability measurement values.

Figure 4.5. Strip 1 (subgrade and median)

Table 4.2. Field testing summary

Strip ID	Date	Location	Soil Type	Test Points	Roller Passes	Amplitude [a]	Strip Length (m)	Roller Points Per Pass
1	10/28	ML 14 at 807+00	Subgrade	20	2	Medium	30	75
2	11/02	WB ML 14, east of 33	Class 5	27	3	High	90	295, 280, 287
3	11/02	WB ML 14, east of 33	Class 5	27	3	Low	90	279, 295, 258
4	11/03	ML 14, parallel to 33	Subgrade	31	2	Medium	45	138, 139
5	11/04	WB ML 14 at 2	Class 5	17	3	Medium	122	374, 383, 374
6, 1	11/07	EB ML 14 at 772+00	Subgrade	11	3	80% Max	60	228, 164, 191
6, 2	11/07	EB ML 14 at 772+00	Subgrade	n/a	3	80% Max	60	236, 163, 189
6, 3	11/07	EB ML 14 at 772+00	Subgrade	n/a	3	High	60	196, 194, 192
6, 4	11/07	EB ML 14 at 772+00	Subgrade	11	3	High	60	197, 196, 193

a Variable amp and freq, except for Strip 6, Tracks 1 and 2; max amp of 2.0 mm, freq from 25 to 35 Hz

Figure 4.6. Strips 2 and 3, side-by-side (Class 5)

(a)
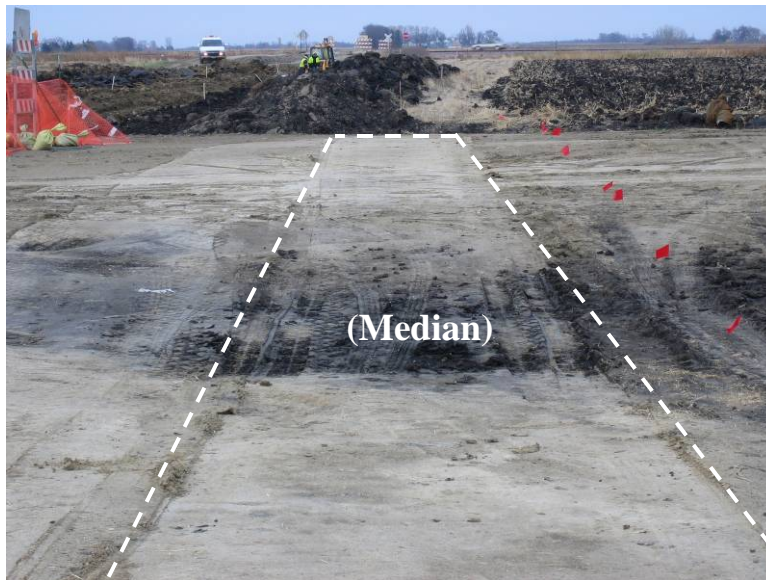
(Median)

(b)

Figure 4.7. Strip 4 (subgrade and median): (a) entire strip and (b) median

Figure 4.8. Strip 5 (Class 5)

(a)

(b)

Figure 4.9. Strip 6 (subgrade): (a) pre-compaction condition and (b) compaction of Track 1

4.5 Test Data

The Ammann k_B output was a list of consecutive measurements, spaced at approximately three pulses per meter. The strip length measurement is therefore based on the number of measured pulses between starting and stopping the data collection system in the roller cab. The in-situ compaction tests were performed at predetermined locations along the test strip, generally at uniformly-spaced intervals (e.g. every 3 m). For Field Study 2, some interpretation in determining the start point for the Ammann data was required. Without using GPS technology to spatially relate k_B data with in-situ compaction measurements, considerable uncertainty in the correlations exist.

Comparisons of k_B and in-situ compaction measurements are provided in the following figures, where all measurements are plotted versus the location along the six test strips. The plots of compaction data show the general trends and potential correlations which are observed between the k_B and the in-situ measurements of soil strength and modulus. In some cases, the k_B trends are not supported by the in-situ test results.
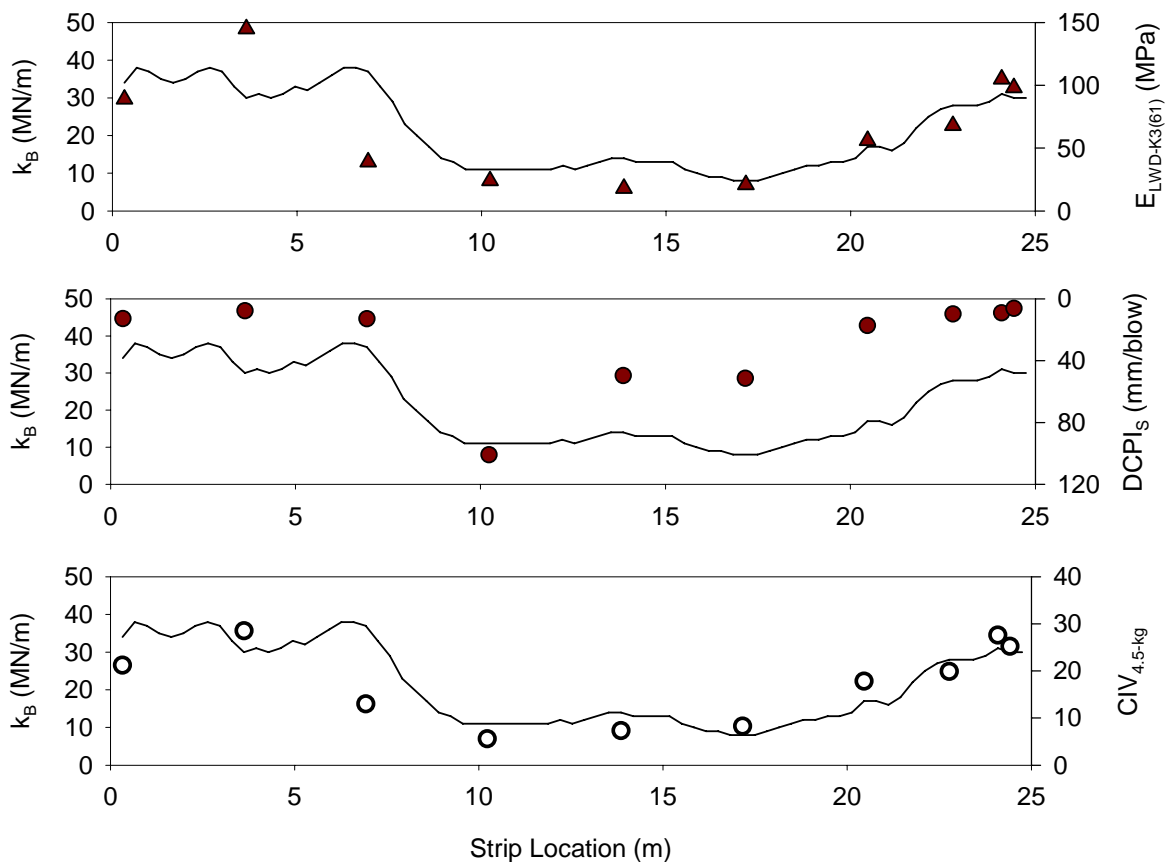
Figure 4.10. Comparison of k_B and in-situ compaction measurements for Strip 1
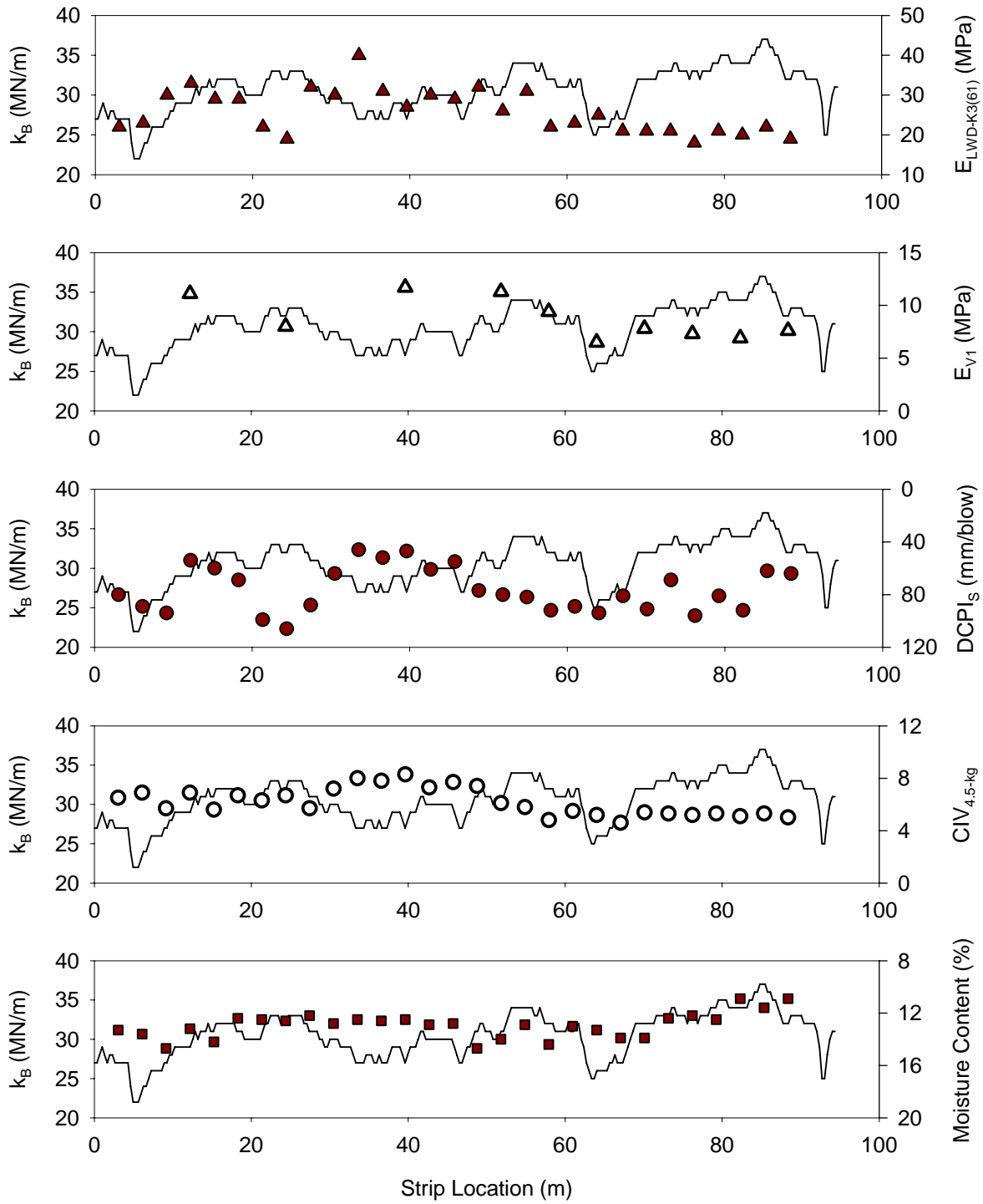
Figure 4.11. Comparison of k_B and in-situ compaction measurements for Strip 2

49
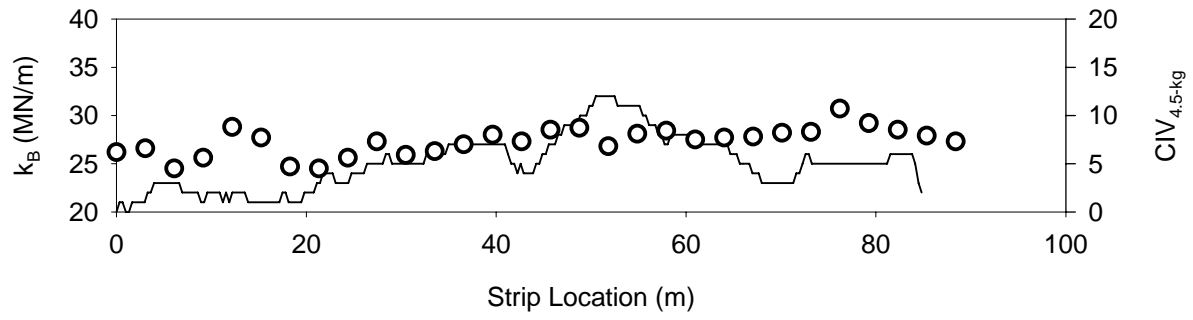
Figure 4.12. Comparison of k_B and in-situ compaction measurements for Strip 3
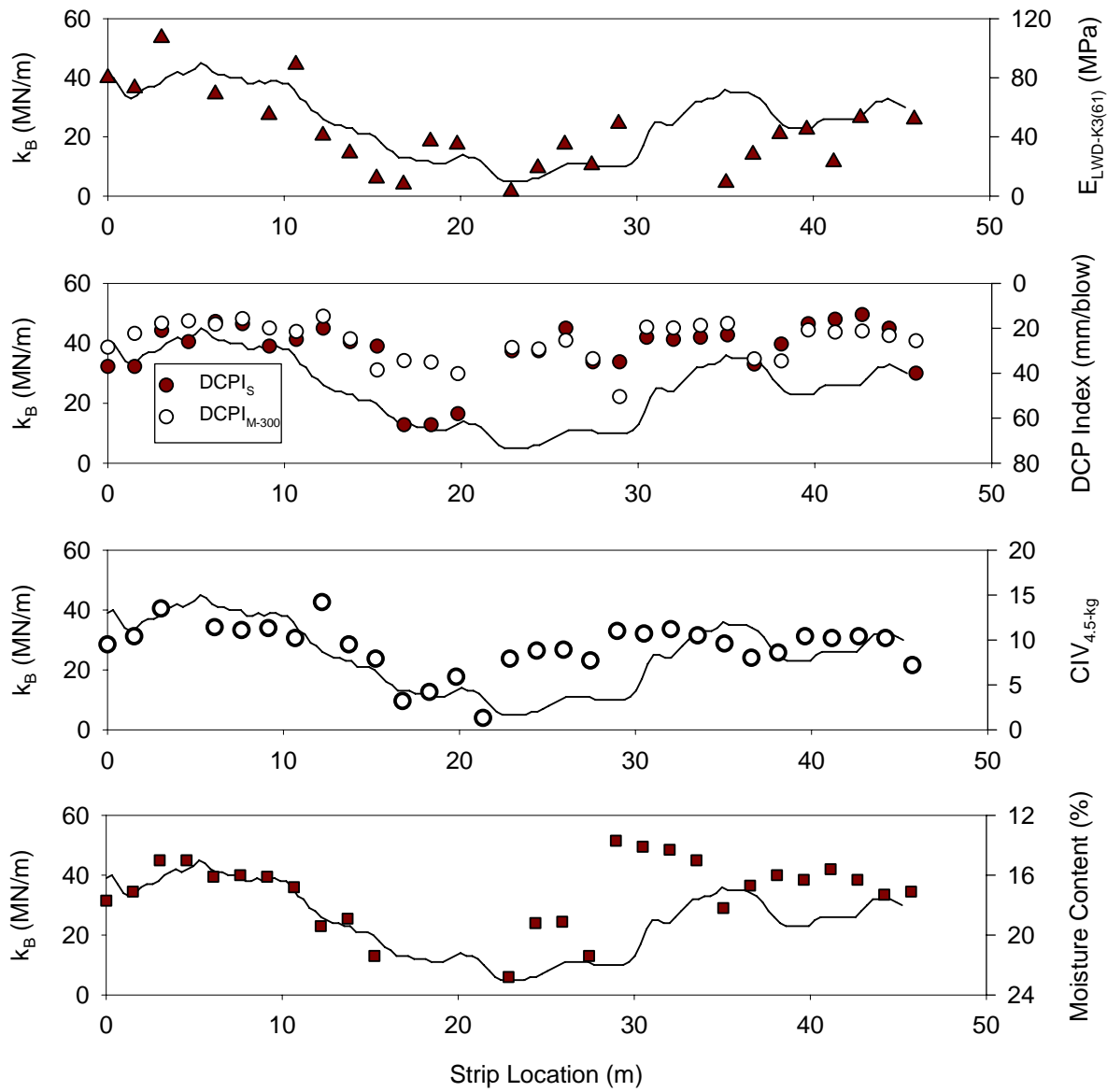
Figure 4.13. Comparison of k_B and in-situ compaction measurements for Strip 4
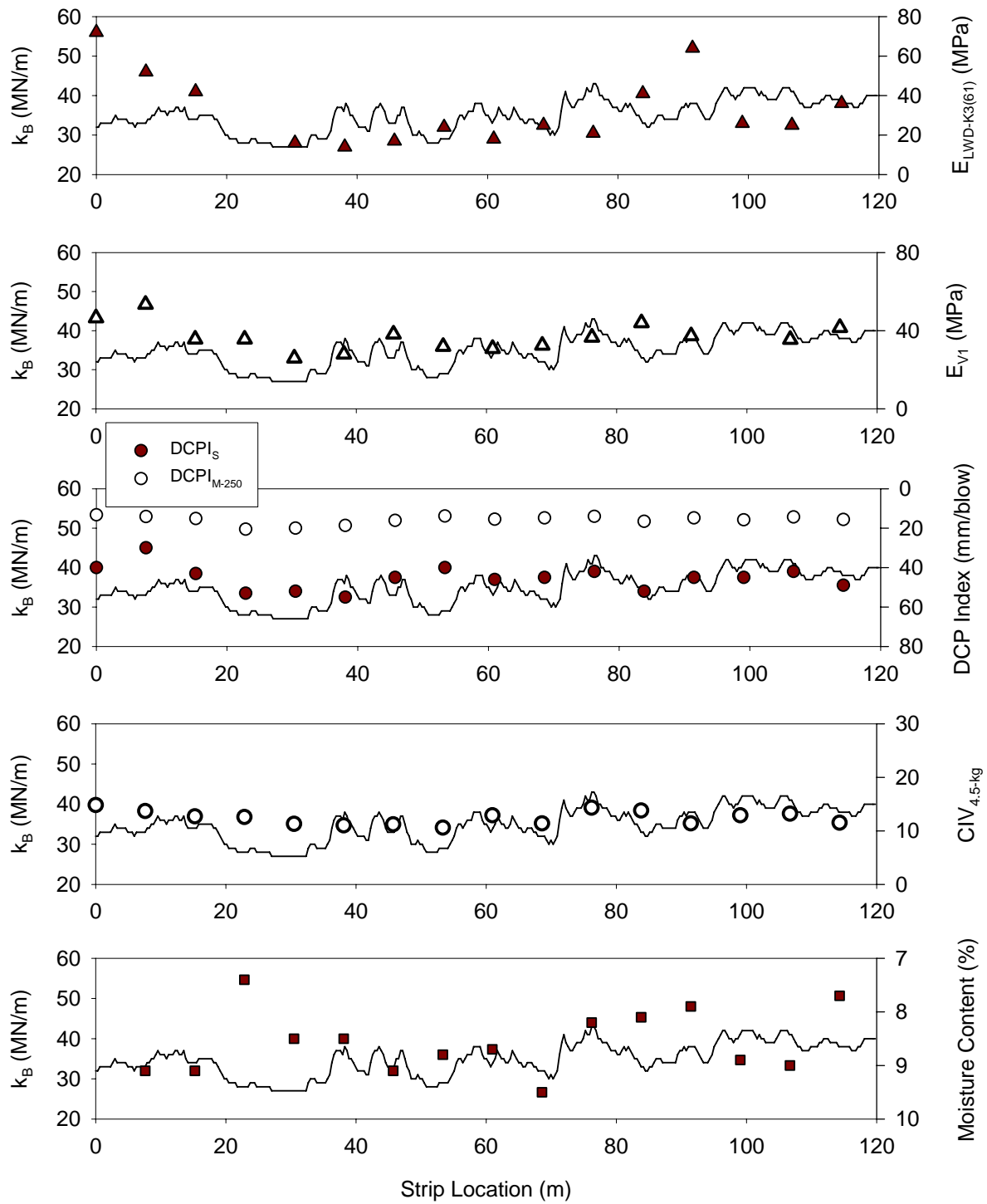
Figure 4.14. Comparison of k_B and in-situ compaction measurements for Strip 5

52
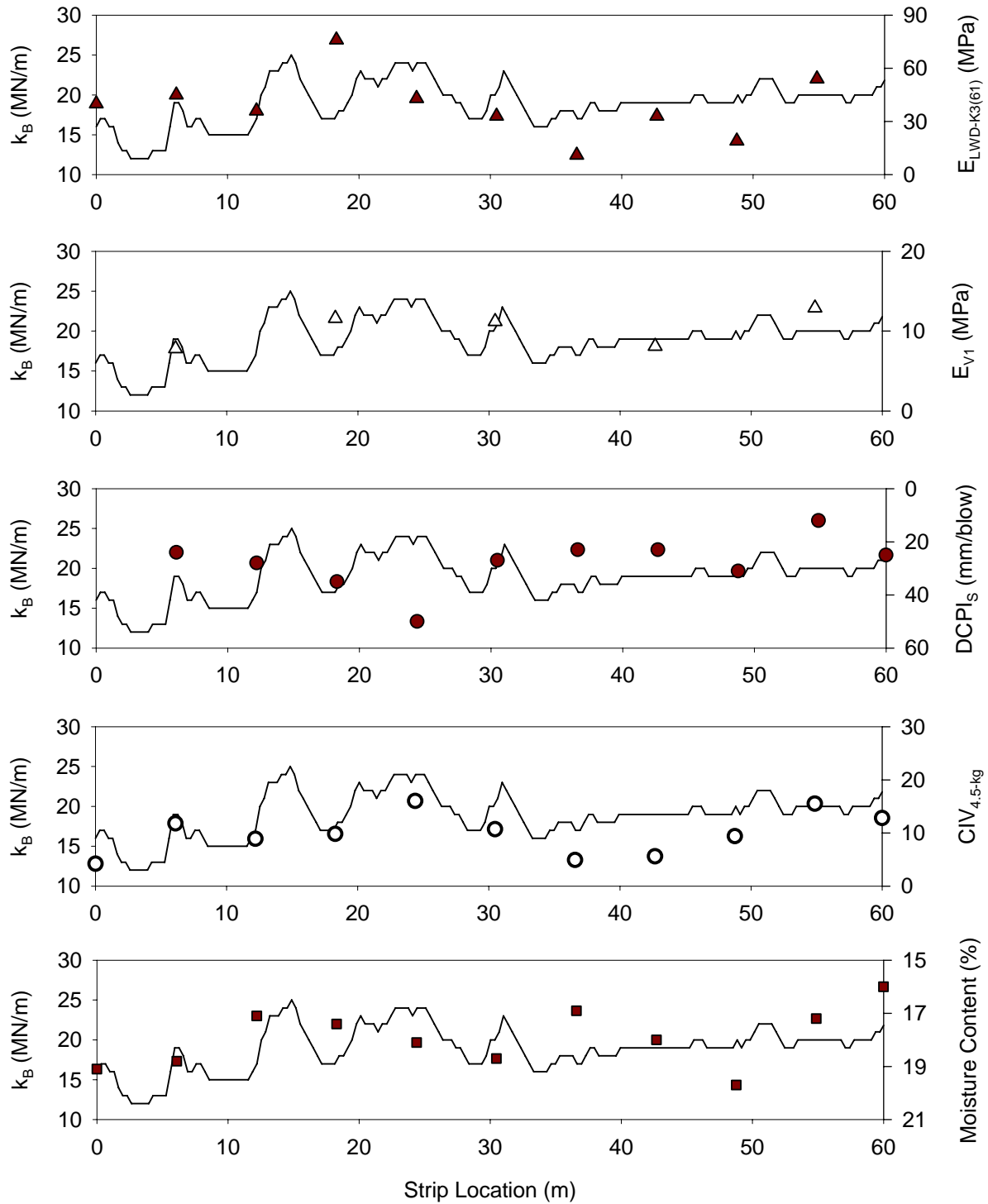
Figure 4.15. Comparison of k_B and in-situ compaction measurements for Strip 6, Track 1
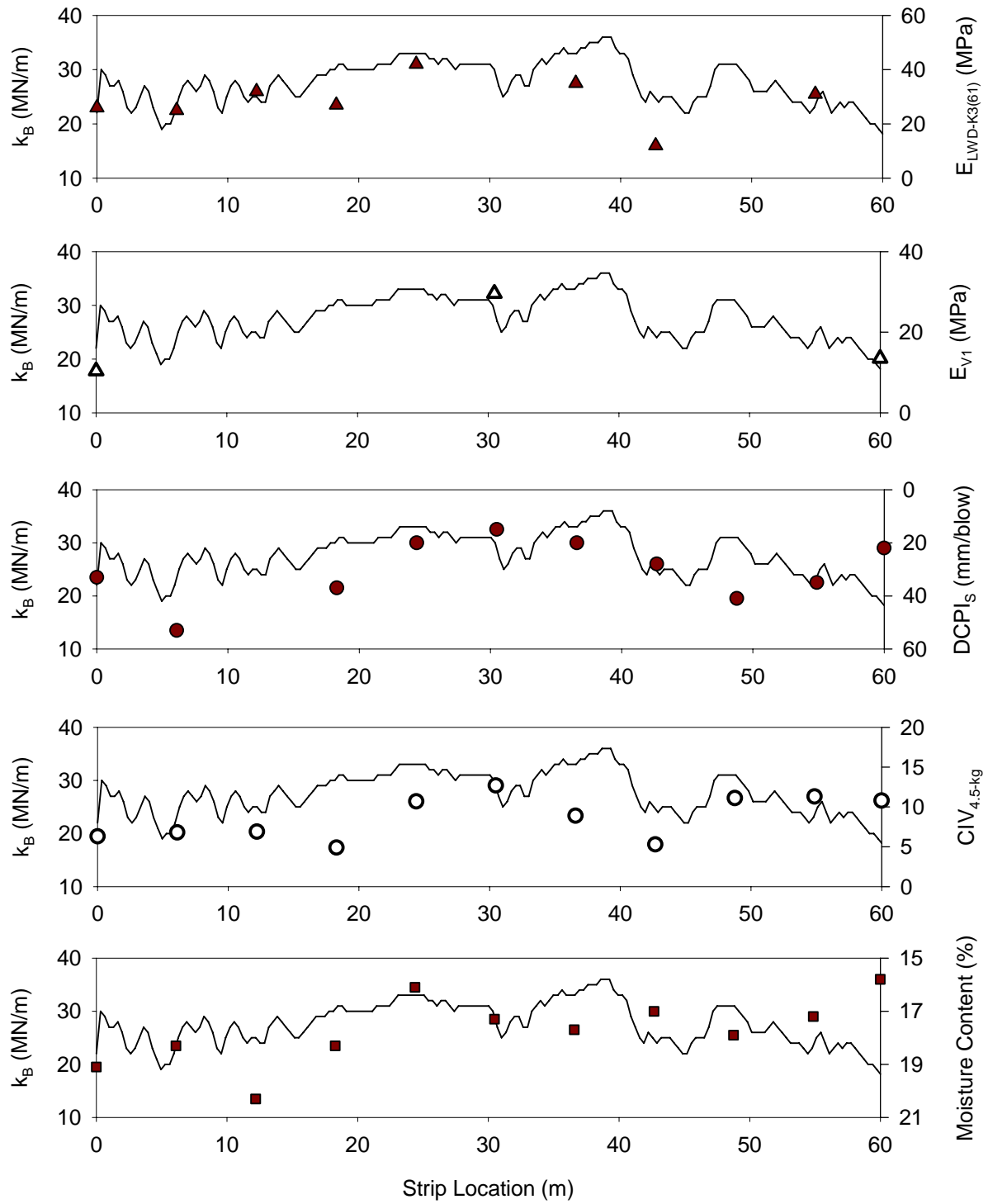
Figure 4.16. Comparison of k_B and in-situ compaction measurements for Strip 6, Track 4

4.6 Data Analysis

To identify the relationships between k_B and soil stability from in-situ test devices, the in-situ compaction measurements were plotted against spatially-nearest k_B measurements. The scatter plots are shown in Figure 4.17 for test strips comprised of subgrade soil (1, 4, and 6). Those for strips comprised of subbase material (2, 3, and 5) are shown in Figure 4.18. The correlations for Strips 1 and 4 – the test strips showing comparatively wide range of stiffness – produce R^2 values ranging from 0.48 to 0.86. Little correlation is observed between k_B and in-situ compaction measurements for the other strips, however, due to the relatively narrow range of stiffness of the test strips. The data from multiple test strips are combined in Figure 4.19. Little improvement is observed by combing data from multiple test strips.

In-situ moisture-density measurements are summarized in Figure 4.20 and Figure 4.21 for subgrade and Class 5 base materials, respectively. The subgrade materials, for having not yet been subject to roller compaction operations, showed relatively high percents compaction. The high dry unit weight measurements are explained by the observed high volume of construction traffic at these locations. The Class 5 subbase was also uncompacted prior to experimental testing, although this material was not subject to construction traffic. Low percents compaction were observed, particularly for Strip 2.

Relationships between percent compaction and k_B for subgrade and Class 5 materials are provided in Figure 4.22 and Figure 4.23, respectively. Only data from Strip 4 (subgrade) was strongly correlated with an $R^2 = 0.56$. Data from other test strips, particularly those strips comprised of Class 5 subbase material, were weakly correlated. As mentioned earlier, the subbase material was relatively uniform, and the range of compaction states (i.e. percent compaction) was narrow. The correlation coefficients would likely increase with a wider range of compaction states. Despite somewhat weak correlation, the data are valuable to the extent that the measurements aid selection of target values for intelligent compaction rollers and other relevant specification criteria.
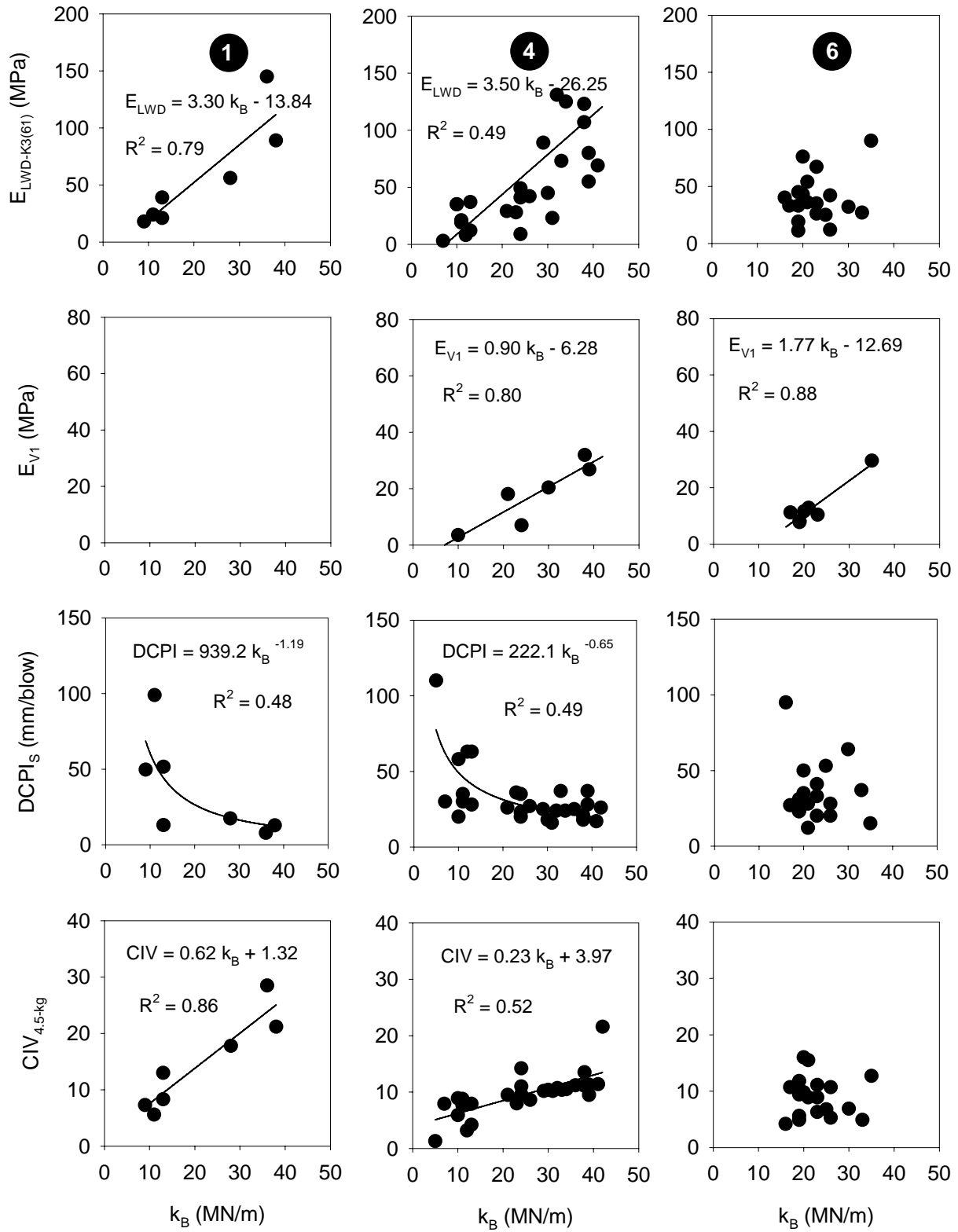
Figure 4.17. Relationships between k_B and in-situ compaction measurements for subgrade soil (Strips 1, 4, and 6)
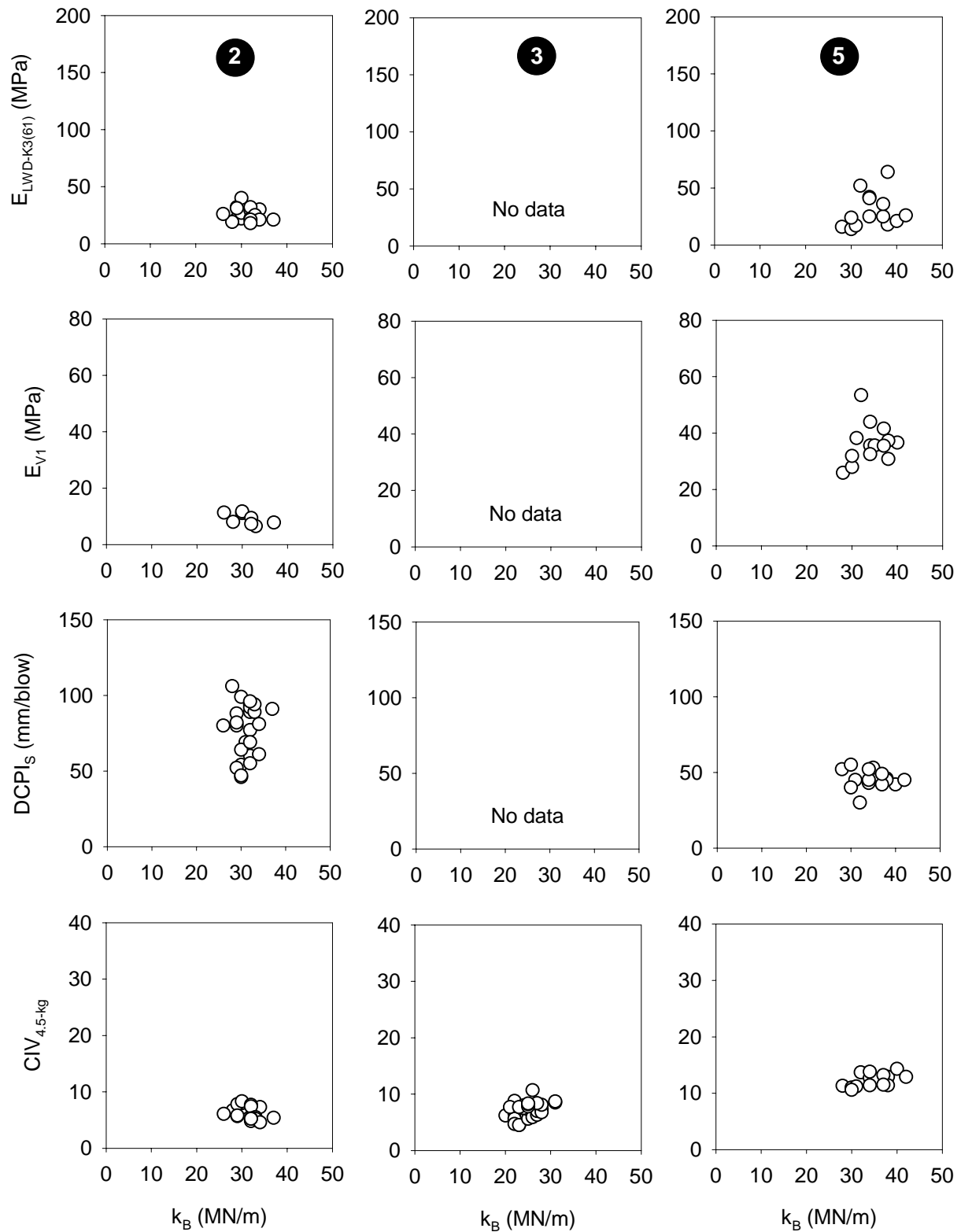
Figure 4.18. Relationships between k_B and in-situ compaction measurements for Class 5 subbase material (Strips 2, 3, and 5)
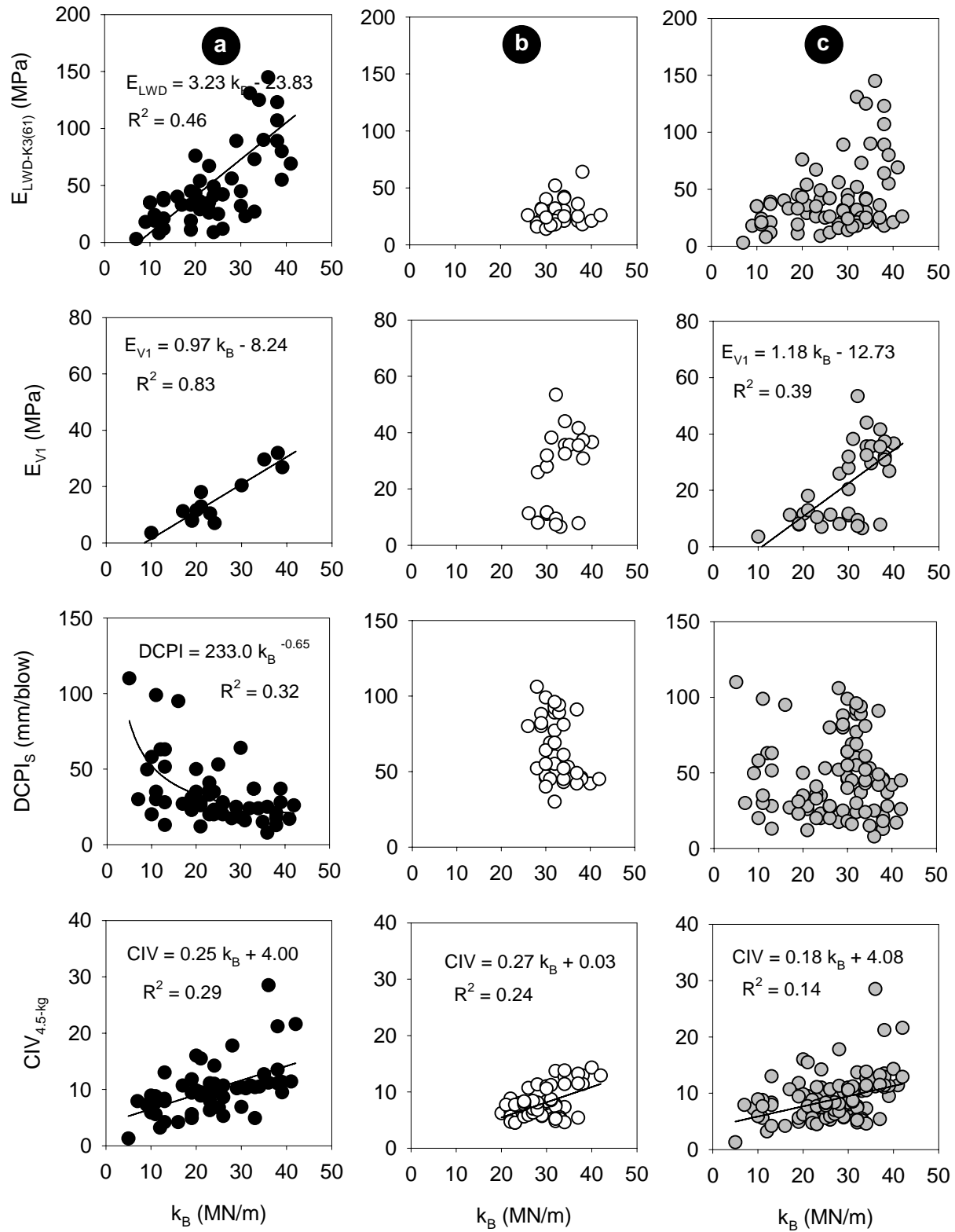
Figure 4.19. Relationships between kB and in-situ compaction measurements for combined data: (a) subgrade soil, (b) Class 5 subbase material, and (c) both soils
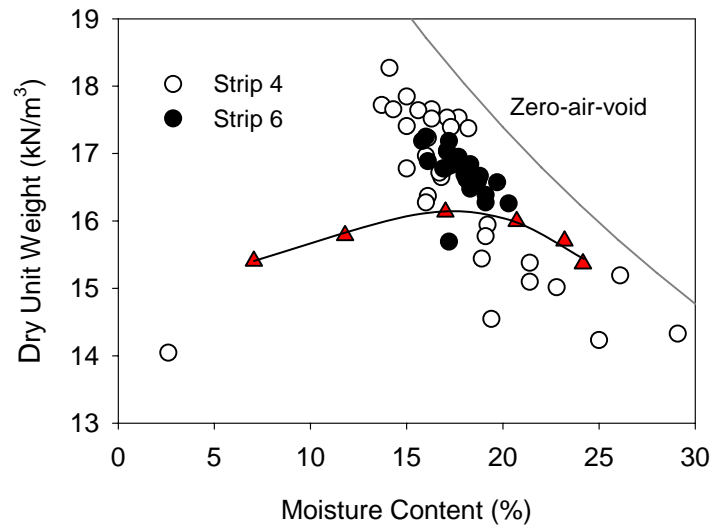
Figure 4.20. Field moisture-density data for subgrade material
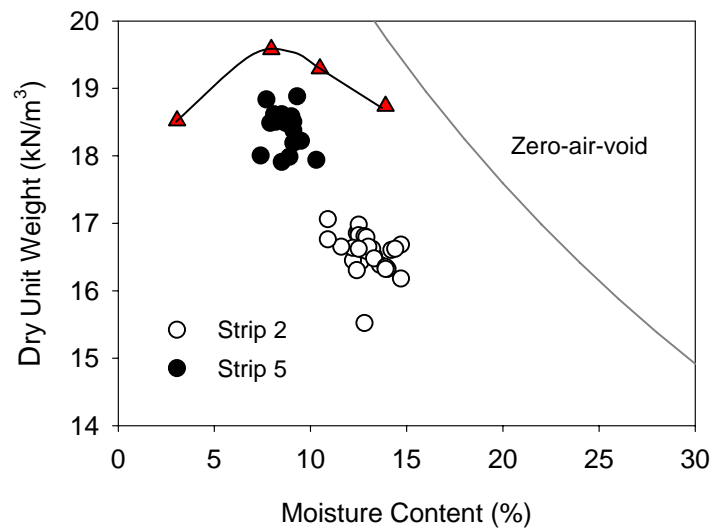
Figure 4.21. Field moisture-density data for Class 5 subbase material
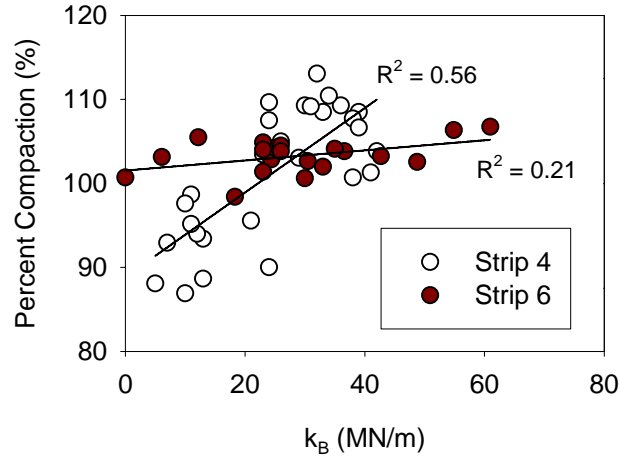
Figure 4.22. Relationship between k_B and percent compaction for subgrade soil
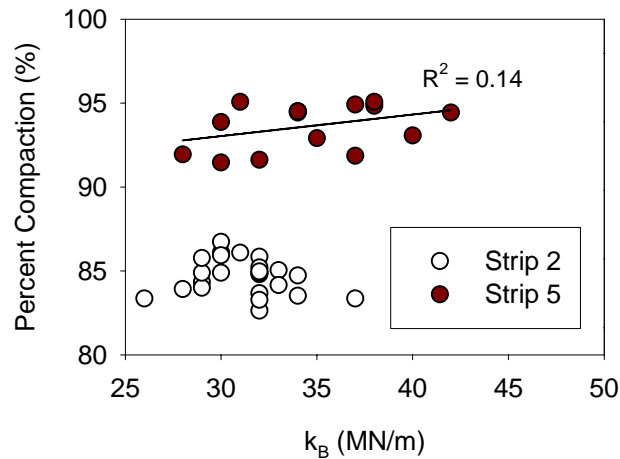
Figure 4.23. Relationship between k_B and percent compaction for Class 5 subbase material

4.6.1 Evaluation of Variable Feedback Control

To evaluate the variable feedback control feature of the Ammann system, distributions of data were observed with particular emphasis on characterizing the measurement variation. Figure 4.24 shows the distribution of k_B for Strip 2 for three roller passes. In operating the roller, variable feedback control was employed at the high amplitude setting. k_B data show that the average soil stiffness decreased slightly for the second roller pass and also that the standard deviation increased with each additional roller pass to give a wider range of k_B stiffness values. Coefficients of variation (C_V) for the data were 5, 7, and 9 percent for the three passes. As the Class 5 material was initially placed with uniform conditions, it is unlikely that soil compaction

60

would produce more uniform soil conditions. Nevertheless, the ability of variable control features in IC technology for achieving more uniform pavement layers was not observed using data from this field study. The performance of variable feedback control features in IC technology must be further investigated, quantified, and documented in future studies.
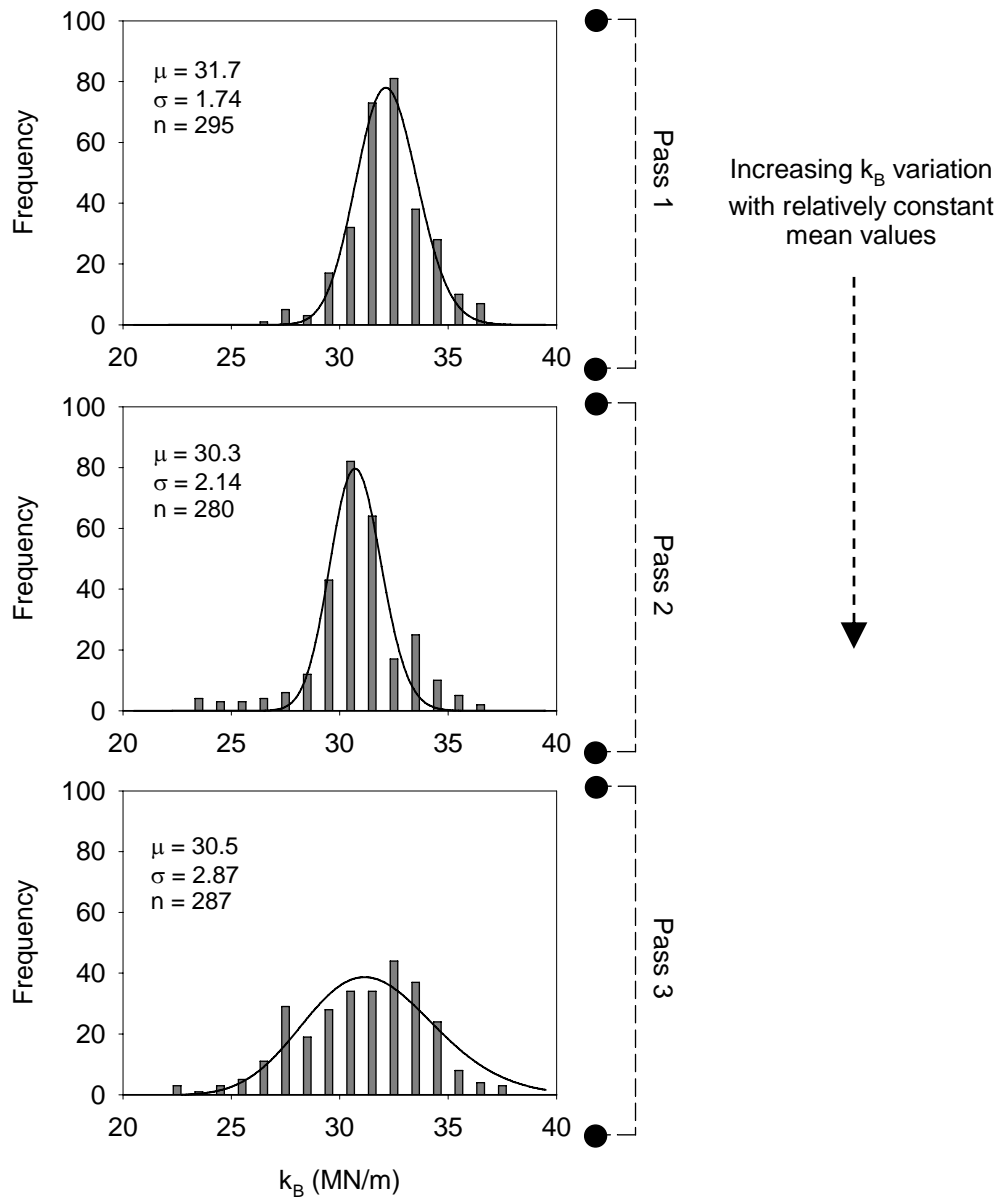
Figure 4.24. Distribution of k_B per roller pass for Strip 2 under variable (control) amplitude operation

The distributions of k_B for two adjacent test strips comprised of Class 5 subbase material (Strips 2 and 3) are shown in Figure 4.25. Strip 2 was tested using a high amplitude setting, while Strip 3 used a low amplitude setting. The variable control feature was engaged for both test strips. Using the high amplitude setting produced a k_B distribution with a higher mean value (31.7 MN/m) than the low amplitude setting (23.0 MN/m). Coefficients of variation for Strips 2 and 3 were 6 and 15 percent, respectively.
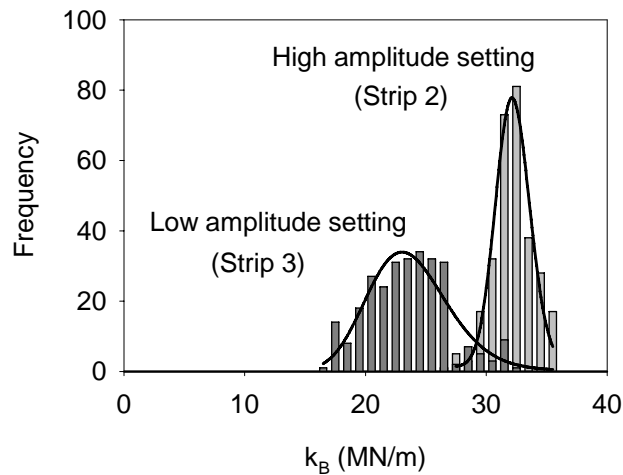
Figure 4.25. Distribution of k_B at two amplitude settings in variable control mode (Class 5)

A direct comparison of k_B distributions using variable and constant amplitudes is shown in Figure 4.26. The distributions of k_B are from Strip 6 in subgrade material. Tracks 1 and 2 employed the constant amplitude setting at 80 percent of the maximum amplitude. Tracks 3 and 4 used variable amplitude. The data do not provide evidence that variable amplitude results in more uniform soil stiffness. Rather, Track 4 (variable amplitude) showed the most variation in k_B measurement with a coefficient of variation equal to 24 percent. However, these results are inconclusive, as the soil at this testing location showed considerable variation. The respective variation reflected in k_B stiffness values between constant and variable amplitude settings does not account for soil variability attributed to construction of the test area.
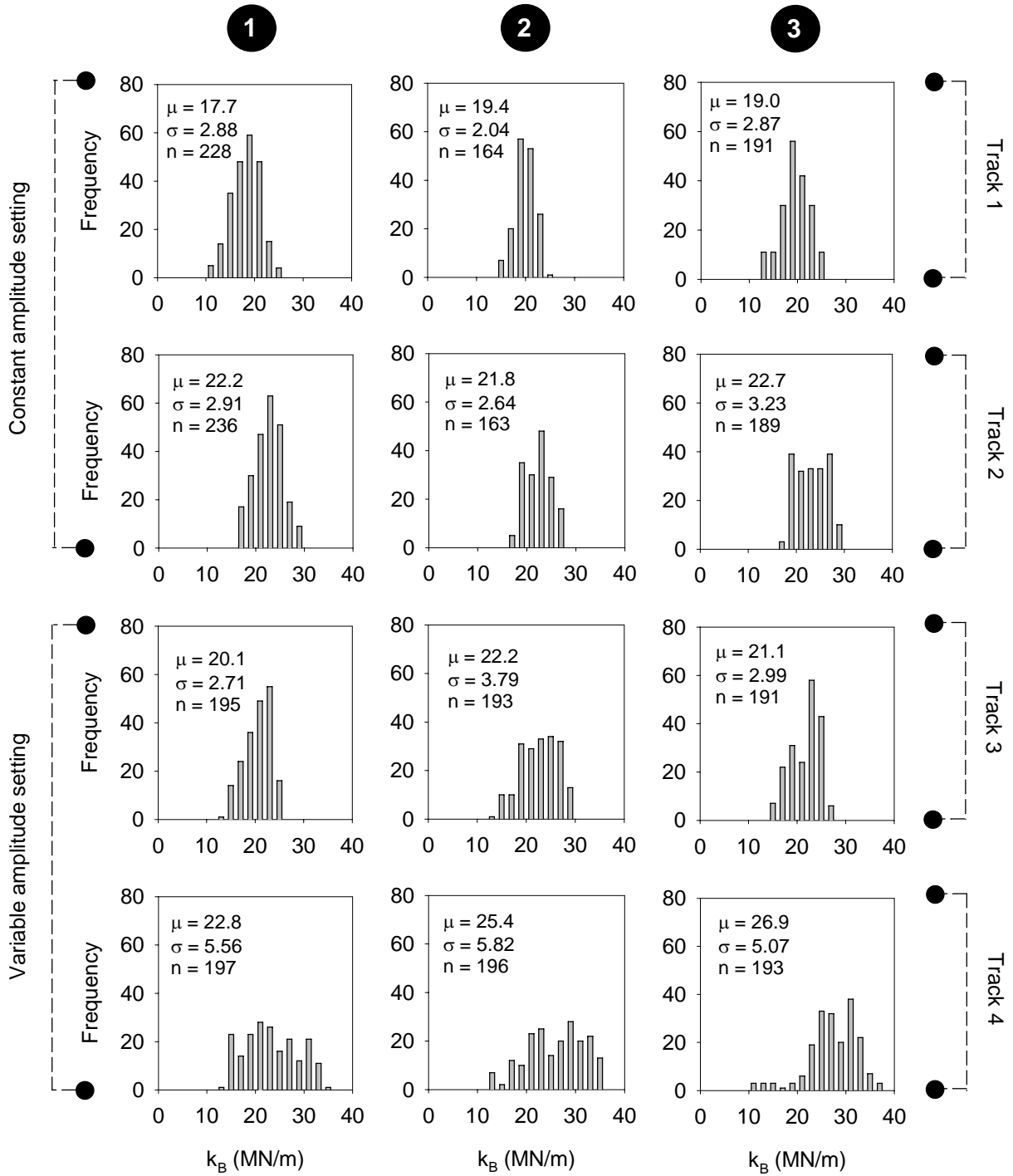
Figure 4.26. Distribution of k_B using variable and constant amplitude setting on Strip 6 (subgrade) for Passes 1, 2, and 3 (left to right)

4.6.2 Intelligent Compaction Comparison to Test Rolling

Test rolling at the US 14 highway reconstruction project served as acceptance testing for the constructed subgrade (see Figure 4.27). To evaluate whether the roller-integrated compaction monitoring system might also identify areas of weak or poorly-compacted soil, the subgrade material at the location of Strip 6 was test rolled following compaction using the Ammann roller and completion of in-situ compaction tests. Significant rutting was observed (see Figure 4.28). Rut depth was measured at each test point, and the ability of the intelligent compaction technology to predict rut depth is shown in Figure 4.29 and Figure 4.30. A linear relationship between rut depth and k_B is observed in Figure 4.31. With the exception of several measurement values, the soil stiffness determined by the Ammann system is supported by measured rut depths as an indicator of soil stability.

Figure 4.27. Test roller for quality assurance

Figure 4.28. Rutting observed following test rolling
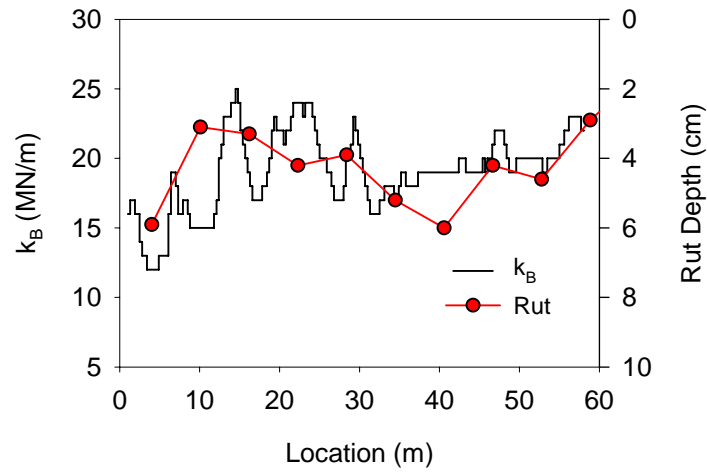
Figure 4.29. Comparison of k_B and rut depth along Strip 6, Track 1 (subgrade)
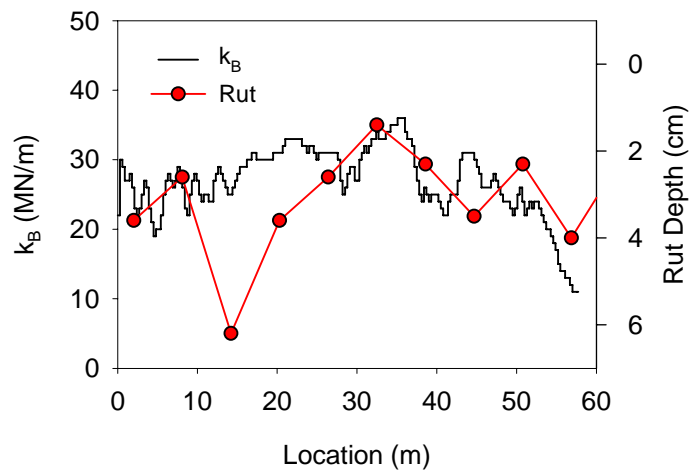
Figure 4.30. Comparison of k_B and rut depth along Strip 6, Track 4 (subgrade)
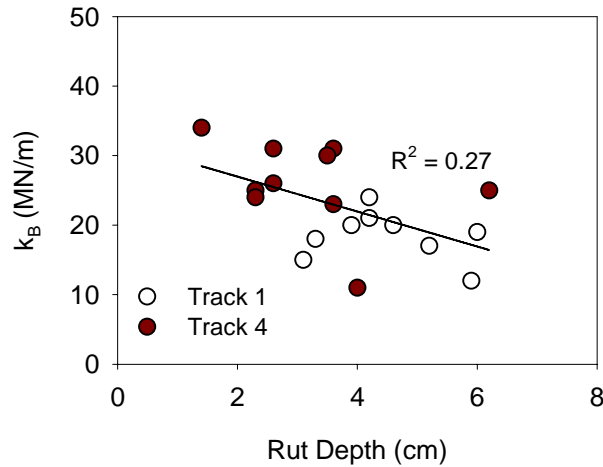
Figure 4.31. Relationship between k_B and rut depth from test rolling

4.7 Project Observations

The following statements summarize the activities of Field Study 2:

- Six test strips with lengths ranging from about 30 to 120 m were compacted using the Ammann vibratory smooth drum roller and tested using a light weight deflectometer, dynamic cone penetrometer, Clegg impact hammer, and static plate load tests.

- Comparisons between Ammann k_B and in-situ compaction measurements were made visually by plotting data with location along the test strip.

- Scatter plots show strong relationships between k_B and in-situ test results for strips with a relatively wide range of soil stiffness (Strips 1 and 4) and comparatively weak relationships for strips with more uniform conditions (Strips 2, 3, 5, and 6). All results are useful for establishing target values for k_B and other relevant specification criteria.

- The ability of variable feedback control of amplitude and frequency to produce more uniform soil conditions was not observed from the limited dataset.

- An area compacted with the Ammann vibratory roller and tested using in-situ test devices was then test rolled to demonstrate the ability of k_B data to identify weak subgrade which are evidenced by rutting by the Mn/DOT test roller.

The following table summarizes intelligent compaction measurement from Field Study 2.

67

Table 4.3. Observed k_B and in-situ compaction measurements (range)

Location	Soil Type	k_B (MN/m)	w (%)	Dry Unit Weight (kN/m^3)	$E_{LWD-K3(61)}$ (MPa)	DCPI$_S$ (mm/blow)
Strip 1	CL [a, b]	30-40	–	–	10-50	5-10
Strip 2	SP-SM [c]	20-35	10-14	16-17	20-40	40-110
Strip 4	CL [a, b]	20-45	15-20	16-18	60-110	10-40
Strip 5	SP-SM [c]	25-40	7-10	18-19	10-70	25-50
Strip 6	CL [a]	10-35	15-20	16-17	10-80	10-60

a w_{opt} = 18%, $\gamma_{d,max}$ = 16.2 kN/m^3
b Excludes median testing
c w_{opt} = 8%, $\gamma_{d,max}$ = 19.6 kN/m^3

Chapter 5
Field Study 3: CCV Evaluation at TH 64

5.1 Project Description

This chapter summarizes in-situ and intelligent compaction measurement values collected on the TH 64 reconstruction project near Akeley, Minnesota from June 20 to 23 and July 18 to 19, 2006. In-situ test measurements of dry unit weight, moisture content, strength, and modulus were compared with *Caterpillar compaction values* (CCV) obtained from a CS-563 vibratory smooth drum roller (see Figure 5.1) during production soil compaction and test rolling on proof sections for quality acceptance. Except for measuring soil moisture content, the intelligent compaction technology applied to the Caterpillar roller was the principal method for quality control. Test rolling was the final quality acceptance method and all sections passed.

Figure 5.1. Caterpillar CS-563 vibratory smooth drum roller

The specific objectives of Field Study 3 include:

- Document specification for use of roller-integrated compaction monitoring technology, including the roller calibration procedure.

- Document all roller-integrated and in-situ compaction measurements collected on the TH 64 project.

- Evaluate the relationships between roller-integrated and in-situ compaction measurements.

Reconstruction of TH 64, shown in Figure 5.2, was comprised of widening 10 km of an existing alignment. The subgrade at select locations of the project was subcut to provide fill material for other areas. Project grading generally classified into two typical sections, including: (1) 0.25-m subcut filled with select granular borrow material and (2) variable subcut up to 1.1 m depth, which is also filled with select borrow material. Fill material was hauled and placed using both trucks and scrapers. Production soil compaction, shown in Figure 5.3, was performed using only the CS-563 vibratory smooth drum roller.

Figure 5.2. TH 64 under construction, looking south at STA 280 (6/28/06)

Figure 5.3. TH 64 soil compaction operation at STA 265 (6/29/06)

5.2 Description of CCV

CCV technology, which is the commercial version of Geodynamik *compaction meter value* (CMV), follows the same theoretical background presented in Chapter 3 for CMV.

Effective use of the intelligent compaction technology is aided in large part by the integration of a GPS system and an on-board compaction monitor which displays the real-time roller location, CCV, vibration amplitude and frequency, and roller speed. The on-board compaction monitor is shown in Figure 5.4. The technology enables a roller operator to make judgments regarding the condition of the compacted fill material.
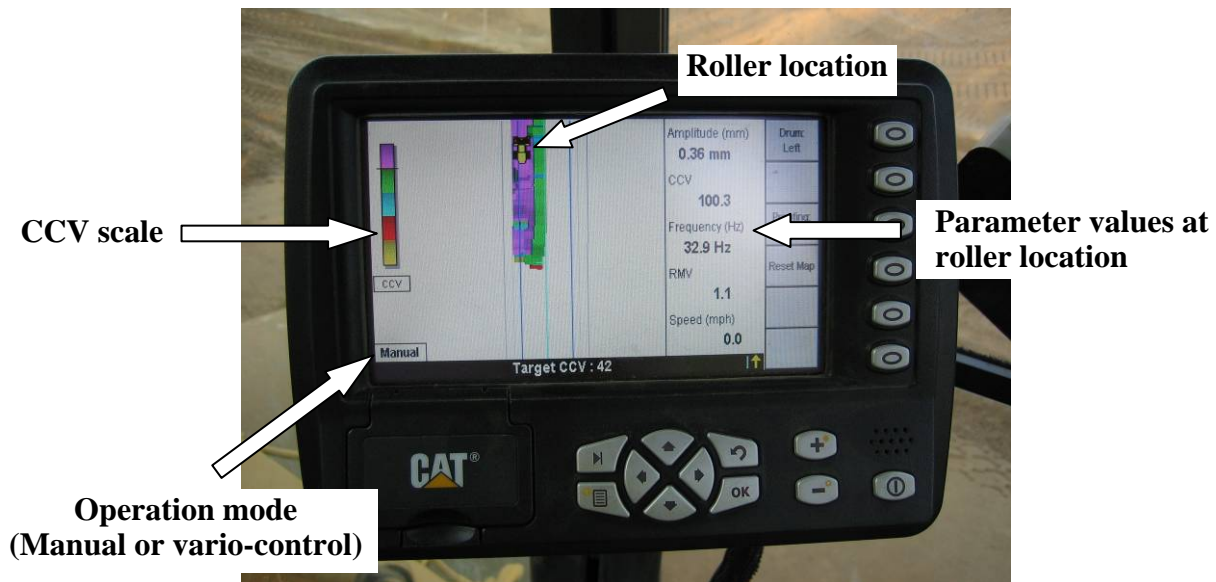
Figure 5.4. On-board compaction monitor

5.3 Description of Specification

The Mn/DOT specification for using intelligent compaction technology for quality control and acceptance is provided as Appendix H. The key attributes of the specification are summarized in Chapter 10.1.

5.4 Material Properties

Fill material for the TH 64 reconstruction project was comprised of sand. Particle size distribution curves for the granular material, which were produced by both Mn/DOT inspectors and Iowa State University researchers, are shown in Figure 5.5. Based on the Iowa State University gradation, the material classifies as SW-SM well-graded sand with silt. Based on the Mn/DOT gradations, the material classifies as SP poorly graded sand.
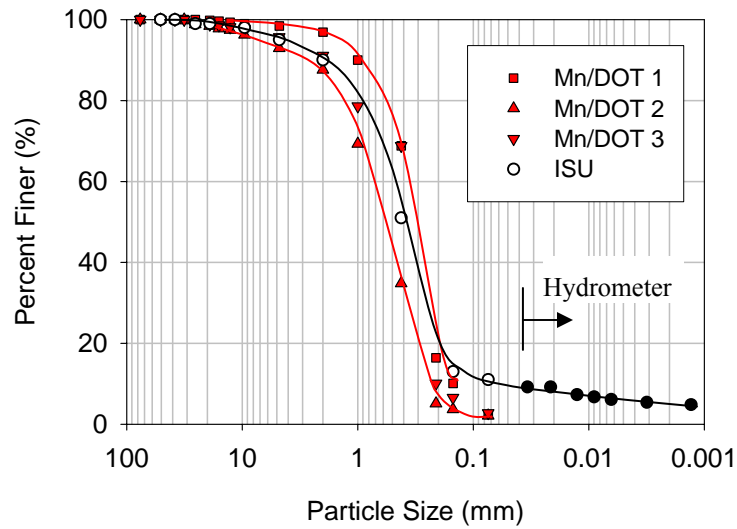
Figure 5.5. ISU and Mn/DOT particle size distribution curves

Moisture-density relations were determined using the standard and modified Proctor tests, as documented in Chapter 2. The Iowa State University moisture-density relationships for standard and modified compaction energies are shown in Figure 5.6. A comparison of standard Proctor moisture-density curves produced by Iowa State University and Mn/DOT is shown in Figure 5.7. Optimum moisture contents at standard compaction energy ranged from 11.4 to 12.4 percent. Maximum dry unit weights for the four tests ranged from 17.03 to 17.86 kN/m^3.
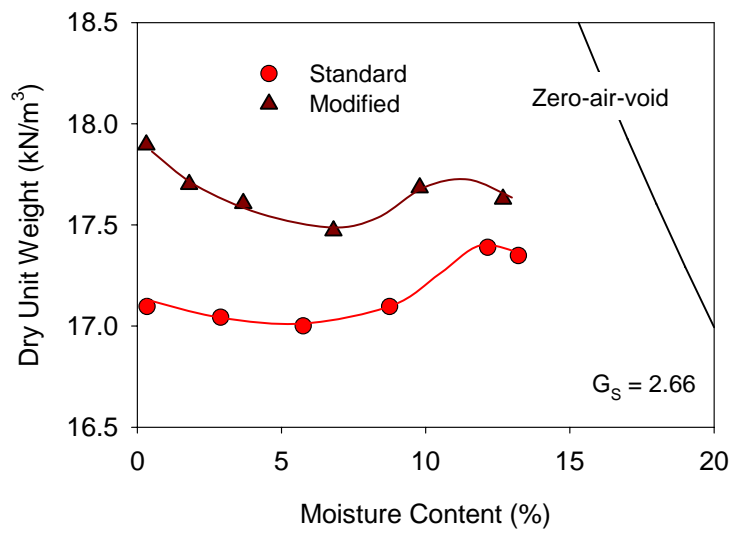
Figure 5.6. ISU standard and modified Proctor moisture-density relationships
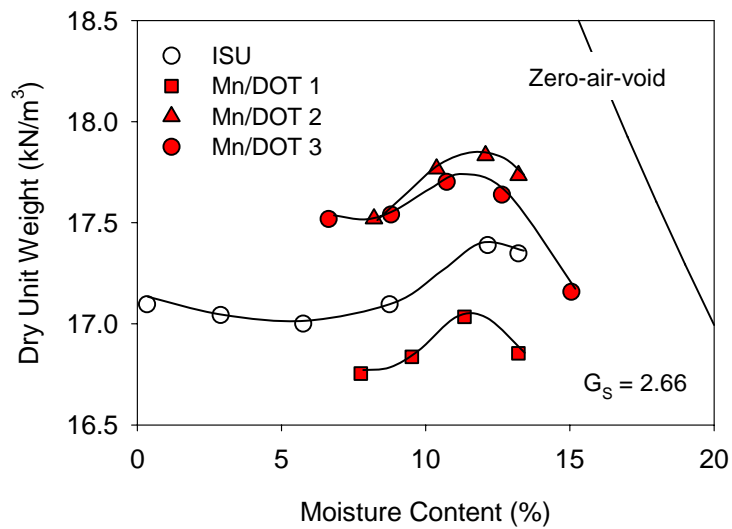
Figure 5.7. ISU and Mn/DOT standard Proctor moisture-density relationships

Table 5.1. Summary of soil properties

Soil Property	Mn/DOT 1	Mn/DOT 2	Mn/DOT 3	ISU
USCS	SP	SP	SP	SW-SM
AASHTO	A-3(0)	A-1-b(0)	A-3(0)	A-3(0)
$F_{3/4}$ (%)	100	98	99	99
$F_{3/8}$ (%)	99	96	98	98
F_4 (%)	98	93	96	95
F_{200} (%)	2	2	3	11
Percent gravel (>4.75mm)	2	7	4	5
Percent sand (>0.075 mm)	96	91	93	84
Percent silt (>0.002 mm)	–	–	–	6
Percent clay (<0.002 mm)	–	–	–	5
Gs	–	–	–	2.66
Standard Proctor				
$\gamma_{d,max}$ (kN/m^3)	17.03	17.83	17.71	17.41
w_{opt} (%)	11.3	11.8	11.3	12.0
Modified Proctor				
$\gamma_{d,max}$ (kN/m^3)	–	–	–	17.75
w_{opt} (%)	–	–	–	10.8

5.5 Testing Methods

Field testing methods for this field study followed procedures documented in Chapter 2.

5.6 Evaluation of Calibration Procedure

Prior to production soil compaction, control sections were constructed with minimum dimensions of 100 m by 10 m to determine target values for CCV. Separate control sections were constructed and tested for the different types of fill sections of the project (e.g. 0.25-m or 1.1-m subcut). For establishing the target value based on CCV data collected during compaction of the control sections, a trial and error method was adopted. Following each roller pass over the control section area, the data were grouped into the following, pre-defined bins: less than 70 percent, 70 to 80 percent, 80 to 90 percent, 90 to 130 percent, and greater than 130 percent of the trial target value. The target value was adopted as quality criteria when the distribution of the data in the five bins met the specification criteria of 90 percent of the data exceeding 90 percent of the target value. With few independent compaction control measurements collected on the control sections, the approach to establishing quality criteria to be used for production soil compaction assumed that the compacted material of the control section was properly compacted. Because Mn/DOT inspectors established these values at the beginning of the project, the contractor was able to reference these measures of fill performance during production compaction operations.

Control Strip 1 was constructed and tested on June 12 to establish the target value for the 0.25-m subcut sections. At five roller passes, the target value was 35. Roller data for this control section is unavailable due to data transfer problems.

Control Strip 2 was constructed and tested on June 16 to establish the target value for the 1.1-m subcut sections. The CCV compaction curve for this control section is shown in Figure 5.8 (a) as a box plot. Box plots display the quartiles (e.g. 25th, 50th, and 75th percentiles) and the minimum and maximum observations of a data group. The length of the box represents the interquartile range (i.e. distance between 25th and 75th percentiles). The vertical lines extend from the largest or smallest value within 1.5 times the interquartile range. Observations outside this range are represented by circular data points. Based on the distribution of CCV, little compaction is observed following the first roller pass. At seven roller passes, the target value was 42.

By late June, the compaction caused by construction traffic was observed to produce distributions of CCV that exceeded considerably the values observed on the control section. Control Strip 3, which was also a 0.25-m subcut section, was constructed and tested. The CCV compaction curve data are shown in Figure 5.8 (b). The target value for this control section following the above procedure was established at 60 at 11 roller passes. Mn/DOT found this value to be unreasonably high, such that the target value for the 0.25-m subcut section remained as 35.

CCV compaction curves for Control Strips 4 and 5 (constructed on June 29 and July 7) are shown in Figure 5.8 (c) and (d), respectively. These control sections also applied to 0.25-m subcut sections. Apparently, the results of the data did not vary significantly from Control Strip 1 results, such that a change in the target value was not adopted.

Last Pass: CTV = 42	
Bin	Percent
>130%	4
90-130%	91
80-90%	3
70-80%	1
<70%	<1

Last Pass: CTV = 60	
Bin	Percent
>130%	5
90-130%	93
80-90%	2
70-80%	< 1
<70%	0

Last Pass: CTV = 45	
Bin	Percent
>130%	8
90-130%	76
80-90%	5
70-80%	3
<70%	7

Last Pass: CTV = 52	
Bin	Percent
>130%	2
90-130%	84
80-90%	8
70-80%	4
<70%	2
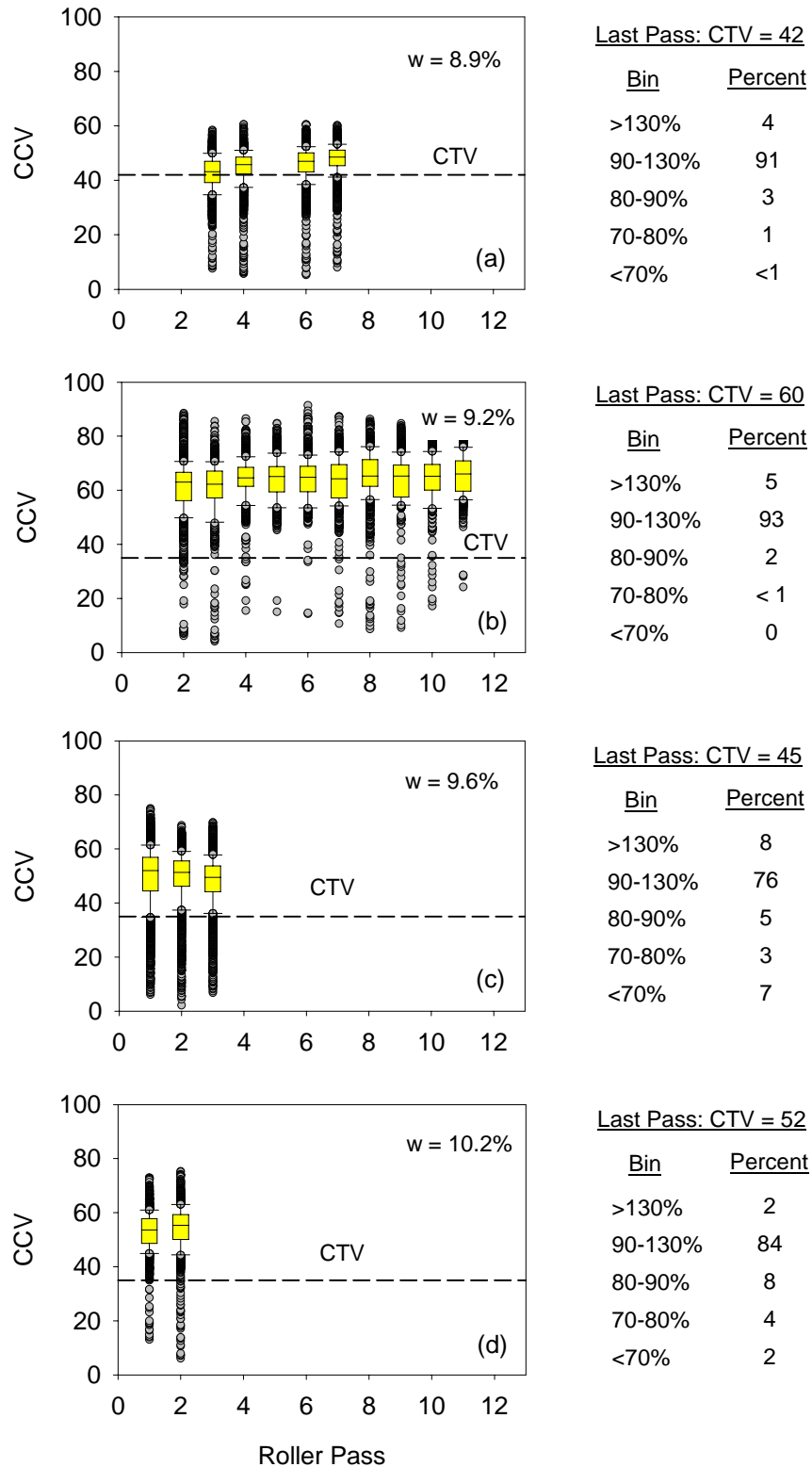
Figure 5.8. CCV compaction curves for Control Strips: (a) 2, (b) 3, (c) 4, and (d) 5

Distribution plots for CCV on Control Strips 2, 3, 4, and 5 are shown from Figure 5.9 to Figure 5.12. Mean values, coefficients of variation (C_V), and tenth percentiles (P_{10}) are additionally provided for each roller pass. Mean values for CCV ranged from 34.7 to 65.9. Coefficient of variation ranged from 12 to 22 percent. A summary of the control section data is provided in Table 5.2. P_{10} for the last roller pass on each control section was approximately equal to 90 percent of the final target value. Thus, given the roller data on a control section, the target value may simply be calculated instead of using the trial and error method of selecting a target value and assessing the data distribution in pre-established bins.
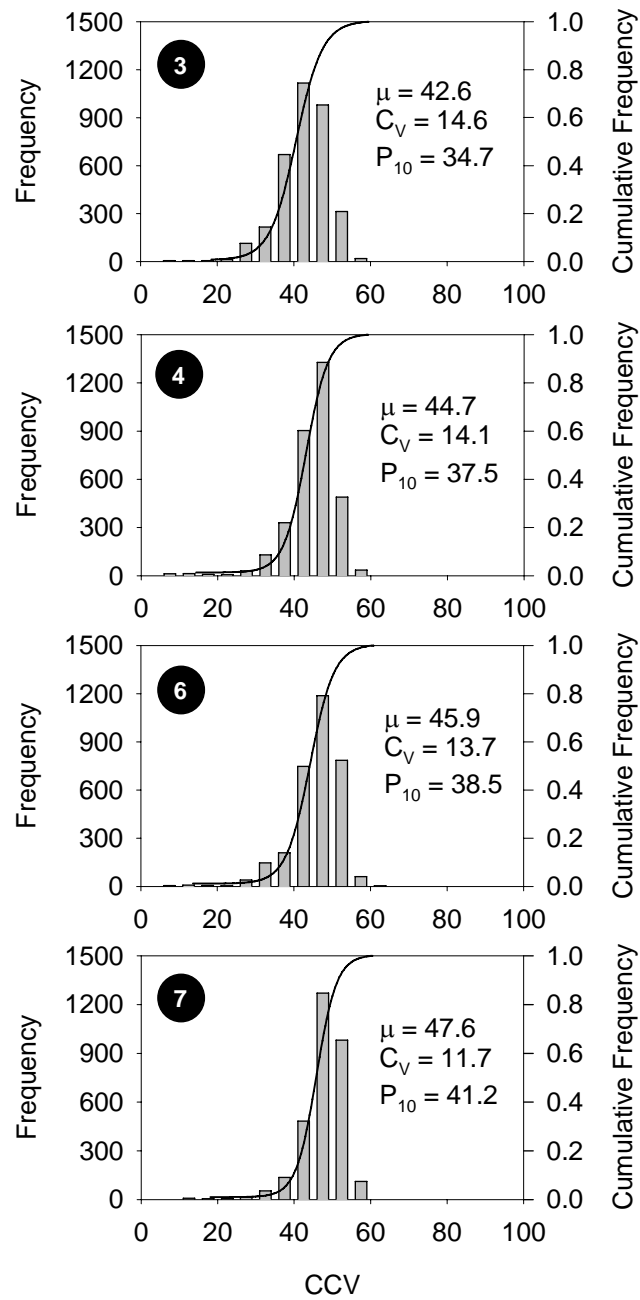
Figure 5.9. Control 2 CCV distribution plots: Passes 3, 4, 6, 7
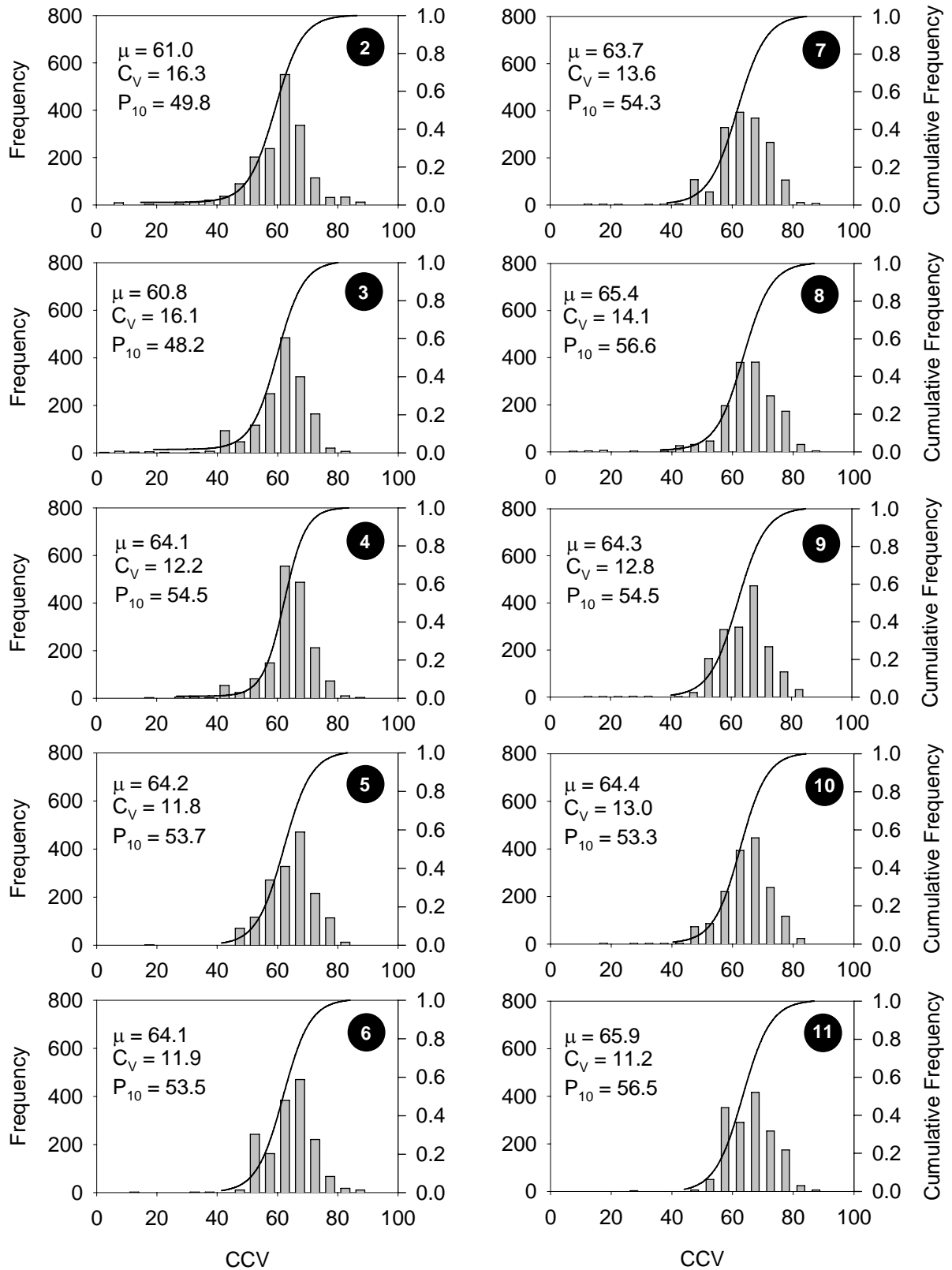
Figure 5.10. Control 3 CCV distribution plots: Passes 2 to 11
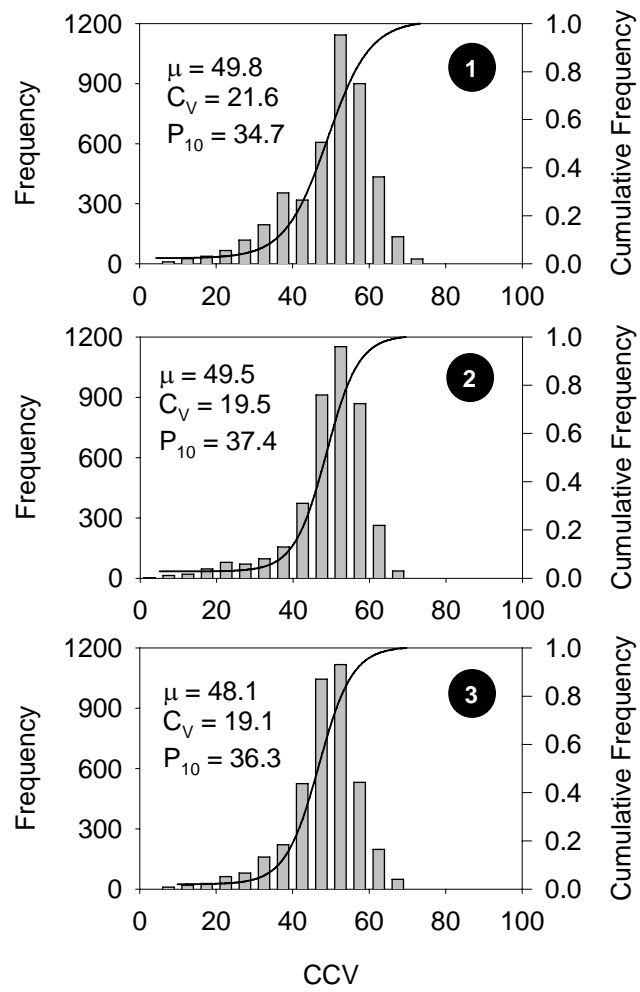
Figure 5.11. Control 4 CCV distribution plots: Passes 1, 2, and 3
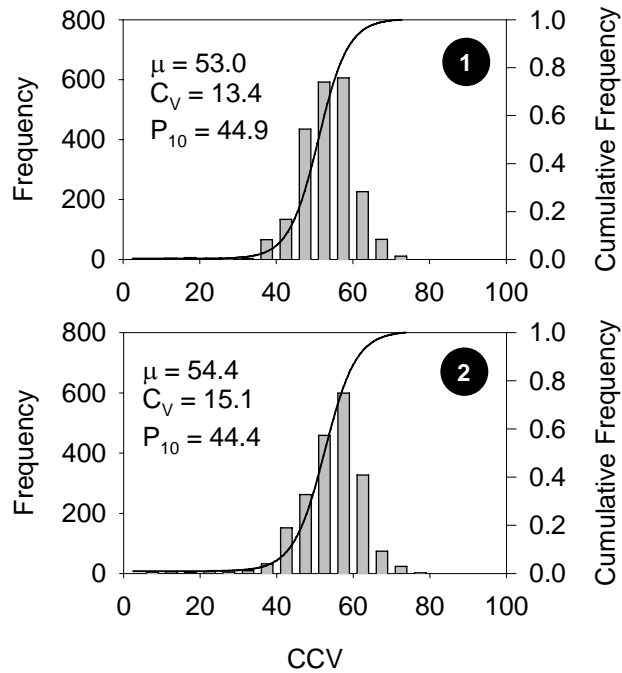
Figure 5.12. Control 5 CCV distribution plots: Passes 1, 2

Table 5.2. Summary of control section data

Control No.	Date	STA	Section Type	IC-CTV	0.9 (CTV)	Last Pass	P_{10}	C_V
1	6/13	148-152	10-in subcut	35	31.5	.	.	.
2	6/16	300-303	42-in subcut	42	37.8	7	41.2	12
3	6/28	255-258	10-in subcut	60	54.0	11	56.5	11
4	6/29	248-253	10-in subcut	45	40.5	3	36.3	19
5	7/7	181-184	10-in subcut	52	46.8	2	44.4	15

5.7 Test Data

Quality acceptance using intelligent compaction technology was accomplished by analyzing CCV data on "proof" sections. These sections, which ranged in length from 90 to 640 m and also varied in width, were prepared by production soil compaction. At the time the operator believed the material to be sufficiently compacted, the moisture content was measured using Speedy moisture oven and the proof area was rolled once without overlapping. Following test

82

rolling, the compaction monitor calculated the percent of the CCV data exceeding 90 percent of the established target value. Provided more than 90 percent of the data exceeded 90 percent of the target value, the proof area was accepted by Mn/DOT inspectors.

A summary of proof sections is provided in Table 5.3.

The proof sections for which there is supplementary in-situ test data are highlighted. Several of the proof sections that were constructed and tested while Iowa State University researchers were on site are shown from Figure 5.13 to Figure 5.15. In these figures, the limits of the proof area are marked with dashed lines.

Mn/DOT and Iowa State University in-situ test data are summarized in Appendix A. In-situ test data collected by Iowa State University for Proofs 14, 15, and 36, however, are also provided in the following figures. Distributions of dry unit weight, modulus, and Clegg impact value are shown for Proof 14 in Figure 5.16. Based on 54 tests (testing frequency = 1 test per 20.6 m^2), the measurements appear to be approximately normally distributed. Proof 15 in-situ test data, comprised of 36 measurements taken between STA 270 to 280 (testing frequency = 1 test per 77.4 m^2), are plotted in Figure 5.17 and shown as distribution plots in Figure 5.18.

Proof 36 was conducted solely by Iowa State University on July 19. The roller was operated on stabilizer material which was placed on the fill material prior to placement of subbase material. The roller was operated in the manual mode at nominal amplitude of 0.7 mm while traveling from STA 160 to 250. The "Auto" mode was used only from STA 178.5 to 179.7 and from STA 230.8 to 232.2. North of STA 250, the GPS signal faded and disallowed mapping of CCV. In operating in the manual mode from STA 250 to 160 along the same travel path at nominal amplitude of 1.1 mm, CCV data were collected to evaluate repeatability of the measurement and identify the influence of amplitude on dynamic roller response. The "Auto" mode was used from STA 178.2 to 180.1 and from STA 197.9 to 198.7. The roller data for Proof 36 are shown in Figure 5.19 and Figure 5.21. The data are discussed in more detail in the next chapter – Chapter 9 Data Analysis. In-situ measurements were collected at 91-m intervals (every three stations) on Proof 36 starting at STA 160. The measurements, which are overlain by CCV data, are shown in Figure 5.23 and Figure 5.24.

Summary statistics were calculated from available CCV and in-situ test data for the proof sections and summarized in Table 5.4. Mean values and coefficients of variation are presented for CCV, E_{LWD}, dry unit weight, moisture content, DPI, and CIV_{20-kg}. The number of observations (n) from which the statistical parameters were calculated is also provided.

Table 5.3. Summary of proof sections

Proof No.	Date	Time (hh.mm)	STA	Lift No.	IC-CTV	w (%)*	Mn/DOT Testing	ISU Testing
1	6/13		311-314		35			
2	6/14		306-309		35			
3	6/14		295-300		35			
4	6/15		275-284		35			
5	6/17	12.36	303-314	2	35	8.7		
6	6/19	08.53	303-314	2	35	8.2		
7	6/21	08.46	311-314	3	35	9.7	x	
8	6/21	09.11	303-311	4	42	11.1	x	
9	6/21	12.40	292-300	2	35	10.4		
10	6/22	18.32	292-300	4	42	11.4		
11	6/22	19.41	287-292	1	35	8.2		
12	6/23	07.51	287-292	1	35	8.2		
13	6/26	10.13	269-287	2	35	8.5		
14	6/27	11.09	269-277	4	42	8.6	x	x
15	6/27	15.26	277-287	4	42	9.8	x	x
16	6/27	18.46	259-269		35	8.0		
17	6/28	18.46	259-266	4	42	10.3		
18	6/28	08.53	243-248	2	35	8.2		x
19	6/29	12.40	253-259	1	60	11.2	x	x
20	7/3	11.00	243-248	4	42	8.9		
21	7/3	13.00	236-243	1	42	8.0		
22	7/4	17.00	224-236	1	42	7.6		
23	7/5	08.00	170-171	2	35	11.4		
24	7/5	10.30	213-223	1	42	8.0	x	
25	7/5	12.30	210-213	1	42	8.2		
26	7/6	10.30	194-208	1	42	8.0	x	
27	7/7	14.21	181-194	1	42	10.7	x	

28	7/8	07.30	138-147	2	35	10.1		
29	7/8	10.30	158-179		42	10.6		
30	7/10	17.20	138-147	4	42	9.8		
31	7/10	18.00	130-138	1	50	8.1		
32	7/11	08.00	147-158	1	50	10.6		
33	7/18	07.00	070-078	2	35	11.1	x	
34	7/18	16.00	085-092		35	10.4		
35	7/19	08.15	067-077	4	42	8.9		x
36	7/19	19.00	160-313					x
37	7/20	10.00	119-130	1	35	11.2		
38	7/20	15.15	106-119	1	42	9.3	x	
39	7/20	17.30	085-106		42	10.9	x	
40	7/25	18.00	077-085	1	42	11.1		
41	7/28	08.30	002-022		35	10.9		
42	7/31	11.00	022-032	1	35	10.9		
43	7/31	11.00	022-032	1	42	10.9		
44	8/2	17.00	032-054	1	38	7.6		
45	8/3	07.45	002-032	1	38	8.7		
46	8/3	09.45	035-041	4	42	8.9		
47	8/3	14.00	054-067	1	42	9.8		

* Mn/DOT speedy moisture prior to proof

Figure 5.13. Proof 14, from STA 269 to 277

Figure 5.14. Proof 15, from STA 277 to 287

Figure 5.15. Proof 18, from STA 243 to 248
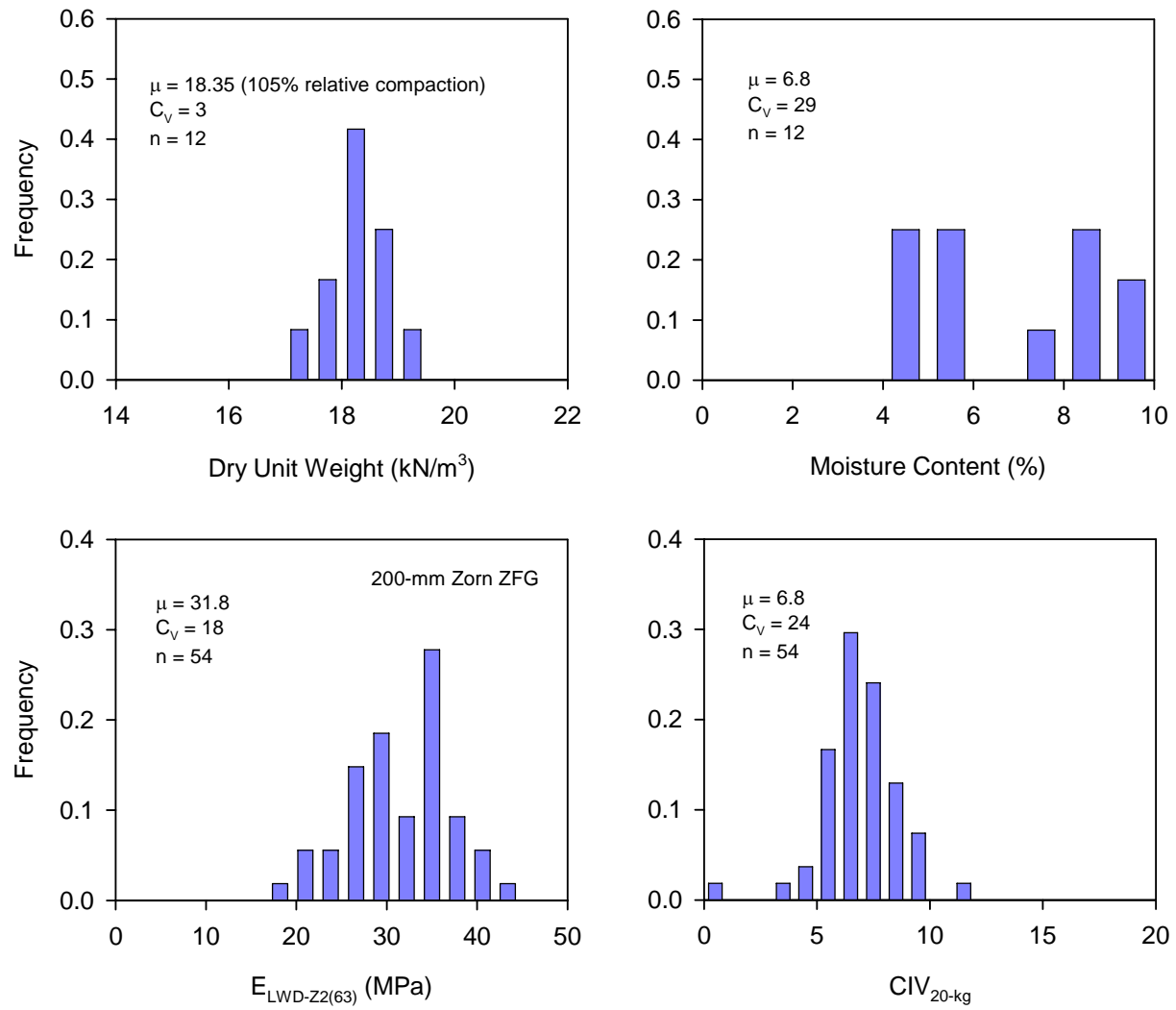
Figure 5.16. Distribution plots for in-situ measurements at Proof 14 (proof area = 1115 m^2)
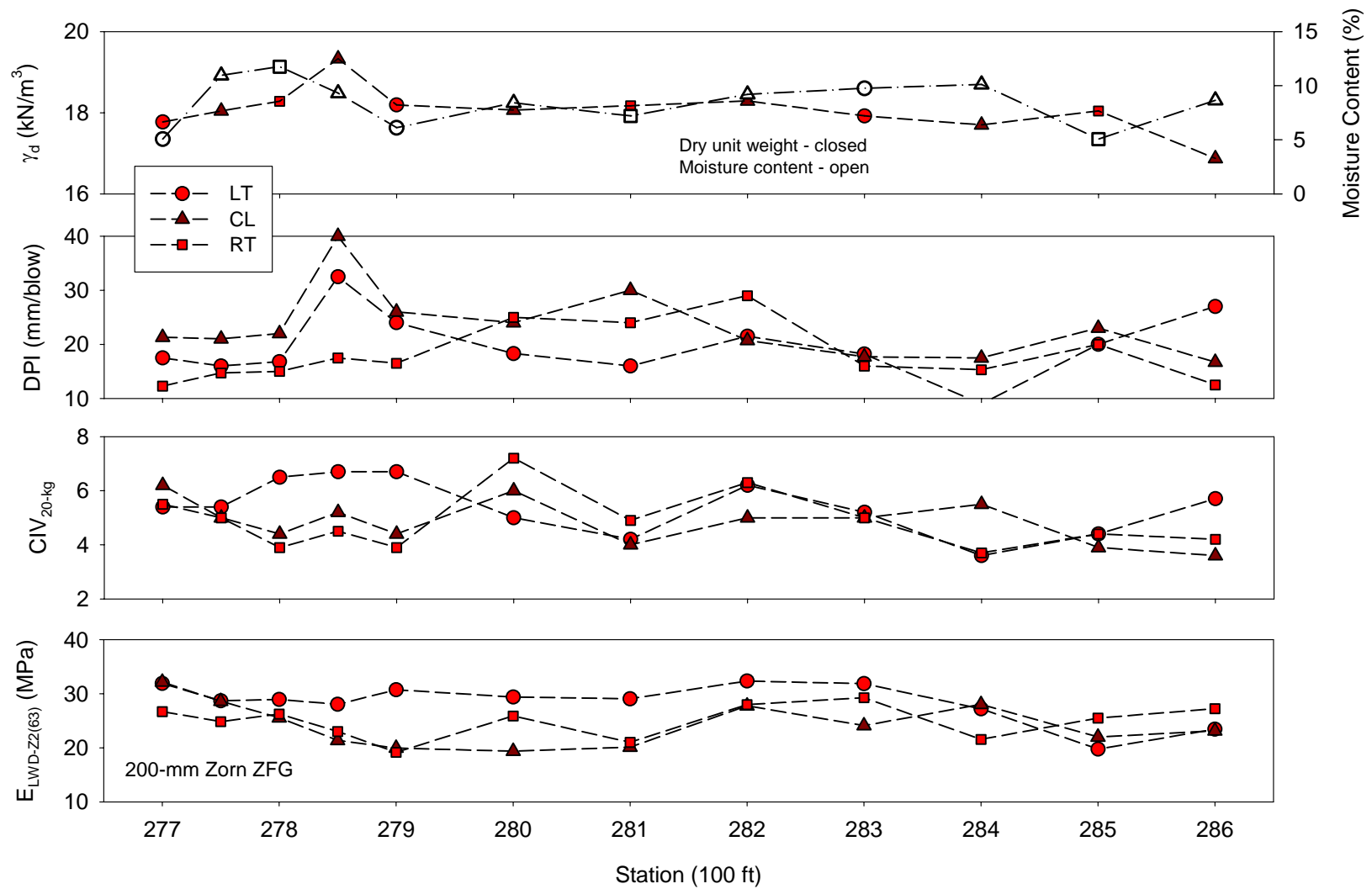
Figure 5.17. Proof 15 dry unit weight, DPI, CIV$_{20\text{-kg}}$, and E$_{LWD}$ data
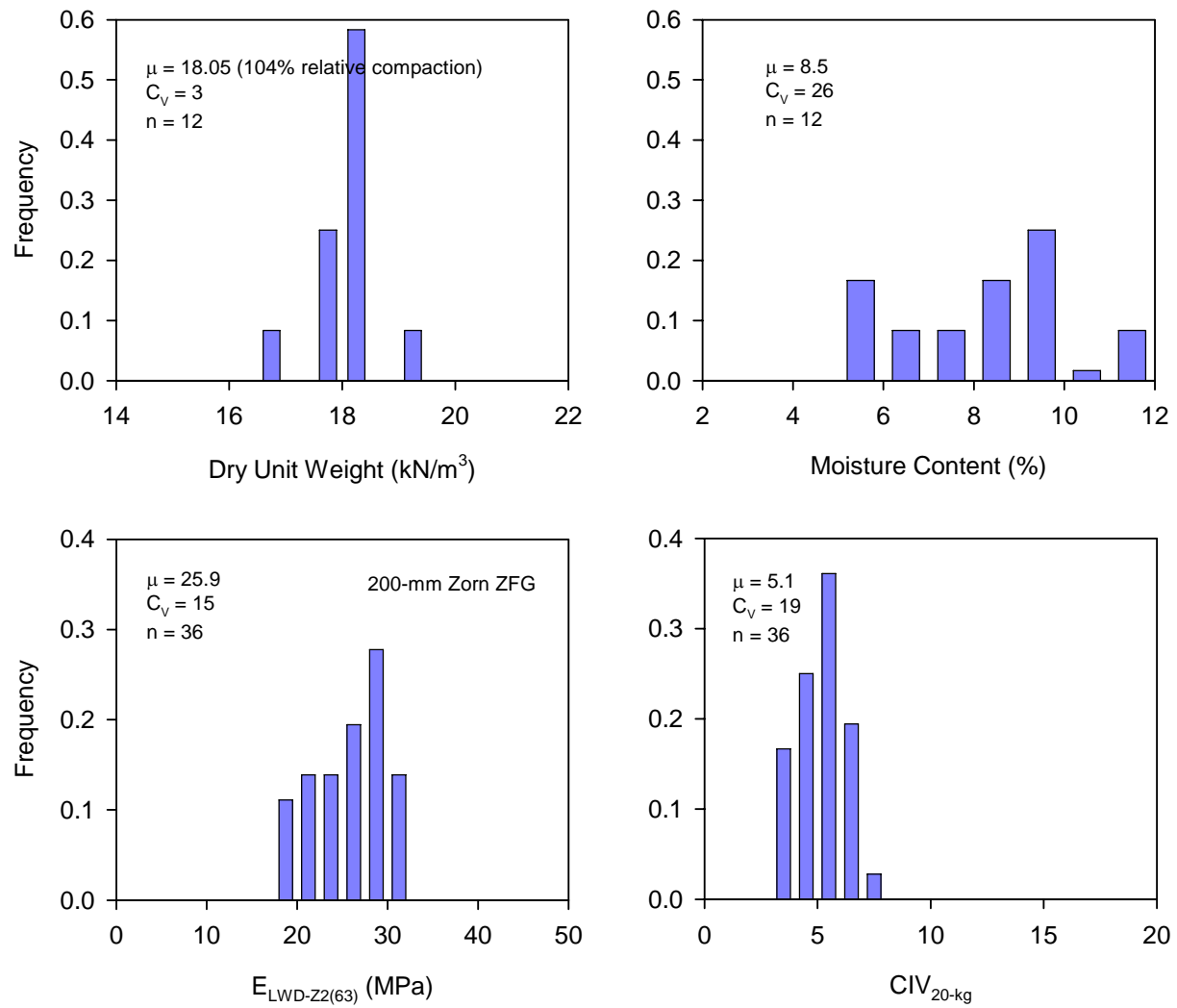
Figure 5.18. Distribution plots for in-situ measurements at Proof 15 (proof area = 2787 m^2)
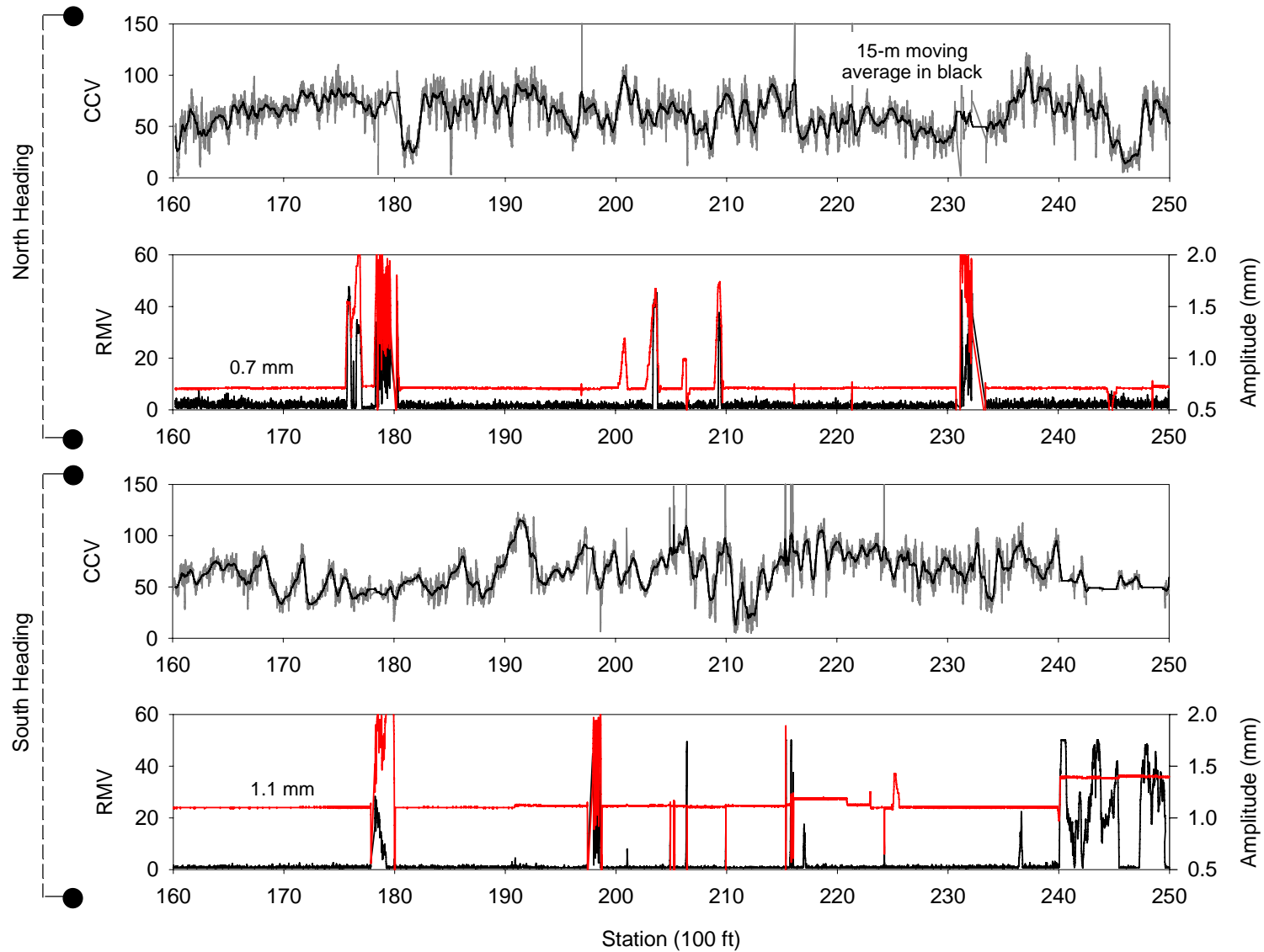
Figure 5.19. Proof 36 CCV, RMV, and amplitude data
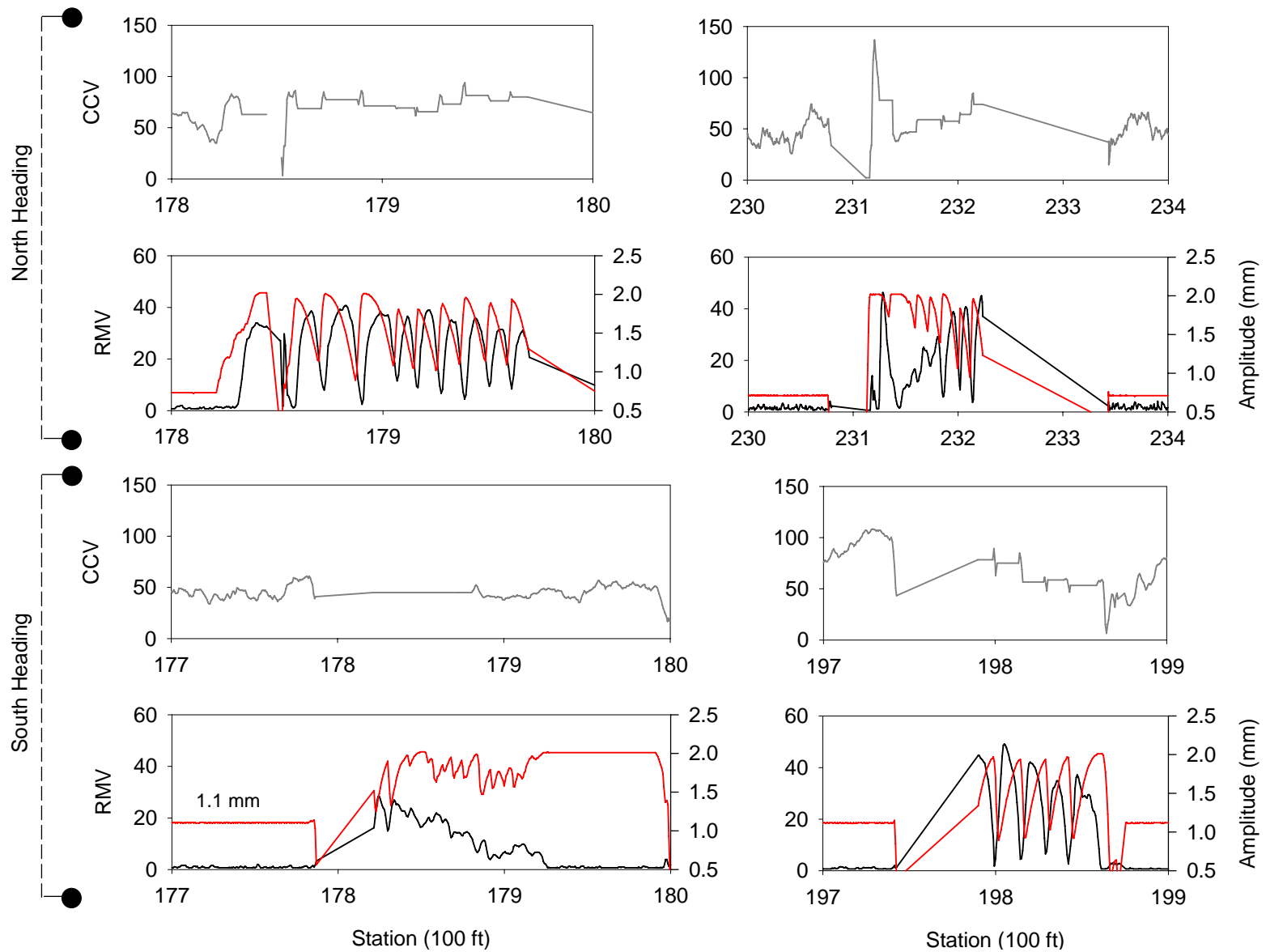
Figure 5.20. Close-up views of Proof 36 CCV, RMV, and amplitude data
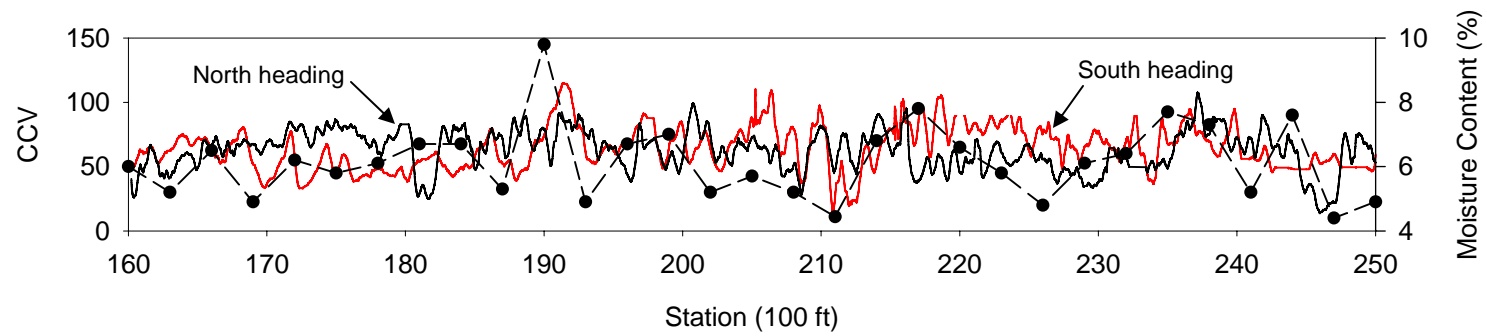
Figure 5.21. Comparison of CCV at two amplitudes and influence of moisture content for Proof 36
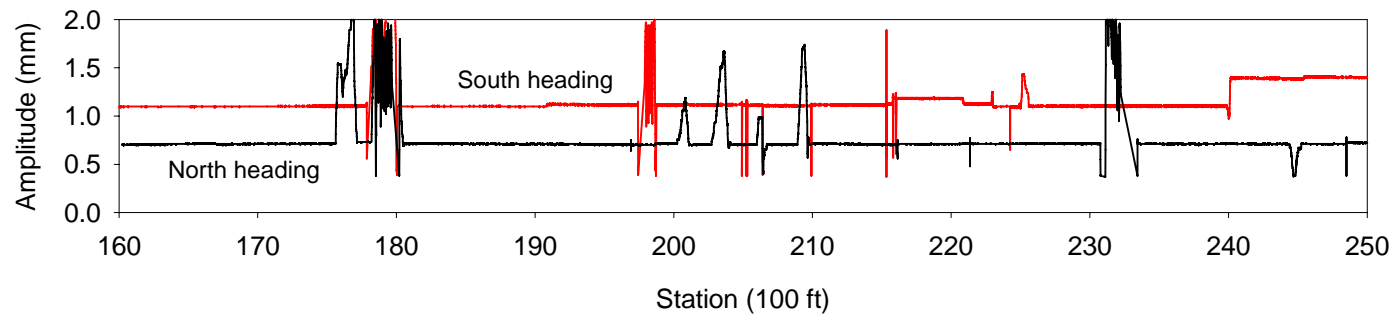
Figure 5.22. Comparison of amplitudes for Proof 36
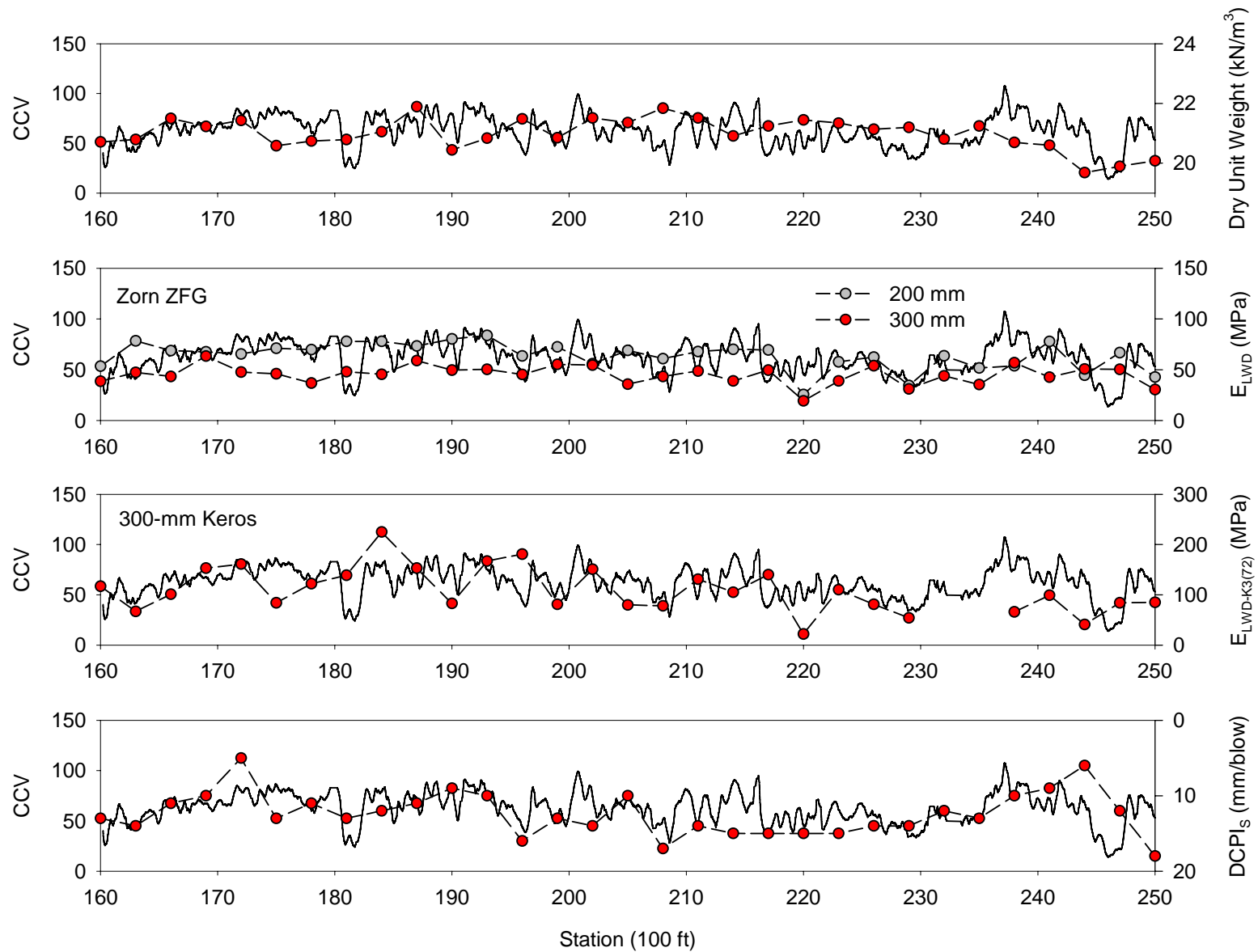
Figure 5.23. Proof 36 CCV (North heading) and in-situ measurement data
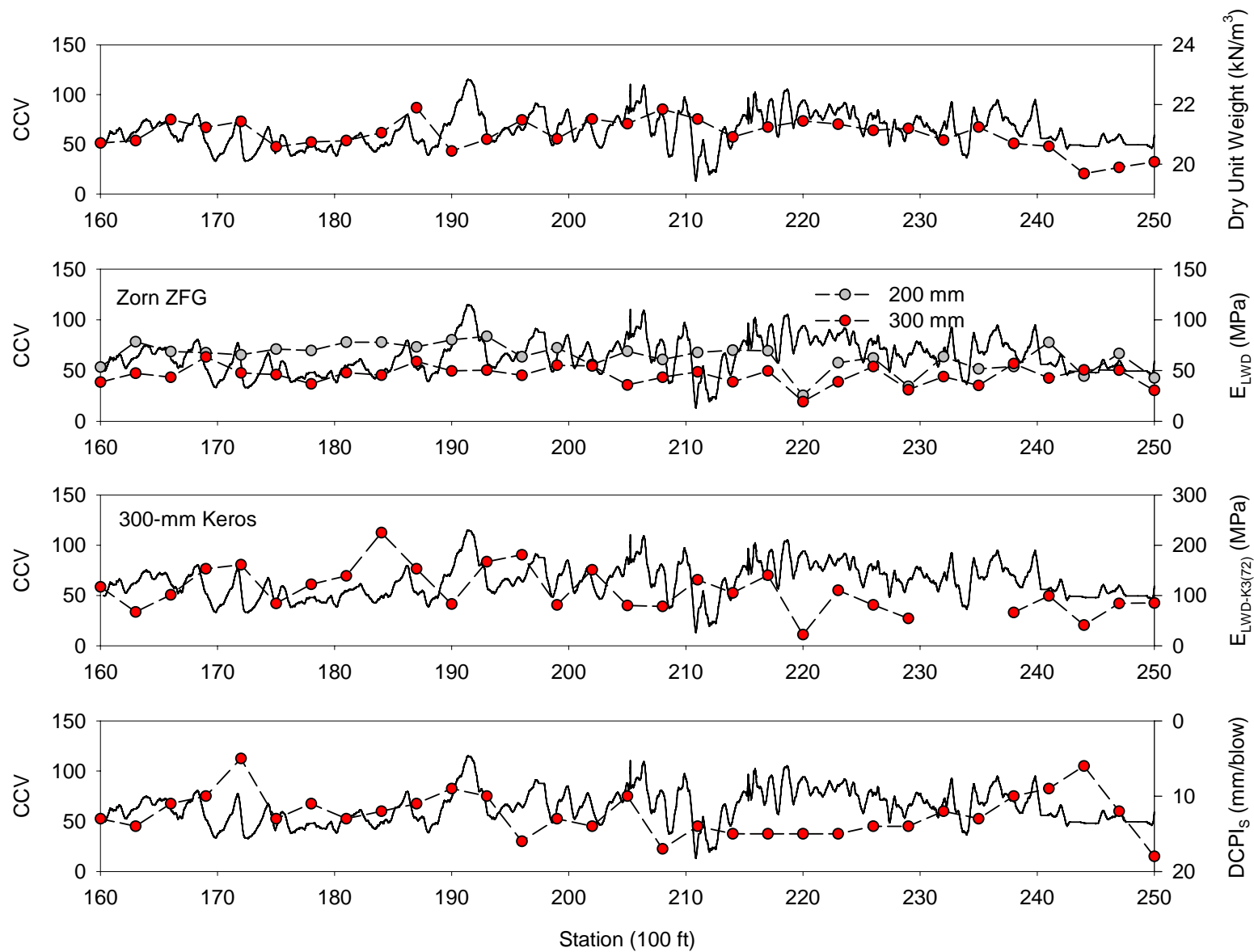
Figure 5.24. Proof 36 CCV (South heading) and in-situ measurement data

Table 5.4. Summary of proof testing results

Proof No.	CCV				$E_{LWD-Z2(63)}$ (MPa)		γ_d (kN/m³)*		w (%)**		DPI (mm/blow)		$CIV_{20\text{-}kg}$	
	n	μ	C_V	n	μ	C_V	μ	C_V	μ	C_V	μ	C_V	μ	C_V
1	–	–	–	–	–	–	–	–	–	–	–	–	–	–
2	–	–	–	–	–	–	–	–	–	–	–	–	–	–
3	–	–	–	–	–	–	–	–	–	–	–	–	–	–
4	–	–	–	–	–	–	–	–	–	–	–	–	–	–
5	13387	40.1	26	–	–	–	–	–	–	–	–	–	–	–
6	15902	44.3	19	–	–	–	–	–	–	–	–	–	–	–
7	4746	42.7	21	2	34.0	37	22.46	–	7.3	–	23	47	–	–
8	10346	47.0	12	3	53.3	4.3	18.40	–	5.8	–	20	31	–	–
9	8214	46.0	24	–	–	–	–	–	–	–	–	–	–	–
10	5441	45.0	15	–	–	–	–	–	–	–	–	–	–	–
11	4700	44.9	27	–	–	–	–	–	–	–	–	–	–	–
12	4795	48.3	24	–	–	–	–	–	–	–	–	–	–	–
13	17475	49.6	18	–	–	–	–	–	–	–	–	–	–	–
14	7924	49.6	16	54	31.8	18	18.35	3	6.8	29	18	26	6.84	24
14	7924	49.6	16	4	62.0	34	18.96	–	8.1	–	17	16	–	–
15	13937	45.3	14	36	25.9	15	18.05	3	8.5	26	20	30	5.05	19

15	13937	45.3	14	4	48.5	14	19.56	–	7.8	–	23	18	–	–
16	10499	55.3	17	–	–	–	–	–	–	–	–	–	–	–
17	–	–	–	–	–	–	–	–	–	–	–	–	–	–
18	5710	49.7	19	6	29.1	15	17.92	2	3.9	4	17	13	5.47	12
19	5045	63.8	14	3	61.0	20	18.66	–	7.3	–	12	45	–	–
20	–	–	–	–	–	–	–	–	–	–	–	–	–	–
21	–	–	–	–	–	–	–	–	–	–	–	–	–	–
22	–	–	–	–	–	–	–	–	–	–	–	–	–	–
23	–	–	–	–	–	–	–	–	–	–	–	–	–	–
24	–	–	–	3	57.3	13	19.43	–	7.4	–	21	5	–	–
25	–	–	–	–	–	–	–	–	–	–	–	–	–	–
26	–	–	–	3	52.5	34	18.22	–	5.0	–	24	34	–	–
27	12599	55.9	16	3	76.3	18	18.93	–	4.4	–	16	19	–	–
28	8241	41.9	24	–	–	–	–	–	–	–	–	–	–	–
29	23387	49.5	21	–	–	–	–	–	–	–	–	–	–	–
30	8970	47.5	17	–	–	–	–	–	–	–	–	–	–	–
31	7524	51.9	16	–	–	–	–	–	–	–	–	–	–	–
32	15701	48.7	22	–	61.3	71	–	–	9.3	–	22	32	–	–
33	12532	43.8	17	2	55.5	19	16.86	–	4.8	–	21	10	–	–
34	9092	37.8	25	–	–	–	–	–	–	–	–	–	–	–
35	17089	40.0	18	14	32.7	12	17.21	2	7.3	30	25	17	–	–

35	17089	40.0	18	3	57.0	17	–	–	6.7	–	20	10	–	–
36a	14994	62.6	33	31	71.4	21	20.99	2	6.1	19	12[a]	24[a]	–	–
36b	14994	65.2	32	31	71.4	21	20.99	2	6.1	19	12[a]	24[a]	–	–
37	11674	39.9	27	3	79.7	39	17.72	–	8.4	–	23	12	–	–
38	12064	46.7	19	3	72.0	34	18.38	–	8.4	–	18	8	–	–
39	19198	46.1	19	6	93.2	20	19.50	–	7.8	–	16	9	–	–
40	8333	46.3	17	–	–	–	–	–	–	–	–	–	–	–
41	19279	41.1	32	–	–	–	–	–	–	–	–	–	–	–
42	15474	41.3	34	–	–	–	–	–	–	–	–	–	–	–
43	–	–	–	–	–	–	–	–	–	–	–	–	–	–
44	20781	43.3	25	–	–	–	–	–	–	–	–	–	–	–
45	20356	46.3	26	–	–	–	–	–	–	–	–	–	–	–
46	5572	45.0	18	–	–	–	–	–	–	–	–	–	–	–
47	14052	44.6	17	–	–	–	–	–	–	–	–	–	–	–

*   Nuclear dry unit weight
**   ISU nuclear moisture or Mn/DOT stove moisture, if no ISU testing
a   Through STA 250

5.8 Data Analysis

The data summarized in Section 5.7 facilitate data analyses that are performed with the following objectives:

- Identify challenges associated with interpreting CCV data collected for fine sand

- Correlate CCV with measures of dry unit weight, strength, and modulus at two spatial scales

- Correlate variation parameters for CCV, dry unit weight, strength, and modulus

From STA 250 to 260, compacted materials were tested for strength and modulus at two depths using the Zorn LWD and the 20-kg Clegg impact tester. The tests were performed at the soil surface and, following careful excavation of the material, at a depth ranging from 110 to 280 mm. Performance of Clegg impact and LWD tests below the soil surface are shown in Figure 5.25 and Figure 5.26, respectively. DCP profiles and the stability measurements at two depths are shown in Figure 5.27. Based on DCP measurements, low strength is observed at the soil surface to a depth of approximately 100 mm. Below this depth, DCP index drops to about 20 percent of the surface measurement (stiffer). Increases in strength and modulus with depth were also supported by Clegg impact and LWD test results, where the respective measurements performed in the excavation were often double those at the soil surface. The test results demonstrate the effect of confining pressure on sand stability and indicate the limited measurement influence depth of many in-situ compaction measurement devices.

Regression analysis of data from STA 250 to 260 shows that both $CIV_{20\text{-kg}}$ and E_{LWD} may be estimated using DCP index data. Figure 5.28 shows a linear relationship between DCPI and $CIV_{20\text{-kg}}$ and a power-function relationship between DCPI and E_{LWD}. Based on these results and the smaller measurement influence depths of Clegg impact tests and the 200-mm LWD device (compared to roller), correlations of DCP index with roller-generated data may be more highly correlated with CCV than CIV or E_{LWD}.

Figure 5.25. Clegg impact tester (20-kg) at 195-mm depth

Figure 5.26. 200-mm Zorn ZFG light weight deflectometer at 220-mm depth
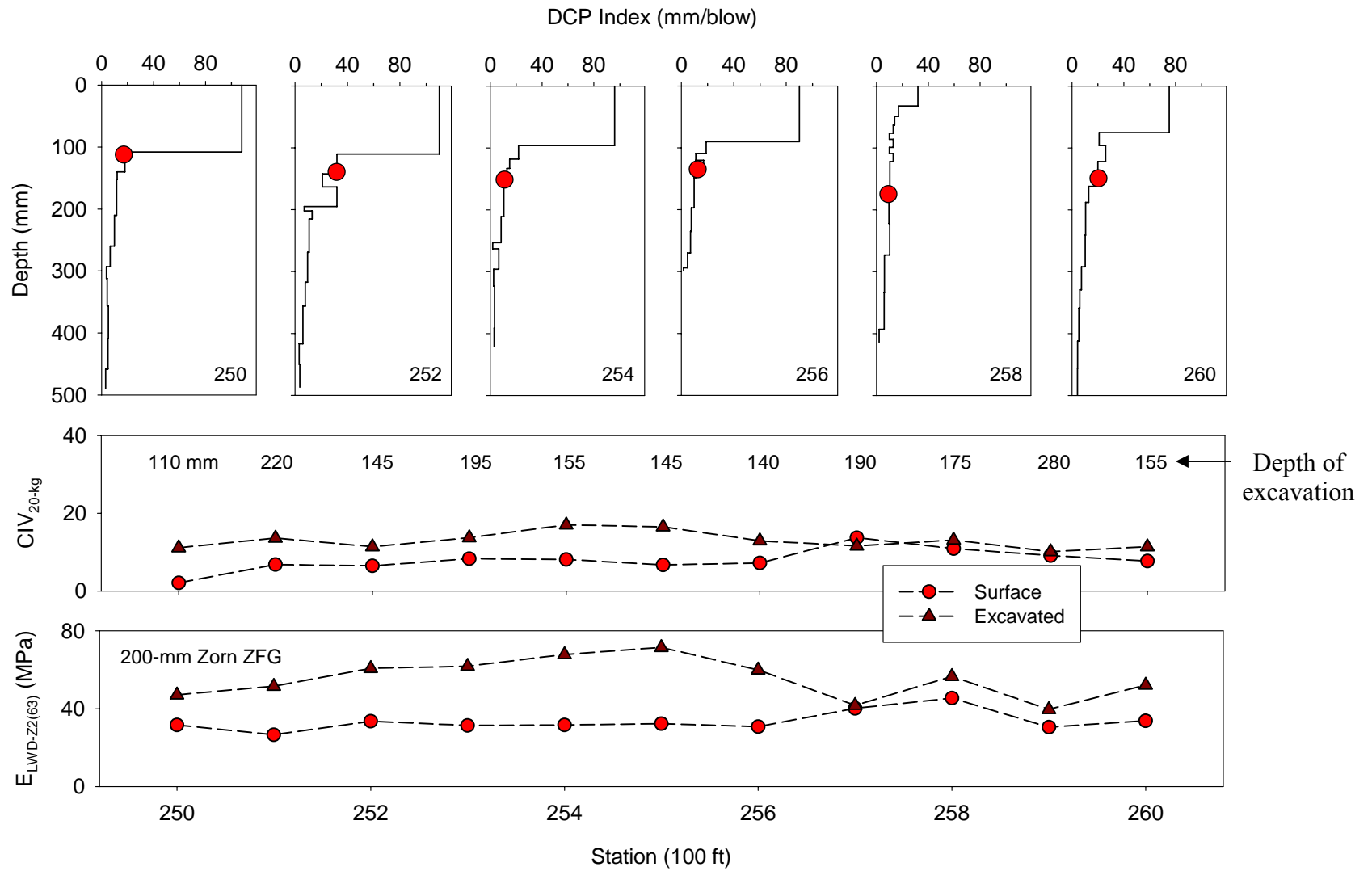
Figure 5.27. In-situ measurements at different depths to show effect of confining pressure on sand stability
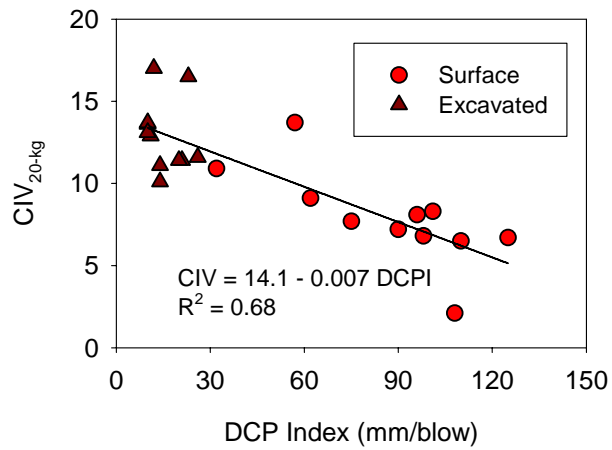
Figure 5.28. Relationships between DCP Index and $CIV_{20\text{-kg}}$ (STA 250 to 260 only)
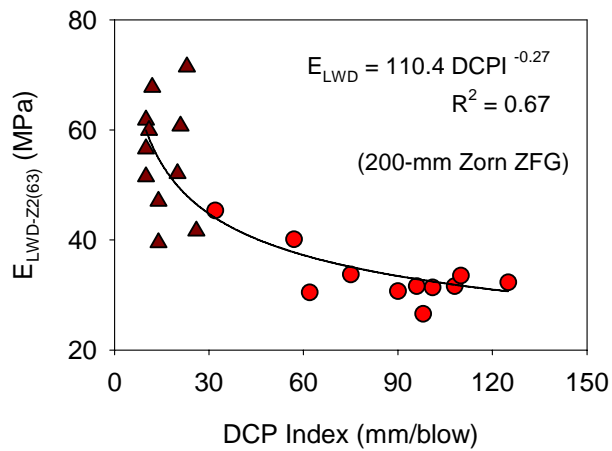
Figure 5.29. Relationship between DCPI and $E_{LWD\text{-}Z2(63)}$ (STA 250 to 260 only)
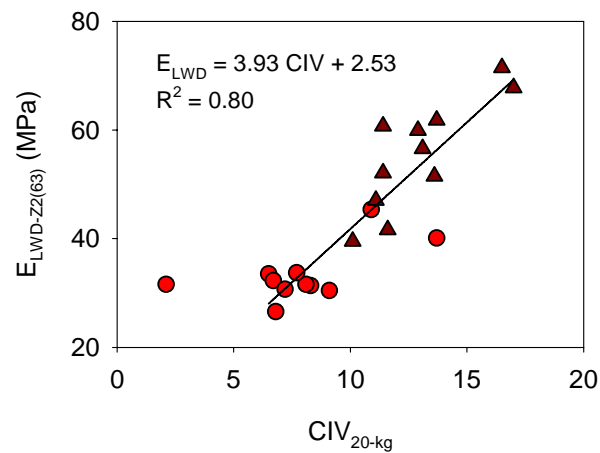
Figure 5.30. Relationship between $CIV_{20\text{-kg}}$ and $E_{LWD\text{-}Z2(63)}$ (STA 250 to 260 only)

102

Correlation analyses were conducted in order to relate CCV to in-situ test device measurement values at the proof scale. For Proofs 14, 15, and 35; dry unit weight, strength, and modulus were compared with the spatially nearest CCV value, the mean CCV for a 3-m square window, and the mean CCV for a 6-m square window. The compaction data and averaging windows are shown in Figure 5.31 for Proof 14. The scatter plots are shown from Figure 5.32 to Figure 5.34. Considerable scatter was observed in the relationships, such that regressions were not fit to these data. Negative relationships are observed between dry unit weight and CCV.

Roller and in-situ test data for the three proofs were combined to produce Figure 5.35. Despite the data scatter, the correct trends were observed and regressions fit to the data. R^2 values ranged from 0.01 to 0.28.
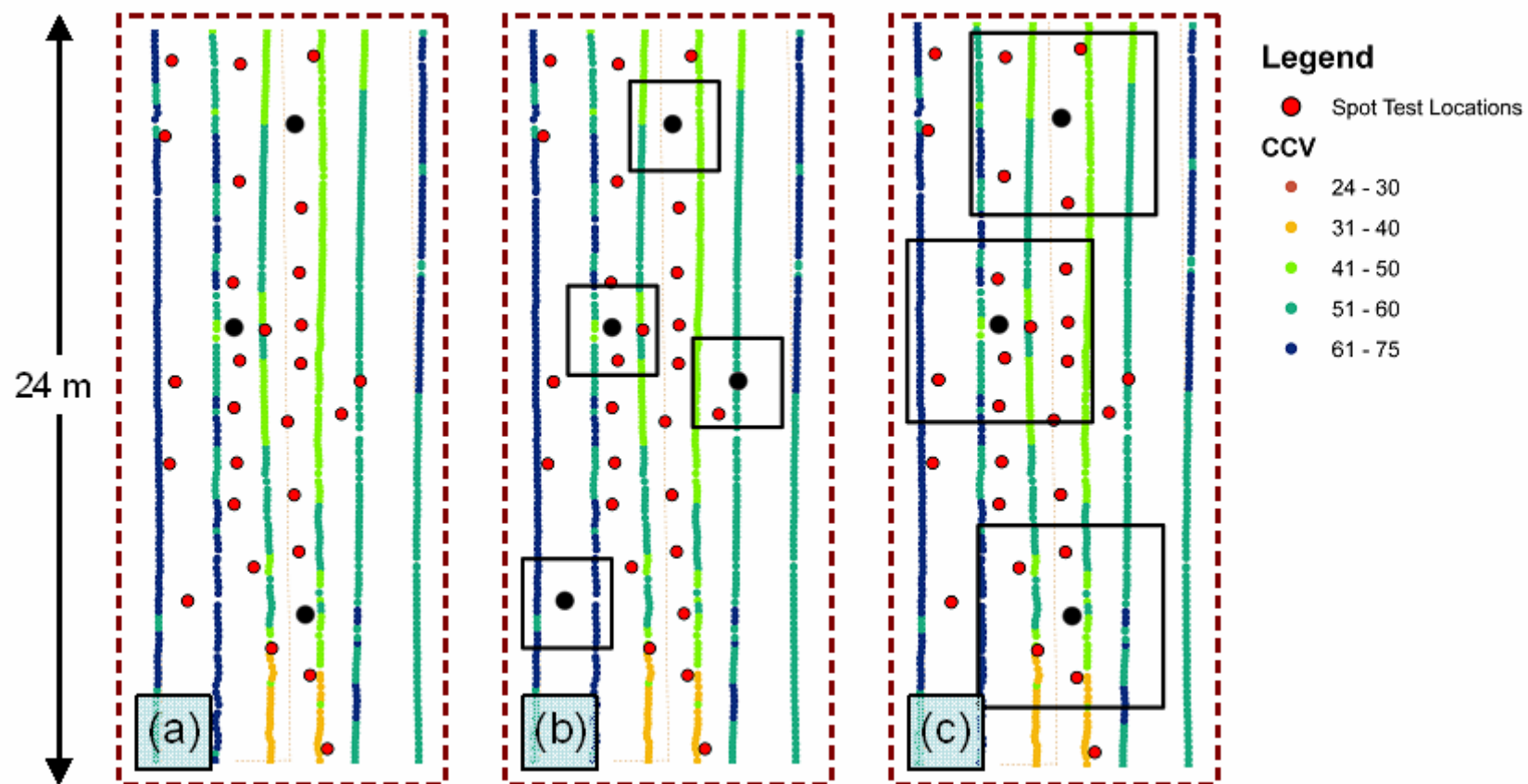
Figure 5.31. Proof 14 compaction measurements and sample averaging windows of: (a) spatially-nearest test point, (b) 3-m CCV average, and (c) 6-m CCV average for developing correlations
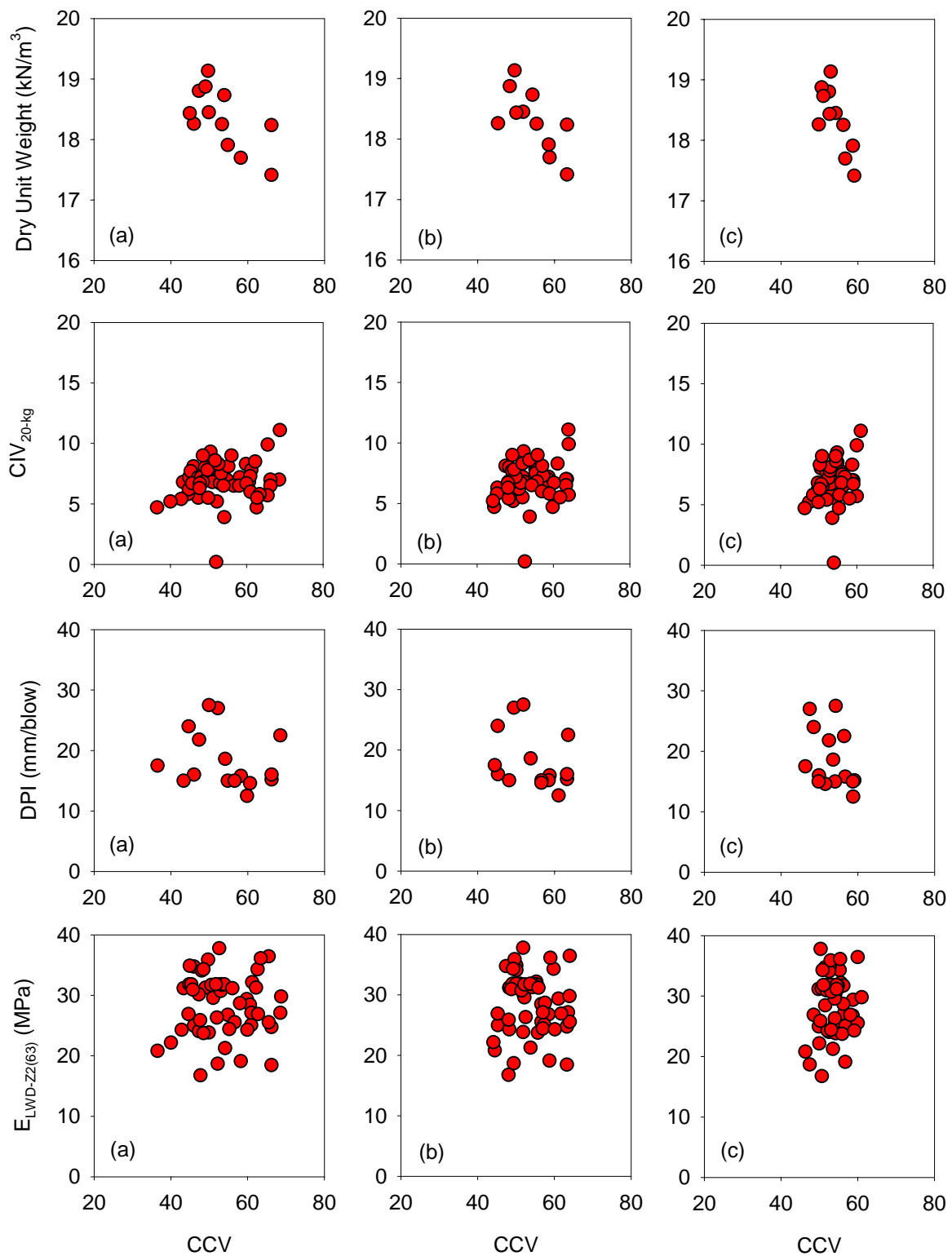
Figure 5.32. CCV correlation with Proof 14 in-situ measurements using: (a) nearest point, (b) 3-m CCV average, and (c) 6-m CCV average
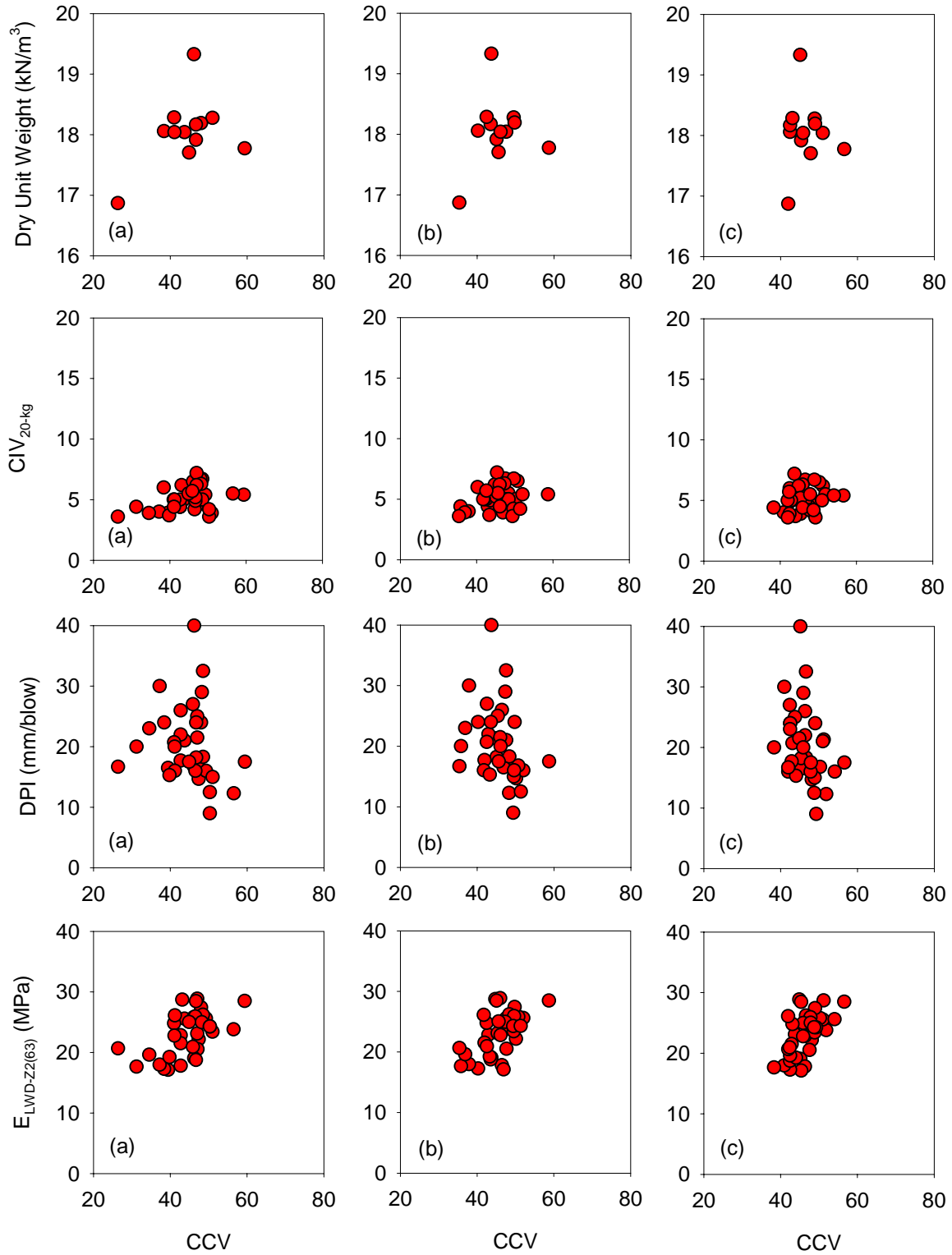
Figure 5.33. CCV correlation with Proof 15 in-situ measurement using: (a) nearest point, (b) 3-m CCV average, and (c) 6-m CCV average
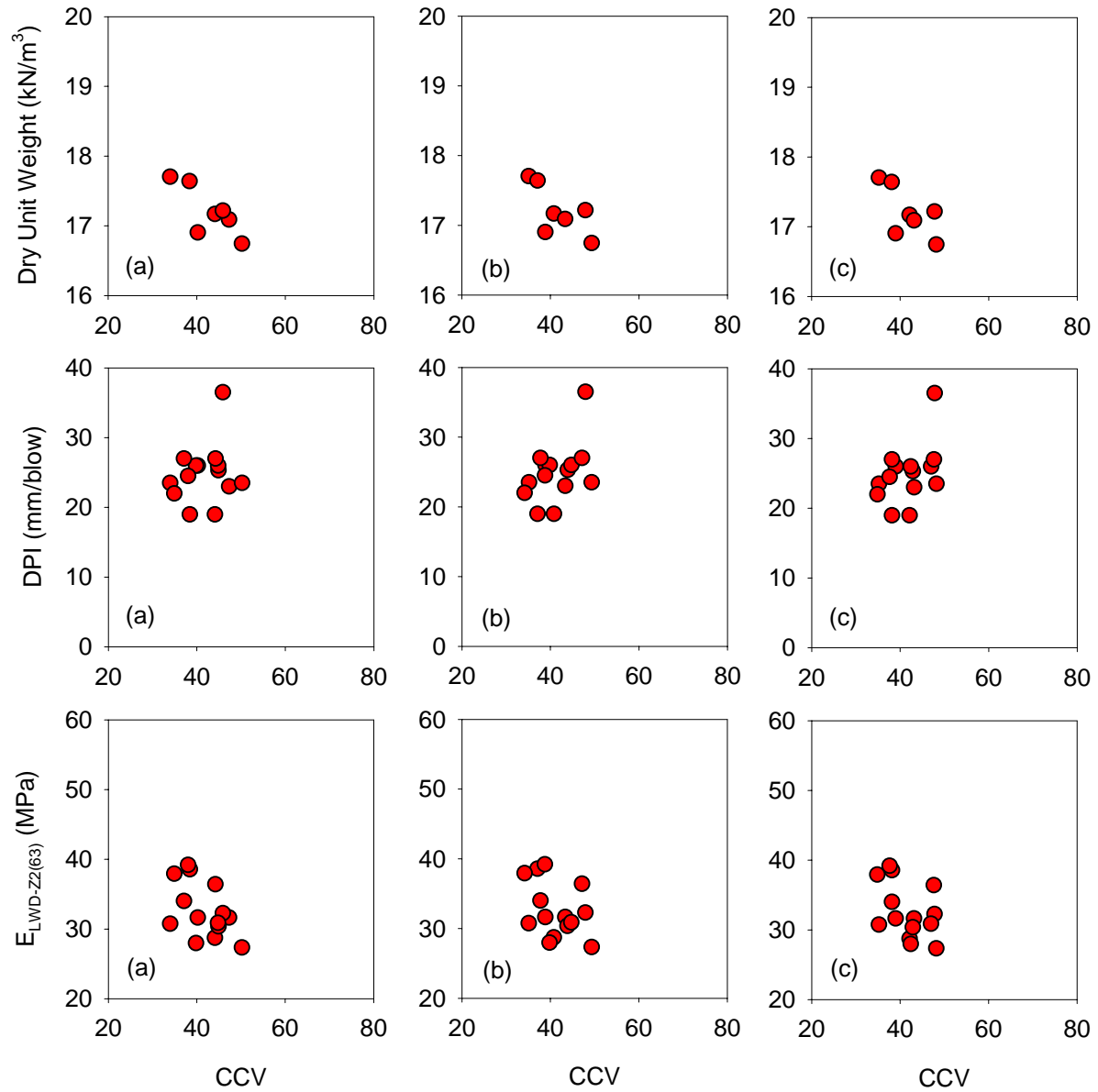
Figure 5.34. CCV correlation with Proof 35 in-situ measurements using: (a) nearest point, (b) 3-m CCV average, and (c) 6-m CCV average
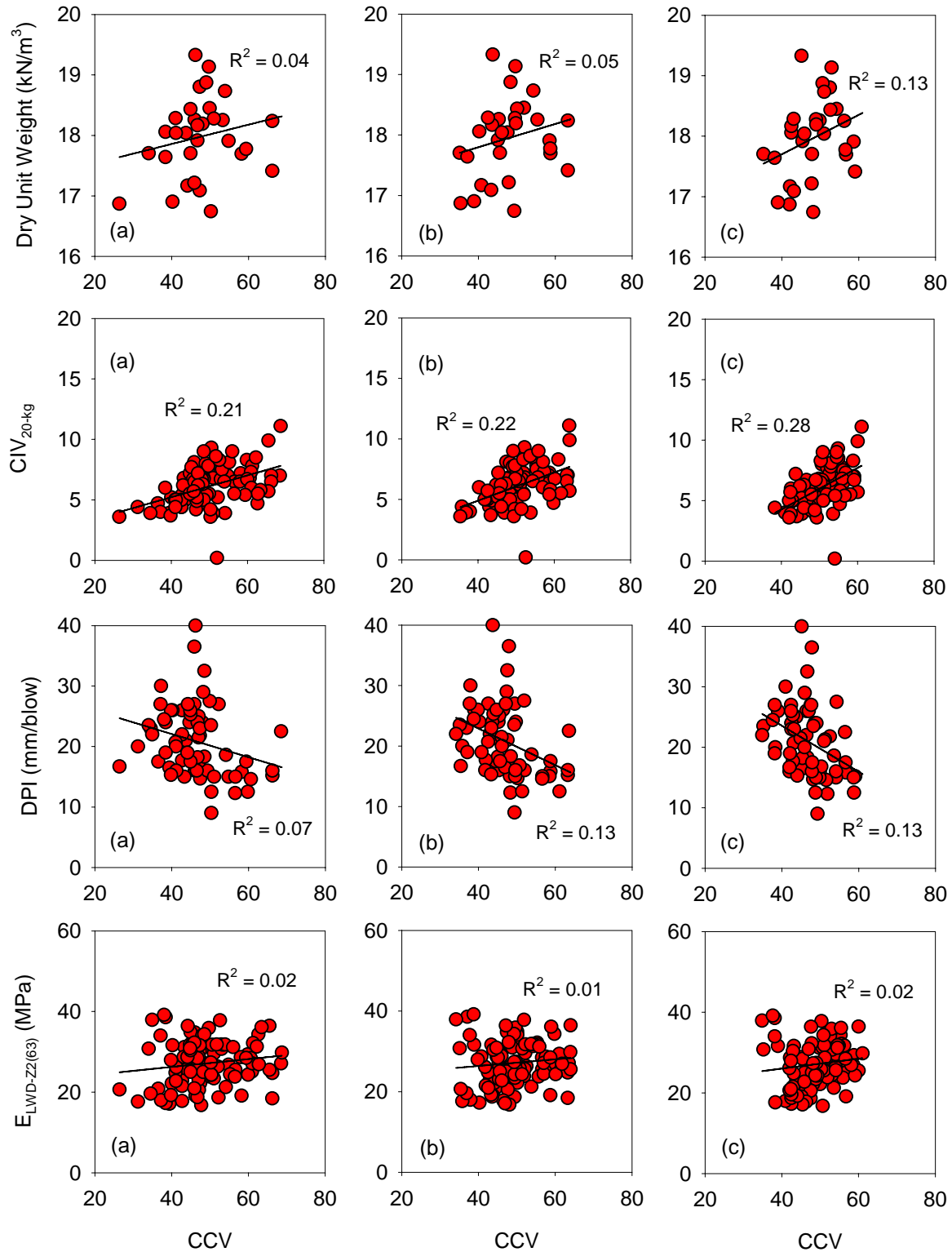
Figure 5.35. Combined proof CCV correlation with in-situ measurements using: (a) nearest point, (b) 3-m average, and (c) 6-m average

108

For investigating the relationships at the project scale, average CCV and in-situ test results for different proof sections (Table 5.4) were compared. Scatter plots are shown in Figure 5.36. By increasing the scale at which the measurements are compared – a measure that incorporates wider range of measurement values, improved correlations are observed. Average dry unit weight and DPI are predicted from average CCV with R^2 values of 0.52 and 0.79, respectively. Considerable scatter was still observed for E_{LWD-Z2}.

As IC technology may be more effective at indicating uniformity of compacted materials than any other test device, relationships between coefficients of variation for CCV and in-situ test measurements were explored. The relationships, which are also shown in Figure 5.36, show some indication that IC technology indicates coefficients of variation similar to DCP and LWD compaction test data.
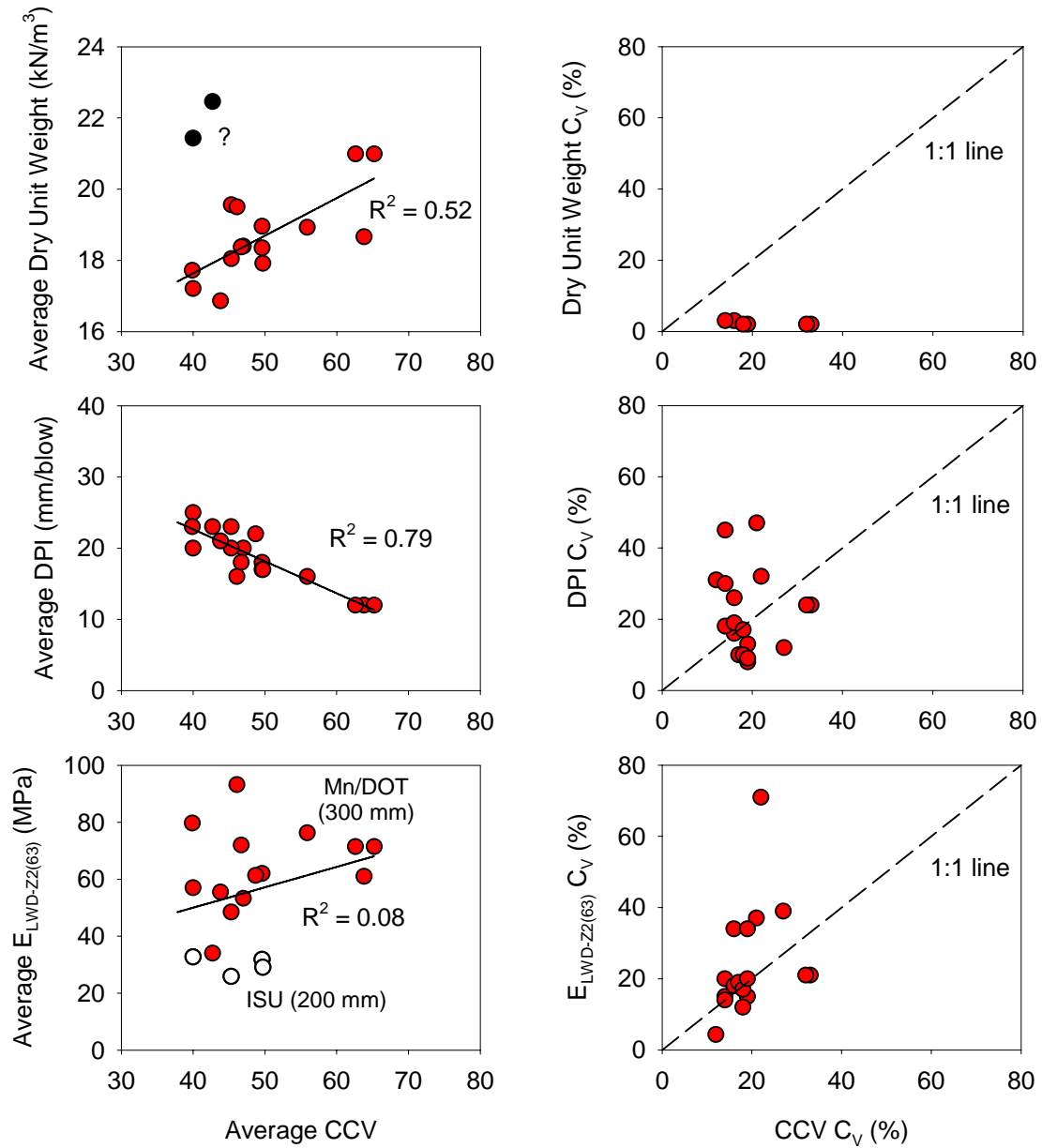
Figure 5.36. Correlation of average CCV and average in-situ measurements and coefficients of variation (combined proofs)

5.9 Project Observations

The following statements summarize the activity of this study.

- Intelligent compaction technology was successfully used as the principal quality control tool on a grading project near Akeley, Minnesota.

- Control sections were constructed and tested in order to establish appropriate quality criteria which were then applied to production areas. Compaction curves observed with control section CCV data show that little compaction occurs after the initial roller pass. This highlights the importance of GPS location and pass information provided to the operator. Target values were approximately the tenth percentile of data collected on the control sections.

- Roller and in-situ test data were collected on proof sections by Mn/DOT inspectors and Iowa State University researchers. These data were analyzed with the objectives of correlating CCV with measures of dry unit weight, strength, and modulus. Variation parameters were also investigated, as intelligent compaction technology may be effective in indicating uniformity of compacted materials.

- CCV and in-situ test results are poorly correlated at the proof scale, likely because insufficient variation is observed in the smaller areas. At the project scale using average values for different proof sections, dry unit weight and DCP index were predicted from CCV with R^2 values of 0.52 and 0.79, respectively. Scatter was still observed for E_{LWD} and attributed to different measurement influence depths of this compaction control device and the roller.

Chapter 6
GIS Database

IC technology provides opportunity to collect and evaluate information for 100 percent of the project area, but it also produces large data files that create analysis, visualization, transfer, and archival challenges. This section of the report describes an approach for managing the data and consists of a "geodatabase" using ArcGIS/ArcInfo modules. IC data archived in this manner is spatially referenced, which can be useful for Mn/DOT as it relates to data management, mapping, etc.

A geodatabase of the TH 64 project IC roller data and in-situ spot test measurements was created as part of this project to demonstrate the application. A brief summary with procedures and structures for creating the geodatabase and a few examples of analysis options in ArcGIS are presented. Further, suggestions for efficient data transfer and storage are provided.

6.1 Introduction

The geodatabase is the common data storage and management framework for ArcGIS (ESRI, 2000). The data types that are supported by the ArcGIS geodatabase system include: point data, line and polygon data, and georeferenced images. Several ArcGIS tools are available to create and manage the geodatabase including:

- ArcCatalog and ArcMap – for creating the geodatabase, visualizing, and data analysis

- ArcPad – a mobile GIS system to collect and analyze data in field, and transfer the data via wireless connections

- ArcIMS – for providing web display of maps

- Python – programming language for customization

The geodatabase can store data that is organized as a "feature class". A feature class is defined as a group of points, lines, or polygons assigned to a geographic X, Y, and Z location (ESRI, 2000). The IC data is typically in point data format that is output in a *.txt, or *.csv, or *.xls format. Data output from the CAT roller used on the TH 64 project was in a *.csv format. The output file consisted of: Time, Left X, Left Y, Left Z (co-ordinates on the left side of the drum), Right X, Right Y, Right Z (co-ordinates on the right side of drum), GPS mode, CCV, RMV, Frequency (Hz), Amplitude (mm), Machine Gear (Forward/Reverse), Auto (ON/OFF), and Vibration (ON/OFF).

A flow chart and procedure used for creating a geodatabase from the raw data is presented in Figures 6.1 to 6.3. Sometimes the IC output files contained unessential data (e.g. data collected when roller is reversing, etc.) which can be filtered before importing into the database. The

filtering criteria are specific to project conditions. For the TH 64 project, data for proof and control sections were filtered for two criteria: (a) machine gear, and (b) vibration mode. Compaction with mapping was specified to be perform in the forward direction and in vibration mode only. Therefore, the filter criteria were selected as "forward" for machine gear and "ON" for vibration mode. After filtering the data, the output file was converted to a *.dbf format. Python scripts are available for which *.csv files can be directly imported in to the geodatabase without conversion.

A personal geodatabase folder is created in ArcCatalog (*see* Figure 6.1). Further, using ArcMap the data files were imported as tables in to the geodatabase folder (*see* Figure 6.2). The imported attribute tables were converted to a feature class using the "Hubbard" county co-ordinate system projections.

6.2 TH 64 Geodatabase Structure

Figure 6.4 shows the geodatabase structure created for the TH 64 project. Data available in the geodatabase includes:

- IC roller data from all control and proof sections organized in "feature data sets" identified by date of compaction, which contains "feature class" identified by time of compaction. Other IC data that is used during compaction is organized by date of compaction. (Note: Only the IC data from control and proof areas were filtered, and all other data is unfiltered).

- Spot test measurements and laboratory Proctor test data by ISU and Mn/DOT.

All data is included in a DVD separate from this report. In addition to the geodatabase data, a few files (*.mxd) showing kriged CCV surface maps, overlaid spot test measurements on the CCV data for proof areas are also included. These files can be viewed using ArcGIS version 9.0, 9.1, or 9.2.

Figures 6.5 to 6.8 show examples of data visualization and analysis performed using ArcGIS tools. Figures 6.5 present CCV data overlaid with ISU spot test measurements for proof nos. 14 and 15. Figure 6.6 shows a histogram plot of the CCV data for proof no. 14. Figure 6.6 shows a semi-variogram model, and Figure 6.7 shows the kriged surface map of CCV for proof no. 14. The semi-variogram and kriging are geostatistical analysis tools described in detail in Chapter 7.

6.3 IC Data Transfer and Storage

Typically, the IC rollers are mounted with an on-board system that collects and stores the data in a memory card. Large data files are generated from IC rollers which should ideally be transferred and stored in real-time. Some important aspects related to efficient data transfer and storage are as follows.

- The type of data collection and storage differ by roller manufacturers. Since implementation of this technology is still new for many contractors and DOT personnel, data management protocols and training by qualified personnel should be required.

- Data back-ups from the memory card should be periodically performed. A practical time limit on the back-up process should be specified in the project specifications.

- Archiving the raw data into a "geodatabase" is an efficient way of storing the data.

- ArcPad technology provided by ESRI (or something similar) potentially could provide real-time wireless data transfer and data archival features, but needs investigation.

- The raw data output contains data points associated with a geographic X, Y, and Z location. Some agencies implement local coordinate systems (e.g. county level coordinate systems) to archive the spatial data. Although, local coordinate systems minimize scale distortions that would occur with larger regional projections, it presents a disadvantage of data transformation using projected coordinates. The current ArcGIS software tools allow for transformation of coordinates; however, minor errors in transformation or projected coordinates could lead to major problems for the end users of the data. These aspects of local coordinate systems should be considered prior to starting the project.

- IC data output files have various formats that include *.xls, *.txt, *.csv, and *.dbf. The Mn/DOT TH 64 IC specification required data output in a *.csv file type. Memory required for data storage will vary with the file type. For example, for a proof section with plan dimensions of approximately 245 m (800 ft) by 11.5 m (38 ft) with compaction performed in 6 roller lanes, the memory required for single point data (assigned to one location across the drum) is about 1.7, 1.0, 1.0, and 1.4 megabytes for *.xls, *.txt, *.csv, and *.dbf file formats, respectively. The total memory required for creating the geodatabase for the TH 64 project was approximately 2GB.

Raw Data

Obtain data output file from IC roller . Typical data file formats include: *.xls, *.txt, and *.csv.
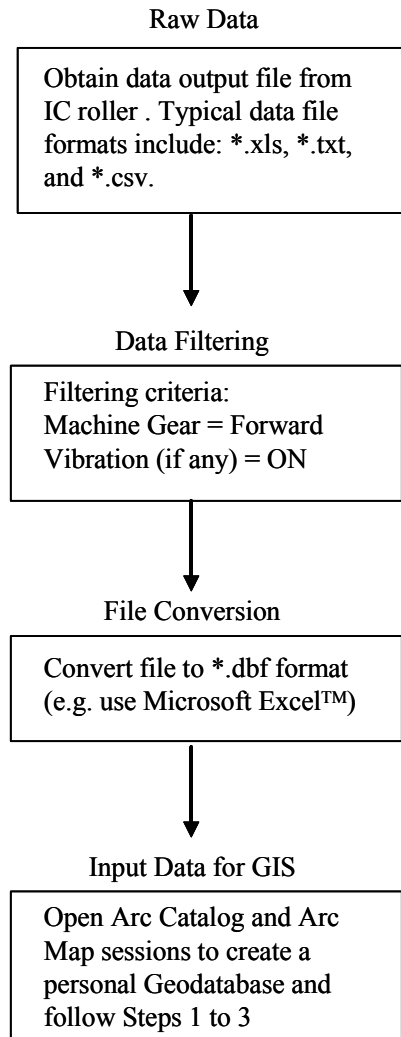
Create a new Personal Geodatabase using Arc Catalog™

Data Filtering

Filtering criteria:
Machine Gear = Forward
Vibration (if any) = ON

File Conversion

Convert file to *.dbf format
(e.g. use Microsoft Excel™)

Input Data for GIS

Open Arc Catalog and Arc Map sessions to create a personal Geodatabase and follow Steps 1 to 3
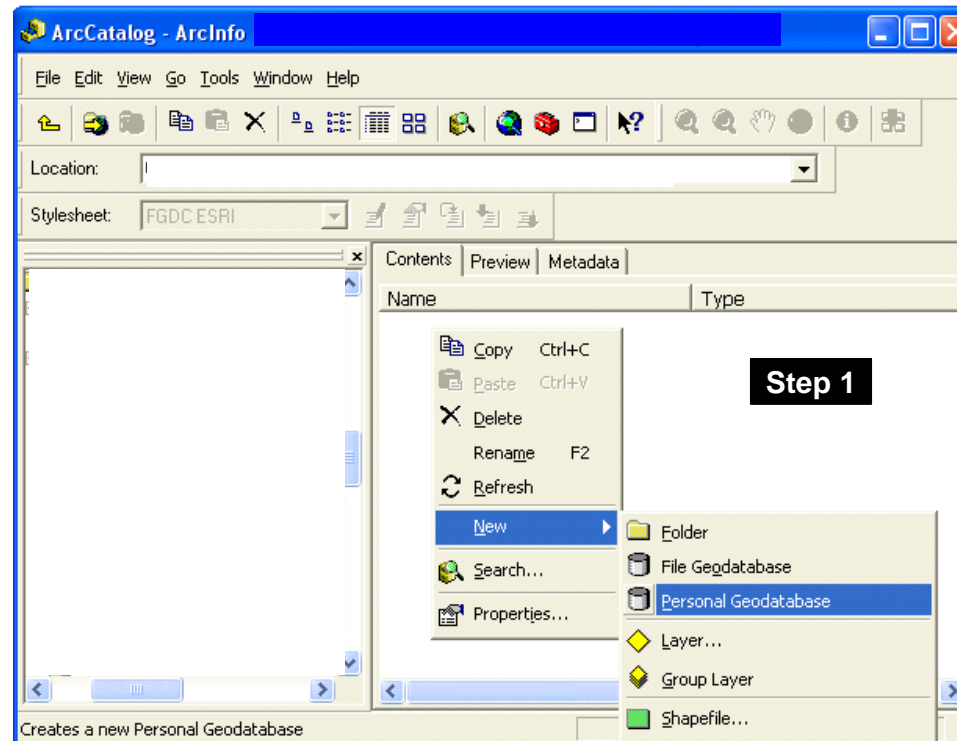
Figure 6.1. Procedure used for importing raw IC data into a geodatabase using ArcGIS interfaces

115
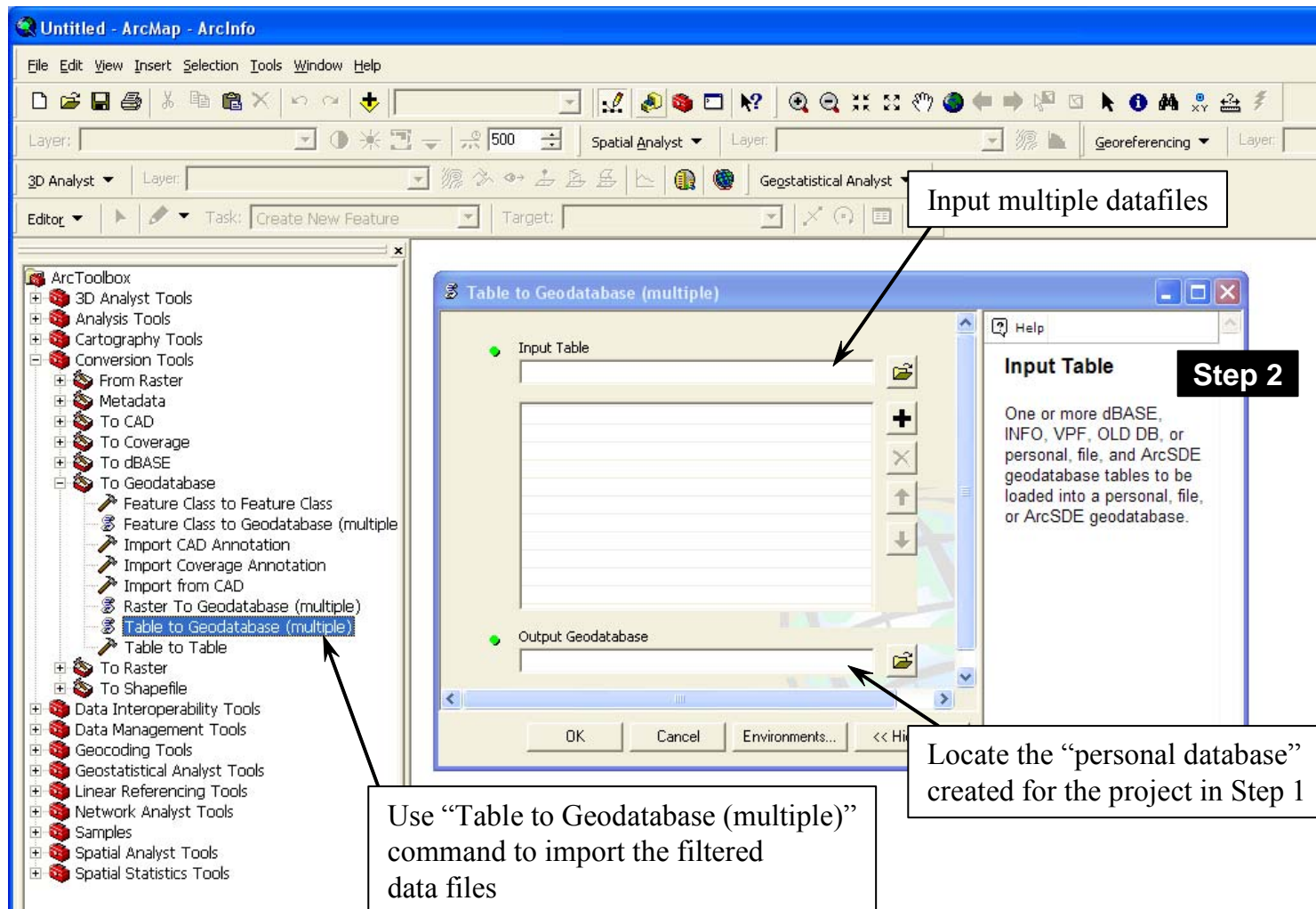
Figure 6.2. Importing filtered data files into geotadabase – ArcCatalog
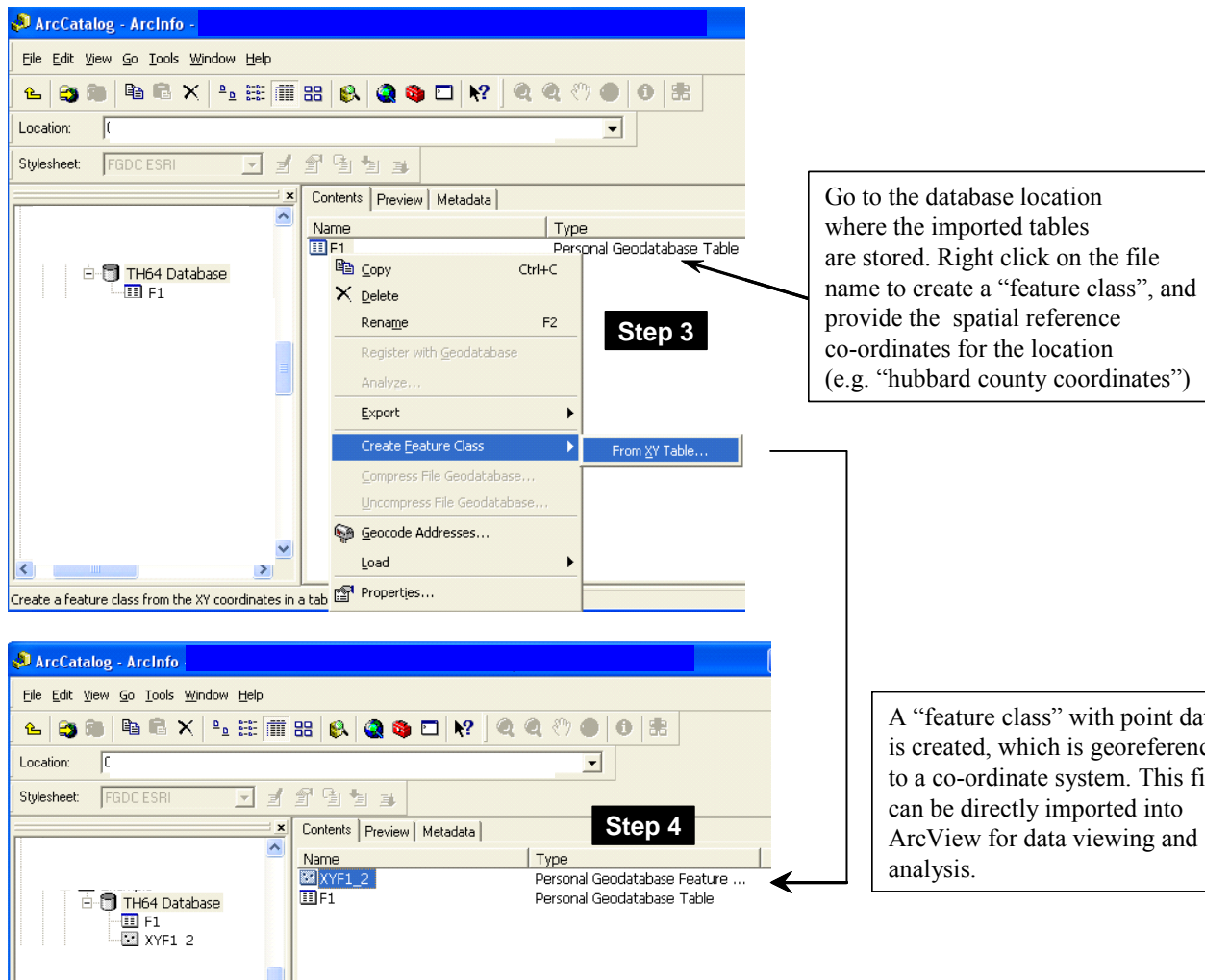
Figure 6.3. Creating "feature class" for imported data tables – ArcCatalog
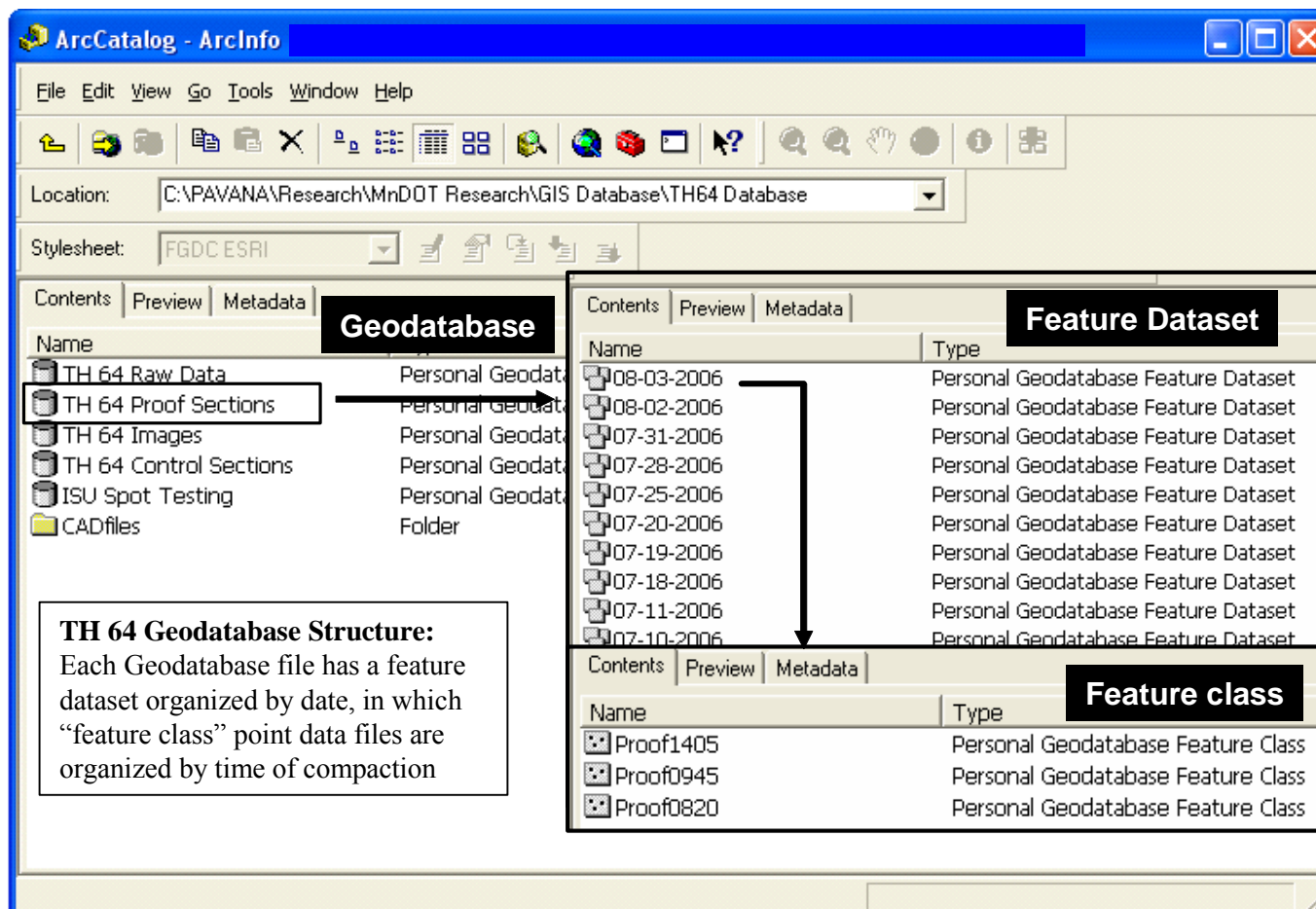
Figure 6.4. Structure of geodatabase created for TH 64 project data – ArcCatalog
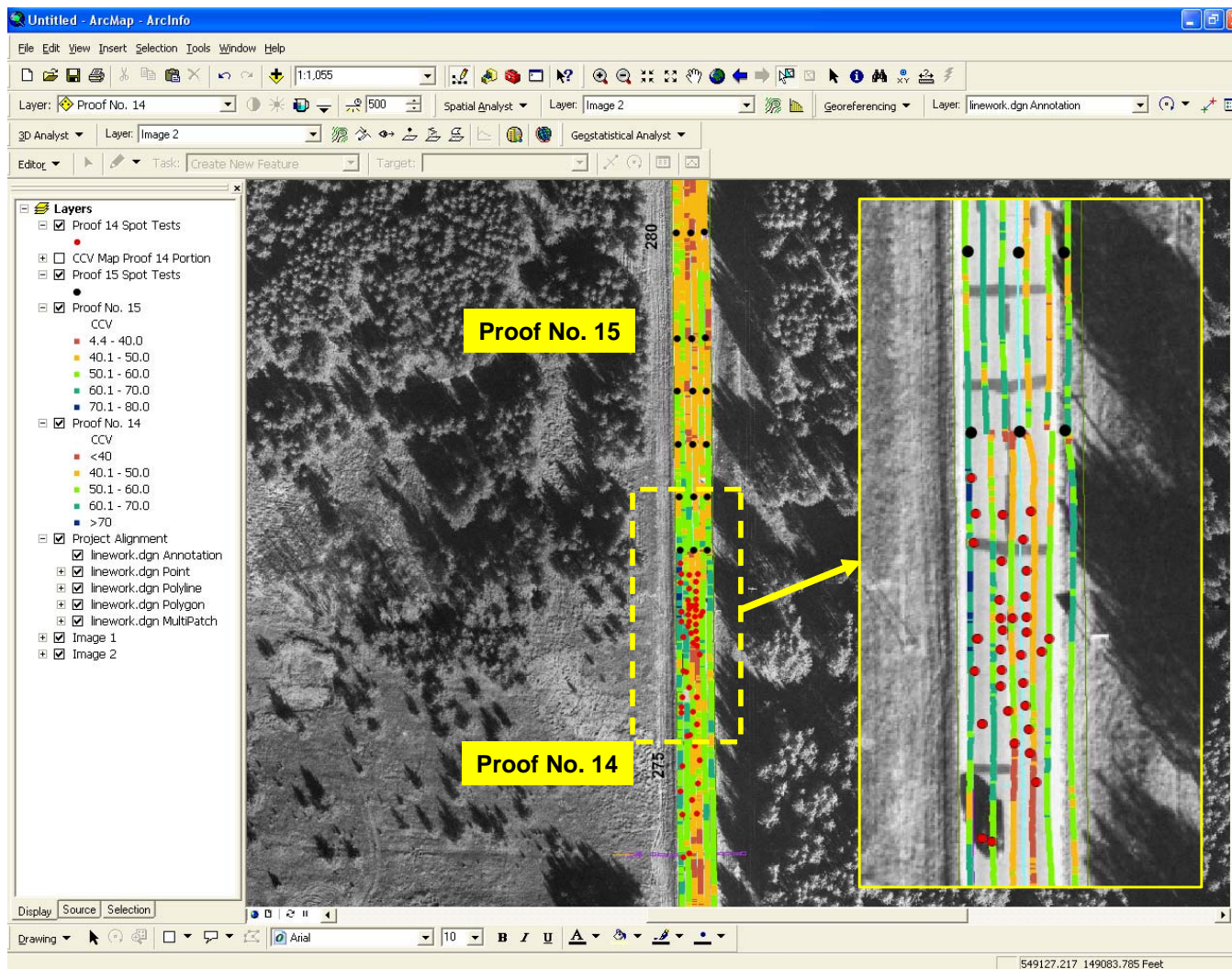
Figure 6.5. Proof Nos. 14 and 15 CCV data and overlaid spot test data in ArcMap

119
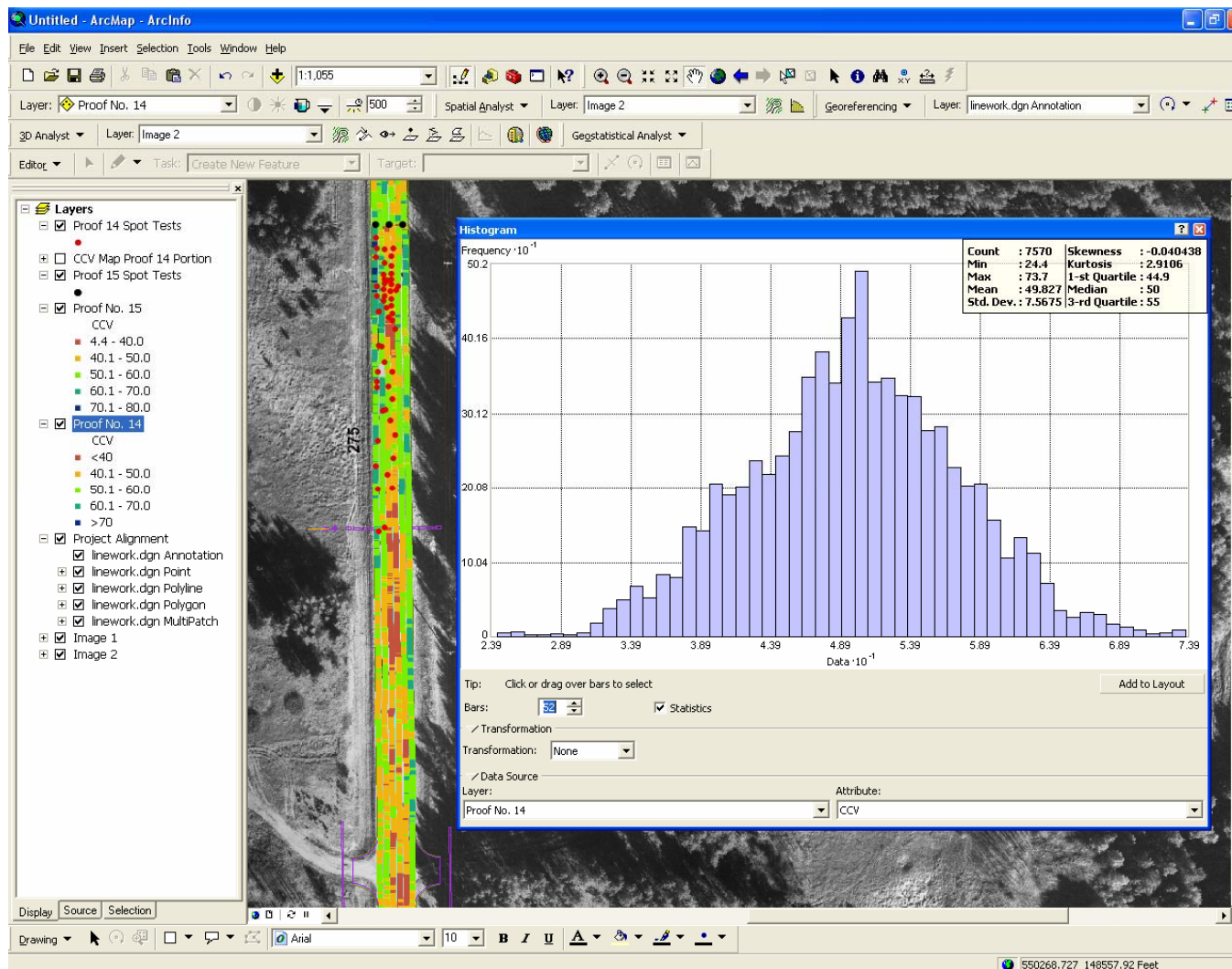
Figure 6.6. Histogram plot of Proof No. 14 CCV data in ArcMap
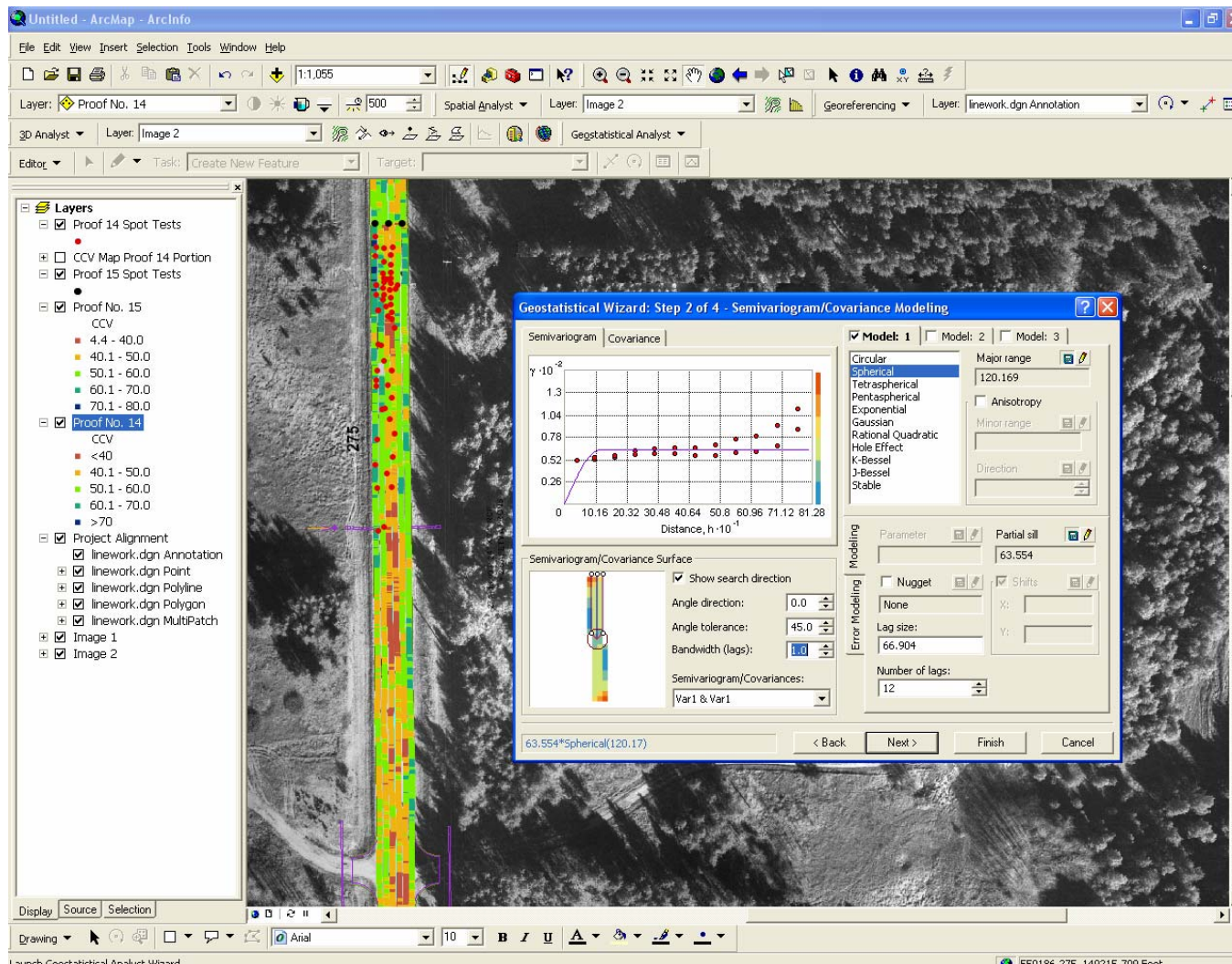
Figure 6.7. Semi-variogram analysis on proof no. 14 CCV data in ArcMap
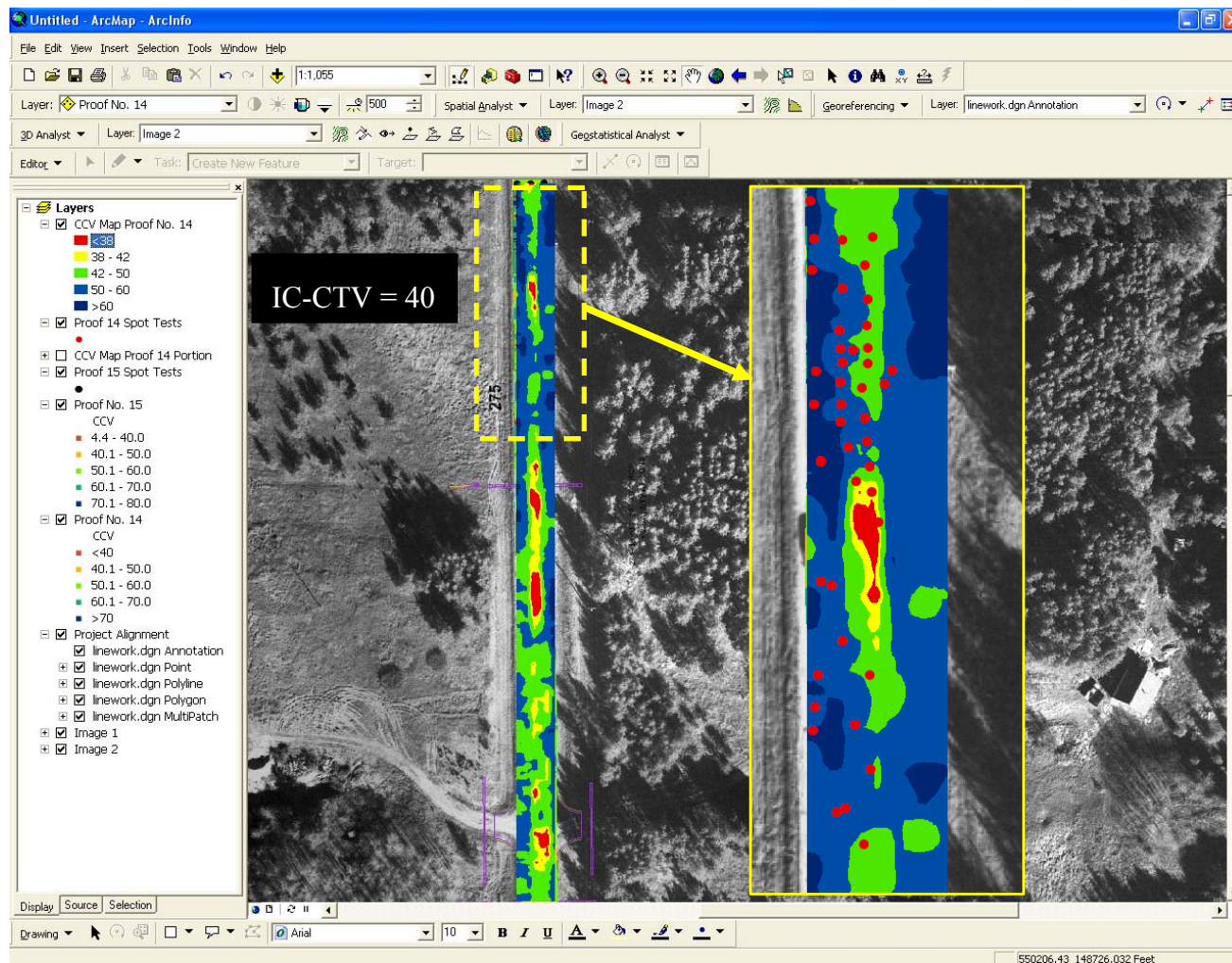
Figure 6.8. Kriged surface map of proof no. 14 CCV data in ArcMap

Chapter 7
Geostatistical Analysis

Applying geostatistical methods in the analysis of IC data has the advantage of quantifying spatial variability, which is not possible with classical statistical analysis. Spatial variability analysis performed using geostatistical tools such as the variogram could potentially be a useful parameter to quantify uniformity for acceptance. Many researchers have demonstrated the importance of uniformity in pavement foundations (e.g. White *et al.* 2004, Doré *et al.* 2001) for good pavement performance. Peterson *et al.* (2007) recently demonstrated Mn/DOT's experience in applying geostatistical analysis where IC was being evaluated.

A brief introduction of geostatistics, its application to IC data, and details of analysis procedures are described in this section. Further, data obtained from selected *control* and *proof* areas from the TH 64 project is analyzed and discussed. Results are compared with univariate statistics and the specified Mn/DOT acceptance criteria. An approach to characterizing uniformity with IC measurement values using spatial statistics and a simplified procedure for implementing geostatistics in quality IC control procedures in conjunction with current Mn/DOT acceptance criterion is proposed. In addition, kriged surface maps for densely spaced spot test measurements (ClV and E_{LWD}) are compared with kriged surface maps of roller integrated measurements (CCV) of the same area along with their spatial statistics.

7.1 Introduction to Geostatistics

Geostatistics is a rapidly evolving branch of applied mathematics that originated in the mining industry in the early 1950's. The field was originally developed for solving ore reserve estimation problems, but by the early 1970's spread into other areas of the earth sciences (Wackernagel 1998). A plethora of papers have been published over the past 30 years with geostatistics applications in geotechnical engineering. Geostatistical analysis differs from conventional statistical analysis such that in addition to the variability and distribution of a parameter, the spatial distribution is quantified. Spatial features of a dataset that identify "hot spots" and the degree of continuity are often of considerable interest in geotechnical engineering. Normally, spatial analysis for geotechnical engineering applications is limited however, by infrequent and widely spaced data points. This is not the case for IC data with virtually 100% coverage.

Spatial continuity can be quantified using spatial variability analysis. The main concept of spatial analysis is that two data points close to each other are more likely to have similar values than two data points that are farther apart. Tools that are available to perform spatial variability analysis include: correlation functions, covariance functions, and variograms. Although these different tools provide different statistical parameters, they primarily describe the spatial relationship between variables. The variogram is a common choice for many earth science applications (Isaaks and Srivastava 1989). Variogram functions were used for the IC data analysis performed in this chapter and is discussed further below.

In addition to quantifying spatial variability, geostatistics can be used as a spatial prediction technique, i.e., for predicting a value at unsampled locations based on values at sampled locations. Geostatistical estimation smoothes, or regresses, and predicts values based on the proportion of total sample variability modeled in a variogram. There are several methods that incorporate spatial relationships into estimating values at unsampled locations. Most methods use an algorithm by which weights are assigned to samples as a function of distance from the location of the desired sample (e.g., inverse-distance, inverse squared distance, etc). Kriging is a stochastic interpolation procedure proposed by Krige (1951), by which the variance between the estimated and known values is minimized using a variogram model. Kriging was used to create IC data maps for analysis of non-uniformity and comparison to maps of different in-situ spot test measurement values and is discussed later.

7.1.2 The Experimental Variogram

A variogram is based on the assumption that the difference in the value between any two positions depends solely upon the separation distance and their relative orientation. For example, assume "m" number of samples, each with a value "S" for the variable of concern and a location defined by some global coordinates, X, Y, and Z. Select a pair of samples, S_1 and S_2 (*see* Figure 7.1), and subtract their variable values to obtain the difference. Depending on the order in which a pair is selected, the result is either positive or negative. To avoid any unnecessary mathematical complication with negative values, the difference is squared. Thus the variability of these two selected pairs can be defined as γ_{12} in equation 7.1 (Houlding 2000).

$$\gamma_{12} = (S_1 - S_2)^2 \tag{7.1}$$

Where:
γ = experimental variance,
S_i = sample value at a point "i"

The distance "h" between the pair of the samples is the length of the vector between their locations referred to as *lag* or *separation distance*. For dense datasets, such as with IC data, several sample pair combinations have a similar separation distance. To generate the semi-variogram, sample pairs with the same lag distances are grouped, which is mathematically expressed in equation 7.2 (Houlding 2000).

$$\gamma(h) = \frac{1}{n}\sum_{i=1}^{n}(S(x_i) - S(x_i + h))^2 \tag{7.2}$$
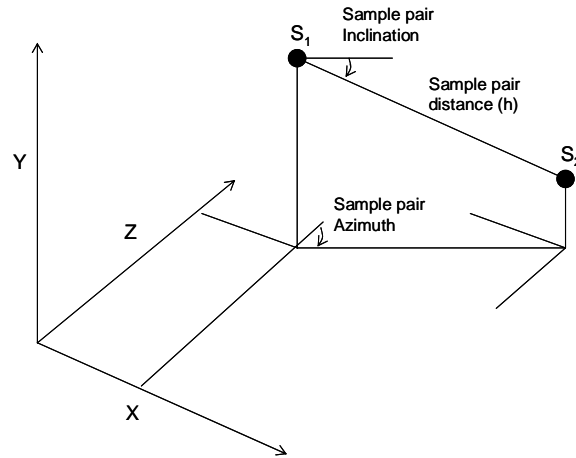
Figure 7.1. Geometry of sample pair (reproduced from Houlding 2000)

If this calculation is repeated for many different values of "h" as the sample data will support, the results can be graphically presented as shown in Figure 7.2 (circles), which constitutes the "experimental variogram plot". From the variogram plot it can seen that, in general, the values increase as distance increases up to approximately 5 m and then levels off and oscillates around a constant value. This can be expected as samples close together have relatively small differences, and those farther apart have larger differences. Theoretically, γ should approach zero as h approaches zero (Isaaks and Srivastava 1989). In practice this seldom happens, because there is invariably some degree of variability (e.g. background noise or inherent soil variability) in the sample.
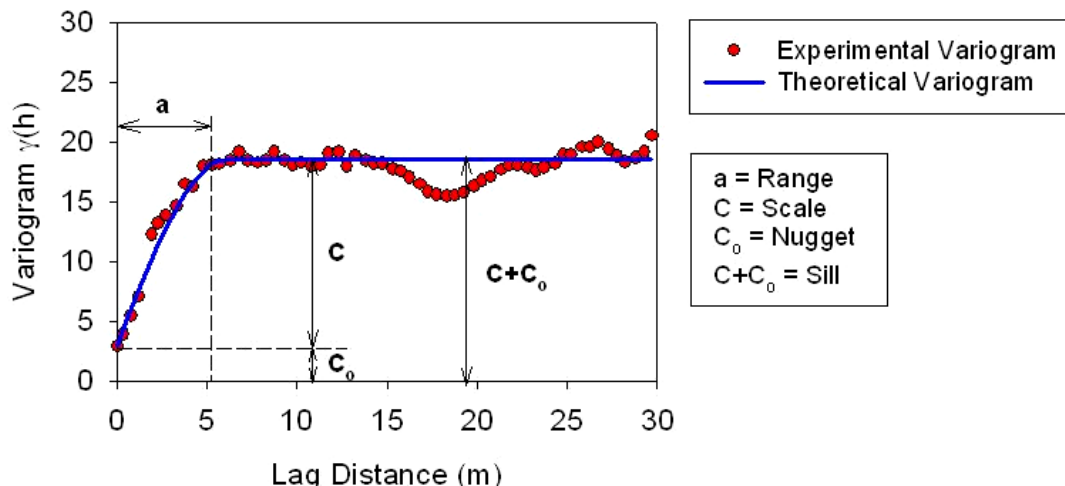
Figure 7.2. Typical sample variogram

Following is a general description of the model parameters from Issaks and Srivastava (1989).

Range of Influence: As the separation distance between pairs increase, the corresponding variogram value will also generally increase. Eventually, however, an increase in the distance no longer causes a corresponding increase in the variogram, i.e. where the variogram reaches a plateau. The distance at which the variogram reaches this plateau is called as *range*.

Sill: The plateau where the variogram reaches at the range is called the *sill*.

Nugget Effect: Though the value of the variogram at zero separation distance is strictly zero, several factors, such as sampling error and very short scale variability, may cause sample values separated by extremely short distances to be quite dissimilar. This causes a discontinuity at the origin of the variogram and is described as *nugget effect*.

7.1.3 Variogram Modeling

The major purpose of fitting a model to the experimental variogram is to give an algebraic formula for the relationship between values at specified distances. There are many possible models to fit an experimental variogram. Some commonly used models include linear, spherical, exponential, and Gaussian models (*see* Figure 7.3). Mathematical expressions of these models are presented in equations 7.3 to 7.11. Detailed descriptions of variogram models are presented in several publications (e.g. Issaks and Srivastava 1989, Clark and Harper 2002, Houlding 2000).

Linear Model:

$$\gamma(0) = 0 \tag{7.3}$$

$$\gamma(h) = C_o + ph, \text{ when } h > 0 \tag{7.4}$$

Spherical Model:

$$\gamma(0) = 0 \tag{7.5}$$

$$\gamma(h) = Co + C\left[\frac{3h}{2a} - \frac{h^3}{2a^3}\right] \text{ when } 0 < h < a \tag{7.6}$$

$$\gamma(h) = Co + C \text{ when } h > a \tag{7.7}$$

Exponential Model:

$$\gamma(0) = 0 \tag{7.8}$$

$$\gamma(h) = Co + C\left[1 - \exp\left(-\frac{h}{a}\right)\right] \quad \text{when } h > 0 \qquad (7.9)$$

Gaussian Model:

$$\gamma(0) = 0 \qquad (7.10)$$

$$\gamma(h) = Co + C\left[1 - \exp\left(-\frac{h^2}{a^2}\right)\right] \quad \text{when } h > 0 \qquad (7.11)$$

where:

a = Range of influence
p = Slope of the line
C_o = Nugget effect
C = Scale
$C + C_o$ = Sill
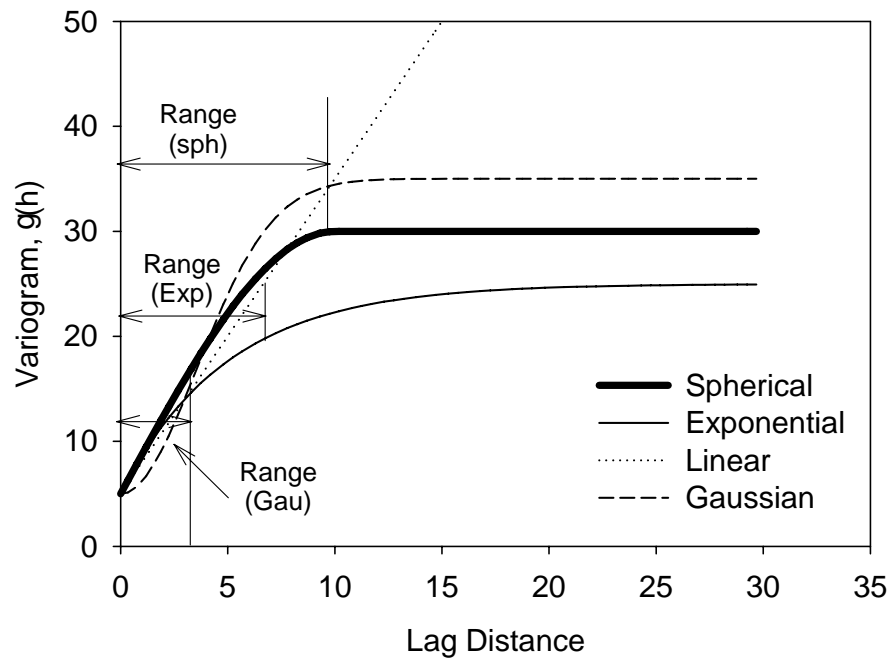
Figure 7.3. Comparison of common theoretical variogram models

The *range* is very well defined in a spherical model, i.e. where the sill reaches its plateau. It should not be interpreted in the same manner for other theoretical models (Clark and Harper, 2002). For example, as shown in Figure 7.3, exponential model and Gaussian models must go at least four to five times above "range (exp)" and "range (gau)" to come close to their asymptotic sills.

One of the challenging tasks in spatial variability analysis is to determine which theoretical model fits a given dataset. There have been many attempts to develop automatic model fitting techniques, least squares methods and other confidence or sensitivity studies (Clark and Harper 2002). Cressie (1993) provided a "goodness of fit" statistic which can be determined using equation 7.12. Clark and Harper (2002) suggested a slight modification to this calculation as shown in equation 7.13 by dividing the statistic with the total number of pairs of samples. Visual assessment of the model fit still remains a key factor in model selection, however.

$$\text{Cressie goodness of fit} = \sum_h N_h \left[\frac{\gamma^*(h) - \gamma(h)}{\gamma(h)} \right]^2 \tag{7.12}$$

$$\text{Modified Cressie goodness of fit} = \frac{1}{\sum_h N_h} \sum_h N_h \left[\frac{\gamma^*(h) - \gamma(h)}{\gamma(h)} \right]^2 \tag{7.13}$$

where:

N_h = Number of pairs at a given lag distance
$\gamma^*(h)$ = Estimated variance at a given lag distance (from the model)
$\gamma(h)$ = Actual variance at a given lag distance
h = total number of lags

The validity of a variogram model can also be checked by estimating values at known locations and comparing them with the measured values at those locations (Houlding 2000). This procedure is referred to as *cross-validation*. Using the known value at a location, the interpolation error is computed using equation 7.14.

$$\text{Error} = \text{interpolated value} - \text{observed value} \tag{7.14}$$

To represent a good variogram model, the graph between interpolated versus actual values should be close to line of unity.

While exercising the process of fitting theoretical models to experimental variograms for the TH 64 data in this study, it was found that an exponential model can fit well with many experimental variograms. In many cases the spherical models also fit the experimental variograms. It is our opinion that considering one unique model for most of the variograms can be helpful in

comparing spatial statistics parameters. Therefore, the sill and range values presented later in this chapter represent only parameters derived from the exponential model.

Variogram modeling also provides an opportunity to investigate the variability in different directions by which principle directions of anisotropy in the data can be determined. IC data can be anisotropic, i.e. differences in variability along roller direction of travel compared to its transverse direction. Variogram changes in different directions for IC dataset and comparisons to omni-directional variograms are presented in detail later in the analysis. While understanding anisotropy is a benefit, changes in variogram parameters with directions complicates the process of fitting a theoretical model. Modeling anisotropy is considered important especially when interpolation processes such as "kriging" are used to interpolate between points that are very farther apart. The IC data is typically very dense and significant errors are not anticipated if interpolated without modeling anisotropy.

7.2 Why Geostatistics in Intelligent Compaction?

Uniformity is a key parameter for achieving long-term pavement performance. Based on numerical analysis, White *et al.* (2004) demonstrated that non-uniform pavement subgrade and subbase stiffness increase localized deflections and cause stress concentrations in the pavement layer which can lead to accelerated pavement distresses. Doré (2001) showed that spatial variation in subgrade material properties can lead to significant frost-heave distress in pavements in colder regions. Univariate statistics of IC measurements alone do not characterize the spatial variability and specifically do not address the issue of uniformity in a spatial standpoint. Two datasets with identical distributions of the data (having similar mean, standard deviation, etc), can have significantly different spatial characteristics. A variogram model in combination with univariate statistics could potentially be utilized to effectively address the issue of uniformity. Figure 7.4 presents a hypothetical illustration of variogram models comparing different uniformity conditions. From a variogram model, a low "sill" and longer "range of influence" can represent best conditions for uniformity, while the opposite represent poor conditions for uniformity (*see* Figure 7.2 for sill/range description).

Mn/DOT implemented an acceptance criterion for the TH 64 project such that a proof area should meet at least 90% of the target value established from a calibration strip for 90% of the area. This approach has the advantage of being relatively simple and easy to implement. However, it should be emphasized that the proof areas may have identical distributions of the data as Control strip, but may not be spatially similar.

During construction of control strips, spot test measurements are performed. The Mn/DOT IC specification required performing three spot tests for control strips. As an alternate, Vennapusa *et al.* (2006) suggested estimating the number of spot tests based on the variability (e.g. considering standard deviation). Spatial statistics can add more value by providing information on the separation distance of the spot tests. The range distance determined from a variogram plot could potentially be used as the maximum separation distance between the spot tests because by definition, a given parameter is not spatially correlated beyond this distance. More reliability in the measurement can be achieved by performing 3 to 5 tests to provide an estimate of mean

value. A strategic sampling plan developed in this manner using geostatistical analysis tools can eliminate under-sampling which can be beneficial for pavement performance. Kestler *et al.* (1994) demonstrated that frequency of FWD testing during pavement evaluation can be optimized to a great extent using variogram models, thus leading to cost and time savings.
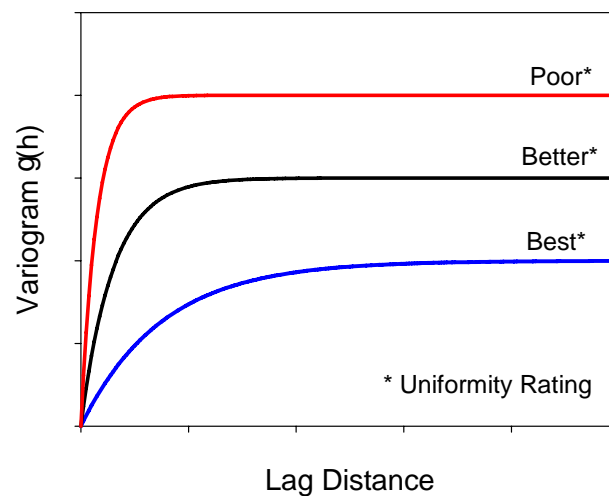
Figure 7.4. Hypothetical illustration of variograms characterizing uniformity

The data output from IC roller is typically in a point data format. Kriging process can be utilized to smooth the data and create color contour plots (or surface maps) based on variogram models which could be potentially used to compare with spatial maps created for spot test measurements.

Based on the discussion above, a summary of key points that provide rationale to implement geostatistics in IC technology are as follows:

1. Variogram models can be used in characterizing uniformity by quantifying spatial variability.

2. The range distance from a variogram plot can be potentially used as a maximum separation distance between spot test measurements. Three to five spot tests within this range could provide a better estimate of mean value of the measurement.

3. Kriging can be used to smooth the point data output from an IC roller by using a variogram model, which can be used to compare with spatial maps of spot test measurements.

7.3 Point Data Representation

Different IC manufacturers present data in different formats to be compatible with software used in the display panel mounted in the roller. Peterson *et al*. 2007 provided a summary of these different data representations. The data output is typically point data each associated with roller integrated measurements, roller operating conditions, time and location. Examples of point data output are as follows:

1. One-point data – data assigned to any one location across roller drum (e.g. left side of the drum, right side of the drum, middle of the drum)

2. Two-point data – data assigned to left and right side of the drum

3. Grid data – showing points in an evenly spaced grid pattern

For spatial analysis of IC data it is important to understand how these different data formats can affect spatial analysis. To investigate this further, several point data types were analyzed as follows:.

1. One-point data – data assigned to one location across the roller drum (e.g. left side of the drum, right side of the drum, middle of the drum

2. Two-point data – data assigned to left and right side of the drum

3. Three-point data – data assigned to left, right, and middle of the drum

4. Seven-point data – data evenly spaced at 0.3 m across the drum width (approximate drum width is 2.1 m)

The data collected from the TH 64 project consisted of a two-point data output points assigned to left and right side of the drum). The other data types listed above are artificially created from the raw data. Data obtained from Control 2 (Sta. 300 to 303) at the third roller pass was randomly selected for the comparison analysis. Control 2 was approximately 12 m wide by 91.5 m long, and consisted of six lanes of roller data. A plan view of the control strip with roller direction of travel in each lane is shown in Figure 7.5.

Surface maps were created using the kriging interpolation technique for the different data types and are presented side-by-side in Figure 7.6. In this case, kriging of the seven-point data is more representative than the other data sets. For quantitative comparison, percent error plots (absolute values) comparing seven point surface maps with other surface maps is shown in Figure 7.7.
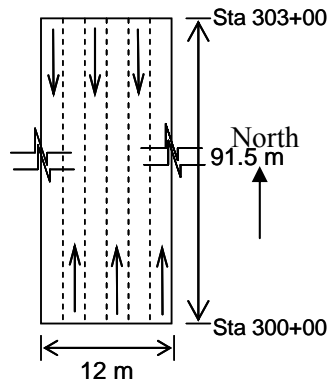
Figure 7.5. Control 2 – 3rd pass showing roller direction of travel in each lane

Based on Figures 7.6 and 7.7 it can be seen that the middle point surface map is more closely comparable to seven point surface map with majority of the area having 5% or less error. The single point assigned to left or right side of the drum and two point data showed significant errors with the majority of the area having 15% or more error. Three point data showed a few concentrated areas of errors over 15%. The reason for significant errors with left/right point maps and two point maps is associated with overlap in points from adjacent lanes. For example, with left point data representation, roller traveling from north to south will assign a point to its east side of the drum. In the adjacent lane, if the roller travels in the opposite direction (which is the case in this control strip, *see* Figure 7.5), the data point is assigned to the west side of the drum, which makes the data points of these two adjacent lanes spaced very close or even overlapped. On the other hand, with a middle point data the points are approximately equally spaced in the direction perpendicular to roller travel with no chance of points overlapping.

Although having seven data points across the roller is more accurate to use for any analysis, it presents challenges in storage, handling, and data transfer. Based on the analysis results described above, it can be concluded that middle point data can be effectively used for analysis purposes without introducing significant error. Therefore, all the spatial analysis performed in this chapter uses single data point assigned to the center of the roller drum (middle point data).
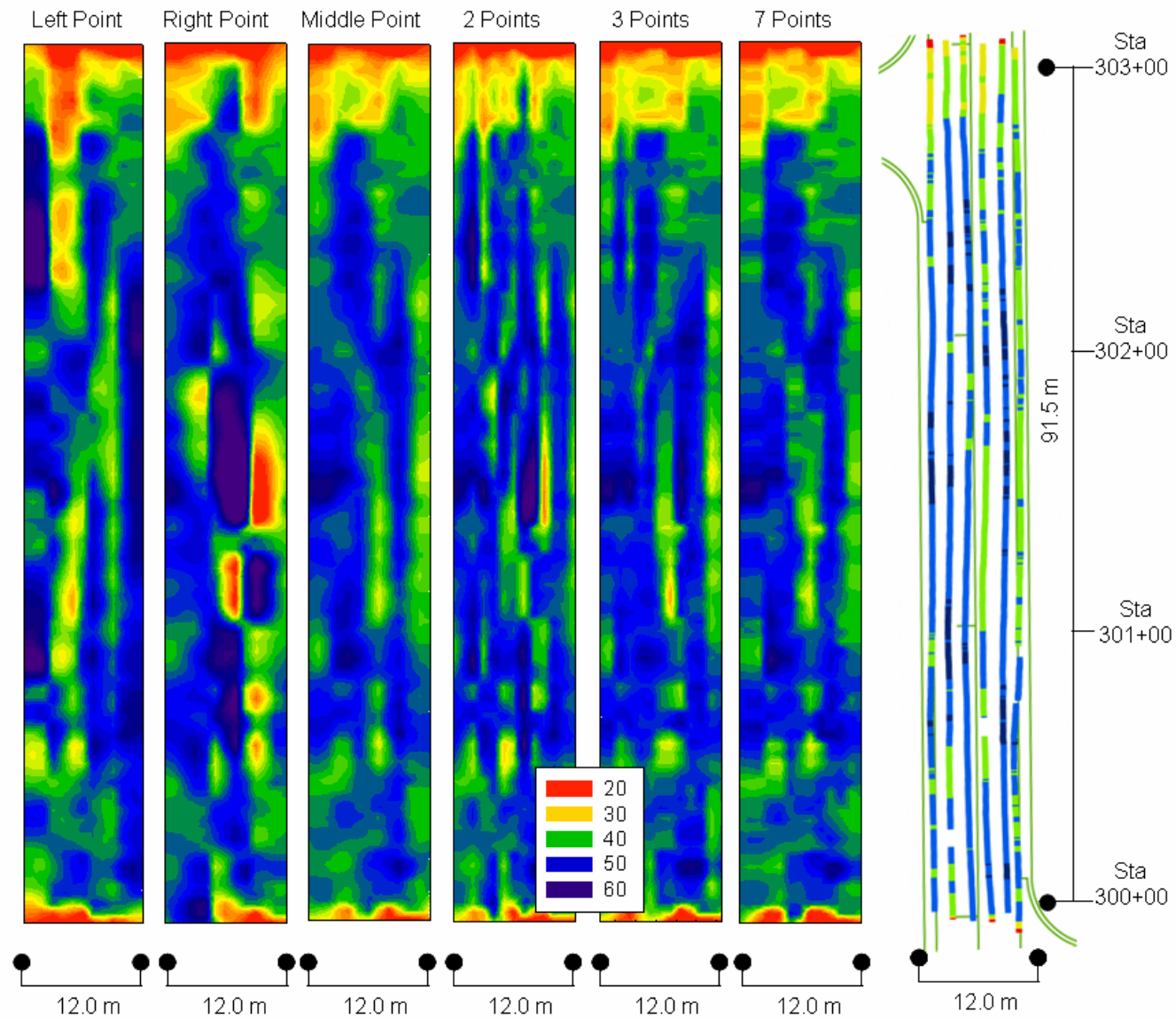
Figure 7.6. Comparison of CCV surface maps using different data representation – Control 2, 3rd roller pass
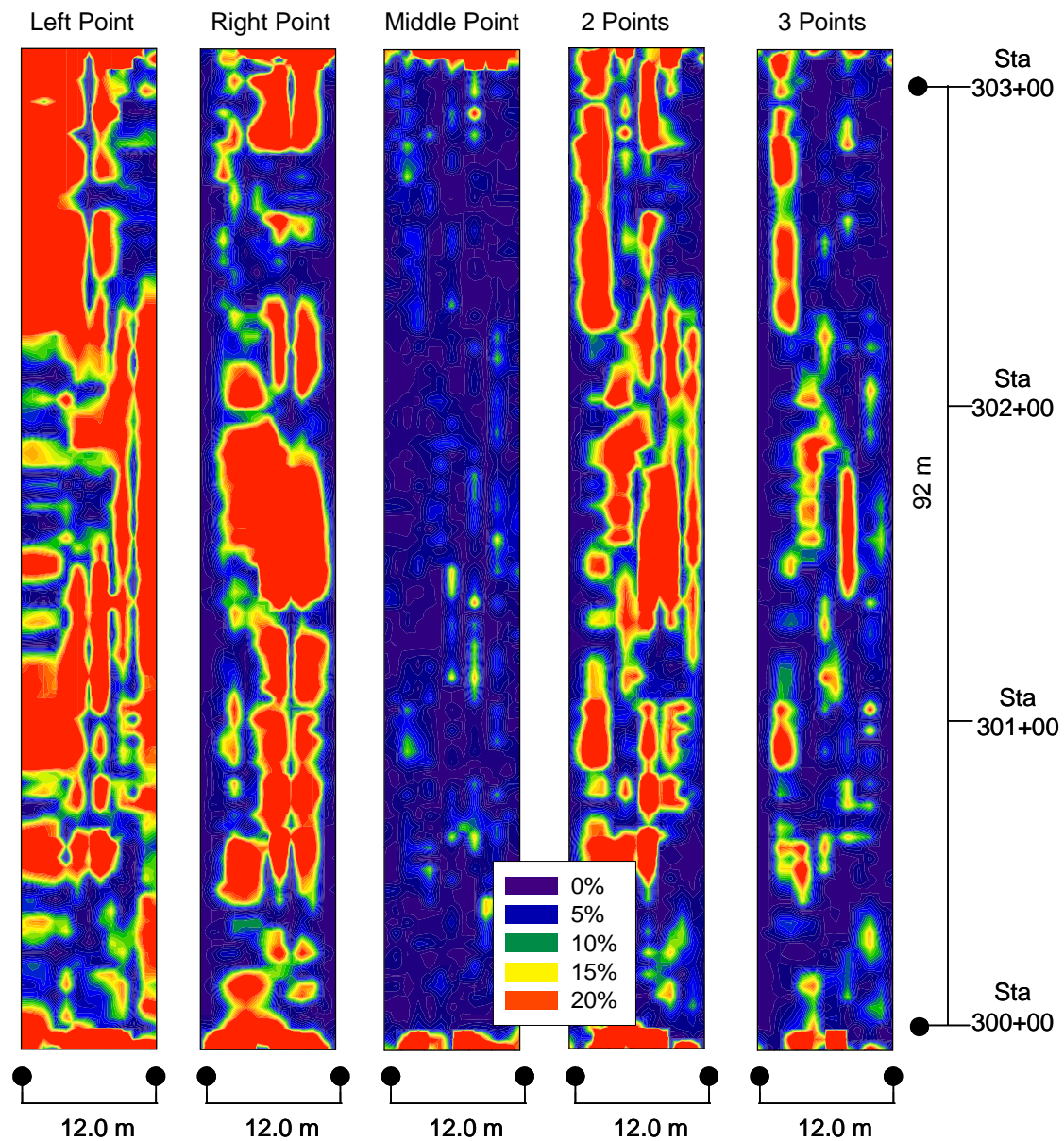
Figure 7.7. Percent error plot with comparison to seven point surface

134

7.4 Spatial Variability Analysis – TH 64 Control Strips

Control strips were constructed prior to production compaction. Target values of CCV were determined from these control strips (e.g. IC-CTV) and used as reference for quality assurance in proof sections. Compaction curves of CCV for control strips using univariate statistical parameters is presented in Chapter 5. Changes in CCV in a spatial perspective for two select control strips are presented below. A summary of control no. 2 and no. 3 is provided in Table 7.1.

Table 7.1. Summary of control sections used for spatial analysis

Control No.	Station	Plan Dimensions (width, m x length, m)	Section Type	No. of Passes	IC-CTV
2	300 – 303	12 x 91.5	1.07 m (42 in.) subcut – 4 lifts	7	42
3	255 – 258	6.4 x 92.0	0.16 m (10 in.) subcut – 1 lift	11	60

Spatial variability analysis involved constructing experimental variograms, fitting theoretical models, comparing spatial statistics (sill and range) with univariate statistics and Mn/DOT acceptance criteria, and creating kriged surface maps of CCV for each roller pass for visual comparison. The sill and range values presented below are based on exponential models that were fit to the experimental variograms. First, a brief summary of each control strip and figures from the analysis are presented, and later a detailed explanation of findings and observations is presented.

7.4.1 Control 2

This control strip was constructed in a 1.07 m subcut, i.e., the existing grade was excavated down to the proposed grade elevation. After reaching the proposed grade elevation, this area was reportedly excavated further to an elevation 1.2 m (4 ft) lower than the proposed grade elevation and then four lifts of select granular fill was placed and compacted. This strip was constructed for use as a reference calibration strip for subsequent proof layers constructed in the fill. Due to data transfer problems, the data from the first three lifts was lost. Only data for the 4th lift (final surface lift) from passes 2 to 7 was analyzed. Compaction operations were performed longitudinally in the north-south direction along six adjacent lanes.

A summary of spatial statistics (sill and range values) and its comparison to univariate statistics and Mn/DOT acceptance criterion is presented in Table 7.2. Sill and range values for omnidirectional variograms and directional variograms with orientation in the direction of roller travel (north-south direction, N-S) and perpendicular to roller travel (east-west direction, E-W) is also presented in Table 7.2. Variogram plots for different roller passes are shown in Figures 7.8 and 7.9. Kriged surface maps of CCV for several roller passes are shown in Figure 7.10.

Comparing the E-W and N-S directional variograms (Figure 7.9), it can be seen that the spatial continuity and variability in E-W direction is lower than the N-S direction as evidenced by lower range and sill values. Comparing the omnidirectional and N-S directional variogram (Figures 7.8 and 7.9), it appears that there is no significant difference between their sill and range values.

Omnidirectional and N-S directional variogram plots show an increasing trend in experimental variance after about 50 feet lag distance. The sill and range values presented for the theoretical model just capture the small scale variability (i.e. within 50 feet).

Figure 7.10 shows the kriged surface maps for CCV from passes 2 to 7. Changes in compaction state of the soil can be clearly seen over the proof area with increasing roller passes. A summary of changes with univariate and spatial statistics as a function of roller passes is presented in Figure 7.11. The mean CCV increased from about 41 to 48 and COV decreased from about 16.7% to 11.7% with increasing roller passes. The percent CCV value in 90%-130% bin for Mn/DOT acceptance criteria increased from about 71% to 89% (*see* Table 7.2) indicating increase in compaction and decrease in variability of CCV from pass 2 to 7. The sill value of all the variograms (omnidirectional, N-S, and E-W) generally decreased with increasing roller passes, thus indicating increasing uniformity. Interestingly, no significant changes in range values are observed.

Table 7.2. Comparison of univariate and spatial statistics of CCV with Mn/DOT acceptance criteria: Control 2 passes 2 to 7

| | | | Univariate Statistics of CCV | | | Spatial Statistics of CCV* | | | | | | Mn/DOT QA Criteria (Percent of CTV) IC-CTV = 60 | | |
| | | | | | | Omni-Directional | | North - South | | East - West | | | | |
Strip	CTV	Pass	Mean, μ	Stdev, σ	COV (%)	Range (m)	Sill $(CCV)^2$	Range (m)	Sill $(CCV)^2$	Range (m)	Sill $(CCV)^2$	> 130%	90% - 130%	< 90%
300-303	42.0	2	41.0	6.9	16.7	5.0	45.0	5.0	45.0	1.0	40.0	1.0	71.2	27.9
300-303	42.0	3	42.6	6.2	14.6	5.0	38.0	5.0	38.0	0.5	30.0	1.2	81.5	17.4
300-303	42.0	4	44.7	6.3	14.1	5.0	36.0	5.0	36.0	1.0	23.0	1.4	87.7	10.9
300-303	42.0	6	45.9	6.3	13.7	5.0	38.0	5.0	38.0	1.0	26.0	3.8	87.0	9.1
300-303	42.0	7	47.6	5.6	11.7	6.0	30.0	6.0	30.0	2.0	20.0	6.0	89.0	5.0

*Note that all the range and sill values are based on exponential variogram

137
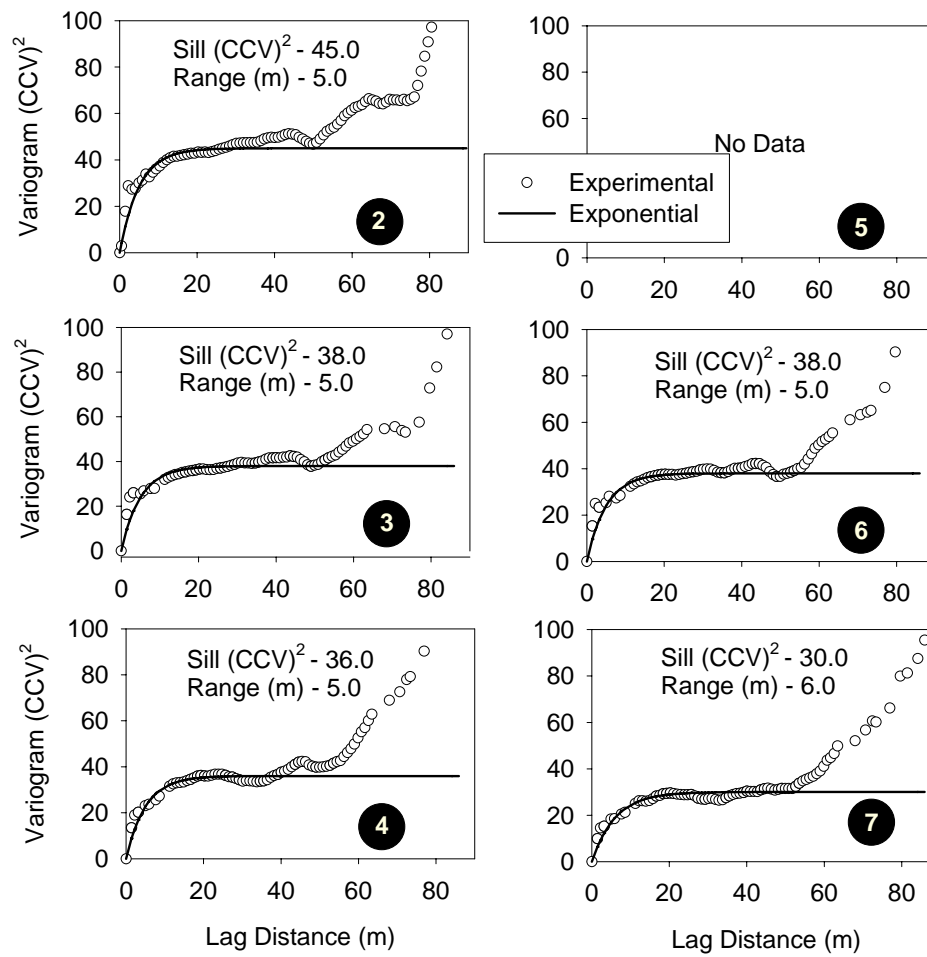
Figure 7.8. Variogram plots for Control 2 (Sta. 300 to 303): Passes 2 to 7
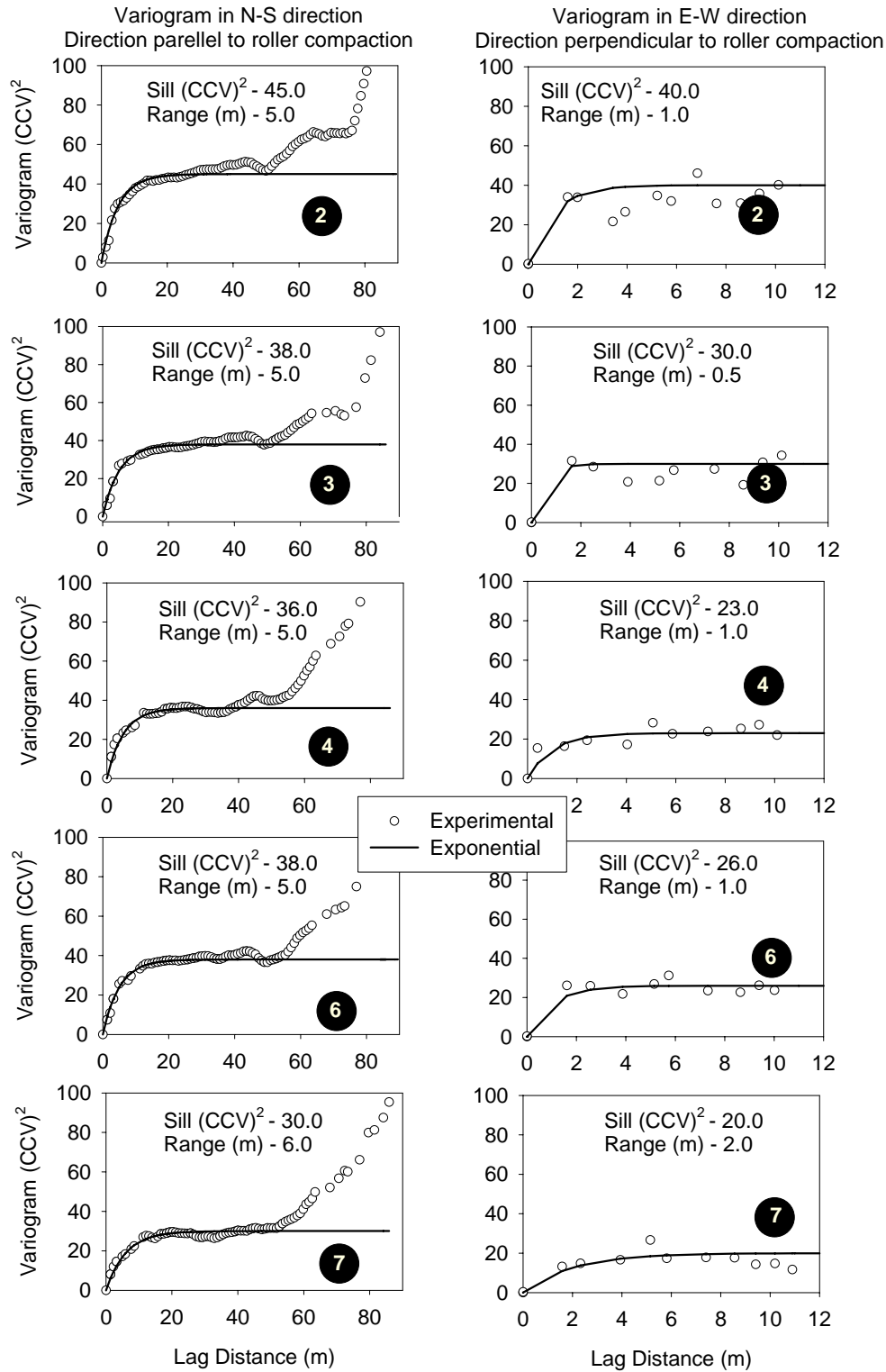
Figure 7.9. Directional variogram plots for Control 2 (Sta. 300 to 303): Passes 2 to 7
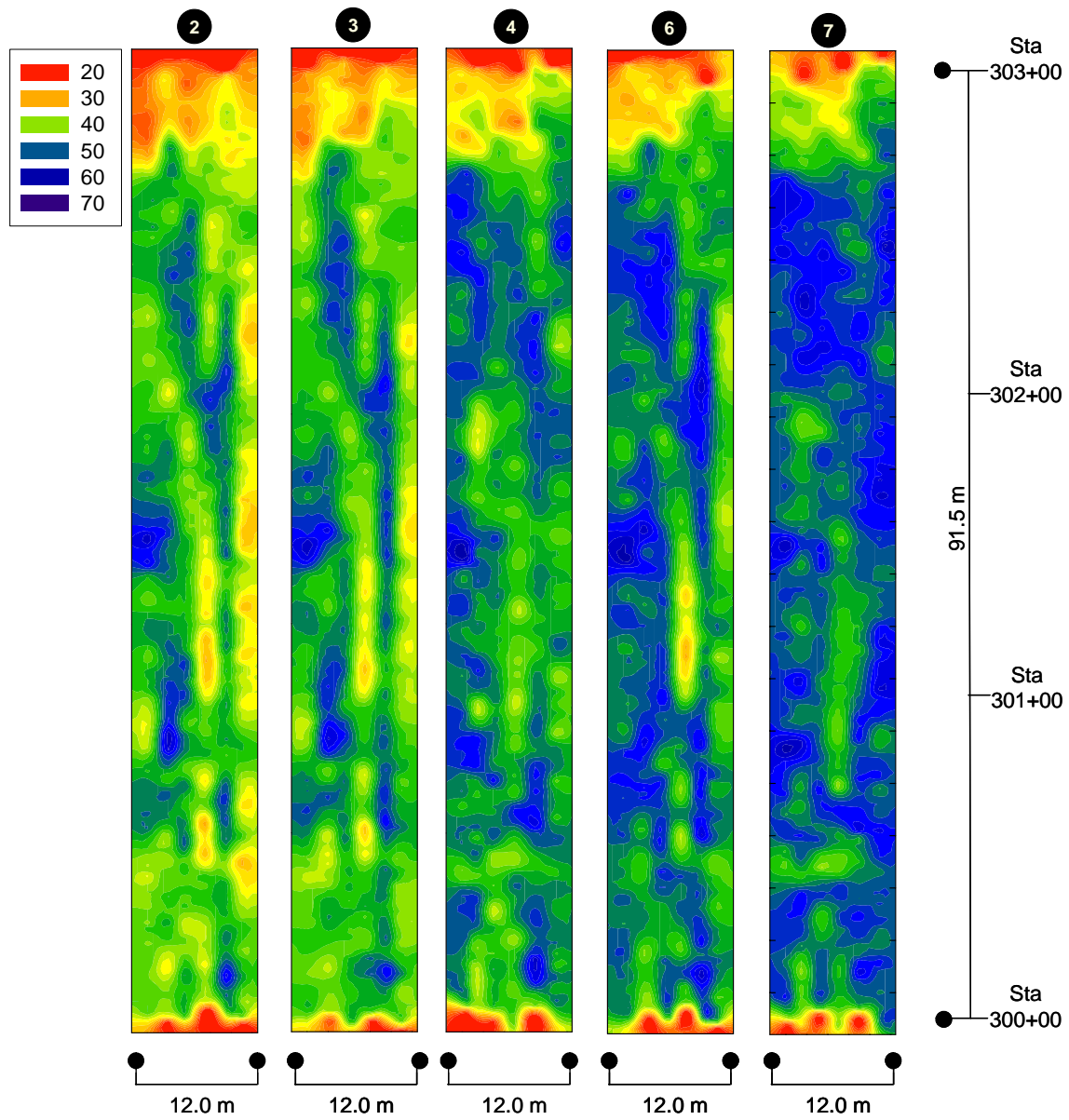
Figure 7.10. CCV surface maps of Control 2 (Sta. 300 to 303): Passes 2 to 7 (CTV = 42)
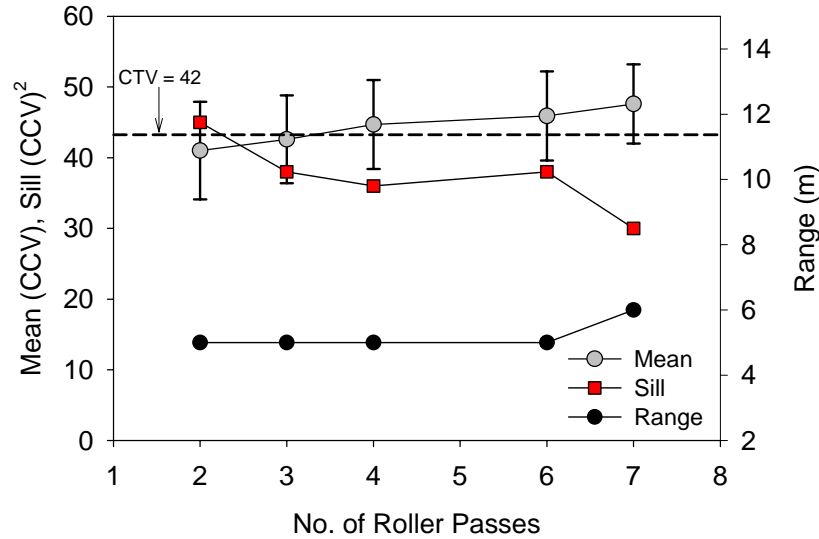
Figure 7.11. Change in mean, sill, and range of CCV with roller passes for Control 2

7.4.2 Control 3

Details of Control 3 are summarized in Table 7.3. This control strip was constructed in a 0.16 m subcut. This section was reportedly excavated down to an elevation of 0.3 m (1 ft) lower than the proposed grade elevation and then one lift of select granular fill was placed and compacted using 11 roller passes. Compaction operations were performed longitudinally along the pavement, i.e. in north-south direction along three adjacent lanes. Although this section was constructed for use as a reference calibration strip for near by proof layers, the target value established was very high (CTV = 60) and was never used for proof areas.

A summary of spatial statistics (sill and range values) and its comparison to univariate statistics and Mn/DOT acceptance criteria is presented in Table 7.3. Sill and range values for omnidirectional variograms and directional variograms with orientation in the direction of roller travel (north-south direction, N-S) and perpendicular to roller travel (east-west direction, E-W) are also presented in Table 7.3. Variogram plots for the different roller passes are shown in Figures 7.12, 7.13, and 7.14. Kriged surface maps of CCV data for several roller passes are shown in Figures 7.15 and 7.16.

Since this control was constructed in only three lanes, a limited number of data points was available for construction of E-W directional variograms. Despite this limitation, trends were observed allowing for fitting of theoretical models. Similar to control No. 2, comparison of E-W and N-S directional variograms (Figures 7.13 and 7.14), the variability and spatial continuity in the E-W direction is generally lower (except for passes 2 and 3) than the N-S direction. Again comparing the omnidirectional and N-S directional variograms (Figures 7.12, and 7.13 and 7.14) shows that there is no significant difference between the sill and range values.

141

Variogram plots presented in Figures 7.12 to 7.14 shows a decreasing trend of variance after about 40 to 50 feet and then an increasing trend after about 75 feet. The sill and range values presented for the theoretical model just capture the small scale variability (i.e. within 40 to 50 feet).

Figures 7.15 and 7.16 show kriged surface maps of CCV from passes 2 to 11. At some concentrated locations (e.g. between Sta. 257 to 258) CCV increased then and decreased with increasing passes. However, changes in compaction state of the soil is visible with more roller passes, and clearly, one can see that the surface after the 11th pass is relatively more uniform than at other passes. A summary of changes with univariate and spatial statistics is presented in Figure 7.17. The mean CCV increased slightly from about 61 to 66 and COV decreased from about 17% to 11% from passes 2 to 11. The percent CCV value in the 90%-130% bin increased from about 75.1% to 92.7% (*see* Table 7.3) which is an indication of decreasing variability and increasing compaction. No definite trend in sill was observed with increasing roller passes. However, the range value showed a strong second-order polynomial increasing trend with R^2 of 0.75 with increasing passes. Increasing range with roller passes indicates increasing spatial continuity in CCV.

Table 7.3. Comparison of univariate and spatial statistics of CCV with Mn/DOT acceptance criteria: Control 3 passes 2 to 11

Strip	Pass	Univariate Statistics of CCV			Spatial Statistics of CCV*						Mn/DOT QA Criteria (Percent of CTV) IC-CTV = 60		
					Omni-Directional		North - South		East - West				
		Mean, μ	Stdev, σ	COV (%)	Range (m)	Sill $(CCV)^2$	Range (m)	Sill $(CCV)^2$	Range (m)	Sill $(CCV)^2$	> 130%	90% - 130%	< 90%
255-258	2	61.0	10.0	16.3	4.5	91.0	5.5	92.0	2.0	120.0	3.7	75.1	21.2
255-258	3	60.8	9.8	16.1	8.0	105.0	7.0	100.0	2.0	100.0	0.8	82.1	17.1
255-258	4	64.1	7.8	12.2	4.5	62.0	4.5	62.0	0.5	50.0	1.6	88.7	9.7
255-258	5	64.2	7.6	11.8	10.0	74.0	11.0	74.0	1.5	50.0	2.6	87.1	10.3
255-258	6	64.1	7.7	11.9	9.0	71.0	10.0	73.0	1.5	45.0	2.4	86.9	10.7
255-258	7	63.7	8.7	13.6	9.0	95.0	10.0	98.0	2.0	70.0	2.4	87.9	9.7
255-258	8	65.4	9.2	14.1	11.0	105.0	11.0	105.0	1.5	100.0	4.5	88.1	7.4
255-258	9	64.3	8.2	12.8	13.0	90.0	13.0	90.0	1.5	40.0	3.2	88.6	8.1
255-258	10	64.4	8.4	13.0	11.0	94.0	11.0	94.0	1.5	50.0	4.1	85.4	10.5
255-258	11	65.9	7.4	11.2	12.0	80.0	12.0	80.0	1.5	40.0	4.9	92.7	2.3

*Note that all the range and sill values are based on an exponential variogram
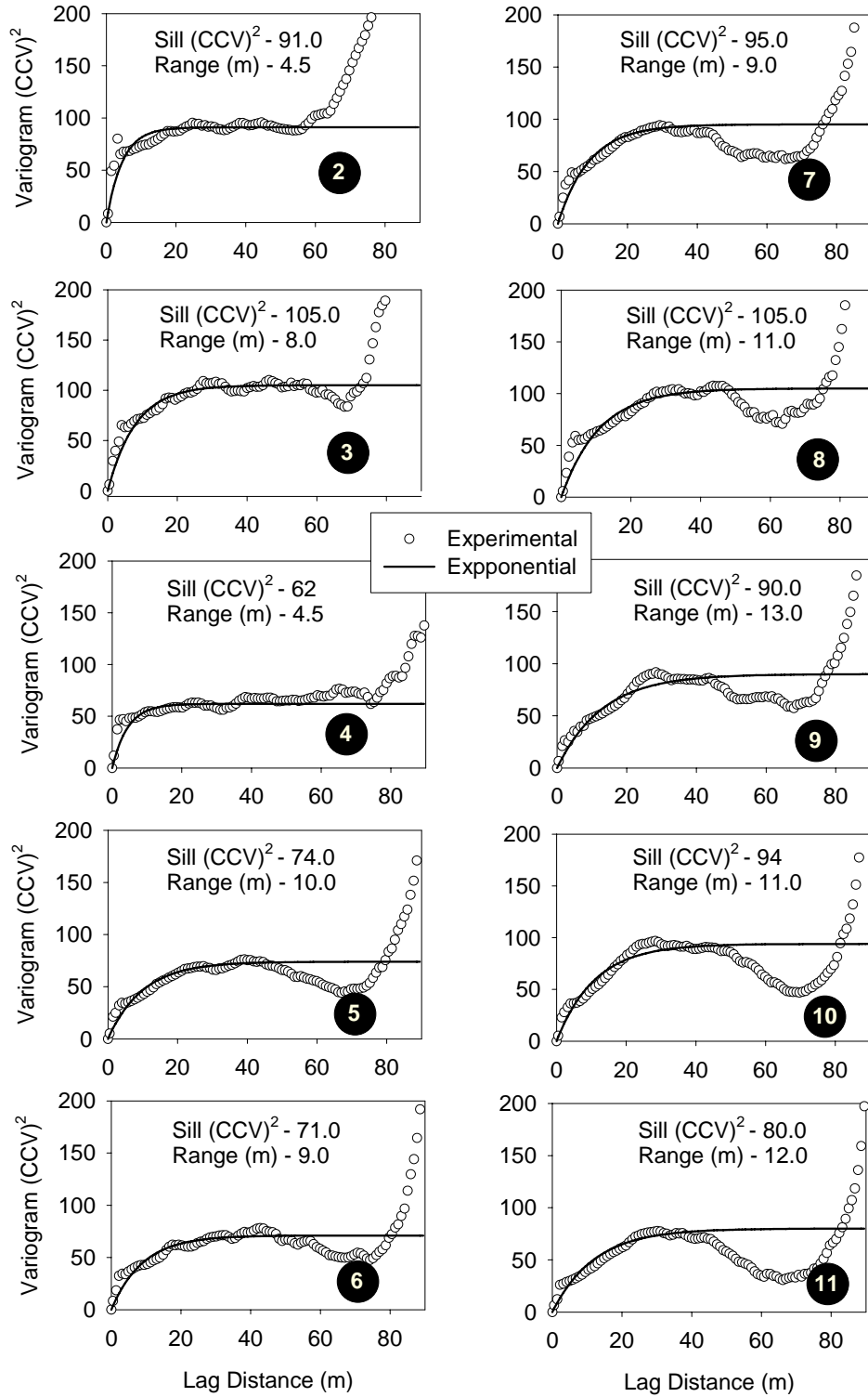
Figure 7.12. Omni-directional variograms for Control 3 (Sta. 255 to 258): Passes 2 to 11 (CTV = 60)
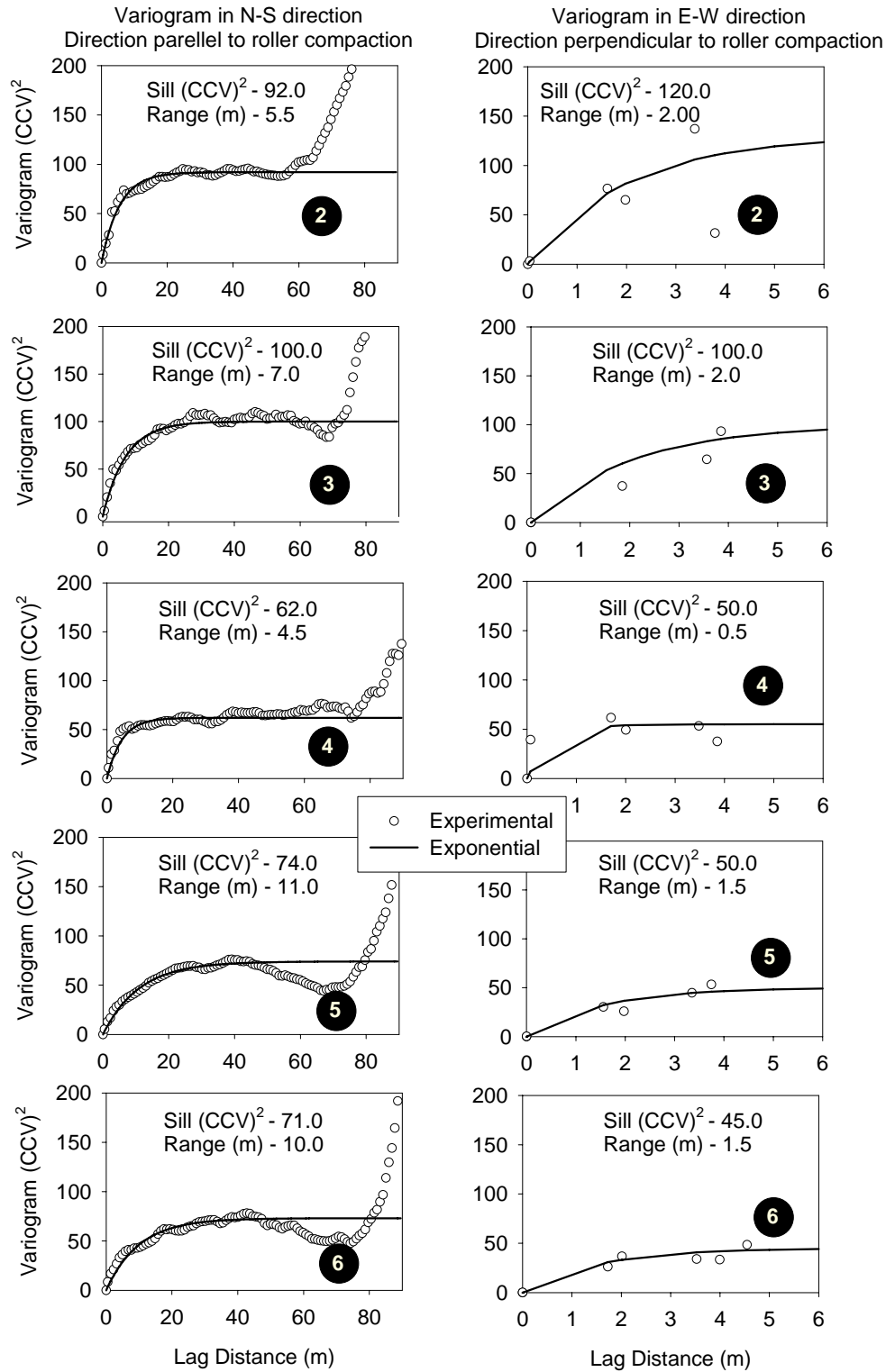
Figure 7.13. Directional variogram plots for Control 3 (Sta. 255 to 258): Passes 2 to 6 (CTV = 60)
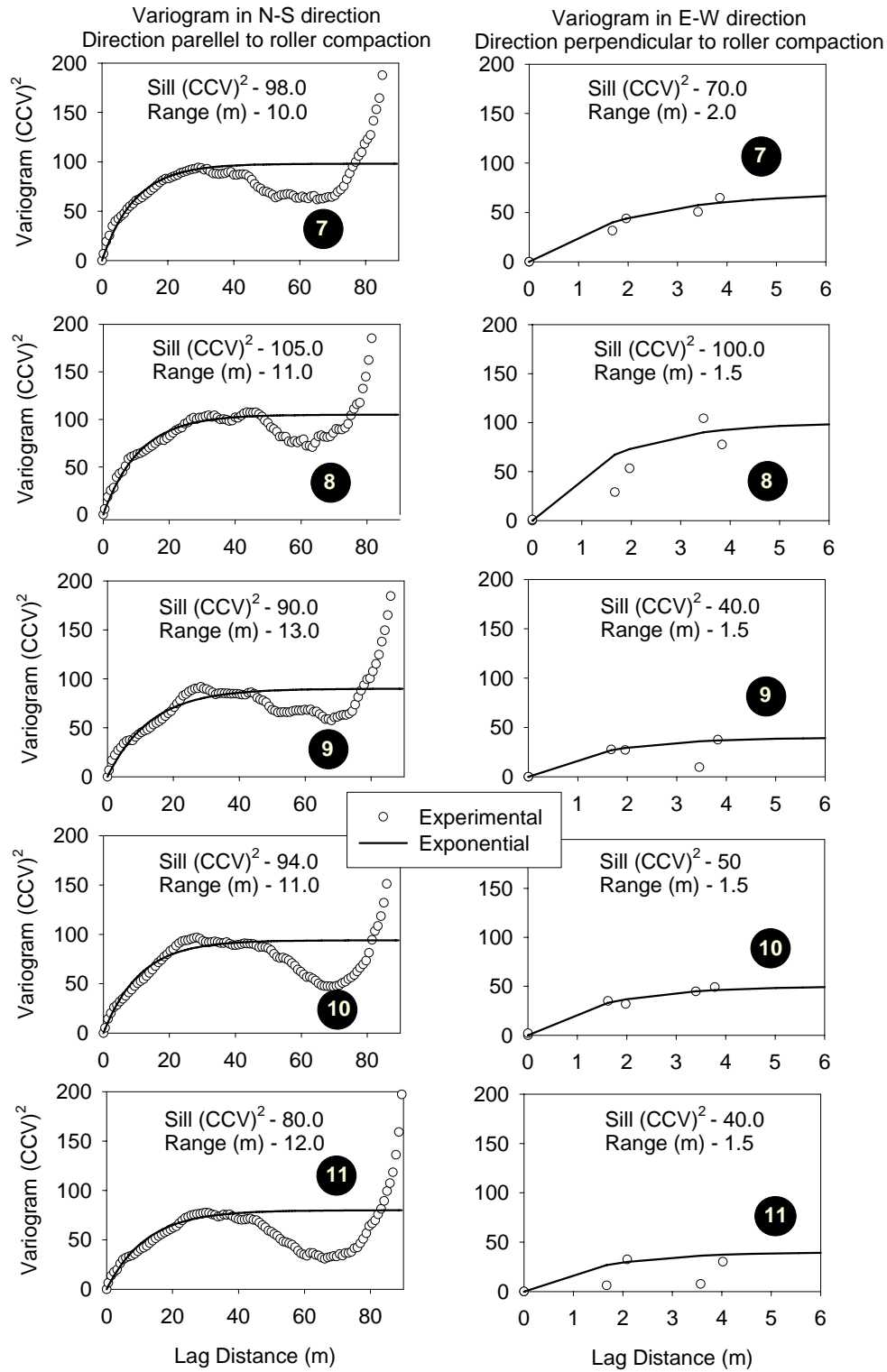
Figure 7.14. Directional variogram plots for Control 3 (Sta. 255 to 258): Passes 7 to 11 (CTV = 60)

146
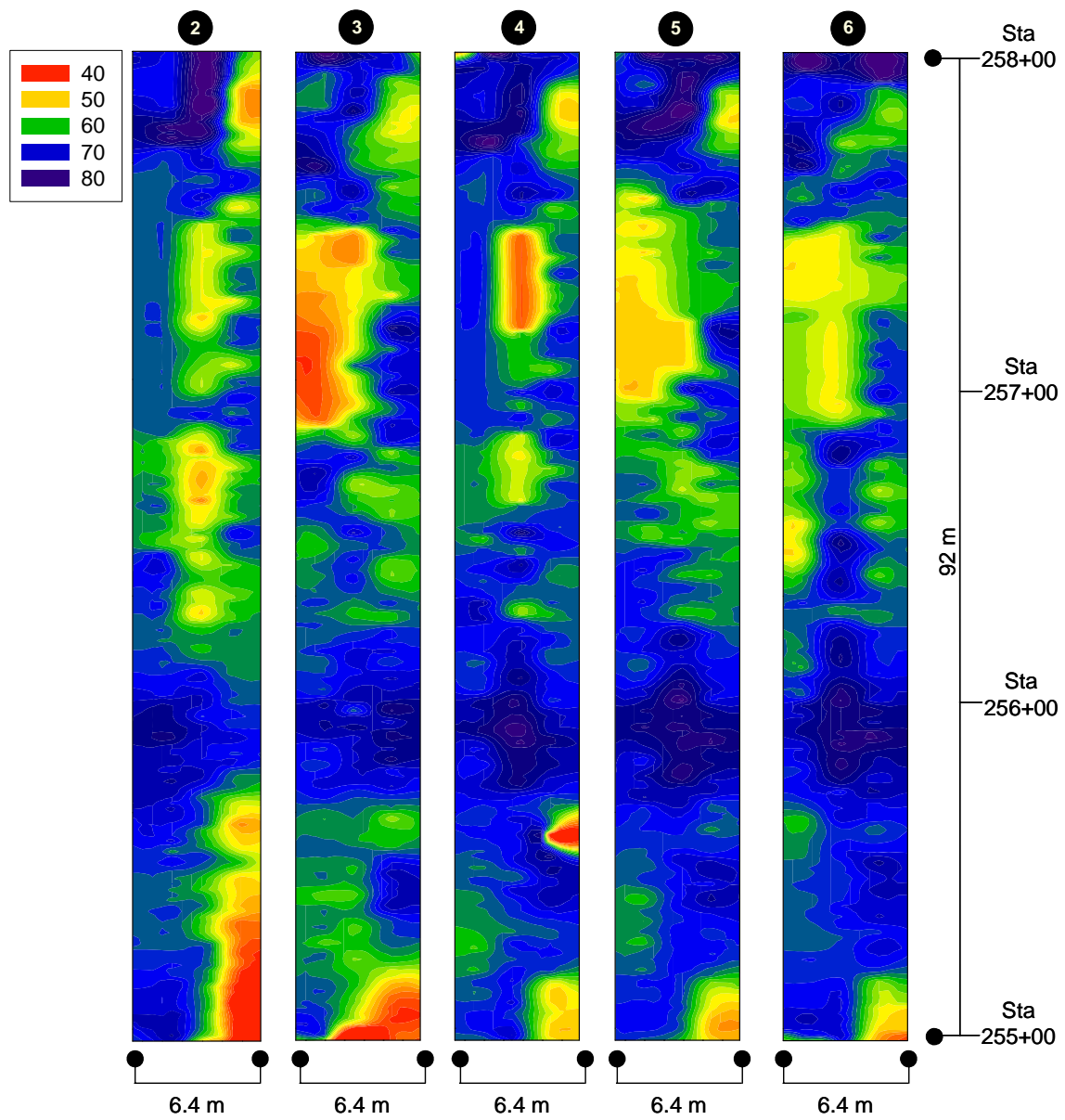
Figure 7.15. CCV surface maps of Control 3 (Sta. 255 to 258): Passes 2 to 6 (CTV = 60)
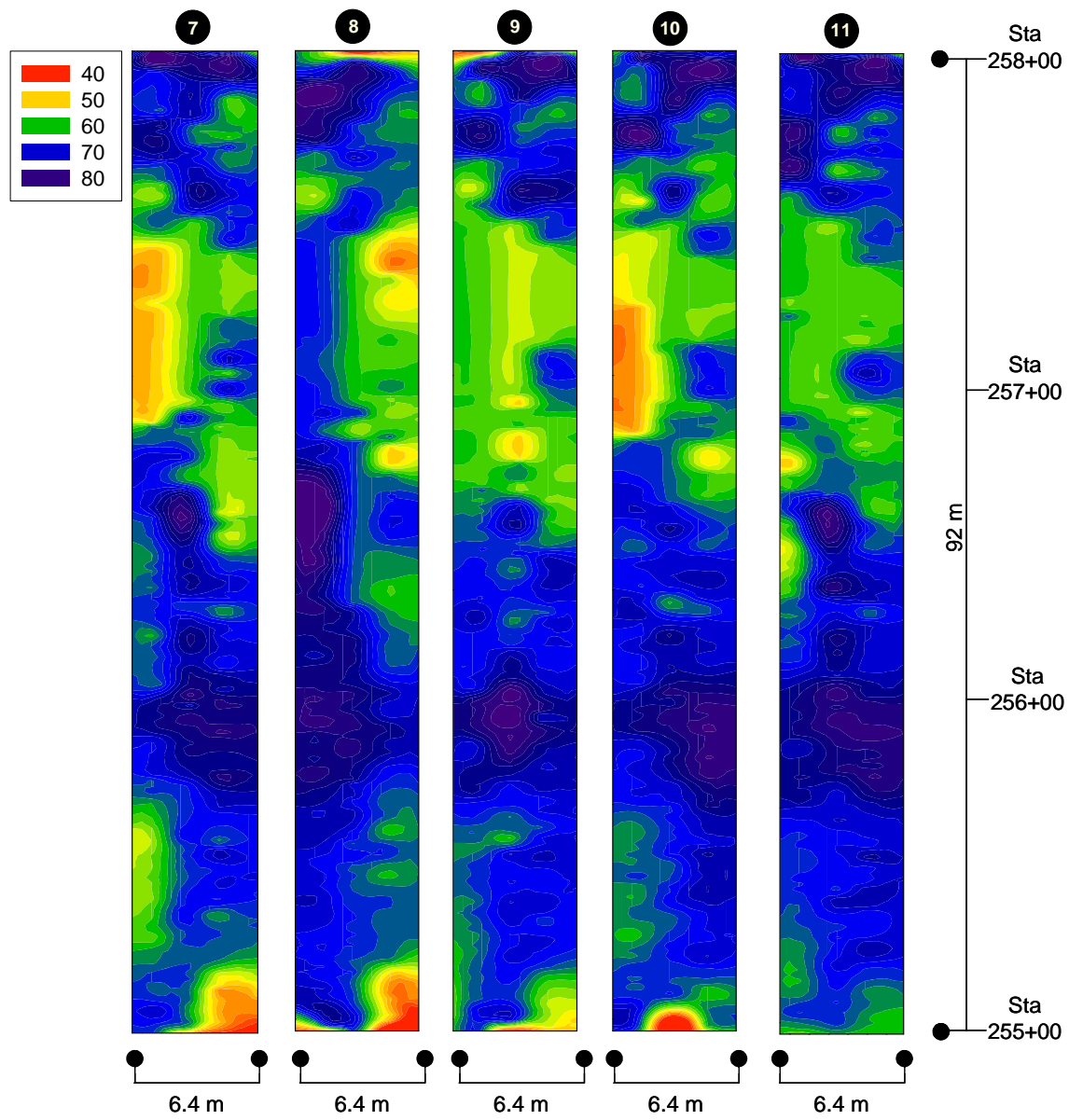
Figure 7.16. Control 3 CCV surface maps: Passes 7 to 11 (CTV = 60)
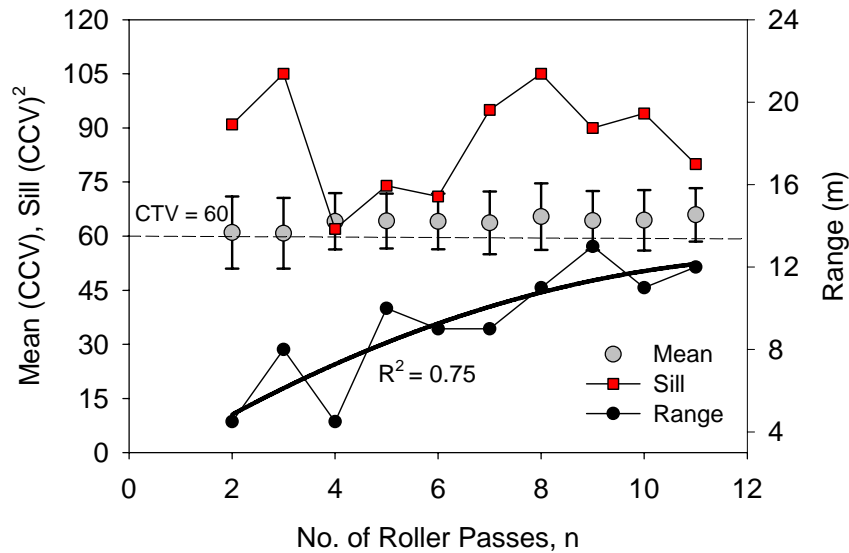
Figure 7.17. Change in mean, sill, and range of CCV with roller passes for Control 3

7.4.3 Summary of Control Strip Evaluation

Some of the key aspects of studying the CCV control strip data that warrant further discussion include: (a) relationships between univariate and spatial statistics; (b) differences in spatial statistical parameters between the two control strips; (c) directional variations in spatial statistics; and (d) small-scale and large-scale spatial correlations.

Univariate versus Spatial Statistics. The mean CCV for control no. 2 and no. 3 increased by about 16% and 8%, respectively, with a decrease in COV of about 5% with increasing passes. The percentage of CCV values in the 90%-130% bin increased with increasing roller passes for both control strips, indicating compaction and decreased variability. The sill value from the variogram for control no. 2 decreased with increasing roller passes, while for control no. 3 no clear trend was observed. With regard to special continuity, control no. 2 showed a relatively constant range value at about 5 m, while the range value for control no. 3 increased substantially from about 5 m to 12 m. The increase in uniformity of CCV over the area can also be visually evidenced from the kriged surface maps.

Differences between Control 2 and 3. Differences observed between control no. 2 and 3 include: higher CCV, higher sill, and longer range values for control no. 3. Based on conversations with Mn/DOT inspectors, it is believed that control no. 3 was subjected to significant construction traffic after fill placement and prior to compaction. Compaction resulting from the combination of construction traffic and subsequent roller passes resulted in comparatively high CCV values for control no. 3 (~ 60) than control no. 2 (~ 42). The sill value in control no. 3.after compaction was about 2.5 times greater, while the range values are approximately 2 times higher for control no. 3 compared to control no. 2. Longer range values in control no. 3 may be related to the differences in underlying subgrade conditions. Control no. 2

149

consisted of 1.2 m (4 lifts) of new fill while control no. 3 consisted of only 0.3 m (1 lift) of new fill material. The underlying subgrade is native sand material. CCV values which are believed to have deeper influence depth of up to 1.5 m (ISSMGE), may be more influenced by native materials in control no. 3 which tend to exhibit greater spatial continuity (i.e., longer range) than fill materials.

Directional Variations. It is observed that the sill values in E-W direction were consistently lower than in N-S direction, which indicates less variability in E-W direction. But longer range values were observed in N-S direction variogram, which suggests greater spatial continuity along the direction of roller travel than the transverse direction.

Directional variograms can help determining principles directions of anisotropy in the IC data; however modeling anisotropy in a variogram involves several complications. Comparison between omnidirectional and N-S directional variograms from two control strips did not show any significant differences in their spatial statistics. This is expected as in an omnidirectional variogram, more data that is oriented in N-S direction is accounted for compared to data in E-W direction. Since omnidirectional variogram accounts for data in all directions and as long as it presents a clearly interpretable structure, it is decided to show only omnidirectional variogram parameters for all the variogram analysis performed later in this chapter.

Small – Scale versus Large – Scale Variations. Variogram plots presented above for control no. 2 showed a decreasing trend of variance after about 40 to 50 feet and then an increasing trend after about 75 feet. Similarly, control no. 3 showed an increasing trend in variance after about 50 feet. The sill and range values presented are based on theoretical models that just captured the small scale variability. Clearly, some large-scale spatial relationships exist in the dataset.

7.5 Spatial Variability Analysis – TH 64 Proof Sections

Proof sections are production compaction areas of the project. IC-TV's established from control sections were used as reference for quality assurance in the proof sections. Two proof sections were selected for spatial variability analysis on CCV data. A summary of the location and dimensions of the proof sections selected for analysis are listed in Table 7.4.

Table 7.4. Brief summary of proof sections used for spatial analysis

Proof No.	Station	Plan Dimensions (width, m x length, m)	Section Type	IC-CTV
14	269 – 277	11.5 x 243.8	Fill – 0.4 m to 1.2 m	42
15	277 – 288	11.5 x 335.3	Fill – 0.3 m to 1.8 m	42

Spatial variability analysis involved constructing experimental variogram, fitting theoretical models, comparing spatial statistics (sill and range) from a theoretical variogram model with univariate statistics and Mn/DOT acceptance criterion, and creating kriged surface maps of CCV. Further, the proof sections are compared with their reference control sections. Note that the sill

150

and range values presented herein represent only the exponential models that were fit to the experimental variograms.

The subgrade conditions in this proof no. 14 consisted of newly placed fill material varying from about 0.4 m to 1.2 m in thickness, underlain by native sand. The subgrade conditions in this proof no. 15 consisted of newly placed fill material varying from about 0.3 m to 1.8 m in thickness, underlain by native sand. Compaction operations for both proof sections were performed longitudinally in north-south direction, along six adjacent lanes. IC-CTV of 42 established from control no. 2 was used as reference for quality assurance.

Variograms for proof nos. 14 and 15 with comparison to control no. 2 along with CCV kriged surface maps are presented in Figures 7.18 and 7.19, respectively. Comparison of univariate statistics and Mn/DOT acceptance criteria is also presented. Note that the lag distance scale on proof no. 14 and proof no. 15 variograms in Figures 7.18 and 7.19 were kept as 90 m for direct comparison with control no. 2 variogram. Full-length variograms for proof nos. 14 and 15 and CCV surface maps are shown in Figure 7.20. Similar to control no. 2, variograms for both proofs showed a trend of increasing variance after about 50 feet lag distance (*see* Figure 7.20) which is not captured by the theoretical variogram.

Both proof nos. 14 and 15 "pass" based on Mn/DOT acceptance criterion. However, if spatial statistics between the proofs and control no. 2 are compared, both of the proofs have failed to achieve the "sill" and "range" values that are achieved in control no. 2. The proof no. 15 sill value was at least closer (~ 33.0) to control 2 sill value (~ 30.0). Both proof nos. 14 and 15 consisted of several concentrated locations of "hot spots" that has CCV < 30, especially at the middle of the pavement. These locations generally match with the locations of grade stakes in the field, and are not subjected to construction traffic and also relatively less compacted.

CCV Statistics	Proof 14	Control 2
Mean, μ	49.8	47.6
Std. Dev, σ	7.6	5.6
COV (%)	15.2	11.7
Sill $(CCV)^2$	51.5	30.0
Range (m)	3.0	6.0
IC-CTV	42.0	42.0
>130% of CTV	25.9	6.0
90 – 130% of CTV	68.3	89.0
<90% of CTV	5.8	5.0
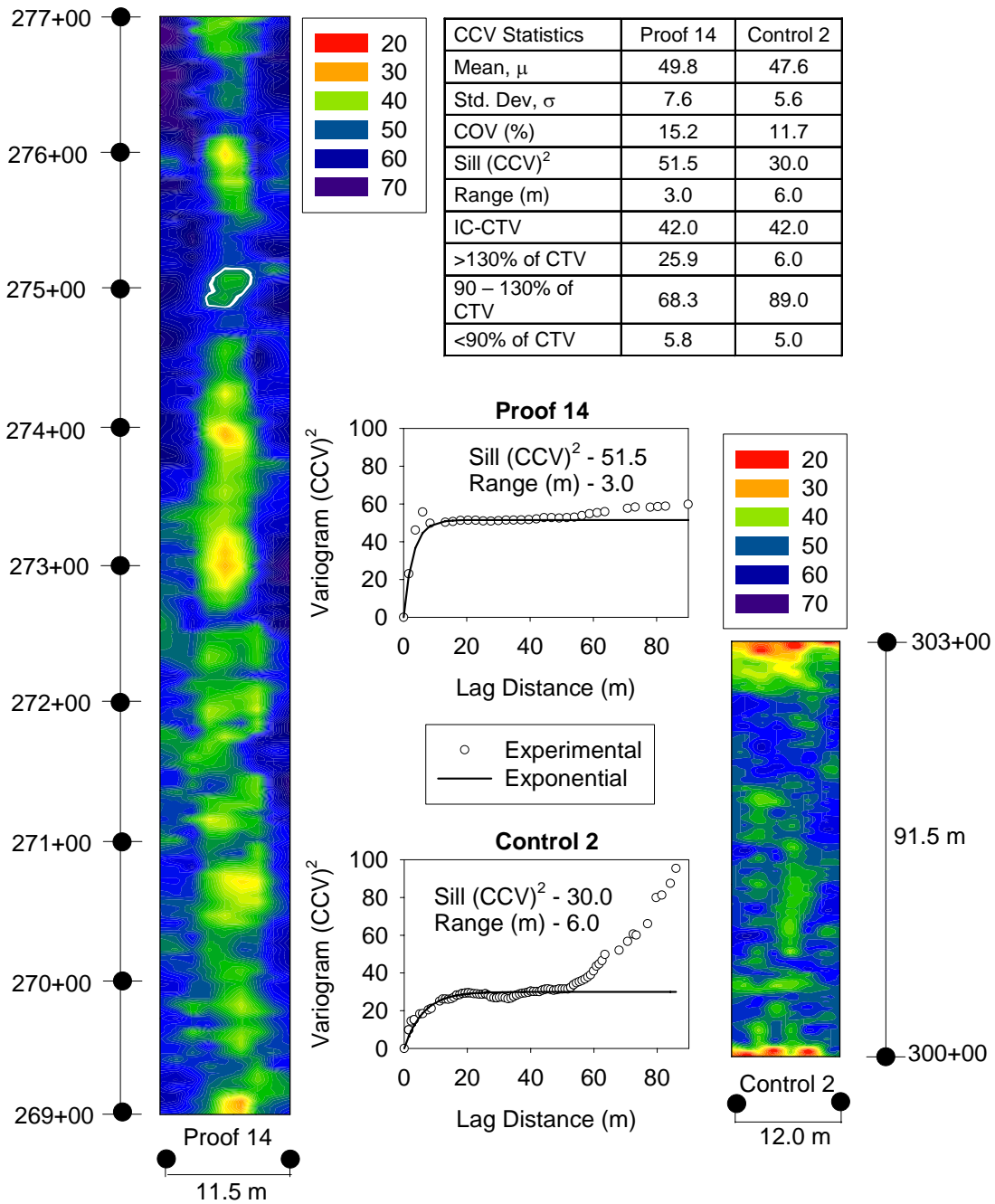
Figure 7.18. Comparison of Proof 14 and Control 2 – CCV surface and variogram plots

152
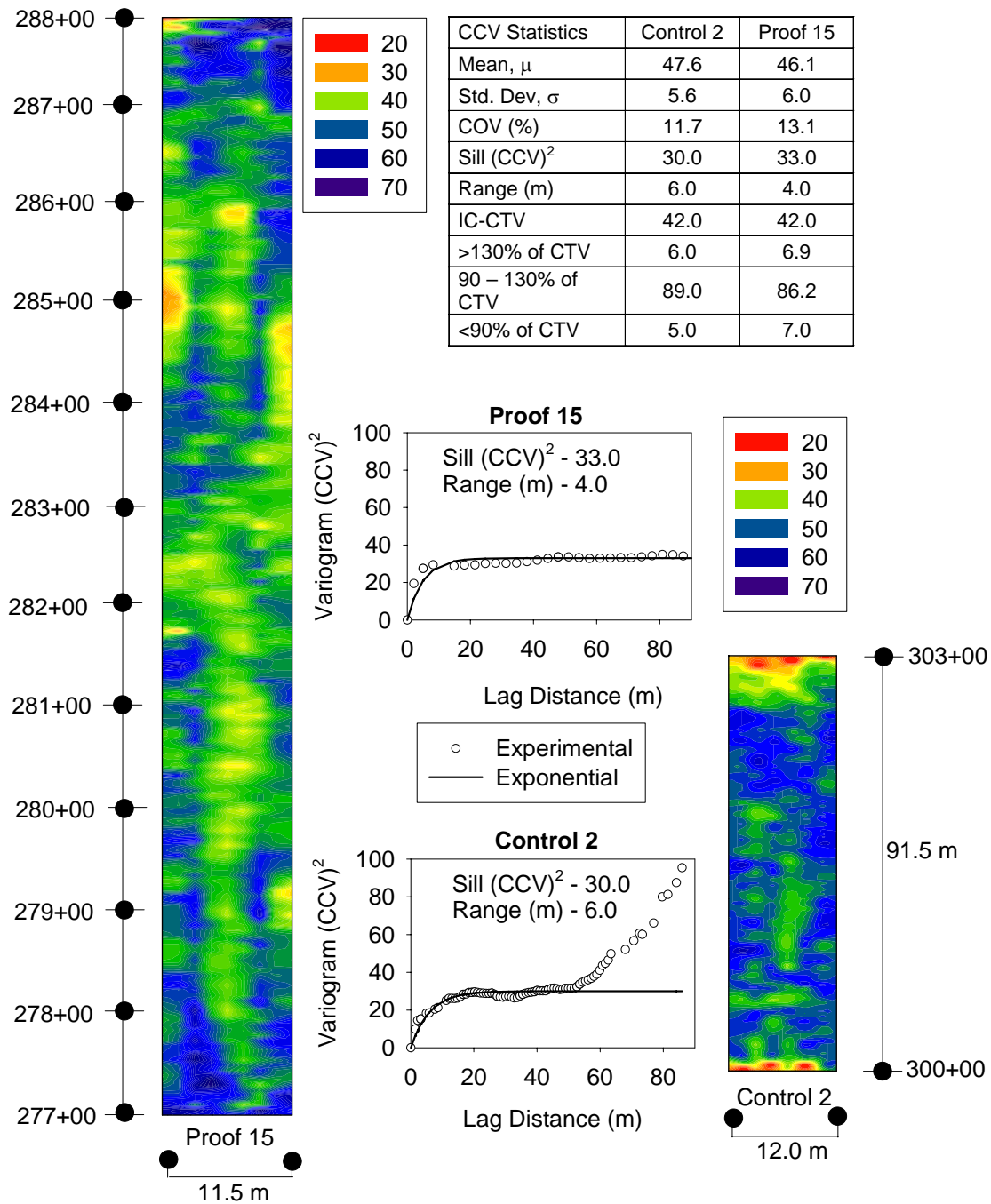
Figure 7.19. Comparison of Control 2 and Proof 15 – CCV surface and variogram plots
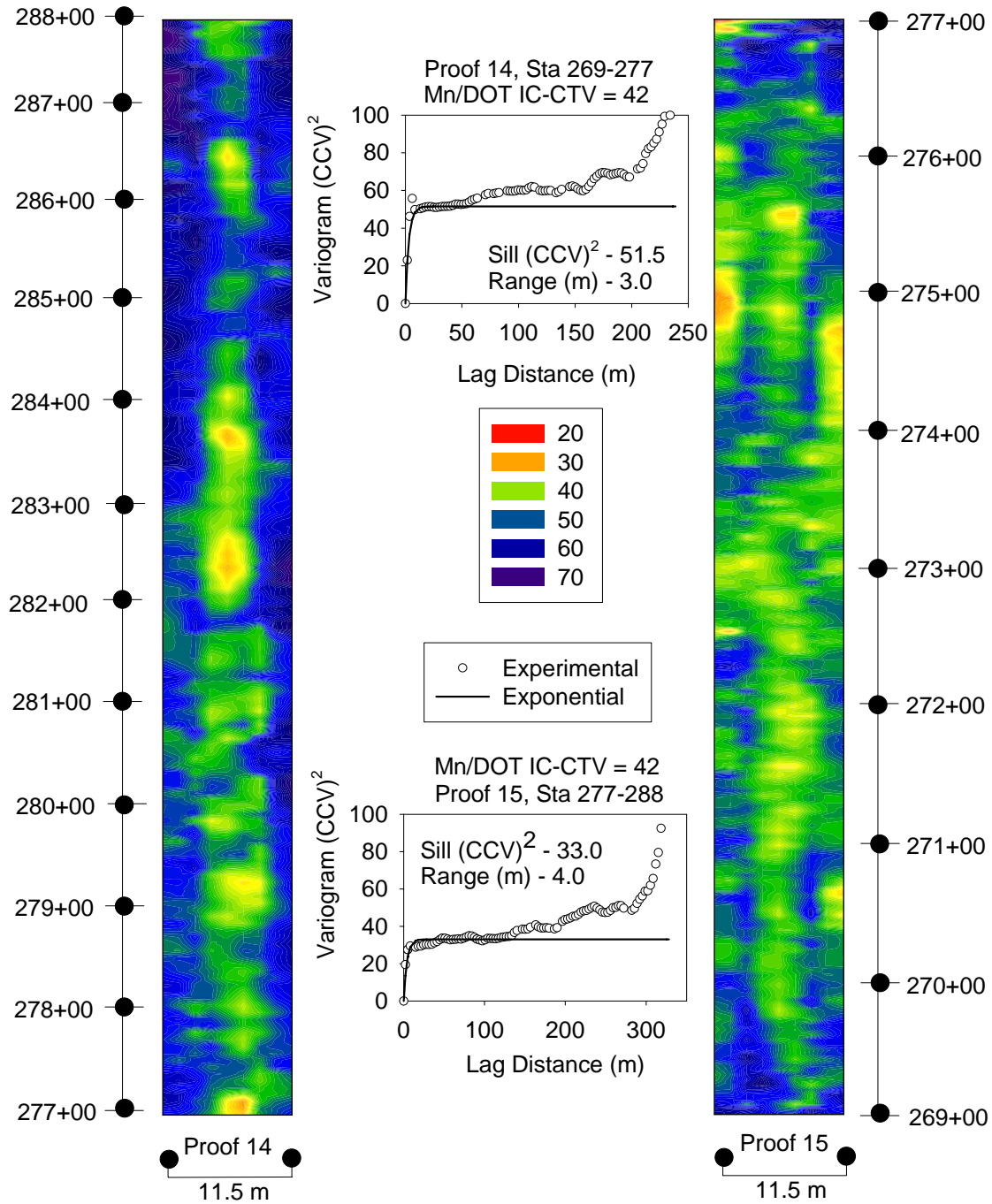
Figure 7.20. CCV surface and variogram plots for Proofs 14 and 15

7.5.1 Evaluation of Proofs at Smaller-Scale

Proof nos. 14 and 15 pass the Mn/DOT acceptance criteria when viewed at a larger scale (250 m to 300 m long). In order to evaluate sections of these proofs separately, proof nos. 14 and 15 were divided in to a total of 19 sections of size 30.5 m long x 11.5 m wide "window" (i.e. separating every station). Univariate, spatial statistics and Mn/DOT acceptance criteria values for these 30.5m long windows are summarized in Table 7.5. Variograms for each window is presented in Figures 7.21 and 7.22. Each variogram is labeled either "pass" or "fail" based on both Mn/DOT and "sill" criteria. To pass the "sill" criteria, the sill value of a given area should meet the sill value from control no. 2. The pass/fail results are also summarized in Table 7.5 for each window.

From Table 7.2 and Figures 7.21 and 7.22 it is evident that at least three 30.5 m long sections of proof nos. 14 and 15 have failed to meet the Mn/DOT acceptance criteria, and at least 12 windows have failed to meet the "sill" criteria.

While portions of proof nos. 14 and 15 "fail" when viewed in a smaller scale, it raises a question on how long or short a proof area should be to evaluate for acceptance. Spatial statistical parameter, "range", achieved in a control can be the minimum size of an area (window size) for evaluation, since from definition the data beyond the range is not spatially correlated. So, at any location over a given proof area, with a window size that is equal to the range, the acceptance criteria (just only with univariate statistics) should be achieved. An example of this approach is presented in Figure 7.23. Figure 7.23b shows pass/fail areas based on 30.5 m windows based on Mn/DOT acceptance criterion. Based on the range from control no. 2, a window size of approximately 6 m x 6 m is used to evaluate between Sta. 273 and 275. Figure 7.23c shows that several isolated areas between these stations failed to meet the Mn/DOT acceptance criteria. Results from these 6 m x 6m widows are summarized in Table 7.6. Results produced using this approach with "pass or fail" map can be simple to understand, and also are more sophisticatedly quantified.

The implication of incremental spatial analysis approach presented above is that is will aid the contractor in identifying localized poorly compacted areas or areas with highly non-uniform conditions, which are often the route cause of pavement problems.

Table 7.5. Comparison of univariate and spatial statistics of CCV with Mn/DOT acceptance criteria and sill criteria with 30.5 m long "windows"

Strip	Univariate Statistics			Spatial Statistics*		Mn/DOT QA Criteria (Percent of CTV)			Pass/Fail Criteria	
	μ	σ	COV (%)	Range (m)	Sill (CCV)^2	> 130%	90% - 130%	< 90%	Mn/DOT	Sill ***
269 - 270	47.3	6.3	13.3	2.5	37.0	9.4	84.3	6.3	Pass	Fail
270 - 271	47.4	5.9	12.5	3.0	38.0	11.2	81.9	6.9	Pass	Fail
271 - 272	48.7	6.4	13.2	2.0	43.0	18.0	79.5	2.6	Pass	Fail
272 - 273	48.5	6.5	13.3	2.5	40.0	16.9	78.2	4.9	Pass	Fail
273 - 274	47.3	8.3	17.5	3.0	62.0	19.1	66.1	14.9	Fail	Fail
274 - 275	52.0	7.4	14.3	2.5	50.0	43.7	51.9	4.4	Pass	Fail
275 - 276	52.6	6.8	13.0	3.0	46.0	38.1	58.1	3.8	Pass	Fail
276 - 277	54.5	8.6	15.8	3.0	75.0	51.5	46.1	2.4	Pass	Fail
277 - 278	51.1	5.9	11.5	2.0	34.0	28.6	71.0	0.4	Pass	Fail
278 - 279	46.8	4.5	9.6	2.0	18.0	3.7	95.7	0.5	Pass	Pass
279 - 280	46.2	5.3	11.6	1.8	27.0	5.8	88.4	5.8	Pass	Pass
280 - 281	44.2	4.3	9.8	2.5	19.0	0.5	91.7	7.8	Pass	Pass
281 - 282	45.1	5.1	11.3	2.5	28.0	2.7	90.3	7.0	Pass	Pass
282 - 283	43.2	3.7	8.6	1.8	15.0	0.0	93.1	6.9	Pass	Pass
283 - 284	45.7	4.0	8.7	2.2	15.5	0.0	96.2	3.8	Pass	Pass
284 - 285	44.5	6.0	13.6	3.0	36.5	1.7	80.9	17.4	Fail	Fail
285 - 286	43.7	6.2	14.1	3.0	39.0	2.1	81.9	16.0	Fail	Fail
286 - 287	46.5	3.8	8.1	2.8	15.5	0.0	97.5	2.5	Pass	Pass
287 - 288	50.2	9.4	18.8	4.0	95.0	30.4	61.4	8.2	Pass	Fail

Notes:
* Spatial statistics are based on exponential onmi-directional variogram
** IC–CTV used for acceptance = 42
*** Sill criteria is to achieve ≤100% sill which is established from Control 2 (i.e. sill = 30)

156
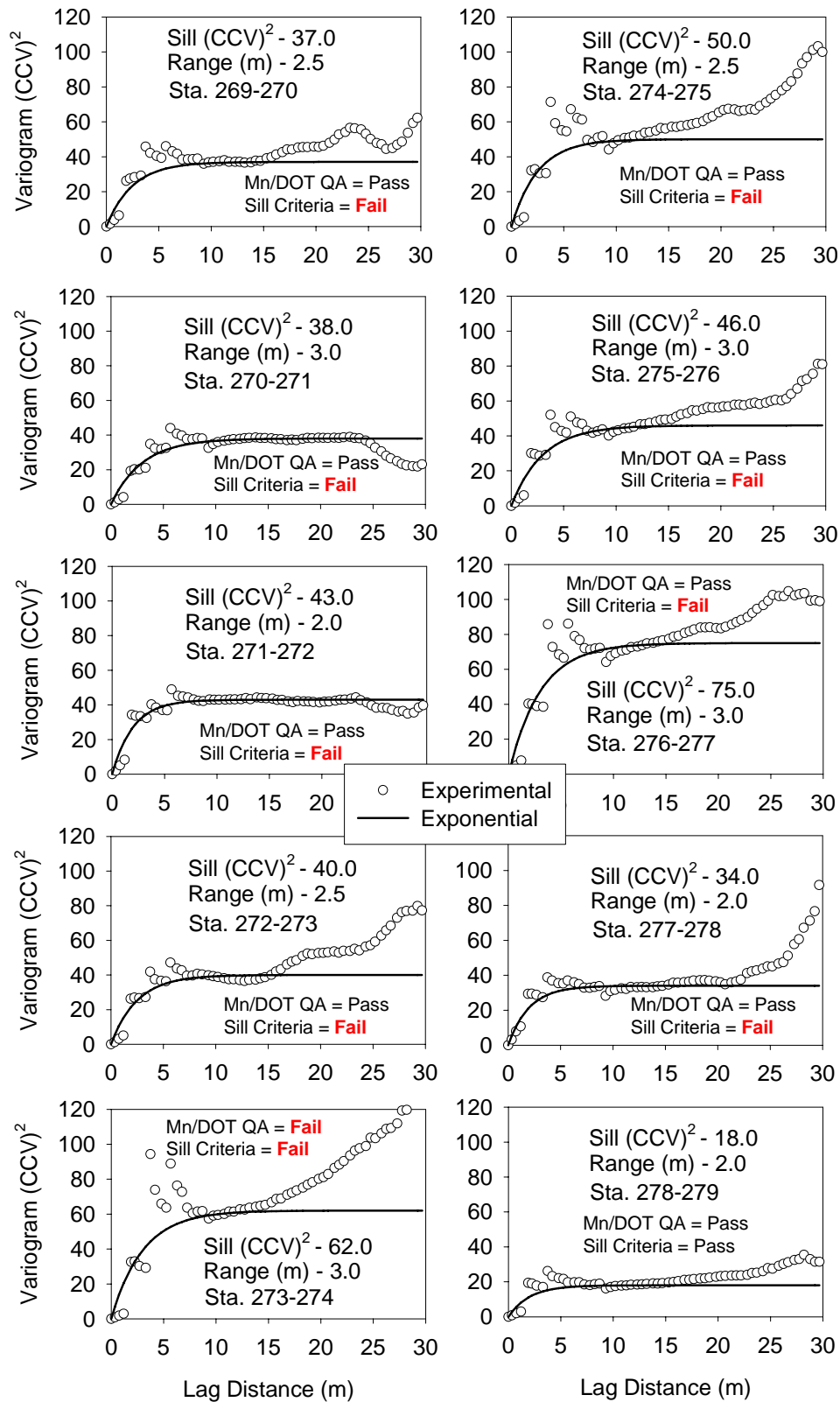
Figure 7.21. 30.5 m x 11.5 m window variograms of Proof 14 and 15 (Sta. 269-279)
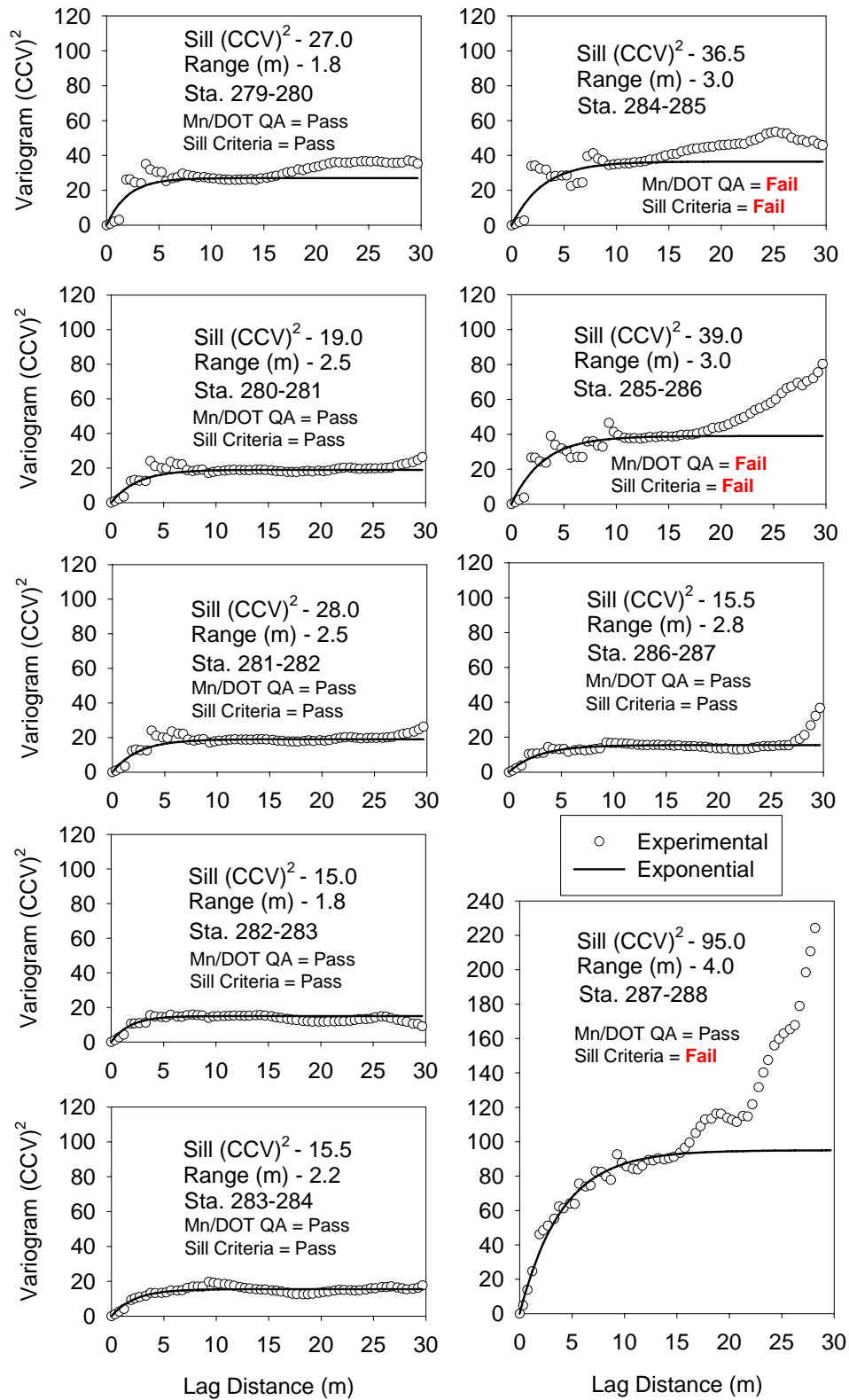
Figure 7.22. 30.5 m x 11.5 m window variograms of Proof 14 and 15 (Sta. 279-288)
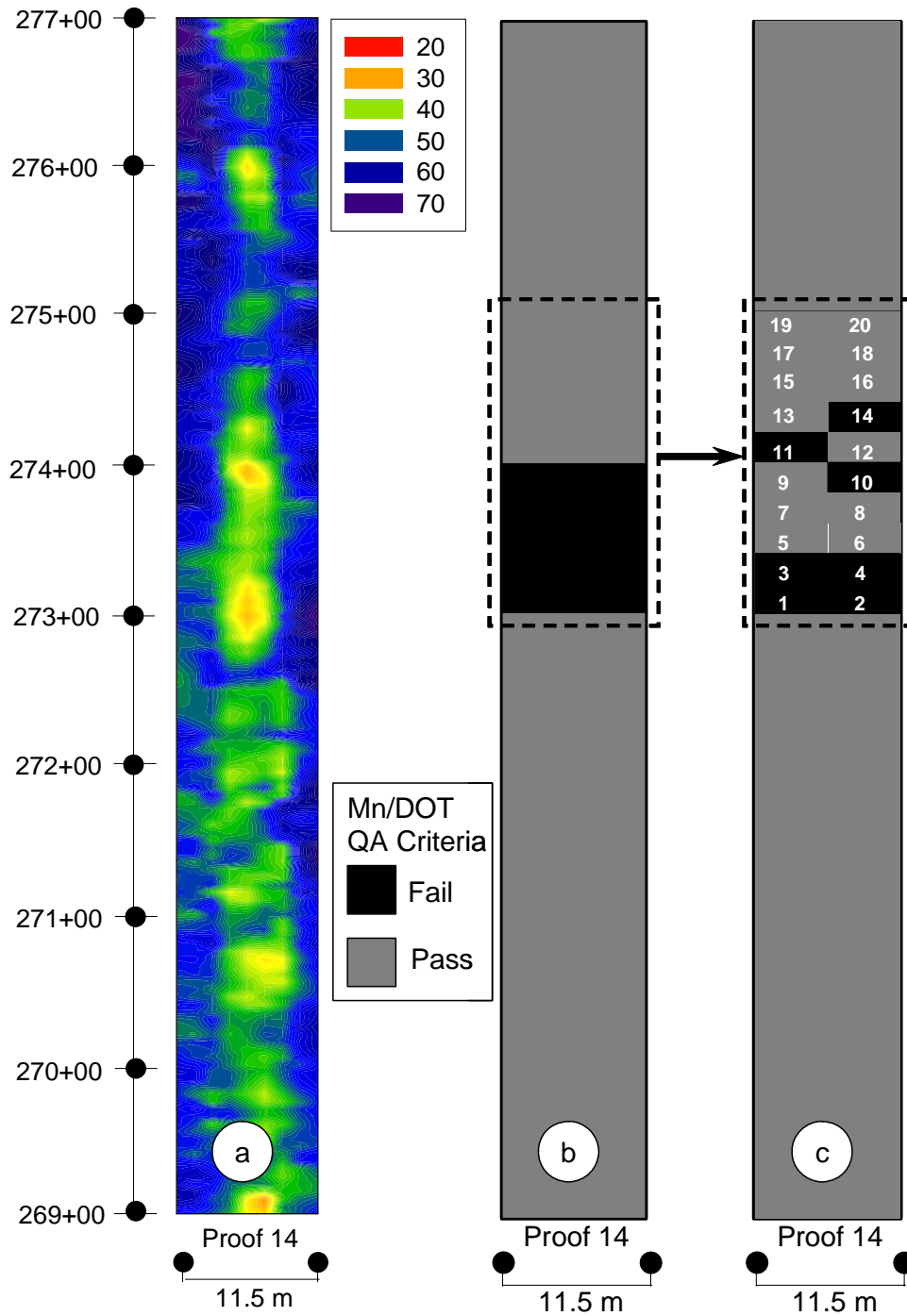
Figure 7.23. Plots showing CCV (a) surface plot (b) 30.5 m x 11.5 m window pass/fail map (c) 6 m x 6 m window pass/fail map between Sta. 273 to 275

Table 7.6. Univariate statistics and Mn/DOT acceptance criteria for 6 m x 6 m size "windows" between Sta. 273 to 275

Strip No.	Univariate Statistics of CCV			Mn/DOT QA Criteria (Percent of CTV)			Pass/Fail
	Mean, μ	Stdev, σ	COV (%)	> 130%	90% - 130%	< 90%	
1	43.9	7.7	17.6	0.0	64.2	35.8	Fail
2	44.8	12.7	28.3	23.1	25.4	51.5	Fail
3	44.2	5.2	27.1	0.0	82.8	17.2	Fail
4	50.0	9.1	18.3	39.6	42.7	17.7	Fail
5	45.9	4.9	10.7	7.3	90.6	2.1	Pass
6	48.2	6.2	12.9	12.5	87.5	0.0	Pass
7	49.6	6.8	13.6	33.0	67.0	0.0	Pass
8	45.7	5.0	10.9	2.0	97.0	1.0	Pass
9	51.5	9.0	17.4	49.5	43.0	7.5	Pass
10	45.2	8.4	18.5	12.9	57.4	29.7	Fail
11	48.4	10.2	21.0	32.3	47.9	19.8	Fail
12	49.0	7.5	15.3	29.3	61.6	9.1	Pass
13	50.7	7.3	14.3	48.9	51.1	0.0	Pass
14	48.9	8.3	16.9	34.0	52.6	13.4	Fail
15	53.0	5.4	10.3	53.8	46.2	0.0	Pass
16	53.0	7.6	14.4	45.8	54.2	0.0	Pass
17	55.7	5.9	10.6	53.2	46.8	0.0	Pass
18	51.4	5.4	10.6	29.0	71.0	0.0	Pass
19	54.5	5.0	9.1	55.8	44.2	0.0	Pass
20	55.1	5.5	10.0	55.9	44.1	0.0	Pass

7.5 Spatial Analysis of Spot Test Data and CCV data – TH 64

A total of 52 spot test measurements using 20 kg Clegg Impact Tester (CIV_{20-kg}), and 200 mm Zorn LWD ($E_{LWD-Z2(63)}$) were conducted on proof no. 14 between Sta. 274 and 277, mostly along the south bound (SB) lane. Only 16 dry unit weight, moisture, and DCP tests were performed in this area, and therefore, were not included in spatial analysis. The total test area has dimensions of about 7.6 m x 91.5 m. A kriged surface map of CCV data is created to compare with the kriged surface maps of CIV_{20-kg} and $E_{LWD-Z2(63)}$ and are shown in Figure 7.24 . These kriged surface maps were created based on variogram models presented in Figure 7.25.

Spot tests between about Sta. 276 to 277 were very closely spaced (about 1 test location per every 7.7 sq. m) compared to spot tests between Sta. 274 to 277 (about 1 test location per every 23.2 sq. m) (*see* Figure 7.24). These spot tests were intentionally spaced at such a frequency to understand scale effects on kriging predictions at untested locations.

Results of correlation analyses to relate CCV to in-situ test results at different window sizes, and comparisons between distributions of CCV data versus in-situ test data is already presented in Chapter 5. Comparison of spatial statistics of CCV data with in-situ test data is shown in Figure 7.25. Some univariate statistics (μ, σ, COV) are also presented in Figure 7.25 for reference. The theoretical variograms presented in Figure 7.25 were checked for its "goodness" using the modified Cressie goodness of fit approach suggested by Clark and Harper (2002) (see equation 7.13) as well as the cross-validation process. A lower Cressie goodness factor indicates a better fit. The best fit model was selected based on Cressie goodness factor, visual assessment, and best possible cross-validation results. The results of cross-validation are also presented in Figure 7.25. The effect of number of samples can be clearly seen in the cross-validation with excellent predictions in case of CCV value versus relatively poor predictions in case of E_{LWD} and CIV.

The nugget effect in the variograms was modeled as suggested by Barnes (2007), by keeping the variance of the measured value from nearest neighbor statistics as the upper bound for the nugget value. As expected, the CCV data did not exhibit any nugget effect because of data points being very closely spaced (approximately 0.06 m) while the CIV and E_{LWD} showed some nugget effect because of no data points within a spacing less than 1.1 m.

Both CIV and E_{LWD} variograms shows greater spatial continuity (longer range values) than CCV. In addition, the spot test measurements have generally showed more locations of low stiffness than CCV values. The reason can be related to the effect of lesser confining stress at the surface which influence the spot tests. Results presented in Chapter 5 have demonstrated the effect of confining pressure on sand stability (*see* Figure 5.26). In addition, the influence depths of spot test and CCV measurements are substantially different. According to Sulewska (1998) and Kulda *et al.* (1991), for Zorn LWD the influence depth is typically equal to its plate diameter which is 200 mm. Also, for 20-kg Clegg it is expected to be less than about 300 m. On the other hand, according to ISSMGE specifications, CCV values can have deeper influence depths of up to 1.5 m. The difference between number of measurements between spot tests and CCV should also be noted. Clearly, denser dataset would produce more reliable spatial predictions.

Considering the influence depth issues, number of data points, and effect of confining stress at surface on spot test measurements, a close match of kriged CCV map to spot test data is not expected. Despite these effects, Figure 7.24 appears to provide a decent spatial comparison by matching some locations of low and high CCV values with some low and high CIV_{20-kg} and $E_{LWD-Z2(63)}$ values, respectively.
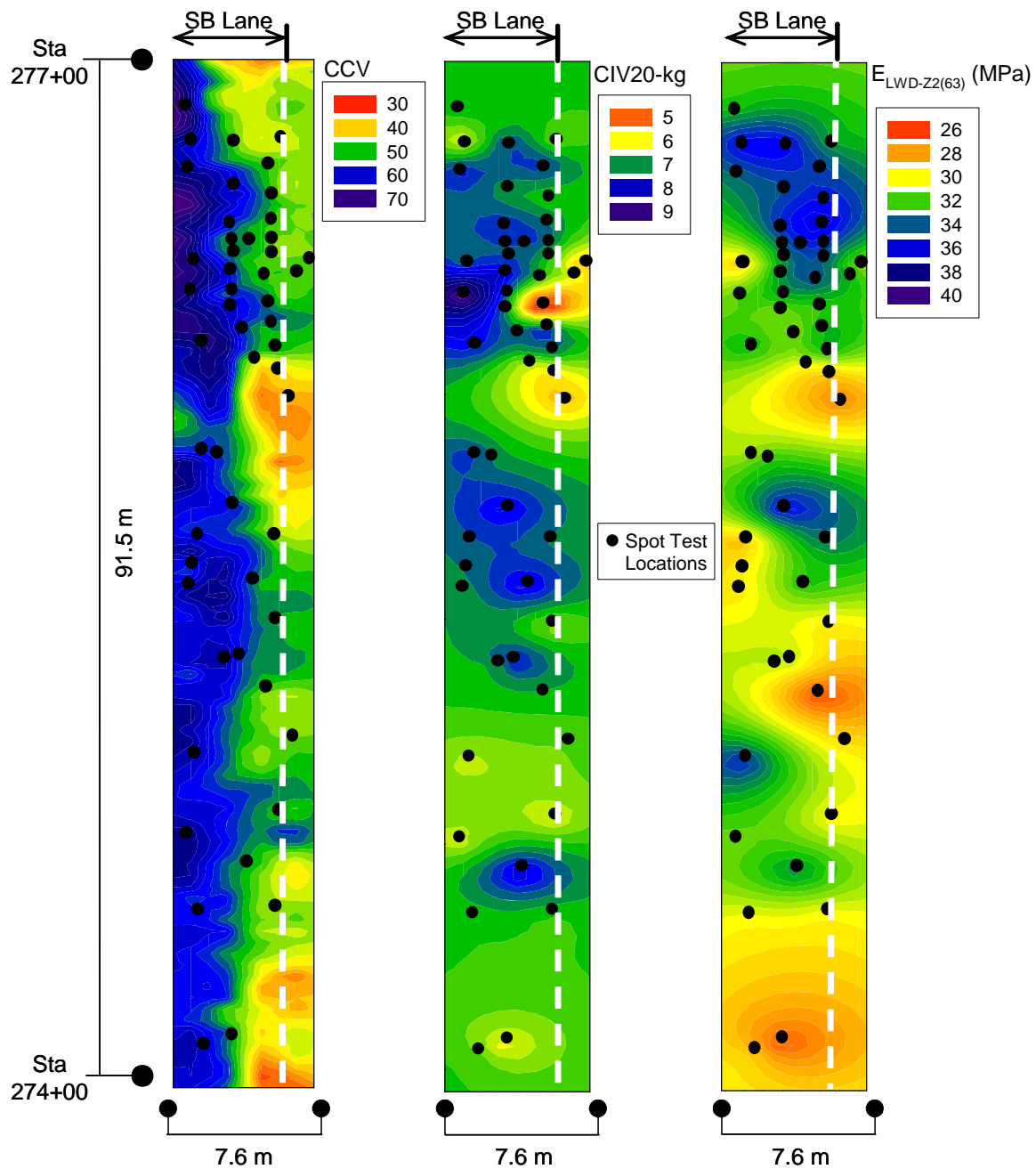
Figure 7.24. Comparison of CCV surface map with CIV_{20-kg} and $E_{LWD-Z2(63)}$ for Proof 14 from Sta. 274 to 277
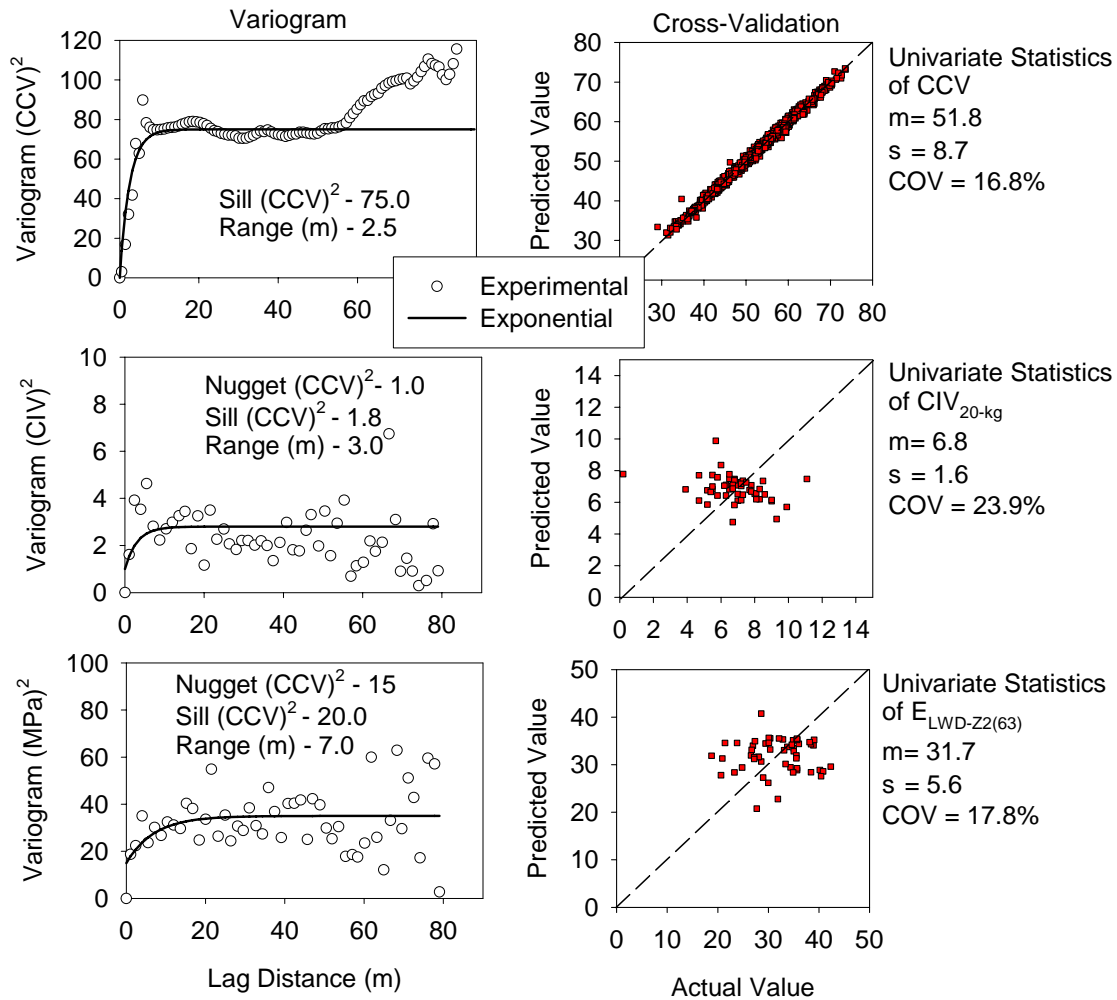
Figure 7.25. Comparison of variograms: CCV, CIV_{20-kg}, and $E_{LWD-Z2(63)}$ for Proof 14 from Sta. 274 to 277

7.6 Summary and Key Findings

A summary of important aspects, conclusions, and key findings from geostatistical analysis include:

- Variogram models can be used in characterizing uniformity by quantifying spatial variability.

- The range distance from a variogram plot can potentially be used as a maximum separation distance between spot test measurements to ensure independent measurements. Three to five spot tests within this range provides an estimate of mean value of the measurement.

163

- Roller data output with data assigned to the center of the drum can provide reliable results in spatial analysis. Single point data assigned to left or right side of the drum or both sides of the drum result in errors greater than 20%.

- Spatial variability analysis on control nos. 2 and 3 identified critical differences including: (1) control no. 3 having a range value about 2 times higher than control no. 2 thus indicating greater spatial continuity; and (2) control no. 2 has a sill value about 2.5 times lower than that of control no. 3, indicating less variability.

- Increasing roller passes in control no. 3 increased the percentage of CCV values in the 90% - 130% bin from 75% to 93%, indicating compaction. With increasing roller passes range also increased indicating increase in spatial continuity. The sill value was variable.

- In the direction transverse to roller travel, the calculated sill values are consistently lower than values determined from the direction of roller travel. Longer range values were observed along direction of travel which suggests greater spatial continuity than the transverse direction.

- Although, proof nos. 14 and 15 "pass" the Mn/DOT acceptance criteria, they failed to meet the alternatively proposed "sill" criteria for uniformity. When proof nos. 14 and 15 are divided into incremental spatial sections, at least three sections about 30.5 m long failed to meet the Mn/DOT acceptance criteria. The implication of incremental spatial analysis is that is will aid the contractor in identifying localized poorly compacted areas or highly non-uniform conditions, which are often the root cause of pavement problems.

- Using "range" as the minimum window size for an area of evaluation, a 60 m long section was analyzed and found that several isolated locations failed to meet the Mn/DOT acceptance criteria. The scale at which acceptance criteria is based is still a question that needs further discussion and analysis.

- Despite the different conditions affecting in-situ spot test measurements and roller-integrated measurements, relatively good spatial comparison of CCV, CIV, and E_{LWD} was observed for a proof area.

Chapter 8
Laboratory Compaction Study

Laboratory compaction of soils should simulate the mechanics and energy delivery system that occurs in the field. This is particularly important as it relates to particle arrangement and structure and measuring engineering properties (e.g. strength and stiffness) of materials compacted in the lab. As part of this research effort, several laboratory compaction techniques were evaluated with comparison measurements of density and resilient modulus. A brief literature review of compaction methods and the influence of these methods on soil strength and stiffness properties is presented. In addition, results from laboratory compaction tests performed using impact, static, gyratory, and vibratory compaction methods for one cohesive soil and one granular soil are presented. Laboratory resilient modulus (M_r) and unconsolidated-undrained (UU) strength tests were also performed on samples prepared using the aforementioned compaction methods to evaluate the effects of compaction method on these soil properties. The implications of this research are important as it relates to development of a database of M_r and UU values for comparison to in-situ LWD and IC measurement values.

8.1 Background

Pavement systems use unbound fill materials for subgrade and base layers whose engineering properties depend on proper compaction and moisture control. To establish target field density values and moisture content limits, a laboratory compaction test is normally performed. Ideally, the laboratory compaction test duplicates the field compaction characteristics of the material. For fine-grained cohesive soils, reproducing lab specimens with a soil fabric/structure similar to the field compacted soils is especially important as the resulting soil-structure can affect the strength properties (Rodriguez *et al.* 1988). Over the past eight decades, several compaction techniques have been developed to determine moisture-density relationships with the purpose of simulating field conditions — static, impact, vibratory, gyratory, and kneading compaction methods.

8.1.1 Laboratory Compaction Methods

Impact Compaction

The impact compaction test was developed by R. R. Proctor during early 1930's based on testing some 200 different soils (Proctor 1933), and the method was standardized by AASHTO and ASTM during early 1940's and is popularly known as the standard Proctor compaction test. During World War II, the Army Corps of Engineers found that for some soils the standard Proctor method produced lower densities than observed in the field (Holtz and Kovacs 1981). For this reason, the method was modified by increasing the compaction energy and later standardized as the modified Proctor method. Since Proctor's work in 1930's, the impact

compaction method has been the most popular and widely implemented method in construction practice, especially for fine-grained cohesive soils. Although there are some limitations, this method has also been applied for use with granular soils.

Proctor's research indicated that each soil has a unique maximum dry density and optimum moisture content for a given compaction energy. On either side of the optimum moisture content, the dry density decreases to a limiting value. A study by Lee and Suedkamp (1972) found that four distinct compaction curves exist: one single peak curve, a one and half peak compaction curve, and a double peak compaction curve, and no distinguishable peak. Irregular shaped curves are found for soils that are typically not within liquid limit range of 30 to 70. Tests on granular soils often do not exhibit a distinguishable peak.

Vibratory Compaction

Based on extensive work by Burmister (1948), Felt (1958), Pettibone and Hardin (1964), it is determined that vibratory compaction methods produce consistently higher maximum densities than the impact method (standard Proctor) for granular materials and also better replicates field densities. Vibratory compaction was standardized by ASTM in the 1960's. According to Lambe (1951), granular free-draining soils do not respond to variations in compacting moisture content and impact energy in the same manner as cohesive soils because of negligible lubrication. Some studies, however, indicate that vibratory compaction can be effective in cohesive soils if compacted at low frequencies (Converse 1956, Lewis 1961).

Static Compaction

Porter (1930) introduced a static compaction test, primarily for granular soils in which a static pressure of about 13,800 kPa (2,000 psi) is applied to a 152 mm diameter (6 inch) specimen. The Porter SOP test method was originally used for California Bearing Ratio (CBR) tests. Although the static compaction method is as old as the impact method, it has not been widely implemented because application of static pressure has been found to be less inefficient for compacting some granular soils (Rodriguez *et al.* 1988). Aguirre (1964) compared results from static and impact compaction methods on 17 different soils. For coarse sands and gravels, moisture-density curves for both static and impact compaction tests were similar. For plastic clay soils, however, the maximum dry unit weights achieved from impact compaction were lower than static compaction.

Bell (1977) showed that static compaction requires less compaction energy than both impact and kneading compaction methods to achieve a target density at a given moisture content. Results from Zhang *et al.* (2000) indicated that the required static compaction energy decreases with increasing moisture content if the dry unit weight is constant, and it increases with increasing dry unit weight if moisture is constant.

Gyratory Compaction

With developments in compaction equipment technology and increasing use of heavy rollers, several researchers have introduced concerns over laboratory impact and vibratory compaction methods in developing moisture-density relationships that simulate field conditions. The Army Corps of Engineers (Coyle and West 1956, McRae 1965) introduced the gyratory compaction test procedure for soils based on extensive testing on silty sand material in the Mississippi area.

Results indicated that gyratory compaction can simulate field compaction characteristics better than impact compaction with standard Proctor energy. Recent work by Kim and Labuz (2006) on recycled granular materials in Minnesota also provided similar conclusions. Based on testing fine sand and silty sand materials, Ping *et al.* (2003) found that the optimum moisture and maximum densities achieved in the field were closer to gyratory compaction results than both impact (modified Proctor) and vibratory compaction. According to Browne (2006) the gyratory compaction method produced maximum dry unit weights greater than modified Proctor method for three different types of soils (A-1-a, A-3, and A-7-6). The gyratory compaction method was standardized by ASTM (ASTM D-3387) based on the work by McRae (1965) for its use for subgrade, base and asphalt mixtures. This method, however, has not been widely implemented for compaction of subgrade and base materials. One reason for slow implementation may be that no standard gyratory variables (e.g. gyration angle, number of gyrations, normal stress, and rate of gyrations) have been developed for subgrade and subbase materials.

Kneading Compaction

Several kneading compaction methods have been developed over the past 50 years. One of the first was developed by S. D. Wilson at Harvard University and is known as the Harvard Miniature Test (Wilson 1950). The intention of this test method was to reproduce the soil-structure that is achieved in the field for sheepsfoot and pneumatic tired rollers. The Harvard test involves compacting the soil in a mold with a standard piston that exerts a constant static pressure and is suitable for cohesive soils only. Other tests have been derived from a similar concept (e.g. Stodjadinovic 1964, Daoud 1996). Recently, Kouassi *et al.* (2000) introduced a new kneading compaction procedure for clay materials in which the soil is compacted using three kneading feet simulating tamping rollers. Results show that the new compaction method generally produces higher densities than impact compaction (standard Proctor), especially on the wet side of optimum and are is in better agreement with field measurements.

8.1.2 Influence of Compaction Method on Strength and Stiffness

According to Lambe (1958), for a given dry density, the compaction method affects the soil-structure, which in turn affects strength properties. Neves (1971) studied the effect of the compaction method on the resulting soil-structure by compacting a cohesive soil to target densities by static, impact, and kneading methods. The effects are presented in Figure 8.1 which show distinctly different soil-structures.

The influence of compaction method on soil strength has been investigated by several researchers; however, studies show contradictory information. Based on tests on a low plasticity sandy salty clay material, Bell (1977) found that static compaction specimens have lower strength than impact compaction specimens of similar moisture content and dry density. Contradictory results are reported by Seed *et al.* (1960). Recent work by Zhang *et al.* (2000) on A-6(11) and A-7(10) soils found that there is no significant difference in unconfined compressive strength of static and impact compaction specimens at similar moisture contents and densities. Bell (1977) found that statically compacted specimens produced lower strengths than kneading compaction specimens, while Mitchell *et al.* (1965) found the opposite for samples on

the wet side of optimum moisture content and no significant changes on the dry side of optimum. A key element of comparing strength measurements from different compaction methods is pore pressure development and largely remains undocumented.

Recently, Lee *et al.* (2007) compared the strength properties and particle arrangements for specimens compacted using gyratory and impact methods with field compacted undisturbed specimens for two types of soils (SM and SW). Results show that specimens prepared using the gyratory method at 400 kPa and 600 kPa vertical pressures more closely match the field compacted strength measurements and particle arrangements compared to the impact method. However, it is not clear how the dry unit weight and moisture contents varied between the specimens for these tests.
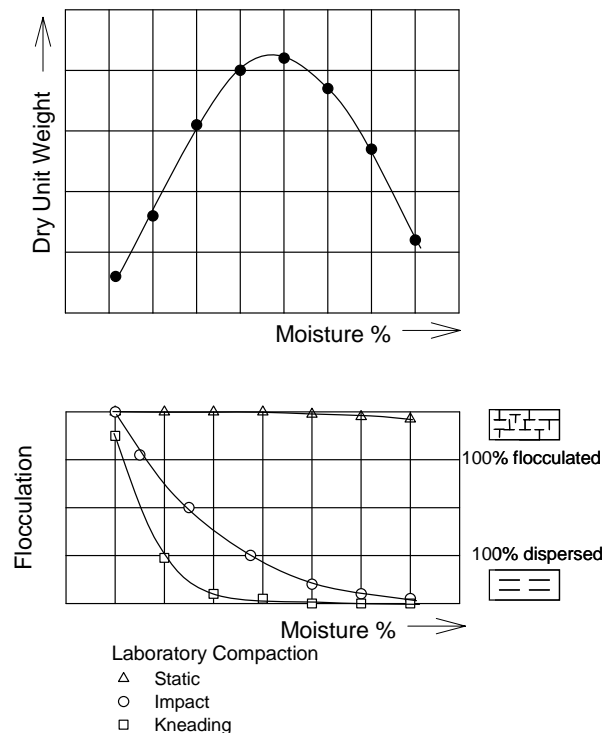
Figure 8.1. Effect of type of compaction on the structure acquired by a compacted soil (Reproduced from Neves (1971))

8.1.3 Resilient Modulus

Resilient modulus (M_r) is used in pavement engineering as a measure of stiffness of unbound materials in the pavement structure. Its concept was first introduced by Seed *et al.* (1962). M_r is defined as the ratio of cyclic deviator stress and resilient strain (Figure 8.2). The M_r parameter is highly stress-dependent (Huang 1993). Many non-linear models have been proposed that incorporate the effects of stress levels and predict resilient modulus. Some of the popular models include the power-law model for granular soils (Monismith *et al.* 1971) and the deviator stress model for cohesive soils (Mohammad and Puppala, 1995). In reality, most soils exhibit the

effects of increasing stiffness with increasing confinement and decreasing stiffness with increasing shear stress (Andrei *et al.* 2004). Witczak and Uzan (1988) provided a "universal" model that combines both of these effects into a single equation (8.1).

$$M_r = k_1 P_a \left(\frac{\theta}{P_a} \right)^{k_2} \left(\frac{\sigma_d}{P_a} \right)^{k_3} \qquad (8.1)$$

where:

k_1, k_2, k_3 = regression coefficients, with $k_1 > 0$, $k_2 \geq 0$, and $k_3 \leq 0$.
θ = sum of principle stresses or bulk stress ($\sigma_1 + \sigma_2 + \sigma_3$)
P_a = atmospheric pressure, same units as M_r and θ
σ_d = deviator stress, same units as M_r and θ
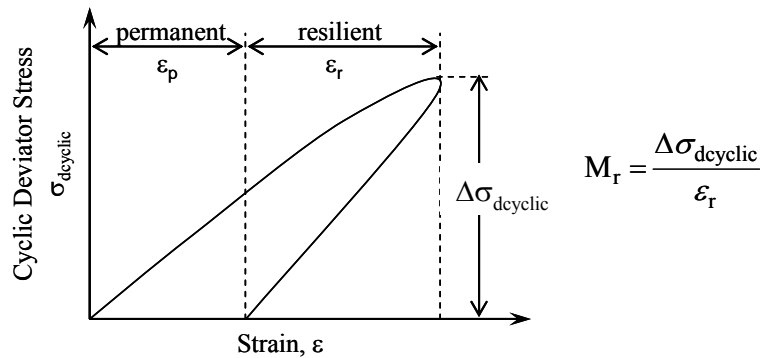
Figure 8.2. Typical stress-strain curve for one loading cycle

A protocol to measure M_r in the laboratory was developed by the Strategic Highway Research Program (SHRP) as LTPP P-46, which was standardized as AASHTO T-307. A revised version of this procedure was released in 2003 as standard protocol NCHRP 1-28. Several modifications were suggested in the new protocol. The most significant of those include application of larger stresses on the specimens, different load pulse durations for base and subgrade materials, and sample preparation methods.

AASHTO T-307 suggests compacting fine-grained cohesive subgrade materials statically in five layers, while the new NCHRP 1-28 procedure implements impact compaction for fine-grained cohesive soils. As an alternate, kneading compaction is suggested in both standards. Vibratory or kneading compaction is suggested for granular materials. However, limited information was found in the literature discussing the influence of compaction type on resilient properties of unbound materials. Elliott and Thornton (1988) found that cohesive soil samples compacted using static compaction have higher resilient modulus than those compacted using kneading

compaction. Results form tests performed on granular materials by Zaman *et al.* (1994) using impact and vibratory compaction methods showed that the compaction type did not significantly influence the resilient modulus. Hoff *et al.* (2004) also indicated that no significant difference was observed between impact, vibratory, and gyratory compaction procedure on M_r of a granular material.

8.2 Objectives and Approach

The primary objectives of this laboratory study were to investigate the relationships between moisture-density, compaction energy, compaction type, and engineering parameter values such as shear strength and resilient modulus. One cohesive soil and one granular soil were selected for this study. The approach to accomplish these objectives involved:

1. Laboratory characterization of soils for index properties,

2. Determining moisture-density relationships using static, impact, vibratory, and gyratory compaction methods with different compaction efforts,

3. Performing resilient modulus (AASHTO T-307) and unconsolidated undrained (UU) shear strength tests on samples compacted using different methods at target moisture contents and densities.

8.3 Test Materials

Materials used in this study include mixed glacial till "sandy lean clay" obtained from the subgrade of test sections 27 and 28 at the MnROAD facility in Albertville, MN, and "well graded sand with silt" material obtained from TH 64 project site located south of Ackley, MN. Index properties of these soils are summarized in Table 8.1. Particle-size distribution curves for these soils are presented in Figure 8.3 and Figure 8.4.

Table 8.1. Index properties of soils used in compaction study

Parameter	Mixed Glacial Till	TH 64 Sand
Material Description	Brown Sandy Lean Clay	Brown Well Graded Sand with Silt
Gravel Content (%) (> 4.75mm)	2	5
Sand Content (%) (4.75mm – 75µm)	37	84
Silt Content (%) (75µm – 2µm)	38	6
Percent Clay Content (%) (<2µm)	22	5
Coefficient of Uniformity (c_u)	—	6.3
Coefficient of Curvature (c_c)	—	1.5
Liquid Limit, LL (%)	32	Non-Plastic
Plasticity Index, PI	19	Non-Plastic
Specific Gravity, Gs	2.69	2.66
AASHTO Classification	A-6 (5)	A-3
Unified Soil Classification (USCS)	CL	SW-SM
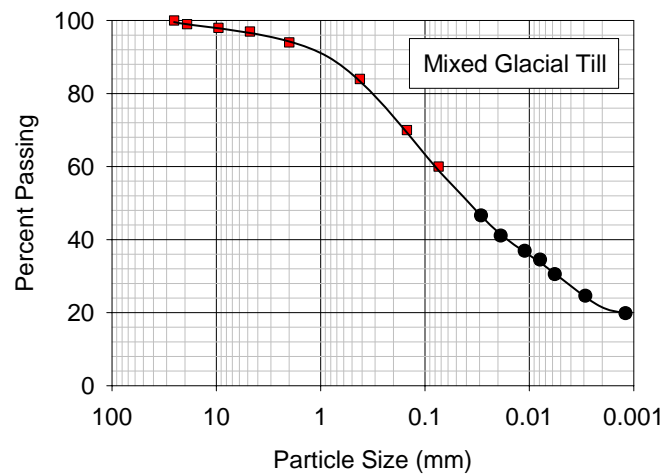
Figure 8.3. Particle-size distribution curve of mixed glacial till material
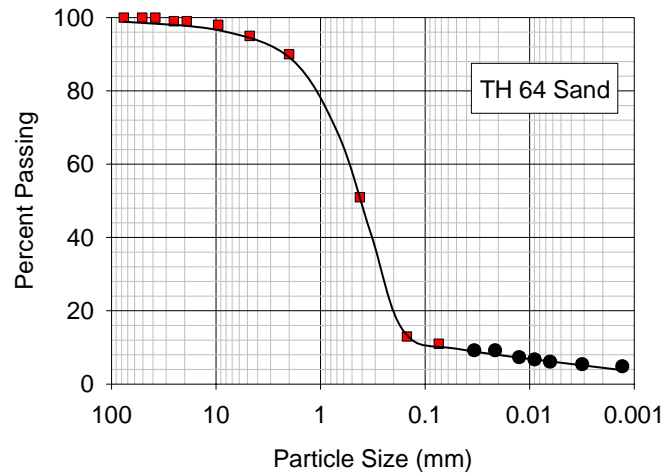
Figure 8.4. Particle-size distribution curve for TH 64 sand

8.4 Compaction Test Results

Procedures to perform laboratory compaction tests using different compaction methods and to determine compaction energies are described in Chapter 2. Relationships between moisture content, dry unit weight, and compaction energy imparted by the different compaction methods for the two selected soils are discussed here.

During static compaction, load and deformation data were recorded. Based on the deformation data, compacted volumes at different load levels were calculated. This way, the relationship between compaction energy and dry unit weight at a particular moisture content is obtained from each test. Similarly, for vibratory compaction, in addition to measuring the deformation after 8 min (according to ASTM D4253), readings were taken at several intervals between 0 and 16 minutes. With this information, compacted volumes at different times were calculated and related to compaction energy and dry unit weights. Results of only select energy levels (for static and vibratory) are presented for clarity. Impact compaction tests were performed at standard Proctor, modified Proctor, and one low, and two intermediate energies. Different energies for each compaction method at which the results are presented are summarized in Table 8.2. Compaction energies for gyratory test could not be determined (see discussion in Chapter 2), and therefore, results are presented below as a function of number of gyrations.

Table 8.2. Compaction energies for different compaction methods

No.	Compaction Energy (kN-m/m^3)		
	Impact	Static	Vibratory
1	0	0	0
2	356	20	10
3	592	50	50
4	996	200	500
5	1660	400	2000
6	2696	600	—

8.4.1 Mixed Glacial Till

Moisture-density relationships for selected compaction energies using impact, static, and vibratory methods are shown below. For static and impact methods, results for "zero" compaction energy were obtained by loosely placing moist soil in the compaction mold in one lift. For vibratory compaction, the minimum index density determined by ASTM D 4254 is reported at "zero" compaction energy. Note that the sample sizes for static and impact compaction methods are similar (101.6 mm diameter), while vibratory compaction was performed on 152.4 mm diameter samples.

Impact Compaction

Figure 8.5 illustrate that for the mixed glacial till soil the higher the impact compaction energy the higher the maximum dry unit weight and lower the optimum moisture content. The curves on the wet side of optimum generally tend to parallel the zero air void line (100% saturation). The points of optimum moisture content at each energy level also tend to parallel the zero air void line. These relationships are common for fine-grained soils subject to impact compaction tests.

Figure 8.6 shows the laboratory compaction energy required to achieve selected target relative compaction values (95%, 98%, and 100% standard Proctor, and 98% and 100% modified Proctor relative compaction) as a function of moisture content. Results plotted in such a manner allow for determination of the "compactability zone". This zone represents the minimum required impact energy and its corresponding moisture content range to achieve the target relative compaction value. For example, for this soil, the minimum energy required to achieving at least 95% of standard Proctor density is approximately 356 kN-m/m^3 (about 60% of standard Proctor energy), at moisture contents between about 15% and 19% (about 0% to 4% above standard

Proctor optimum moisture content). Also indicated in Figure 8.6 is the region of the plot where soil conditions are susceptible to "over-compaction". In this area of the compaction curve, applying additional compaction energy does not increase the relative compaction value and can often result in development of unwanted shear planes and excess pore pressures.
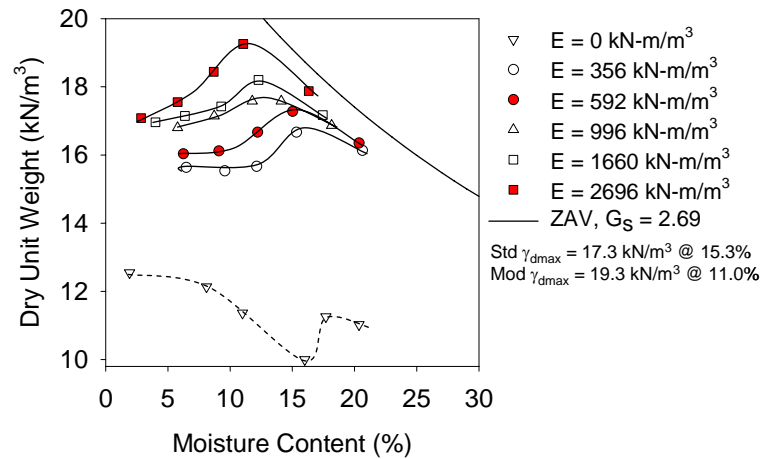
Figure 8.5. Moisture-density curves for different "impact" compaction energies for mixed glacial till
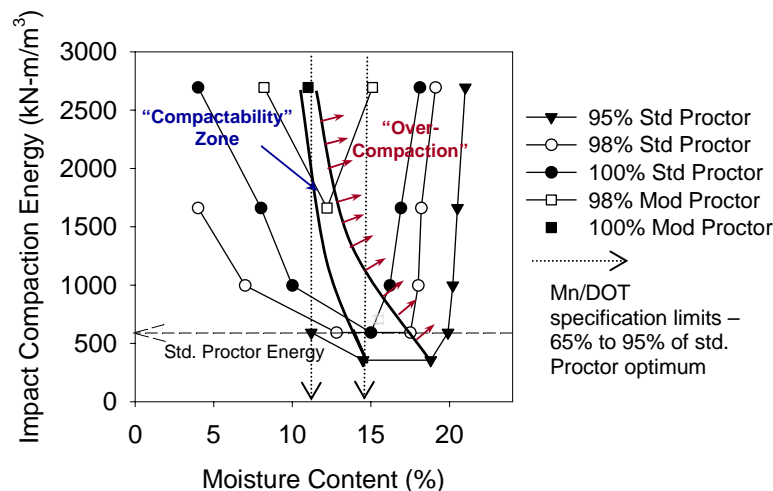
Figure 8.6. Relationship between impact compact energy and moisture content at target dry densities for mixed glacial till

Figure 8.7 shows the dry unit weight growth curves as a function of compaction energy at selected moisture contents. Plotting the results in these terms shows that below standard Proctor compaction energy, the dry unit weight is higher for moisture contents close to standard Proctor optimum or slightly wet of optimum. Between standard Proctor compaction energy and modified Proctor compaction energy, the growth curves show that at high moisture contents, no increase in dry unit weight is realized, while at low moisture contents dry unit weight increases almost linearly with increasing compaction energy.

174
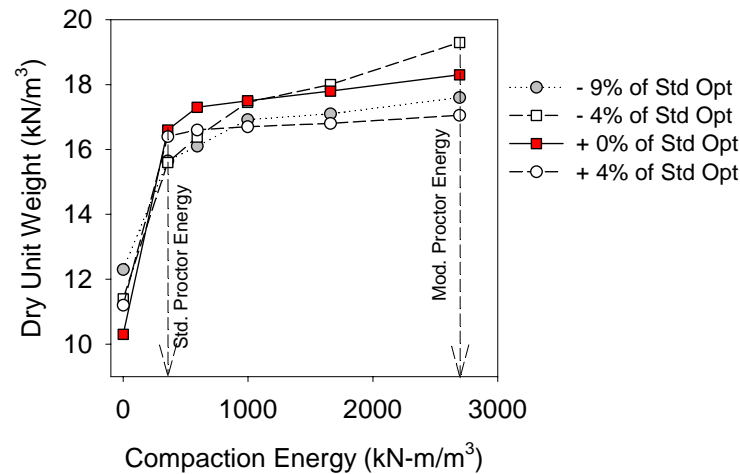
Figure 8.7. Relationship between dry unit weight and compaction energy at different moisture contents for mixed glacial till

Static Compaction

The moisture-density curves from static compaction tests at different energies are shown in Figure 8.8. The results show that increasing the static compaction energy increases the maximum dry unit weight. Optimum moisture contents are not observed in the range of moisture contents used in the tests. With increase in moisture, the compaction energy required to achieve a dry unit weight tends to decrease. In contrast with impact compaction curves, for this soil at >50 kN-m/m^3 static compaction energy the curves tend to approach the zero air void line as the moisture increases. Very similar phenomenon was observed by Bell (1977), and Zhang *et al.* (2000). Data showing load versus deformation curves (*see* Figure 8.9) show noticeably different shapes of the compaction energy curves as the moisture increases.
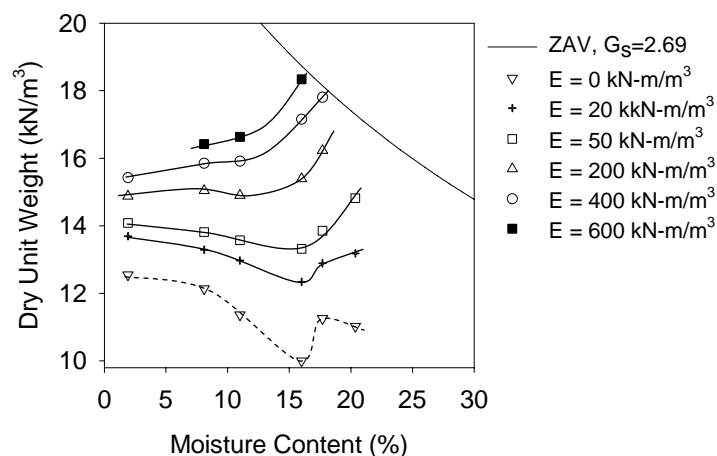
Figure 8.8. Moisture-density curves for different "static" compaction energies for mixed glacial till
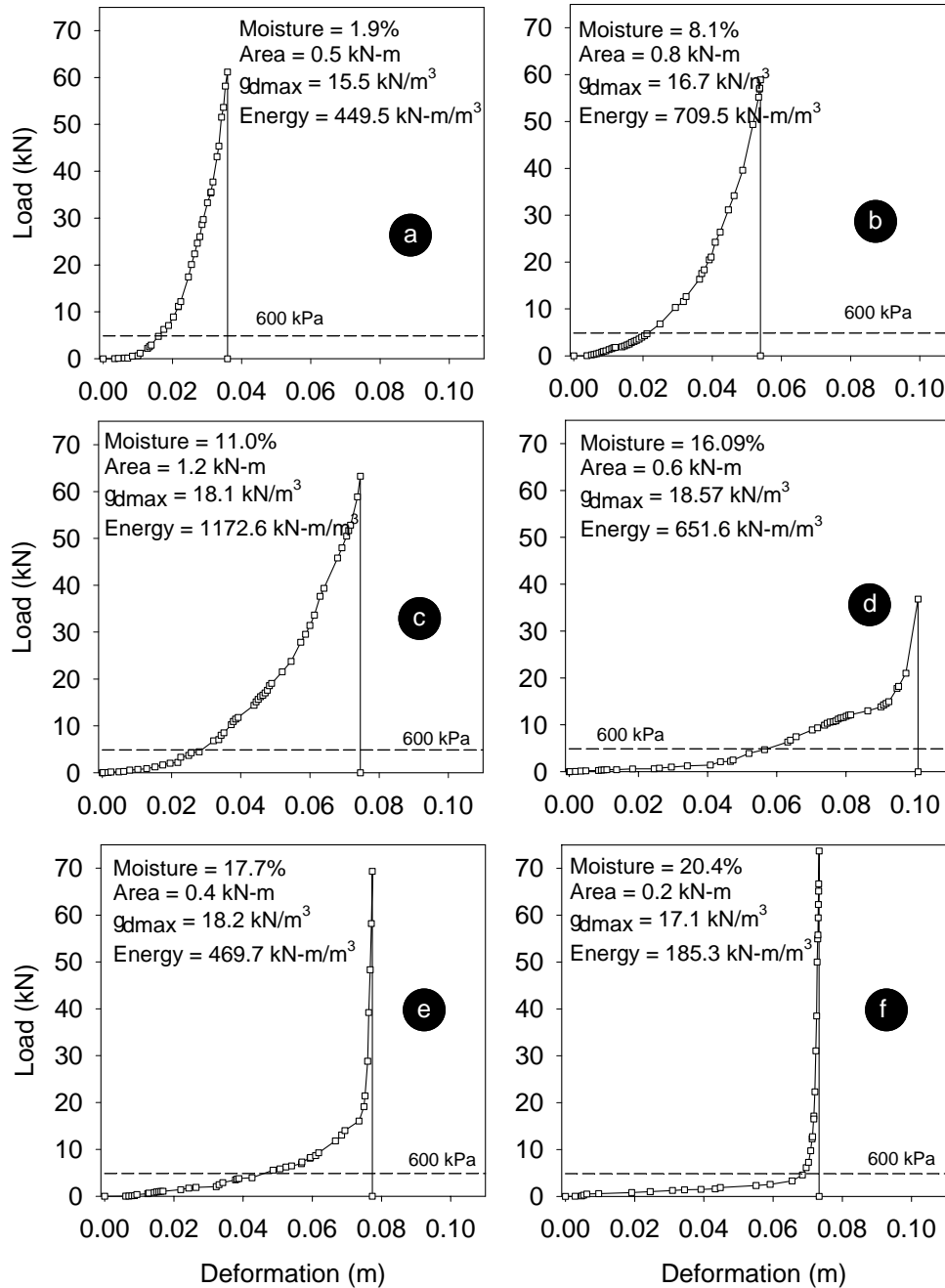
Figure 8.9. Load versus deformation curves during static compaction test at different moisture contents for mixed glacial till

Vibratory Compaction

Figure 8.10 illustrates the moisture-density relationships at different vibratory compaction energies. Results from the standard 8 min vibration time are also shown. The compaction energy imparted at 8 min depends on the volume of the compacted sample; therefore, the range of energy is also shown. Unusual moisture density curves are observed from this test. The

176

densities generally decreased up to about 15% moisture content (which is close to standard Proctor optimum moisture content) and then increased thereafter up to about 23% and then again decreased with increasing moisture content. The curves above 23% moisture content tend to parallel the zero air void line. Low densities at moisture contents dry of optimum moisture are typically observed in granular sands due to "bulking" phenomenon. This phenomenon is not typically expected for fine-grained cohesive soils. The dry unit weights increased significantly with increased compaction energy from 0 to 50 kN-m/m^3 at all moisture contents, and thereafter no noticeable increase was observed. This trend can be seen in Figure 8.11, where at least 95% to 98% of the maximum dry unit weight (at that particular moisture content) is achieved within less than 1 min. A maximum dry unit weight of 16.51 kN/m^3 was achieved for the air dry sample at 2.7% moisture, which is about 95% of the standard Proctor maximum dry unit weight.

Webster (1984) performed similar tests using a vibratory compactor instead of a vibratory table on fine-grained cohesive soils (soil classified as CL), and showed a similar moisture-density curve as found in this study with maximum densities at air dry moistures.
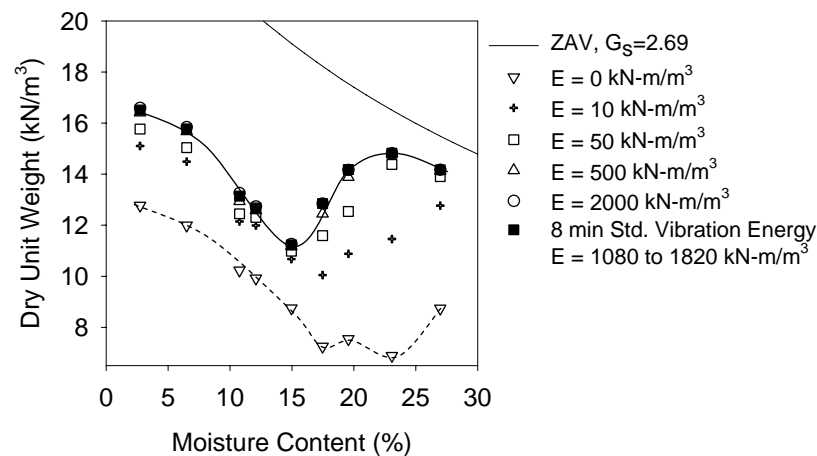
Figure 8.10. Moisture-density curves for different "vibratory" compaction energies for mixed glacial till
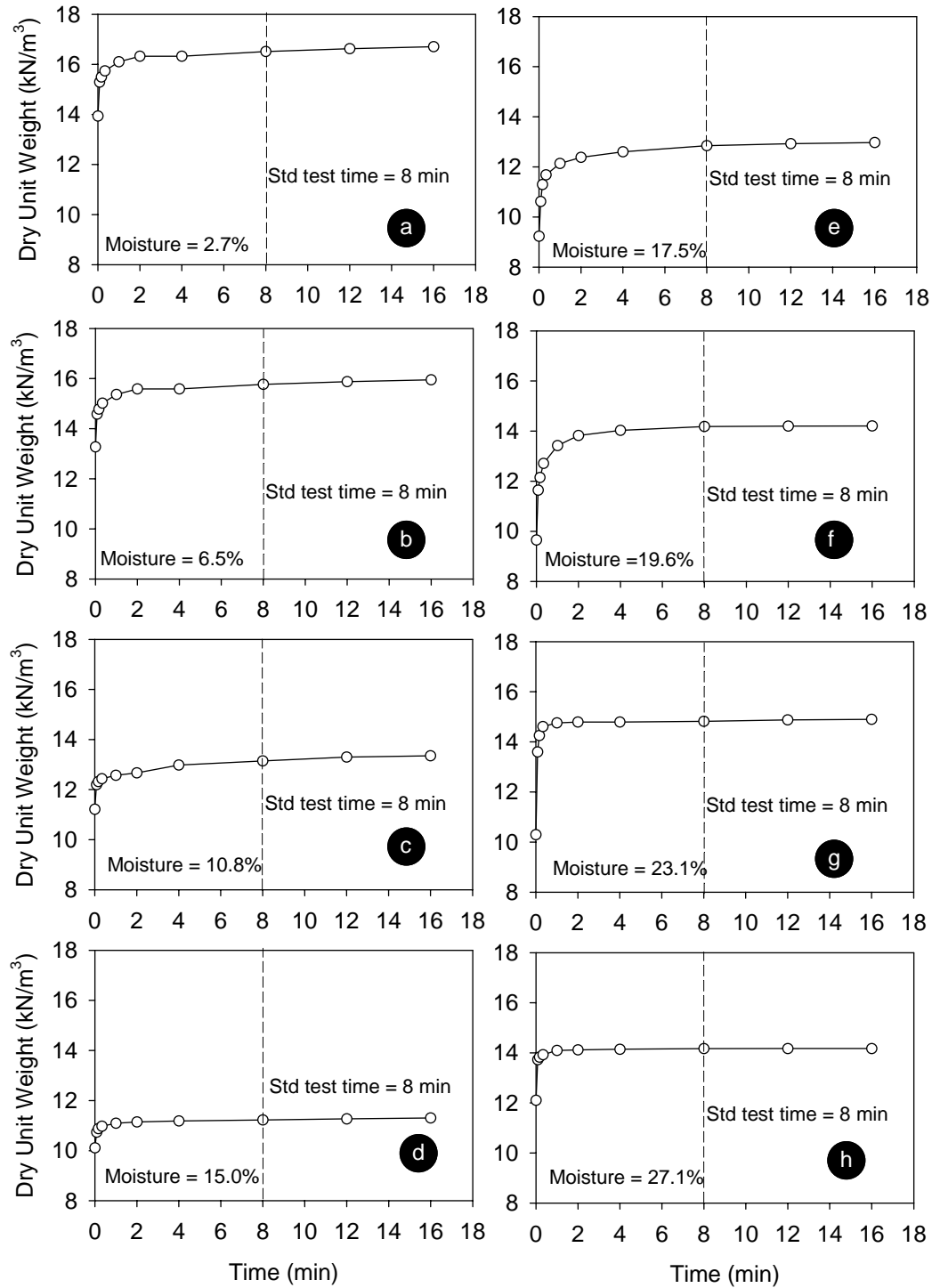
Figure 8.11. Increase in dry unit weight with time in vibratory compaction test at different moisture contents for mixed glacial till

178

Gyratory Compaction

The moisture-dry unit weight curves from gyratory compaction tests as a function of number of gyrations (0 to 50) are shown in Figure 8.12. Note that at "0" gyrations a static pressure of 600 kPa is applied on the sample. Maximum dry unit weight and optimum moisture content at 50 gyrations are noted on Figure 8.12. The maximum dry unit weight observed is about 109% standard Proctor γ_{dmax} and 103% modified Proctor γ_{dmax}, and the optimum moisture content is about -2% of standard Proctor optimum +2% of modified Proctor optimum moisture contents. Density growth curves at different moisture contents are presented in Figure 8.13. The results show that dry unit weight increases with the number of gyrations at all moisture content; however, dramatic changes in the rate of increase in dry unit weights are noticed with changes in moisture content. For example, the dry unit weight at w = 14.7% (close to optimum) tends to level off after about 10 gyrations and at w = 18.1% tends to level off within in < 10 gyrations, while at w = 10.9% the dry unit weight increases rapidly after 10 gyrations and almost linearly from about 20 to 50 gyrations.
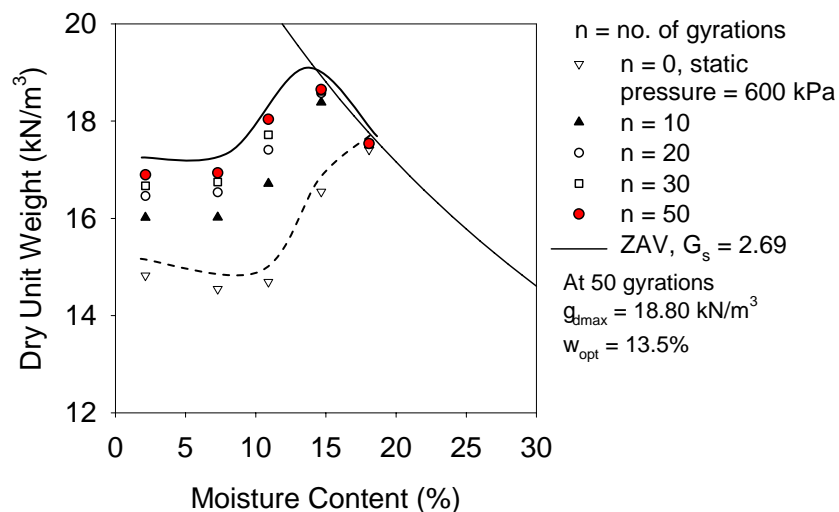
Figure 8.12. Moisture-density curves for mixed glacial till using gyratory compaction test at various number of gyrations
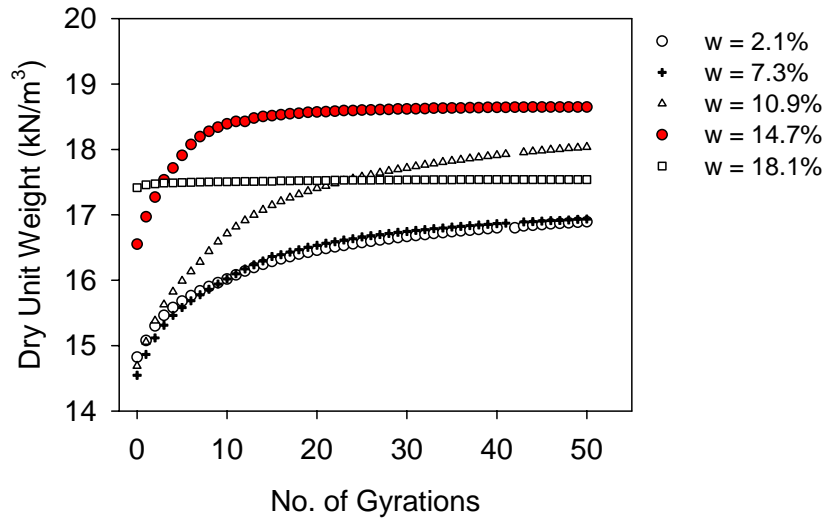
Figure 8.13. Dry unit weight growth curves using gyratory compaction test for mixed glacial till

Comparison and Discussion

Figure 8.14 shows comparison density growth curves as a function of compaction energy on a volume basis for static, impact, gyratory, and vibratory methods at – 3%, 0%, and +2.5% of standard Proctor optimum moisture content. Results show that for standard Proctor to modified Proctor energy the density growth at wet of optimum conditions is not significant, while at dry of optimum, dry unit increases with increasing impact compaction energy following the trend of a linear-rate function. The density growth curves for static compaction follows closely with the impact compaction curves at dry of optimum moisture content, but deviates as the moisture content increases. No significant growth in dry unit weight is realized with increase in vibratory compaction energy over 50 kN-m/m^3. The vibratory method resulted in consistently low dry unit weights.

Also shown on Figure 8.14 are the density growth curves from the gyratory compaction test as a function of number of gyrations. The curves generally follow the path of static compaction. The maximum dry unit weights achieved after 50 gyrations are greater than the standard Proctor and lower than the modified Proctor dry unit weights at the three moisture contents.

The compaction energy needed to achieve at least 95% of standard Proctor maximum density by static and impact methods is presented in Figure 8.15. This figure demonstrates that the required static and impact compaction energies to achieve this density decreases almost linearly on the dry side of optimum. On the wet side of optimum, the impact compaction energy required increases due to greater remolding of the soil. On the other hand, the required static compaction energy decreases as the moisture content increases. This figure also shows that at close to standard Proctor optimum moisture content (i.e. within 0% to -2%), the static and impact compaction energies required is similar. When the soil is dry or wet of optimum, the required static compaction energy is lower than the impact compaction energy.

180

Figure 8.16 shows the static compaction energy required to achieve the standard Proctor moisture-density relationship. Obviously, the standard Proctor energy is constant (592 kN-m/m^3). The figure shows that the required static compaction energy is consistently lower than the impact compaction energy at any moisture content; however, the phenomenon on the dry and wet side of standard Proctor optimum moisture content is different. On the dry side of optimum (up to about -2% of optimum), the static compaction energy required is almost constant, and then with increase in moisture content the required compaction energy decreases substantially.
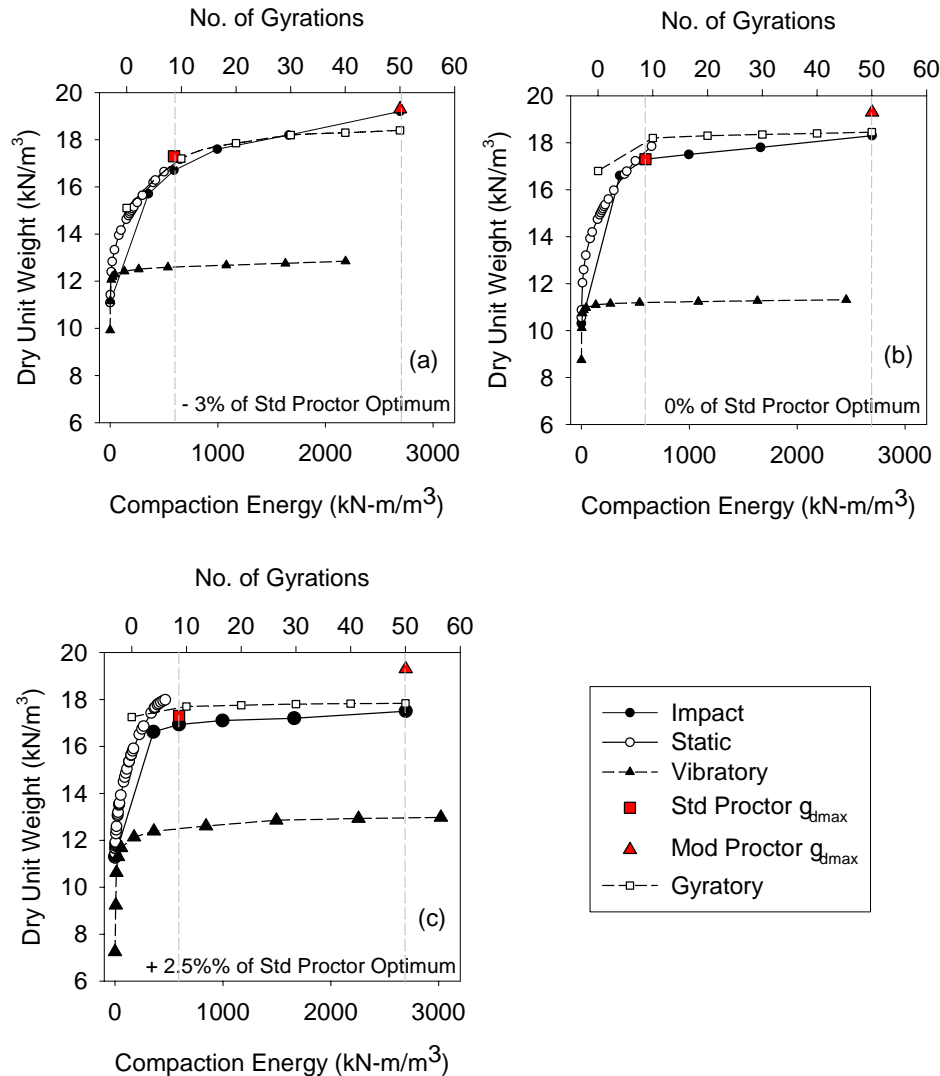
Figure 8.14. Comparison of relationship between dry unit weight and impact, static, and vibratory compaction energy for mixed glacial till at (a) dry of optimum, (b) optimum, (c) wet of optimum moisture content from standard Proctor test
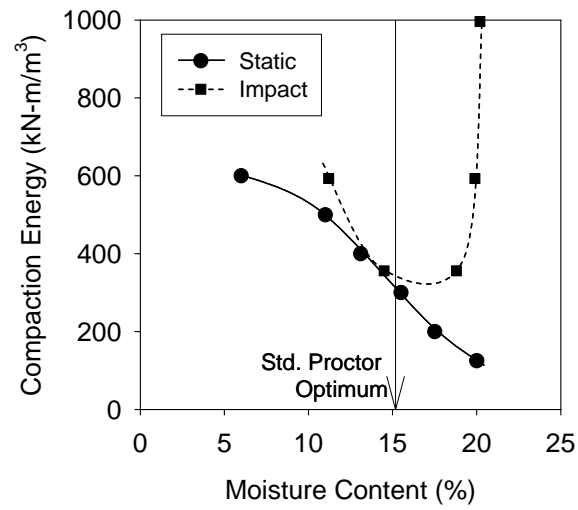
Figure 8.15. Compaction energy (static and impact) required to achieve 95% γ_{dmax} of standard Proctor test
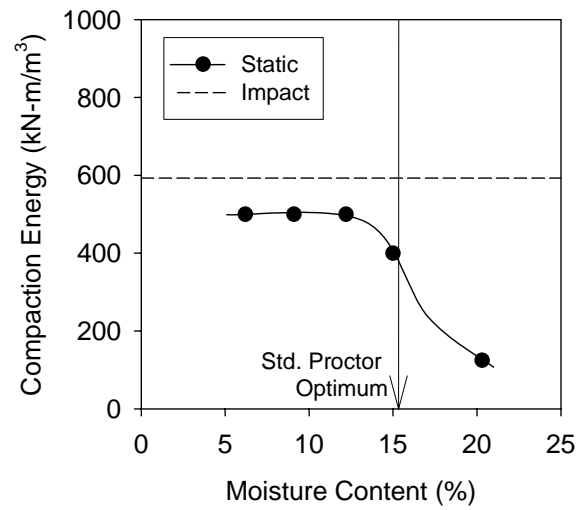
Figure 8.16. Static compaction energy required to achieve standard Proctor densities at various moisture contents

8.4.2 TH 64 Sand

Moisture-density relationships as a function of compaction energy using impact, static, gyratory, and vibratory methods are shown below for the TH64 sand. For static and impact methods, results for "zero" compaction energy were obtained by loosely placing the moist material in the compaction mold. For vibratory compaction, the minimum index density determined using ASTM D 4254 is reported at "zero" compaction energy. Note that the sample sizes for static and impact compaction methods were similar (101.6 mm diameter), while vibratory compaction was performed using a 152.4 mm diameter sample.

Impact Compaction

Figure 8.17 shows the relationship between moisture content and dry unit weight as a function of compaction energy for the impact compaction method. No significant variations in density with increasing moisture content and compaction energy was observed. Maximum dry unit weight determined by modified Proctor method ($E = 2694$ kN-m/m^3) is only about 102% of maximum dry unit weight determined by standard Proctor method ($E = 593$ kN-m/m^3). "Bulking" phenomenon is noticeable at "zero" compaction energy at about 6% moisture content. Although not as significant, "bulking" phenomenon is also observed at other compaction energies at close to 6% moisture content.
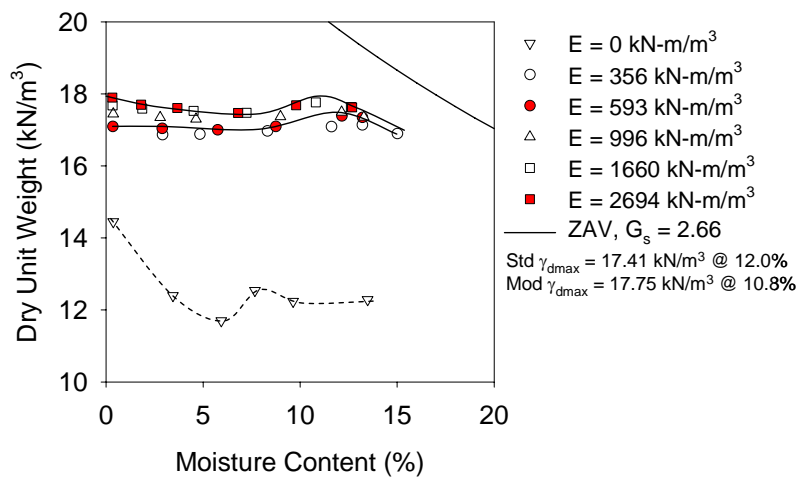
Figure 8.17. Moisture-density curves for selected impact compaction energies for TH 64 sand

Static Compaction

The moisture-density curves from static compaction tests are shown in Figure 8.18. As expected, this data shows that dry unit weight increases with increasing static compaction energy. Porter (1930) reported that with the Porter SOP static compaction test device with a static pressure of about 13,800 kPa, the moisture-density results were similar to impact compaction tests. The maximum stress applied in the current study varied between 6150 to 9250

kPa. Higher stresses were not attempted with the current setup. Load versus deformation curves for different moisture contents are presented in Figure 8.19.
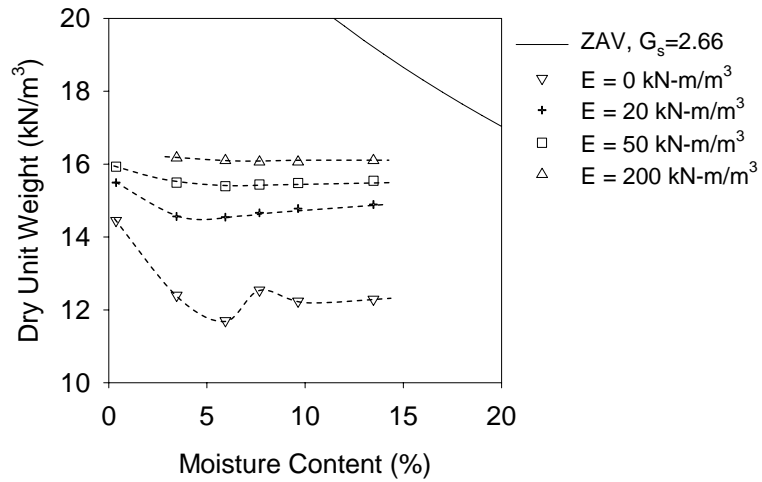
Figure 8.18. Moisture-density curves for selected static compaction energies for TH 64 sand
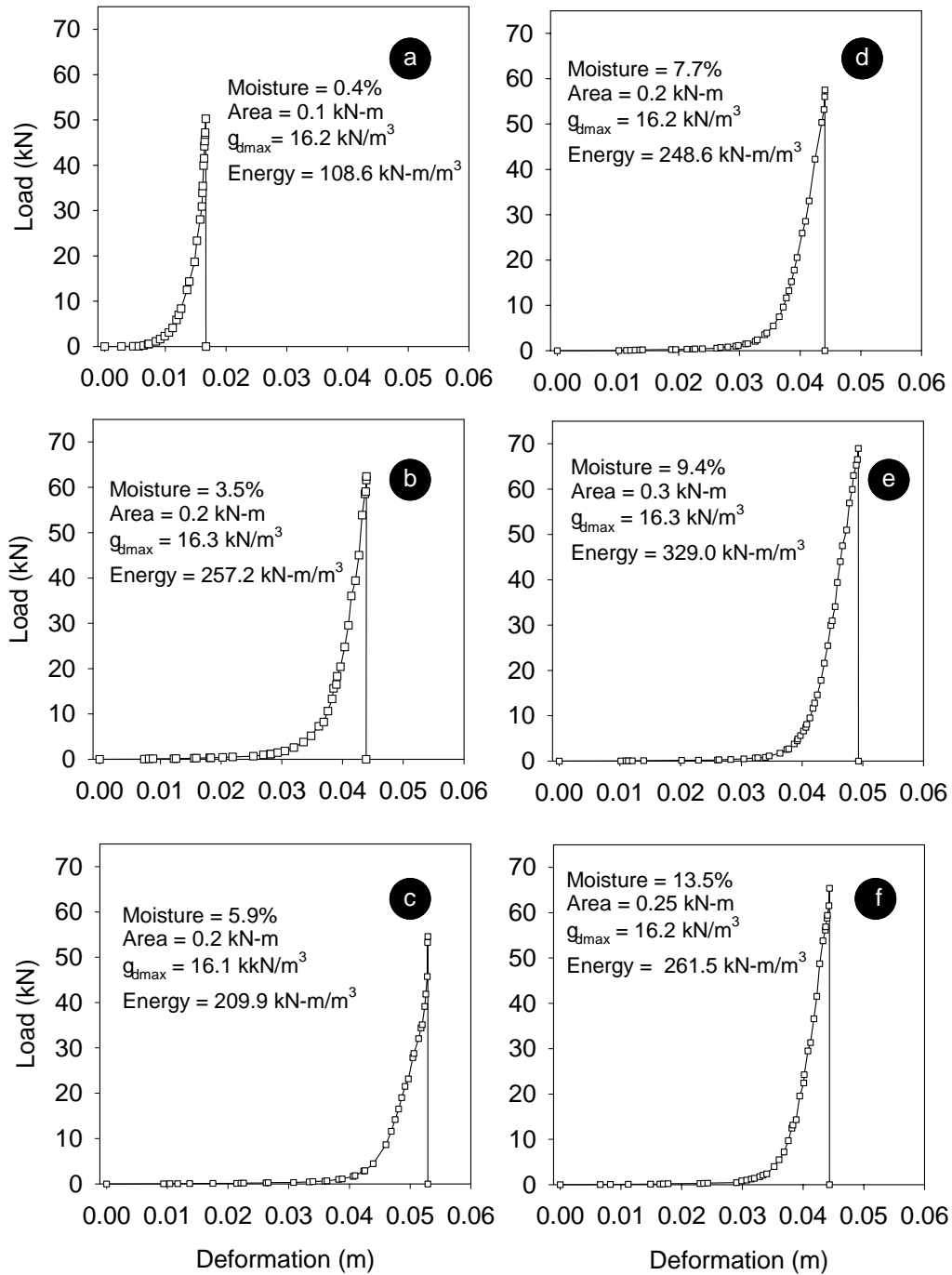
Figure 8.19. Static compaction load versus deformation curves for TH 64 sand

185

Vibratory Compaction

Figure 8.20 illustrates the moisture-density curves for a range of compaction time intervals using vibratory compaction. Results from the standard 8 min vibration time are also shown. Bulking phenomenon at about 6% moisture content can be observed. The maximum and minimum dry unit weights from the tests are noted. Density growth curves with increasing vibration compaction time at selected moisture contents are shown in Figure 8.21.

Results show that dry unit weight increases significantly with increasing compaction energy (or compaction time) from 0 to 200 kN-m/m^3 at any moisture content, and thereafter no significant increase is observed. This can also be seen in Figure 8.18, where at least 95% to 97% of the maximum dry unit weight (at that particular moisture content) is achieved within less than 1 min of vibration time.
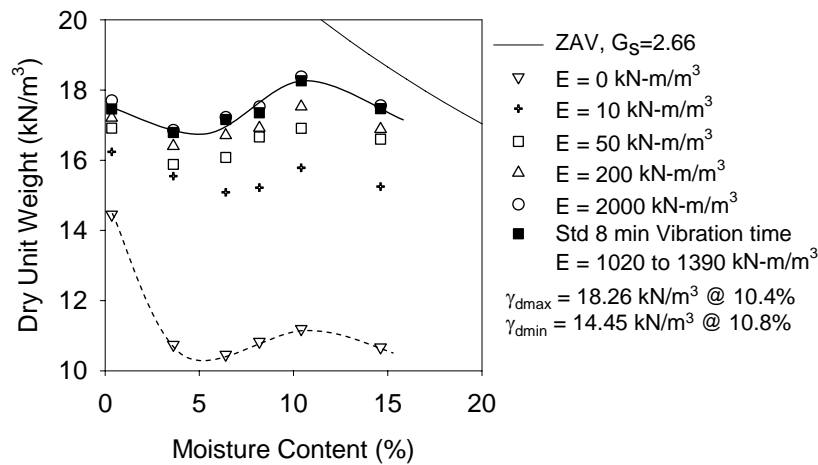
Figure 8.20. Moisture-density curves for selected vibratory compaction energies for TH 64 sand
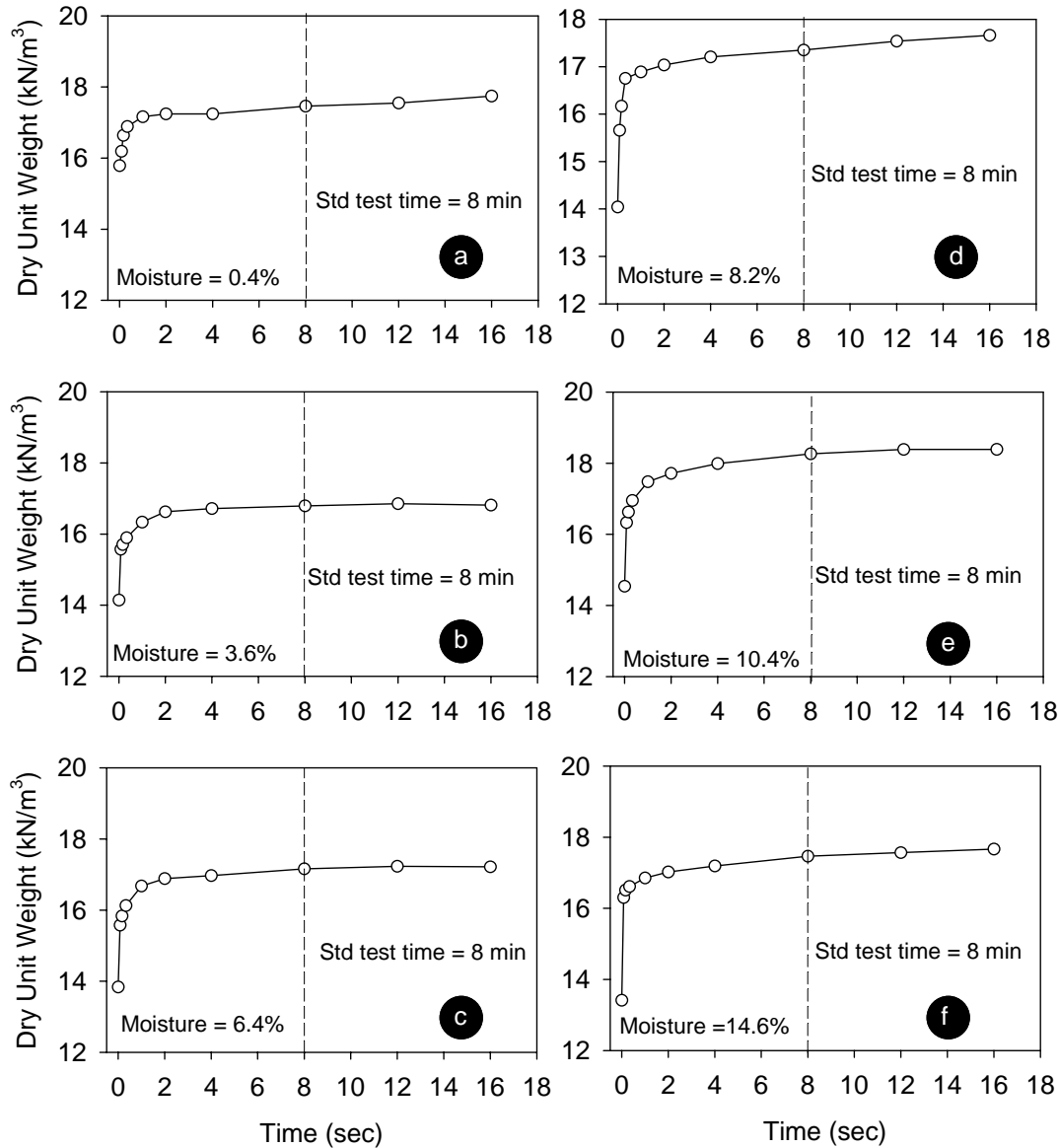
Figure 8.21. Vibratory compaction curves for TH 64 sand

Gyratory Compaction

The moisture-dry unit weight curves from gyratory compaction tests as a function of number of gyrations are shown in Figure 8.22. Note that at "0" gyrations a static pressure of 600 kPa is applied on the sample. Maximum dry unit weight and optimum moisture content at 50 gyrations are noted on Figure 8.22. The maximum dry unit weight observed is about 105% of standard Proctor γ_{dmax} and 103% of modified Proctor γ_{dmax}, and the optimum moisture content is about -1% of standard Proctor optimum and close to modified Proctor optimum moisture contents. "Bulking" phenomenon is not noticeable in the moisture-dry unit weight curves. Density growth curves at different moisture contents are presented in Figure 8.23. The results show that dry unit weights increases with increasing number of gyrations. The rate of increase in dry unit weight is related to the moisture contents.
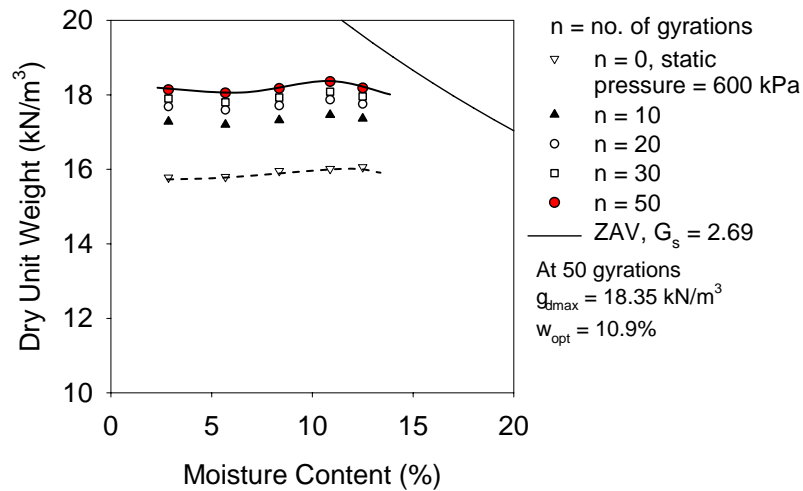
Figure 8.22. Gyratory compaction test moisture-density curves for TH 64 sand
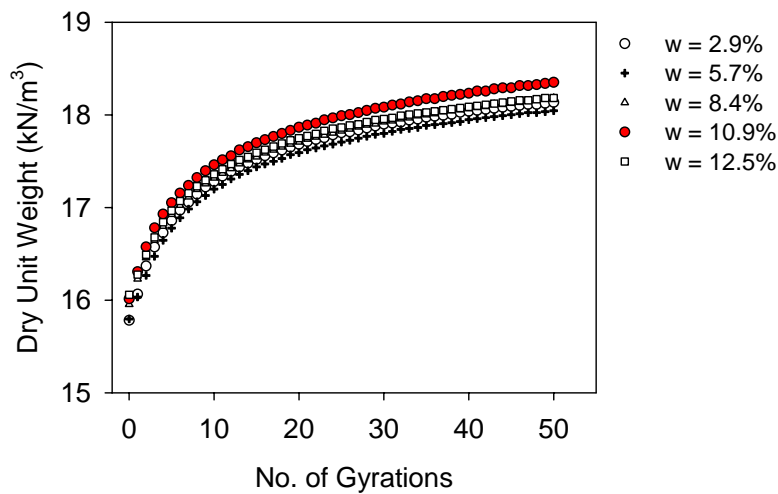
Figure 8.23. Gyratory compaction test dry unit weight growth curves for TH 64 sand

Comparison between different methods

Figure 8.24 shows density growth curves relating to compaction energy comparing static, impact, and vibratory methods at – 3%, 0%, and +2% of standard Proctor optimum moisture content. Results show that there is no significant density growth with an increase in impact compaction energy above 356 kN-m/m^3 (lower than standard Proctor). The shape of the density growth curves with vibratory compaction appears to closely match the impact compaction curves. No significant growth in dry unit weight is realized with an increase in vibratory

compaction energy over 200 kN-m/m^3. At 3% dry of optimum and optimum moisture contents, the densities achieved with vibratory compaction are slightly greater than impact compaction densities. Wet of optimum, no significant difference was observed between impact and vibration compaction. The densities achieved with 200 kN-m/m^3 of static compaction energy are lower than the densities achieved using standard impact and vibratory compaction methods.

Also shown in Figure 8.24 are the density growth curves from gyratory compaction as a function of number of gyrations. Although it is more logical to interpret and compare these results with other compaction methods in compaction energy terms, it appears that the curves generally follow the path of static compaction density growth curves. The maximum dry unit weights achieved after 50 gyrations are greater than the standard and modified Proctor dry unit weights at the three moisture contents.

The compaction energy needed to achieve 100% standard Proctor maximum density at various moisture contents by impact and vibratory methods is presented in Figure 8.25. Results show that the required vibratory compaction energy to achieve 100% standard Proctor density between 1.5% and 7.5% moisture content increases by at least 10 times. With increase in moisture from 7.5 to 11%, the amount of vibratory energy required decreases to about 100 kN-m/m^3. On the other hand, with impact compaction, the energy required to achieve the target density remained constant up to about 9% moisture content, and then decreases at optimum moisture content. On the wet side of optimum, the required impact compaction energy increases almost linearly.

Figure 8.26 shows the vibratory compaction energy required to achieve standard Proctor moisture-density relationship (592 kN-m/m^3). Results show that the required vibratory compaction energy is high within the moisture content range of 4% to 6% and low at other moisture contents. As explained earlier, with the bulking moisture content close to 6%, high capillary stresses inhibit compaction.
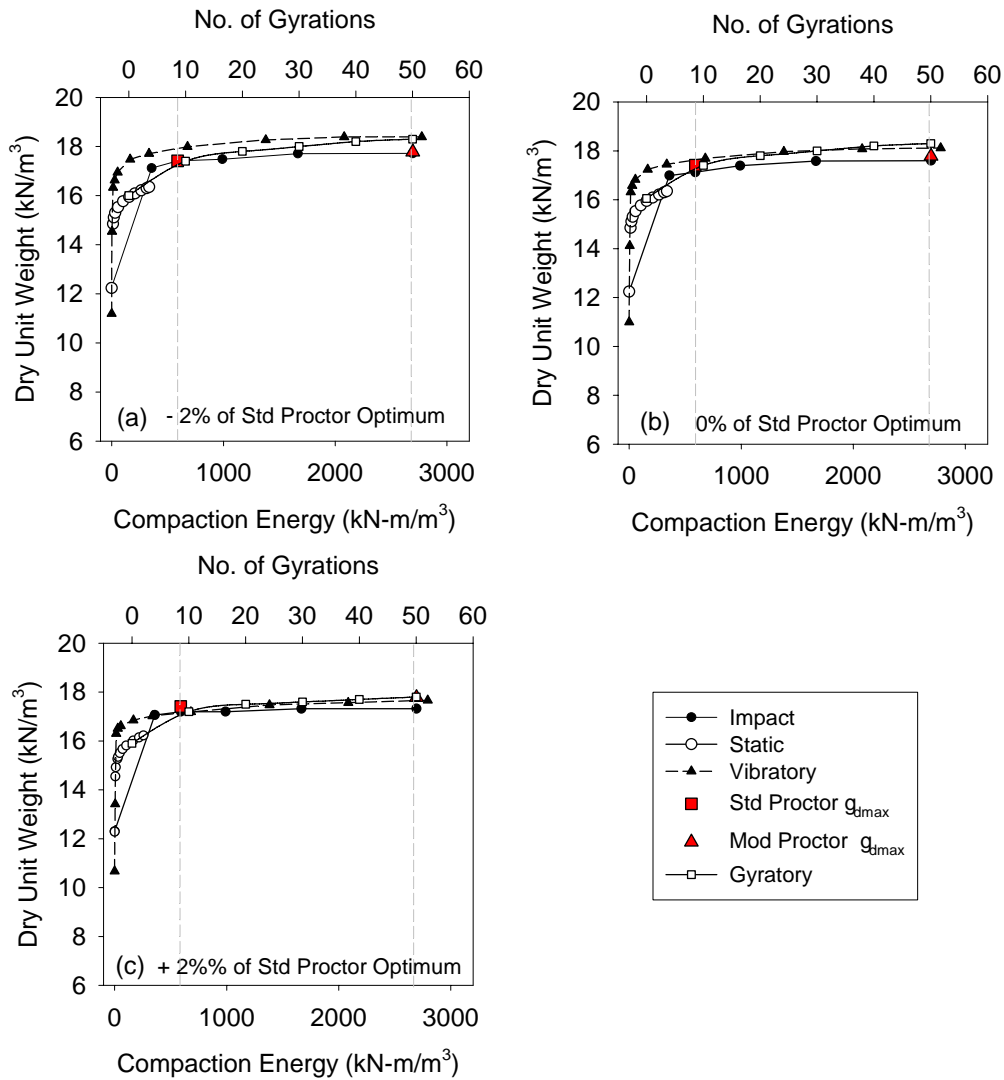
Figure 8.24. Comparison of relationship between dry unit weight and impact, static, and vibratory compaction energy for TH 64 Sand at (a) dry of optimum, (b) optimum, (c) wet of optimum moisture content from standard Proctor test
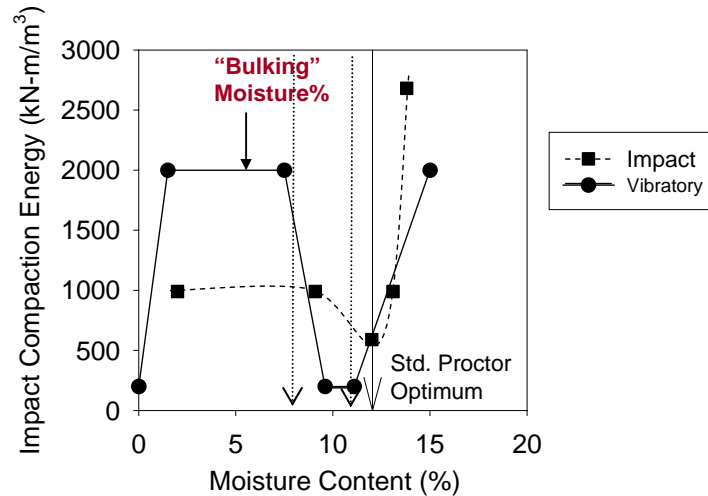
Figure 8.25. Compaction energy (static and impact) required to achieve 95% γ_{dmax} of standard Proctor test
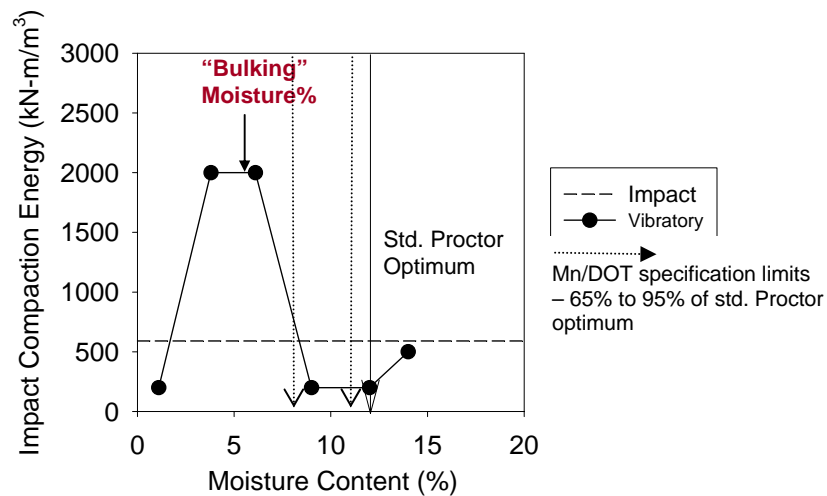
Figure 8.26. Static compaction energy required to achieve standard Proctor densities at various moisture contents

8.4.2 TH 64 Sand Laboratory versus Field Compaction

The sand used in this study was obtained from the roadway subgrade of the TH 64 project at about Sta. 70+00. Mn/DOT and ISU crews performed field density measurements in the vicinity of the sample location. A summary of the field test results are presented in Table 8.3. The field measurements are plotted in Figure 8.27 along with dry unit weight curves from standard and modified Proctor, vibratory compaction, and static compaction at E = 200 kN-m/m³.

191

Table 8.3. Comparison of field and laboratory dry unit weights

Station	Dry Unit Weight (kN/m3)	Moisture (%)	Moisture Method	Relative Compaction (%)		
				Std Impact	Mod Impact	Vibratory
74+00	16.9	5.5	Speedy	96.8	95.0	92.3
71+37	21.5	6.8	Speedy	123.4	121.1	117.7
69+00	17.2	6.9	Nuke	98.6	96.7	94.0
69+50	17.1	5.3	Nuke	98.2	96.3	93.6
70+00	17.2	3.7	Nuke	98.9	97.0	94.3
70+50	16.7	8.4	Nuke	96.2	94.3	91.7
71+00	16.9	7.9	Nuke	97.1	95.2	92.6
71+50	17.7	9.1	Nuke	101.7	99.7	97.0
72+00	17.6	9.8	Nuke	101.3	99.4	96.6
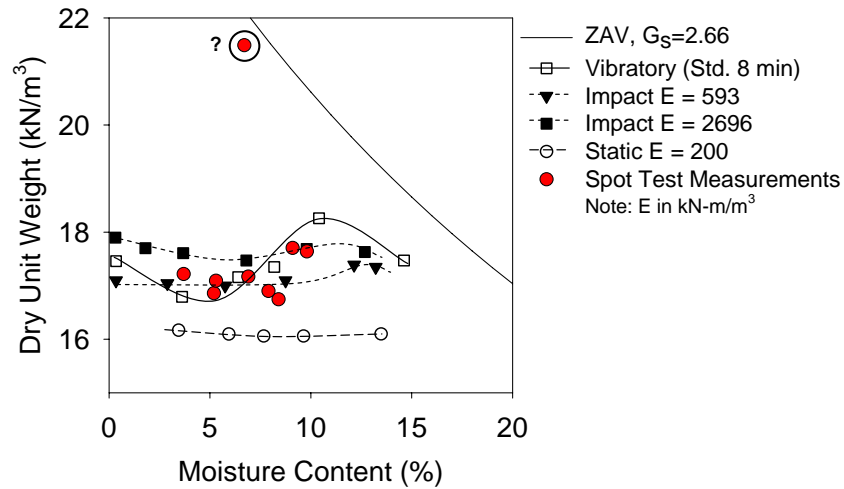
Figure 8.27. Static compaction energy required to achieve standard Proctor densities at various moisture contents

Figure 8.27 shows that the field densities match closely with the laboratory densities determined by vibratory and impact methods. The density curve from static method is lower than other methods and also densities observed in field, thus indicating the inadequacy of the method within the applied energies to compact the soil representing field densities.

8.5 Resilient Modulus Test Results

Resilient modulus tests and UU shear strength tests were conducted on the two selected soils following the AASHTO T-307 standard procedure. Specimens were compacted to target moisture contents and dry unit weights using different compaction methods. Static, impact, and vibratory compaction methods were used for the glacial till material and impact and vibratory method for the TH 64 sand.

Different loading sequences are suggested in the AASHTO standard for cohesive subgrade soils and granular base course materials. For the mixed glacial till material, the loading sequences for cohesive soils was used, and for TH 64 sand the loading sequences for granular materials was used. For all samples, the conditioning sequence was kept constant as 1000 load cycles. A brief overview of sample preparation methods and laboratory setup is presented in Chapter 2.

Results for the mixed glacial till and TH 64 sand materials are discussed below. Regression coefficients presented are based on the Witczak and Uzan (1988) "universal" model shown in equation 8.1.

8.5.1 Mixed Glacial Till

Samples were compacted to achieve a target of 100% standard Proctor maximum density (17.3 kN/m^3) at moistures -3%, 0%, and +3% of optimum moisture content (15.3%). Table 8.4. provides the dry unit weights achieved for the triaxial M_r samples. The average M_r value was calculated as the mean of the values resulting from fifteen loading sequences and is reported in this table along with its coefficient of variation (COV). Witczak and Uzan (1988) model coefficients k_1, k_2, k_3 and the R^2 value for the model are provided in Table 8.4. Results for all M_r values for each sequence and all tests are provided in Appendix I.

Plots of deviator stress versus resilient modulus are shown in Figure 8.28 to Figure 8.30 for the selected moisture contents. Figure 8.31 shows the change in average M_r as a function of moisture content and compaction method. On average, M_r for statically compacted samples is lower than that for samples compacted using impact or vibratory compaction. This difference is substantial on the dry side of optimum moisture content. The static compaction sample resulted in lower M_r values by a factor of two time compared to impact or vibratory methods. On the wet side of optimum, the impact and static compaction specimens have similar M_r values, while vibratory compaction produced M_r values about 1.3 times higher than the other two methods. No significant difference in M_r was realized between impact and vibratory compacted samples.

Measurements of maximum shear strength, τ_{max}, are shown in Table 8.4. Figure 8.32 shows the change in shear strength with increasing moisture content for the various compaction methods. The static compaction specimens have consistently lower shear strengths (about 1.2 to 1.4 times) than impact compaction specimens. Bell (1977) also found that static compaction specimens result in lower strengths. Although the average M_r values for impact and vibratory compaction

samples were similar on the dry side of optimum, the τ_{max} of vibratory compaction sample was lower than that of the impact compaction samples. No significant differences are observed between these two compaction methods on the wet side of optimum.

The differences in τ_{max} and M_r between the compaction methods is likely due to variations in the resulting soil structure and potential differences of pore pressures in the specimen resulting from compaction. According to Lambe and Whitman (1969) different compaction methods can affect the total stresses and pore pressures within a compacted soil, which can alter the strength properties of the soil. Based on tests on compacted kaolonite, Lambe (1961) found that at a given density and moisture content the negative pore pressures developed in the sample compacted by static compression are greater than those compacted using kneading method.

For all compaction methods, the mean M_r decreased with increasing moisture content with one exception, which was for samples compacted using the static method. The static compaction samples yielded average M_r from dry of optimum to optimum moisture content that were similar, but showed a trend of decreasing M_r with increasing moisture content above optimum. The average M_r for impact and vibratory compaction samples decreased by about 1.5 and 2.0 times with increasing moisture from about -3% to +3% of optimum moisture content. The τ_{max} values decreased linearly with increasing moisture content from dry to wet side of optimum for all compaction methods. The static, impact, and vibratory compaction samples resulted in a strength reduction of 2.4, 2.7, and 1.8 times, respectively, with increasing moisture from about -3% to +3% of optimum moisture content.

Table 8.4. Summary of resilient modulus and shear strength results for glacial till

Method	Dry Unit Weight (kN/m^3)	Moisture (%)	Mean M_r (MPa)	COV (%)	Model Coefficients*	τ_{max} (kPa)	Strain at failure (%)
Static	17.34	11.7	72.5	16.3	$k_1 = 679.7$ $k_2 = 0.38$ $k_3 = 0.03$ $R^2 = 0.72$	269.4	2.2
Impact	17.32	11.4	144.8	16.7	$k_1 = 1069.2$ $k_2 = 0.45$ $k_3 = -0.17$ $R^2 = 0.64$	373.5	1.6
Vibratory	17.41	12.5	148.3	17.7	$k_1 = 1219.7$ $k_2 = 0.39$ $k_3 = -0.08$ $R^2 = 0.50$	250.4	1.2
Static	17.45	14.3	96.3	21.1	$k_1 = 859.1$ $k_2 = -0.01$ $k_3 = -0.08$ $R^2 = 0.10$	193.3	2.7
Impact	17.53	15.2	130.2	17.3	$k_1 = 1011.5$ $k_2 = -0.02$ $k_3 = -0.21$ $R^2 = 0.61$	187.0	8.0
Vibratory	17.88	14.2	131.3	31.8	$k_1 = 1571.0$ $k_2 = 0.54$ $k_3 = -0.32$ $R^2 = 0.77$	-	-
Static	17.36	17.2	72.1	23.4	$k_1 = 448.0$ $k_2 = 0.37$ $k_3 = -0.34$ $R^2 = 0.77$	111.1	6.0
Impact	17.39	17.4	74.1	15.2	$k_1 = 527.7$ $k_2 = 0.36$ $k_3 = -0.22$ $R^2 = 0.77$	136.2	10.0
Vibratory	17.6	17.1	96.9	17.6	$k_1 = 976.6$ $k_2 = 0.15$ $k_3 = 0.04$ $R^2 = 0.22$	139.9	10.0
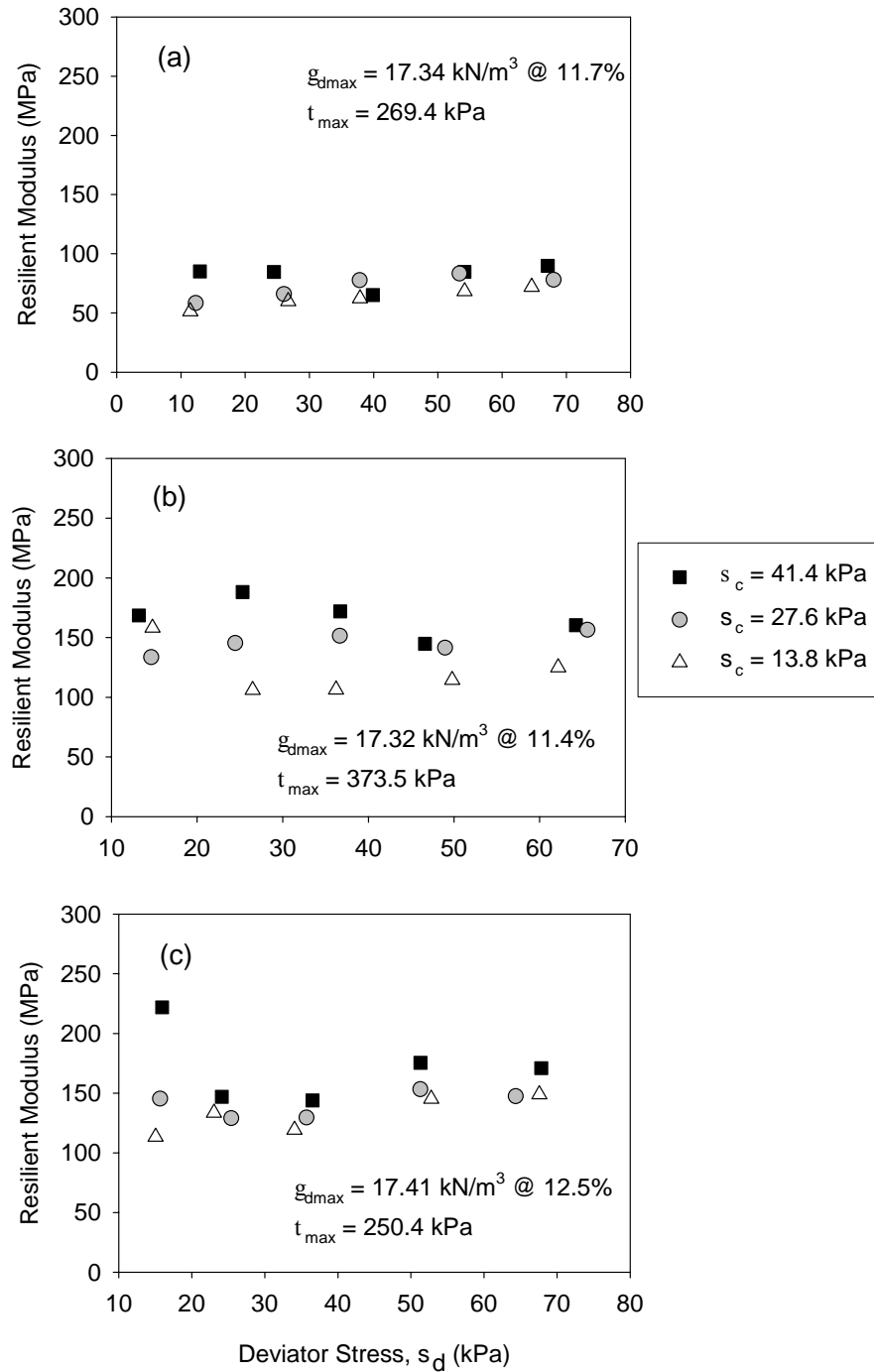
Figure 8.28. Deviator stress versus resilient modulus at about -3% of standard optimum moisture content compacted using (a) static (b) impact (c) vibratory compaction method
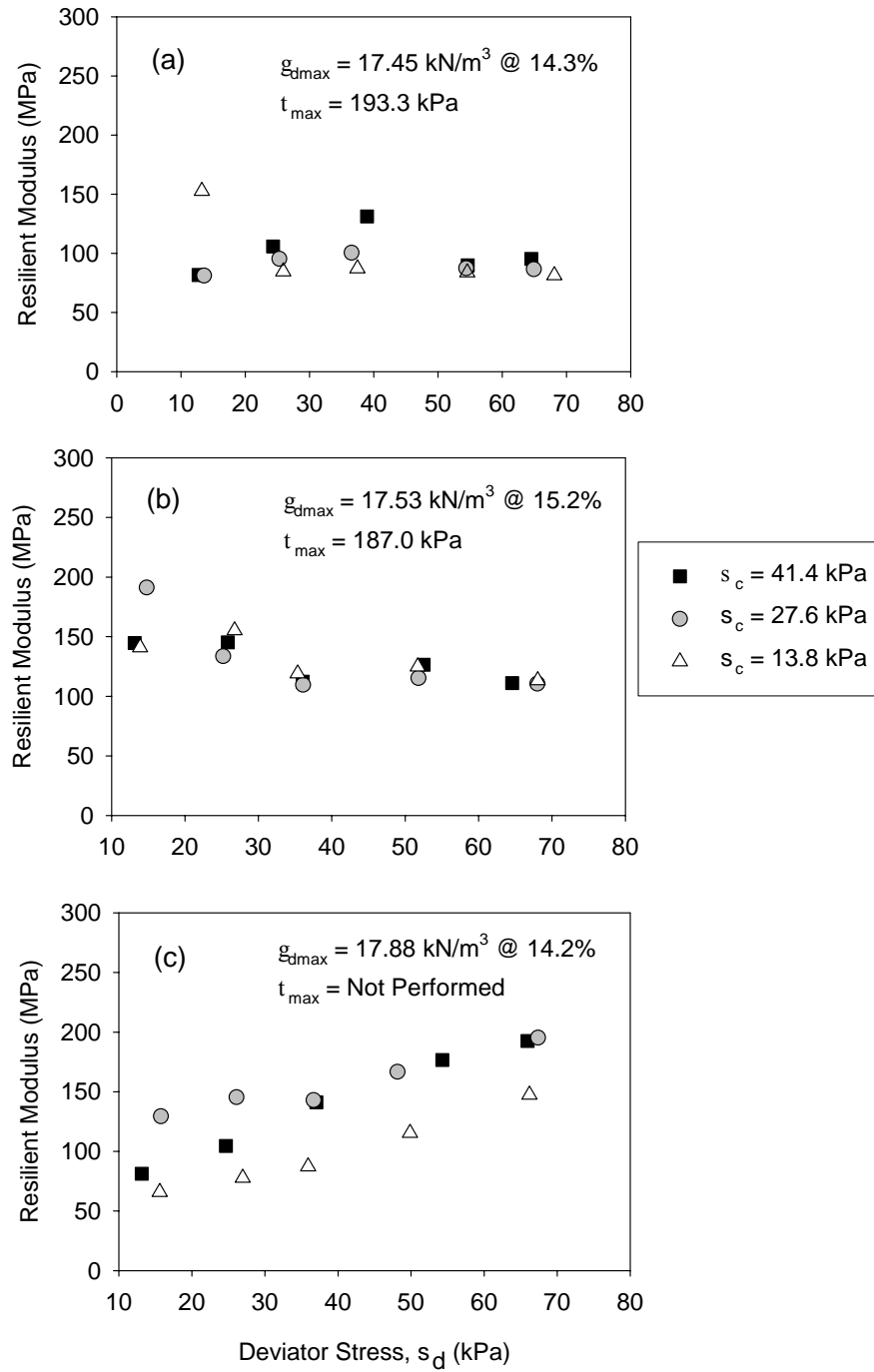
Figure 8.29. Deviator stress versus resilient modulus at about standard optimum moisture content compacted using (a) static (b) impact (c) vibratory compaction method
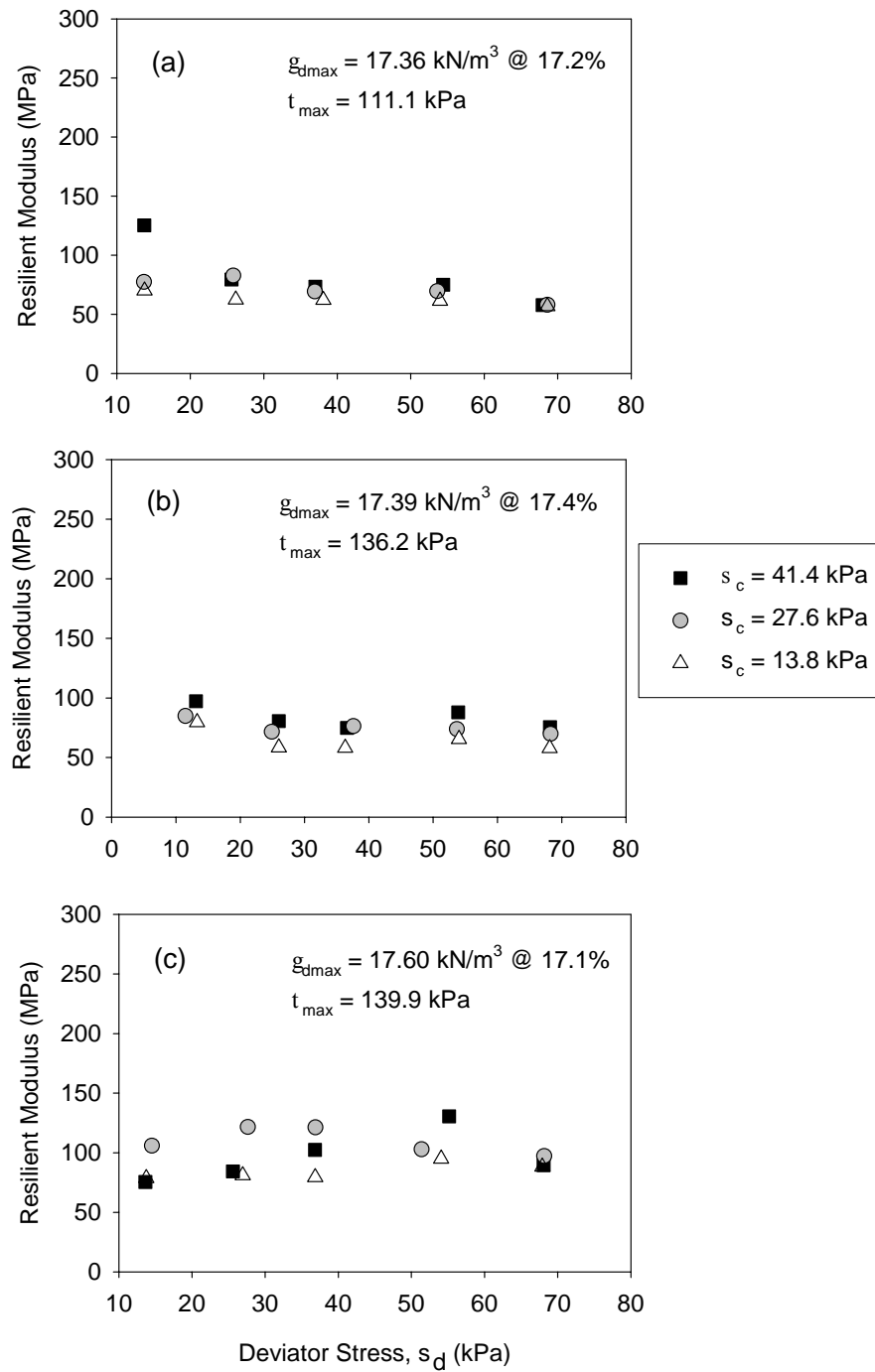
Figure 8.30. Deviator stress versus resilient modulus at about +3% of standard optimum moisture content compacted using (a) static (b) impact (c) vibratory compaction method
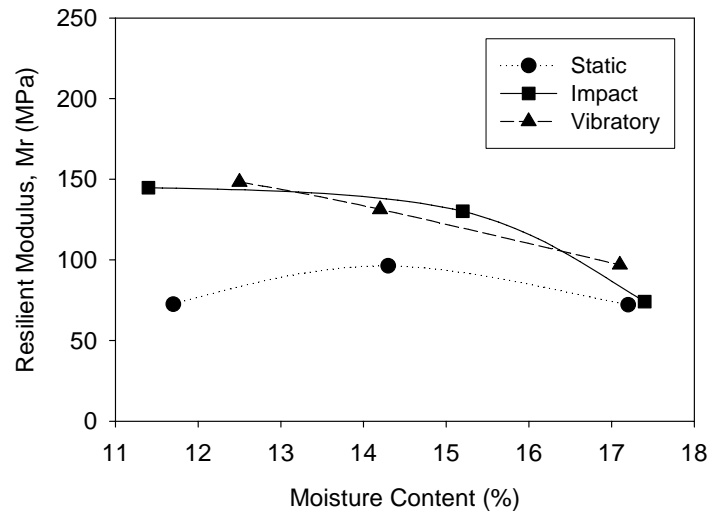
Figure 8.31. Change in average resilient modulus with moisture for specimens compacted using different methods
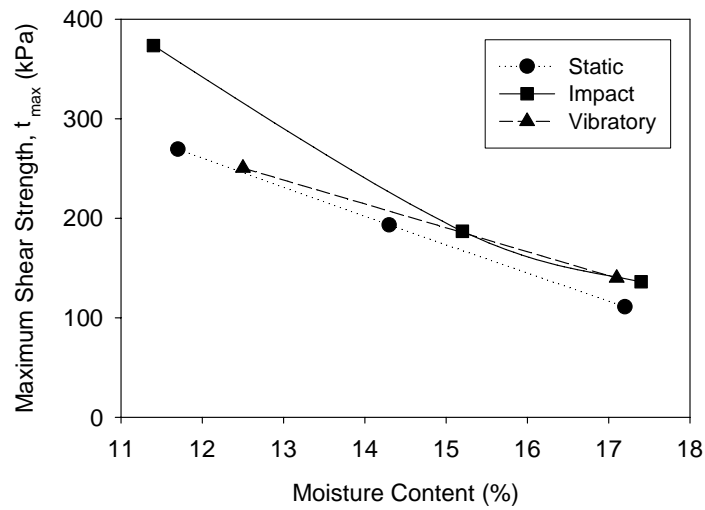
Figure 8.32. Change in maximum shear strength with moisture for specimens compacted using different methods

8.5.1 TH 64 Sand

Samples were compacted to achieve a target of 100% maximum dry density determined by vibratory compaction method (18.26 kN/m^3) at 6%, 8%, and 10% target moisture contents. These moisture contents were selected based on the field measurements. Dry unit weights for the triaxial M_r samples are presented in Table 8.5. Average M_r values were calculated from the fifteen loading sequences and are reported in this Table 8.5 along with coefficient of variation (COV). Witczak and Uzan (1988) model coefficients, k_1, k_2, k_3 and R^2 values for the models are also provided in the Table 8.5. Results for all M_r values for each loading sequence for all tests are provided in Appendix I.

Figure 8.33, 8.35, and 8.37 show plots of deviator stress versus resilient modulus for three different moisture contents. Results generally show that with increasing confining stress, M_r increases and that M_r is influenced more by confining stress than deviator stress (Figure 8.34,Figure 8.36, and Figure 8.38). The Witzack and Uzan (1988) "universal" model appears to fit well for the data set as evidenced by R^2 values of 0.82 to 0.98.

Figure 8.39 shows the change in average M_r as a function of moisture content and compaction method. On average, vibratory compaction samples produced higher M_r values (5 to 20 percent) than impact compaction, with greater differences at higher moisture contents.

Maximum shear strength, τ_{max}, are shown in Table 8.5. Figure 8.40 shows the change in shear strength with increasing moisture content for different compaction methods. Although not significant, vibratory compaction samples generally exhibited higher shear strengths than impact compaction specimens.

No profound influence of moisture content is observed in M_r and τ_{max} within the 6% to 10% moisture ranges.

Table 8.5. Summary of resilient modulus and shear strength values for TH 64 sand

Method	Dry Unit Weight (kN/m^3)	Moisture (%)	Mean M_r (MPa)	COV (%)	Model Coefficients*	τ_{max} (kPa)	Strain at failure (%)
Impact	18.36	5.6	135.4	36.7	$k_1 = 570.0$ $k2 = 0.77$ $k3 = -0.01$ $R^2 = 0.98$	45.0	2.0
Vibratory	18.39	5.5	144.3	42.5	$k1 = 629.7$ $k2 = 0.65$ $k3 = 0.00$ $R^2 = 0.96$	73.1	1.5
Impact	18.31	7.9	143.9	37.4	$k1 = 681.0$ $k2 = 0.64$ $k3 = -0.03$ $R^2 = 0.96$	70.1	2.2
Vibratory	18.36	7.6	161.3	32.3	$k1 = 806.3$ $k2 = 0.60$ $k3 = -0.05$ $R^2 = 0.96$	68.5	1.9
Impact	18.33	9.8	138.2	32.3	$k1 = 686.6$ $k2 = 0.63$ $k3 = -0.20$ $R^2 = 0.82$	70.6	2.2
Vibratory	18.35	9.6	167.9	30.8	$k1 = 891.5$ $k2 = 0.56$ $k3 = -0.07$ $R^2 = 0.94$	87.3	1.5

* Model coefficients are based on Witczak and Uzan (1988) model
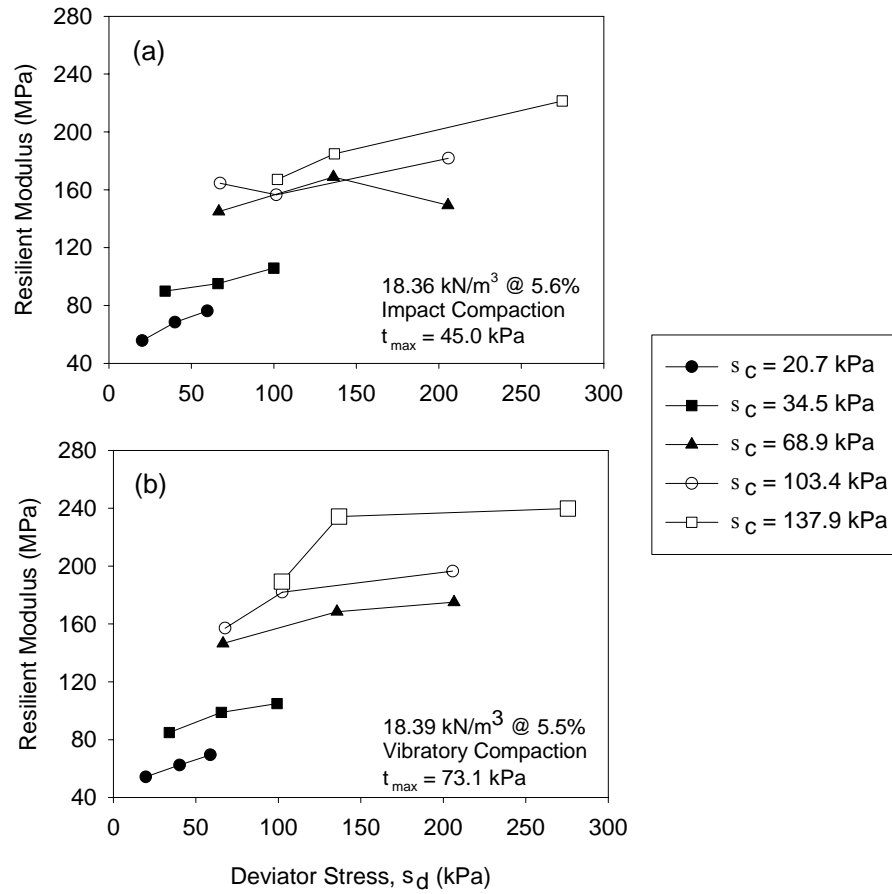
Figure 8.33. Deviator stress versus resilient modulus at 6% target moisture: (a) impact compaction (b) vibratory compaction
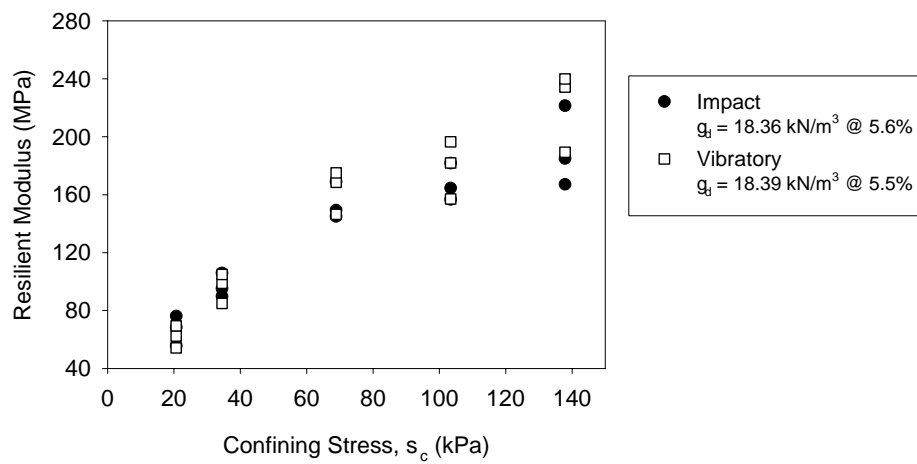
Figure 8.34. Confining stress versus resilient modulus at 6% target moisture using impact and vibratory compaction
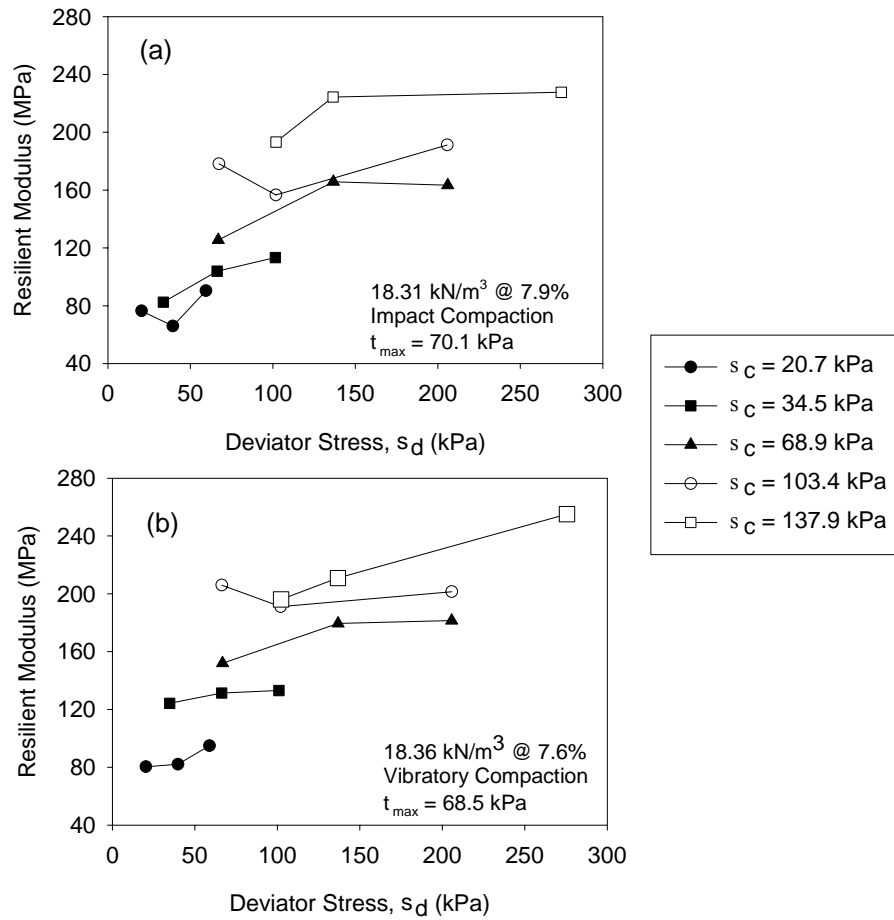
Figure 8.35. Deviator stress versus resilient modulus at 8% target moisture: (a) impact compaction (b) vibratory compaction
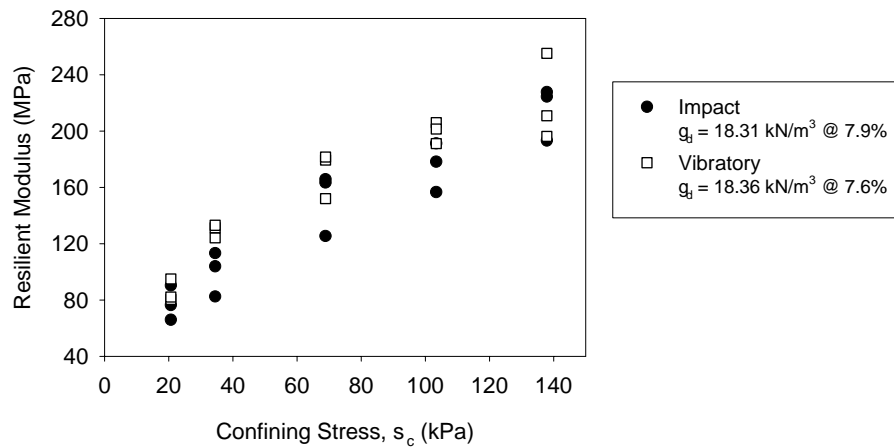
Figure 8.36. Confining stress versus resilient modulus at 8% target moisture using impact and vibratory compaction
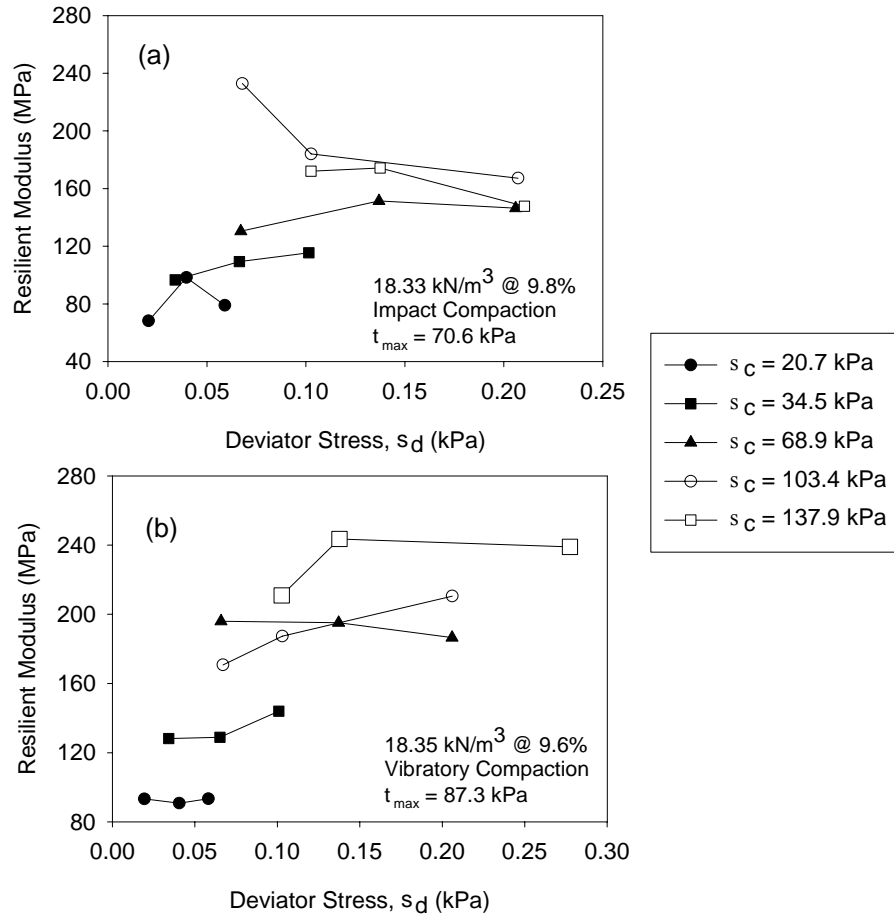
Figure 8.37. Deviator stress versus resilient modulus at 10% target moisture: (a) impact compaction (b) vibratory compaction
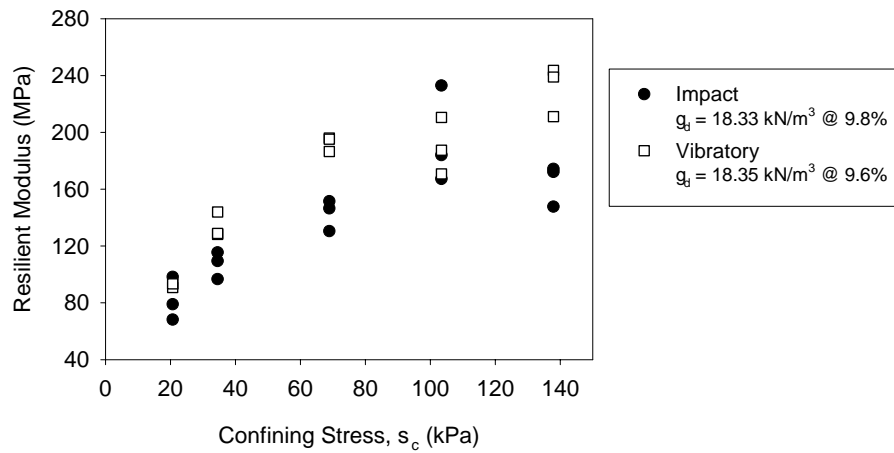
Figure 8.38. Confining stress versus resilient modulus at 10% target moisture using impact and vibratory compaction
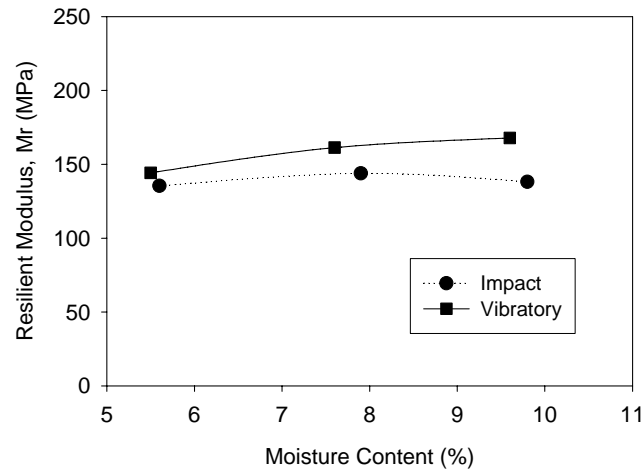
Figure 8.39. Change in average resilient modulus with moisture for specimens compacted using different methods
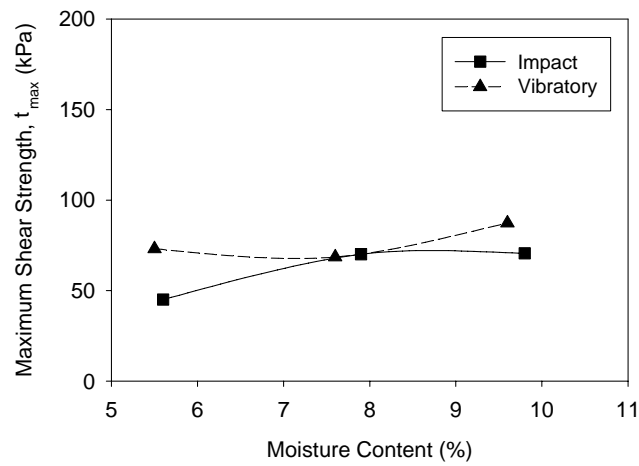
Figure 8.40. Change in maximum shear strength with moisture for specimens compacted using different methods

8.6 Summary and Key Findings

Some of the key findings from the literature include:

- There is increasing concern over laboratory impact and vibratory compaction methods in duplicating the mechanics and energy delivery system that occurs in the field. Several studies indicate promising results with gyratory and kneading compaction techniques, however, they have not been widely implemented for unbound fill materials.

- For cohesive soils, different compaction methods can result in distinctly different soil-structure in the compacted samples, which in turn affects the strength properties.

- A key element of comparing strength measurements from different compaction methods is capillary stress development and largely remains undocumented.

- Influence of compaction method on strength properties were studied by several researchers, however, contrasting results were published in the literature. Limited data is available describing the influence of compaction method on stiffness properties (e.g. resilient modulus).

Some of the key findings from the laboratory testing performed as part of this study include:

- Distinctly different moisture-density curves were realized between static, impact, gyratory, and vibratory compaction methods for the two materials.

- Vibratory compaction was inadequate to effectively characterize the moisture-density relationships for the cohesive soil. This method, however, provided effective for the granular material.

- Changes in moisture-density relationships with increasing impact energy were apparent for the cohesive soil but not for the granular material. The dry unit weight of granular material increased only slightly (about 1% to 2%) with increasing impact energy from standard to modified Proctor energy for the range of tested moisture contents.

- Optimum moisture contents are not observed with the static compaction method.

- For the granular material, the maximum dry unit weight achieved using 200 kN-m/m^3 static compaction energy was only 94% of the standard Proctor maximum dry unit weight. Application of additional compaction energy required static pressures greater than about 9200 kPa (1300 psi), which are considered significantly higher than what is applied in the field.

- For the cohesive soil, the static compaction energy required to achieve a target dry unit weight at any given moisture content is lower than the required impact compaction energy.

- The vibratory compaction energy required to achieve a target dry unit weight for the granular soil is significantly higher than the impact energy at "bulking" moisture contents, while it is lower at other moisture conditions. Therefore the moisture content during field production compaction should be greater than the "bulking" moisture content.

- For the granular soil, the field densities matched closely with the laboratory densities determined by standard Proctor, modified Proctor, and vibratory compaction methods. A narrow range of densities is observed between these methods for this soil.

- On average for the cohesive soil, vibratory and impact compaction methods resulted in greater M_r values by a factor of 1.3 to 2 times compared to the static method.

- No significant difference in M_r was realized between impact and vibratory methods for both soils.

- For the cohesive soil, static compaction samples resulted in lower τ_{max} (about 1.2 to 1.4 times) compared to the impact method. τ_{max} resulting from vibratory compaction was about 1.5 times lower compared to the impact method on the dry side, while there was no noticeable difference on the wet side of optimum moisture content.

- Vibratory compaction samples exhibited similar or slightly higher (0.97 to 1.2 times) τ_{max} than impact compaction samples for the granular soil.

- Differences in τ_{max} and M_r between compaction methods are attributed to the variations in the resulting soil structure and potential differences in capillary stresses.

- A profound influence of moisture content on the τ_{max} is realized for the cohesive soil with a strength reduction of about 1.8 to 2.7 times with increasing moisture content from -3% to +3% of optimum moisture content, for the three compaction methods. The average M_r reduced by about 1.3 to 2.0 times with increasing moisture content for the cohesive soil, for the three compaction methods.

- The influence of moisture content is not significant on M_r and τ_{max} values within the 6% to 10% moisture ranges for the granular soil.

Chapter 9
Comparison of Light Weight Deflectometers

9.1 Introduction

Light weight deflectometers (LWDs) are increasingly being considered by state and federal agencies in the U.S. and several countries around the world in earthwork QC/QA testing. Mn/DOT is in the process of evaluating and implementing LWD as a QC/QA tool on a state wide basis. Currently, different LWD devices are commercially available from at least four manufacturers (i.e., http://www.zorn-online.de, http://www.pavement-consultants.com, http://www.dynatest.com, http://www.al-engineering.fi). To successfully implement use of these devices, it is important to understand for what conditions they provide reliable measurements and also if differences exist between calculated elastic modulus values between the various devices. LWD elastic modulus (E_{LWD}) is calculated using elastic half-space theory knowing plate contact stress and deflection. Although most of the devices exhibit similarities in operation and methodology, they differ in how the plate contact stress and deflections are determined leading to variations in the calculated E_{LWD}. The LWD device components generally consist of a 100 to 300 mm diameter plate with a 10 kg to 20 kg drop weight, an accelerometer or geophone to determine deflection, and a load cell or calibrated drop height to determine plate contact stress.

A number of technical articles have been published over the past 20 years describing different LWD devices along with test results from lab and field for pavement foundation materials and correlations to several other in-situ test measurements. A review of basic principles, comparisons between different LWD devices, correlations between E_{LWD} to other in-situ test measurements and laboratory resilient modulus tests was conducted and presented in the following subsections.

Further, as part of this study two LWD devices (ZFG 2000 manufactured by Zorn Stendal from Germany, and the Keros manufactured by Dynatest in Denmark) with different plate diameters were used side-by-side for testing various pavement subgrade and base layers in Minnesota to observe the influences of plate diameter and calculated E_{LWD} values. At a few LWD test locations, tube samples were obtained from a compacted subgrade to evaluate the relationship between in-situ E_{LWD} and laboratory resilient modulus.

9.2 Literature Review

The application of a concentrated vertical load to a horizontal surface of any solid body produces a set of vertical stresses on horizontal planes within the body. The intensity of vertical pressures on any horizontal plane through the loaded soil decrease from a maximum at the point located directly beneath the load (contact point) to zero at a very large distance from this point. A pressure distribution of this kind is represented by a bell or dome shaped space (*see* Terzaghi and Peck 1967). These applied stresses cause immediate or elastic settlement beneath the contact

point directly after the application of the load. The magnitude of this settlement and the contact stress distribution will depend on the flexural rigidity of the base that is in contact with the soil (Das, 1998). Based on the well known Bousinnesq elastic solution, the relationship between applied stresses and displacement in the soil for the case of a rigid or flexible base resting on an elastic half-space can be derived as provided in equation 9.1.

$$E = \frac{(1-v^2).\sigma_0.a}{d_0} \times f$$

(9. 1)

where:
d_0 = Measured settlement (mm)
v = Poisson's Ratio
σ_0 = Applied Stress (MPa)
a   = Radius of the plate (mm)
E = Young's Modulus (MPa)
f = Shape factor (see Table 9.1)
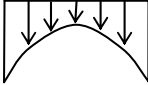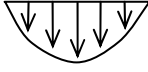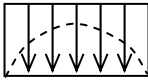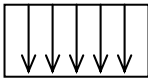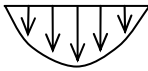
Table 9.1. Summary of shape factors in E_{LWD} estimation (Terzaghi and Peck 1967, Das 1998)

Plate Type	Soil Type	Stress Distribution		Shape factor (f)
Rigid	Clay (elastic material)	Inverse Parabolic		$\pi/2$
Rigid	Cohesionless sand	Parabolic		8/3
Rigid	Material with intermediate characteristics	Inverse Parabolic to Uniform		$\pi/2$ to 2
Flexible	Clay (elastic material)	Uniform		2
Flexible	Cohesionless Sand	Parabolic		8/3

All of the LWD devices utilize this simple elastic theory and assumptions of stress distribution to calculate elastic modulus from a measured (or assumed) contact stress and peak deflections of the loading plate or the soil directly under the center of the plate. Some LWD manufactures leave the option of selecting the shape factor to the user (e.g. Prima, Keros, etc.) while such option is not available with other manufacturers (e.g. Zorn and Loadman assumes a fixed stress distribution factor of 2). According to Terzaghi and Peck (1967), the stress distribution under a

plate depends on both plate rigidity and soil type. Three different stress distributions are generally possible (inverse parabolic, parabolic, and uniform) as shown in Table 9.1. Results presented in Mooney and Miller (2007) show that the stress distribution under a "rigid" LWD plate is dependent on soil type as well as the soil profile. Tests performed over a sand layer (250 mm thick) underlain by a clay layer showed a uniform stress distribution, while tests performed over two sand layers (250 mm thick) underlain by a clay layer showed close to a parabolic stress distribution. The E_{LWD} results can vary by up to 170% depending on the assumed stress distribution factor (Mooney and Miller 2007). (A stress distribution factor of 2 was assumed for tests performed on granular materials, and $\pi/2$ for tests performed on cohesive materials for this study.)

The LWD devices listed below are those that are commonly addressed in the literature, and of which the details are presented in the following sub-sections. A brief comparison between LWD devices is provided in Table 9.2. Correlations reported in the literature between LWD devices and to other in-situ test devices and laboratory tests are also summarized. The results and discussions presented in the following sections use the nomenclature shown below (in parenthesis) to be consistent with the nomenclature used elsewhere in this report (Note: "x" indicates the LWD plate diameter, e.g., 3 for a 300mm diameter plate).

- Light Drop Weight Tester ZFG2000 by Zorn Stendal, Germany (E_{LWD-ZX})

- Keros Portable FWD by Dynatest, Denmark (E_{LWD-KX})

- Prima 100 Light Weight Deflectometer by Carl Bro Pavement Consultants, Denmark (E_{LWD-PX})

- Loadman by AL-Engineering Oy, Finland (E_{LWD-LX})

- Light Drop Weight Tester by ELE (E_{LWD-EX})

- TRL Foundation Tester (TFT), a working prototype at the Transport Research Laboratory, United Kingdom (E_{LWD-TX})

- Truck-mounted Falling Weight Deflectometer test (E_{FWD-X})

- Static Plate Load Test – initial and reload modulus (E_{V1}, and E_{V2})

- Geogauge Modulus (E_{SSG})

- Dynamic Cone Penetrometer Test (DCPI)

- Laboratory Resilient Modulus Test (M_r)

- Resilient Modulus Test estimated from FWD test (M_{R-FWD})

Table 9.2. Brief comparison between different LWD devices

Device	Plate Diameter (mm)	Falling Weight (kg)	Maximum Applied Force (kN)	Load Cell	Total Load Pulse (ms)	Deflection Transducer	
						Type	Location
Zorn Zorn (2003)	150, 200, 300	10, 15	7.07	No	18 ± 2	Accelero-meter	Plate
Keros Keros (2003)	100, 200, 300	10, 15	15.0	Yes	15 – 30	Velocity	Ground
Prima Fleming *et al.* (2002)	100, 200, 300	10, 20	15.0	Yes	15 – 20	Velocity	Ground
Loadman Livneh *et al.* (1997)	110, 200	10	17.6	No	Unknown	Accelero-meter	Plate
ELE van Gurp *et al.* (2000)	300	10	Unknown	No	Unknown	Velocity	Plate
TFT Fleming *et al.* (2002)	200, 300	10	8.5	Yes	15 – 25	Velocity	Ground

9.2.1 Factors Influencing E_{LWD}

Factors that influence the estimation of E_{LWD} include: plate size, plate rigidity, plate contact stress, type and location of deflection transducer, measurement of load via transducer, loading rate, and buffer stiffness. Additional details on how these factors influence the modulus are discussed below.

Influence of Plate Size

Deng-Fong *et al.* (2006) conducted field studies using the Prima LWD and found that the size of the loading plate affects the calculated modulus. E_{LWD} estimated from a 100 mm plate is found to be about 1.5 times higher than those from a 300 mm plate. Based on experimental work using the TFT device, Chaddock and Brown (1995) demonstrated that a 200 mm plate results in modulus approximately 1.3 to 1.5 times higher than that from a 300 mm plate for the same applied stress condition. Terzaghi (1955) proposed a linear rate equation (see equations 9.2 and 9.3 for clay and sand, respectively) to estimate modulus of subgrade reaction (k_s) for different footing sizes from plate load tests of different diameter. According on this equation, modulus from a 200 mm plate is approximately 1.45 times (for sand) to 1.5 times (for clay) greater than that from a 300 mm plate. Based on experimental work, Stranton (1944) demonstrated that a 200 mm plate can result in a modulus that is approximately 1.3 times higher than with 300 mm plate (*see* Figure 9.1).

$$k_s = k_1\left(\frac{B_1}{B}\right) \quad \text{[for footings on clay]} \tag{9.2}$$

$$k_s = k_1\left(\frac{B+B_1}{2B}\right)^2 \quad \text{[for footings on sand]} \tag{9.3}$$

where:
B_1 = size of plate used in plate load test (m)
B = size of footing (m)
k_s = modulus of subgrade reaction (kPa/m)
k_1 = stiffness estimated from plate load test (kPa/m)

Modulus of Subgrade Reaction, k, expressed as
Percentage of 760 mm (30 in) dia plate value
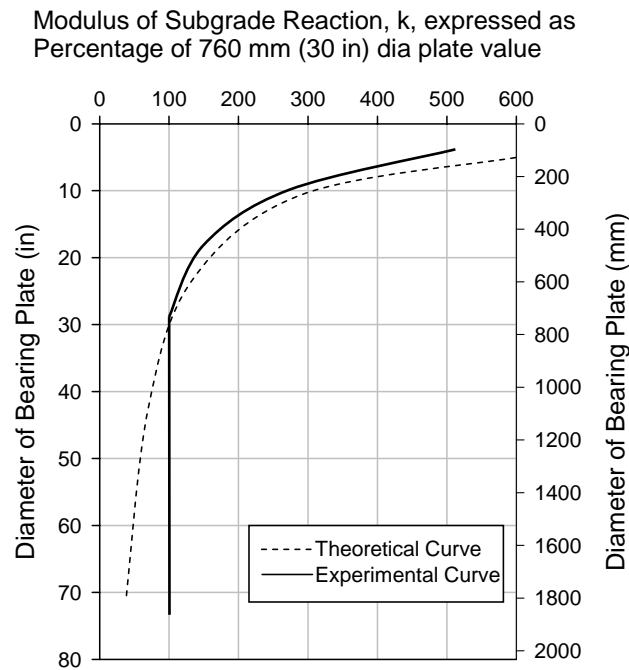
Figure 9.1. Relationship between modulus of subgrade reaction and diameter of bearing plate (Reproduced from Stranton (1944))

Plate Contact Stress

Contrasting information is available in the literature on the effect of plate contact stress on the calculated E_{LWD}. Fleming *et al.* (2000) investigated the influence of plate contact stress on E_{LWD} using the TFT and the Prima LWD by altering the drop height. Results showed that E_{LWD-P3} increased by about 15% while E_{LWD-T3} increased by about 33% with increasing plate contact stress from 35 kPa to 120 kPa. In contrast, Deng-Fong *et al.* (2006) concluded that the effect of drop height on E_{LWD} is insignificant based on Prima LWD tests over a natural sandy soil deposit. Results presented by Camargo *et al.* (2006) showed that increased drop height from 25 to 75 cm

increased the modulus values on average (based on 12 points) by only 1.1 times. Based on tests performed on very stiff self-cementing material, van Gurp *et al*. (2000) also found that variation in plate contact stress (from about 140 to 200 kPa) did not produce significant variation in the calculated E_{LWD}.

Type and Location of Deflection Sensor

Fleming *et al*. (2002) provided a discussion on the influence of the type and location of the deflection measuring sensor, i.e. on the plate versus on the ground. The Zorn device, for example, has an accelerometer built into the plate that is twice integrated to calculate deflection of the plate, while Keros, Prima, and TFT devices use a geophone that is placed in direct contact with the ground surface through a hole in the center of the plate (measuring deflections on the ground). The differences between these devices in type and location of deflection transducers may be expected to further affect their respective measurements. Van Gurp *et al*. (2000) investigated this issue and concluded that measurement on the ground was more comparable to laboratory triaxial measurements at in-situ stress levels. It was observed therein that velocity measurement on the bearing plate produced larger deflections relative to measurement on the ground. Fleming *et al*. (2002) indicated that the transducer mounted on the bearing plate will also record the initial acceleration of the plate, as opposed to one mounted on the soil. Therefore, devices that use transducers that measure deflections in the plate are expected to measure larger deflections as evidenced by many field studies (Weingart 1993, ZTVA -StB 1997, Shahid *et al*. 1997, Fleming *et al.* 1998, Fleming 1998 and 2001).

Plate Rigidity

Stress distribution under a LWD plate varies with the rigidity of the plate (*see* Table 9.1). Discussion presented above on deflections observed over a plate versus directly on the soil, also calls in a question whether the LWD plates are truly rigid. Theoretically, a true rigid plate should not deflect under a load. Mooney and Miller (2007) showed a stress distribution that falls between inverse parabolic and uniform when tested over a clay subgrade. It is indicated therein that it may explain the tendency of soil reaching failure where the stress distribution is uniform. However, this also may suggest some influence on plate rigidity, because theoretically (according to Das (1998)) a flexible plate would show uniform stress distribution when loaded on a clay subgrade. Different LWD manufacturers produce plates of different thicknesses and materials, which obviously can have differences in their rigidity. A clear understanding of each LWD plate's rigidity is needed as it relates to the selection of an appropriate shape factor in E_{LWD} calculation.

Load Transducer

Some devices (e.g., Zorn and Loadman) assume a constant applied force based on calibration tests performed on a concrete surface, while other devices (e.g., Prima and Keros) measure the actual applied load during the test using a load cell. Theoretically, the applied force on a surface cannot be constant as it clearly depends on the stiffness of the material. However, as the LWDs are commonly utilized for testing compacted layers which are relatively stiff, any error associated with the assumption of a constant applied force in calculations may not be practically significant. Brandl *et al*. (2003) performed field and laboratory tests using the Zorn LWD and

demonstrated that the assumption of constant applied force is reasonable. Kopf and Adam (2004) also provided similar conclusions. Davich (2005) reported laboratory test measurements to investigate error introduced from using an assumed applied load and concluded that the assumption of constant force can lead to an over-estimation of modulus of only 4% to 8%, based on testing soft to very stiff materials.

Loading Rate and Stiffness of Buffer

With using elastic theory in the E_{LWD} estimation procedure, the maximum transient deflection is assumed equivalent to the maximum deflection from a static plate of similar diameter and applied stress. Some studies however, indicate that the rate of loading can affect E_{LWD}. The loading rate can be controlled by varying the spring stiffness of the buffer placed between the drop weight and contact plate. Fleming (2000) reports that a comparatively lower stiffness buffer provides more efficient load transfer and better simulates static plate loading conditions. Lenngren (1992) reports that with using a stiffer buffer, the load pulse time history is shortened and the resulting E_{FWD} is increased by 10 to 20% on some asphalt concrete pavements while other locations showed little or no difference. Based on FWD tests conducted over asphalt pavements, Lukanen (1992) indicated that the shape of the load pulse and its rise and dwell time affect the magnitude of the measured deflections to some extent. According to Adam and Kopf (2002), the applied load pulse can vary by about 30% with a change in rubber buffer temperature from 0 to 30°C, while it remains more constant for a steel spring buffer. Our recent conversation with the Zorn manufacturer indicates that rubber buffers are prohibited for use in Germany.

9.2.2 Comparison between different LWD's and other In-situ Test Devices

Siekmeier *et al.* (2000) presented results of side-by-side in-situ test measurements performed using the DCP, Loadman LWD, and FWD over several pavement granular base layers constructed in Minnesota. Results from this study showed a strong correlation between E_{LWD} and E_{FWD} values and indicated that it is important to consider the stress conditions imposed by the instruments when stress dependent materials are tested. Results also showed a "decent" correlation between shear strength estimated from DCP and Loadman E_{LWD}.

Sulewska (1998) presented correlations between Zorn modulus (E_{LWD-Z3}) and relative compaction (R%) based on standard proctor maximum dry density and E_{V1} and E_{V2} from static plate load tests on sand-gravel mixture. Regression analysis showed significant dependencies between E_{LWD-Z3} and E_{V1} and E_{V2} as well as R%, which is evidenced by R^2 values greater than 0.8. Sulewska (2004) also reported results of calibration tests using a 300 mm plate Zorn LWD device that were conducted on a field project site consisting of a 5 m thick sand-gravel mix embankment. In-situ density and LWD tests were performed at 28 test locations for comparison. It was reported that E_{LWD-Z3} increased with relative compaction with a "good" correlation.

German specifications for road construction (ZTVA-StB 1997) provide target values as shown in Table 9.3 for use in field projects where site-specific correlations are not available. In addition to minimum E_{LWD} target values, Weingart (1993) suggested considering some observations from the Zorn LWD test that include: (a) the value of "time of acceleration" s/v ratio, where s =

settlement under impact load, and v = speed of settlement, which gives additional information on soil compaction; and (b) at proper compaction in field $2.2 \leq E_{V2}/E_{LWD-Z3} \leq 2.6$ should be satisfied. Some limiting values and additional conditions for acceptance testing based on field tests on granular base and sub-base materials were proposed as shown in Table 9.4 (Weingart 1993).

Table 9.3. Recommended values of E_{V2} and LWD dynamic modulus for acceptance (ZTVA -StB 1997)

E_{V2} (MPa)	120	100	80	45
E_{LWD} (MPa)	60	50	40	25

Note: Values represent 300 mm diameter plate modulus

Table 9.4. Recommended values of E_{V2} and dynamic modulus using Zorn LWD for acceptance (Weingart 1993)

E_{V2} (MPa)	150	120	100	80	60	45	Additional Conditions: s/v < 3.5ms
E_{LWD-Z3} (MPa)	70	55	45	40	30	25	

Notes:
- These values do not refer to fine-grained soils that are sensitive to moisture content
- s/v ratio is "time of acceleration" from Zorn LWD test

Fleming *et al*. (2000) presented correlations between three different LWD devices (Zorn, TFT, and Prima) and conventional 300 mm FWD measurements. A wide range of material types and stiffnesses including soft clay subgrade materials to very dense granular base capping layers were tested. An important conclusion from this study was that the results from different devices can be dramatically different and so are the correlations, depending on the soil type and stiffness. Several correlations are summarized below for different LWD and FWD devices:

For a range of subgrade materials (silty clays, oxford clay, glacial till, silty sand, and stabilized oxford clays) and granular capping materials (sandstone, mixture of sand, gravel and limestone):

$$E_{LWD-Z3} = 0.43 \text{ to } 1.41 \text{ x } E_{FWD-3} \text{ (with majority between 0.4 to 0.7 times)} \qquad (9.4)$$

$$E_{LWD-T3} = 0.81 \text{ to } 1.40 \text{ x } E_{FWD-3} \text{ (with majority within 0.8 to 1.2 times)} \qquad (9.5)$$

For a controlled field section consisting of silty clay subgrade and granular sub-base:

$$E_{LWD-P3} = 0.97 E_{FWD-3} \qquad (9.6)$$

$$E_{LWD-Z3} = 0.63 E_{FWD-3} \qquad (9.7)$$

$$E_{LWD-T3} = 1.13 E_{FWD-3} \qquad (9.8)$$

A similar correlative ratio between E_{LWD-Z3} and E_{FWD} in the range of 0.5 to 0.6 has been reported by others (Shahid *et al.* 1997, Fleming *et al.* 1998, Fleming 1998, and Fleming 2001). These correlations are similar to what is suggested between E_{v2} and E_{LWD-Z3} in the German specifications (ZTVA -StB 1997). Some of the differences observed in moduli from different LWD's are attributed to different load pulse shapes, while some are attributed to differences in deflection transducers (Fleming *et al.* 2000). Fleming (2000) indicated that most of the correlations published in the literature have significant scatter, and therefore it is suggested that many tests be performed and with some statistical analysis to ensure appropriate acceptance testing decisions are made on-site.

Livneh and Goldberg (2001) indicated that E_{LWD-Z3} is about $0.3 - 0.4$ times the conventional FWD moduli. A relationship between E_{LWD-Z3} and E_{V2} was derived as shown in equation 9.9. The estimated E_{V2} from this equation is about 0.55 to 0.85 times E_{FWD}:

$$E_{V2} = 600 - \frac{300}{300 - E_{LWD-Z3}} \tag{9.9}$$

Hildebrand (2003) presented a comparison study between static plate load test, FWD, and three portable LWD's (Loadman, Keros, and Zorn) on a granular base layer construction project. Results showed that there is a "good" correlation between static plate load test and E_{FWD}. E_{LWD-K3} and to some lesser degree E_{LWD-LM} were well correlated with the E_{FWD} and static plate load test modulus. E_{LWD-Z3} values were considerably lower than those measured with other methods. On an average of about 20 measurements, relationships between FWD and other LWD devices are as follows:

$$E_{FWD-3} = 1.53 E_{LWD-LM} \tag{9.10}$$

$$E_{FWD-3} = 2.48\ E_{LWD-Z3} \tag{9.11}$$

$$E_{FWD-3} = 1.26 E_{LWD-K3} \tag{9.12}$$

$$E_{LWD-K3} = 1.22\ E_{LWD-LM}\ \text{and}\ 1.97\ E_{LWD-Z3} \tag{9.13}$$

$$E_{PLT} = 1.49 E_{LWD-LM} \tag{9.14}$$

$$E_{PLT} = 2.41\ E_{LWD-Z3} \tag{9.15}$$

$$E_{PLT} = 1.23 E_{LWD-P3} \tag{9.16}$$

(Note: It is unknown whether the plate load modulus indicated below (E_{PLT}) is initial or re-load modulus)

Nazzal *et al.* (2004) conducted a field study with the Prima LWD device by testing selected highway project sections in Louisiana, as well as some test sections constructed at Louisiana Transportation Research Center (LTRC). In conjunction with Prima LWD measurements, FWD and static plate load tests were performed. Tests were conducted on a wide-range of subgrade materials (un-stabilized, cement-stabilized, and lime-stabilized clayey soil, and crushed limestone base material). Relationships between E_{LWD-P3} and M_{R-FWD}, and E_{v1} and E_{v2} are presented below. These relationships reflect the modulus values of only the tested layer. Due to

the effect of varying influence depths by different devices, e.g., PLT has an influence depth of 2 times the diameter of plate, and 300 mm plate LWD has an influence depth of 280 mm (Nazzal 2003), a multi-layered system solution referred to as "Method Equivalent Thickness" described in Odemark (1949), was utilized to backcalculate individual layer moduli from LWD and FWD tests.

$$M_{R\text{-}FWD} = 0.97\ E_{LWD\text{-}P3}\ (R^2 = 0.94 \text{ and standard error} = 33.1 \text{ MPa}) \tag{9.17}$$

$$E_{V1} = 22 + 0.70\ E_{LWD\text{-}P3}\ (R^2 = 0.92 \text{ and standard error} = 36.4 \text{ MPa}) \tag{9.18}$$
$$\text{for } 12.5 \text{ MPa} < E_{LWD\text{-}P3} < 865 \text{ MPa}$$

$$E_{V2} = 20.9 + 0.69\ E_{LWD\text{-}P3}\ (R^2 = 0.94 \text{ and standard error} = 29.8 \text{ MPa}) \tag{9.19}$$
$$\text{for } 12.5 \text{ MPa} < E_{LWD\text{-}P3} < 865 \text{ MPa}$$

Alshibli *et al*. (2005) conducted comprehensive laboratory testing on compacted layers of silty clay, clayey silt, cement-treated clay, sand, gravel, recycled asphalt pavement, and limestone aggregates using the 300 mm Prima, 300 mm static plate load test, soil stiffness gauge, and DCP tests. "Good" statistical correlations were obtained between $E_{LWD\text{-}P3}$ and E_{v1} and E_{v2}, as well as DCP index (DCPI) as shown below. A wide scatter and poor repeatability was observed in the E_{LWD} values when testing weak subgrade layers. Reportedly, both E_{LWD} and E_{SSG} yielded unreliable measurements for the cement-treated clay materials due to development of shrinkage cracks. Relationships presented in this paper include:

$$E_{V1} = 0.907\ E_{LWD\text{-}P3} - 1.812\ (R^2 = 0.84) \tag{9.20}$$

$$E_{V2} = 25.25\ e^{0.006 E_{LWD\text{-}P3}}\ (R^2 = 0.90) \tag{9.21}$$

$$E_{LWD\text{-}P3} = 2191.4/DCPI\ (R^2 = 0.72) \tag{9.22}$$

Based on field and laboratory tests using the Prima LWD device, Nazzal *et al.* (2007) reported that E_{v1}, E_{v2}, E_{FWD}, and DCPI values can be predicted from E_{LWD} with significant confidence. Reportedly, prediction models can be improved when soil properties such as moisture content and void ratio are included in the model.

Groenedijk *et al*. (2000) performed comparison field tests using the Prima and ELE LWDs along with FWD testing. The ELE LWD employs a geophone sensor placed on the loading plate at the center, while the Prima and FWD devices used a geophone sensor placed in the center of the loading plate directly in contact with the ground. Based on an average of about five test measurements performed before the base layer was constructed, and 1, 7, 28, 90 days after construction, the following relationships were observed for a granular base layer (Groenedijk *et al*. 2000):

$$E_{FWD} = 1.4 \text{ to } 2.5\ E_{LWD\text{-}E3}\ (\text{Avg. } 2.0\ E_{LWD\text{-}E3}) \tag{9.23}$$

$$E_{FWD} = 0.6 \text{ to } 1.6\ E_{LWD\text{-}P3}\ (\text{Avg. } 1.0\ E_{LWD\text{-}P3}) \tag{9.24}$$

9.2.3 Typical E_{LWD} Values

White *et al.* (2006) and White *et al.* (2007) carried out field testing programs using the Keros and Zorn LWDs on a wide-range of cohesive and cohesionless soils. Ranges of E_{LWD} values for different soil types and conditions are presented in Table 9.5. The mean and coefficient of variation of E_{LWD} are presented relating to the range of moisture deviation from optimum and percent relative compaction based on standard Proctor test. The E_{LWD} values reported for cohesive soils have higher coefficient of variation (COV range from 46 to 71%), than compared to cohesionless soils (COV range from 5 to 27%). The values on cohesive soils are also relatively more moisture sensitive than cohesionless soils. This can be evidenced by COV of 46% for the E_{LWD} values in case of the sandy lean clay soil within a range of moisture deviation of 1% and increase in relative compaction of 4%.

9.2.4 Correlations between E_{LWD} and Laboratory M_r

To date, very limited literature is available showing correlations between E_{LWD} and laboratory M_r. This is not surprising considering the time and complications involved in performing the laboratory resilient modulus test, variations between in-situ and laboratory stress conditions, problems with representing actual field conditions. Siekmeier *et al.* (2000) presented a comparison between resilient modulus tests performed on granular base samples that were prepared and compacted close to in-situ moisture content and density with FWD tests. It was indicated that the backcalculated E_{FWD} values compared favorably with laboratory M_r values at lower bulk stresses, but diverged at higher bulk stresses.

Groenedijk *et al.* (2000) compared E_{LWD-P3} to lab M_r test results for very stiff self-cementing granular materials, by using a "forward calculation" procedure. This procedure involved modeling a soil layer system in KENLAYER modeling software using a M_r-θ model for base and subgrade materials, applying vertical stresses similar to plate contact stresses from a LWD test, and predicting resilient modulus (M_{r-pred}) of the surface layer. The predicted resilient modulus from this procedure was then compared to the measured E_{LWD}. Comparison results showed good statistical correlations with R^2 values ranging from 0.78 to 0.98. Combining all the tests performed in that study, the following equation was derived:

$$E_{LWD-P3} = 0.989\ M_{r-pred} - 44.1\ (MPa) \tag{9.25}$$

where: M_{r-pred} = predicted resilient modulus. Swenson *et al.* (2006) performed comparison testing between E_{LWD-P2} and laboratory M_r (at σ_c = 14 kPa and σ_d = 27 kPa) on four different types of soils (L, C, Si, SiCL according to Mn/DOT textural classification). Linear relationships are presented between the two moduli as $E_{LWD-P2} = \alpha.M_r$, where α values were observed as 0.55, 0.53, 0.85, and 0.85, for L, C, Si, and SiCL soils, respectively. Significant scatter in the data was observed, however. Ping *et al.* (2002) compared in-situ E_{FWD} to laboratory M_r for stress conditions simulating a FWD test. Results suggest that the E_{FWD} is about 1.65 times higher than laboratory M_r with an R^2 of about 0.3. This relationship is in general agreement with AASHTO (1991) which suggest that the E_{FWD} is approximately two to three times higher than laboratory M_r.

Table 9.5. Range of LWD modulus values published in literature

Soil Name	USCS	Loose Lift Thickness (mm)	Moisture Deviation[1] (% Range[2])	Relative Compaction[3] (% Range[2])	LWD Modulus[4] (MPa) (COV)	Parameter	Reference
Cohesive Soils							
Silt	ML	300	-2.5 to -3.0	94 to 98	47 (-)	$E_{LWD-K3(61)}$	White *et al.* (2006)
		200	-1.5 to -4.0	96 to 102	127 (71)		
Lean Clay With Sand	CL	250	+1.0 to +3.5	87 to 95	49 (58)		
		250	-4.0 to + 0.5	86 to 93	59 (62)		
Sandy Lean Clay	CL	250	- 6.0 to -5.0	84 to 88	45 (46)		
		250	-3.0 to -1.5	85 to 90	65 (58)		
Cohesionless Soils							
Well Graded Sand With Silt	SW-SM	360	-5.0 to -3.5	96 to 99	24 (27)	$E_{LWD-K3(61)}$	White *et al.* (2006)
		250	-6.0 to -4.5	96 to 100	28 (22)		
Silty Gravel With Sand	GM	350	-0.5 to 0.0	88 to 90	33 (15)	$E_{LWD-K3(61)}$	White *et al.* (2007)
Silty Sand With Gravel	SM	280	-6.0 to -5.5	95 to 100	33 (8)		
Poorly Graded Gravel	GP	300	-	95 to 103	41 (17)		
Silty Sand	SM	360	-1.5 to -1.0	91 to 95	19 (24)		
Clayey Gravel With Sand	GC	340	-2.0 to -1.5	86 to 92	37 (12)		
Well Graded Sand With Silt	SW-SM	200	-0.5 to +2.0	99 to 102	8 (5)		
		200	-5.0 to -4.5	99 to 101	33 (21)	$E_{LWD-Z2(63)}$	
		200	-2.5 to -1.5	97 to 102	27 (33)		

Notes:
[1] Moisture deviation from optimum moisture content determined by standard Proctor test or relative density test
[2] Range indicates mean ± one standard deviation
[3] Percent compaction relative to standard Proctor maximum density or 100% relative density
[4] For x (y) LWD modulus values, x – mean, and y – coefficient of variation.

9.3 Comparison of Zorn ZFG and Keros LWD Devices

9.3.1 Light Drop Weight Tester – ZFG 2000

The ZFG 2000 LWD device is manufactured by Zorn Stendal, Germany http://www.zorn-online.de, and complies with German specifications for road construction (*see* TP BF-StB 1992). The dynamic deflection modulus is calculated using equation 9.1. The equation assumes a Poisson's ratio of 0.5 and that the stress distribution under the plate is uniform. Based on the manufacturer's calibration test on a concrete slab, the drop height is set at 72 cm to achieve an applied load of 7.07 kN (Zorn 2003). Deflections are measured during the test using an accelerometer that is built-in to the load plate. Deflection measurements are recorded during the execution of the last three load pulses and averaged. Using equation 9.1 and knowing the deflection and contact stress the dynamic deflection modulus is calculated (TP BF-StB 1992, and Zorn 2003). Technical details of the device are summarized in Table 9.2.

From conversations with a representative from the manufacturer, it is understood that if the user chooses to use a different drop-height, the constant force value can be estimated using equation 9.26. According to this formula, the drop height to achieve an applied force of 7.07 kN is 70.3 cm. However, based on the manufacturer's calibration tests on a concrete pad, an applied force of 7.07 kN was experimentally found to be 72 cm. The difference between the theoretical and experimental determined drop height is apparently attributed to non-linearity in the spring buffers during dynamic loading. A relationship between drop height and estimated applied force for a 10 kg drop weight using equation 9.26 with comparison to calibrated applied forces (provided by manufacturer) is shown in Figure 9.2.

$$F = \sqrt{2 \times m \times g \times h \times k} \qquad\qquad (9.26)$$

Where:
F = Applied force (kN)
m = mass of falling weight (kg)
g = acceleration due to gravity, 9.81 (m/s^2)
h = drop height (m)
k = spring constant (362396.2 N/m)
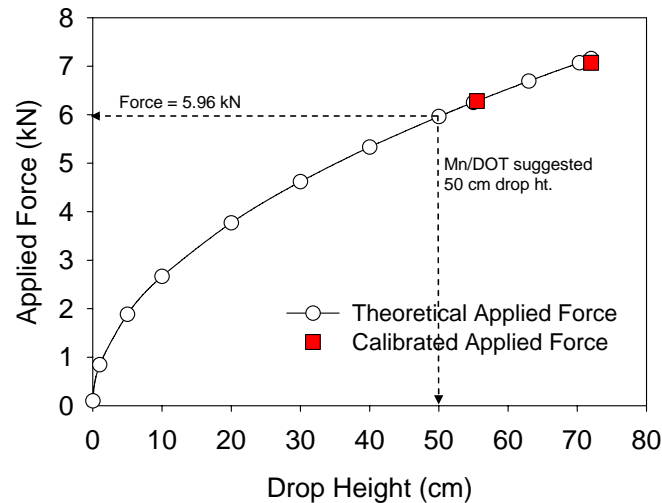
Figure 9.2. Relationship between drop height and applied force for 10 kg drop weight (Zorn LWD)

Kopf and Adam (2004) indicated that the tuning and resulting design of the Zorn device is based on extensive model calculations and parametric studies performed by Weingart (1977). This device is recommended for use on stiff cohesive soils, mixed soils and coarse-grained soils up to 63 mm in size (Zorn, 2003). Field tests should be performed by placing the plate on flat ground in a way that full contact between the plate and the surface is achieved. The manufacturer suggests using a thin layer of sand at locations where a flat contact surface cannot be obtained.

9.3.2 Keros Portable Falling Weight Deflectometer

The Keros LWD device is manufactured by Dynatest, Denmark http://www.dynatest.com. The device is equipped with a load cell to measure the impact force from the falling weight and a geophone to measure induced deflections at the ground surface. Two additional geophones can be added to obtain the deflection away from the loading point. The load and geophone sensors are connected to an electronic box to store and transmit the data to either a pocket PC or a laptop with Bluetooth capability. The software provided with the device allows the user to enter Poisson's ratio and an appropriate stress distribution factor ($\pi/2$, 2, or 8/3) depending on the anticipated contact stress distribution. The dynamic surface modulus is calculated using equation 9.1 (Dynatest 2004). Technical details of the device are listed in Table 9.2.

9.3.3 Zorn – Keros Comparison Field Test Results

The Zorn and Keros LWD devices were compared in this study during summer 2006 for a pavement subgrade layer and base layer at the MnROAD facility and a subgrade layer at the TH64 project site south of Ackley, MN. Comparison tests at these project sites were performed

within a spacing of approximately 2 feet or less to minimize variation in soil properties between test locations. Tests were performed by preloading with three load pulses, and measuring the average deflection for the succeeding three load pulses. Test results from each project site are summarized below.

MnROAD Facility

A photo of each device is shown in Figure 9.3. Both devices were setup with 200 mm diameter plates. To investigate the differences in E_{LWD} values, the assumptions made in the calculations (i.e., Poisson's ratio and stress influence factors) and the test procedures (such as drop height and drop weight) were kept identical. Table 9.6 lists the field test procedures and the parameters used in the calculations. Average applied stress for the last three drops was used in the modulus estimation for the Keros device, while an assumed force of 6.96 kN was used for the Zorn device (force estimated based on 63 cm drop height from Figure 9.2).

Comparison results of deflection and E_{LWD} are shown in Figure 9.4. Figure 9.4a and 9.4b show the difference in the deflection measurements and estimated modulus for the two devices for cohesive and cohesionless soils, respectively. Soil index properties are presented in Table 9.7. Figure 9.4c shows differences in the deflection measurements and estimated modulus values combining both cohesive and cohesionless soils. Linear regression relationships between the deflection measurements and estimated modulus values for the two devices are also shown with R^2 values of 0.89 and higher. Note that Figure 9.4c includes deflection measurements on asphalt and concrete layers as a reference. The number of tests in this study included 13 tests on cohesive soil, 113 tests on cohesionless soil, two tests on asphalt pavement, and one test on a Portland cement concrete pavement.

| (a) | (b) |
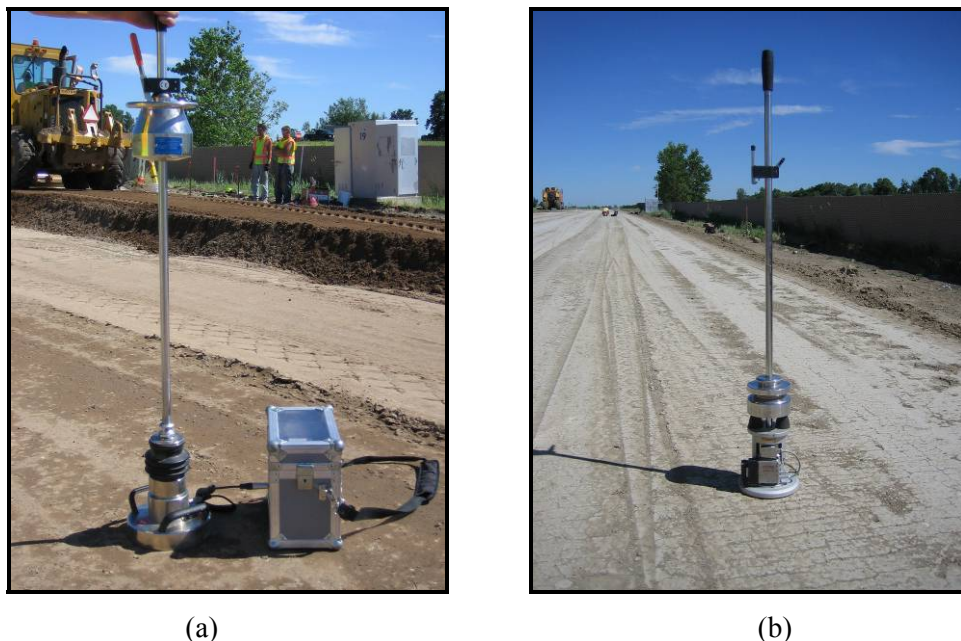
Figure 9.3. (a) Zorn ZFG 2000 LWD (b) Keros LWD

Table 9.6. Summary of Zorn and Keros LWD test conditions

Description	Keros	Zorn ZFG 2000
Drop Weight	10 kg	10 kg
Drop Height	630 mm – 200 mm plate[1] 720 mm – 300 mm plate[2]	630 mm – 200 mm plate[3] 720 mm – 300 mm plate[4]
Diameter of Plate	200 and 300 mm	200 and 300 mm
Load Sensor	Load Cell Range: 0 – 19.6 kN	None (Assumes constant applied force of 6.69 kN for 200 mm plate and 7.07 kN for 300 mm plate)
Deflection Sensor	Geophone	Accelerometer
Modulus Estimation	Use Equation 9.1 Assume a Poisson's ratio of 0.4 $f = \pi/2$ for cohesive soils $f = 2$ for cohesionless soils	

Notes:
[1]Modulus values are denoted as $E_{LWD-K2(63)}$
[2]Modulus values are denoted as $E_{LWD-K3(72)}$
[3]Modulus values are denoted as $E_{LWD-Z2(63)}$
[4]Modulus values are denoted as $E_{LWD-Z3(72)}$
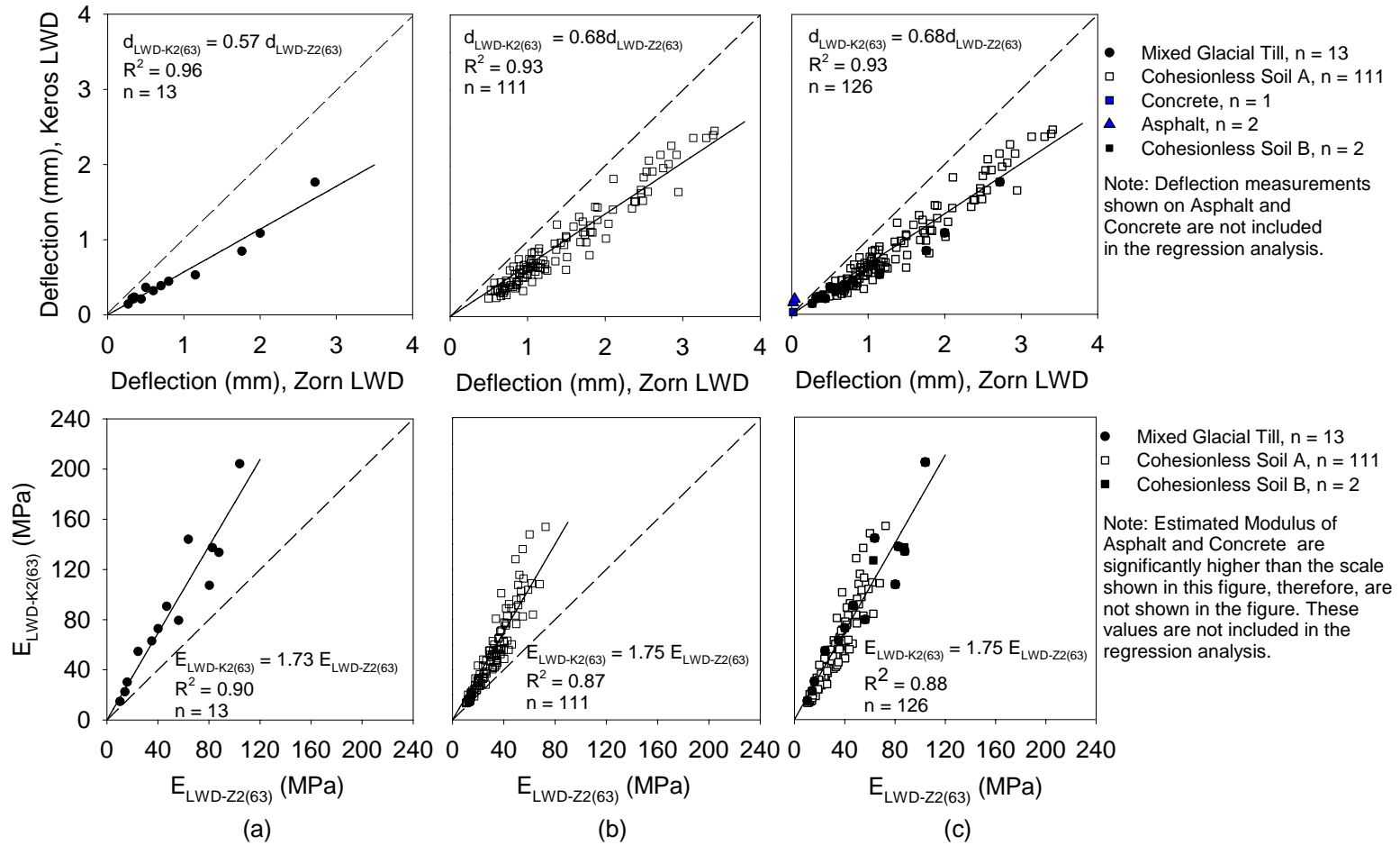
Figure 9.4. Relationships between deflection measurements and E_{LWD} by 200 mm Zorn and Keros devices for (a) cohesive soils, (b) cohesionless soils, and (c) combined results.

Table 9.7. Index properties of the soils at MnROAD project site

Parameter	Mixed Glacial Till	Cohesionless Soil A
Material Description	Brown Sandy Lean Clay	Brown Poorly Graded Sand With Silt and Gravel
Maximum Dry Unit Weight (kN/m^3) and Optimum Moisture Content (%)		
Standard Proctor	18.0 (14.6 %)	21.3 (7.2 %)
Modified Proctor	19.7 (11.3 %)	21.9 (6.2 %)
Gravel Content (%) (> 4.75mm)	6	30
Sand Content (%) (4.75mm – 75μm)	47	60
Silt Content (%) (75μm – 2μm)	31	7
Clay Content (%) (< 2μm)	16	3
Coefficient of Uniformity (c_u)	—	22.07
Coefficient of Curvature (c_c)	—	0.90
Liquid Limit, LL (%)	31	Non - Plastic
Plasticity Index, PI	13	Non - Plastic
AASHTO Classification	A-6 (5)	A-1-b
Unified Soil Classification (USCS)	CL	SP-SM

On average, E_{LWD-K2} is approximately 1.75 times greater than E_{LWD-Z2}. A similar trend of lower modulus (by factor of about 2 times) from the Zorn device was observed in a study conducted by the Danish Road Directorate (*see* Hildebrand 2003) when compared with the Keros. Others have also reported that the moduli from Zorn is generally in the range of about 0.5 to 0.6 times lower compared to other LWD devices with load cell and geophone displacement sensors (Fleming *et al*. 2000 and 2002).

Based on the results presented in Figure 9.4, deflections from the Zorn are on average about 1.5 times higher than the Keros. In short, the differences in E_{LWD} between these devices are believed to be related to: (a) the higher estimated deflections from the Zorn (or lower from Keros), and (b) the assumption of constant applied force of 6.96 kN in the case of the Zorn device versus measured loads for the Keros. The primary contributor to differences in E_{LWD} values is the difference in deflection values, as the constant assumed load of 6.69 kN by Zorn is very comparable to the average load from the Keros (6.56 kN) (*see* Figure 9.5). Figure 9.6 shows the comparison between predicted E_{LWD-K2} using an assumed load of 6.69 kN and the measured E_{LWD-K2}, which also indicates that the assumption of constant load in the test does not lead to significant errors in the measured values.
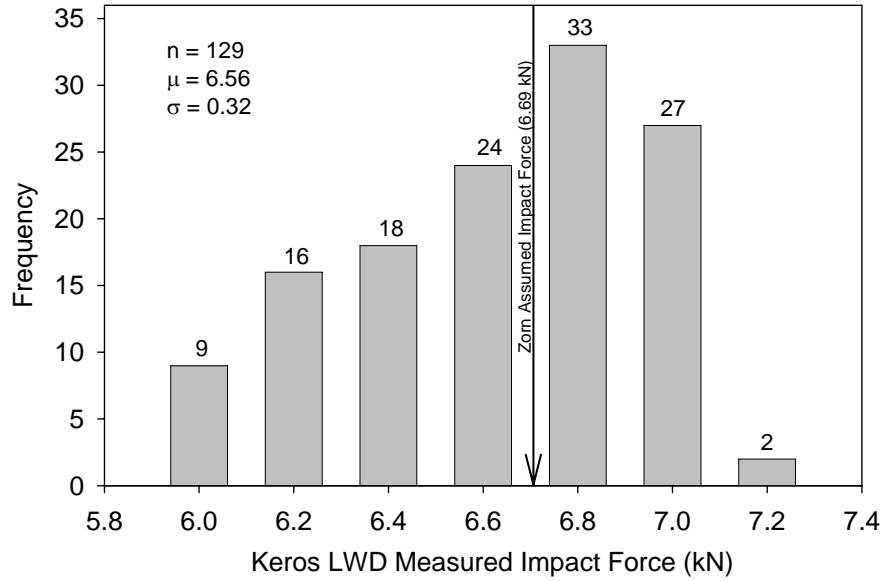
Figure 9.5. Frequency distribution of impact force by Keros LWD device
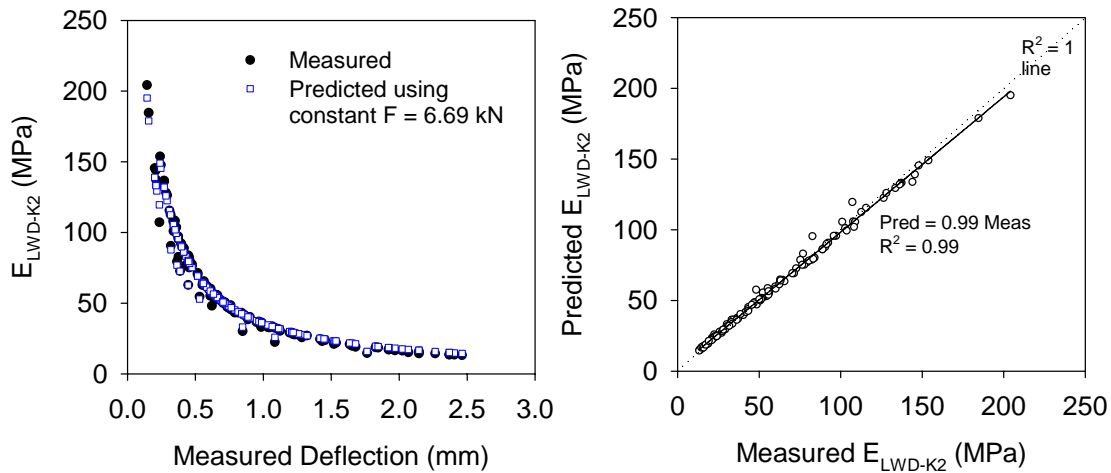
Figure 9.6. Comparison between Keros measured and predicted E_{LWD} moduli (assumption of constant force)

TH 64 Project Site

The LWD devices used at this project site are shown in Figure 9.7. Both devices were setup with 300 mm diameter plates. At some locations, a 200 mm diameter Zorn device was also used (shown in Figure 9.3a). The two primary objectives at this project site include investigating: (a)

the influence of plate diameter on modulus, and (b) differences between 300 mm plate diameter Zorn and Keros LWD devices.

A total of 46 tests were conducted on a capping layer which is two inches in thickness underlain by poorly graded fine sand. Soil index properties of the fine sand material are provided in Chapter 5 under section 5.4. To investigate the differences in E_{LWD}, the assumptions made in the calculations (i.e., Poisson's ratio and stress influence factors) were kept constant. A comparison between parameters used in the calculations and test procedures are provided in Table 9.6. Average applied stress for the last three drops was used in the modulus estimation for the Keros device, while an assumed force of 6.96 kN and 7.07 kN were used for the 200 mm and 300 mm Zorn devices due to 63 cm versus 72 cm drop heights, respectively.

Comparison results of modulus are presented in Figure 9.8 and 9.9. Figure 9.8 shows the difference between E_{LWD-Z2} and E_{LWD-Z3}. Linear regression relationship between the two values is also shown with R^2 value of 0.63. Figure 9.9 shows the difference between E_{LWD-Z2}, E_{LWD-Z3}, and E_{LWD-K3}. A relatively poor R^2 value of 0.37 is observed between these two values.

Figure 9.7. 300 mm plate Zorn and Keros LWD devices
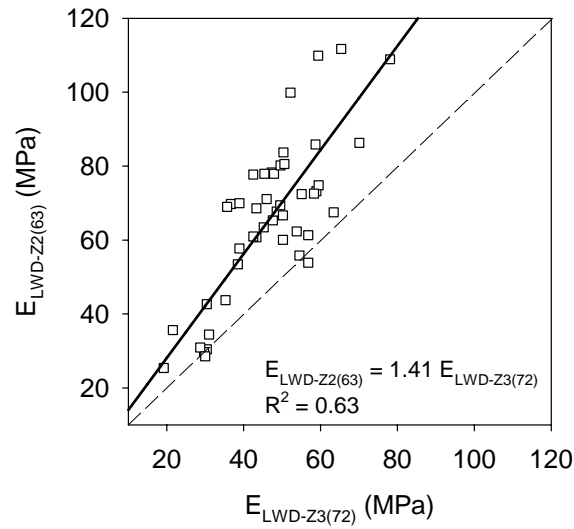
Figure 9.8. Comparison between 300 to 200 mm plate Zorn E_{LWD}
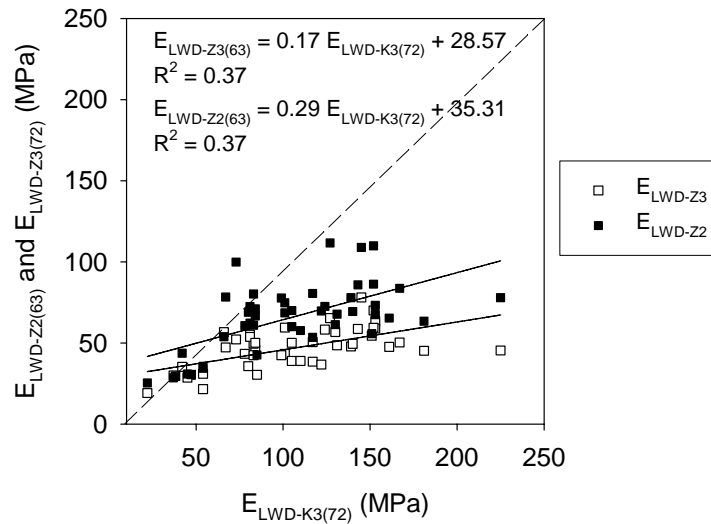
Figure 9.9. Comparison between 300 mm and 200 mm plate Zorn and Keros E_{LWD}

On average, E_{LWD-Z2} is approximately 1.4 times greater than E_{LWD-Z3}. This difference in E_{LWD} between two plate diameters is in general agreement with the linear rate equation proposed by Terzaghi (1955) (*see* equation 9.3 for which a 200 mm plate modulus can be approximately 1.45 times greater than a 300 mm plate modulus). Results presented in Chaddock and Brown (1995) also showed that a 200 mm plate E_{LWD} is approximately 1.3 to 1.5 times higher than that from a 300 mm plate.

A poor relationship with R^2 of 0.37 is observed between E_{LWD-Z3}, E_{LWD-Z2}, and E_{LWD-K3} (Figure 9.9). Deflection measurement comparison for this data was not possible as data was lost due to

problems with the Bluetooth device. However, based on the results from the MnROAD facility presented earlier, it is clear that the difference in deflection measurements is the primary contributor for the differences in estimated E_{LWD} between these devices. On average, E_{LWD} from 300 mm Keros is approximately 2.2 times greater than that from 300 mm Zorn. This ratio is in general agreement with the values reported by others (Hildebrand 2003, Fleming *et al.* 2000 and 2002).

9.4 Comparison of LWD Modulus and Resilient Modulus

To date very limited data showing relationships between in-situ LWD modulus and laboratory resilient modulus is available in the literature (Groenedijk *et al.* 2000, Swenson *et al.* 2006). An effort has been made in this study to build this relationship by obtaining shelby tube samples from a few select LWD test locations on compacted subgrade of test sections 27 and 28 at the MnROAD facility. Figure 9.10 shows the process of obtaining four inch diameter tube samples. Figure 9.11 shows an extracted sample. Resilient modulus and unconsolidated-undrained (UU) tests were performed on the tube samples in accordance with AASHTO T 307 standard procedure (*see* AASHTO 1999). For very dense and dry samples, a very thin layer (< 3mm) of fine sand was placed on the top and bottom of the extracted sample (*see* Figure 9.11 b) to create a level surface prior to placing the sample in the triaxial chamber.

Soil index properties of the subgrade soil are presented in Table 9.7 under mixed glacial till. LWD tests were performed adjacent to the shelby tube locations using the 200 mm plate diameter Zorn and Keros devices. Additional details on these devices and test conditions are provided in Table 9.6. Moisture content and dry density of the tube samples and LWD test results at the sample locations are presented in Table 9.8. Following the AASHTO T 307 procedure, the resilient modulus test is performed at several confining and deviator stress conditions that result in a range of resilient moduli. A high and a low resilient modulus for each sample is presented in Table 9.9 (see Tables in Appendix J) for resilient modulus results at all sequences along with Witczak and Uzan (1988) model coefficients). Maximum undrained shear strength (or at 5% strain), τ_{max}, and shear strength at 1% strain, $\tau_{1\%}$, are presented in Table 9.9.

(a)   (b)

Figure 9.10. Figures showing tube extraction process (a) Mn/DOT drill rig pushing a 4 inch diameter shelby tube, and (b) LWD and tube locations
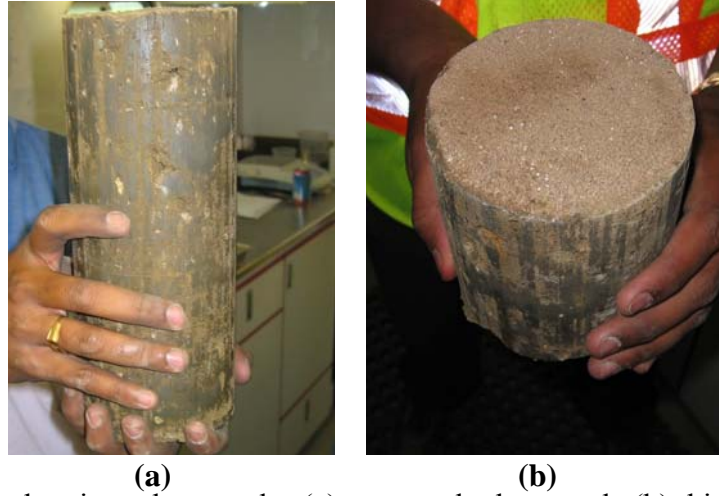
(a) **(b)**
Figure 9.11. Figure showing tube samples (a) extracted tube sample (b) thin layer of sand at the sample surface

Table 9.8. Brief summary of LWD modulus and shelby tube samples

Sample	Moisture (%)	Dry Density (kN/m³)	E_{LWD-Z2} (MPa)	E_{LWD-K2} (MPa)
27 # 1B	11.8	17.6	92.8	133.5
27 # 2	12.0	18.5	67.5	144.0
28 # 2	11.1	16.8	59.4	79.4
28 # 3	14.5	17.5	16.9	30.2
28 # 4	15.4	17.7	10.9	14.8
28 # 5	14.6	17.9	14.8	22.5
28 # 6	13.5	17.9	32.4	57.0

Table 9.9. Summary of resilient and deformation modulus and undrained shear strength of tube samples

Sample	M_r (MPa) High*	M_r (MPa) Low*	M_s (MPa) High*	M_s (MPa) Low*	M_r (MPa)**	M_s (MPa)**	Max. Shear Strength τ_{max} (kPa)	Shear Strength at 1% strain $\tau_{1\%}$ (kPa)
27 # 1B	194.8	75.7	107.3	41.7	148.2	89.2	290.6	290.6
27 # 2	151.5	78.6	52.5	16.4	151.5	44.0	332.5	280.0
28 # 2	101.9	63.6	37.4	13.5	88.0	35.0	84.2	80.0
28 # 3	102.4	57.7	21.3	6.0	71.2	19.8	135.2	80.0
28 # 4	89.2	34.3	12.7	3.9	48.0	12.7	104.2	55.0
28 # 5	74.0	32.0	20.5	4.2	55.2	13.0	142.6	45.0
28 # 6	95.7	54.1	34.3	8.3	81.8	24.8	128.9	85.0

Notes:
* High and low modulus values from the AASHTO T-307 resilient modulus test
** Values at σ_d = 68.9 kPa and σ_c = 41.4 kPa

As described earlier, E_{LWD} is a function of maximum deformation (or strain) under an applied plate contact stress. On the other hand, resilient modulus (M_r) is a function of resilient strain under a controlled cyclic deviator stress. Although it can be reasoned that a stiffer material can have a higher deformation and resilient moduli, practically the two moduli cannot be the same. Therefore, secant modulus (M_s) was also calculated from the permanent strain and resilient strain data from the resilient modulus test for comparison to E_{LWD}. E_{LWD}, M_r, and M_s are shown in Figure 9.13. Table 9.9 shows the high and low secant modulus values for each sample.

Although comparison between E_{LWD} and a range of laboratory M_r and M_s (shown as High and Low) gives a good approximation, it is probably more appropriate to develop these relationships for similar stress conditions (i.e. simulate the in-situ LWD stress conditions in the lab test). With the LWD setup used in this study, a maximum contact stress of approximately 210 kPa was applied at the ground surface. The maximum applied deviator stress during the resilient modulus test for subgrade soils on the other hand is about 68.9 kPa (following AASHTO T 307). For this reason, a deviator stress of 68.9 kPa and confining stress of 41.4 kPa (highest values following test protocol) were selected for M_r and M_s comparison to E_{LWD} and are shown in Table 9.9.

Comparison plots of Zorn and Keros 200 mm plate modulus with high/low resilient and secant modulus are shown in Figure 9.13. Comparisons with resilient and deformation modulus at a σ_d of 68.9 kPa and σ_c of 41.4 kPa are presented in Figure 9.14 and 9.15, and with maximum shear strength and shear strength at 1% strain are presented in Figure 9.16.   Some studies (e.g. Gupta *et al.* 2007 and Lee *et al.* 1972) indicate that resilient moduli and shear strength at 1% strain are well correlated. Results presented in Figure 9.15 show that LWD moduli are better correlated with shear strength at 1% strain compared to at failure or 5% strain, as well as resilient moduli at the selected deviator stress.
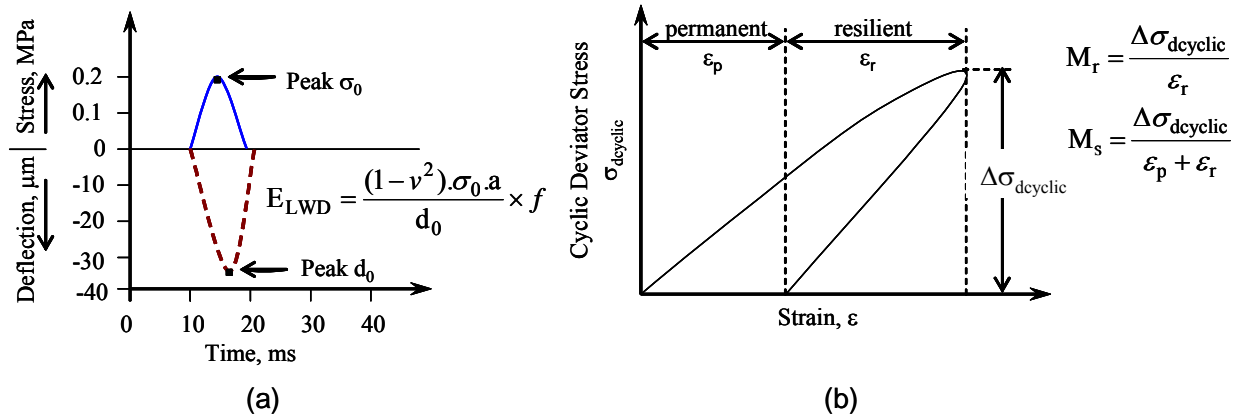
Figure 9.12. (a) typical load-deflection response in a LWD test (b) typical stress-strain response for one-loading cycle in a M_r test.
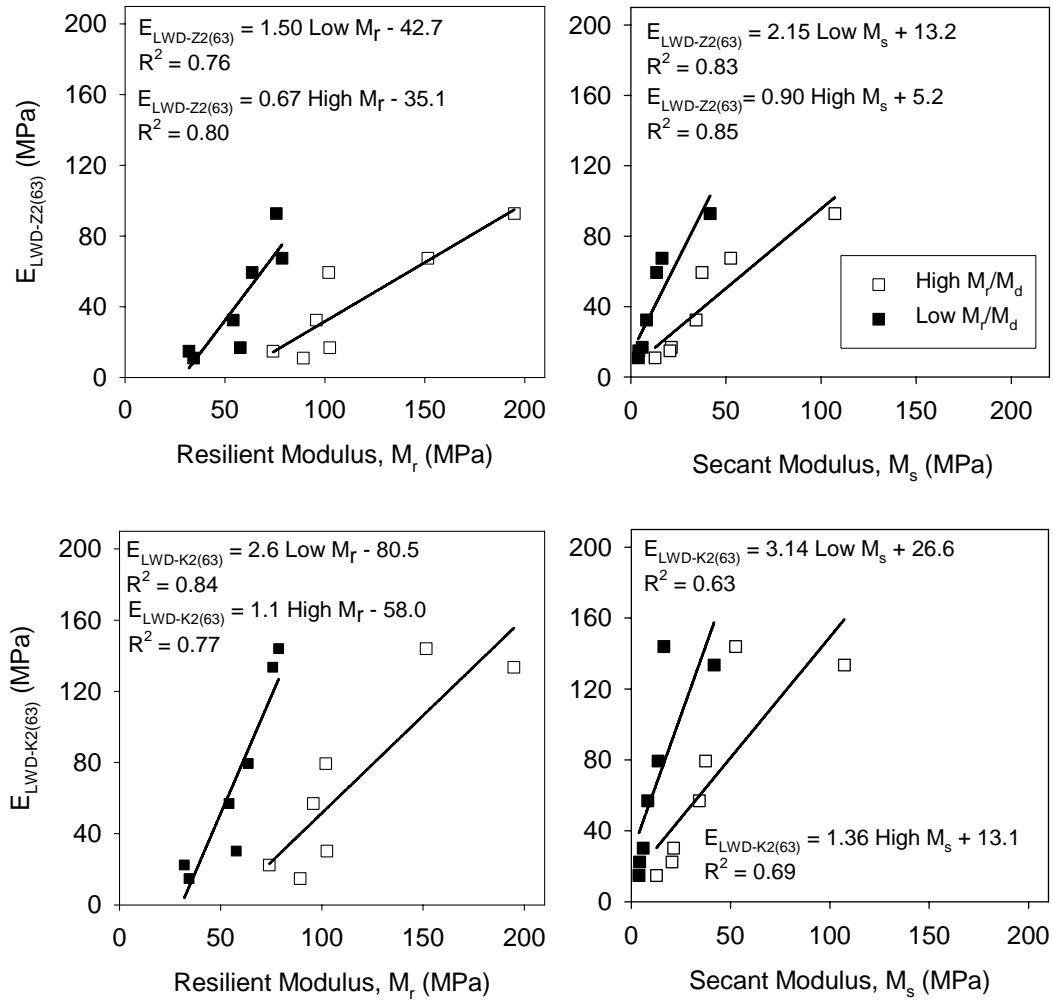
Figure 9.13. Relationship between Keros and Zorn E_{LWD} and higher and lower M_r and M_s
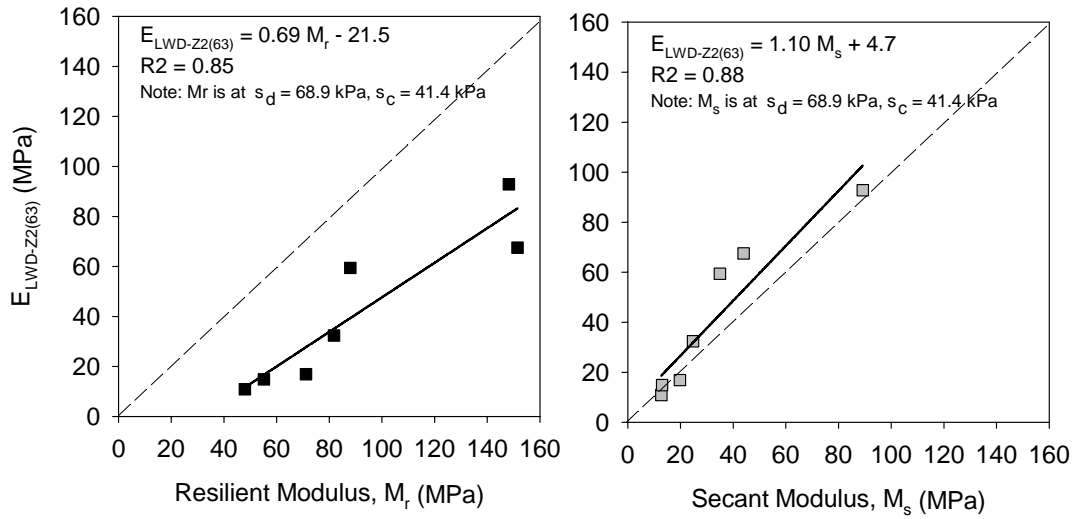
Figure 9.14. Relationship between 200 mm Zorn E_{LWD} and laboratory M_r and M_s
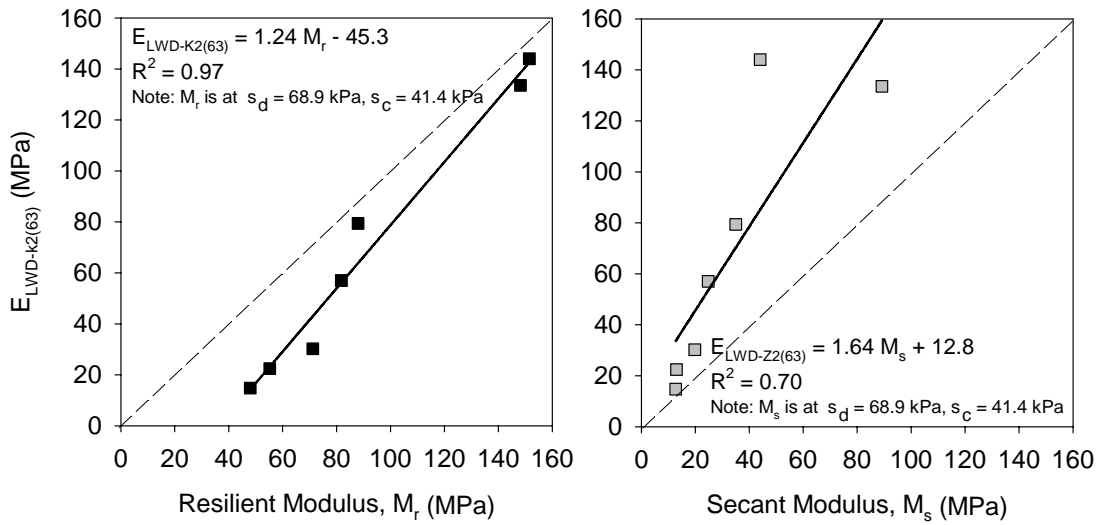
Figure 9.15. Relationship between 200 mm Keros E_{LWD} and laboratory M_r and M_s
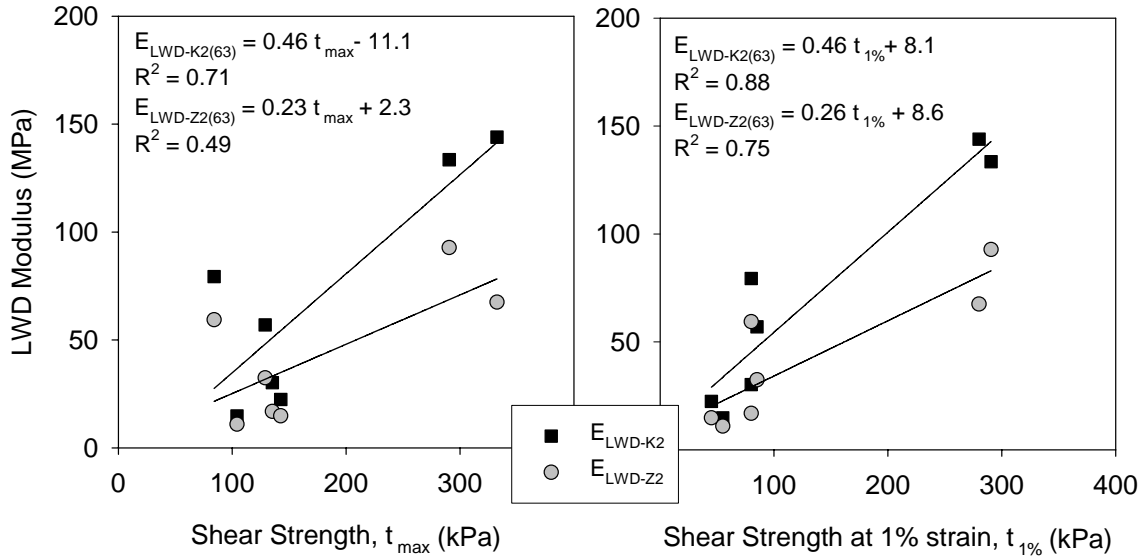
Figure 9.16. Relationship between E_{LWD} and (a) maximum shear strength, τ_{max}, and (b) shear strength at 1% strain, $\tau_{1\%}$

At the selected deviator and confining stress condition ($\sigma_d = 68.9$ kPa and $\sigma_c = 41.4$ kPa), on average, E_{LWD} from Zorn is approximately 0.5 times M_r and 1.2 times M_s, while E_{LWD} from Keros is approximately 0.7 times M_r and 2.0 times M_s. A strong correlation is observed for these relationships with R^2 coefficients between 0.70 and 0.97. It can be seen that the relationship between M_r and E_{LWD} has a comparatively larger intercept, while for M_s the intercept values are smaller (*see* Figures 9.12 and 9.13). A smaller intercept and a linear relationship were expected between M_s and E_{LWD}, as both parameter values are calculated using the peak deformation and peak stress. In the case of M_r, larger intercept values suggest a non-linear relationship at low moduli, i.e. at softer soil conditions with secant modulus < 10 MPa. The relationship derived between laboratory M_r and 300 mm Keros E_{LWD} is very similar to a correlation equation proposed between 300 mm Prima E_{LWD} and M_r by Groenedijk *et al.* (2000) (*see* equation 9.26).

Figure 9.14 presents the relationship between shear strength and E_{LWD}. Comparisons with maximum shear strength, which is determined from shear strength at failure or 5% strain, shows wide scatter in the data. When shear strength at 1% strain is compared with E_{LWD}, the correlation is improved with R^2 values between 0.75 and 0.88.

All the relationships described above show relatively strong correlations that warrant further data collection and analysis. The significance of this type of relationship is that it provides the opportunity to develop specifications that relate to pavement design parameters (i.e. M_r).

234

9.5 Key Findings and Conclusions

Some of the key findings from the literature review include:

- Factors that influence the estimation of E_{LWD} include: plate size, plate contact stress, type and location of deflection transducer, usage of load transducer, loading rate, and buffer stiffness. Contrasting information is available in the literature on the effect of plate contact stress on E_{LWD}.

- According to theoretical equations and experimental investigations by researchers, a 200 mm plate modulus can be approximately 1.3 to 1.5 times higher than that of a 300 mm plate.

- Differences in type and location of sensors used in the LWD devices lead to variations in E_{LWD}. LWD devices that use accelerometers that measure deflection of the plate (e.g. Zorn) are expected to measure larger deflections compared to devices that measure deflections on the ground with a geophone (e.g. Keros and Prima).

- Assumption of constant applied force does not lead to significant variations in the estimated modulus, as the LWD devices are commonly utilized to test stiff compacted layers.

- Correlations between E_{LWD} and other in-situ measurements (DCP, E_{SSG}, and E_{FWD}) are presented by several authors, for a wide variety of pavement foundation materials. Only limited data is available with correlations to laboratory resilient modulus.

Some of the key findings and conclusions from field and laboratory testing performed as part of this study include:

- The Keros E_{LWD} is on average 1.9 to 2.2 times greater than Zorn E_{LWD}. Strong linear relationship was observed between 200 mm plate Zorn and Keros with R^2 value between 0.87 and 0.9. A relatively poor correlation was observed between 300 mm plate Zorn and Keros E_{LWD} with R^2 of 0.37.

- The constant applied force of 6.69 kN in the 200 mm Zorn device was very comparable with average loads by 200 mm Keros device (6.56 kN). Therefore, primary contributor for differences in E_{LWD} values is the difference in measured deflections. On average, Zorn deflections are 1.5 times greater than Keros.

- The E_{LWD} of a 200 mm plate Zorn is approximately 1.4 times greater than of a 300 mm plate Zorn.

- A linear relationship between E_{LWD} and laboratory M_r was observed at a selected stress condition ($\sigma_d = 68.9$ kPa and $\sigma_c = 41.4$ kPa) with a strong correlation – R^2 values ranging from 0.85 to 0.97.

- A linear relationship between E_{LWD} and estimated secant modulus (M_s) was observed at a selected stress condition ($\sigma_d = 68.9$ kPa and $\sigma_c = 41.4$ kPa) with a strong correlation – R^2 values ranging from 0.75 to 0.88.

- Larger intercept values in relationships between E_{LWD} and M_r suggest a non-linear relationship at low moduli, i.e. at softer soil conditions with secant modulus about < 10 MPa. A smaller intercept values are observed as expected between M_s and E_{LWD}, as both parameter values are calculated using the peak deformation and peak stress.

- The correlations between shear strength and E_{LWD} are improved when compared at 1% strain ($R^2 = 0.75$ to 0.88) than with maximum shear strength ($R^2 = 0.49$ to 0.71).

Chapter 10
Specifications for IC Quality Management

10.1 Review of Existing Intelligent Compaction Specifications

Brief details of selected international roller-integrated compaction monitoring specifications and the 2006 TH64 Mn/DOT specification are summarized below. A comparison of the specifications is provided in Table 10.1.

10.1.1 Mn/DOT (2006 TH 64))

Equipment Specifications: Use smooth drum or padfoot vibratory roller weighing at least 11,300 kg (25,000 lbs.). Equipment must use a global positioning system to allow continuous recording of roller location and corresponding compaction-related output (e.g., number of roller passes and roller-generated materials stiffness measurements). Contractor shall provide at least one intelligent compaction (IC) instrumented roller during roadbed embankment construction. The IC roller must be the final roller used to obtain compaction on the proof layers.

Location Specifications (including size, depth, and track overlap): Each control (calibration) strip must be at least 100 m (300 ft) x 10 m (32 ft) at its base (or other size approved by Engineer). Thickness should equal that of the planned granular treatment thickness being constructed (maximum 1.2 m (4.0 ft)). Construct one control strip for each different type/source of grading material used on the construction site.

Compaction Process and Acceptance Specifications: Contractor and Engineer save material sample from each control strip for comparison to embankment material. Compaction and mixing shall be uniform from bottom to top and for the entire length and width of the embankment. Optimum compaction is reached when the Engineer determines that additional compaction passes do not result in a significant increase in stiffness. Intelligent Compaction Target Values (IC-TV) for all proof layers shall be the values obtained on the 1.2 m (4.0 foot) layer of each control strip—unless the layer thickness is < 0.75 m (2.5 ft). In that case, IC-TV is value obtained on the 0.6 m (2.0 ft) layer of the strip. All segments shall be compacted so at least 90% of the IC stiffness measurements are at least 90% of the IC-TV prior to placing the next lift. If localized areas have IC stiffness of less than 80% of the IC-TV, the areas shall be re-compacted. If a significant portion of the grade is more than 30% in excess of the selected IC-TV, the Engineer shall re-evaluate the IC-TV.

Misc. Specs (moisture, speed, frequency, etc.): Moisture should be 65%–100% of Optimum Moisture, as determined by the Standard Proctor Density Method. Contractor shall add water, and/or perform blending as needed to meet the moisture requirements. Control strips constructed at each moisture content extreme can be used to determine a linear IC-TV correction trendline. Engineer may order contractor to provide a light weight deflectometer and/or electronic moisture

meter or other moisture testing device. Engineer grants final approval, based on observation of final compaction/stiffness recording pass, approval of Weekly QC Reports, moisture tests, and test rolling requirements.

Documentation Requirements: Weekly QC Report must document all compaction results, IC stiffness measurements, moisture testing results, QC activities, and corrective construction actions taken in order to meet specs. Roller output must be immediate to allow for real-time corrections, must be available for review on demand, and must include a plan-view, color-coded plot of roller stiffness and/or pass number measurements (or other approved data format).

(Note: The 2007 Mn/DOT intelligent compaction projects will implement new/revised specifications for granular and cohesive materials including a light weight deflectometer (LWD) quality compaction pilot specification.)

10.1.2 ISSMGE

Equipment Specifications: Measuring system must enable a clear presentation of the required values, displayed directly to the roller driver. Roller should be chosen by experience, considering parameters of the specific construction site.

Location Specifications (including size, depth, and track overlap): Surface should be homogenous and even, allowing drum to have full ground contact. Contractor and controller should jointly determine the measuring field. Sizes of measuring fields and tracks should correspond to those of the test field. Usually, a section 100 m long by the width of the road (or embankment) is selected as a test field within the construction section. Overlap of roller tracks should not exceed 10% drum width.

Compaction Process and Acceptance Specifications: On a compacted test field, a forward measuring pass and then a reverse static pass must occur at least twice on each track. If any track differs widely from the average of the others, further passes must be performed to attempt additional compaction. Measuring passes for construction should be continued until the mean of a pass is no more than 5% higher than the mean of the preceding pass. Immediately after test compaction passes, nine measurements of the E_{v1} value must be performed at areas with low, medium, and high measuring values, where no double jump occurred. The "tester" selects measurement points.

The common calibration procedure involves the correlation of dynamic measuring values with the modulus of the static load plate test (E_{v1}); other tests are allowed. A linear regression must show a correlation coefficient ≥ 0.7. The minimum must be $\geq 95\%$ of the required E_{v1} value, and the mean must be $\geq 105\%$ (or $\geq 100\%$ during jump operation).

No more than 90% of the track should be below the specified minimum for each measuring pass. The measured minimum must be $\geq 80\%$ of the specified minimum. The percent standard deviation (relative to the mean) must be $\leq 20\%$ within a measuring pass.

Misc. Specifications (moisture, speed, frequency, etc.): Rollers must be operated at a constant travel speed (2–6 km/h, $\pm$ 0.2 km/h). The exciter frequency must be kept constant during each

measuring pass (tolerance range ± 2 Hz). If the fine grained portion (< 0.006 mm) exceeds 15%, special attention must be given to the water content.

Documentation Requirements: Calibration must document the following: rolling pattern, sequence of compaction and measuring passes; change of amplitude and/or travel speed (with reasons), comparative tests (locations, allocation to the specific measuring pass). Prior to each measuring pass, a track plot of the dynamic measuring values must be recorded (and must be printable). The minimum, maximum, mean, deviation, and other values must also be automatically documented for the following: dynamic measuring values, theoretical amplitude, frequency, travel speed, and jump operation. Area plot must be printed. Values must have assigned coordinates, stored for future review, and guaranteed free of manipulation.

10.1.3 Earthworks (Austria)

Equipment Specifications: Vibrating roller compactors with rubber wheels and smooth drums that can also be propelled are preferred, but other configurations are acceptable in certain circumstances. The vibration behavior of the drum must be reproducible.

Location Specifications (including size, depth, and track overlap): Sizes of measuring fields and tracks should correspond to those of the test field—usually 100 m long and the width of the site. Test section should be characteristic of the entire site. Track overlap should be ≤ 10% drum width. These factors should be attended to: evenness, inhomogeneities of materials or water content, loose surface, and location correspondence of the measurement locations (between the roller and the plate test).

Compaction Process and Specifications: On a compacted test field, a forward measuring pass and then a reverse static pass must occur twice on each track. If the result on a track differs widely from the average of the others, further passes must be performed to attempt additional compaction. Measuring passes for construction should continue until the mean of a pass is no more than 5% higher than the mean of the preceding pass.

Calibration involves the correlation of dynamic measuring values with the modulus of the static 30-cm load-bearing plate test (Ev1). In the test field, E_{v1} values should be measured immediately after the measurement run in locations with low, medium, and high dynamic measurement values (9 runs in places where no jump mode occurred). A linear regression must show a correlation coefficient ≥ 0.7. The minimum value must be ≥ 95% of the required E_{v1} value, and the mean must be ≥ 105% (or ≥ 100% during jump operation). No more than 90% of the track should be below the specified minimum for each measuring pass. The measured minimum must be ≥ 80% of the specified minimum. The percent standard deviation (relative to the median) must be ≤ 20% within a measuring pass. The measured maximum within a run cannot exceed the set maximum (i.e., 150% of the determined minimum).

Misc. Specifications (moisture, speed, frequency, etc.): Excitation frequency should be kept constant (tolerance ± 2 Hz). Forward travel velocity should be constant (2–6 km/h, ± 0.2 km/h). When the fraction of fine particles smaller than 0.06 mm is larger than 15%, special emphasis is laid on water compliance.

Documentation Requirements: Measurements must be linked to location coordinates, clearly displayed to the driver, and available for future review. Surface and track plots must be printable. The following should be recorded during calibration: compaction run plan, sequence of compaction and measurement runs, change in amplitude and/or speed (with explanation), and inter-comparison (location and allocation for every measurement run). For measurement runs, the system should automatically document the minimum, maximum, median, and deviation of dynamic measuring values, amplitude, frequency, speed, and jump mode.

10.1.4 Research Society for Road and Traffic (Germany)

Equipment Specifications: Self-propelled rollers with rubber tire drive are preferred; towed vibratory rollers with towing vehicle are suitable. Acceleration transducer must be correctly fitted at the drum of the roller. Operator must be able to read the measuring value, travel speed, and frequency on a display or recording unit.

Location Specifications (including size, depth, and track overlap): Surface must be level and free of puddles. Conditions of the calibration area must be almost identical to that of the testing area in regards to soil type, water content, layer thickness, bearing capacity of the support ground, type of compaction equipment and measuring roller, measuring system, and rest time after compaction. Track overlap should not exceed 10% machine width.

Compaction Process and Specifications: Calibration field is compacted over the full width, outside strips first. Each calibration area must cover at least 3 partial fields approx. 20 m. in length and have areas of light, medium, and high (full) compaction. Testing drives should occur in the same direction as calibration drives, must cover entire area to be evaluated, and cannot be performed during or immediately after heavy rain. Values detected during jump operation cannot be used if not auto-corrected by the system. Calibration available from a similar construction site may be used with customer agreement.

Calibration is based on either (1) the correlation of the dynamic measuring value and the static modulus of deformation Ev2 or (2) the degree of compaction. The correlation coefficient resulting from a regression analysis must be ≥ 0.7 for the calibration to be valid. Individual area units (the width of the roller drum) must have a dynamic measuring value within 10% of adjacent area units to be suitable for calibration measurements. After the test, poorly compacted spots must be subsequently compacted and re-tested. If widespread, the calibration may no longer be valid. Further examination of soil characteristics may be required.

Misc. Specifications (moisture, speed, frequency, etc.): Frequency and travel speed should be kept constant.

Documentation Requirements: Data must be recorded in a contractually agreed form and must be associated with the exact location of the testing lot, including the measuring value, speed, frequency, jump operation, amplitude, travel distance, time of measurement, roller type, soil type, water content, and layer thickness. Test report also includes purpose of test drive; date, time, file name, or registration number; weather conditions; position of test tracks and rolling direction in test lot; application position or absolute height; local conditions and embankments in

marginal areas; machine parameters; and any perceived deviations that occurred in the test drive. Graphical presentations of measuring data should be provided.

10.1.5 Vägverket (Sweden)

Equipment Specifications: Roadbases shall be compacted using a vibratory or oscillating single-drum roller exerting a linear load of at least 15–30 kN/m.

Location Specifications (including size, depth, and track overlap): Compaction shall be done on homogenous layers of non-frozen material. Thickness of largest layer is typically 0.2–0.6 m. The allowable deviation of surface levelness depends on layer type. An accepted layer must be inspected again if (1) intervening frost season occurs before placement of next layer, (2) surface has been used by traffic, or (3) adjustment is performed after the inspection. Protective layers < 0.5 m may be compacted with the sub-base.

Compaction Process and Specifications: Gravel wearing courses shall be compacted by two passes of a roller exerting a static linear load $\geq$ 15 kN/m. For unbound roadbases of surfaced roads in evenness classes 1–2 and for gravel roads, roller shall make at least 4 passes if a compaction meter with documentation system is used. Areas exhibiting bearing-capacity growth shall be compacted further.

Requirements for bearing capacity or degree of compaction should be met for the following objects: protective layers > 0.5 m thick and $\leq$ 6000 m^2, sub-bases $\leq$ 6000 m^2, and roadbases $\leq$ 4500 m^2. When a roller-mounted compaction meter is employed during compaction of unbound pavements, the bearing capacity or degree of compaction should be measured at two points in the inspection object—at the weakest sections, as indicated by the compaction meter (see "Surface-coverage compaction control" procedure).

Requirements for compaction and for the bearing capacity ratio (Ev2:Ev1) of the static plate loading test are dependent upon layer type. The mean of the two bearing capacity ratio values must be $\geq$ 40 for individually compacted protective layers, $\geq$ 110 for sub-bases under roadbases < 100 mm in thickness, $\geq$ 95 for sub-bases under roadbases $\geq$ 100 mm in thickness, and $\geq$ 130 for roadbases. The mean of the two degree of compaction values should be $\geq$ 89% for protective layers > 0.5 m thick and for any sub-base under a roadbase, and the mean should be $\geq$ 90% for roadbases. Other formulas are also in effect for determining the acceptability of measured Ev2:Ev1 values and ratios.

Misc. Specifications (moisture, speed, frequency, etc.): Best compaction is achieved if moisture content is close to optimal (as determined by separate procedure). Compactor must move at a constant speed of 2.5–4.0 km/h, and low amplitude should be used during compaction. Dry density may be measured via isotope meter (see other procedures for determining maximum dry density).

Documentation Requirements: None specified.

Table 10.1. Summary of intelligent compaction specifications

	Equipment	Field Size	Location Specs	Documentation	Compaction Specs	Speed	Freq.
Mn/DOT (2006 TH 64)*	Smooth drum or padfoot vibratory roller (25,000 lbs.)	300 ft x 32 ft (minimum at base). Max 4 ft. thick.	One calibration/ control strip per type or source of grading material	Compaction, stiffness, moisture, QC activities, and corrective actions (weekly report)	90% of the stiffness measurements must be at 90% of the compaction target value.	Same during calibration and production compaction	
ISSMGE	Roller chosen by experience	100 m by the width of the site	Homogenous, even surface. Track overlap ≤ 10% drum width.	Rolling pattern, sequence of compaction and measuring passes; amplitude, speed, dynamic measuring values, frequency, jump operation, and corresponding locations	Correlation coefficient ≥ 0.7. Minimum value ≥ 95% of E_{v1}, and mean should be ≥ 105% (or ≥ 100% during jump mode). Dynamic measuring values should be lower than the specified minimum for ≤ 10% of the track. Measured minimum should be ≥ 80% of the specified minimum. Standard deviation (of the mean) must be ≤ 20% in one pass.	Constant 2–6 km/h (± 0.2 km/h)	Constant (± 2 Hz)
Earthworks (Austria)	Vibrating roller compactors with rubber wheels and smooth drums suggested	100 m long by the width of the site	No inhomogeneities close to surface (materials or water content). Track overlap ≤ 10% drum width.	Compaction run plan, sequence of compaction and measurement runs, velocity, amplitude, frequency, speed, dynamic measuring values, jump operation, and corresponding locations	Correlation coefficient ≥ 0.7. Minimum value ≥ 95% of E_{v1}, and median should be ≥ 105% (or ≥ 100% during jump mode). Dynamic measuring values should be lower than the specified minimum for ≤ 10% of the track. Measured minimum should be ≥ 80% of the set minimum. Measured maximum in a run cannot exceed the set maximum (150% of the determined minimum).Standard deviation (of the median) must be ≤ 20% in one pass.	Constant 2–6 km/h (± 0.2 km/h)	Constant (± 2 Hz)
Research Society for Road and Traffic (Germany)	Self-propelled rollers with rubber tire drive are preferred; towed vibratory rollers with towing vehicle are suitable.	Each calibration area must cover at least 3 partial fields ~20 m. long	Level and free of puddles. Similar soil type, water content, layer thickness, and bearing capacity of support layers. Track overlap ≤ 10% machine width.	Dynamic measuring value; frequency; speed; jump operation; amplitude; distance; time of measurement; roller type; soil type; water content; layer thickness; date, time, file name, or registration number; weather conditions; position of test tracks and rolling direction; absolute height or application position; local conditions and embankments in marginal areas; machine parameters; and perceived deviations	The correlation coefficient resulting from a regression analysis must be ≥ 0.7. Individual area units (the width of the roller drum) must have a dynamic measuring value within 10% of adjacent area to be suitable for calibration.	Constant	

	Equipment	Field Size	Location Specs	Documentation	Compaction Specs	Speed	Freq.
Vägverket (Sweden)	Vibratory or oscillating single-drum roller. Min. linear load 15–30 kN. Roller-mounted compaction meter optional.	Thickness of largest layer 0.2–0.6 m.	Layer shall be homogenous and non-frozen. Protective layers < 0.5 m may be compacted with sub-base.	—	Bearing capacity or degree of compaction requirements may be met. Mean of compaction values for two inspection points ≥ 89% for sub-base under roadbase and for protective layers over 0.5 m thick; mean should be ≥ 90% for roadbases. Required mean for two bearing capacity ratios varies depending on layer type.	Constant 2.5–4.0 km/h	—

* Note: The 2007 Mn/DOT intelligent compaction projects will implement new/revised specifications for granular and cohesive materials including a light weight deflectometer (LWD) quality compaction pilot specification.

10.1.6 Key Attributes for Quality Management Using IC: Equipment Requirements

Intelligent compaction specifications and intelligent compaction rollers should be established to provide the following capabilities.

- Real-time corrections in the compaction process by the roller operator and inspection personnel.

- On-demand visual review of in-cab monitor by inspector.

- Data provided to inspector in a timely manner in the form of printed, plan-view color maps.

- Data provided to inspector in a timely manner in the form of comma delimited ASCII data files identified by fixed format filenames containing the data, time and location of the proof layer.

- Summary of quality control parameters that include, roller compaction value (e.g. IC-TV), resonance meter value (RMV), operation parameters (amplitude, frequency, speed), and roller pass number.

- Roller position for each data record accurate to the frequency of the drum (x, y, z) coordinates for each end of the drum in UTM NAD 1983.

- Includes timestamp for each data record to the frequency of the drum.

10.2 Conceptual Approach to Quality Acceptance (and Database Population) Using Intelligent Compaction

10.2.1 Method Overview

The preceding sections on key attributes for quality management using intelligent compaction, combined with the results from field studies and subsequent analyses, provide the basis for a conceptual process for quality acceptance and database development using intelligent compaction technology. As with any instrumented system, some level of calibration is required. The detailed process of on-site calibration is outlined in Figure 10.1 and is comprised of five primary steps that include: (1) roller data collection on a calibration area, (2) semivariogram modeling to determine sampling requirements, (3) in-situ testing using other approved testing devices on calibration area parallel with compaction process, (4) regression analysis to determine target values, and (5) evaluation of production soil compaction using target machine values and semivariogram parameters as indicators of quality.

The process starts by compacting a calibration area (control strip) with intelligent compaction technology to collect roller data (Step 1). Using this data, the semivariogram parameters may be fit to a model (Step 2). As described in Chapter 7, the semivariogram describes how measurements are related considering their spatial distribution. At *lag* or *separation* distances (distance between pairs of data) beyond the range, measurements are no longer spatially related. Therefore, the range value may be used as an interval for in-situ testing to ensure that soil property measurements are independent, which is important for assessing the reliability of the these measurements.

As compaction of the calibration area continues, in-situ compaction measurements using other approved devices will also be collected over the compaction area (Step 3). At each test location, several in-situ tests will be performed across the width of the roller and averaged to generate one regression point. This measure increases the reliability associated with the measurement and also helps account for variation across the drum width, which is averaged by the roller in providing a machine measurement value at a particular location. In order to improve the regressions, the collection of intelligent compaction and in-situ measurements should occur over a wide range of states of compaction (i.e. low to high number of roller passes). Clearly, as the range over which regression data is obtained increases, the correlations improve.

Regressions which use average in-situ compaction measurements over the width of the drum and roller data that is averaged over a 1-m length in the direction of roller travel are developed (Step 4). In addition to a least-squares best fit line, confidence intervals may also be plotted to indicate the reliability of the regression equation. For a given C property value, the upper confidence interval for obtaining a target value will be the minimum machine value that, with the desired confidence, will achieve the specified E_{LWD-Z2} property. It is noted that by either developing the regression over the widest possible range of values or by increasing the in-situ testing (regression points), the confidence intervals may "tighten up" to potentially reduce the target value. In other words, it may be to the contractor's and/or owner's benefit to make an increased initial investment in performing more spot tests to calibrate the roller.

In moving towards applying quality acceptance criteria to data collected during production compaction operations (Step 5), the results from semivariogram modeling and regression analyses will be used. As was used for TH 64, evaluation criteria may include a desired percent of the data within an evaluation window must exceed the target value. The performance of the compacted materials will be ensured by specifying that the majority of data within a window empirically corresponds to the specified soil property (e.g. modulus, dry unit weight). In terms of uniformity, one might specify that the variance, which is the square of the standard deviation, be less than twice the *sill* value from Step 2. For an evaluation window with dimensions the size of the range, the *sill* value, which is half of the variance, is a lower limit of acceptable uniformity (provided the calibration area was constructed using acceptable practices).
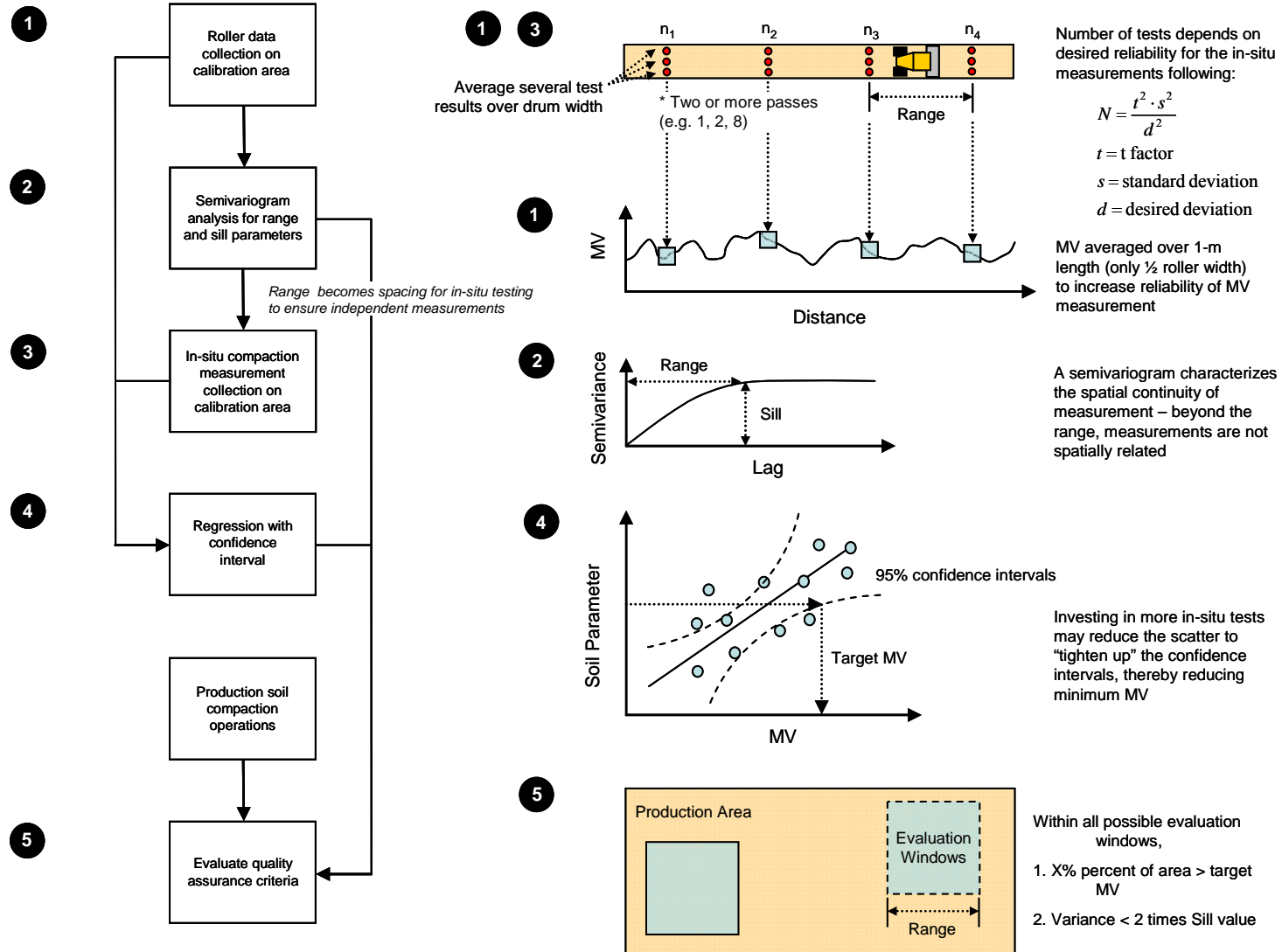
Figure 10.1. Conceptual process for quality assurance (database population) using intelligent compaction technology

10.2.2 Level 1: Statistically-Rigorous Roller Calibration

The most statistically-rigorous roller calibration will be achieved with a relatively large quantity of roller and other in-situ device compaction data. The need for many data results from several sources of variability and measurement error that influence the precision and bias and also several factors affecting intelligent compaction measurements. Possible sources of variability and measurement error include: (1) inherent soil variation, (2) GPS location measurement error (for matching intelligent compaction data with in-situ test results), (3) intelligent compaction sensor measurement error, and (4) test device/operator measurement error. The factors which affect intelligent compaction measurements differently than in-situ test results include: (1) measurement influence depth, (2) multi-layered soil with variable stiffness, (3) roller-induced confining pressure during IC measurement, (4) stress-dependent soil behavior, and (5) roller operational conditions (e.g. amplitude, frequency). These issues complicate generating relationships between intelligent compaction data and in-situ test results, and therefore, additional data will be collected to produce more meaningful interpretation of the results.

Large datasets allow for statistical averaging that increases the reliability of a measurement at a particular location and also for improved correlation between measurement systems. For example, Field Study 3 (Chapter 5) and previous studies have found that single measurements do not provide a high level of confidence in being representative of the average, particularly when addressing variable compaction parameters and intelligent compaction data. In combining averaged data from a small, uniform areas (e.g. proof at TH 64), however, the correlations between different measurements improve (e.g. proof-scale regression versus project-scale regression in Chapter 5).

Guidelines for establishing calibration data requirements apply principally to in-situ testing, as intelligent compaction data are monitored and stored nearly continuously. As was described in Section 10.2.1 and shown in Figure 10.1, in-situ testing using approved devices should occur at three locations across the drum width to account for soil variability, the influence of rear tire compaction, and also to increase the measurement reliability. These data may be collected at three to five test locations within the calculated (geostatistical) range interval (nine to 15 tests performed per range interval). Then, in building a regression from data collected throughout the entire compaction process (e.g. 1, 2, 4, 8 passes), the data within each range interval (three to five points) may be averaged – in which case intelligent compaction data are also averaged over the range interval – or treated as individual test points. If desired, the in-situ test data may be analyzed to characterize spatial uniformity.

10.2.3 Level 2: Reduced Roller Calibration Requirements

Level 1 roller calibration admittedly requires significant initial investment in collecting in-situ compaction measurements. Provided the contractor and/or owner are willing to accept greater risk, the sampling requirements may be reduced (Level 2). Level 2 roller calibration may also be used at later stages of an earthworks project after the initial calibration relationships have been

developed. An inspector may overlay the regressions from calibration with reduced sampling over those generated from more frequent sampling to evaluate whether significant changes (if any) are attributed to changes in material type, construction operations, etc. Calibration that does not appear to reflect the new conditions may indicate the need to re-calibrate the intelligent compaction measurements (Level 1) for the new conditions.

The in-situ testing requirements may be reduced to only one test at each location (i.e. not three across the drum width) and only one test location per range interval. These data may still allow for regression model development or verification, but may disallow geostatistical analysis. Use of the semivariogram for a particular measurement generally requires at least three to five data points spaced closer than the range distance.

10.2.4 Level 3: Options for Eliminating Roller Calibration

The current Mn/DOT intelligent compaction specification (and the approach documented above) requires the construction of control strips in order to determine target values. Continued construction of control strips is not desired by Mn/DOT, such that new methods of establishing target values are needed. In recognizing that an owner runs greater risk by not incorporating calibration into the quality acceptance process, the following options are provided as alternatives to constructing control/calibration strips.

1. Database of target machine parameters (see Table 10.2 to Table 10.5). Mn/DOT may initially incorporate calibration on projects. With time and experience, the agency may populate a database of target machine parameters that includes different intelligent compaction technologies and roller configurations, soil types, and representative lift sections. Later, inspectors may simply pull out target values from the database that correspond to conditions of their project. Some supplemental in-situ verification testing for quality assurance may be used during production soil compaction to verify that the target value is providing reasonable estimates of in-situ performance parameters.

2. Laboratory procedure for estimating target values for the roller and other in-situ devices machine parameters. New laboratory testing protocols may be developed that allow for some empirical relation to in-situ compaction/stiffness measured by the roller and other in-situ devices.

3. Existing relationships between machine parameters and material properties. Relationships between in-situ and roller-integrated compaction measurements have been documented in this report and in other literature (White *et al*. 2006, White *et al*. 2007). These relationships might be extrapolated for use on an earthwork construction project, but must consider the influence of moisture content, lift thickness, variable stiffness of underlying layers, and roller operational conditions (e.g. amplitude, frequency, speed) on soil compaction and machine response.

Table 10.2. Values for MDP, dry unit weight, and E_{LWD}, and DCP index for different soils (mean, coefficient of variation)

Soil Type	Roller Configuration	MDP (kJ/s)	w (%)	Dry Unit Weight (kN/m^3)	$E_{LWD-K3(61)}$ (MPa)	DCP Index (mm/blow)	Dataset Reference
ML [a]	Static Padfoot	8.8, 44	23, 7	15.3, 3	24, 52	92, 14	White *et al*. (2006)
ML [a]	Static Padfoot	9.6, 46	22, 5	15.2, 3	27, 57	87, 17	White *et al*. (2006)
ML [a]	Static Padfoot	3.8, 97	18, 6	15.2, 2	47	38	White *et al*. (2006)
ML [a]	Static Padfoot	2.6, 84	17, 8	15.7, 3	127, 71	36, 18	White *et al*. (2006)
ML [a]	Static Padfoot	2.9, 92	15, 7	14.6, 2	49, 23	28, 23	White *et al*. (2006)
ML [a]	Static Padfoot	1.7, 99	16, 5	14.8, 4	49, 37	28, 49	White *et al*. (2006)
CL [b]	Static Padfoot	11.9, 30	21	–	22	139	White *et al*. (2006)
CL [b]	Static Padfoot	2.4, 72	15, 11	15.6, 4	49, 58	36, 28	White *et al*. (2006)
CL [b]	Static Padfoot	7.5, 43	18, 6	15.8, 4	59, 62	94, 27	White *et al*. (2006)
CL [c]	Static Padfoot	3.1, 59	8, 5	16.1, 2	65, 33	18, 15	White *et al*. (2006)
CL [c]	Static Padfoot	2.1, 80	8, 5	15.8, 2	45, 46	29, 17	White *et al*. (2006)
CL [c]	Static Padfoot	12.0, 35	17, 6	17.1, 2	18, 59	147, 15	White *et al*. (2006)
CL [c]	Static Padfoot	7.9, 94	15, 8	17.3, 4	–	77, 35	White *et al*. (2006)
CL [c]	Static Padfoot	4.1, 128	11, 9	15.4, 8	102, 38	34, 22	White *et al*. (2006)
SW-SM [d]	Static Padfoot	15.1, 20	7, 6	16.6, 2	41, 19	123, 12	White *et al*. (2006)
SW-SM [d]	Static Padfoot	10.3, 39	10, 8	17.9, 2	24, 27	70, 4	White *et al*. (2006)
SW-SM [d]	Static Padfoot	11.7, 24	11, 7	17.8, 2	28, 22	62, 13	White *et al*. (2006)
CL [c]	Vibratory Padfoot	10.6	14	17.2	51	–	White *et al*. (2006)

CL [c]	Vibratory Padfoot	8.9	8	17.8	31	–	White *et al*. (2006)
GM [e]	Vibratory Smooth	5.3	8, 10	17.2, 4	38, 38	17, 21	White *et al*. (2007)
SM [f]	Vibratory Smooth	4.2	4, 15	19.4, 3	34, 18	17, 10	White *et al*. (2007)
GP [g]	Vibratory Smooth	5.4	3, 15	15.0, 6	–	–	White *et al*. (2007)
SM [h]	Vibratory Smooth	5.7	6, 14	18.7, 3	23, 25	45, 20	White *et al*. (2007)
GC [i]	Vibratory Smooth	4.1	8, 11	18.5, 2	40, 49	19, 31	White *et al*. (2007)
SW-SM	Vibratory Smooth	0-20	5-15	16-19	–	–	Field Study 1

a w_{opt} = 15%, $\gamma_{d,max}$ = 17.2 kN/m^3

b w_{opt} = 14%, $\gamma_{d,max}$ = 18.1 kN/m^3

c w_{opt} = 7%, $\gamma_{d,max}$ = 19.9 kN/m^3

d $\gamma_{d,max}$ = 18.8 kN/m^3

e w_{opt} = 8%, $\gamma_{d,max}$ = 19.5 kN/m^3

f $\gamma_{d,max}$ = 20.1 kN/m^3

g Standard Proctor not applicable

h w_{opt} = 8%, $\gamma_{d,max}$ = 19.8 kN/m^3

i w_{opt} = 10%, $\gamma_{d,max}$ = 20.0 kN/m^3

Table 10.3. Values for CMV, dry unit weight, and E_{LWD}, and DCP index for different soils (mean, coefficient of variation)

Soil Type	Roller Configuration	CMV	w (%)	Dry Unit Weight (kN/m³)	E_{LWD} (MPa)	DCP Index (mm/blow)	Dataset Reference
GM [a]	Vibratory Smooth	10.3	8, 10	17.2, 4	38, 38	17, 21	White *et al*. (2007)
SM [b]	Vibratory Smooth	17.3	4, 15	19.4, 3	34, 18	17, 10	White *et al*. (2007)
GP [c]	Vibratory Smooth	21.5	3, 15	15.0, 6	–	–	White *et al*. (2007)
SM [d]	Vibratory Smooth	15.1	6, 14	18.7, 3	23, 25	45, 20	White *et al*. (2007)
GC [e]	Vibratory Smooth	14.9	8, 11	18.5, 2	40, 49	19, 31	White *et al*. (2007)
SW-SM	Vibratory Smooth	0-50	5-15	16-19	–	–	Field Study 1
SP [f]	Vibratory Smooth	40-65	7-12	17-21	35-90 [h]	10-25 [i]	Field Study 3

a w_{opt} = 8%, $\gamma_{d,max}$ = 19.5 kN/m³

b $\gamma_{d,max}$ = 20.1 kN/m³

c Standard Proctor not applicable

d w_{opt} = 8%, $\gamma_{d,max}$ = 19.8 kN/m³

e w_{opt} = 10%, $\gamma_{d,max}$ = 20.0 kN/m³

f w_{opt} = 10%, $\gamma_{d,max}$ = 20.0 kN/m³

g $E_{LWD-K3(61)}$

h $E_{LWD-Z2(63)}$

i Mn/DOT DPI calculation

Table 10.4. Values for k_B, dry unit weight, and E_{LWD}, and DCP index for different soils (range)

Soil Type	Roller Configuration	k_B (MN/m)	w (%)	Dry Unit Weight (kN/m³)	$E_{LWD-K3(61)}$ (MPa)	DCP Index (mm/blow)	Dataset Reference
CL [a, b]	Vibratory Smooth	30-40	–	–	10-50	5-10	Field Study 2
SP-SM [c]	Vibratory Smooth	20-35	10-14	16-17	20-40	40-110	Field Study 2
CL [a, b]	Vibratory Smooth	20-45	15-20	16-18	60-110	10-40	Field Study 2
SP-SM [c]	Vibratory Smooth	25-40	7-10	18-19	10-70	25-50	Field Study 2
CL [a]	Vibratory Smooth	10-35	15-20	16-17	10-80	10-60	Field Study 2
a w_{opt} = 18%, $\gamma_{d,max}$ = 16.2 kN/m³ b Excludes median testing c w_{opt} = 8%, $\gamma_{d,max}$ = 19.6 kN/m³							

Table 10.5. Values for E_{VIB}, dry unit weight, and E_{LWD}, and DCP index for different soils (mean, coefficient of variation)

Soil Type	Roller Configuration	E_{VIB} (MPa) [a]	w (%)	Dry Unit Weight (kN/m^3)	$E_{LWD-K3(61)}$ (MPa)	DCP Index (mm/blow)	Dataset Reference
SM [b]	Vibratory Smooth	46.6, 91	10, 28	19.6, 4	–	40, 77	Petersen (2005)
GW-GM [c]	Vibratory Smooth	46.6, 91	4, 25	20.6, 4	–	23, 18	Petersen (2005)
a Values for combined soils b w_{opt} = 10%, $\gamma_{d,max}$ = 19.3 kN/m^3 c w_{opt} = 11%, $\gamma_{d,max}$ = 20.7 kN/m^3							

Chapter 11
Summary and Conclusions

11.1 Summary

The successful implementation of intelligent compaction technology and performance related specifications into earthwork construction practice requires knowledge of the roller-integrated compaction measurements and their relationships with the engineering and index properties of materials used for pavement design (e.g. resilient modulus). These relationships were studied at three earthwork construction projects in Minnesota. In these field studies, intelligent compaction and in-situ test data were collected to demonstrate use of the various technologies, characterize the variation associated with each measurement system, aid performance of regression analyses, and ultimately to provide recommendations that improve current specifications.

IC technology provides opportunity to collect and evaluate information for 100 percent of the project area, but it also produces large data files that create analysis, visualization, transfer, and archival challenges. An approach for managing large quantities of data is to create a "geodatabase" using ArcGIS modules. A geodatabase of the TH 64 project IC data and in-situ spot test measurements was created to demonstrate this application.

Applying geostatistical methods in the analysis of IC data has the advantage of quantifying spatial variability, which is not possible with classical statistical analysis. An approach to characterize uniformity with IC data using spatial statistics and a simplified procedure for implementing geostatistics in IC quality control procedures in conjunction with current Mn/DOT acceptance criteria is proposed.

Laboratory compaction of pavement foundation materials should simulate the mechanics and energy delivery system that occurs in the field. This is particularly important as it relates to fabric/structure and measuring engineering properties (e.g. strength and stiffness) of materials compacted in the lab. Laboratory compaction tests were performed using impact, static, gyratory, and vibratory compaction methods for one cohesive soil and one granular soil to examine the differences in moisture-density relationships between these methods. Laboratory resilient modulus (M_r) and unconsolidated-undrained (UU) strength tests were also performed on samples prepared using the aforementioned compaction methods to evaluate the effects of compaction method on these mechanistic properties.

Mn/DOT is in the process of evaluating and implementing the LWD as a QC/QA tool on a state-wide basis. To successfully implement these devices, it is important to understand the conditions for which they provide reliable measurements and also if differences exist between calculated elastic moduli values between the various devices. Two LWD devices (ZFG 2000 manufactured by Zorn Stendal from Germany, and the Keros manufactured by Dynatest in Denmark) with different plate diameters were used side-by-side for testing various pavement subgrade and base layers to observe the differences in E_{LWD} between the devices, and the influence of plate

diameter on the E_{LWD} values. Shelby tube samples were also obtained from a compacted subgrade to evaluate the relationship between in-situ E_{LWD} and laboratory resilient modulus.

11.2 Conclusions

The conclusions drawn from field studies with intelligent compaction technology are:

- Bringing intelligent compaction technology to field projects of transportation agencies helps to transfer the technology to both agency and contractor personnel that will benefit in the future.

- Intelligent compaction technology effectively identifies areas of weak or poorly-compacted materials with real-time readings and 100-percent coverage.

- Comparisons between Ammann k_B and in-situ compaction measurements showed strong relationships between k_B and in-situ test results for strips with a relatively wide range of materials stiffness and comparatively weak relationships for strips with more uniform conditions. The results can be used to establish target values for k_B and other relevant specification criteria.

- The ability of variable feedback control of amplitude and frequency by the Ammann roller (used at the US 14 project) to produce more uniform compaction was not clear from the limited dataset.

- An area compacted with the Ammann vibratory roller and tested using in-situ test devices was then test rolled to demonstrate the ability of k_B data to identify weak subgrade which are evidenced by rutting of the Mn/DOT test roller.

- Intelligent compaction technology was successfully implemented by the Mn/DOT as the principal quality control tool on the TH 64 grading project near Akeley, Minnesota. The entire project passed the test rolling acceptance criteria.

- Control sections were constructed and tested in order to establish appropriate quality criteria which were then applied to production areas. Compaction curves observed with control section CCV data for fine sand material show that little compaction occurs after the initial roller pass.

- CCV and in-situ test results are poorly correlated at the proof scale, because insufficient variation is observed in the smaller areas. At the project scale using average values for different proof sections, dry unit weight and DCP index were predicted from CCV with R^2 values of 0.52 and 0.79, respectively. Scatter was still observed for E_{LWD} and attributed to different measurement influence depths of this compaction control device and the roller.

255

A summary of key findings and conclusions from geostatistical analysis on the TH 64 IC data include:

- Roller data output with data assigned to the center of the drum can provide reliable results in spatial analysis. Single point data assigned to left or right side of the drum or both sides of the drum result in significant errors (> 20%).

- Variogram models can be used in characterizing uniformity by quantifying spatial variability and continuity.

- The "range" distance from a variogram plot can potentially be used as a separation distance between spot test measurements to ensure independent measurements.

- Anisotropy in the IC data is realized with greater spatial continuity along the direction of roller travel than the transverse direction.

- Proof Nos. 14 and 15 which "pass" the Mn/DOT acceptance criteria have failed to meet the alternatively proposed "sill" criteria for uniformity. When these proofs are divided into incremental spatial sections, at least three sections about 30.5 m long failed to meet the Mn/DOT acceptance criteria. The implication of such incremental spatial analysis is that it will aid the contractor in identifying localized poorly compacted areas or highly non-uniform conditions, which are often the root cause of pavement problems.

- Using "range" as the minimum window size for an area of evaluation, a 60 m long section was analyzed and found that several isolated locations failed to meet the Mn/DOT acceptance criteria. The scale at which the acceptance criteria is based is still a question that needs further evaluation.

- Despite the different conditions affecting in-situ spot test measurements and roller-integrated measurements, relatively good spatial comparison of CCV, CIV, and E_{LWD} was observed for a proof area.

The conclusions drawn from the laboratory compaction study on one cohesive and one granular soil are:

- Distinctly different moisture-density curves were realized between static, impact, gyratory, and vibratory compaction methods for the two materials.

- The vibratory compaction method was inadequate to effectively characterize the moisture-density relationships for the cohesive soil. This method provided effective results with the granular soil.

- Changes in moisture-density relationships with increasing impact energy are apparent for the cohesive soil but not for granular soil. The dry unit weight of granular soil increased only slightly (about 1% to 2%) with increasing impact energy from standard to modified Proctor energy at any moisture content.

- Optimum moisture contents are not observed with the static compaction method. Increase in static compaction energy showed increase in the maximum dry unit weight for the two soils.

- For the granular soil, the maximum dry unit weight achieved using static compaction energy of 200 kN-m/m^3 was only 94% of the standard Proctor maximum dry unit weight. Application of additional compaction energy required static pressures greater than about 9200 kPa (1300 psi), which are considered significantly greater application stresses than what is applied during construction in the field.

- For the cohesive soil, the static compaction energy required to achieve a target dry unit weight at any given moisture content is lower than the required impact compaction energy.

- The vibratory compaction energy required to achieve a target dry unit weight for the granular soil is significantly higher than the impact energy at "bulking" moisture contents, while it is lower at other moisture conditions. Therefore the moisture content during field production compaction should be greater than the "bulking" moisture content.

- For the granular soil, the field densities matched closely with the laboratory densities determined by standard Proctor, modified Proctor, and vibratory compaction methods. A narrow range of densities is observed between these methods for this soil.

- On average for the cohesive soil, vibratory and impact compaction methods resulted in greater M_r values by a factor of 1.3 to 2 times than the static method.

- No significant difference in M_r was realized between impact and vibratory methods for the two materials tested.

- For the cohesive soil, static compaction samples resulted in lower τ_{max} (about 1.2 to 1.4 times) than impact method. τ_{max} with vibratory method was about 1.5 times lower than impact method on the dry side, while there was no noticeable difference on the wet side of the optimum moisture content.

- Vibratory compaction samples exhibited similar or slightly higher (0.97 to 1.2 times) τ_{max} than impact compaction samples of the granular soil.

- Differences in τ_{max} and M_r between compaction methods are attributed to the variations in the resulting soil structure and potential differences of capillary tension in the specimen resulting from compaction.

- A profound influence of moisture content is realized for the cohesive soil on the τ_{max} with a strength reduction of about 1.8 to 2.7 times with increasing moisture content from -3% to +3% of optimum moisture content, for the three compaction methods. The average M_r reduced by about 1.3 to 2.0 times with increasing moisture content of the cohesive soil, for the three compaction methods.

- Influence of moisture content is not significant on M_r and τ_{max} values within the 6% to 10% moisture ranges for the granular soil.

Some of the key findings and conclusions from the LWD comparison study include:

- The Keros E_{LWD} is on average 1.9 to 2.2 times greater than Zorn E_{LWD}. Strong linear relationship was observed between 200 mm plate Zorn and Keros with R^2 value between 0.87 and 0.9. A relatively poor correlation was observed between 300 mm plate Zorn and Keros E_{LWD} with R^2 of 0.37.

- The constant applied force of 6.69 kN in the 200 mm Zorn device was very comparable with average loads by 200 mm Keros device (6.56 kN). Therefore, the primary contributor for differences in E_{LWD} values is the difference in measured deflections. On average, Zorn deflections are 1.5 times greater than Keros.

- The E_{LWD} of a 200 mm plate Zorn is approximately 1.4 times greater than of a 300 mm plate Zorn.

- A linear relationship between E_{LWD} and laboratory M_r was observed at a selected stress condition ($\sigma_d = 68.9$ kPa and $\sigma_c = 41.4$ kPa) with a strong correlation – R^2 values ranging from 0.85 to 0.97.

- A linear relationship between E_{LWD} and estimated secant modulus (M_s) was observed at a selected stress condition ($\sigma_d = 68.9$ kPa and $\sigma_c = 41.4$ kPa) with a strong correlation – R^2 values ranging from 0.75 to 0.88.

- Larger intercept values in relationships between E_{LWD} and M_r suggest a non-linear relationship at low moduli, i.e. at softer soil conditions with secant modulus about < 10 MPa. Smaller intercept values are observed as expected between M_s and E_{LWD}, as both parameter values are calculated using the peak deformation and peak stress.

- The correlations between shear strength and E_{LWD} are improved when compared at 1% strain ($R^2 = 0.75$ to 0.88) than with maximum shear strength ($R^2 = 0.49$ to 0.71).

11.3 Recommendations for Implementation

The following recommendations are based on the study findings and communication with representatives from Mn/DOT personnel, industry, and contractors. The recommendations have been separated into categories of Education and Future Research.

11.3.1 Education

- Prepare a condensed field inspector's guide to intelligent compaction technologies, testing, documentation, and operations.

- Develop training curriculum for using intelligent compaction rollers, as well as other in-situ testing methods used for calibration and verification testing.

- Begin implementing IC specifications on a limited basis with on-site training/seminars for inspectors and contractors. A research team may further facilitate technology transfer/training and speed up the implementation process. Such demand will additionally increase the availability of IC rollers in Minnesota.

- Educate designers on how to use intelligent compaction technology to refine/validate pavement design and, ultimately, participate in establishing quality criteria for IC rollers.

- Facilitate discussion between roller manufacturers for the purpose of establishing some level of consistency between roller usage – a measure that will help eliminate bias towards a specific technology and enabling the users to select from a wide range of manufacturers.

11.3.2 Future Research

- Continue research in identifying and quantifying all the factors affecting intelligent compaction measurements. Continue evaluating the relationships between in-situ test results and intelligent compaction data for different pavement foundation conditions.

- Continue development of database of relationships between design parameters (e.g. M_r) to in-situ LWD values.

- Develop new or refine existing roller calibration procedures.

- The appropriate scale at which the acceptance criteria is based remains unresolved and needs further research.

- Continue research in the areas of modulus-based QC/QA protocols implicit to performance-based specifications.

- Monitor construction expediency and cost of projects using IC technology. Favorable comparison with conventional construction methods would warrant more rapid implementation. In the long term, pavement performance may further support the effectiveness of IC technology.

- Document/verify that use of intelligent compaction technology produces a higher quality product than does the conventional approach. This task may involve comparing IC output with test rolling results or may involve, in the longer term, comparison of performance of road sections constructed using different technologies/methods.

- Investigate how intelligent compaction technologies and specifications can be used to improve conventional earthwork operations (e.g. improved compaction efficiency, improved material uniformity).

- Develop standard methods for managing, analyzing, and archiving the large quantities of intelligent compaction data produced throughout a project.

References

AASHTO (1991). *Interim method of test for resilient modulus of subgrade soils and untreated base/subbase materials*, AASHTO T 292, American Association of State Highway and Transportation Officials, Washington, D.C.

AASHTO (1999). *Standard method of test for determining the resilient modulus of soils and aggregate materials*, AASHTO T 307. American Association of State Highway and Transportation Officials, Washington, D.C.

Adam, D., and Kopf, F. (2002). "Messtechnische und theoretische untersuchungen als grundlage für die weiterentwicklung und normative anwendung der dynamischen lastplatte (leichtes fallgewichtsgerät)." *Inhaltsverzeichnis Heft-Nr.68*: *Messen in der Geotechnik* (in German).

Aguirre, M. L. M. (1964). *Correlación entre las pruebas estáticas y dinámicas de compactación de suelos en el laboratorio*, MS Thesis, National University of México.

Alshibli, K. A., Abu-Farsakh, M., and Seyman, E. (2005). "Laboratory evaluation of the geogauge and light falling weight deflectometer as construction control tools." *J. Mat. in Civ. Engrg.,* ASCE, 17(5), 560-569.

Amini, F. (2004). "Dynamic cone penetrometer in quality control of compaction, state-of-the-art report." *Proc., Geo-Trans 2004 – Geotechnical Engineering for Transportation Projects*, Geotechnical Special Publication No. 126, Yegian and Kavazanjan, eds., ASCE, Los Angeles, Ca., 1023-1031.

Ampadu, S., and Arthur, T (2006). "The dynamic cone penetrometer in compaction verification on a model road pavement." *Geotech. Test. J.*, ASTM, 29(1), 70-79.

Anderegg, R (2000). "ACE Ammann compaction expert – Automatic control of the compaction." *Proc., European Workshop on Compaction of Soils and Granular Materials*, Paris, 229-236.

Andrei, D., Witczak, M. W., Schwartz, C. W., and Uzan, J. (2004). "Harmonized resilient modulus test method for unbound pavement materials." *Transportation Research Record No. 1874*, Transportation Research Board, Washington, D. C., 29-37.

Barnes, R. (2007). *Variogram Tutorial*, Golden Software, Inc., <http://www.goldensoftware.com/variogramTutorial.pdf> (Jan. 1, 2007).

Bell, J. R. (1977). "Compaction energy relationships of cohesive soils." *Transportation Research Record No. 641*, Transportation Research Board, Washington, D.C., 29-34.

Brandl, H., Adam, D., Kopf, F., and Niederbrucker, R. (2003). "Der dynamische lastplattenversuch mit dem leichten fallgewischtesgerät." *Bundesministerium für Verkehr: Innovation und Technologie*, Straßenforschung, Heft 528, Wien.

Browne, M. J. (2006). *Feasibility of using a gyratory compactor to determine compaction characteristics,* MS Thesis, Montana State University, Bozeman, MT.

Burmister, D. M (1948). "The importance of practical use of relative density in soil mechanics." *Proc., of American Society of Testing Materials*, 48: 1249-1251.

Burnham, T., and Johnson, D. (1993). *In-Situ foundation characterization using the dynamic cone penetrometer*, Final report MN/RD-93/05, Minnesota Department of Transportation, St. Paul, Mn.

Camargo, F., Larsen, B., Chadbourn, B., Roberson, R., and Siekmeier, J. (2006). "Intelligent compaction: A Minnesota case history." *Proc., 54th Annual University of Minnesota Geotechnical Conference*, St. Paul, Mn.

Chaddock, B. C. J., and Brown. A. (1995). "In-situ tests for road foundation assessment." *Proc., Unbound Aggregates in Roads – UNBAR 4*, Dawson and Jones, eds., Nottingham, U.K.

Clark, I., and Harper, W. (2002). *Practical geostatistics 2000*, 3rd reprint, Ecosse North America Llc, Columbus, Oh.

Clegg, B. (1986). "Correlation with California bearing ratio." *News Letter 2*, <http://www.clegg.com.au/information_list12.asp > (Mar. 1, 2007).

Converse, F. J. (1956). "Compaction of cohesive soil by low-frequency compaction." *ASTM Special Publication No. 206*, American Society for Testing and Materials, 75-82.

Coyle, H. M., and West, E. C. (1956). *Laboratory compaction of a silty clay to simulate field density curves*, MS Thesis, Massachusetts Institute of Technology, Ma.

Cressie, N. A. C. (1993). *Statistics for spatial data*. Revised Ed., John Wiley & Sons, Inc., New York.

Das, B. M. (1998). *Principles of geotechnical engineering*. 4th Ed., PWS Publishing Company, Boston, MA.

Daoud, F. (1996). *La perméabilité des sols fins compactés (Permeability of compacted clays)*, PhD Dissertation. I.N.P.L. Ecole Nationale Supérieure de Géologie de Nancy.

Davich, P. (2005). *Analysis of LWD load estimation from measurements of deflection*, Final Report, Minnesota Department of Transportation, St. Paul, Minn.

Deng-Fong, L., Chi-Chau, L., and Jyh-Dong, L (2006). "Factors affecting portable falling weight deflectometer measurements." *J. Geotech. and Geoenvir. Engrg.*, ASCE, 132(6), 804-808.

Doré, G., Flamand, M., and Tighe, S. (2001). "Prediction of winter roughness based on analysis of subgrade soil variability." *Transportation Research Record No. 1755*, Transportation Research Board, Washington, D.C., 90-96.

Dynatest. (2004). *Keros portable FWD – Instruction manual for use and maintenance*, Issue No. 010704, Denmark.

Elliott, R. P., and Thornton, S. (1988). "Simplification of subgrade resilient modulus testing." *Transportation Research Record No. 1192*, Transportation Research Board, Washington, D. C., 1-7.

ESRI. (2000). *Getting to know ArcGIS*, ESRI Publishers, California.

Felt, E. J. (1958). "Laboratory methods of compacting granular materials." *ASTM STP 239*, American Society of Testing Materials, West Conshohocken, Pa.

Fleming, P. R., Rogers, C. D. F., and Frost, W. (1998). "Performance parameters and target values for construction of UK road foundations". *Proc., 5th Intl. Conf. on Bearing Capacity of Roads and Airfields*, Vol. 3, Trondheim, Norway, 1491-1502.

Fleming, P. R. (1998). "Recycled bituminous planings as unbound granular materials for road foundations in the UK." *Proc., 5th Intl. Conf. on Bearing Capacity of Roads and Airfields*, Vol. 3, Trondheim, Norway, 1581-1590.

Fleming, P. R. (2000). "Small-scale dynamic devices for the measurement of elastic stiffness modulus on pavement foundations." *Nondestructive Testing of Pavements and Backcalculation of Moduli: Third Volume*, ASTM STP 1375, Tayabji and Lukanen, eds., American Society of Testing and Materials, West Conshohocken, Pa., 41-58.

Fleming, P. R., Frost, M.W., and Rogers, C. (2000). "A comparison of devices for measuring stiffness in-situ." *Proc., Unbound Aggregates in Road Construction – UNBAR 5*, Dawson, A. R., ed., Balkema, Rotterdam, 193-200.

Fleming, P. R. (2001). "Field measurement of stiffness modulus for pavement foundations." *Proc., 80th Annual Transportation Research Board Meeting*, Washington D.C., Paper No. 01-2145.

Fleming, P. R., Lambert J. P., Frost M. W., and Rogers, C. (2002). "In-situ assessment of stiffness modulus for highway foundations during construction." *Proc., 9th Intl. Conf. on Asphalt Pavements*, Copenhagen, Denmark (CD-ROM).

Gabr, M., Hopkins, K., Coonse, J., and Hearne, T. (2000). "DCP criteria for performance evaluation of pavement layers." *J. Perf. of Constr. Facil.*, ASCE, 14(4), 141-148.

Gabr, M. A., Coonse, J., and Lambe, P.C. (2001). "A potential model for compaction evaluation of piedmont soils using dynamic cone penetrometer (DCP)." *Geotech. Test. J.*, 24(3), 308-313.

Groenendijk, J., van Haasteren, C. R., and van Niekerk, A. (2000). "Comparison of stiffness moduli of secondary road base materials under laboratory and in-situ conditions." *Proc., Unbound Aggregates in Road Construction – UNBAR5*, Dawson, A. R. ed., Balkema, Rotterdam, 201-208.

Gupta, S., Ranaivoson, A., Edil, T., Benson, C., Sawangsuriya, A. (2007). *Pavement design using unsaturated soil technology*, Minnesota Department of Transportation Research Report, Submitted by University of Minnesota in St. Paul, Minnesota and University of Wisconsin, Madison (in preparation).

Hildebrand, G. (2003). "Comparison of various types of bearing capacity equipment." *Nordic Road and Transportation Research*, 15(3), Danish Road Directorate, 12-14.

Hoff, I., Bakløkk, L. J., and Aurstad., J. (2004). "Influence of laboratory compaction method on unbound granular materials." *Proc., 6th International Symposium on Pavements Unbound – UNBAR 6*, Dawson, A. R., ed., Nottingham, U.K.

Holtz, R. D., and Kovacs, W. D. (1981). *An introduction to geotechnical engineering*, Prentice-Hall, Inc., Englewoods Cliffs, New Jersey.

Houlding, S. W. (2000). *Practical geostatistics: Modeling and spatial analysis*, Springer-Verlag, Germany.

Huang, Y. (1993). *Pavement analysis and design*, 1st Ed., Prentice-Hall, Inc., Englewood Cliffs, New Jersey.

Humboldt Mfg. Co. (2000). *Geogauge (soil stiffness/modulus) user guide*. Ver. 3.8.

Isaaks, E.H., and R. M. Srivastava. (1989). *An introduction to applied geostatistics*. Oxford University Press, New York.

ISSMGE. (2005). *Geotechnics for pavements in transportation infrastructure, roller-integrated continuous compaction control (CCC)*, Technical Contractual Provisions – Recommendations, International Society for Soil Mechanics and Geotechnical Engineering.

Kestler, M, A., Harr, M. E., Berg, R. L., and Johnson, D. (1994). "Spatial variability of falling weight deflectometer data: A geostatistical analysis." *Proc., Bearing Capacity of Roads and Airfields Conference*, Minneapolis, Mn, 318-330.

Kim, W., and Labuz, J. (2006). *Resilient modulus and strength of base course with recycled bituminous material*, Final Report submitted to Minnesota Department of Transportation, University of Minnesota, St. Paul., Mn.

Komandi, G. (1999). "An evaluation of the concept of rolling resistance." *J. Terramechanics*, 36: 159-166.

Konrad, J. and Lachance, D. (2001). "Use of in-situ penetration tests in pavement evaluation." *Can. Geotech. J.,* 38: 924-935.

Kopf, F., and Adam, D. (2004) "Load plate test with the light falling weight device." *Proc., 16th European Young Geotechnical Engineers Conference – EYGEC*, Vienna.

Kouassi, P., Breysse, D., Girard, H., and Poulain, D. (2000) "A new technique of kneading compaction in the laboratory." *Geotech. Test. J.,* 23(1), 72-82.

Krige, D. G. (1951). *A statistical approach to some mine valuations and allied problems at the Witwatersrand*, MS Thesis, University of Witwatersrand, Johannesburg, S.A.

Kudla, W., Floss, R., and Trautmann, Ch. (1991). "Dynamic test with plate – Quick method of quality assurance of road layers without binder (Dynamischer plattendruckversuch – Schnellprüfverfahren für die qualitätssicherung von ungebundenen schichten)." *Streets and Highways (Strasse and Autobahn)*, Vol. 2, Bonn, 66-71 (in German).

Lambe, T. W. (1951). *Soil testing for engineers*, John Wiley and Sons, New York.

Lambe, T. W. (1960). "A mechanistic picture of shear strength of clay." *Proc., Research Conf. on the Shear Strength of Cohesive Soils*, ASCE, New York, 437.

Lambe, T. W. (1961). "Residual pore pressures in compacted clay." *Proc., 5th Intl. Conf. Soil Mechanics and Foundation Engineering*, Vol. 1, Paris, 207.

Lambe, T. W, and Whitman, R. V. (1969). *Soil mechanics*, John Wiley & Sons, New York.

Lee, K., M. Prezzi, and Kim, N. (2007). "Subgrade design parameters from samples prepared with different compaction methods." *J. of Transp. Engrg*, ASCE, 133(2), 82-89.

Lee, P. Y., and Suedkamp, R. J. (1972). "Characteristics of irregularly shaped compaction curves of soil." *Highway Research Record No. 381*, Washington, D.C., 1-9.

Lenngren, C. (1992). "Discussion: Effects of buffers on falling weight deflectometer loadings and deflections, By Lukanen, E.O", *Transportation Research Record No. 1355*, Transportation Research Board, Washington, D. C., 51.

Lewis, W.A. (1961). "Recent research into the compaction of soil by vibratory compaction equipment." Proc., *5th Intl. Conf. of Soil Mechanics and Foundation Engineering*, Paris, Vol. 2, 261-268.

Livneh, M., Livneh, N., and Ishai, I. (2000). "The Israeli experience with the regular and extended dynamic cone penetrometer for pavement and subsoil-strength evaluation." *Nondestructive Testing of Pavements and Backcalculation of Moduli: Third Volume*, ASTM STP 1375, Tayabji and Lukanen, eds., American Society of Testing and Materials, West Conshohocken, Pa., 189-213

Livneh, M., and Goldberg, Y. (2001)."Quality assessment during road formation and foundation construction: Use of falling-weight deflectometer and light drop weight." *Transportation Research Record No. 1755*, Transportation Research Board, Washington D.C., 69-77.

LTPP P46. (1996). *Resilient modulus of unbound granular base/subbase materials and subgrade soils – Long term pavement performance (LTPP) protocol 46*, FHWA Pavement Performance Division.

Lukanen, E. O. (1992). "Effects of buffers on falling weight deflectometer loadings and deflections." *Transportation Research Record No. 1355*, Transportation Research Board, Washington D.C., 37-51.

Marr, W. A., Hankour, R., and Werden, S. (2003) "A fully automated computer controlled resilient modulus testing system." *Resilient Modulus Testing for Pavement Components*, ASTM STP 1437, ASTM International, West Conshohocken, Pa., 141-151.

McRae, J. L. (1965). *Gyratory testing machine technical manual for bituminous mixtures, soils, and base course materials*, Engineering Developments Company, Inc., Vicksburg, Ms.

Mitchell, J. K., Hooper, D. R., and Campanella, R. G. (1965). "Permeability of compacted clay." *J. Soil Mech. and Found. Div.,* ASCE, 91(4), 41-66.

Mohammad, L.N., Puppala, A., and Alavilli, P. (1995). "Resilient properties of laboratory compacted subgrade soils." *Transportation Research Record No. 1504*, Transportation Research Board, Washington, D.C., 87-102.

Monismith, C.L., Hicks, R.G., and Salam, Y. (1971). "Basic properties of pavement components." Final Report FHWA-RD-72-19, Federal Highway Administration, Berkeley, Ca.

Mooney, M. A., and Miller, P. K. (2007) "Analysis of falling weight deflectometer." *J. Geotech. and Geoenvir. Engrg.*, ASCE (under review).

Muro, T, and O'Brien, J. (2004). *Terramechanics*, A.A. Balkema Publishers, Exton, Pennsylvania.

Nazzal, M. D. (2003). *Field evaluation of in-situ test technology for QC/QA during construction of pavement layers and embankments*, MS Thesis, Department of Civil Engineering, Louisiana State University, Baton Rouge, La.

Nazzal, M. D, Abu-Faraskh, M., Alshibli, K., and Mohammad, L. (2004). "Evaluating the potential use of a portable LFWD for characterizing pavement layers and subgrades", *Proc., Geo-Trans 2004 – Geotechnical Engineering for Transportation Projects*, Vol. 1, Geotechnical Special Publication No. 126, , Los Angeles, Ca.

Nazzal, M. D, Abu-Faraskh, M., Alshibli, K., and L. Mohammad. (2007). "Evaluating light falling-weight deflectometer device for in-situ measurement of elastic modulus of pavement layers", *Proc., 86th Annual Transportation Research Board Meeting*, Washington D.C., Paper No. 07-0035.

NCHRP 1-28A. (2002). *Recommended standard method for routine resilient modulus testing of unbound granular base/subgrade materials and subgrade soils – NCHRP protocol 1-28A,* National Cooperative Highway Research Program.

Neves, M. E. (1971). *Influencia das tensoes neutras negativas nas caracteristicas estructurais dos solos compactados,* Report No. 386, National Laboratory of Civil Engineering, Public Works Ministry, Libson, Portugal.

Odemark, (1949). "Investigations as to the elastic properties of soils and design of pavements according to the theory of elasticity." *Statens Väginstitut*, Mitteilung No. 77, Stockholm, Sweden.

Petersen, L. (2005) *Continuous compaction control MnROAD demonstration*, Final Report MN/RC-2005-07, Minnesota Department of Transportation, St. Paul, Mn.

Peterson, D. L., Erickson, M. L., Roberson, R., and Siekmeier, J. (2007). "Intelligent soil compaction: Geostatistical data analysis and construction specifications." *Proc., 86th Annual Transportation Research Board Meeting*, Washington, D.C., Paper No. 07-2858.

Pettibone, H. C., and Hardin, J. (1964). "Research on vibratory maximum density test for cohesionless soils." *Compaction of Soils*, ASTM Special Publication No. 377, West Conshohocken, Pa., 3-19.

Ping, V.W., Yang, Z., and Gao, Z. (2002). "Field and laboratory determination of granular subgrade moduli." *J. of Perf. of Constr. Facil.,* ASCE, 16(4), 149-159.

Ping, W. V., Xing, G., Leonard, M., and Yang, Z. (2003). *Evaluation of laboratory compaction techniques for simulating field soil compaction – Phase II*, Research Report No. FL/DOT/RMC/BB – 890 (F), Florida State University, Tallahassee, Fl.

Porter, O. J. (1930). *Method of determining relative compaction and shrinkage of soil materials,* Research Department, California Division of Highways, Ca.

Proctor, R. R. (1933). "Fundamentals principles of soil compaction." *Engineering News Record*, 3(9), 245-248.

Proctor, R. R. (1948). "Relationship between the foot pounds per cubic foot of compactive effort and subsequent consolidation under various loadings." *Proc., 2nd Intl. Conf. on Soil Mechanics and Foundation Engineering*, Vol. 5, Rotterdam, 223.

Rodriguez, R. A., Castillo, H., and Sowers, G. (1988). *Soil mechanics in highway engineering*, Trans Tech Publications, Federal Republic of Germany, Germany.

Sandstrom, A. and Pettersson, C. (2004). "Intelligent systems for QA/QC in soil compaction." *Proc., 83rd Annual Transportation Research Board Meeting*, Washington, D.C.

Seed, H. B., Mitchell, J. K., and Chan, C. (1960). "The strength of compacted cohesive soils." *Proc., Research Conf. on Shear Strength of Cohesive Soils*, Vol. 2, ASCE, University of Colorado, Boulder, Co., 877-964.

Seed, H. B., Chan, C. K., and Lee, C. (1962). "Resilience characteristics of subgrade soils and their relation to fatigue failures in asphalt pavements." *Proc., 1st Intl. Conf. on the Structural Design of Asphalt Pavements,* Ann Arbor, Mi.

Shahid, M. A., Thom, N. H., and Fleming, P. (1997). "In situ assessment of road foundations." *J. Institute of Highways and Transportation and IHIE*, 44(11), 15-17.

Siekmeier, J.A., Young, D., and Beberg, D. (2000). "Comparison of the dynamic cone penetrometer with other tests during subgrade and granular base characterization in Minnesota." *Nondestructive Testing of Pavements and Backcalculation of Moduli: Third Volume*, ASTM STP 1375, Tayabji and Lukanen, eds., ASTM, West Conshohocken, Pa., 175188.

Smith, D. M. (2000). *Response of granular layers in flexible pavements subjected to aircraft loads*, PhD Dissertation, Louisiana State University, Baton Rouge, La.

Stojadinovic, M. R. (1964). "Etude des conditions de compactage des sols avec les rouleaux à pieds de mouton et les rouleaux àpneus (Study of compacting conditions with sheepsfoot compactors and tire compactors)." *Ann. I.T.B.T.P.*, No. 195-196, 301-334.

Stranton, J. H. (1944). "Military airfields – Construction and design Problems." *Proc., American Society of Civil Engineers*, 70(1), 28-54.

Sulewska, M. J. (1998). "Rapid quality control method of compaction of non-cohesive soil embankment." *Geotechnical Hazards*, Marić et al., eds., Balkema, Rotterdam, 283-286.

Sulewska, M. J. (2004). "The application of the modern method of embankment compaction control." *J. Civil Engineering and Management*, Vol X(1), 45-50.

Swenson, J., Guzina, B., Labuz, J., and Drescher, A. (2006). *Moisture effects on PVD and DCP measurements,* Report # MN/RC-2006-26, Minnesota Department of Transportation, St. Paul, Mn.

Terzaghi, K. (1955). "Evaluation of coefficient of subgrade reaction." *Geotechnique*, 5(4), 297-326.

Terzaghi, K., and Peck, R. B. (1967). *Soil mechanics in engineering practice*, 2nd Ed., John Wiley & Sons, Inc., New York.

TP BF-StB Teil B 8.3. (1992). *Technical specification for soil and rock in road construction (Technische prüfvorschrift für boden und fels im straßenbau – TP BF-StB Teil B 8.3)*, Dynamischer Plattendruckversuch mit Hilfe des Leichten Fallgewichtsgerates, Road and Transportation Research Association, Köln (in German).

van Gurp, C., Groenendijk, J., and Beuving, E. (2000) "Experience with various types of foundation tests." *Proc., Unbound Aggregates in Road Construction – UNBAR5*, Dawson, A. R., ed., Balkema, Rotterdam, 239-246.

Vennapusa, P., White, D. J., and Jahren, C.T. (2006). "In-situ permeability of unbound granular bases using the air permeameter test." *Proc., 85th Annual Transportation Research Board Meeting*, Washington, D.C., Paper No. 06-1729.

Wackernagel, H. (1998). *Multivariate geostatistics - An introduction with applications*, 2nd Ed, Springer-Verlag, Germany.

Webster, C. R. (1984). *Laboratory investigation of vibratory compaction of dry soils,* MS Thesis, Texas A&M University, College Station, Texas.

Weingart, W. (1977). *Theoretische und experimentelle untersuchungen zur bestimmung der elastizität, viskosität und festigkeit von erdstabilisierungen mit hilfe einer registrierenden kleinschlagsonde*. PhD Dissertation. Technische Hochschule Leipzig, Germany.

Weingart, W. (1993). "Control of road layers without binder using light drop-weight tester." *Transactions in Mineral Materials in Road Construction (Tagungsband Minerallstoffe in Strassenbau)*, Vol. 6, Köln, 50-53 (in German).

White, D. J, Jaselskis, E., Schaefer, V., Cackler, E., Drew, I. and Li, L. (2004a). *Field evaluation of compaction monitoring technology: Phase I*, Final report, Iowa Department of Transportation Project No. TR-495, Iowa State University, Ames, Ia.

White, D. J., Rupnow, T., and Ceylan, H. (2004b) "Influence of subgrade/subbase non-uniformity of pavement performance." *Proc., Geo-Trans 2004 – Geotechnical Engineering for Transportation Projects*, Geotechnical Special Publication No. 126, ASCE, Los Angeles, Ca., 1058-1065.

White, D. J, Jaselskis, E. J, Schaefer, V. R., and Cackler, E. T. (2005). "Real-time compaction monitoring in cohesive soils from machine response." *Transportation Research Record No. 1936*, Transportation Research Board, Washington, D.C., 173-180 .

White, D. J, and Thompson, M. (2006). "Relationships between in-situ and roller-integrated compaction measurements for cohesionless soils." *J. Geotech. and Geoenvir. Engrg.,* ASCE (under review).

White, D. J., Thompson, M. T., Jovaag, K., Jaselskis, E. J., Schaefer, V. R., and Cackler, E. T. (2006). *Field evaluation of compaction monitoring technology – Phase II*, CTRE Project 04-171, Center of Transportation Research and Education, Iowa State University, Ames, Ia.

White, D. J., Thompson, M. T., and Vennapusa, P. (2007). *Field study of compaction monitoring systems – Tamping foot 825 and vibratory smooth drum CS-533E rollers*, Center of Transportation Research and Education, Iowa State University, Ames, Ia.

Wilson, S. D. (1950). "Small scale compaction apparatus duplicates field results closely." *Engineering News Record*, 145(18), 34-36.

Witczak, M. W., and Uzan, J. (1988). "The universal airport design system – Report I of IV: Granular material characterization." Department of Civil Engineering, University of Maryland, College Park. Md.

Zaman, M., Chen, D-H, and Laguros, J. (1994). "Resilient moduli of granular materials." *J. of Transp. Engrg*, ASCE, 120(6), 967-988.

Zhang, Z., Tao, M., and Tumay, M. (2005). "Absorbed energy and compacted cohesive soil performance – Technical Note." *Geotech. Test. J.,* 28(4), ASTM, 404-409.

Zorn, G. (2003). *Operating manual: Light drop-weight tester ZFG2000*, Zorn Stendal, Germany.

ZTVA-StB. (1997). *Additional technical requirements and instructions for excavations in road constructions (Zusätzliche technische vertragsbedingungen und richtlinien für erdarbeiten im straßenbau)*, Road and Transportation Research Association, Köln (in German).

Appendix A: DCP Calculation Methods – Example Calculations

Blows	Reading	Depth	DCPI	Cum Blows
0	75	0	(150)	0
1	225	150	150	1
1	325	250	100	2
2	450	375	62.5	4
4	525	450	18.8	8
2	600	525	37.5	10
3	700	625	33.3	13

DCPI (mm/blow)

Cumulative Blows
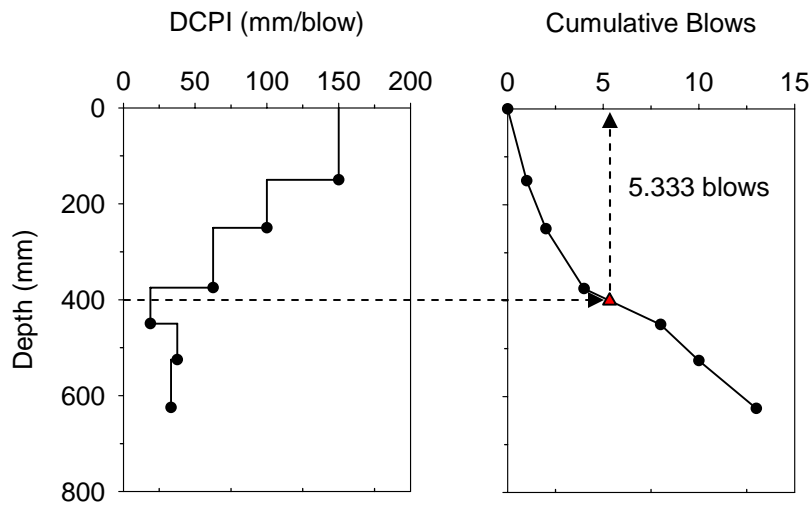
Calculation depth: 400 mm

$$DCPI_{A\text{-}400} = \frac{\text{Penetration}}{\text{Blows to Pen.}} = \frac{400 \text{ mm}}{5.333 \text{ blows}} = 75 \text{ mm/blow}$$

$$DCPI_{M\text{-}400} = \frac{PI_1 \cdot z_1 + PI_2 \cdot z_2 + \ldots + PI_n \cdot z_n}{\Sigma z_n}$$

$$= \frac{150 \cdot 150 + 100 \cdot 100 + 62.5 \cdot 12.5 + 18.8 \cdot 25}{400 \text{ mm}} = 102 \text{ mm/blow}$$

$$DCPI_S = 150 \text{ mm/blow}$$

Appendix B: Field Study 2 In-Situ Compaction Measurements

Table B. 1. Strip 1 at ML 14 STA 807+00; 0 Roller Passes

Test Point (Location)	Nuclear Gauge (kN/m^3, %)		Oven (%)	Clegg	DCP	E$_{LWD}$ (MPa)			E$_V$ (MPa)	
	γ_d	w$_g$	w$_g$	CIV	PI (mm/blow)	Keros	Keros	Zorn	E$_{V1}$	E$_{V2}$
1	---	---	---	19.8	12	95	79	---	---	---
2	---	---	---	27.8	8	60	51	---	---	---
3	---	---	---	12.7	15	23	78	---	---	---
4	---	---	---	5.9	91	19	12	---	---	---
5	---	---	---	9.6	41	3	42	---	---	---
6	---	---	---	9.0	43	58	71	---	---	---
7	---	---	---	18.4	15	86	86	---	---	---
8	---	---	---	20.3	10	43	79	---	---	---
9	---	---	---	18.4	10	11	50	---	---	---
10	---	---	---	18.8	11	35	52	---	---	---

Table B. 2. Strip 1 at ML 14 STA 807+00; 1 Roller Pass

Test Point (Location)	Nuclear Gauge (kN/m^3, %)		Oven (%)	Clegg	DCP	E_{LWD} (MPa)			E_V (MPa)	
	γ_d	w_g	w_g	CIV	PI (mm/blow)	Keros	Keros	Zorn	E_{V1}	E_{V2}
1	---	---	---	21.2	13	101	89	---	---	---
2	---	---	---	28.5	8	---	145	---	---	---
3	---	---	---	13.0	13	27	39	---	---	---
4	---	---	---	5.6	101	7	24	---	---	---
5	---	---	---	7.3	50	14	18	---	---	---
6	---	---	---	8.3	52	12	21	---	---	---
7	---	---	---	17.8	17	73	56	---	---	---
8	---	---	---	19.9	10	59	68	---	---	---
9	---	---	---	27.6	9	119	105	---	---	---
10	---	---	---	25.2	6	83	98	---	---	---

Table B. 3. Strip 2 at WB ML 14, east of County 33; 3 Roller Passes

Test Point (Location)	Nuclear Gauge (kN/m³, %)		Oven (%)	Clegg	DCP	E_{LWD} (MPa)			E_V (MPa)	
	γ_d	w_g	w_g	CIV	PI (mm/blow)	Keros	Keros	Zorn	E_{V1}	E_{V2}
10	16.51	13.3	---	6.5	80	24	22	7.3	---	---
20	16.38	13.6	---	6.9	89	10	23	12.1	---	---
30	16.18	14.7	---	5.7	94	19	30	16.5	---	---
40	16.62	13.2	---	6.9	54	20	33	18.4	11.1	---
50	16.60	14.2	---	5.6	60	11	29	15.2	---	---
60	16.86	12.4	---	6.7	69	17	29	25.3	---	---
70	16.86	12.5	---	6.3	99	---	22	21.6	---	---
80	16.43	12.6	---	6.7	106	6	19	20.1	8.0	---
90	16.45	12.2	---	5.7	88	---	32	20.5	---	---
100	15.52	12.8	---	7.2	64	11	30	19.9	---	---
120	16.98	12.5	---	8.0	46	16	40	29.0	---	---
130	16.62	12.6	---	7.8	52	17	31	18.5	11.7	---
140	16.82	12.5	---	8.3	47	11	27	27.1	---	---
150	16.59	12.9	---	7.3	61	---	30	23.6	---	---
160	16.81	12.8	---	7.7	55	---	29	23.8	---	---

170	16.68	14.7	---	7.4	77	15	32	29.6	11.3	---
180	16.32	14.0	---	6.1	80	12	26	26.3	---	---
190	16.79	12.9	---	5.8	82	12	31	29.8	9.4	---
200	16.62	14.4	---	4.8	92	10	22	15.8	---	---
220	16.65	13.0	---	5.5	89	24	23	16.9	---	---
230	16.48	13.3	---	5.2	94	15	25	19.1	6.5	---
240	16.35	13.9	---	4.6	81	8	21	13.9	---	---
250	16.32	13.9	---	5.4	91	9	21	14.4	7.8	---
260	16.31	12.4	---	5.3	69	7	21	15.2	---	---
270	16.64	12.2	---	5.2	96	---	18	14.8	7.3	---

Table B. 4. Strip 3 at WB ML 14, east of County 33; 3 Roller Passes

Test Point (Location)	Nuclear Gauge (kN/m³, %)		Oven (%)	Clegg	DCP	E_LWD (MPa)			E_V (MPa)	
	γ_d	w_g	w_g	CIV	PI (mm/blow)	Keros	Keros	Zorn	E_{V1}	E_{V2}
10	---	---	---	6.2	---	11.0	21.0	---	---	---
20	---	---	---	6.6	---	---	---	---	---	---
30	---	---	---	4.5	---	6.0	12.0	---	---	---
40	---	---	---	5.6	---	---	---	---	---	---
50	---	---	---	8.8	---	---	---	---	---	---
60	---	---	---	7.7	---	---	---	---	---	---
70	---	---	---	4.7	---	8.0	---	---	---	---
80	---	---	---	4.5	---	---	---	---	---	---
90	---	---	---	5.6	---	---	19.0	---	---	---
100	---	---	---	7.3	---	---	---	---	---	---
120	---	---	---	5.9	---	---	---	---	---	---
130	---	---	---	6.3	---	9.0	29.0	---	---	---
140	---	---	---	7.0	---	---	---	---	---	---
150	---	---	---	8.0	---	8.0	27.0	---	---	---
160	---	---	---	7.3	---	---	---	---	---	---

170	---	---	---	8.5	---	9.0	28.0	---	---	---
180	---	---	---	8.7	---	---	---	---	---	---
190	---	---	---	6.8	---	9.0	26.0	---	---	---
200	---	---	---	8.1	---	---	---	---	---	---
220	---	---	---	8.4	---	---	23.0	---	---	---
230	---	---	---	7.5	---	---	---	---	---	---
240	---	---	---	7.7	---	---	27.0	---	---	---
250	---	---	---	7.8	---	---	---	---	---	---
260	---	---	---	8.2	---	6.0	23.0	---	---	---
270	---	---	---	8.3	---	---	---	---	---	---

Table B. 5. Strip 4 at ML 14, east of County 33; 3 Roller Passes

Test Point (Location)	Nuclear Gauge (kN/m³, %)		Oven (%)	Clegg	DCP	E_{LWD} (MPa)			E_V (MPa)	
	γ_d	w_g	w_g	CIV	PI (mm/blow)	Keros	Keros	Zorn	E_{V1}	E_{V2}
0	17.53	17.7	---	9.5	37	66	80	24.8	---	---
5	17.53	17.1	---	10.4	37	78	73	40.0	---	---
10	17.41	15.0	---	13.5	21	157	107	37.7	31.9	---
15	16.78	15.0	---	21.6	26	207	201	55.1	---	---
20	16.37	16.1	---	11.4	17	62	69	31.6	---	---
25	16.27	16.0	---	11.1	18	134	123	34.2	---	---
30	17.23	16.1	---	11.3	28	34	55	25.4	26.8	---
35	16.65	16.8	---	10.2	25	84	89	18.3	---	---
40	14.55	19.4	---	14.2	20	21	41	21.2	---	---
45	15.44	18.9	---	9.5	26	25	29	10.3	18.0	---
50	15.10	21.4	---	7.9	28	16	12	---	---	---
55	15.19	26.1	---	3.2	63	9	8	---	---	---
60	14.33	29.1	---	4.2	63	1	37	---	---	---
65	14.04	2.6	---	5.9	58	45	35	---	3.5	---
70	14.23	25.0	---	1.3	110	5	Overload	---	---	---

75	15.02	22.8	---	7.9	30	45	3	---	---	---
80	15.94	19.2	---	8.8	30	21	19	---	---	---
85	15.77	19.1	---	8.9	20	39	35	---	---	---
90	15.38	21.4	---	7.7	35	20	21	---	---	---
95	17.72	13.7	---	11.0	35	68	49	---	7.0	---
100	18.27	14.1	---	10.7	24	147	131	---	---	---
105	17.66	14.3	---	11.2	25	260	219	---	---	---
110	17.85	15.0	---	10.5	24	113	125	---	---	---
115	17.37	18.2	---	9.6	23	85	9	---	---	---
120	16.71	16.7	---	8.0	36	33	28	---	---	---
125	16.97	16.0	---	8.6	27	53	42	---	---	---
130	17.66	16.3	---	10.4	18	47	45	---	20.4	---
135	17.64	15.6	---	10.2	16	19	23	---	---	---
140	17.52	16.3	---	10.4	14	68	53	---	---	---
145	17.39	17.3	---	10.2	20	259	241	---	---	---
150	17.03	17.1	---	7.2	40	67	52	---	23.5	---

Table B. 6. Strip 5 at WB ML 14; 3 Roller Passes

Test Point (Location)	Nuclear Gauge (kN/m³, %)		Oven (%)	Clegg	DCP	E_{LWD} (MPa)			E_V (MPa)	
	γ_d	w_g	w_g	CIV	PI (mm/blow)	Keros	Keros	Zorn	E_{V1}	E_{V2}
0	17.94	10.3	---	14.8	40	---	72	24.8	46.5	---
25	18.50	9.1	---	13.7	30	---	52	40.0	53.4	---
50	18.19	9.1	---	12.7	43	---	42	37.7	35.6	---
75	18.00	7.4	---	12.6	53	---	163	55.1	35.6	---
100	17.91	8.5	---	11.3	52	---	16	31.6	25.9	---
125	18.61	8.5	---	11.0	55	---	14	34.2	27.9	---
150	18.38	9.1	---	11.2	45	---	17	25.4	38.2	---
175	18.57	8.8	---	10.6	40	---	24	18.3	31.9	---
200	18.49	8.7	---	12.9	46	---	18	21.2	30.8	---
225	18.22	9.5	---	11.4	45	---	25	10.3	32.5	---
250	18.50	8.2	---	14.3	42	---	21	27.2	36.6	---
275	18.61	8.1	---	13.8	52	---	41	23.0	44.0	---
300	18.49	7.9	---	11.4	45	---	64	27.4	37.3	---
325	17.99	8.9	---	12.9	45	---	26	33.3	---	---
350	18.58	9.0	---	13.2	42	---	25	33.7	35.5	---

| 375 | 18.83 | 7.7 | --- | 11.5 | 49 | --- | 36 | 34.8 | 41.6 | --- |
| 400 | 18.88 | 9.3 | --- | 16.6 | 40 | --- | 44 | 38.3 | 45.4 | --- |

Table B. 7. Strip 6, Track 1 at WB ML 14; 3 Roller Passes

Test Point (Location)	Nuclear Gauge (kN/m³, %)		Oven (%)	Clegg	DCP	E_{LWD} (MPa)			E_V (MPa)	
	γ_d	w_g	w_g	CIV	PI (mm/blow)	Keros	Keros	Zorn	E_{V1}	E_{V2}
0	16.27	19.1	---	4.2	95	61	40	9.9	---	---
20	16.67	18.8	---	11.8	24	40	45	13.5	7.8	---
40	17.04	17.1	---	8.9	28	29	36	9.7	---	---
60	1.59	17.4	---	9.8	35	85	76	16.6	11.6	---
80	16.62	18.1	---	16.0	50	56	43	11.6	---	---
100	16.59	18.7	---	10.7	27	41	33	12.2	11.2	---
120	16.78	16.9	---	4.9	23	7	11	12.9	---	---
140	16.68	18.0	---	5.6	23	40	33	11.1	8.1	---
160	16.57	19.7	---	9.4	31	20	19	17.7	---	---
180	17.19	17.2	---	15.5	12	71	54	14.5	12.9	---
200	17.25	16.0	---	12.8	25	225	169	39.1	---	---

Table B. 8. Strip 6, Track 4 at WB ML 14; 3 Roller Passes

Test Point (Location)	Nuclear Gauge (kN/m³, %)		Oven (%)	Clegg	DCP	E_{LWD} (MPa)			E_V (MPa)	
	γ_d	w_g	w_g	CIV	PI (mm/blow)	Keros	Keros	Zorn	E_{V1}	E_{V2}
0	16.38	19.1	---	6.3	33	30	26	20.6	10.4	---
20	16.84	18.3	---	6.8	53	28	25	21.5	---	---
40	16.26	20.3	---	6.9	64	42	32	20.4	---	---
60	16.48	18.3	---	4.9	37	20	27	13.6	---	---
80	16.89	16.1	---	10.7	20	37	42	12.5	---	---
100	16.82	17.3	---	12.7	15	98	90	18.4	29.6	---
120	16.95	17.7	---	8.9	20	38	35	21.8	---	---
140	16.78	17.0	---	5.3	28	10	12	9.2	---	---
160	16.81	17.9	---	11.1	41	46	67	13.9	---	---
180	15.69	17.2	---	11.3	35	24	31	14.3	---	---
200	17.19	15.8	---	10.8	22	---	84	11.8	13.5	---

Appendix C: Field Study 2 Static Plate Load Test Load-Deflection Data
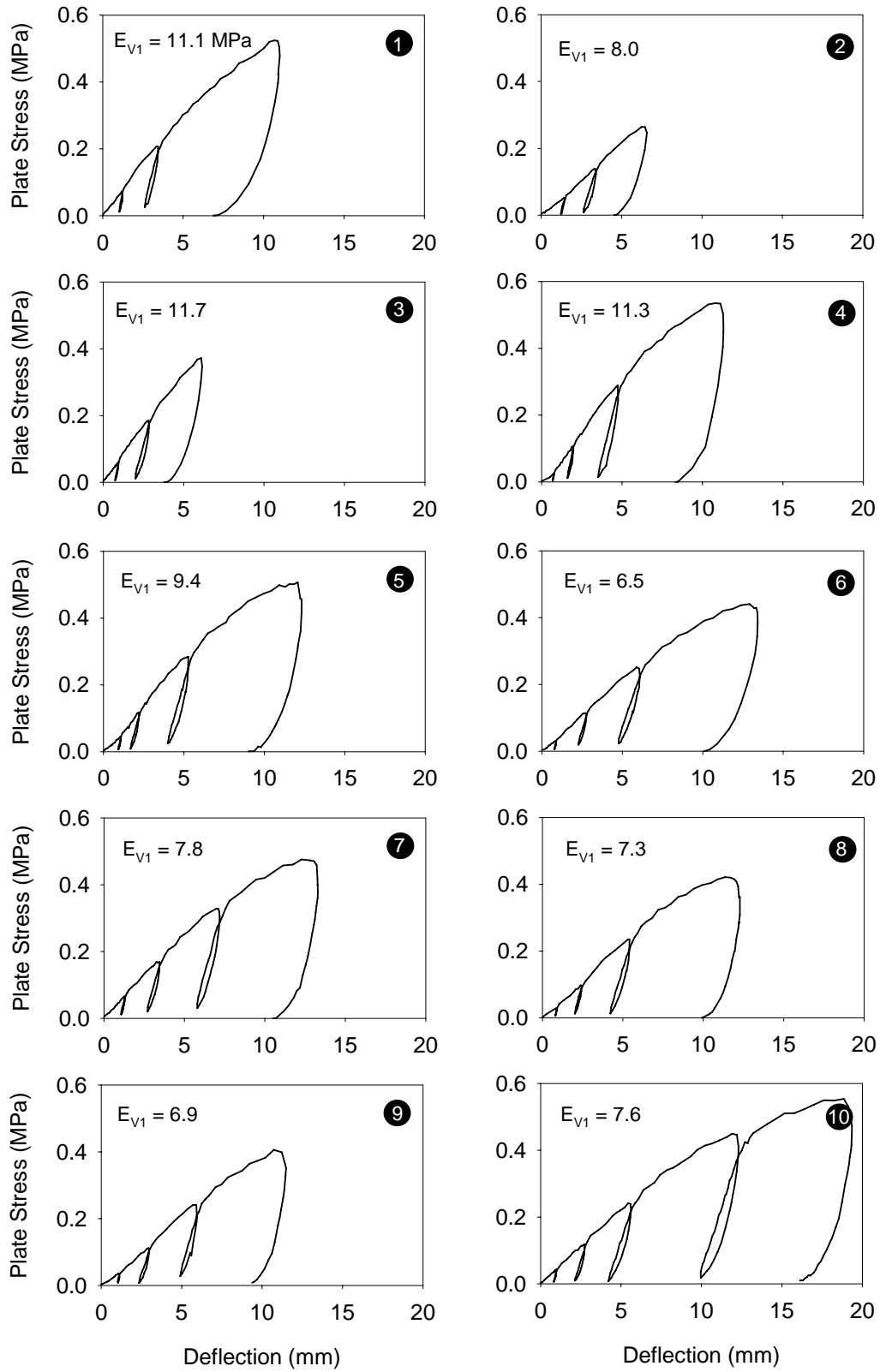
Figure C. 1. Strip 2 load-deflection curves (subbase material)
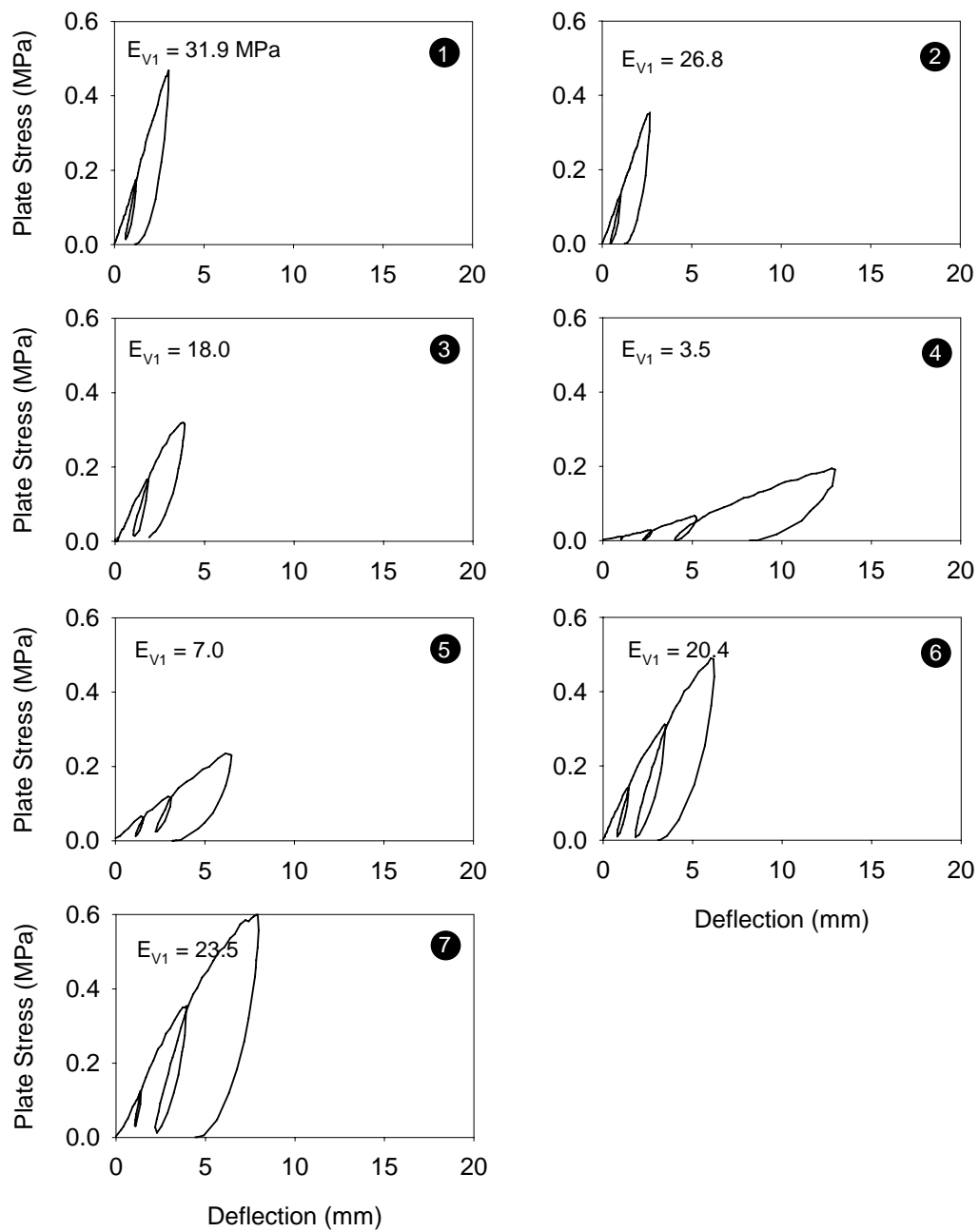
Figure C. 2. Strip 4 load-deflection curves (subgrade material)
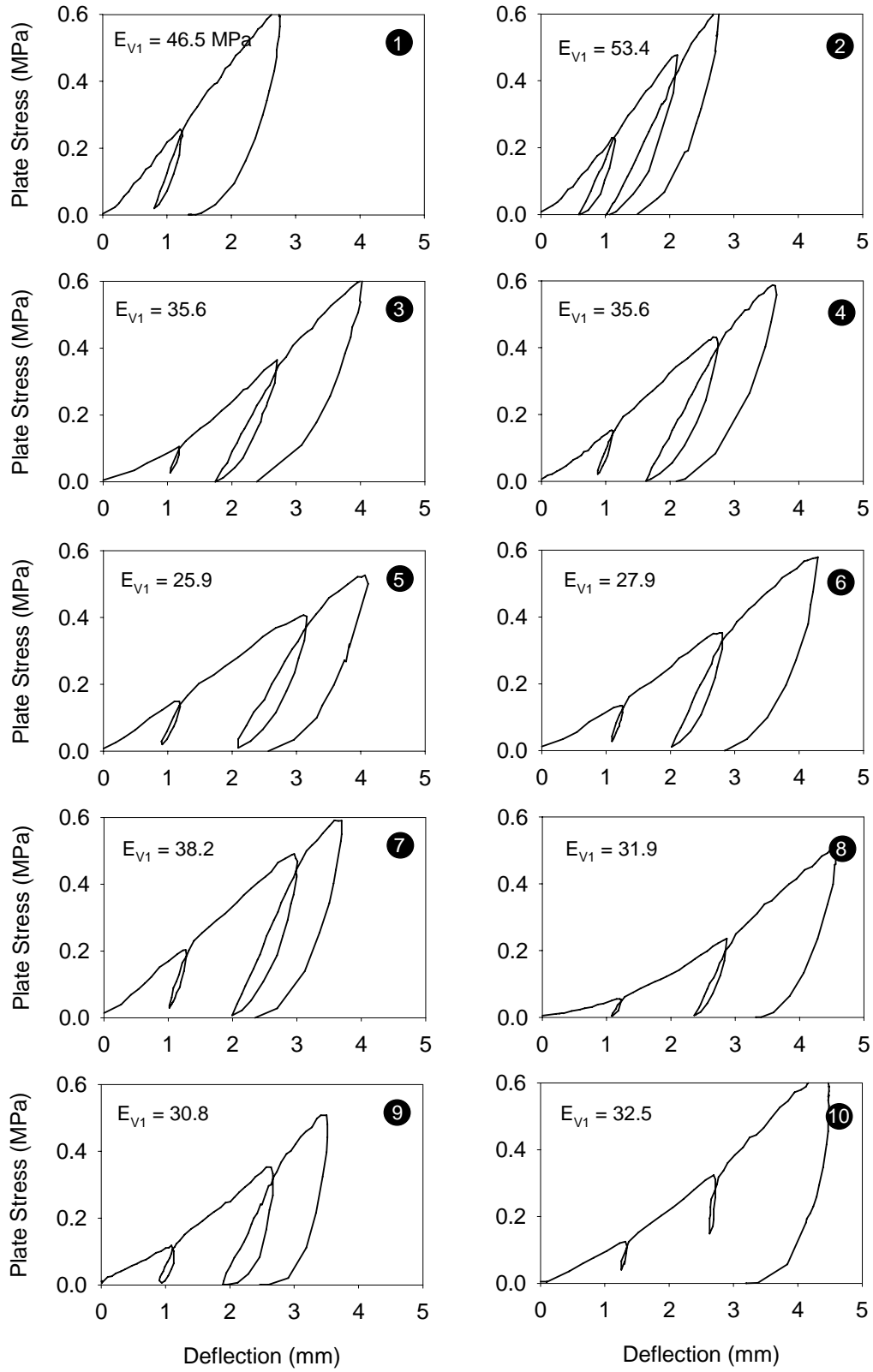
Figure C. 3. Strip 5 load-deflection curves (1 of 2) (subbase material)
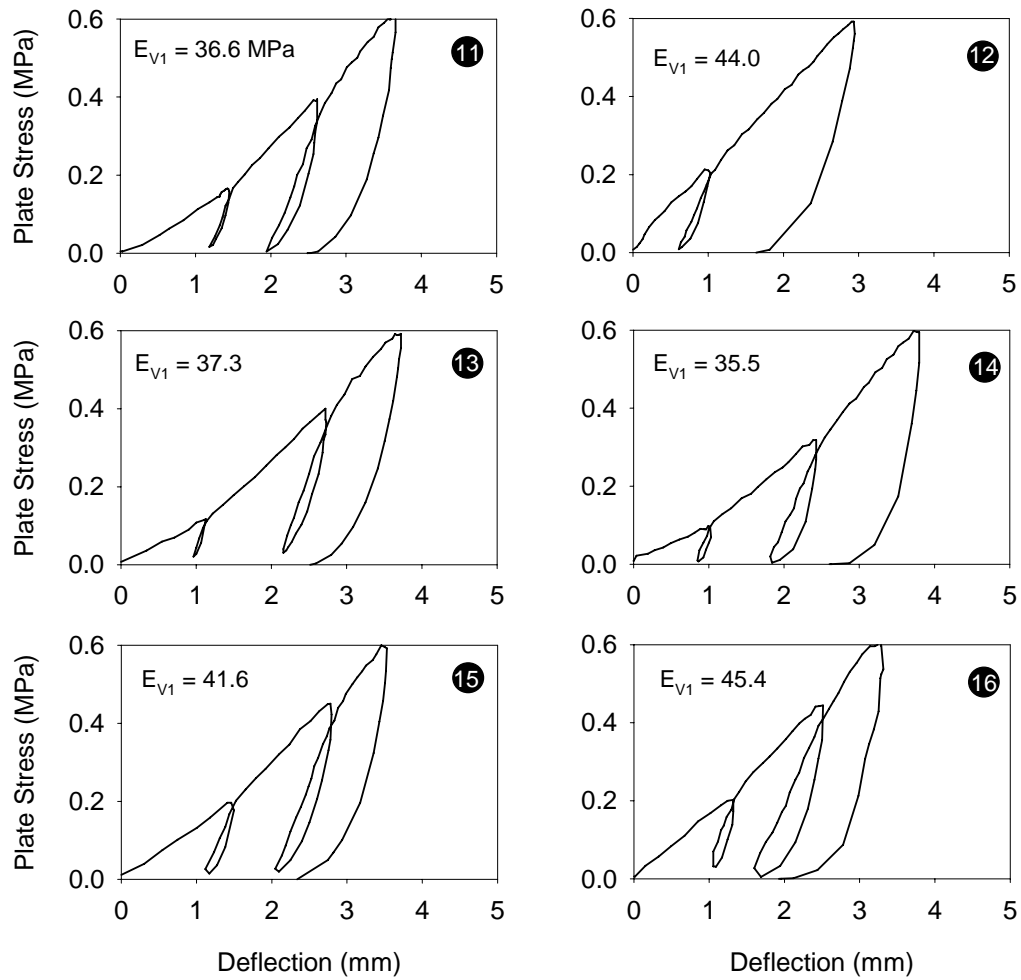
Figure C. 4. Strip 5 load-deflection curves (2 of 2) (subbase material)
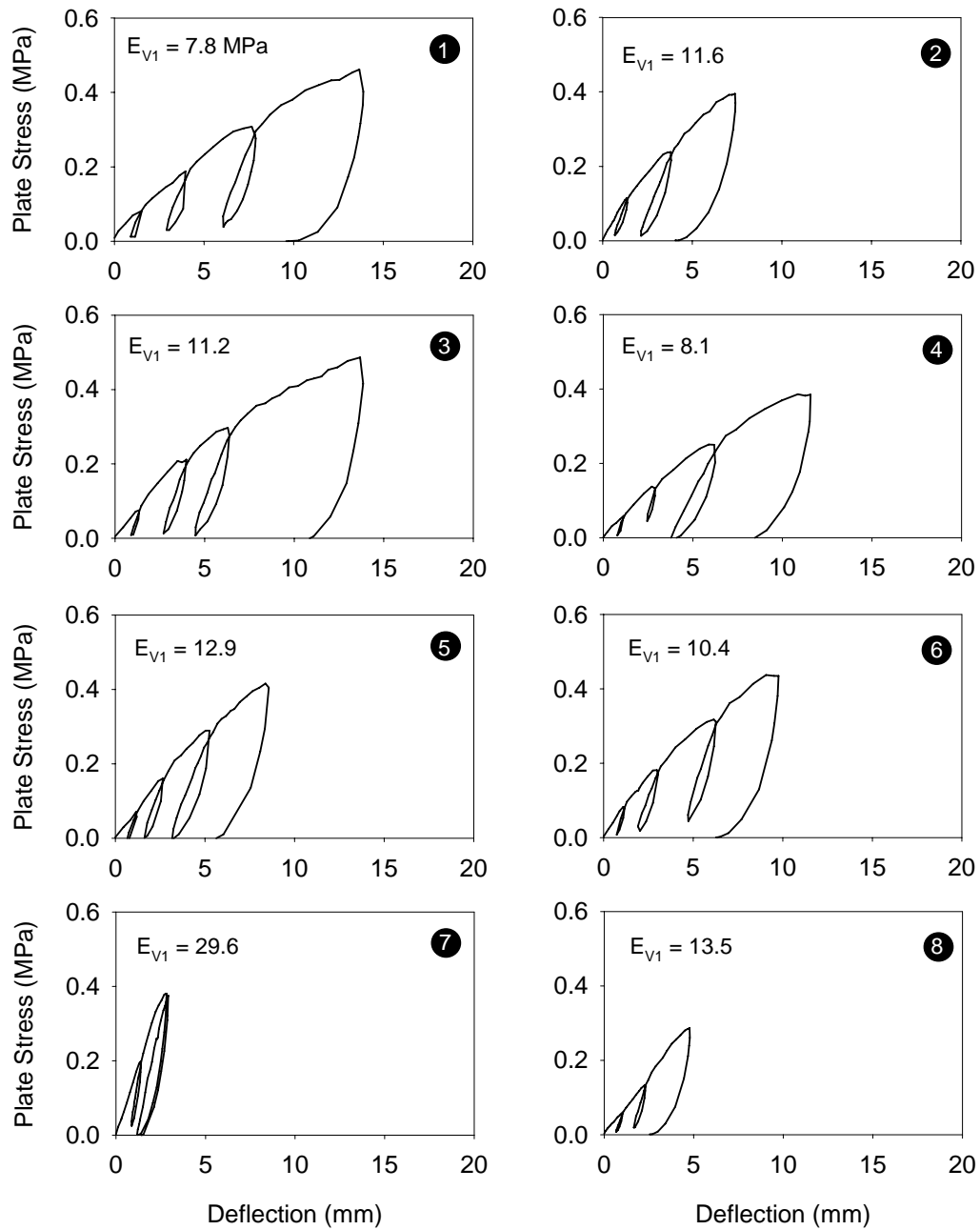
Figure C. 5. Strip 6 load-deflection curves (subgrade material)

Appendix D: Field Study 2 k_B Data Summary
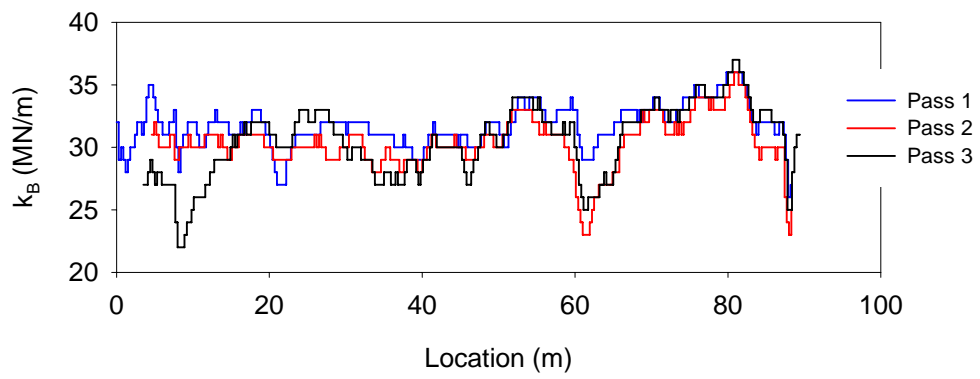
Figure D. 1. Ammann data for Strip 2
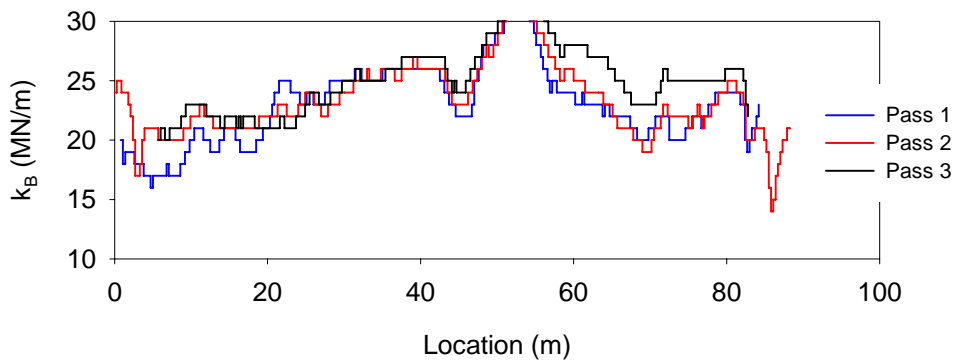
Figure D. 2. Ammann data for Strip 3
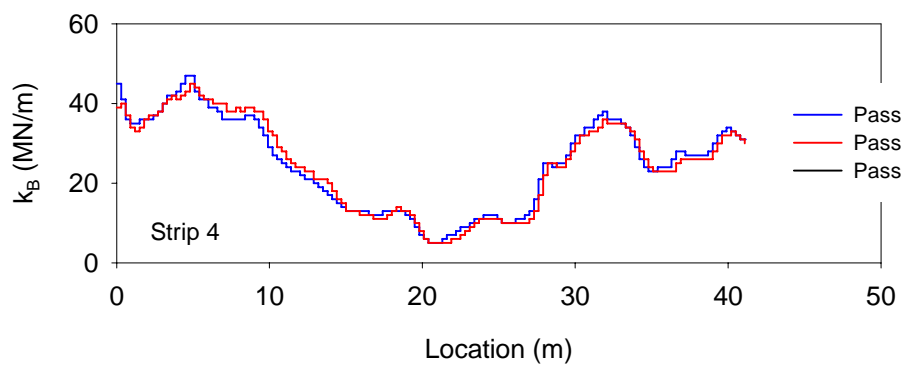
Figure D. 3. Ammann data for Strip 4
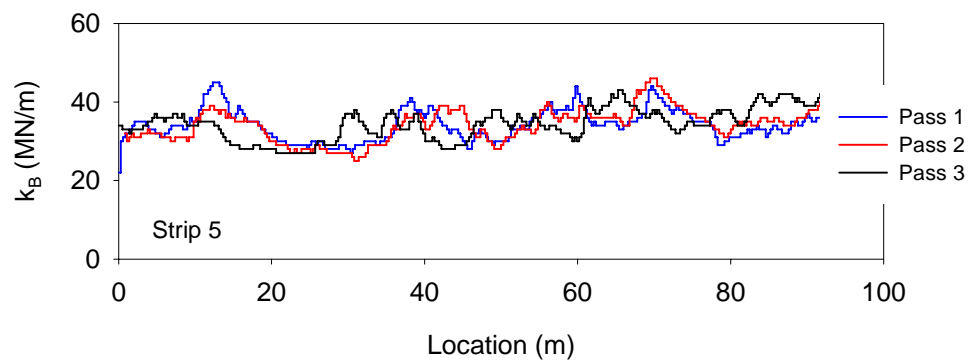
Figure D. 4. Ammann data for Strip 5
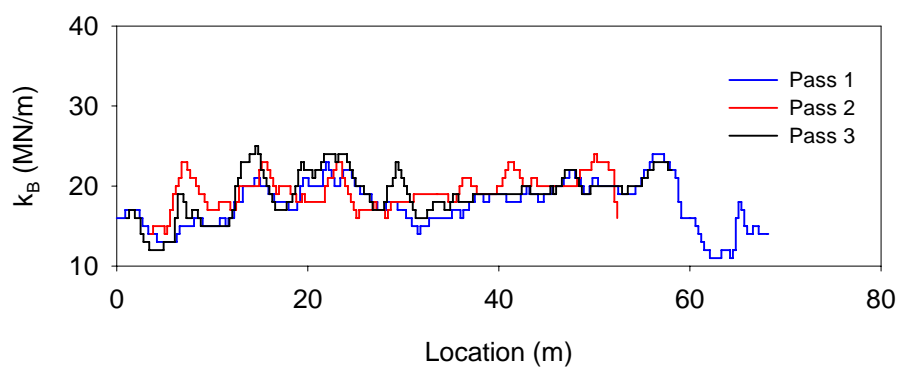
Figure D. 5. Ammann data for Strip 6, Track 1
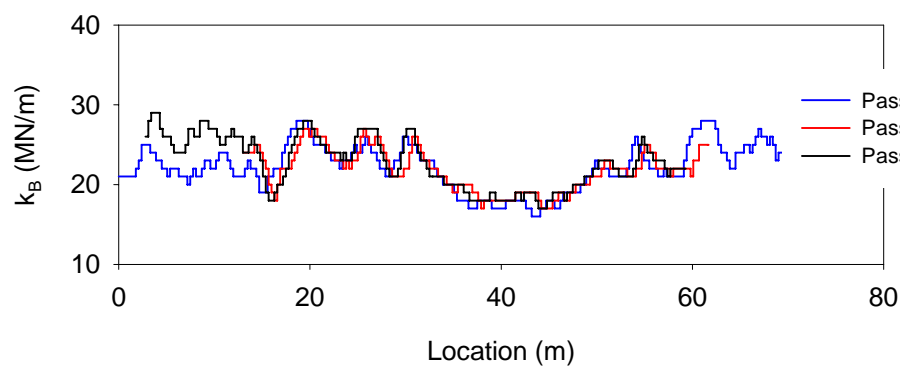
Figure D. 6. Ammann data for Strip 6, Track 2
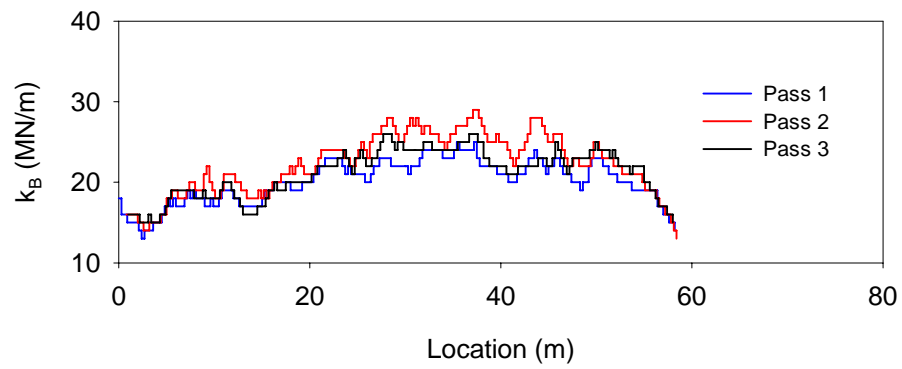
Figure D. 7. Ammann data for Strip 6, Track 3
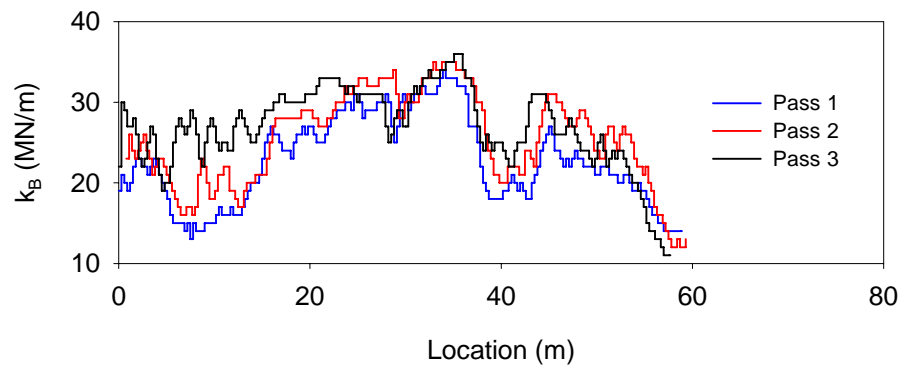
Figure D. 8. Ammann data for Strip 6, Track 4

Appendix E: Field Study 3 In-Situ Compaction Measurements

Table E. 1. Summary of in-situ testing for Proof 14

Test No.	Northing	Easting	E_{LWD-Z} (MPa)	γ_d (lb/ft^3)	w (%)	CIV_{20-kg}
1	4599.88	5043.22	30.37	.	.	7.0
2	4581.55	5043.55	32.89	17.41	4.7	8.3
3	4554.68	5044.40	27.72	18.24	4.4	7.0
4	4554.68	5044.46	20.66	17.70	5.7	6.5
5	4473.99	5044.84	21.42	17.91	4.4	7.2
6	4465.52	5044.30	29.99	.	.	7.0
7	4363.91	5045.12	28.60	.	.	6.5
8	4324.20	5045.90	31.88	.	.	6.8
9	4327.31	5049.65	20.92	18.26	5.4	5.2
10	4364.88	5055.65	27.97	18.80	5.9	6.3
11	4392.87	5056.26	26.96	18.45	7.2	5.5
12	4449.14	5055.77	26.71	.	.	5.5
13	4474.01	5055.57	34.90	.	.	6.8
14	4514.52	5057.50	23.31	.	.	4.7
15	4554.75	5060.32	23.81	.	.	3.9
16	4590.34	5056.31	30.11	.	.	5.8
17	4589.44	5050.02	38.93	.	.	8.1
18	4589.82	5044.14	38.43	18.87	8.4	4.7
19	4582.69	5054.65	35.03	.	.	8.0
20	4576.60	5049.92	32.13	.	.	6.5
21	4573.73	5055.25	35.66	18.43	9.1	6.2
22	4566.63	5055.09	39.06	.	.	7.2
23	4565.54	5049.39	36.04	.	.	7.8
24	4560.89	5055.26	35.66	.	.	7.7
25	4560.36	5052.15	35.66	.	.	7.3
26	4560.50	5049.60	33.77	.	.	7.2

27	4556.68	5055.22	34.65	.	.	6.7
28	4557.01	5049.97	33.14	.	.	6.8
29	4551.16	5058.70	34.40	.	.	6.7
30	4550.33	5054.07	38.18	.	.	7.2
31	4551.84	5049.49	35.03	18.25	9.8	8.5
32	4545.83	5049.72	35.53	.	.	7.5
33	4545.70	5043.95	33.39	.	.	11.1
34	4542.30	5054.64	29.48	.	.	0.2
35	4541.28	5049.50	28.10	.	.	7.3
36	4536.10	5055.05	35.53	.	.	9.3
37	4534.40	5051.17	26.59	19.13	8.1	6.8
38	4529.31	5055.69	40.19	.	.	7.8
39	4525.52	5052.72	27.22	.	.	5.4
40	4530.73	5045.52	28.60	.	.	5.7
41	4530.70	5045.50	40.82	.	.	9.9
42	4522.57	5056.00	24.82	.	.	5.2
43	4498.74	5045.49	27.34	18.73	8.8	8.1
44	4497.91	5047.64	35.66	.	.	6.5
45	4483.15	5049.86	42.34	.	.	8.3
46	4460.85	5052.53	35.66	.	.	8.6
47	4459.43	5043.81	27.22	.	.	6.7
48	4438.83	5050.64	34.90	.	.	9.0
49	4437.56	5048.64	30.37	.	.	6.0
50	4429.14	5054.43	18.77	.	.	6.7
51	4414.80	5058.00	28.98	.	.	6.3
52	4409.90	5044.60	40.45	.	.	5.8
53	4386.22	5043.38	30.11	.	.	5.5
54	4377.74	5051.73	38.43			9.0

Table E. 2. Summary of in-situ testing for Proof 15

Test No.	Northing	Easting	E_{LWD-Z} (MPa)	γ_d (lb/ft^3)	w (%)	CIV_{20-kg}
1	4638.13	5043.65	31.90	17.77	5.1	5.4
2	4626.57	5055.40	32.17	.	.	6.2
3	4626.91	5070.80	26.68	.	.	5.5
4	4673.55	5071.72	24.84	.	.	5.0
5	4675.01	5054.47	28.61	18.04	11.0	5.0
6	4675.32	5042.98	28.68	.	.	5.4
7	4724.27	5042.16	28.92	.	.	6.5
8	4723.31	5058.56	25.56	.	.	4.4
9	4723.40	5071.48	26.23	18.28	11.8	3.9
10	4777.73	5072.19	23.01	.	.	4.5
11	4779.12	5055.81	21.36	19.33	9.3	5.2
12	4779.95	5042.46	28.04	.	.	6.7
13	4823.29	5042.29	30.73	18.19	6.1	6.7
14	4825.37	5059.14	19.93	.	.	4.4
15	4825.42	5071.81	19.17	.	.	3.9
16	4923.74	5069.42	25.87	.	.	7.2
17	4923.66	5057.39	19.35	18.06	8.4	6.0
18	4922.95	5041.69	29.37	.	.	5.0
19	5023.48	5039.88	29.05	.	.	4.2
20	5023.54	5056.60	20.13	.	.	4.0
21	5023.60	5069.54	21.00	18.17	7.2	4.9
22	5030.56	5069.37	27.98	.	.	6.3
23	5124.41	5056.18	27.77	18.29	9.2	5.0
24	5124.00	5037.00	32.34	.	.	6.2
25	5223.32	5038.62	31.87	17.92	9.8	5.2
26	5224.21	5049.83	24.09	.	.	5.0

27	5223.13	5066.84	29.26	.	.	5.0
28	5324.43	5067.98	21.54	.	.	3.7
29	5326.77	5049.60	28.02	17.70	10.1	5.5
30	5325.33	5037.48	27.19	.	.	3.6
31	5422.35	5035.49	19.77	.	.	4.4
32	5424.08	5053.04	21.99	.	.	3.9
33	5423.71	5065.23	25.51	18.04	5.1	4.4
34	5523.40	5062.50	27.21	.	.	4.2
35	5523.71	5051.54	23.13	16.87	8.7	3.6
36	5523.96	5035.48	23.43	.	.	5.7

Table E. 3. Summary of in-situ testing for Proof 18

Test No.	Northing	Easting	E_{LWD-Z} (MPa)	γ_d (lb/ft^3)	w (%)	CIV_{20-kg}
1	1260.29	5042.84	34.02	17.68	4.0	6.0
2	1268.66	5047.87	28.85	.	.	5.7
3	1251.01	5048.38	28.35	18.15	3.8	6.3
4	1253.71	5055.88	34.40	.	.	5.2
5	1258.70	5035.04	23.69	.	.	4.4
6	1285.93	5055.94	25.20	.	.	5.2

Table E. 4. Summary of in-situ testing for Proof 35

Test No.	STA	Offset (ft)	$E_{LWD\text{-}Z\,200}$ (MPa)	$E_{LWD\text{-}Z\,300}$ (MPa)	γ_d (lb/ft^3)	w (%)
1	269+00	-6	28.73	38.86	17.17	6.9
2	269+50	-6	31.63	30.24	17.09	5.3
3	270+00	-6	32.26	31.58	17.22	3.7
4	270+50	-6	27.34	33.82	16.75	8.4
5	271+00	-6	31.63	35.06	16.90	7.9
6	271+50	-6	30.74	40.99	17.70	9.1
7	272+00	-6	38.56	41.22	17.64	9.8
8	269+00	-12	30.37	42.34	.	.
9	269+50	-12	27.97	32.70	.	.
10	270+00	-12	30.87	40.99	.	.
11	270+50	-12	36.41	45.36	.	.
12	271+00	-12	34.02	45.70	.	.
13	271+50	-12	37.93	48.16	.	.
14	272+00	-12	39.19	48.72	.	.

Table E. 5. Summary of in-situ testing for Proof 36

Test No.	STA	Offset (ft)	γ_d (lb/ft^3)	w (%)	$E_{LWD-Z-200}$ (MPa)	$E_{LWD-Z-300}$ (MPa)	$E_{LWD-K-300}$ (MPa)
1	160	-11	20.71	6.0	59.85	43.12	131
2	163	-12	20.79	5.2	87.70	52.98	75
3	166	-10	21.49	6.5	76.86	48.50	113
4	169	-10	21.23	4.9	75.60	71.01	171
5	172	-9	21.43	6.2	73.21	53.31	180
6	175	-11	20.58	5.8	79.63	51.52	94
7	178	-9	20.74	6.1	78.12	41.10	137
8	181	-8	20.79	6.7	87.32	53.65	156
9	184	-5	21.05	6.7	87.32	50.85	252
10	187	-9	21.89	5.3	82.03	65.97	171
11	190	-9	20.44	9.8	89.84	55.55	93
12	193	-10	20.83	4.9	93.74	56.38	187
13	196	-8	21.48	6.7	71.06	50.62	203
14	199	-10	20.85	7.0	81.14	61.71	91
15	202	-10	21.51	5.2	62.50	61.04	169
16	205	-8	21.35	5.7	77.24	39.98	90
17	208	-9	21.84	5.2	68.04	48.50	87
18	211	-13	21.51	4.4	75.85	54.43	147
19	214	-11	20.91	6.8	78.37	43.57	118
20	217	-10	21.24	7.8	77.74	55.44	157
21	220	-10	21.45	6.6	28.48	21.50	25
22	223	-11	21.34	5.8	64.64	43.57	123
23	226	-12	21.13	4.8	69.80	60.26	91
24	229	-12	21.19	6.1	38.56	34.72	60
25	232	-8	20.80	6.4	71.32	49.17	.
26	235	-8	21.24	7.7	57.83	39.54	.

27	238	-9	20.69	7.3	60.35	63.62	74
28	241	-10	20.60	5.2	87.07	47.60	111
29	244	-9	19.69	7.6	49.77	56.67	46
30	247	-12	19.89	4.4	74.72	56.22	94
31	250	-12	20.08	4.9	47.75	34.05	95
32	253	-13	19.04	4.8	37.67	66.64	56
33	256	-13	20.75	5.0	68.67	63.62	146
34	259	-13	19.64	4.9	68.29	47.60	93
35	262	-13	20.30	5.2	90.22	56.67	131
36	265	-13	19.43	5.5	67.28	56.22	118
37	268	-15	18.40	4.9	34.15	34.05	53
38	271	-8	20.68	4.9	83.79	66.64	113
39	274	-8	20.55	4.4	123.10	66.53	170
40	277	-9	20.22	5.2	125.12	73.25	142
41	280	-9	20.74	5.1	111.89	58.46	82
42	283	-14	19.81	4.7	49.01	39.54	47
43	286	-11	20.55	5.5	102.19	67.87	.
44	289	-8	19.26	4.9	72.20	50.62	.
45	292	-13	17.99	4.4	39.94	24.19	60
46	295	-8	21.15	4.8	96.14	65.74	160
47	298	-8	19.84	4.1	121.97	87.47	162
48	301	-10	19.62	4.0	96.64	78.51	170
49	304	-13	19.67	4.5	81.27	65.30	139
50	307	-16	17.91	3.2	33.26	33.26	43
51	310	-16	18.74	3.1	34.65	32.14	50
52	313	-15	18.82	3.6	32.00	33.60	41

Table E. 6. Summary of Mn/DOT quality acceptance testing

Test No.	STA	Offset (ft) [a]	Proof No.	E_{LWD} (MPa)	γ_d (lb/ft^3)	w (%)	DPI$_{Mn/DOT}$
1	151+00	+3		93		11.0	
2	150+00	+6		109	115.8	5.4	22
3	149+00	-10		97		4.9	21
4	302+00	0		28		10.5	22
5	301+60	+7		21	120.0	6.4	20
6	300+55	-8		25		9.2	19
7	312+00	-2	7	43	143.0	4.3	30
8	315+21	+8	7	25		10.3	15
9	309+77	-12	8	56		5.0	25
10	306+17	0	8	52	117.1	6.1	21
11	303+26	-13	8	52		6.4	13
12	292+35	+12		64	117.2	4.8	22
13	295+39	-7		65		6.4	23
14	299+65	0		64	116.5	7.8	22
15	297+00	+3		44		8.2	29
16	276+65	-2	14	71	116.5	10.5	15
17	274+45	-18	14	38		3.8	18
18	272+12	+8	14	86	124.9	8.0	14
19	269+51	0	14	53		10.1	20
20	277+08	-14	15	55		5.3	19
21	279+03	-5	15	52	124.5	10.8	20
22	283+00	+9	15	39		5.8	28
23	285+65	-8	15	48		9.2	23
24	243+26	-13		45		3.7	22
25	245+62	+8		65	115.7	7.5	16
26	257+80	+6		81		6.9	13

27	257+05	+10		75		7.4	10
28	255+31	+2		98	112.5	5.8	12
29	253+15	+8	19	52		5.4	18
30	255+29	0	19	56		9.5	12
31	258+29	-10	19	75	118.8	7.1	7
32	221+00	-9	24	54		10.3	20
33	218+00	+10	24	66	123.7	7.4	21
34	214+00	+5	24	52		4.6	22
35	206+00	0	26	52		3.1	26
36	202+00	-7	26	62	116.0	6.4	12
37	199+00	+1	26	28		4.3	31
38	196+00	-4	27	68		6.4	26
39	192+00	+4	27	68		3.6	19
40	190+00	+7	27	69	120.5	5.0	17
41	187+00	-6		92		4.7	13
42	154+00	+11		24		10.7	29
43	150+00	-2		109		8.8	15
44	147+00	-3		51	121.7	8.4	22
45	075+75	+8	33	63		4.4	22
46	074+00	-6	33	48	107.3	5.2	19
47	069+00	+3	35	54		4.2	21
48	071+37	-7	35	68	136.4	6.7	22
49	075+95	+8	35	49		9.1	18
50	127+00	-10	37	67		8.1	22
51	124+00	+8	37	57	112.8	10.7	21
52	121+00	+5	37	115		6.3	26
53	117+00	-1	38	44		6.8	19
54	110+00	+4	38	83		9.9	17
55	108+00	-2	38	89	117.0	8.6	

56	103+00	-11	39	120		7.6	16
57	100+00	+7	39	87	123.6	6.6	14
58	096+00	-10	39	70		5.7	17
59	093+00	-4	39	103		9.8	18
60	090+00	+9	39	102	124.7	8.9	16
61	088+00	+1	39	77		8.2	15
62	095+62	+10		78		8.7	14
63	098+42	-6		113		5.0	14
64	122+63	-18		105	119.6	6.6	16

[a] Positive = right of CL; negative = left of CL

Appendix F: Field Study 3 DCP Profiles
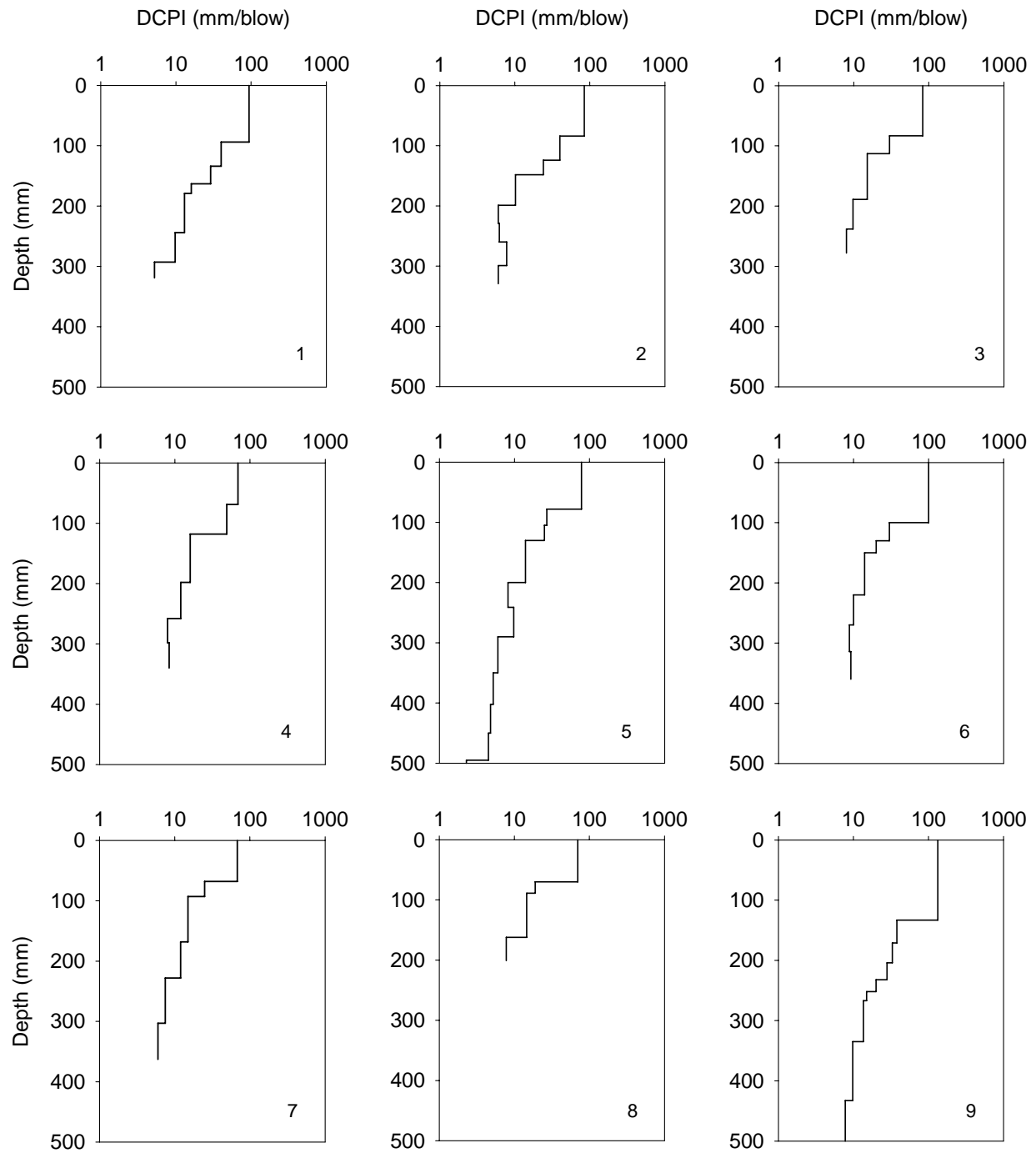
Figure F. 1. Proof 14 DCP profiles

F-1
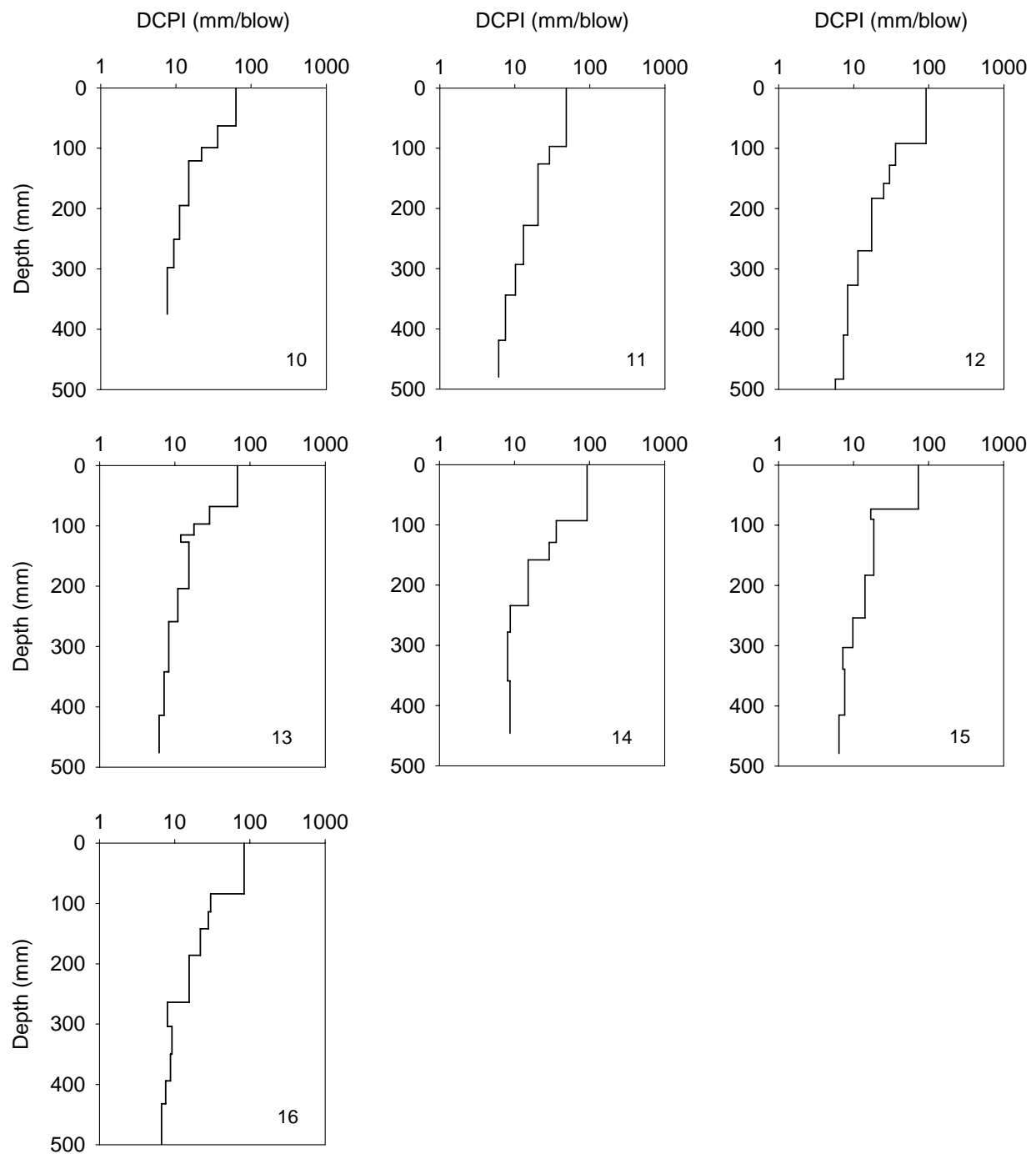
Figure F. 2. Proof 14 DCP profiles (continued)
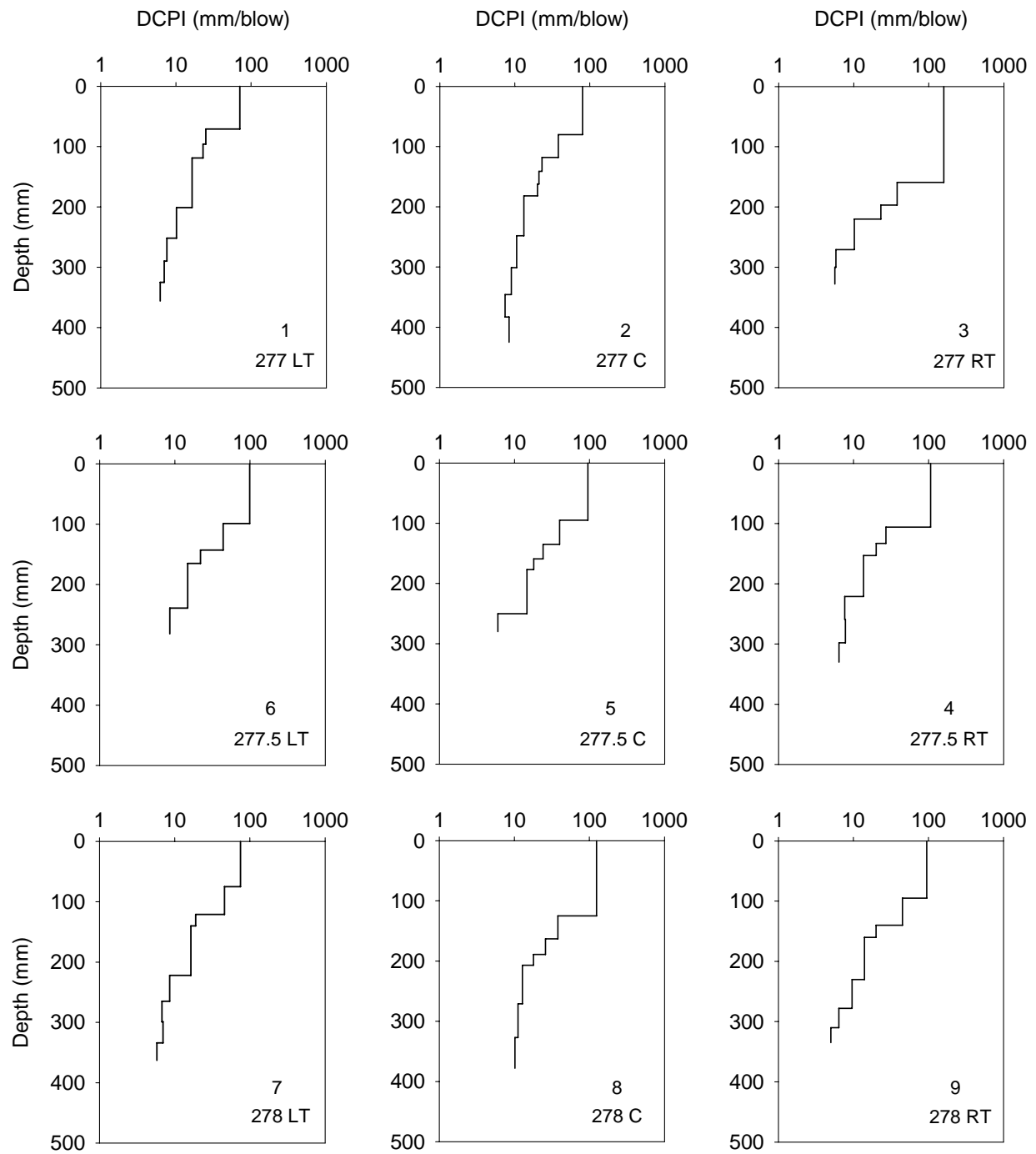
Figure F. 3. Proof 15 DCP profiles
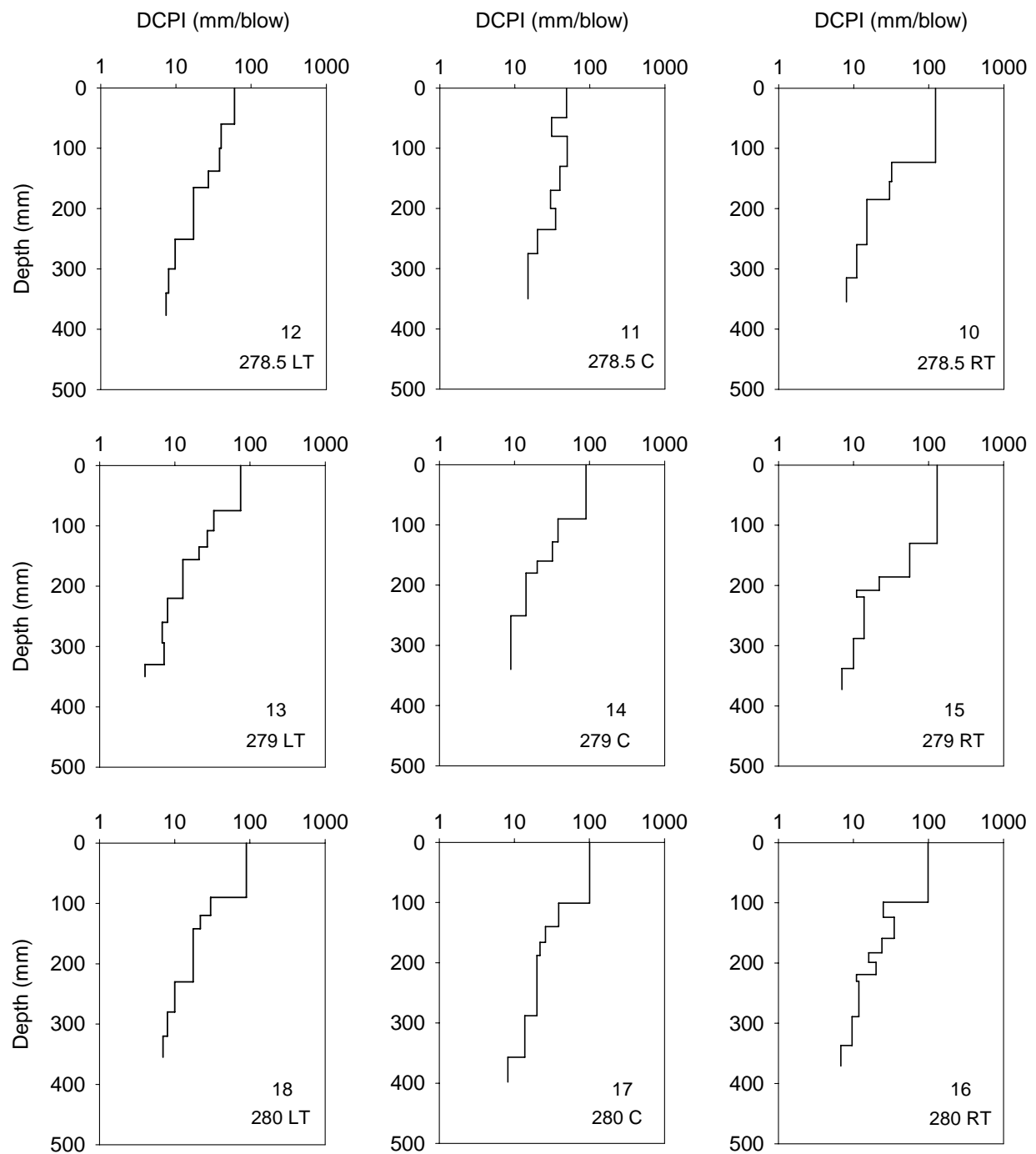
Figure F. 4. Proof 15 DCP profiles (continued)
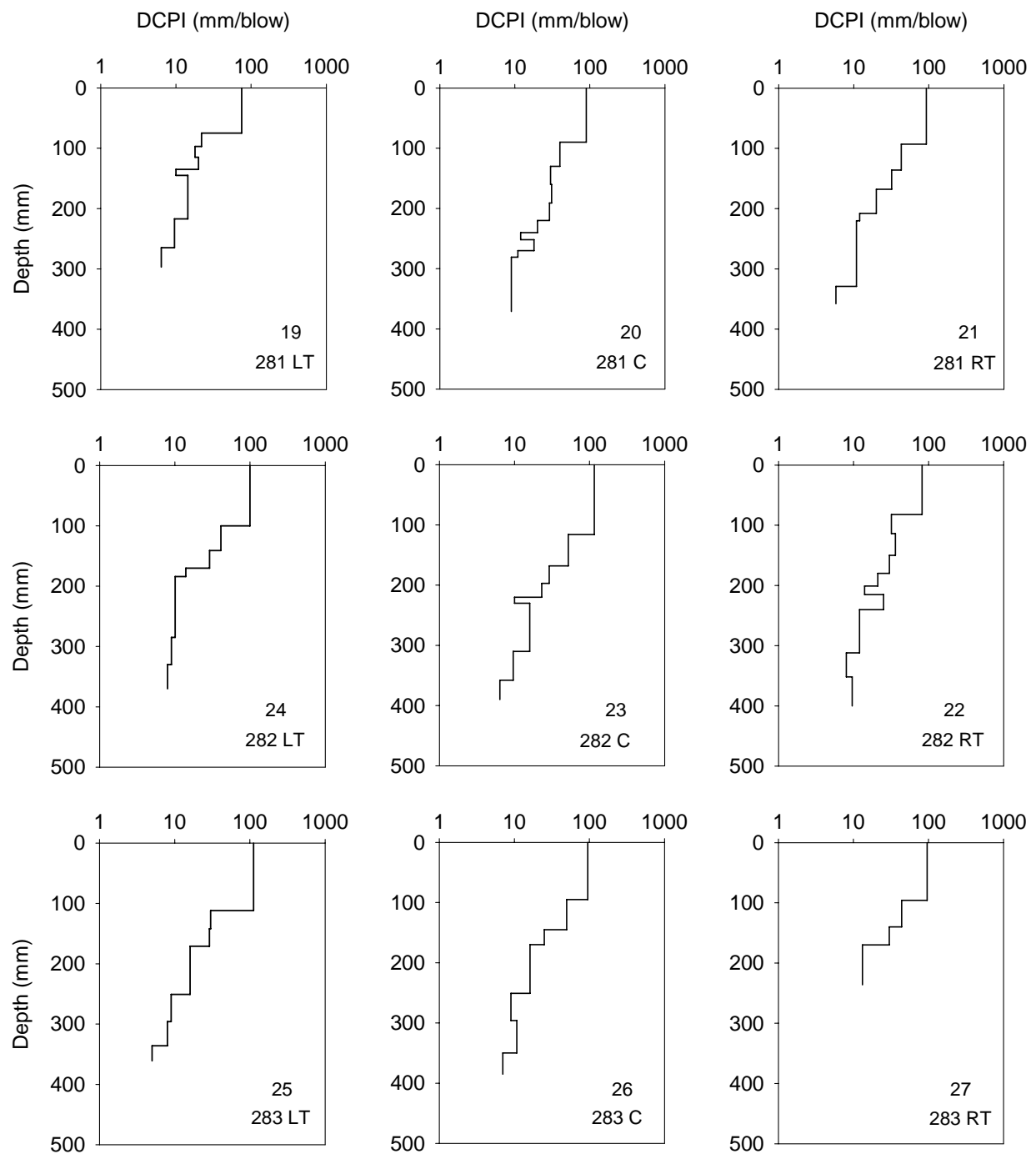
Figure F. 5. Proof 15 DCP profiles (continued)
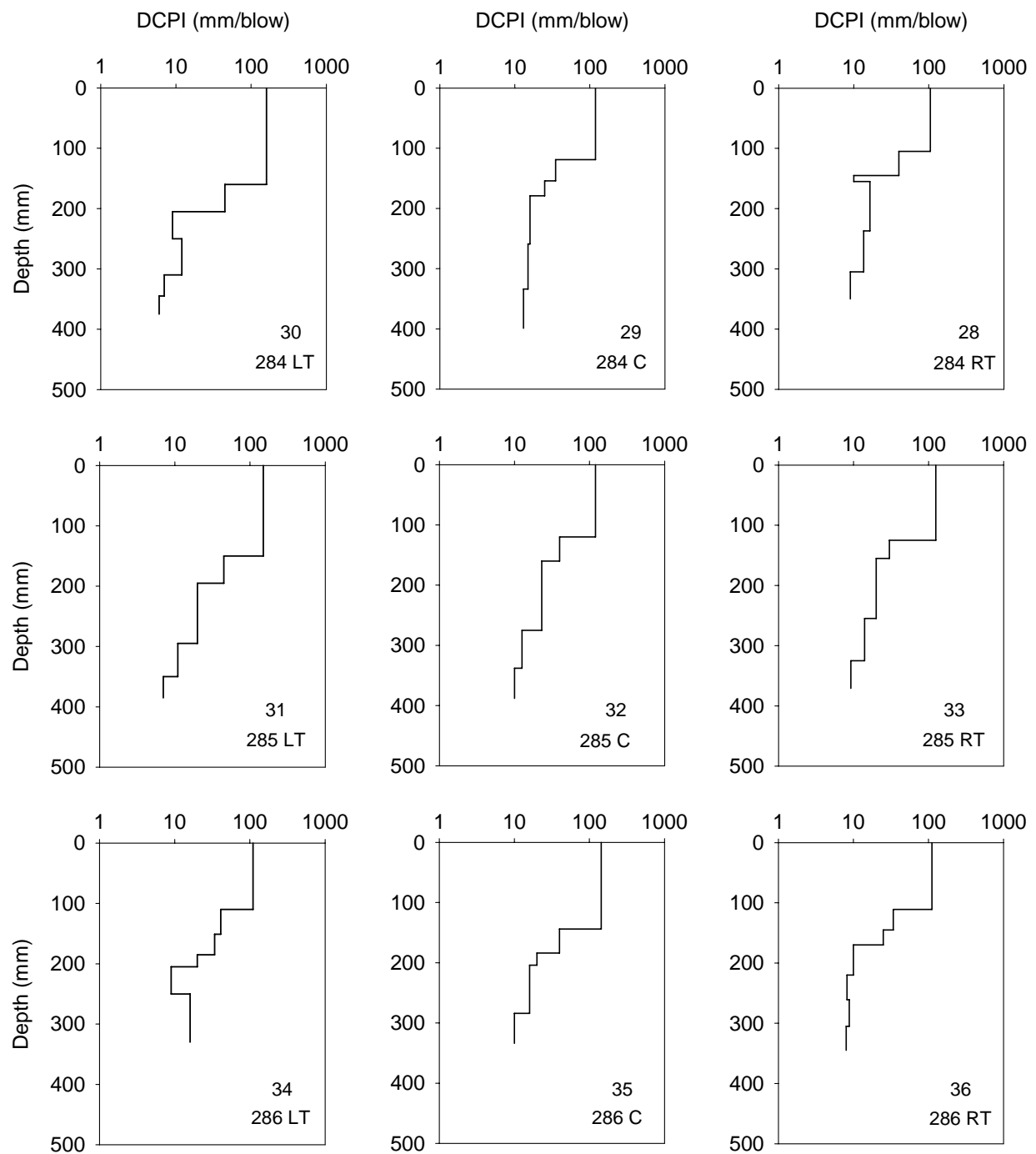
Figure F. 6. Proof 15 DCP profiles (continued)
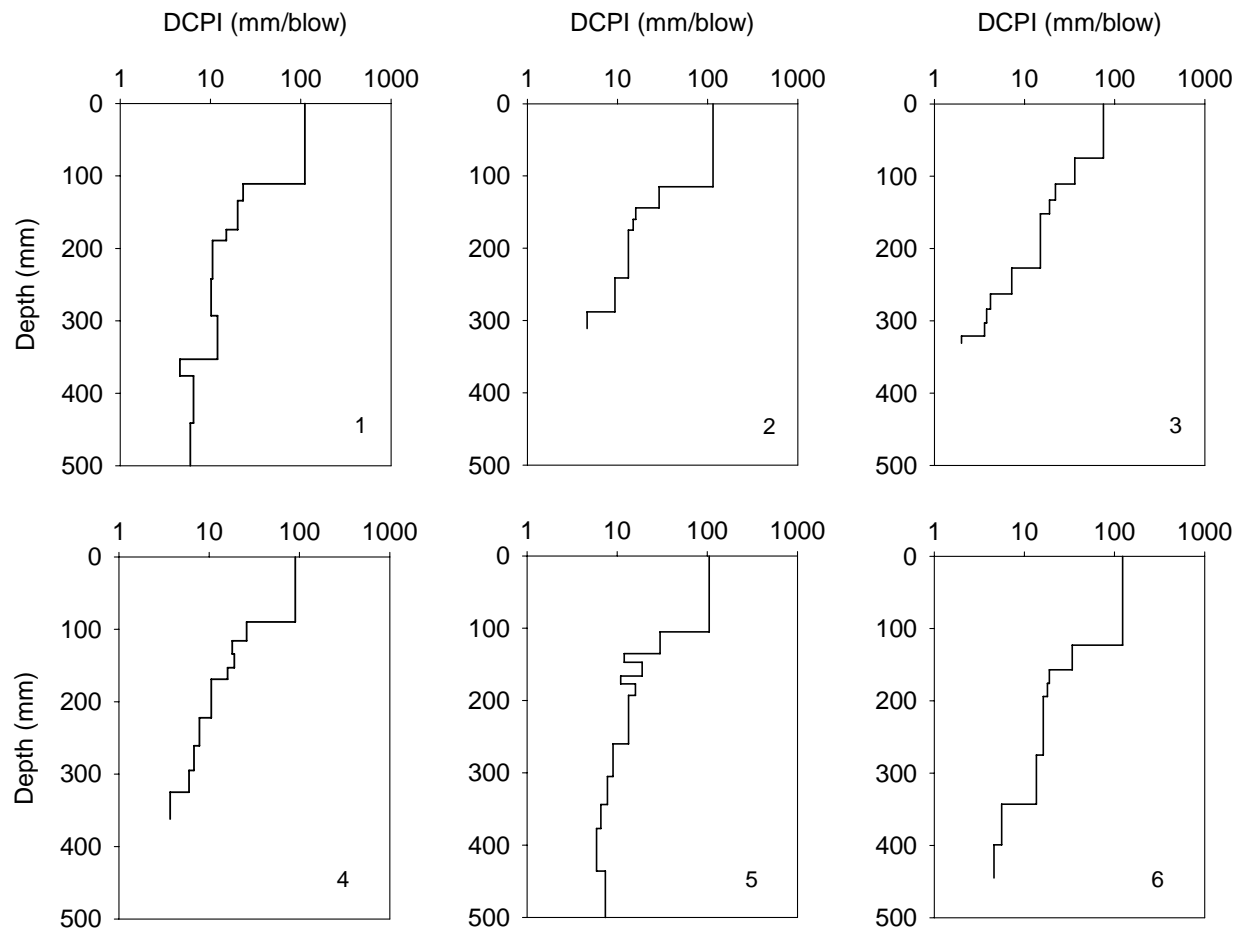
Figure F. 7. Proof 18 DCP profiles
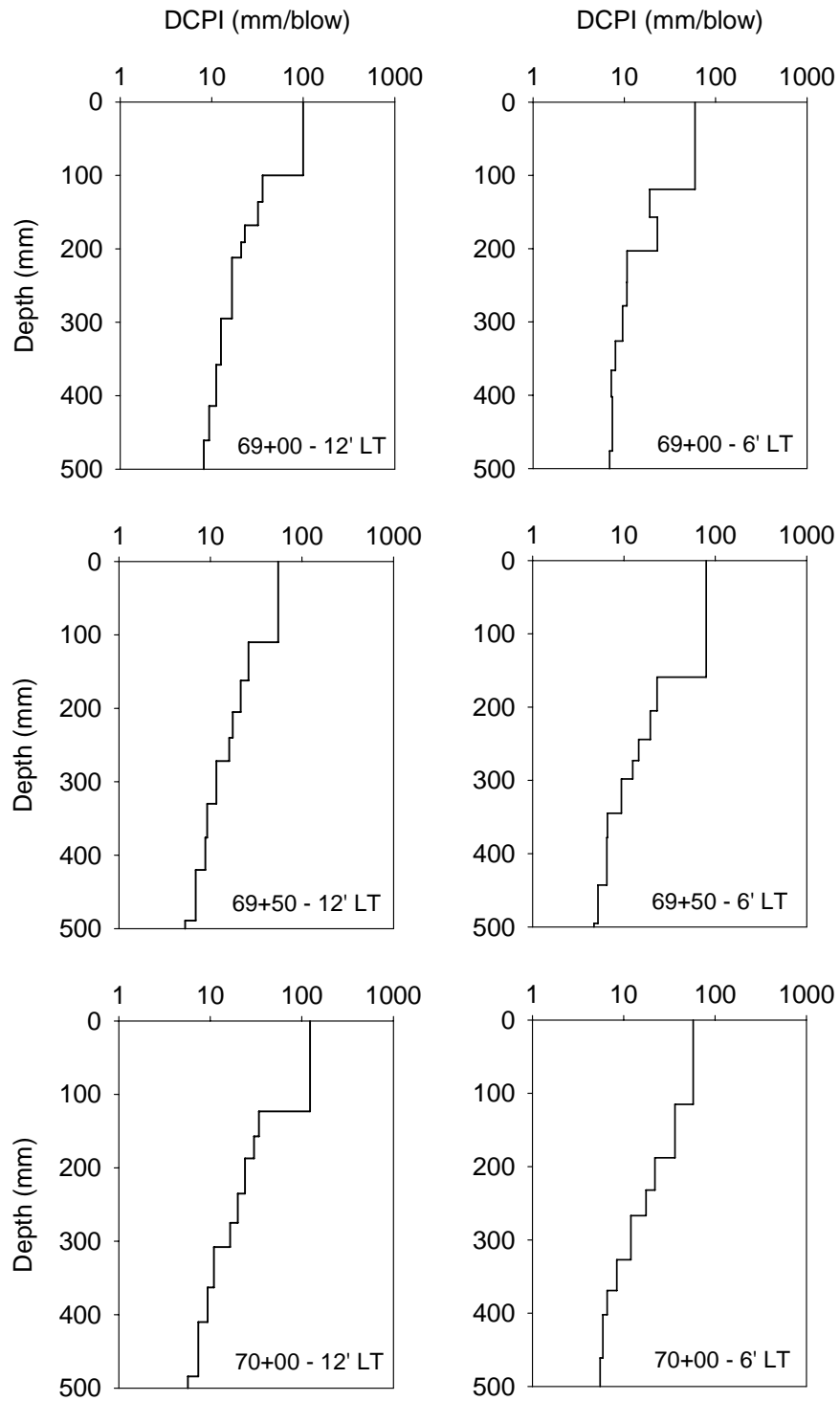
Figure F. 8. Proof 35 DCP profiles
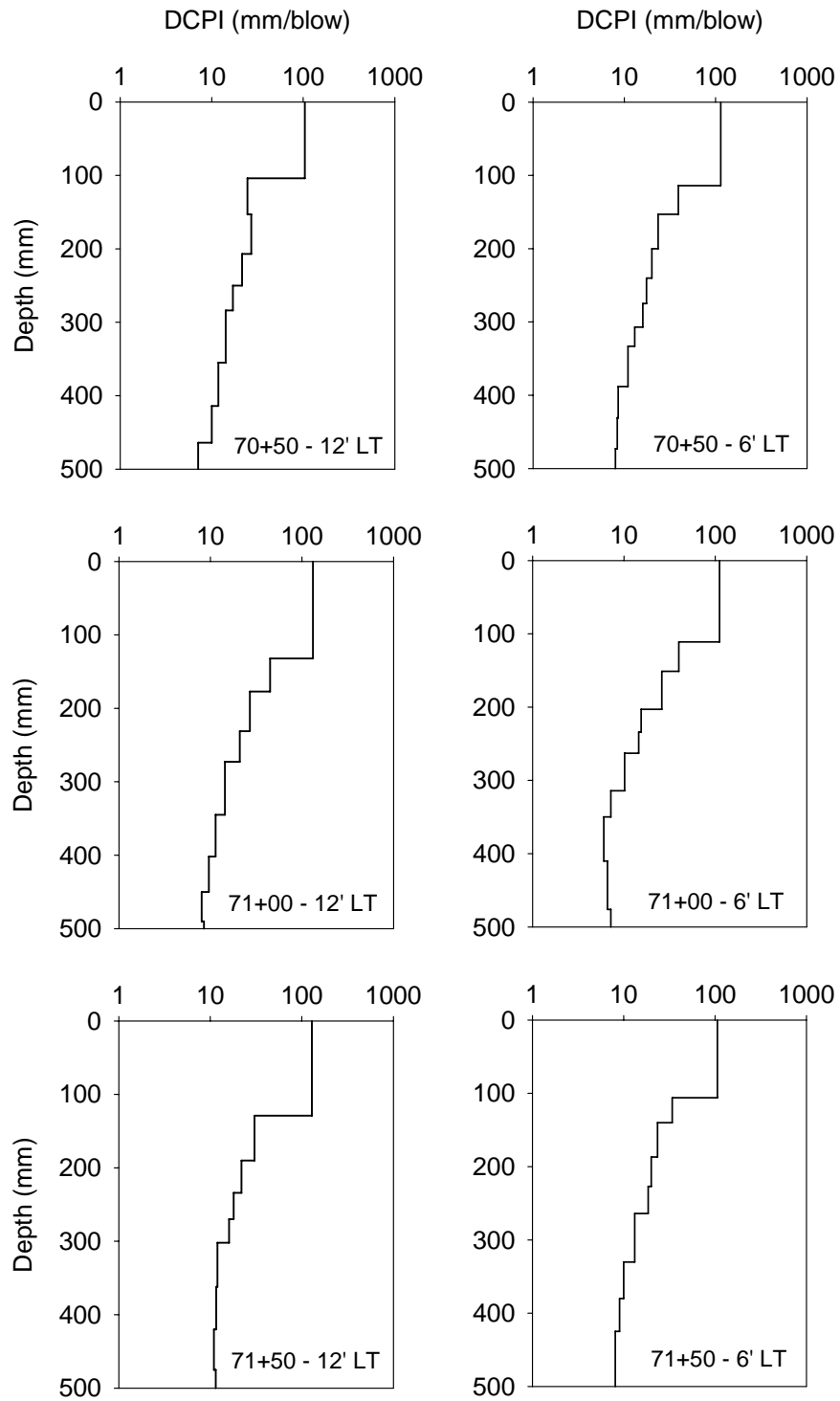
Figure F. 9. Proof 35 DCP profiles (continued)
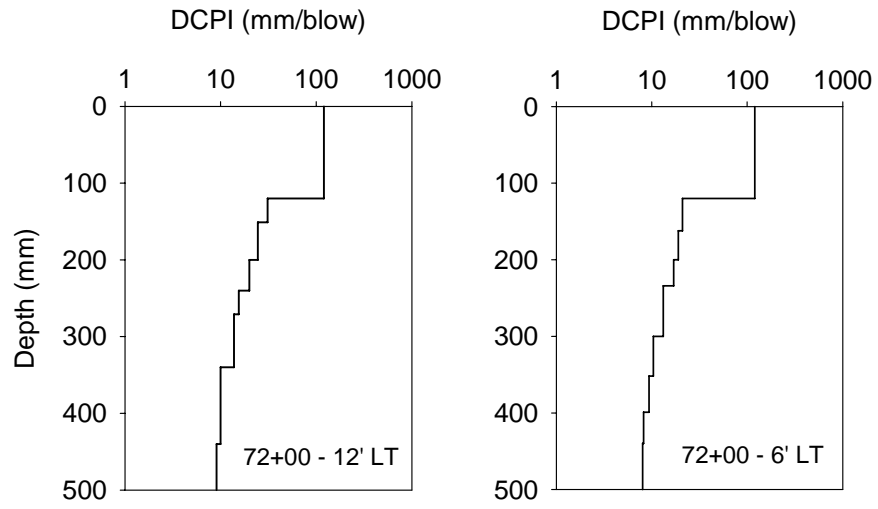
Figure F. 10. Proof 35 DCP profiles (continued)
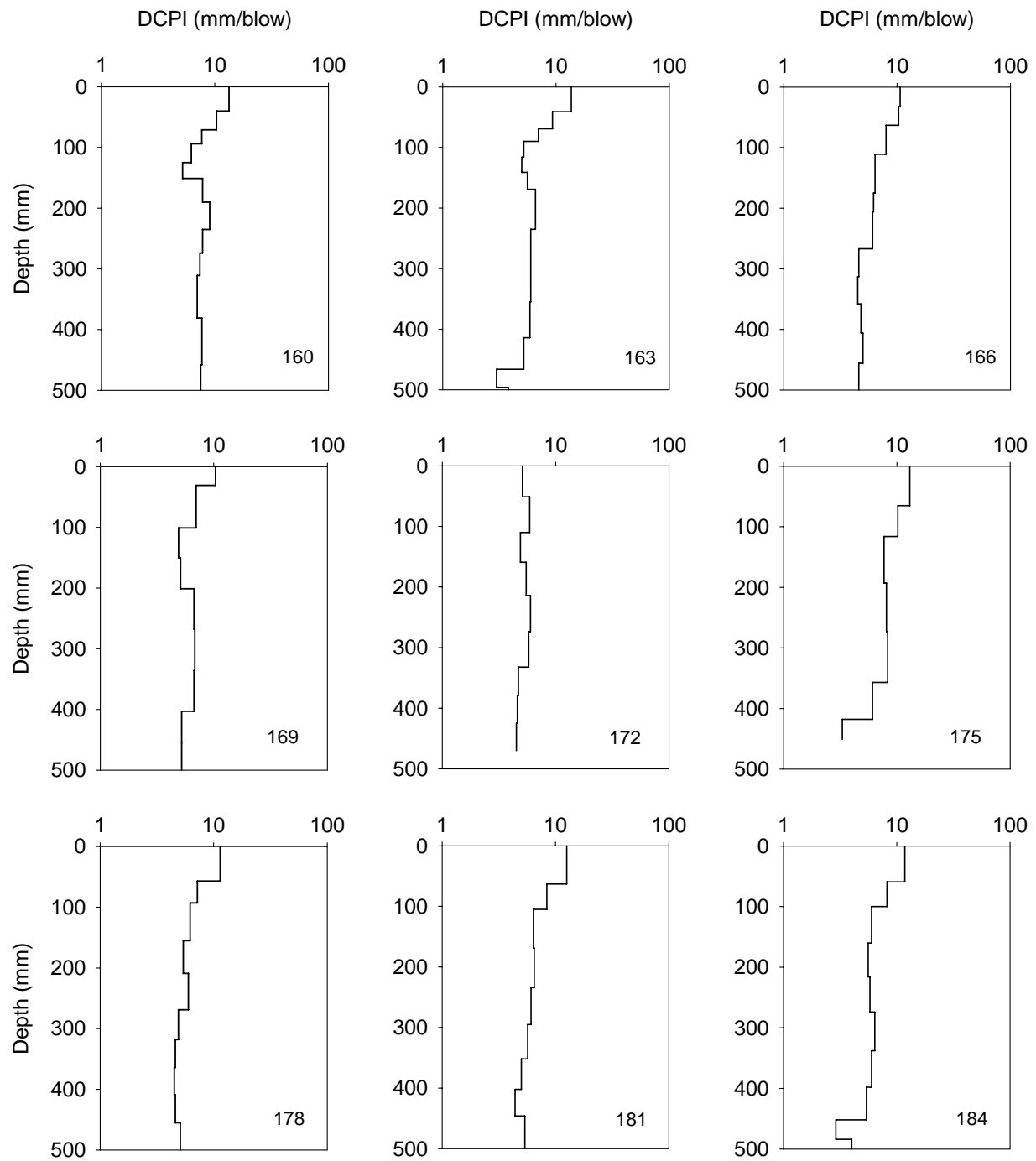
Figure F. 11. Proof 36 DCP profiles
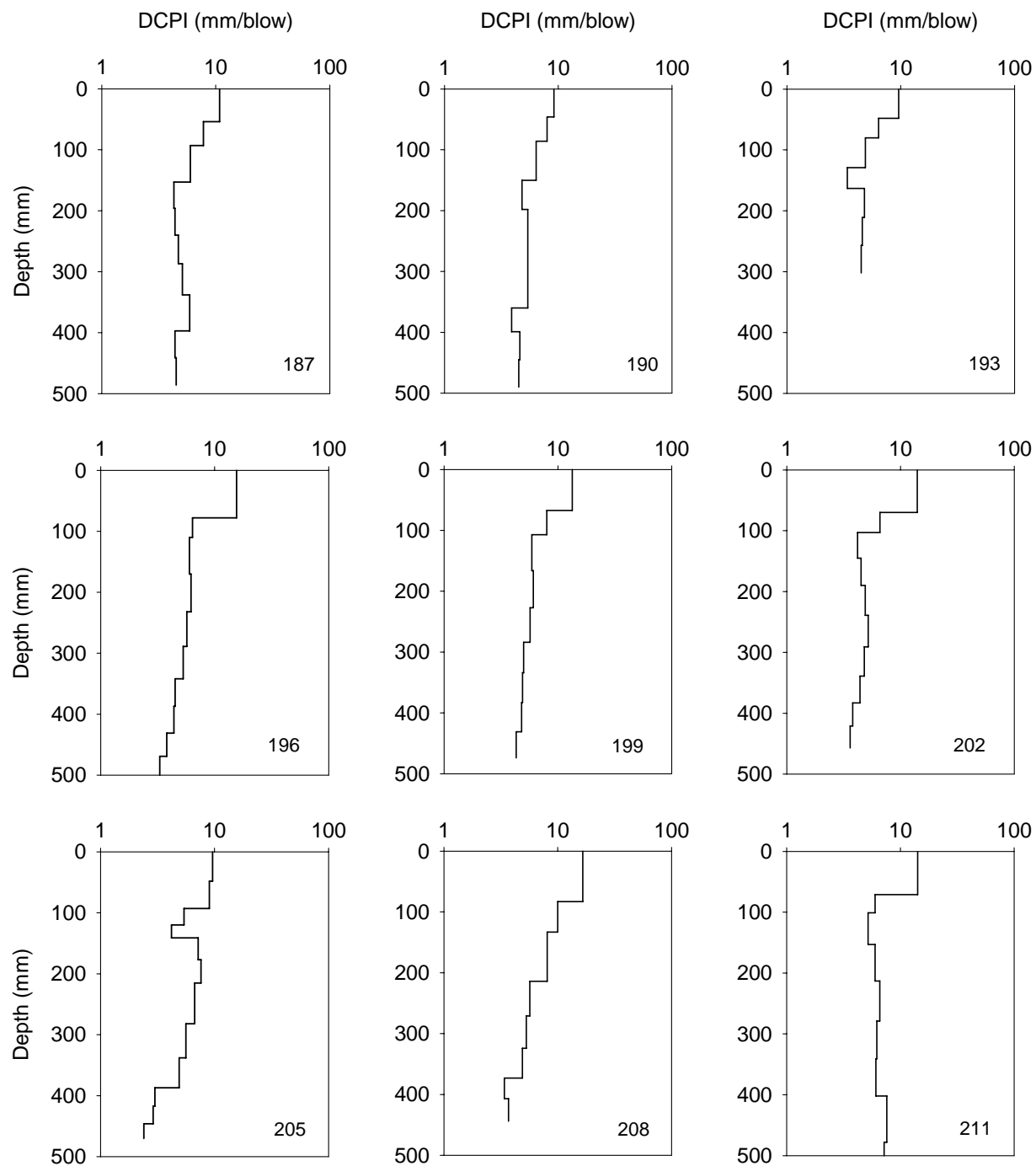
Figure F. 12. Proof 36 DCP profiles (continued)
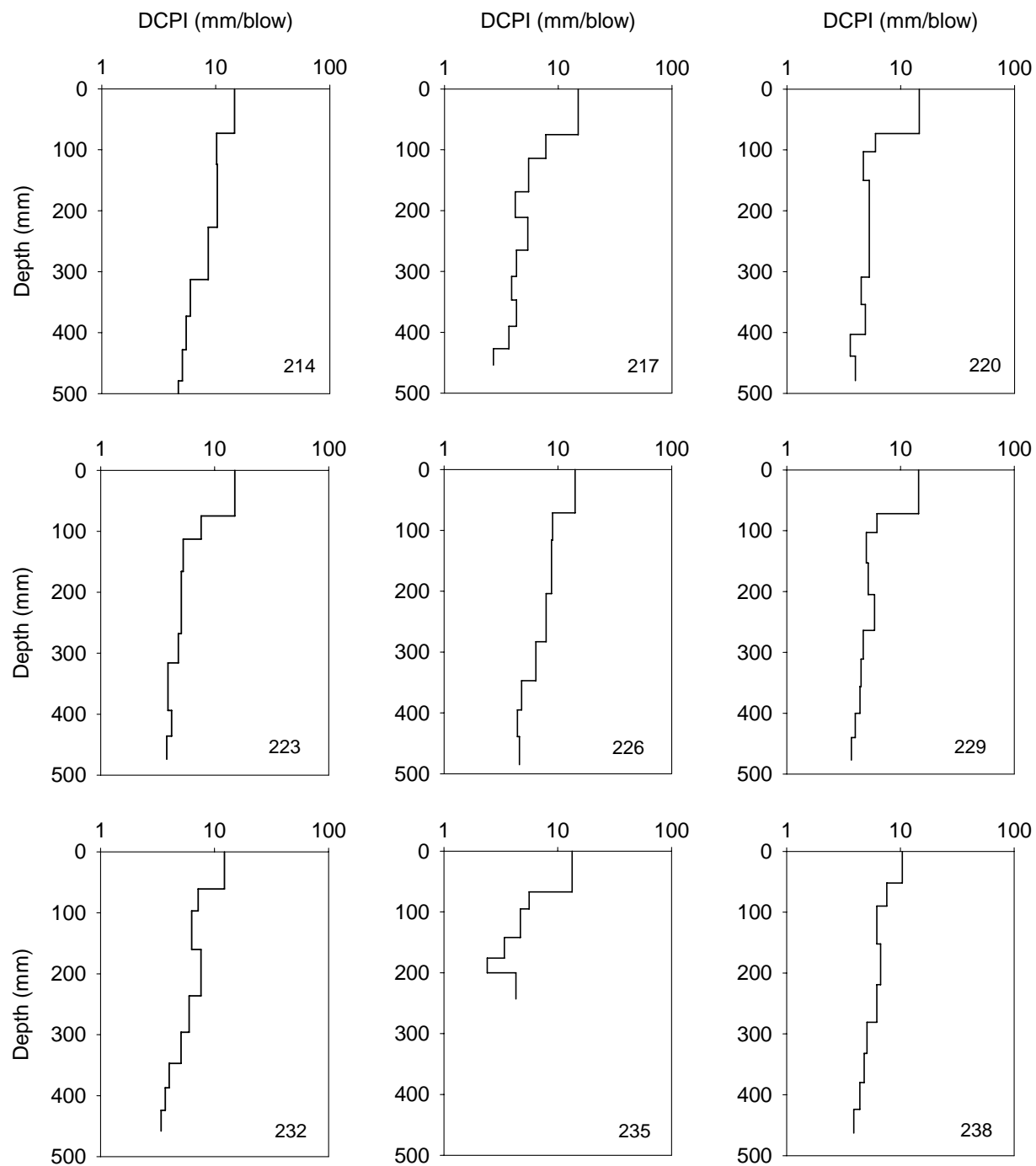
Figure F. 13. Proof 36 DCP profiles (continued)
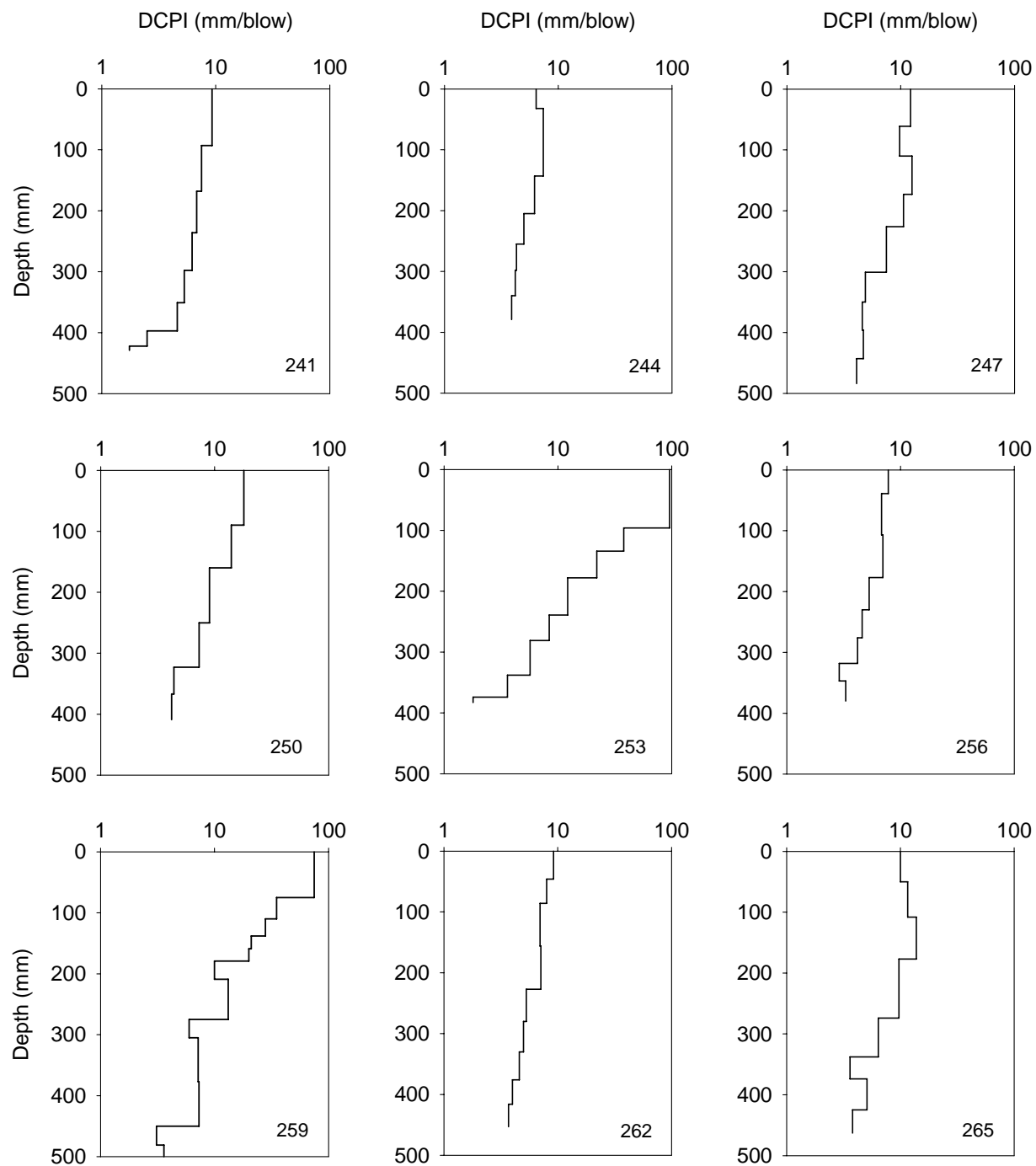
Figure F. 14. Proof 36 DCP profiles (continued)
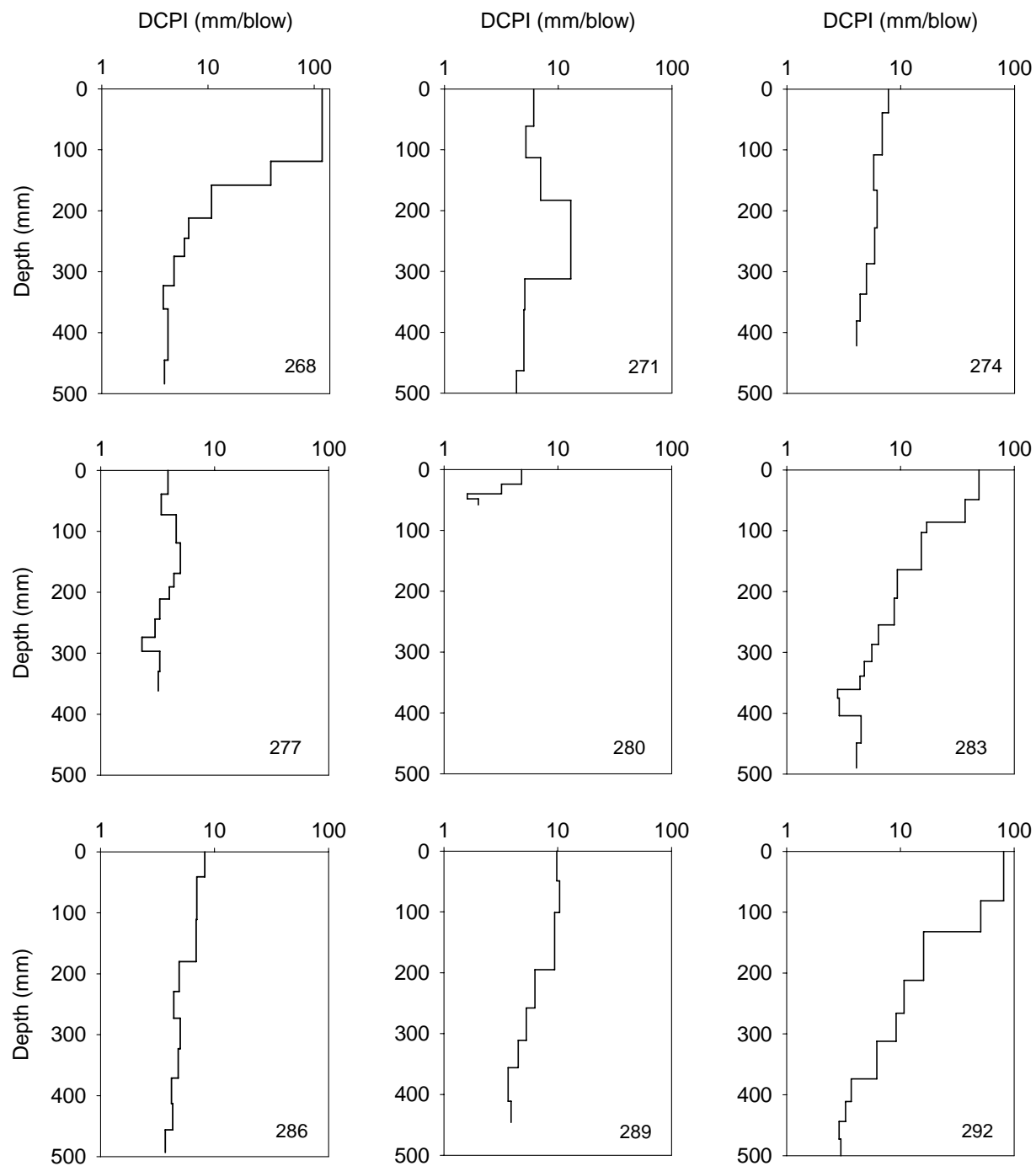
Figure F. 15. Proof 36 DCP profiles (continued)
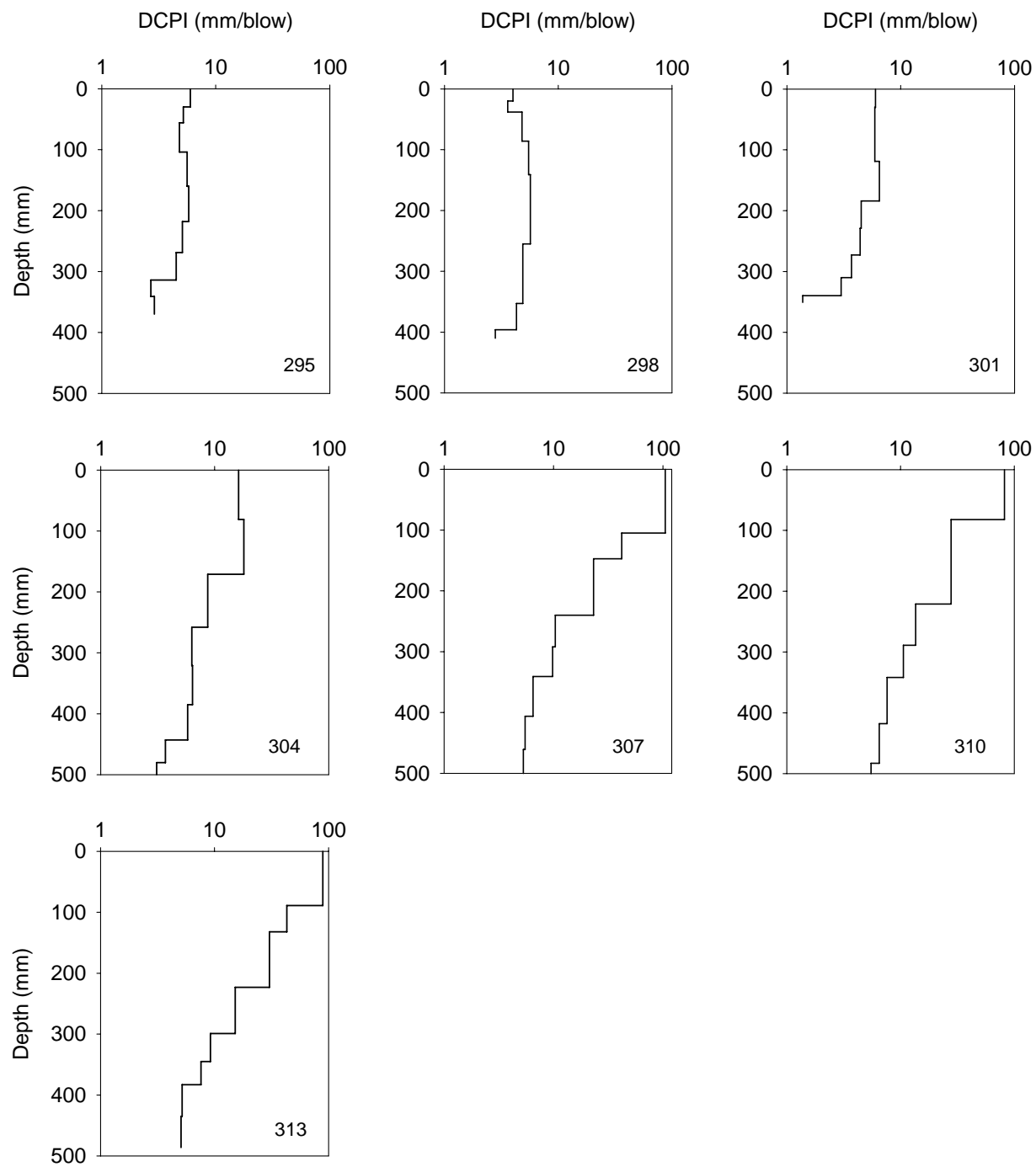
Figure F. 16. Proof 36 DCP profiles (continued)
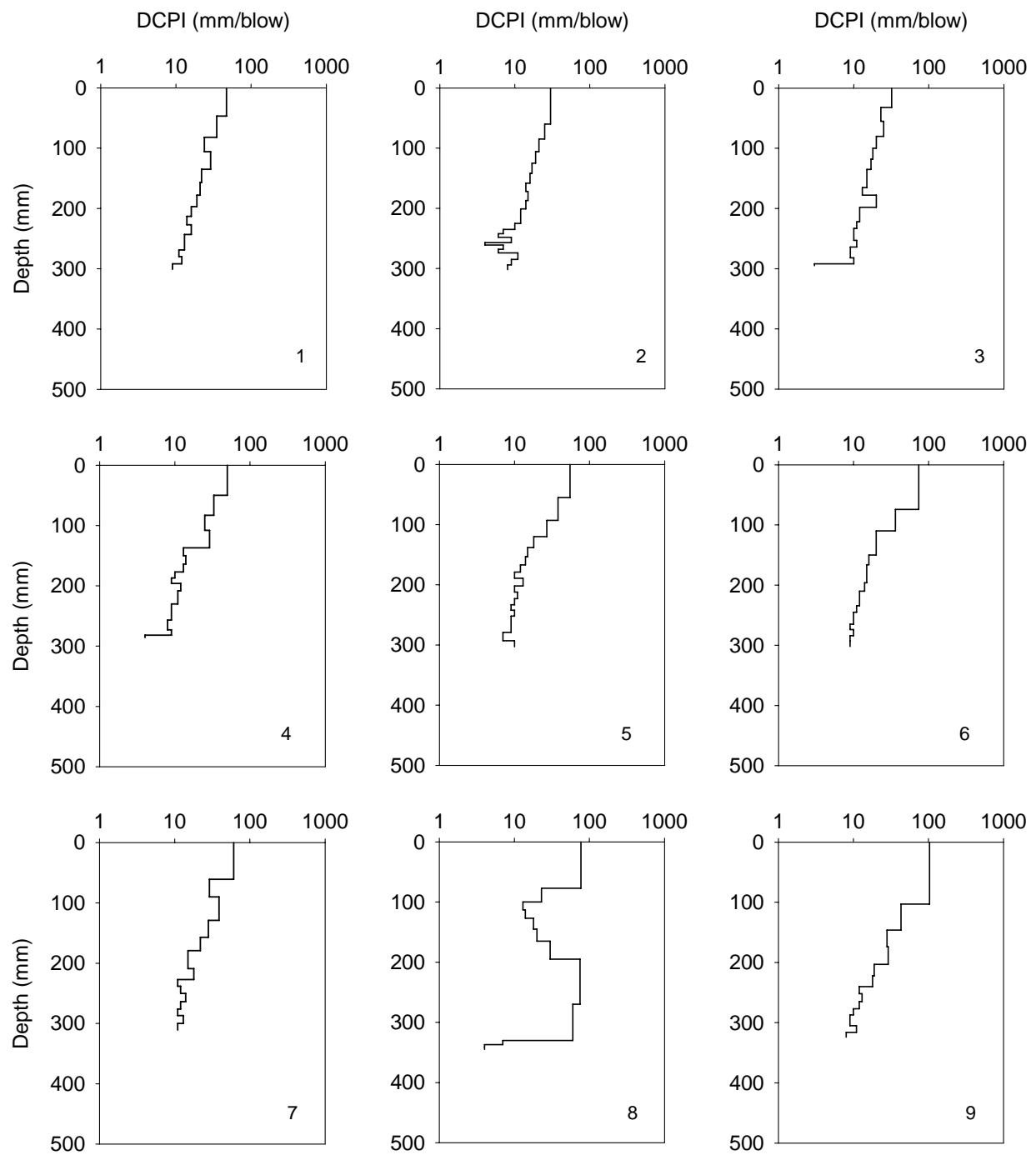
Figure F. 17. Mn/DOT DCP profiles
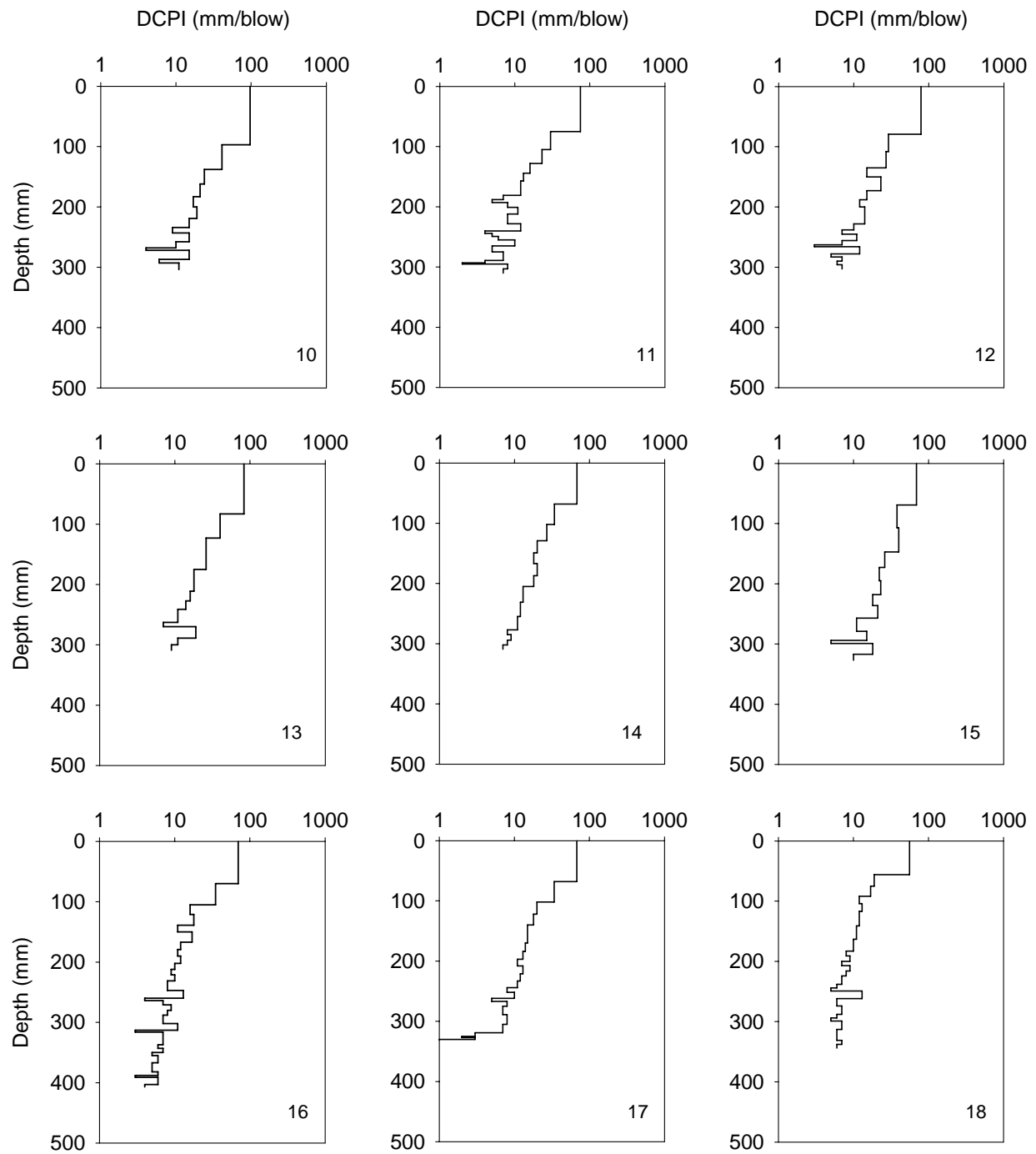
Figure F. 18. Mn/DOT DCP profiles (continued)
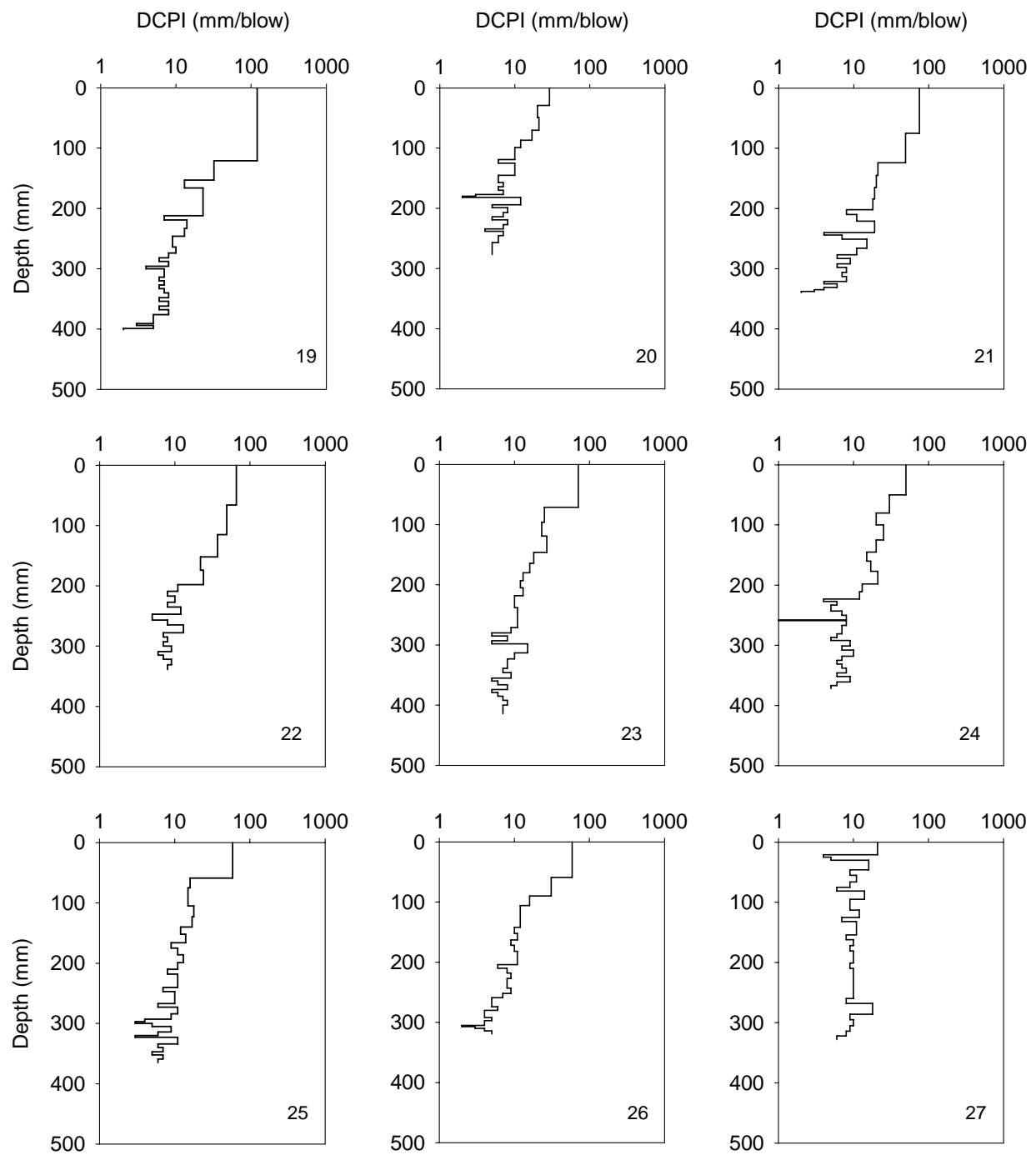
Figure F. 19. Mn/DOT DCP profiles (continued)
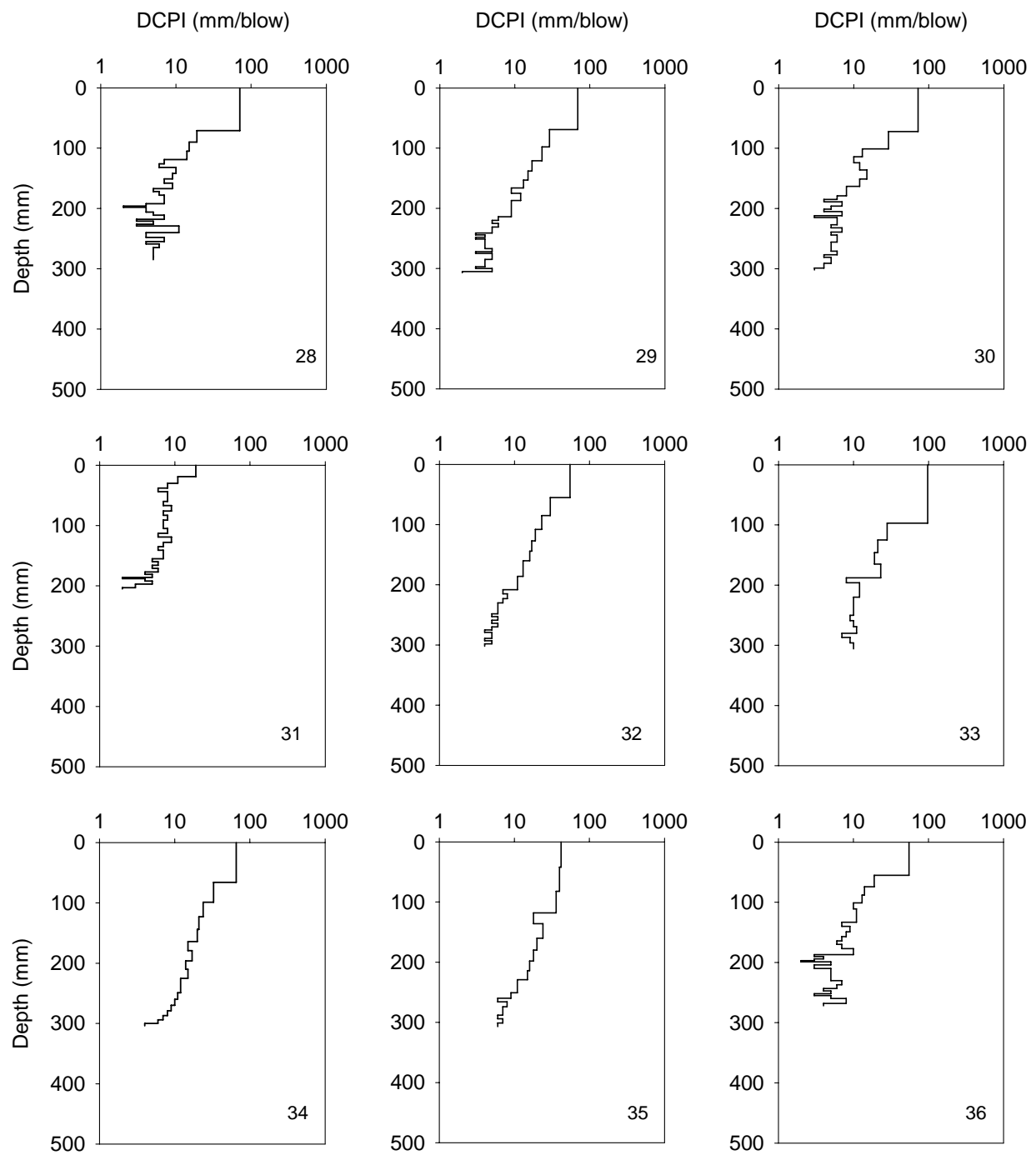
Figure F. 20. Mn/DOT DCP profiles (continued)
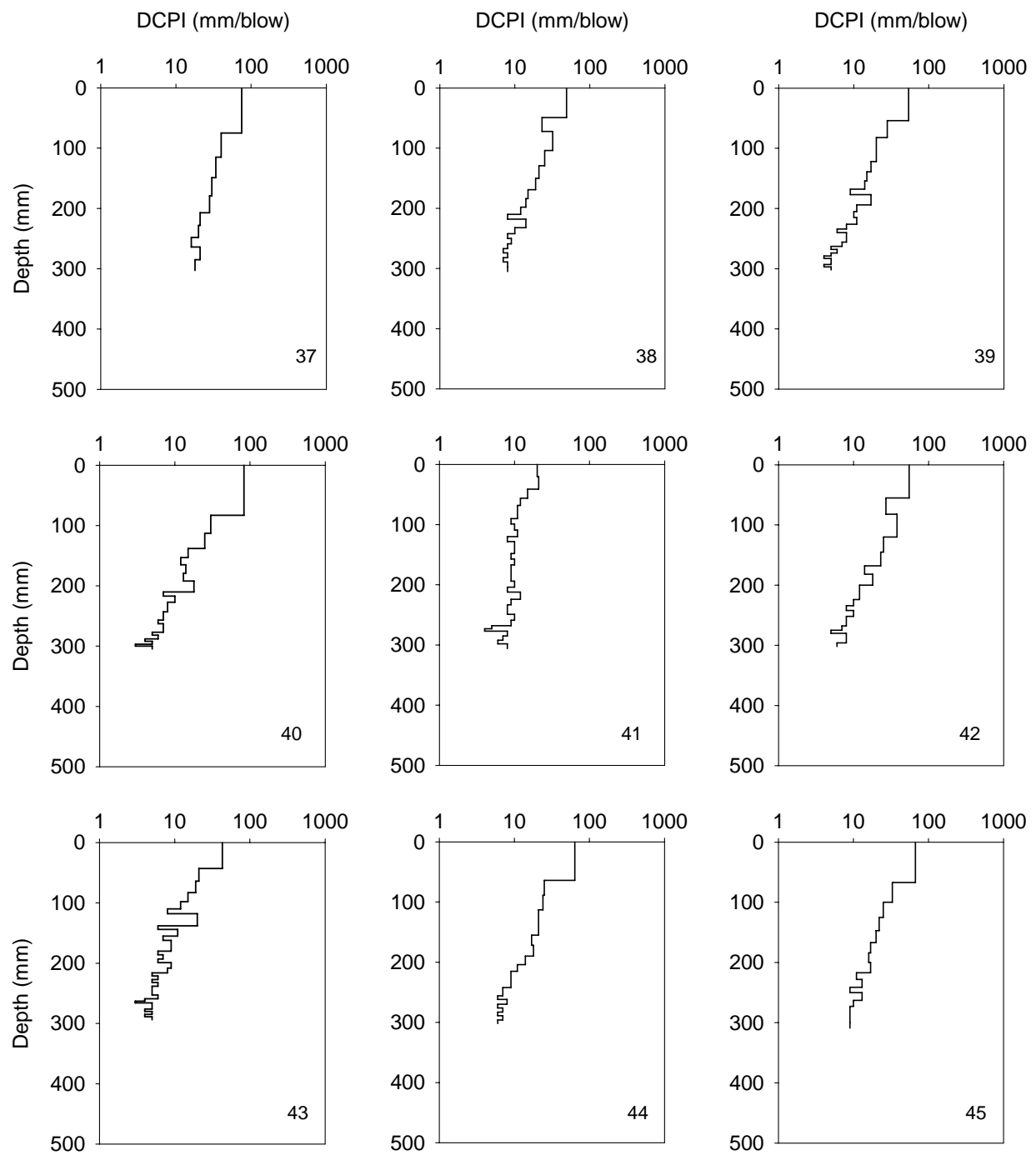
Figure F. 21. Mn/DOT DCP profiles (continued)
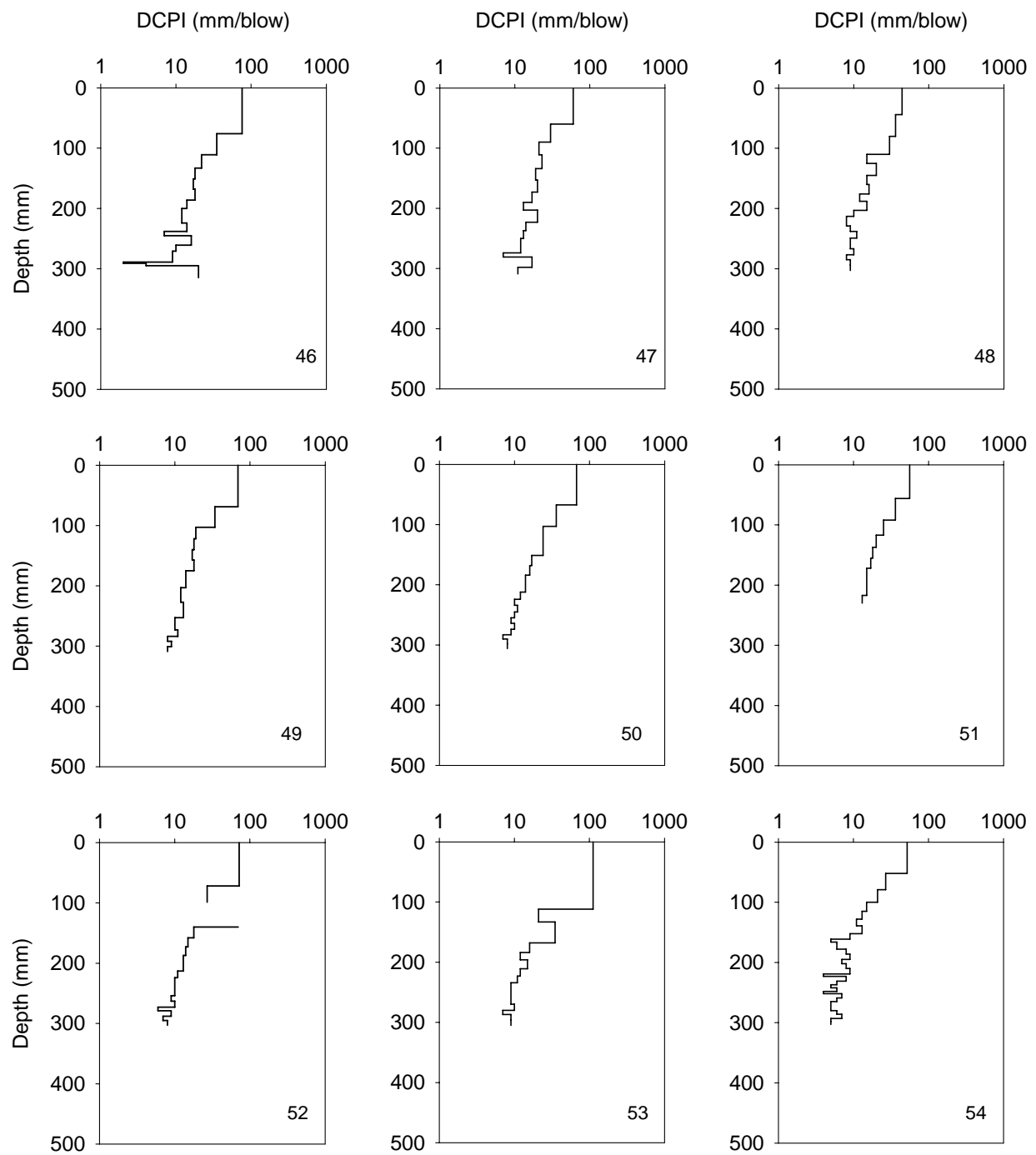
Figure F. 22. Mn/DOT DCP profiles (continued)

DCPI (mm/blow)

DCPI (mm/blow)

56

57

DCPI (mm/blow)

Depth (mm)

58

59

60

Depth (mm)

61

62

63
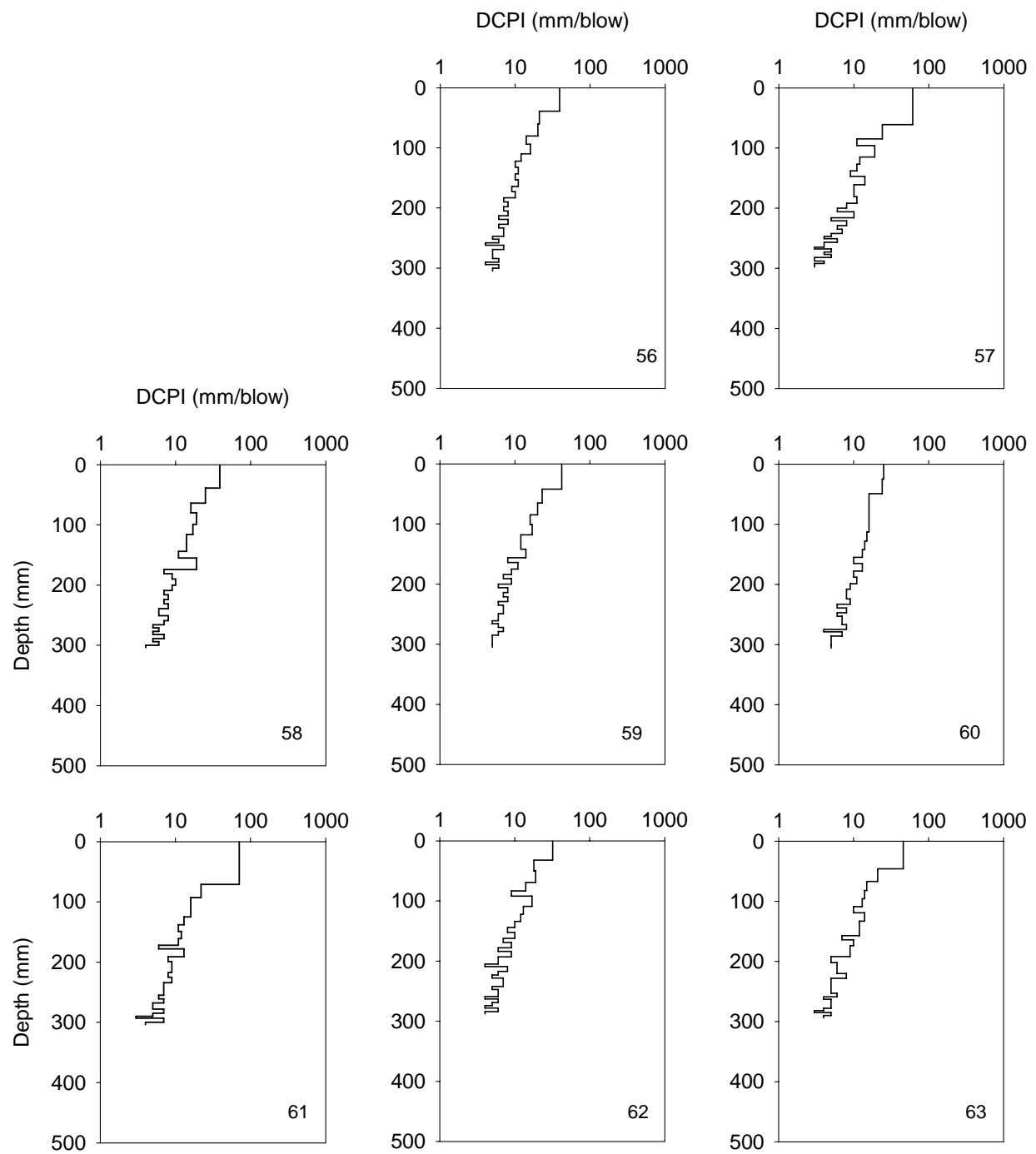
Figure F. 23. Mn/DOT DCP profiles (continued)

Appendix G: Field Study 3 CCV Data Summary
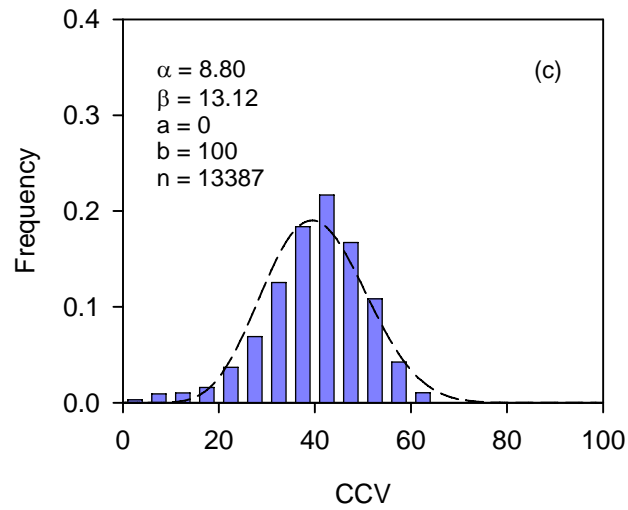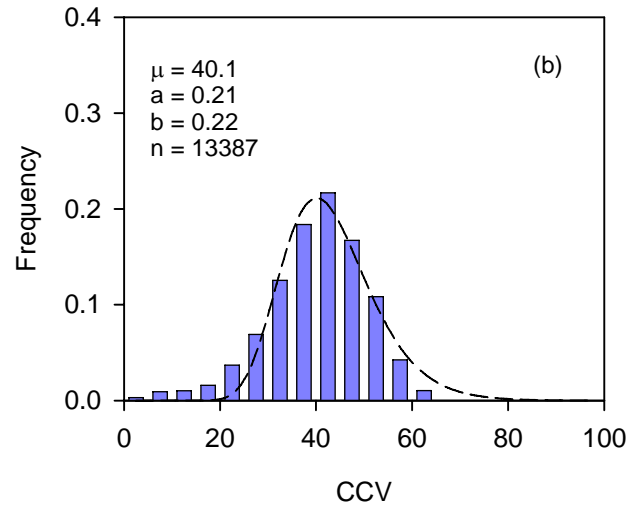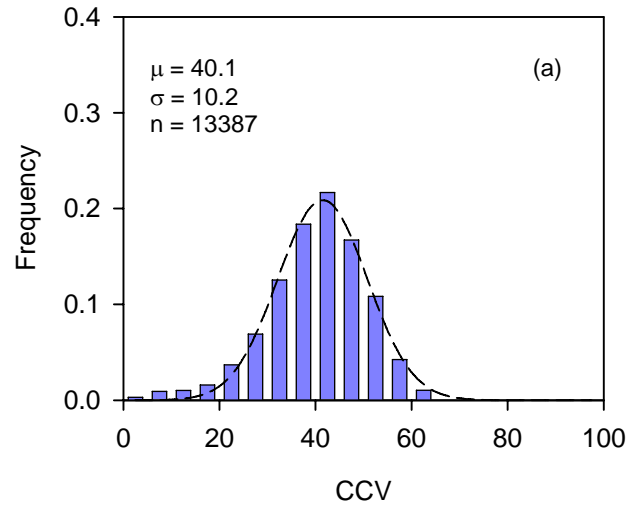
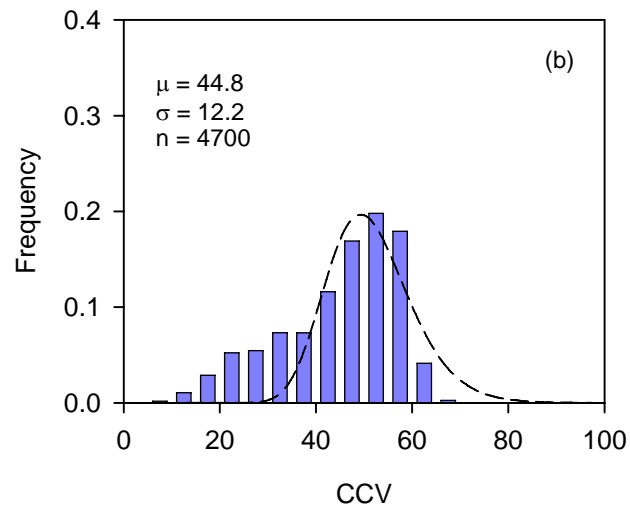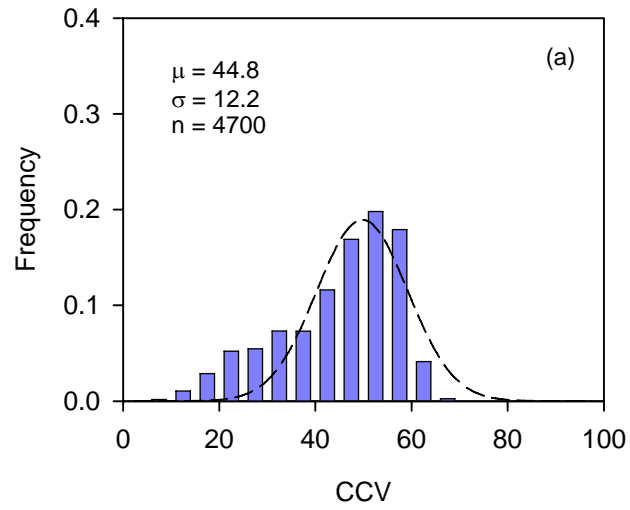Figure G. 1. Proof 5 CCV distribution plot: (a) normal, (b) log normal, and (c) beta
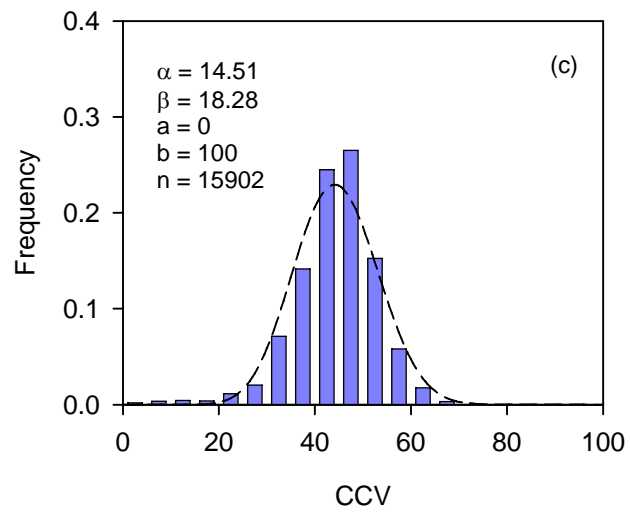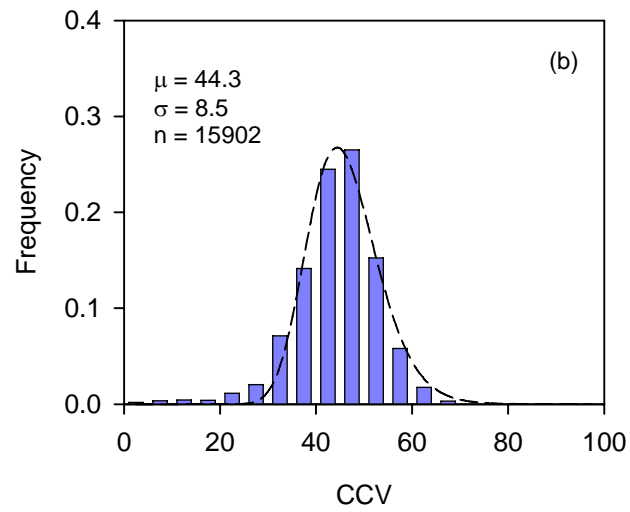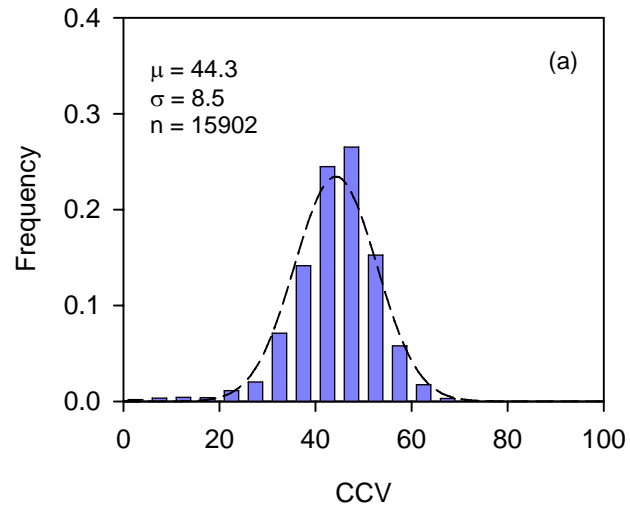
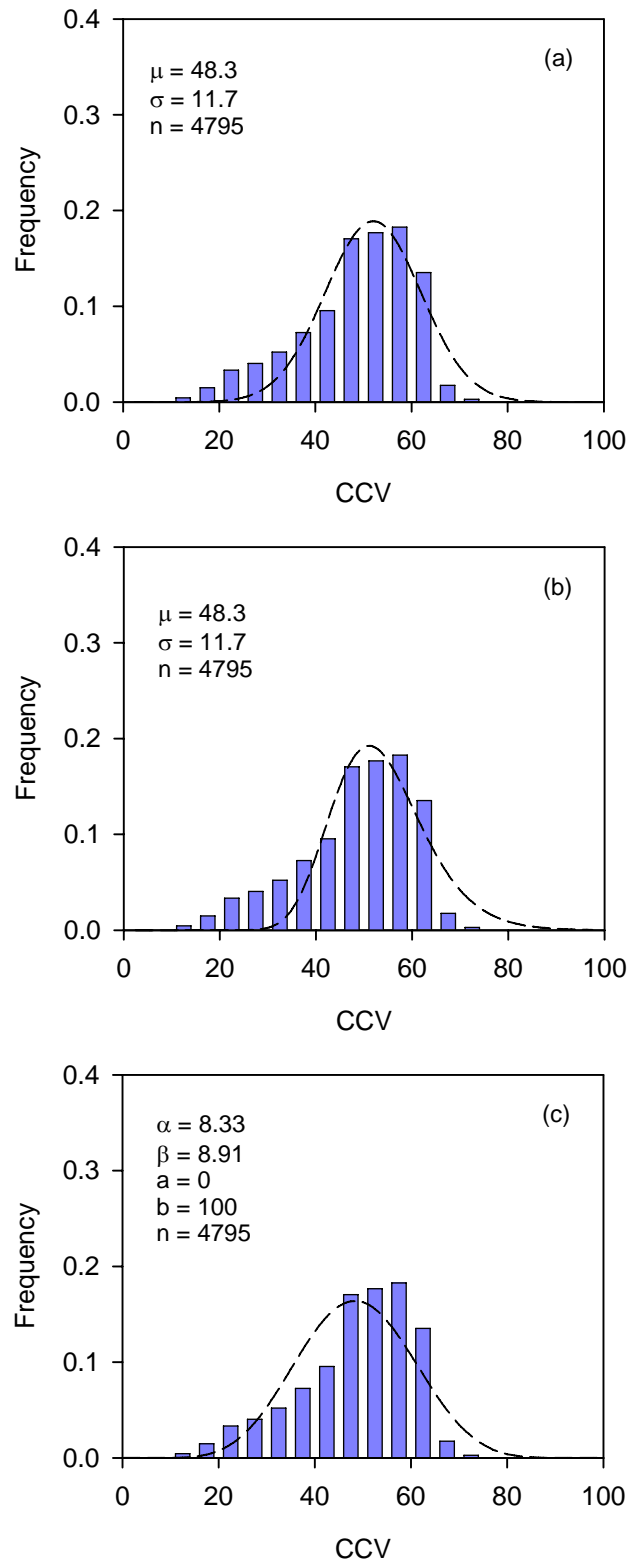Figure G. 2. Proof 6 CCV distribution plot: (a) normal, (b) log normal, and (c) beta
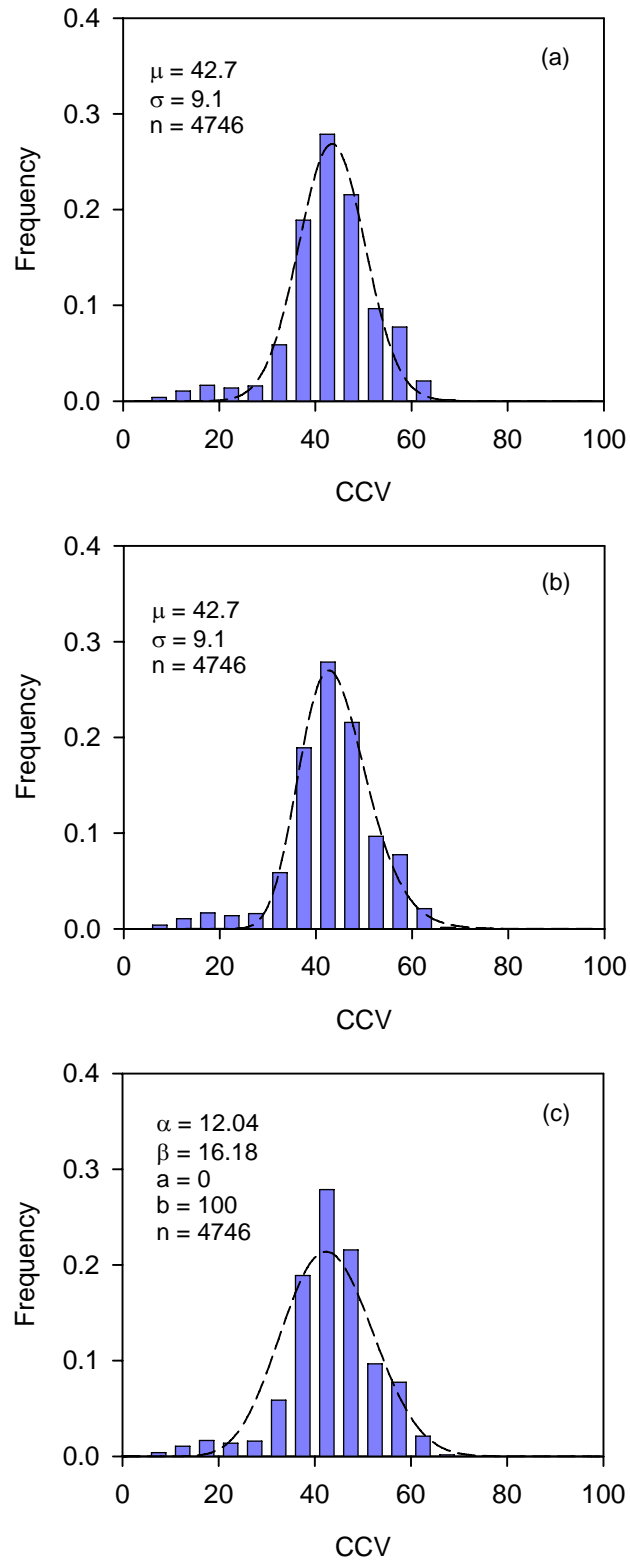
Figure G. 3. Proof 7 CCV distribution plot: (a) normal, (b) log normal, and (c) beta
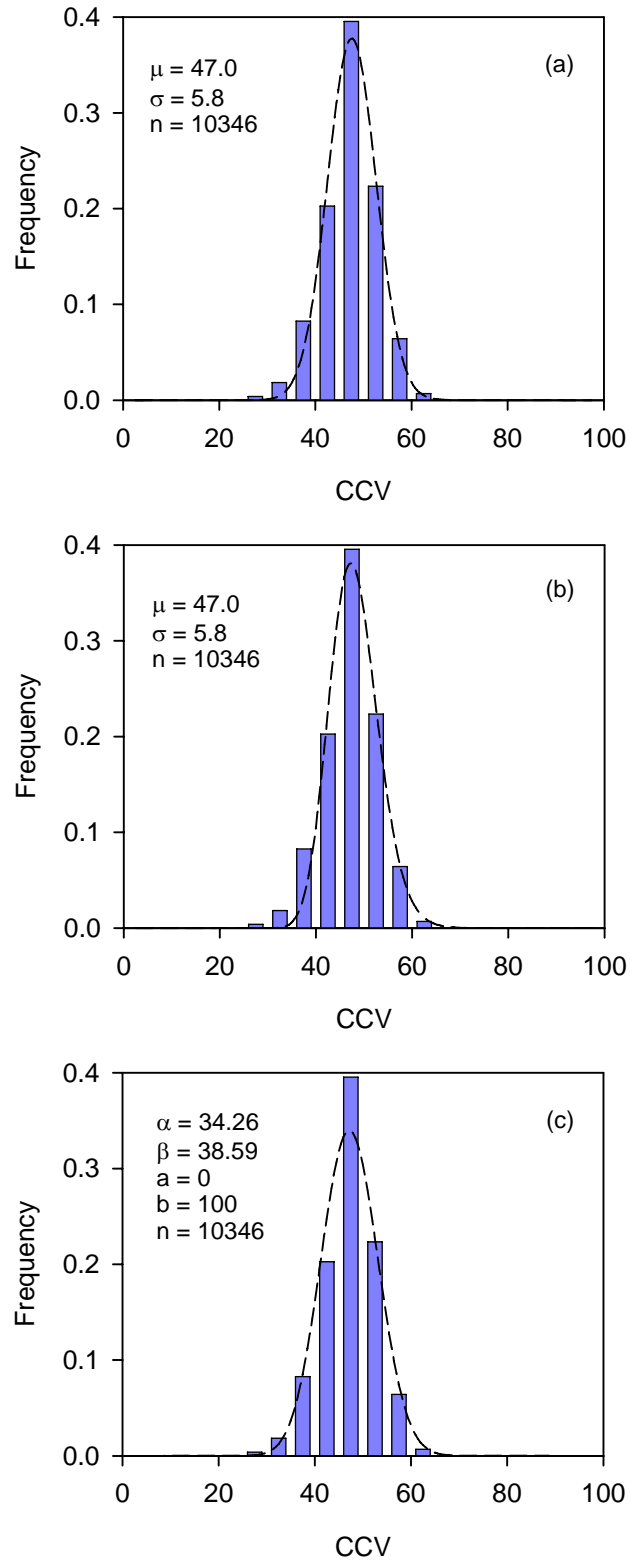
Figure G. 4. Proof 8 CCV distribution plot: (a) normal, (b) log normal, and (c) beta
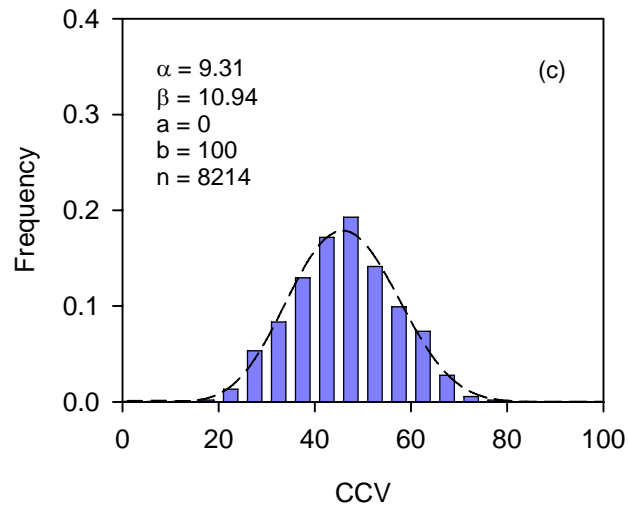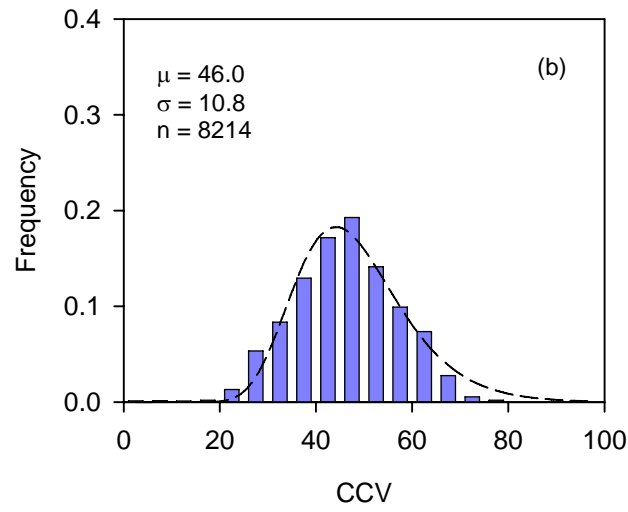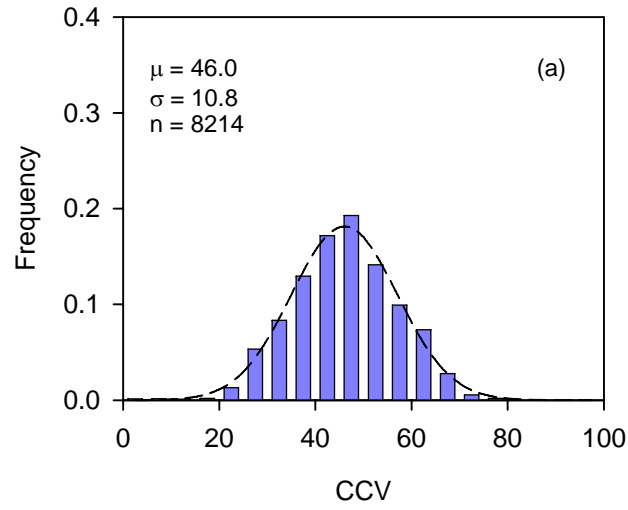
Figure G. 5. Proof 9 CCV distribution plot: (a) normal, (b) log normal, and (c) beta
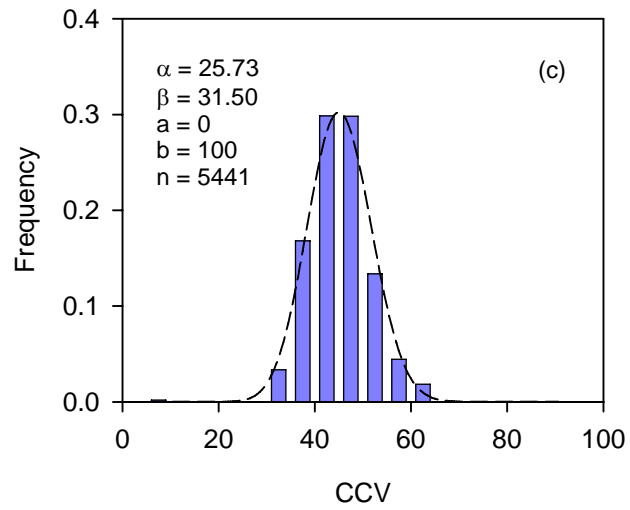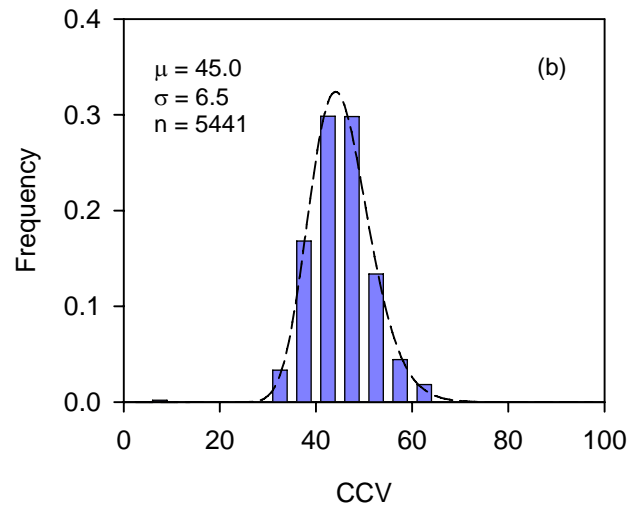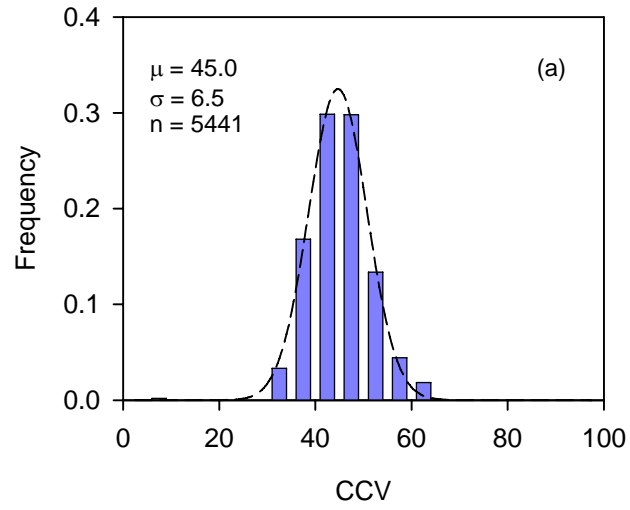
Figure G. 6. Proof 10 CCV distribution plot: (a) normal, (b) log normal, and (c) beta
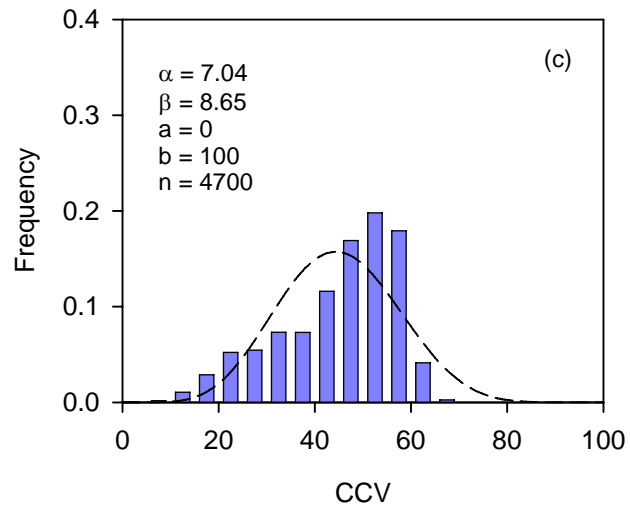
Figure G. 7. Proof 11 CCV distribution plot: (a) normal, (b) log normal, and (c) beta

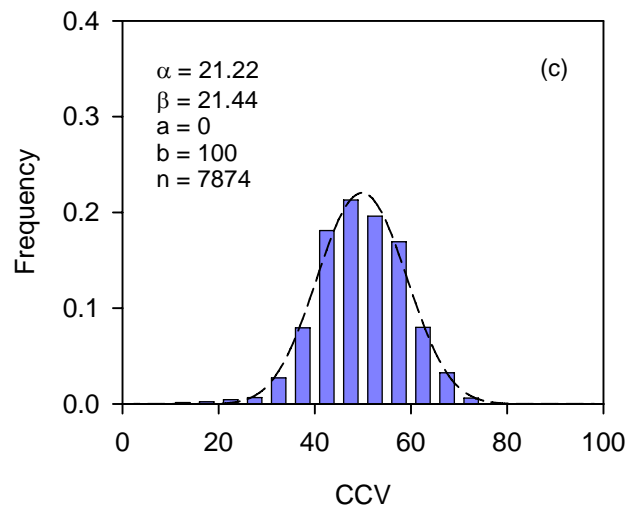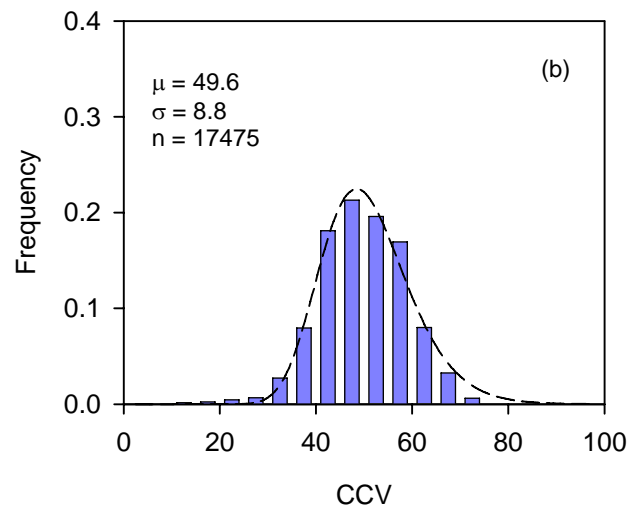Figure G. 8. Proof 12 CCV distribution plot: (a) normal, (b) log normal, and (c) beta
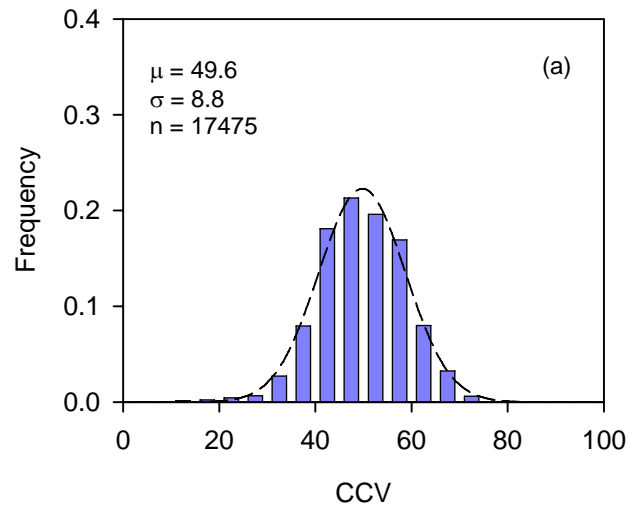
Figure G. 9. Proof 13 CCV distribution plot: (a) normal, (b) log normal, and (c) beta
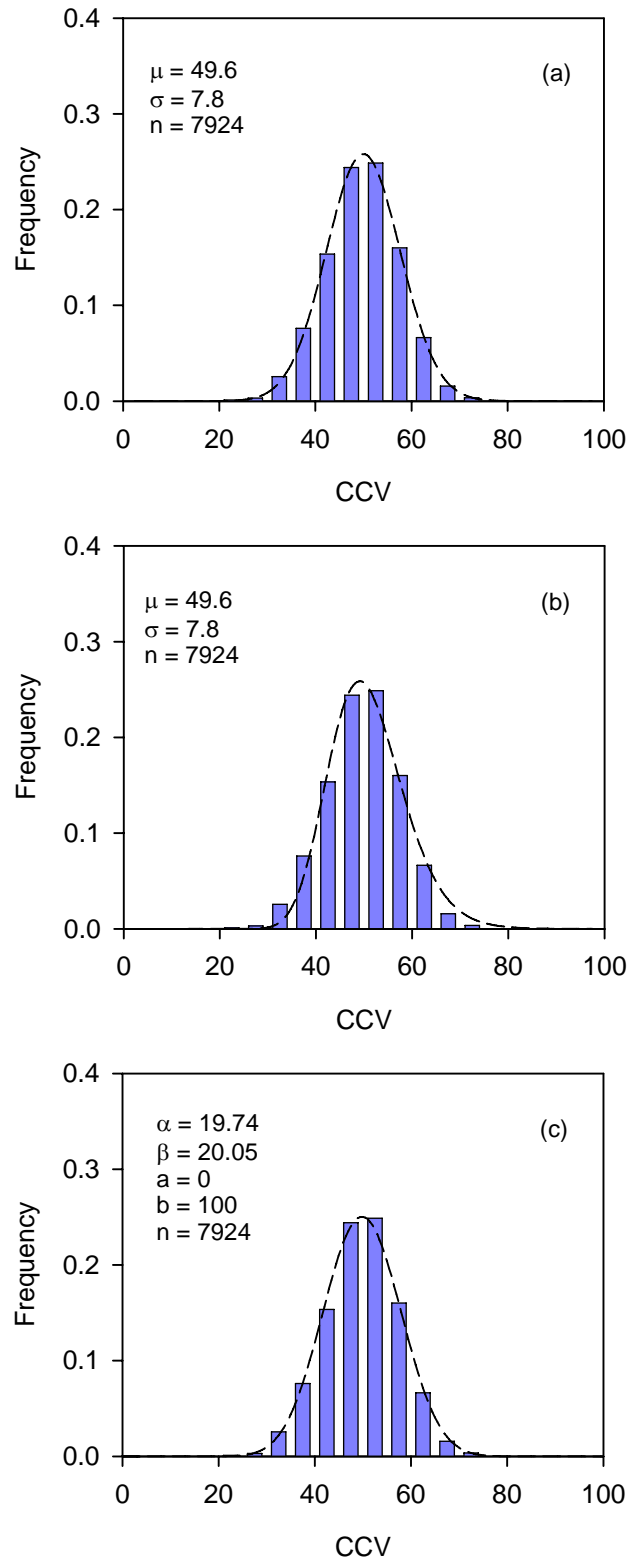
Figure G. 10. Proof 14 CCV distribution plot: (a) normal, (b) log normal, and (c) beta

Figure G. 11. Proof 15 CCV distribution plot: (a) normal, (b) log normal, and (c) beta

Figure G. 12. Proof 16 CCV distribution plot: (a) normal, (b) log normal, and (c) beta

Figure G. 13. Proof 18 CCV distribution plot: (a) normal, (b) log normal, and (c) beta
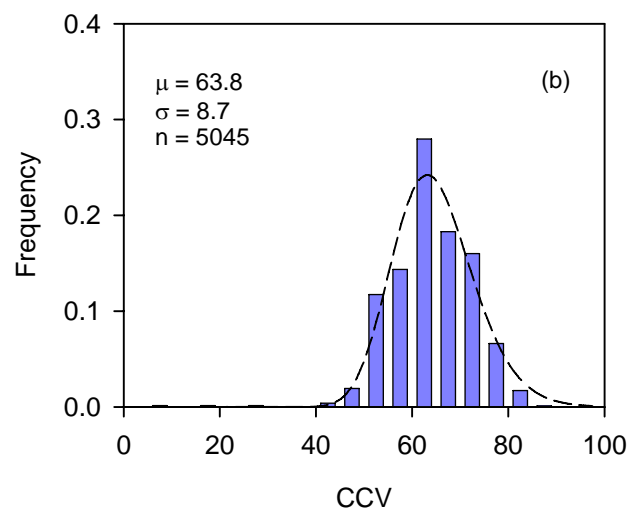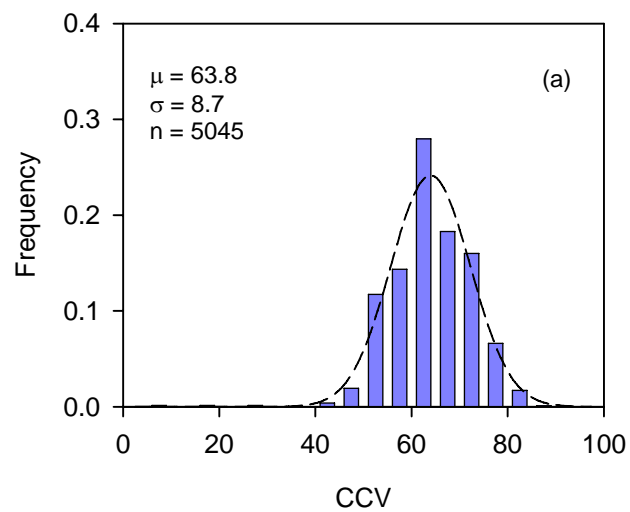
Figure G. 14. Proof 19 CCV distribution plot: (a) normal, (b) log normal, and (c) beta
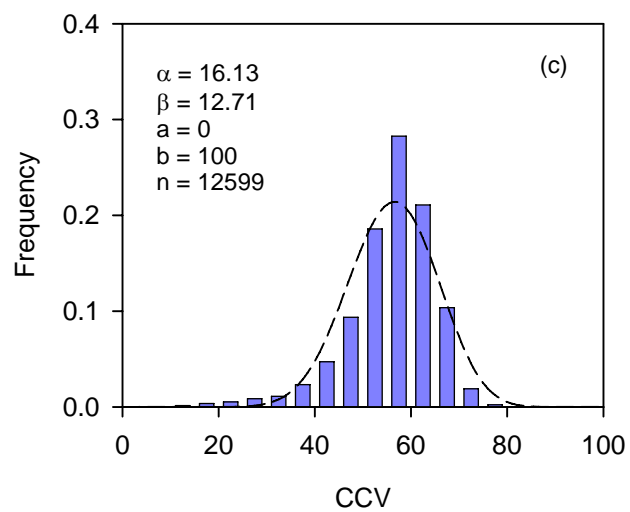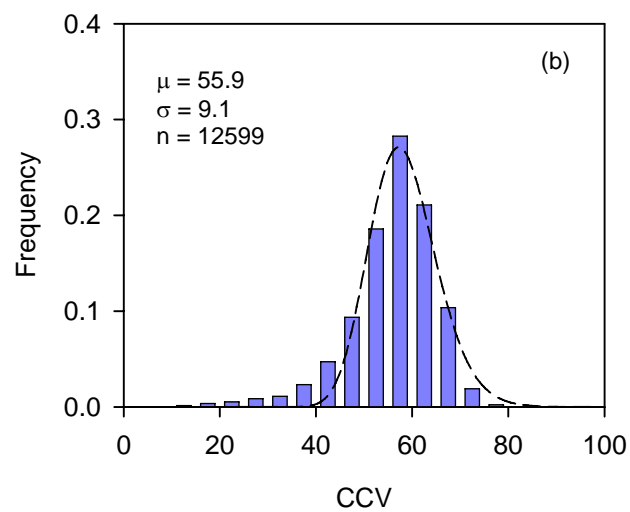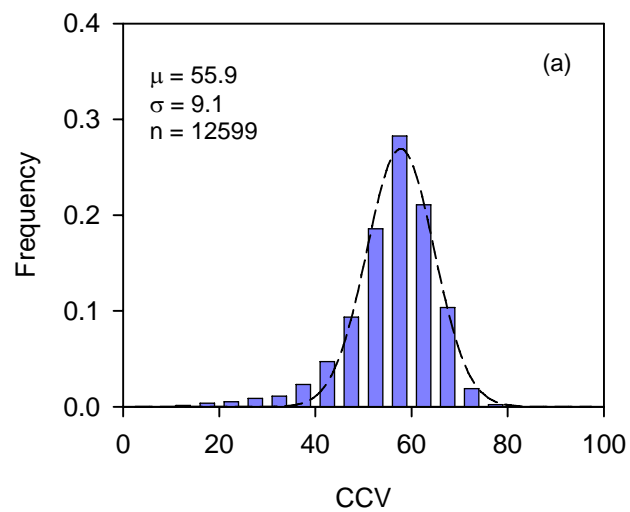
Figure G. 15. Proof 27 CCV distribution plot: (a) normal, (b) log normal, and (c) beta
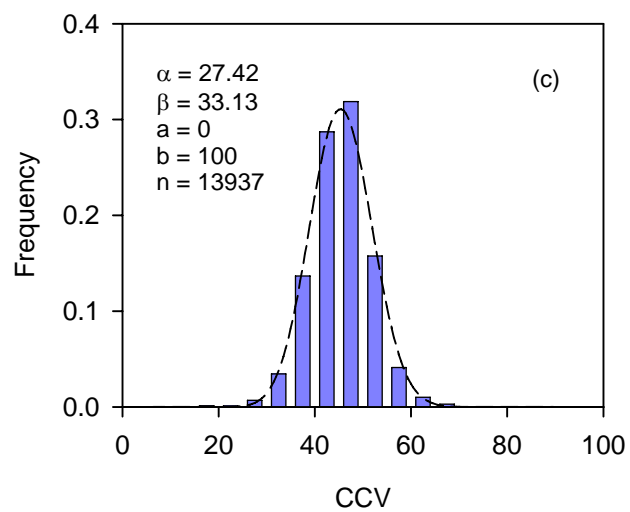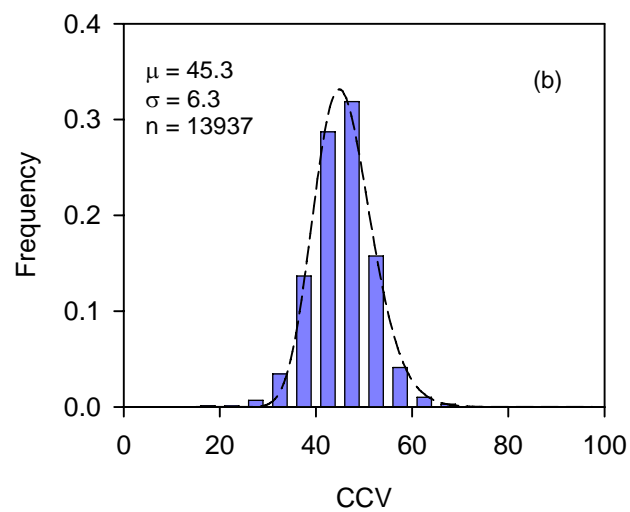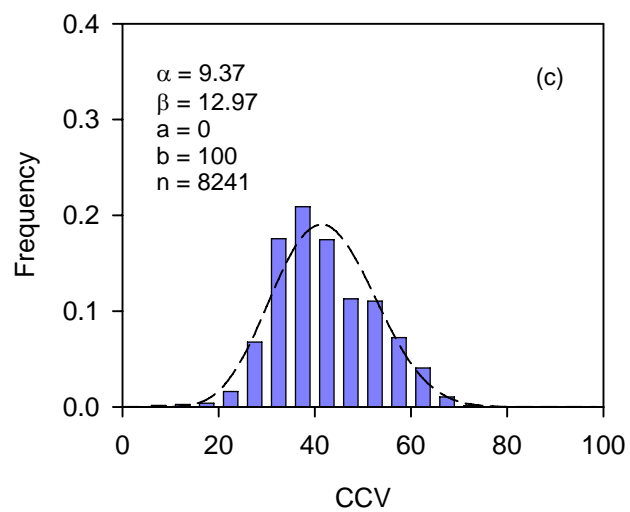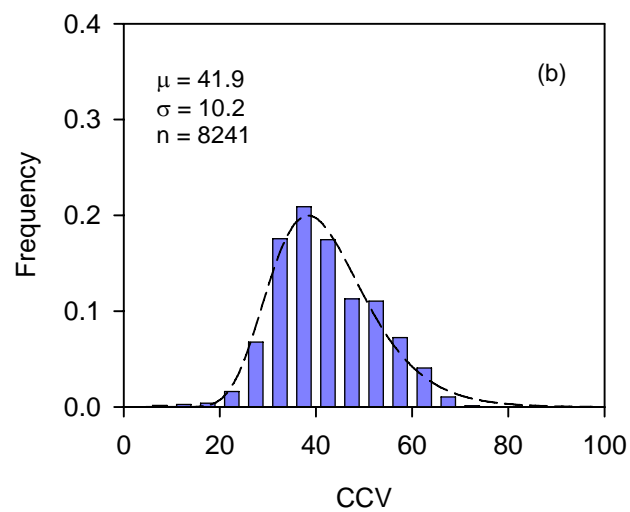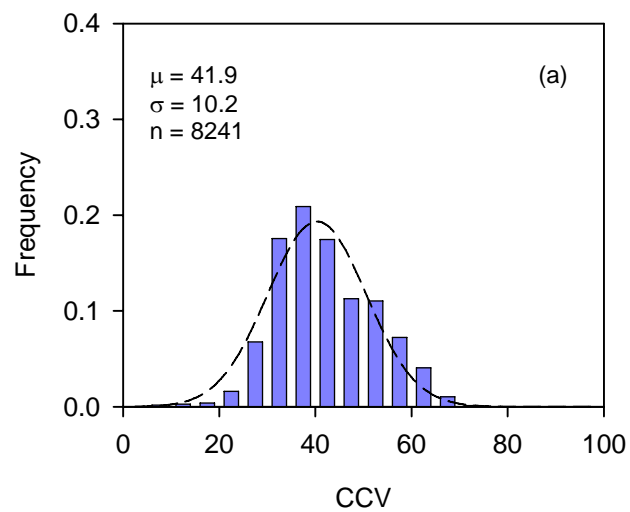
Figure G. 16. Proof 28 CCV distribution plot: (a) normal, (b) log normal, and (c) beta
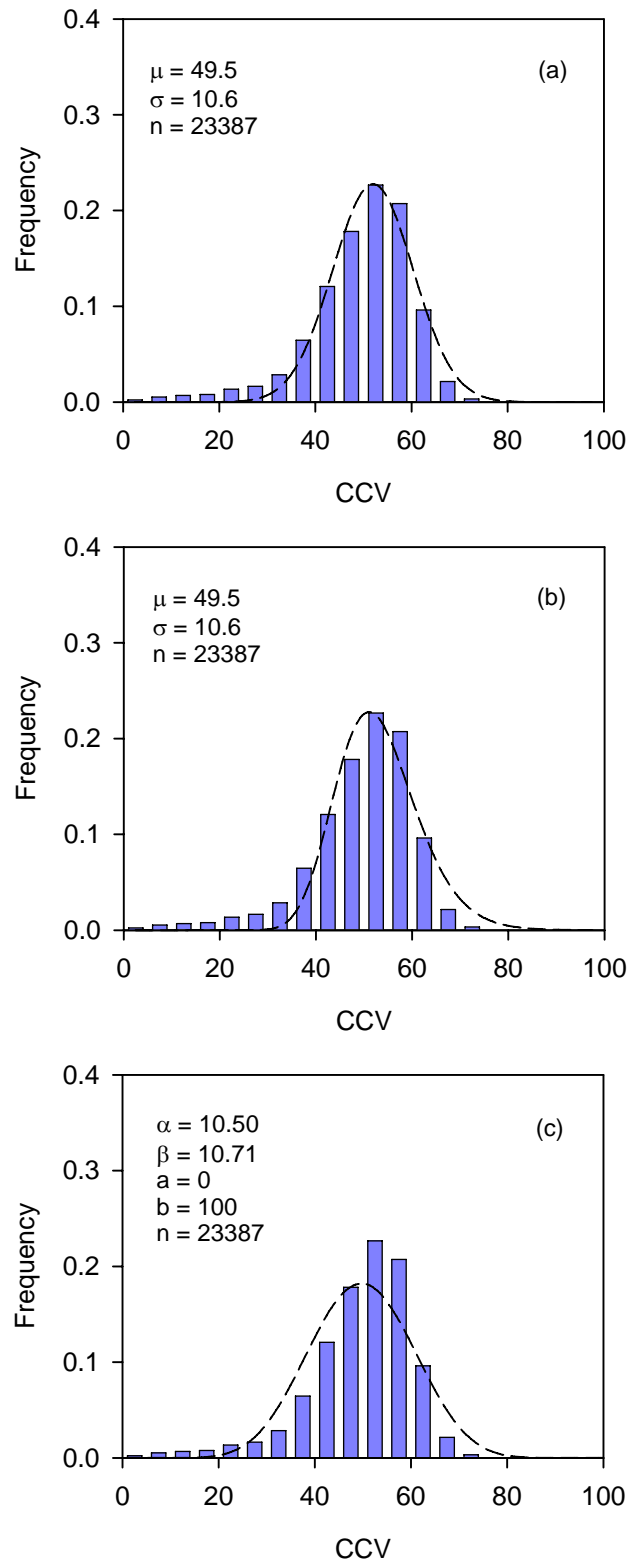
Figure G. 17. Proof 29 CCV distribution plot: (a) normal, (b) log normal, and (c) beta
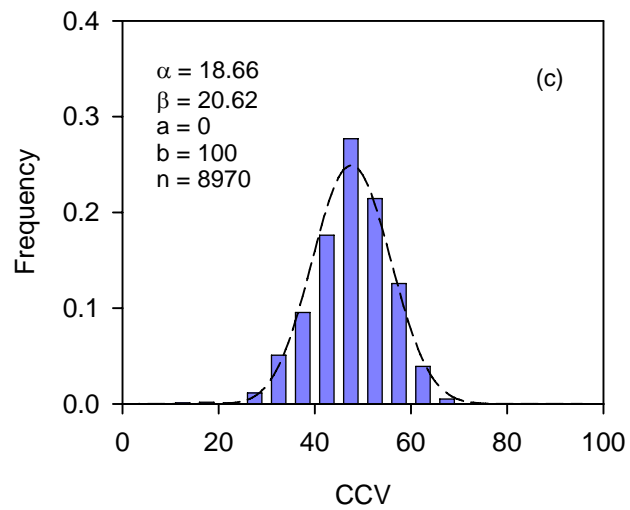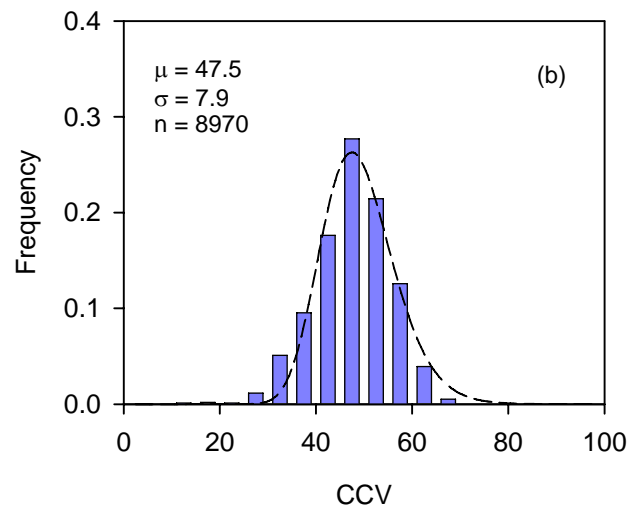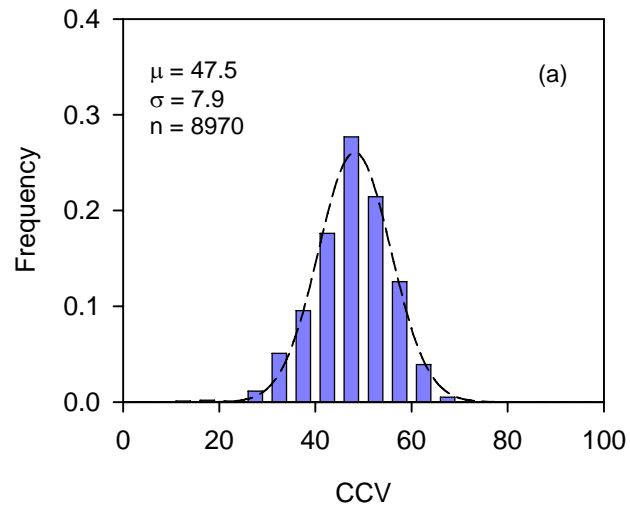
Figure G. 18. Proof 30 CCV distribution plot: (a) normal, (b) log normal, and (c) beta
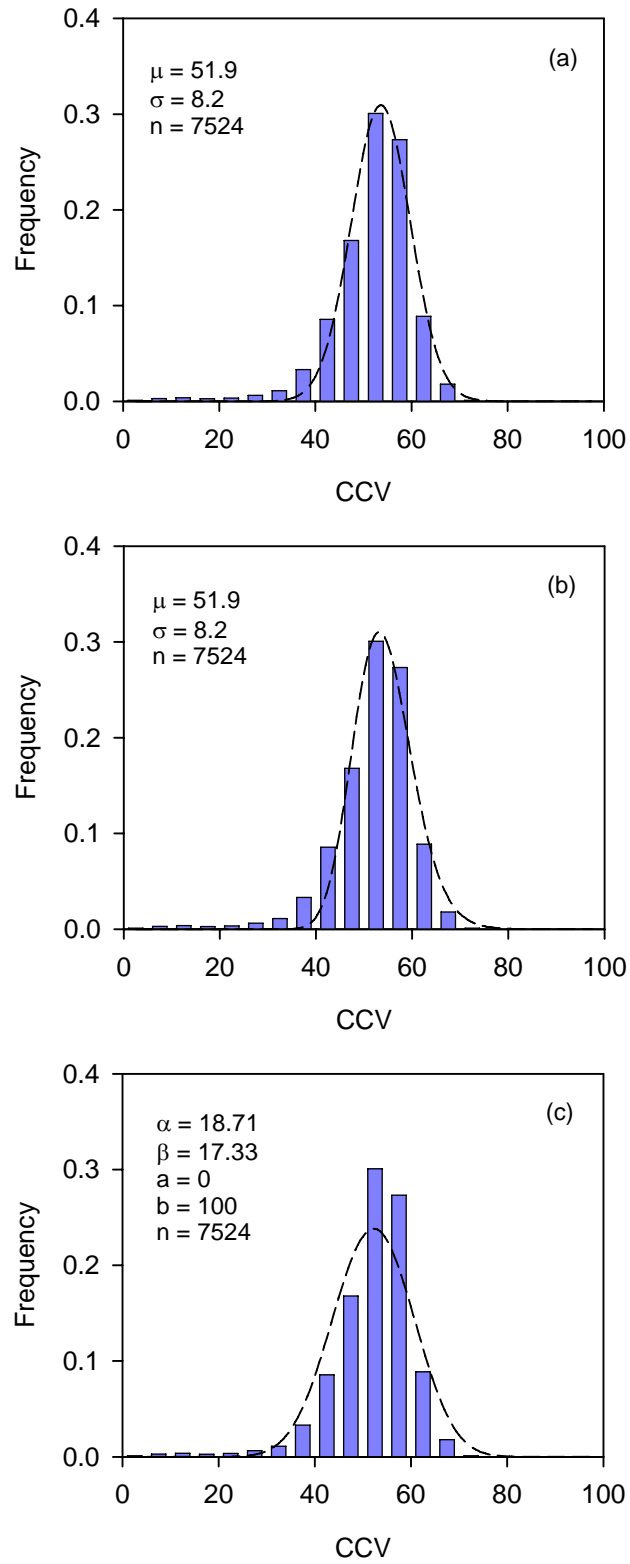
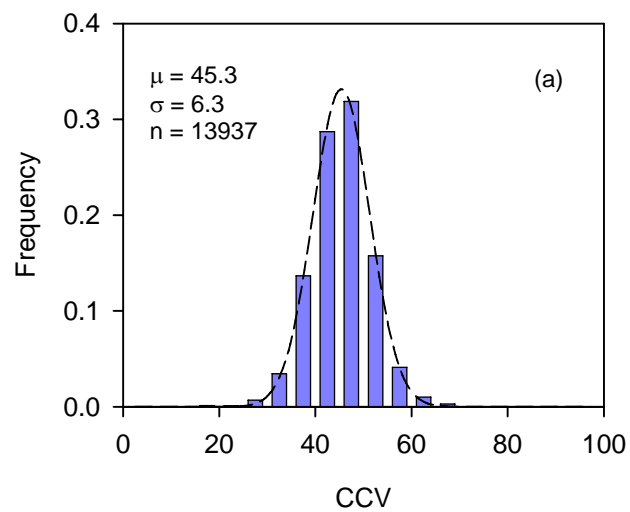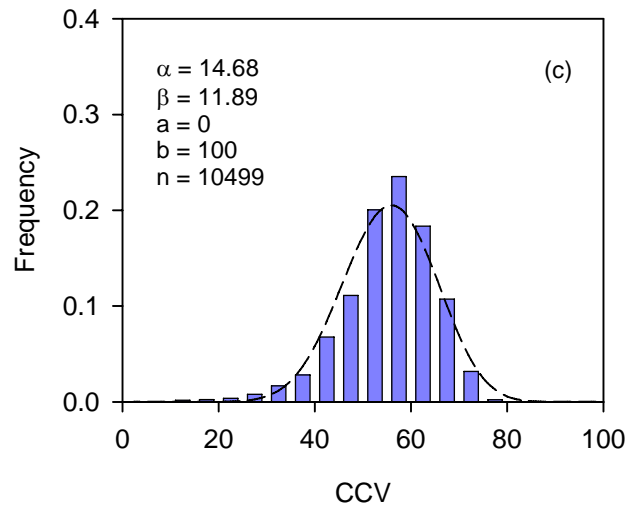Figure G. 19. Proof 31 CCV distribution plot: (a) normal, (b) log normal, and (c) beta
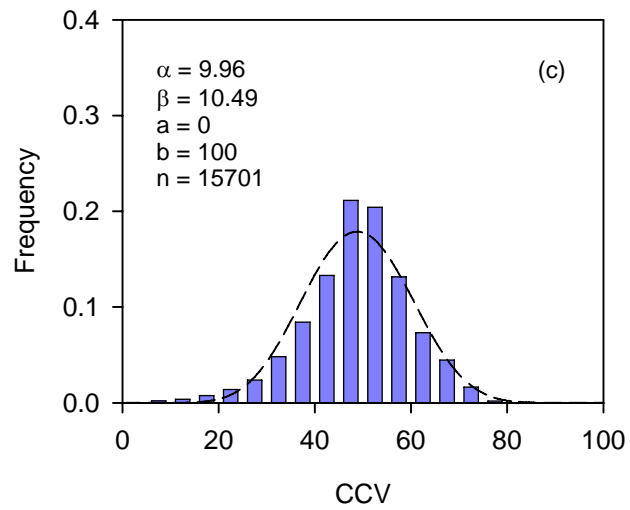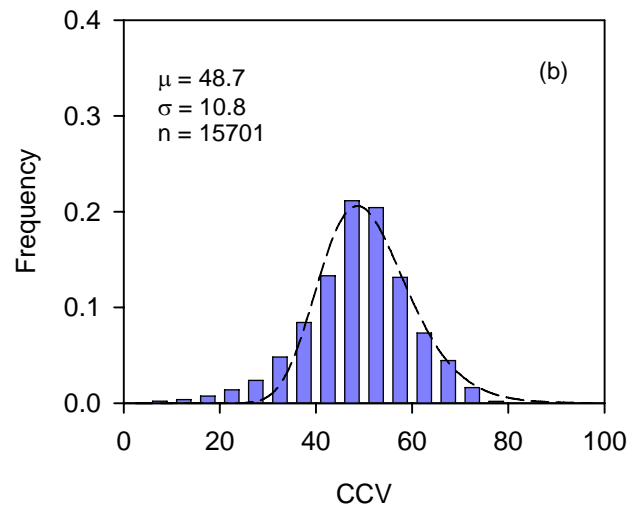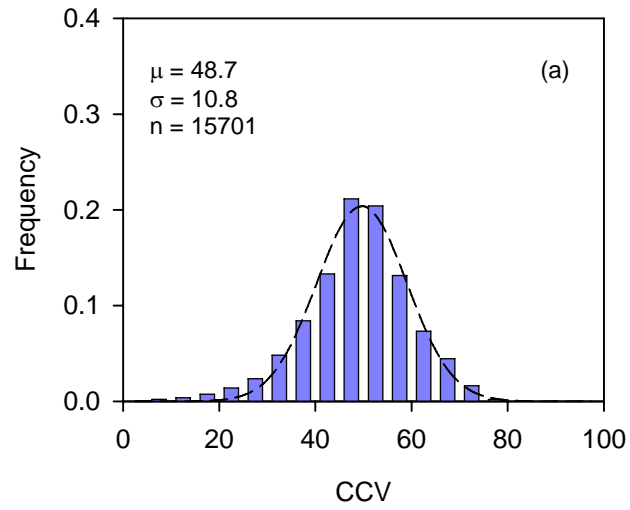
Figure G. 20. Proof 32 CCV distribution plot: (a) normal, (b) log normal, and (c) beta
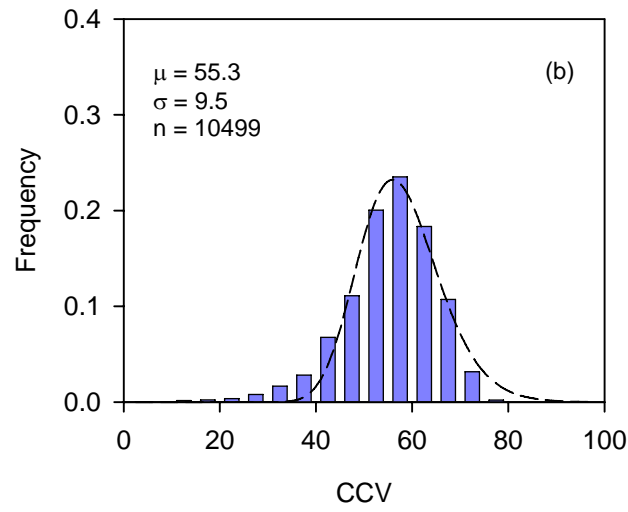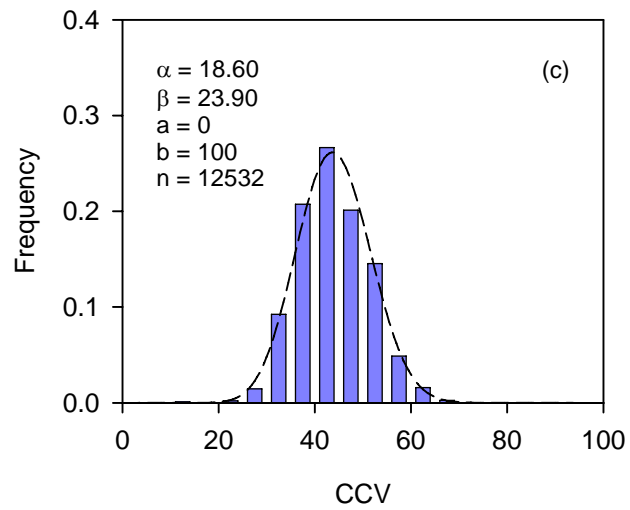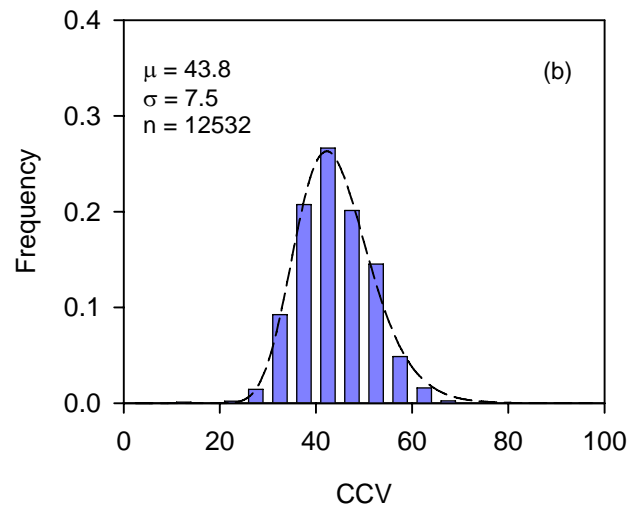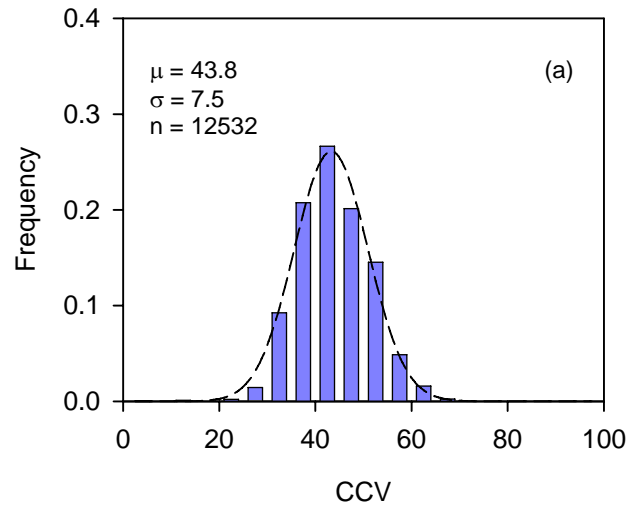
Figure G. 21. Proof 33 CCV distribution plot: (a) normal, (b) log normal, and (c) beta

G-21
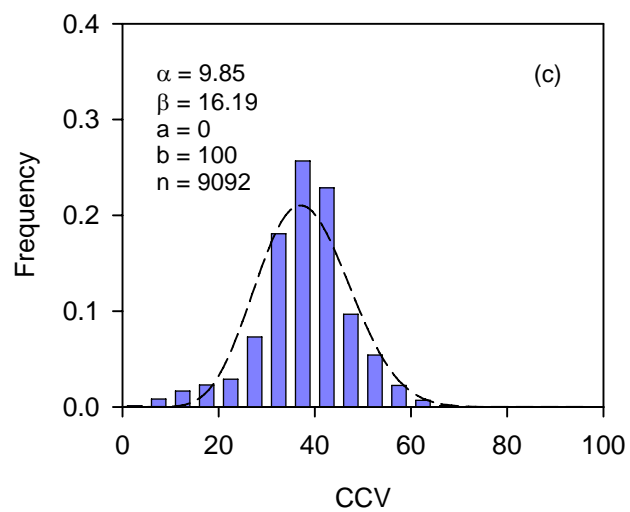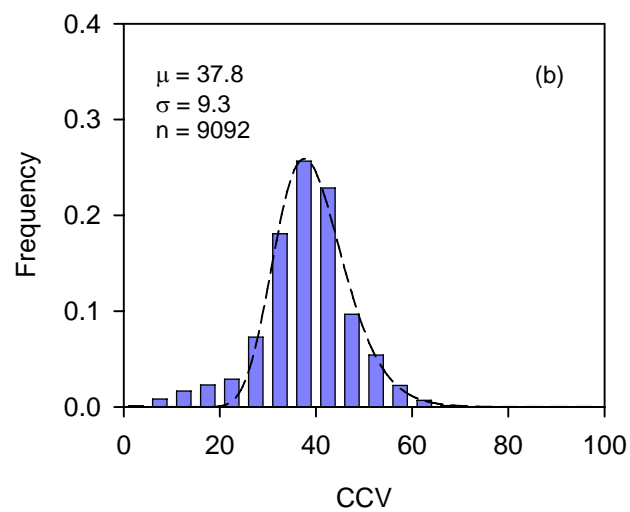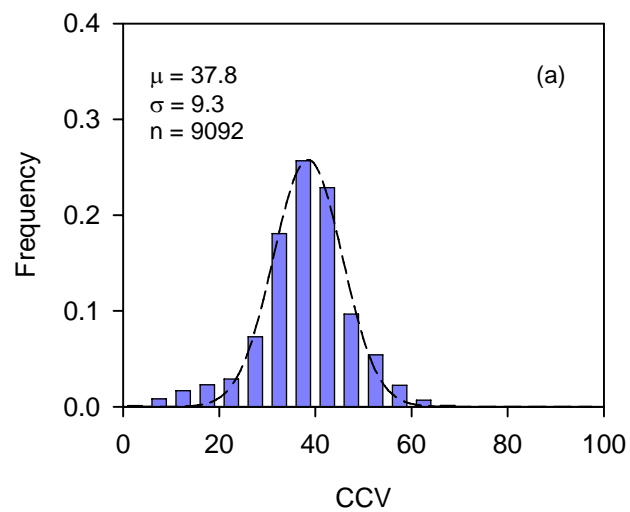
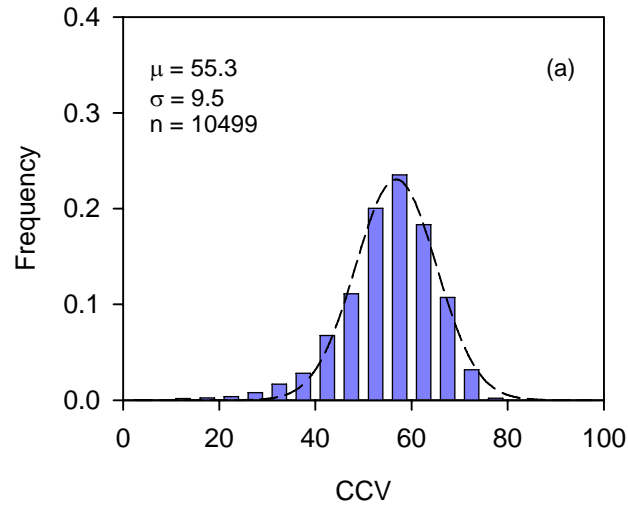Figure G. 22. Proof 34 CCV distribution plot: (a) normal, (b) log normal, and (c) beta
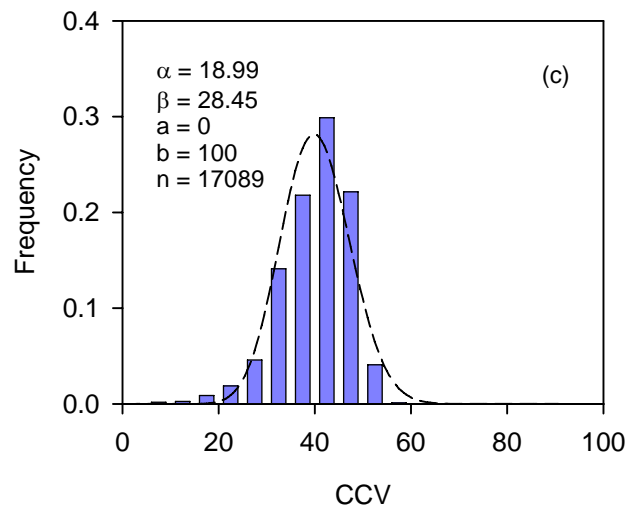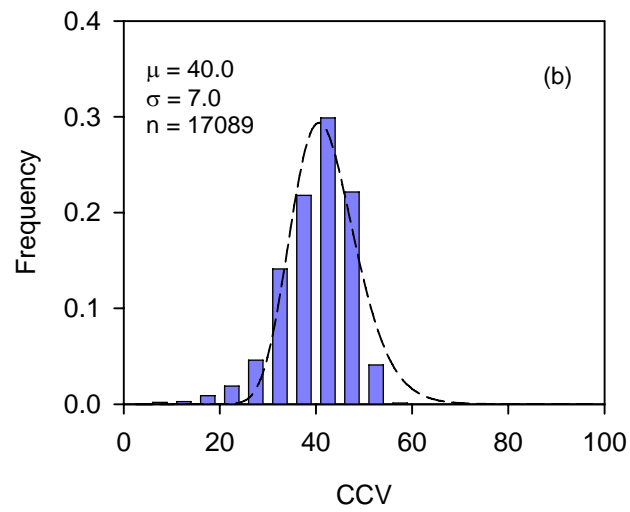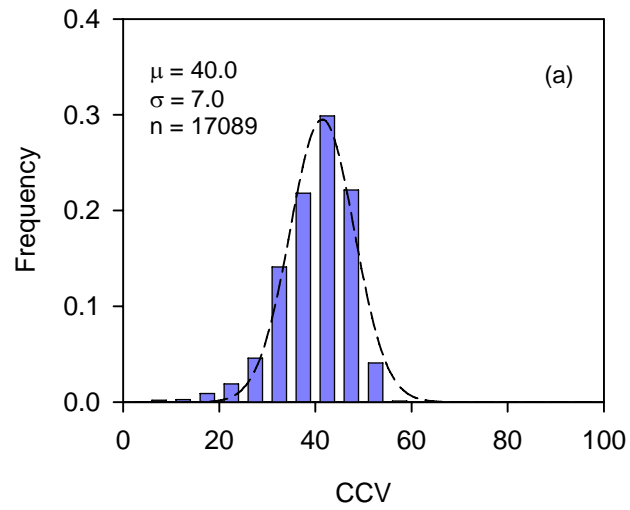
Figure G. 23. Proof 35 CCV distribution plot: (a) normal, (b) log normal, and (c) beta
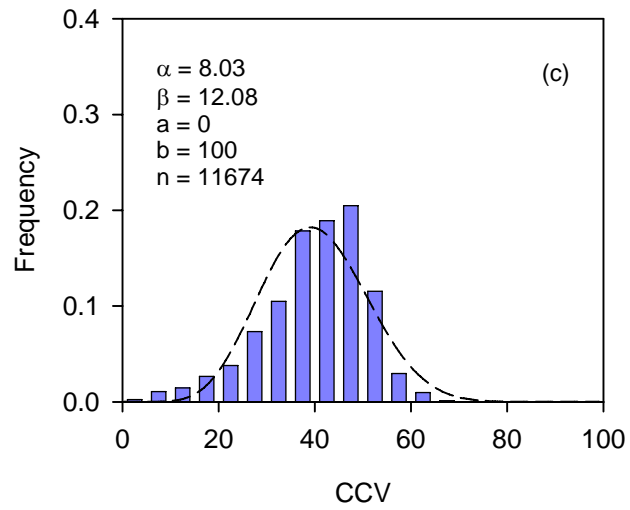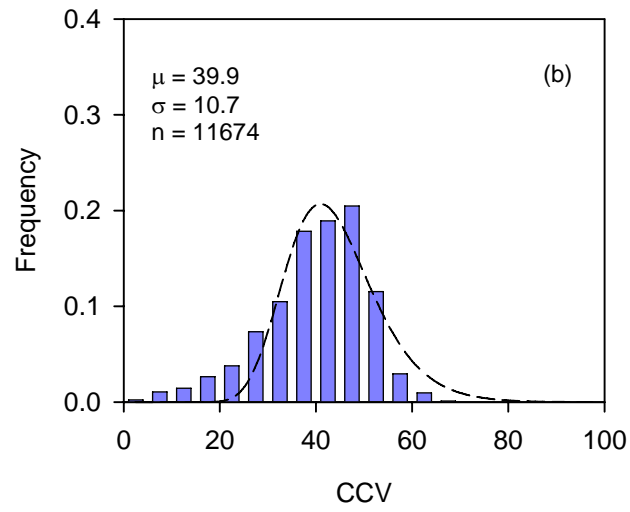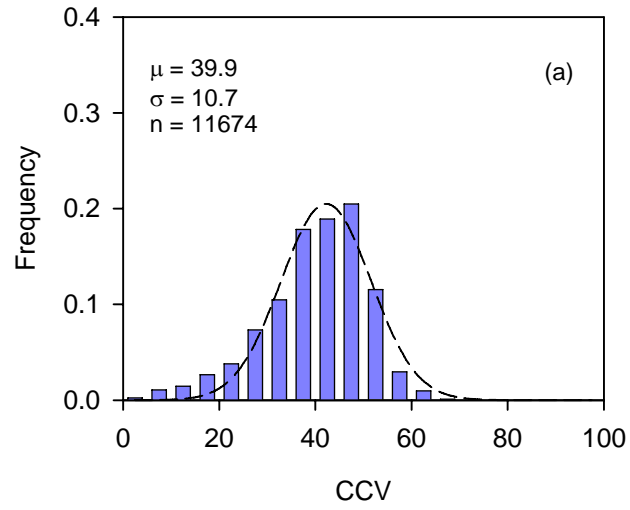
Figure G. 24. Proof 37 CCV distribution plot: (a) normal, (b) log normal, and (c) beta
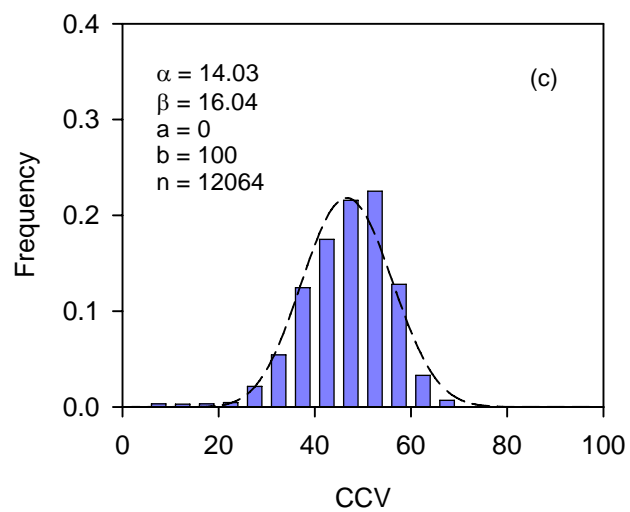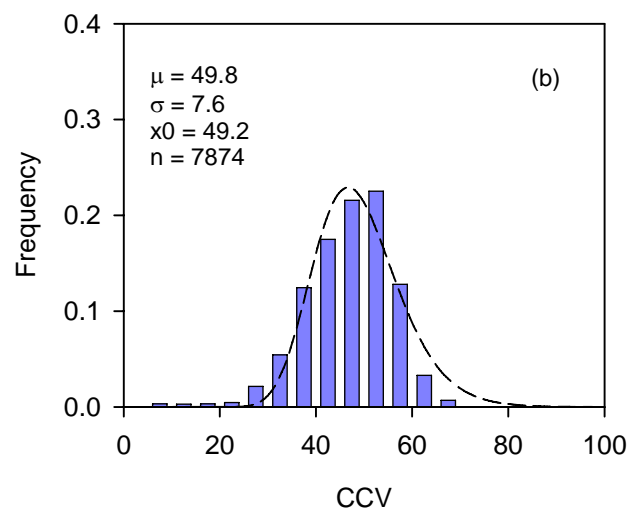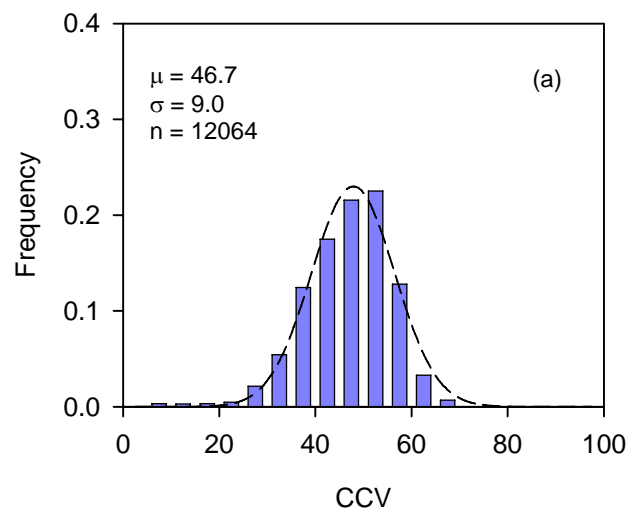
Figure G. 25. Proof 38 CCV distribution plot: (a) normal, (b) log normal, and (c) beta
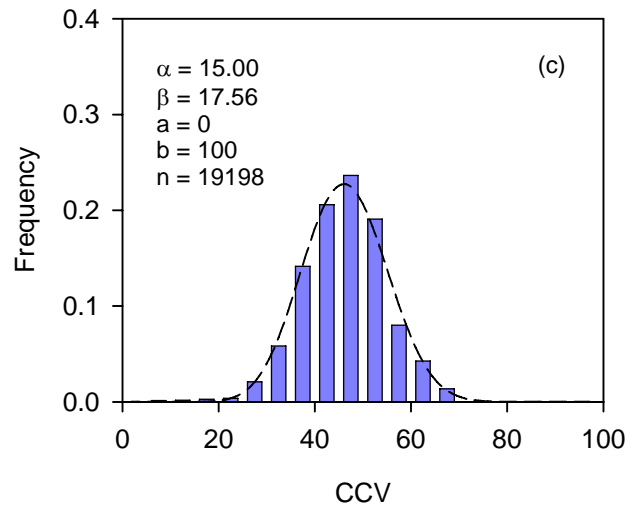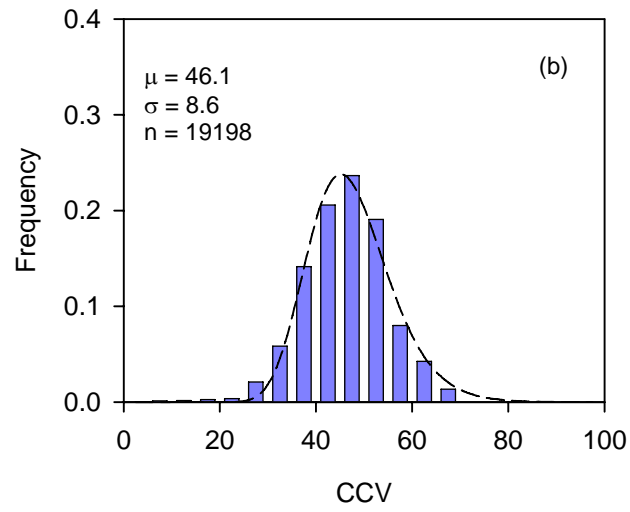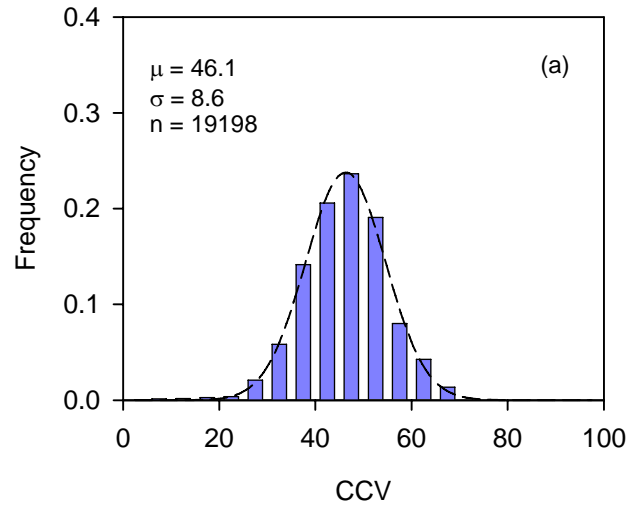
Figure G. 26. Proof 39 CCV distribution plot: (a) normal, (b) log normal, and (c) beta
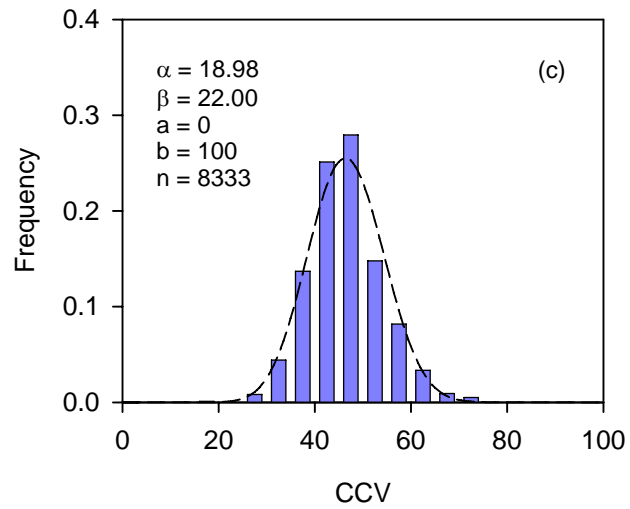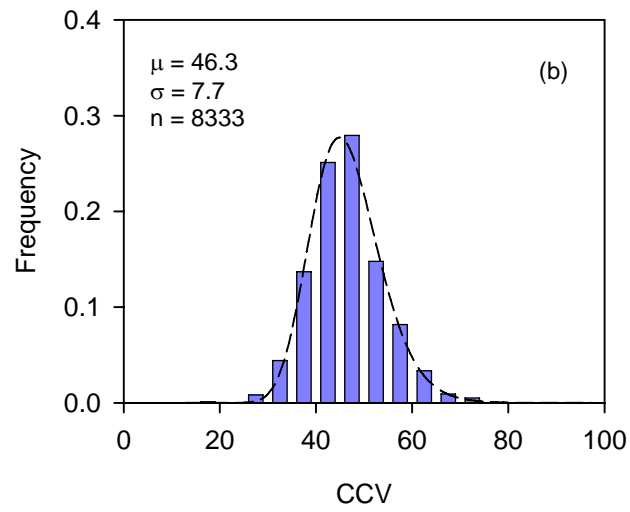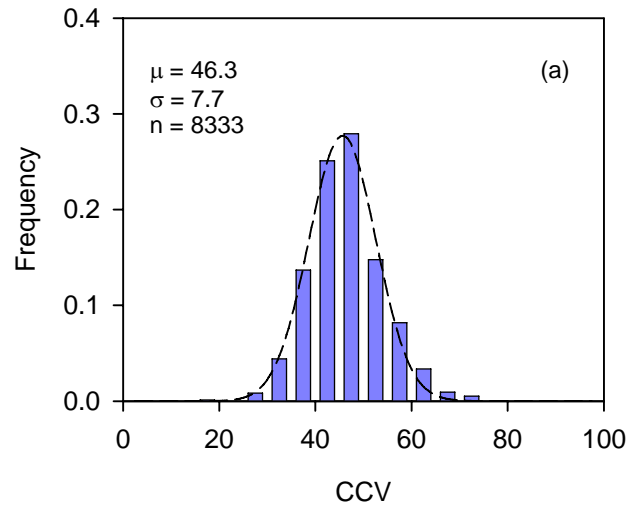
Figure G. 27. Proof 40 CCV distribution plot: (a) normal, (b) log normal, and (c) beta
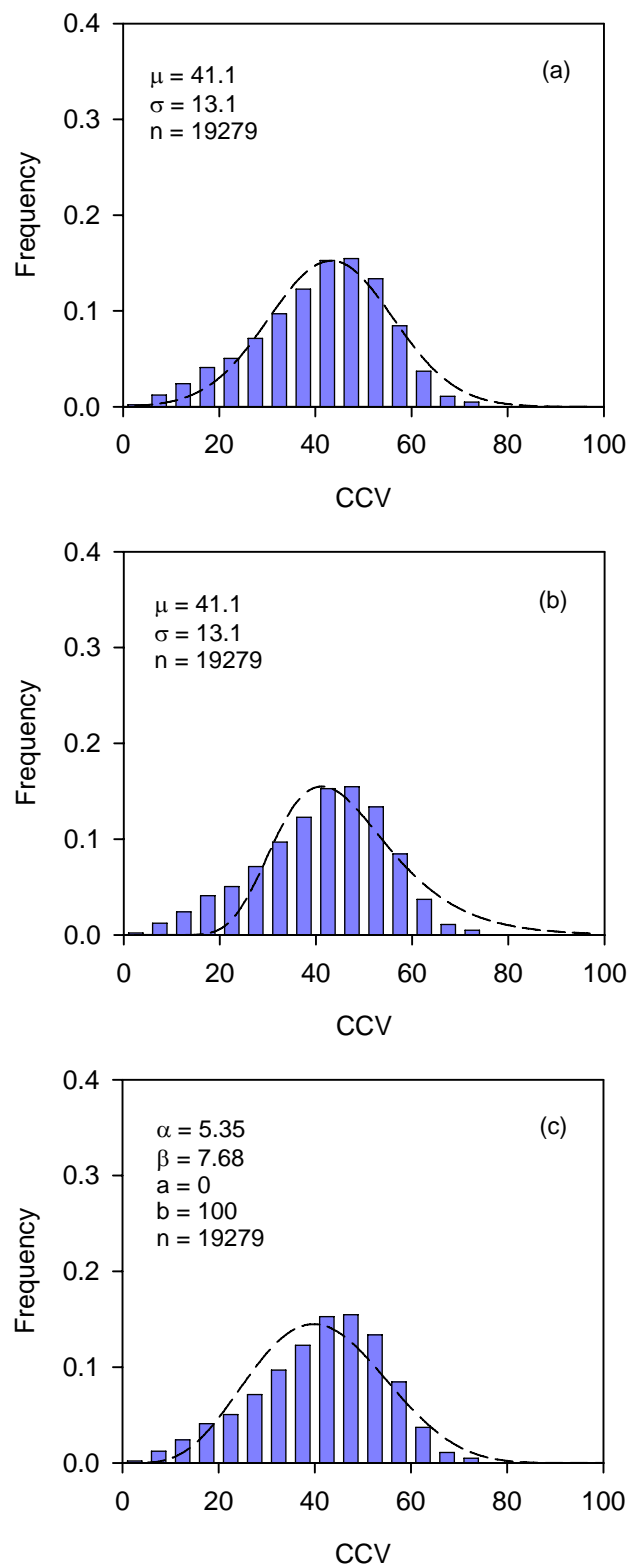
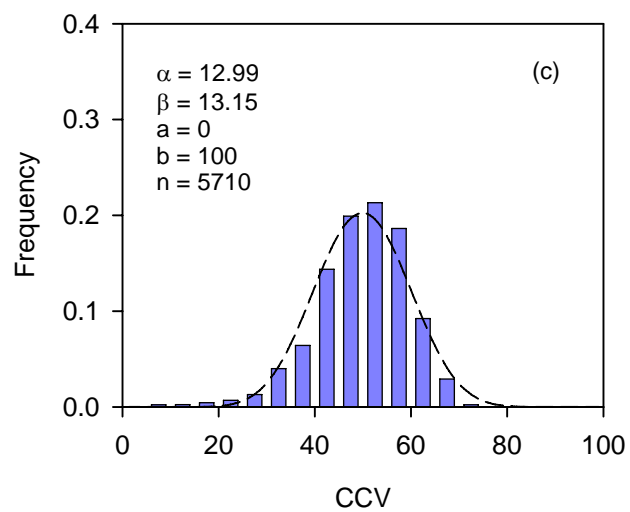Figure G. 28. Proof 41 CCV distribution plot: (a) normal, (b) log normal, and (c) beta
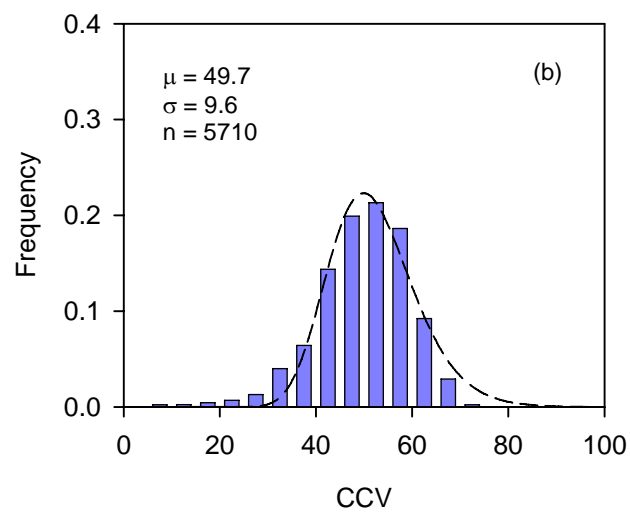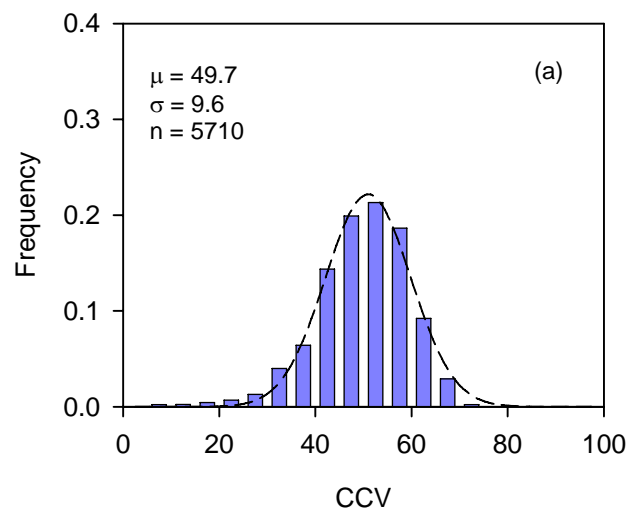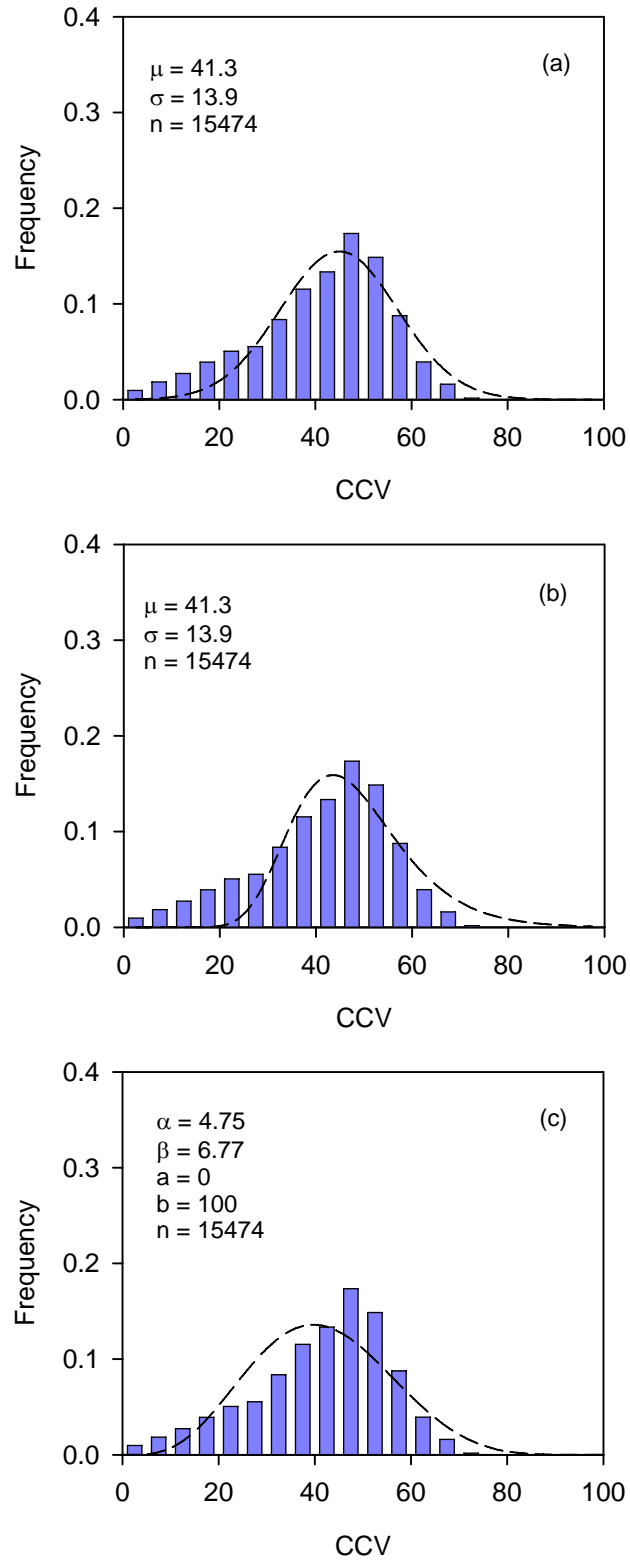
Figure G. 29. Proof 42 CCV distribution plot: (a) normal, (b) log normal, and (c) beta
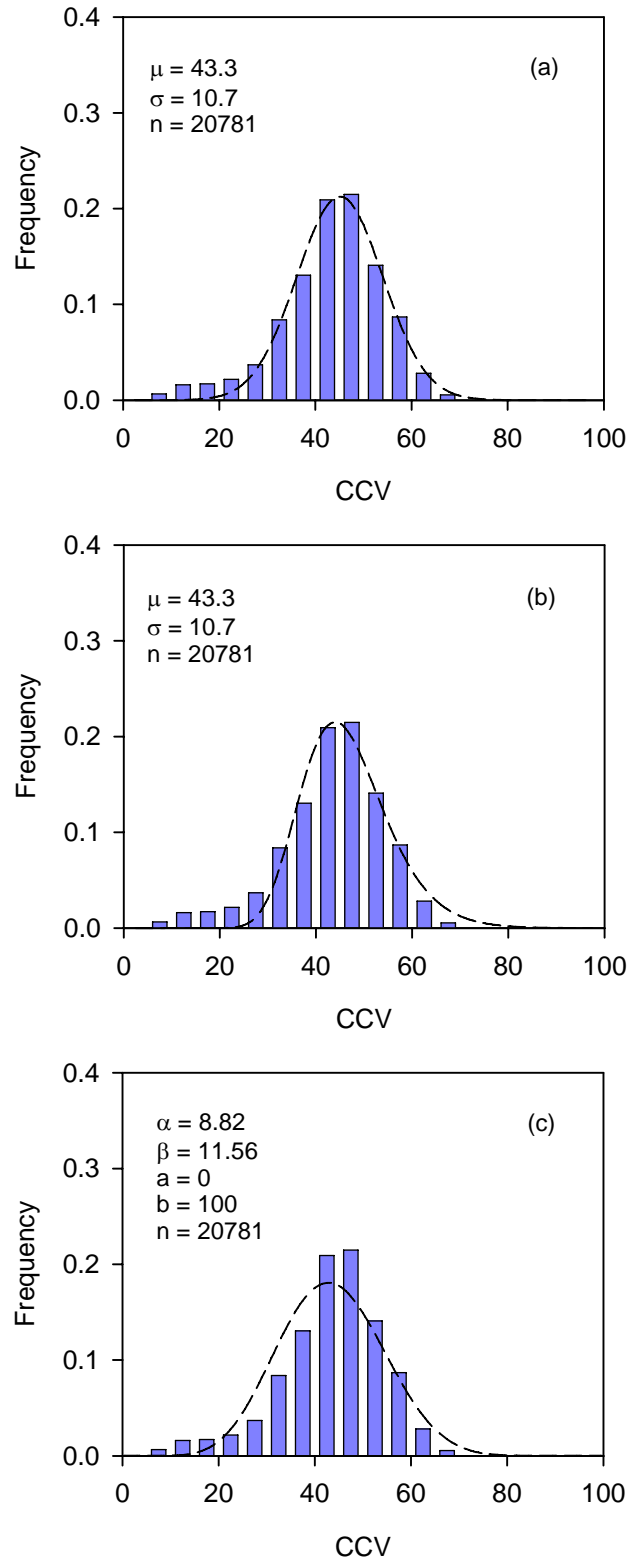
Figure G. 30. Proof 44 CCV distribution plot: (a) normal, (b) log normal, and (c) beta
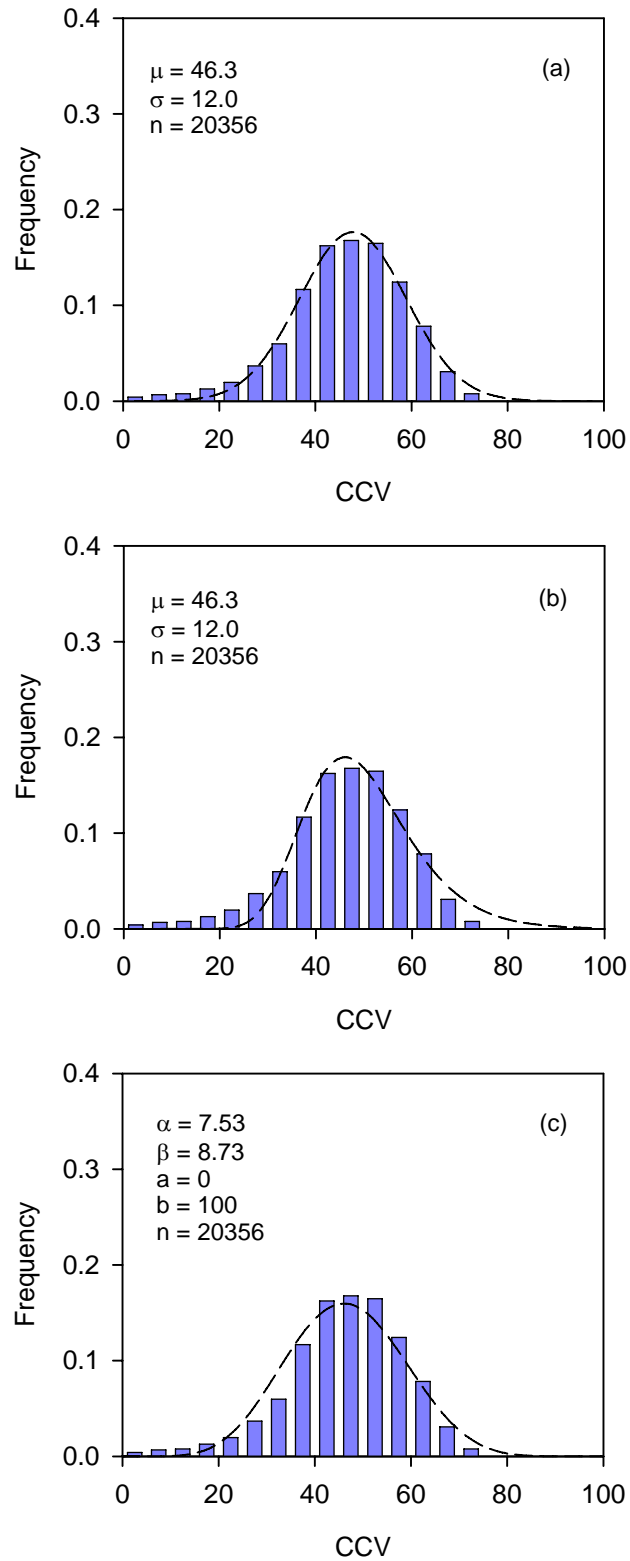
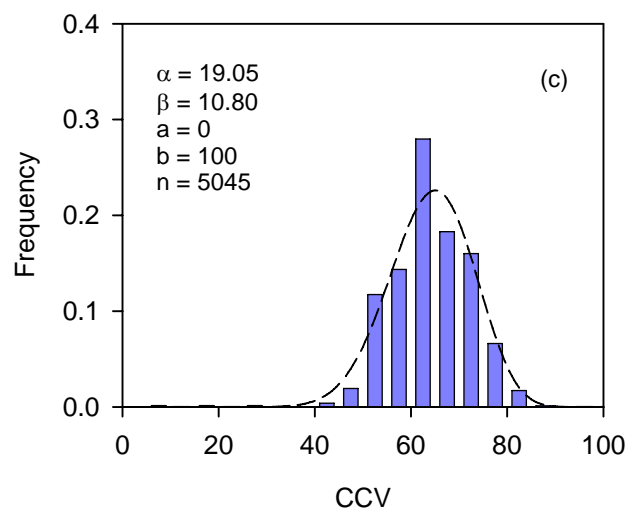Figure G. 31. Proof 45 CCV distribution plot: (a) normal, (b) log normal, and (c) beta
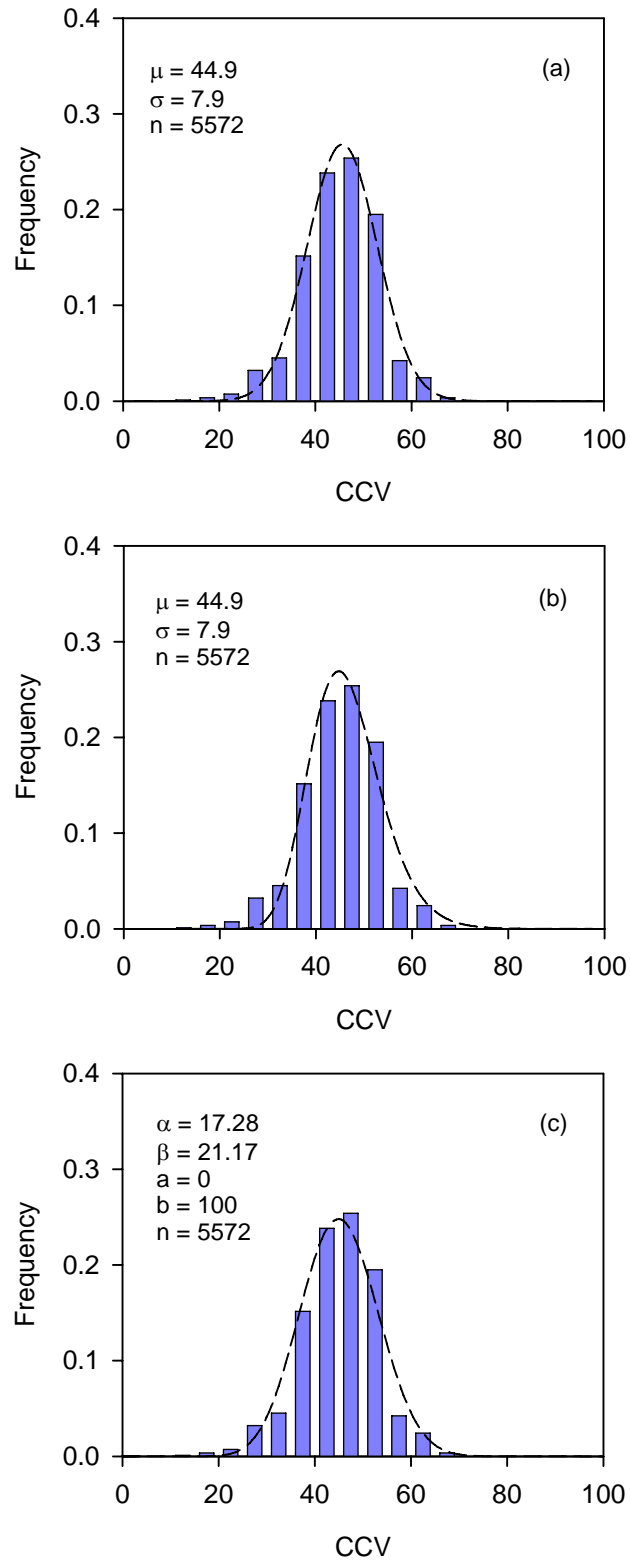
Figure G. 32. Proof 46 CCV distribution plot: (a) normal, (b) log normal, and (c) beta
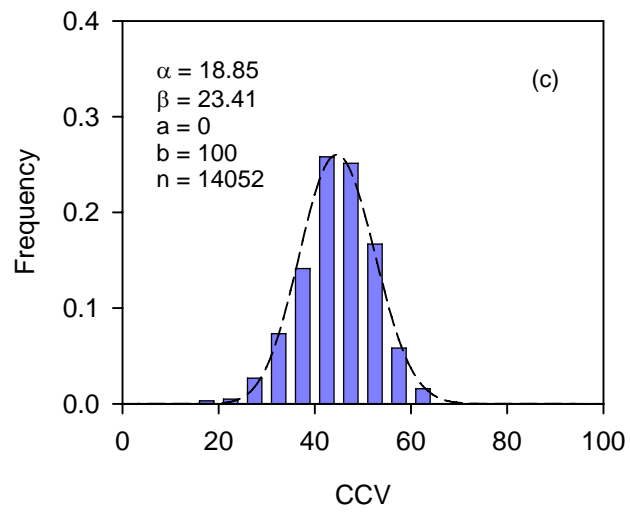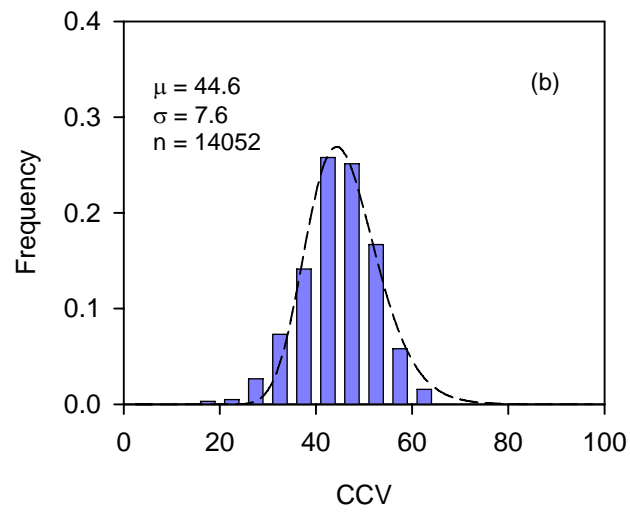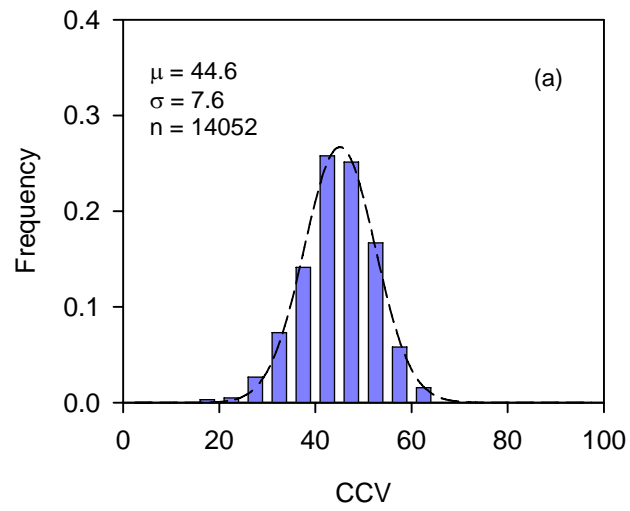
Figure G. 33. Proof 47 CCV distribution plot: (a) normal, (b) log normal, and (c) beta

Appendix H : 2006 Mn/DOT Intelligent Compaction Specification

S-xx (2105) EXCAVATION AND EMBANKMENT – (QC/QA) IC Quality COMPACTION (pilot specification)

S-xx.1 (QC/QA) IC Quality Compaction Method

The Engineer will develop IC-CTV's (Intelligent Compaction – Compaction Target Values), from control strips constructed by the Contractor. The Contractor will develop and implement a project specific Quality Control Procedure for embankment construction that is based on Contractor IC stiffness measurements, moisture testing and other Quality Control practices; and will provide ongoing Quality Control data to the Engineer. Final acceptance by the Engineer will be based on observation of the final stiffness recording pass of the Intelligent Compactor, review and approval of the Contractor's Quality Control data, Mn/DOT performed companion and verification moisture assurance testing, and test rolling specification requirements.

Within 15 days after award of the Contract, the Contractor needs to specify the manufacturer of the IC equipment he intends to utilize on the Project. The Contractor shall make available an on-site equipment manufacturers representative for construction of the initial control strip and as required or requested by the Engineer throughout the course of that portion of the Project which utilizes IC.

   The Contractor shall allow access for viewing by the Engineer, the IC equipment display panels at all times during the course of that portion of the Project which utilizes IC.

S-xx.2 Definitions

          The term "roadbed embankment materials" as used in this specification shall mean any granular, select granular, select granular modified, or non-granular grading soils (borrow or select grading soils) to be placed in the roadbed sub-grade as indicated in the Plan. The roadbed shall be the zone under the base, pavement and curb structures bounded by the roadbed slopes shown in the Plan or 1:1 slopes from the shoulder PI (point of intersection) (1.0 vertical to 1.5 horizontal slopes for fills over 10 meters **(30 feet)** in height).

          "Quality Compaction" shall be as defined in Specification 2105.3F2 Quality Compaction (Visual Inspection) Method.

          "Quality Control" shall be defined as a procedure whereby the Contractor develops, utilizes, and documents Quality Control activities that govern how embankment is constructed on this project.

          "Quality Assurance" shall be defined as a procedure whereby the Engineer monitors the Contractor's Quality Control activities and performs assurance monitoring and/or testing for final acceptance of all embankment construction.

"IC" refers to Intelligent Compaction. This process involves measuring and recording the time, location and stiffness of the material being compacted during the compaction process with a vibratory roller that is equipped with an accelerometer-based measuring system and a GPS positioning system.

"IC-CTV" is the IC compaction target value, which is the target stiffness reading for each grading material type obtained using the IC measuring and recording capabilities of the Intelligent Compactor on the control strip(s) constructed on this project.

"Proof layer" shall be defined as a predetermined layer that requires Quality Control measurements by the Contractor and Quality Assurance by the Engineer to ensure compliance with the Compaction Target Value prior to placing successive lifts. The proof layers described herein are general in nature and may be adjusted by the Engineer.

S-xx.3 Quality Control/Quality Assurance (QC/QA)

        A)   Quality Control Procedure Development by the Contractor.

The Contractor shall incorporate data gathered from the control strip constructed using IC technology to develop a Quality Control Procedure for embankment construction. This procedure shall detail how Quality Control will be accomplished, which could include identifying IC equipment and procedures, collecting and reporting IC stiffness measurement results, ensuring uniformity of grading material, confirming acceptable moisture and compaction results on embankment lifts between proof layers, determining the anticipated number, pattern and speed of roller passes to obtain optimum compaction results on all layers, not just the proof layers, and other items that may contribute to an effective Quality Control Procedure.

In addition, the Quality Control Procedure should include any corrective construction actions that may be required as a result of Quality Control measurements, such as adding water and/or drying soils, re-compacting non-compliant embankments or other corrective actions that may be undertaken.

Included in the Quality Control Procedure shall also be the manner in which these efforts will be documented in order to meet the requirements of the Weekly Quality Control Report. The Quality Control Procedure shall be submitted to the Engineer for approval prior to embankment construction.

        B)   Quality Control Procedure Implementation by the Contractor.

The Contractor will perform all IC stiffness measurements required by the approved Quality Control Procedure, and will modify construction operations so that acceptable compaction results are obtained. The Contractor shall also document, in the form of a Weekly Quality Control Report, all Quality Control IC compaction results, Quality Control activities and corrective construction actions taken as a result of the Quality Control measurements to meet the

requirements of this specification. The documentation shall be submitted to the Engineer for acceptance on a weekly basis.

C)   Quality Assurance by Mn/DOT.

The Engineer will observe the final stiffness recording pass of the Intelligent Compactor on each proof layer, review and approve the Contractor's Quality Control data documenting that acceptable compaction results were obtained, submitted in the form of the Weekly Quality Control Report as described in Section S-xx.8, perform companion and verification moisture testing and observe test rolling results to ensure compliance with the requirements of Mn/DOT Specification 2111, for final acceptance of the compacted embankment.

S-xx.4 Compaction Requirements

Location	Method
Bottom of sub-cuts, excavations, and embankment foundations.	Quality Compaction with IC Base Map
All roadbed embankments	(QC/QA) IC Quality Compaction
Embankment outside of the roadbed	Quality Compaction
Embankment adjacent to retaining walls (not part of the roadbed)	Quality Compaction
Aggregate Bedding under drainage structures	Modified Penetration Index Method
Culvert and Sewer Trench Backfill	Modified Penetration Index Method
Backfill under roadbed near structures	Modified Penetration Index Method

S-xx-5 Equipment Requirements for Control Strip Construction

A)   Smooth Drum or Padfoot Vibratory Roller

The vibratory roller shall weigh at least 11,300 kg (**25,000 pounds**).

The IC roller shall be a Mn/DOT approved IC roller equipped with a measurement and documentation system that allows continuous recordation, through an accurate global positioning system, of roller location and corresponding compaction-related output, such as number of roller passes and roller-generated materials stiffness measurements.

The output is the continuous measurement of the stiffness of the material being compacted as the roller moves along during the compaction process and must 1) enhance the ability of the roller operator and/or project inspection personnel to make real-time corrections in the compaction process, 2) be available for inspector review on demand, and 3) allow for a plan-view, color-coded plot of roller stiffness and/or roller pass number measurements throughout a designated section of roadway or other approved data submittal format

S-xx.6 Compaction Target Value - (IC-CTV)

The Contractor shall construct compaction control strips to determine the IC Compaction Target Value (IC-CTV) for each identifiable different type and/or source of grading material. Additional control strips shall be constructed for materials with observable and/or quantifiable variations in material properties that affect the IC-CTV, as determined by the Engineer. Each control strip shall be constructed with acceptable grading materials having the moisture content within the required range.

The compactor used for control strip construction shall be instrumented with an approved IC accelerometer-based measuring system that measures and records stiffness values of the compacted soil and the corresponding locations, using global positioning devices, within the accuracy specified by the Engineer.

 The Contractor and the Engineer shall both save a material sample from each control strip for comparison to the embankment material being compacted during QC/QA procedures in order to determine the applicable control strip IC-CTV.

The control strip shall be at least 100 m (**300 feet**) long and at least 10 m (**32 feet**) wide at the base, or as otherwise determined by the Engineer. The lift thicknesses for the control strip and the constructed embankment shall be limited to the maximum lift thickness allowed in Mn/DOT Specification 2105. The total thickness of the granular treatment control strip shall equal the planned granular treatment thickness being constructed. The total thickness of the select grading soils control strip shall be a maximum of 1.2 m (4.0 feet).

The control strip for select grading soils shall be constructed on an excavated surface that is compacted with Quality Compaction procedures prior to the start of the control strip compaction activities.   The control strip for granular embankments shall be constructed on top of a previously constructed control strip from select grading soils, or on top of an excavated surface similar to what will be encountered in actual construction. This surface shall be compacted with Quality Compaction procedures prior to the start of the control strip compaction activities. After the excavation bottom has been compacted by Quality Compaction procedures, the IC roller shall be used to record the stiffness of the excavation bottom prior to placing additional material. This data shall be utilized as an IC Quality Compaction Base Map to determine uniformity of the subgrade soils and to identify any inherent soft spots.

The following requirements for designation of proof layers in the control strip construction are general in nature and may require modification by the Engineer to meet specific project conditions.

 For granular treatments more than 0.75 m (2.5 feet) in thickness, the proof layers of the control strip shall be designated as the midpoint and the top of the planned granular treatment thickness. For granular treatments less than or equal to 0.75 m (2.5 feet) in thickness, the proof layer of the control strip shall be designated as the top of the planned thickness.

For select grading soils, the proof layers of the control strip shall be designated as the 0.6 m (2.0 foot) thickness of embankment and the 1.2 m (4.0 foot) thickness.

During construction of the control strip, the Contractor shall make repeated compaction passes on each lift, using a roller pattern approved by the Engineer, with continuous stiffness measurements being recorded by the Intelligent Compactor. When additional roller or compactor passes do not result in a significant increase in stiffness values on that lift, as determined by the Engineer, the next lift shall be placed.

The proof layer IC-CTV will be the optimum value obtained from the IC stiffness measurements on the designated proof layer during construction of the control strip. The optimum value is reached when additional passes do not result in a significant increase in stiffness values, as determined by the Engineer.

The costs of constructing the control strip for each identifiable different type and/or source of grading material, for each material with observable and/or quantifiable variations in material properties that affect the IC-CTV, or for each compaction method, shall be part of the work required for this specification with no direct compensation made therefore.

S-xx.7 Moisture Requirements

At the time of compaction, both for the construction of the control strip(s) and during production compaction, the moisture content of the portion of the embankment materials that are to be compacted under (QC/QA) IC Quality Compaction requirements shall be not less than 65% or more than 100% of Optimum Moisture as determined by the Standard Proctor Density Method. The Standard Proctor Density will be determined by the Engineer.

The Contractor shall add water, and /or perform blending as needed to meet the moisture requirements. The Engineer may order the application of additional water for compaction if necessary. If any embankments are constructed with materials that contain excessive moisture, the Contractor shall dry or replace it with material having the required moisture content.

Additional water ordered by the Engineer, or efforts to dry materials or replace soils that are excessively wet which are taken by the Contractor to meet Quality Control procedures or otherwise ordered by the Engineer, will not be considered extra work, but shall be considered part of the work required for this specification with no direct compensation made therefore.

S-xx.8 <u>Quality Control Procedure</u>

The Contractor shall perform and document Quality Control measurements as required elsewhere in this specification. In addition, as a result of the information gained by the Quality Control measurements, the Contractor shall conduct, modify and correct embankment construction activities so that all moisture and compaction requirements are met prior to final Quality Assurance by the Engineer.

IC stiffness measurements, moisture testing results, Quality Control activities and corrective construction actions taken as a result of Quality Control activities shall be submitted to the Engineer for acceptance each week as a written Weekly Quality Control Report. This report shall be the basis for determining whether all contract requirements were met by the Contractor. The completeness and accuracy of this report shall be certified by the Project Superintendent or other responsible Contractor's representative. In the event the Engineer needs clarification or disputes the accuracy or completeness of any Weekly Quality Control Report, a compliance review shall be held to resolve these issues prior to acceptance of the report by Mn/DOT.

As part of the Quality Control Procedure, the Contractor will perform moisture tests on the embankment material being compacted as needed to determine the moisture content for compliance with the moisture requirements of this specification. Contractor performed moisture tests will be performed by a project calibrated electronic moisture meter, reagent method, field moisture oven, oven dry method, or other gravimetric methods as approved by the Engineer. The rate of Contractor moisture testing shall be the minimum of that shown in the Schedule of Materials Testing for Specified Density testing. Additional moisture tests may be performed as determined by the Engineer.

The Contractor will also record IC stiffness measurements as shown in the Contractor's Quality Control Procedure and on the designated proof layers at the required locations of each embankment material as part of the Quality Control activities.

The Contractor shall provide at least one IC instrumented roller during roadbed embankment construction. Additional compactors that are utilized may be non-instrumented, but the IC roller must be the final roller used to obtain compaction on the proof layers. When using non-instrumented rollers, the actual compaction efforts, such as number of passes, type of drum, moisture content, and speed of the roller during compaction shall be shown in the Quality Control Procedure as determined by the information gathered during control strip construction.

The Weekly Quality Control Report shall indicate how these requirements are met on embankments compacted with non-instrumented compactors.

The (QC/QA) IC Quality Compaction Method shall apply to all roadbed embankment construction.

The (QC/QA) IC Quality Compaction Method shall meet the requirements of Specification 2105.3F2 Quality Compaction (Visual Inspection) Method and the additional requirements as shown below:

Compaction and mixing efforts shall be complete and uniform from bottom to top of all roadbed embankments, and for the entire length and width of the roadbed embankment.

The following requirements for designation of proof layers in the QC/QA procedures are general in nature and may require modification by the Engineer to meet specific project conditions.

The selection of the applicable IC-CTV shall be by visual comparison, or other acceptable comparison method, of the material properties of the embankment being constructed and the material properties of saved material samples from the control strip construction.

For granular treatments more than 0.75 m (2.5 feet) in thickness, the proof layers shall be designated as the midpoint and the top of the planned granular treatment thickness. For granular treatments less than or equal to 0.75 m (2.5 feet) in thickness, the proof layer shall be designated as the top of the planned thickness. The IC-CTV for each proof layer shall be the value obtained on the corresponding proof layer (i.e. midpoint or top) of the applicable control strip.

For select grading soils, the proof layers shall be successive 1.2 m (4.0 foot) layers in thickness from the bottom of the embankment up, plus the top of the planned select grading soils thickness. If the top of the select grading soils is within 1.5 m (5.0 feet) of the previous proof layer, the next proof layer shall be the top surface instead of at the next 1.2 m (4.0 foot) increment. If the planned select grading soils thickness is less than 1.2 m (4.0 feet), the proof layer shall be designated as the top of the planned select grading soils thickness. The IC-CTV for all proof layers shall be the value obtained on the 1.2 m (4.0 foot) layer of the applicable control strip, unless the planned select grading soils thickness is less than 0.75 m (2.5 feet). In that case, the IC-CTV shall be the value obtained on the 0.6 m (2.0 foot) layer of the applicable control strip.

The Contractor shall provide a relatively smooth uniform surface that has been shaped to approximate line and grade of each proof layer for the purpose of recording all IC stiffness measurements, as part of the work required for this specification with no direct compensation made therefore.

IC stiffness measurements will be recorded on all proof layers of embankment construction continuously by the Intelligent Compactor.

For acceptance of compaction at each proof layer during general production operations, all segments of the embankment shall be compacted so that at least 90% of the IC stiffness measurements are at least 90% of the applicable IC-CTV prior to placing the next lift. The Contractor shall re-compact (and dry or add moisture as needed) all areas that do not meet these

requirements. Additional IC stiffness measurements shall be taken for acceptance of the re-compacted areas.

If localized areas have an IC stiffness measurement of less then 80% of the IC-CTV, the Contractor shall re-compact (and dry or add moisture as needed) these areas to at least 90% of the IC-CTV prior to placing the next lift.

If a significant portion of the grade is more than 30% in excess of the selected IC-CTV, the Engineer shall re-evaluate the selection of the applicable control strip IC-CTV. If an applicable IC-CTV is not available, the Contractor shall construct an additional control strip to reflect the potential changes in compaction characteristics.

If, according to the visual inspection method, the Contractor appears to be doing work that results in acceptable compaction, but the IC stiffness measurements consistently do not meet the applicable IC-CTV, the Engineer shall re-evaluate the selection of the applicable control strip IC-CTV. If an applicable IC-CTV is not available, the Contractor shall construct an additional control strip to reflect the potential changes in compaction characteristics.

Quality Assurance Procedures

The Engineer will observe the final compaction recording pass of the Intelligent Compactor and review the Contractor's Quality Control data taken on all proof layers, as described elsewhere in these specifications.

In addition, the Engineer will perform and companion and verification moisture tests on a random basis or in areas that visually appear to be non-compliant, as deemed necessary by the Engineer and test rolling in accordance with Mn/DOT Specification 2111.

Mn/DOT companion and verification moisture tests shall be evenly distributed throughout the duration of the Contractor's testing and will be taken utilizing the procedures as shown in this specification.

Final Acceptance shall be determined when the following criteria are met:

> A) The final stiffness pass observed by the Engineer meets the requirements of this specification.
>
> B) The Contractor has submitted Weekly Quality Control Reports documenting that acceptable compaction results were obtained for all embankment construction.
>
> C) All companion and verification tests meet specification requirements.
>
> D) The Engineer has reviewed the IC stiffness measurements taken on all proof layers and has approved the Weekly Quality Control Reports.

E)   Test rolling meets the requirements of Mn/DOT specification 2111.

S-xx.10   <u>Testing Equipment</u>

The Engineer may order the contactor to provide a Light Weight Deflectometer and/or electronic moisture meter or other moisture testing device with payment to be made as Extra Work.

Appendix I: Resilient Modulus Test Results

Table I. 1. Comparison of resilient modulus test results at -3% of optimum moisture content for mixed glacial till

Static Compaction Samples			Impact Compaction Samples			Vibratory Compaction Samples		
σc (kPa)	σd (kPa)	Mr (MPa)	σc (kPa)	σd (kPa)	Mr (MPa)	σc (kPa)	σd (kPa)	Mr (MPa)
41.4	13.0	85.1	41.4	13.2	168.6	41.4	15.9	221.8
41.4	24.5	84.7	41.4	25.3	188.1	41.4	24.1	147.0
41.4	39.9	65.1	41.4	36.7	171.9	41.4	36.5	143.9
41.4	54.1	84.8	41.4	46.6	144.8	41.4	51.3	175.5
41.4	67.1	89.8	41.4	64.2	160.4	41.4	67.8	170.9
27.6	12.3	58.4	27.6	14.6	133.5	27.6	15.7	145.3
27.6	26.0	66.0	27.6	24.4	145.3	27.6	25.4	129.1
27.6	37.8	77.6	27.6	36.7	151.5	27.6	35.7	129.5
27.6	53.4	83.3	27.6	48.9	141.5	27.6	51.3	153.3
27.6	68.0	78.0	27.6	65.6	156.5	27.6	64.3	147.5
13.8	11.5	51.4	13.8	14.8	158.1	13.8	15.0	113.5
13.8	26.7	60.0	13.8	26.5	106.0	13.8	23.0	133.5
13.8	37.9	62.3	13.8	36.2	106.4	13.8	34.1	119.4
13.8	54.2	68.3	13.8	49.8	114.4	13.8	52.8	145.3
13.8	64.6	72.1	13.8	62.2	125.0	13.8	67.6	149.0

Table I. 2. Comparison of resilient modulus test results at optimum moisture content for mixed glacial till

Static Compaction Samples			Impact Compaction Samples			Vibratory Compaction Samples		
σc (kPa)	σd (kPa)	Mr (MPa)	σc (kPa)	σd (kPa)	Mr (MPa)	σc (kPa)	σd (kPa)	Mr (MPa)
41.4	12.8	81.7	41.4	13.2	144.7	41.4	13.1	81.1
41.4	24.3	105.9	41.4	25.8	145.2	41.4	24.7	104.5
41.4	38.9	131.2	41.4	36.0	112.2	41.4	37.0	141.2
41.4	54.6	89.8	41.4	52.5	126.5	41.4	54.3	176.5
41.4	64.5	95.3	41.4	64.6	111.1	41.4	65.9	192.5
27.6	13.6	81.2	27.6	14.8	191.2	27.6	15.8	129.4
27.6	25.3	95.3	27.6	25.2	133.6	27.6	26.1	145.4
27.6	36.6	100.5	27.6	36.1	109.5	27.6	36.7	142.9
27.6	54.4	87.4	27.6	51.8	115.3	27.6	48.1	166.6
27.6	64.9	86.6	27.6	68.0	110.5	27.6	67.4	195.3
13.8	13.2	152.7	13.8	13.9	141.0	13.8	15.6	65.8
13.8	25.9	84.7	13.8	26.8	155.2	13.8	27.0	77.7
13.8	37.5	87.3	13.8	35.3	119.1	13.8	35.9	87.2
13.8	54.6	83.9	13.8	51.7	124.9	13.8	49.9	115.4
13.8	68.1	81.5	13.8	68.0	113.4	13.8	66.2	147.5

Table I. 3. Comparison of resilient modulus test results at +3% of optimum moisture content for mixed glacial till

Static Compaction Samples			Impact Compaction Samples			Vibratory Compaction Samples		
σc (kPa)	σd (kPa)	Mr (MPa)	σc (kPa)	σd (kPa)	Mr (MPa)	σc (kPa)	σd (kPa)	Mr (MPa)
41.4	13.7	125.3	41.4	13.1	97.3	41.4	13.6	75.4
41.4	25.6	79.5	41.4	26.0	80.6	41.4	25.6	84.3
41.4	37.0	73.3	41.4	36.6	74.8	41.4	36.8	102.4
41.4	54.4	75.0	41.4	53.9	87.8	41.4	55.2	130.5
41.4	67.9	57.9	41.4	68.2	75.5	41.4	68.1	89.5
27.6	13.7	77.4	27.6	11.5	84.8	27.6	14.5	105.9
27.6	25.8	82.9	27.6	24.9	71.5	27.6	27.6	121.6
27.6	36.9	69.3	27.6	37.6	76.3	27.6	36.9	121.3
27.6	53.6	69.7	27.6	53.7	73.8	27.6	51.4	102.9
27.6	68.6	58.0	27.6	68.3	69.9	27.6	68.1	97.1
13.8	13.8	70.1	13.8	13.3	79.6	13.8	13.7	78.7
13.8	26.2	62.5	13.8	26.0	58.4	13.8	26.9	81.1
13.8	38.1	62.2	13.8	36.3	58.0	13.8	36.8	79.5
13.8	54.0	61.5	13.8	54.0	65.5	13.8	54.1	95.0
13.8	68.6	56.9	13.8	68.1	57.8	13.8	67.9	88.2

Table I. 4. Comparison of resilient modulus test results at 6% target moisture content for TH 64 sand

Impact Compaction Samples			Vibratory Compaction Samples			
σc (kPa)	σd (kPa)	Mr (MPa)	σc (kPa)	σd (kPa)	Mr (MPa)	Percent Difference*
20.7	20.2	55.7	20.7	19.6	54.2	-2.7
20.7	40.0	68.4	20.7	40.1	62.4	-9.6
20.7	59.6	76.2	20.7	58.8	69.5	-9.7
34.5	34.0	89.9	34.5	33.9	84.9	-5.9
34.5	66.1	95.1	34.5	65.4	98.8	3.8
34.5	100.0	105.8	34.5	99.2	104.9	-0.9
68.9	66.6	144.9	68.9	66.4	146.5	1.1
68.9	136.1	168.9	68.9	135.6	168.5	-0.2
68.9	205.6	149.3	68.9	206.5	175.1	14.7
103.4	67.4	164.5	103.4	67.7	157.1	-4.7
103.4	101.5	156.6	103.4	102.3	182.0	14.0
103.4	205.8	181.8	103.4	205.7	196.5	7.5
137.9	102.2	167.1	137.9	102.1	189.4	11.7
137.9	136.7	184.9	137.9	136.9	234.3	21.1
137.9	274.8	221.4	137.9	275.6	239.9	7.7

Note: *percent difference is relative to vibratory compaction sample Mr

Table I. 5. Comparison of resilient modulus test results at 8% target moisture content for TH 64 Sand

Impact Compaction Samples			Vibratory Compaction Samples			Percent Difference*
σc (kPa)	σd (kPa)	Mr (MPa)	σc (kPa)	σd (kPa)	Mr (MPa)	
20.7	20.4	76.4	20.7	20.3	80.4	5.0
20.7	39.3	66.0	20.7	39.7	82.1	19.6
20.7	59.4	90.4	20.7	58.9	94.9	4.8
34.5	33.5	82.5	34.5	34.7	124.2	33.6
34.5	66.2	103.9	34.5	66.2	131.4	20.9
34.5	101.5	113.3	34.5	101.0	133.1	14.9
68.9	66.9	125.5	68.9	66.8	152.0	17.5
68.9	136.7	165.8	68.9	136.9	179.5	7.6
68.9	206.0	163.4	68.9	205.7	181.5	10.0
103.4	67.3	178.2	103.4	66.4	206.0	13.5
103.4	101.8	156.6	103.4	102.0	191.2	18.1
103.4	205.7	191.2	103.4	205.8	201.5	5.1
137.9	101.9	193.3	137.9	102.3	196.2	1.5
137.9	136.5	224.4	137.9	136.8	210.9	-6.4
137.9	274.9	227.7	137.9	275.6	255.2	10.8

Note: *percent difference is relative to vibratory compaction sample Mr

Table I. 6. Comparison of resilient modulus test results at 8% target moisture content for TH 64 Sand

Impact Compaction Samples			Vibratory Compaction Samples			Percent Difference*
σc (kPa)	σd (kPa)	Mr (MPa)	σc (kPa)	σd (kPa)	Mr (MPa)	
20.7	20.5	68.2	20.7	19.4	93.3	26.9
20.7	39.6	98.3	20.7	40.5	90.8	-8.2
20.7	59.1	79.0	20.7	58.2	93.4	15.4
34.5	34.0	96.7	34.5	34.1	128.2	24.6
34.5	66.4	109.3	34.5	65.2	128.9	15.2
34.5	101.5	115.5	34.5	100.9	144.0	19.8
68.9	67.1	130.4	68.9	65.8	196.0	33.5
68.9	136.9	151.5	68.9	137.2	195.1	22.4
68.9	206.0	146.5	68.9	206.0	186.5	21.5
103.4	67.9	232.9	103.4	67.1	170.7	-36.4
103.4	102.7	184.0	103.4	103.0	187.4	1.8
103.4	207.2	167.2	103.4	206.1	210.5	20.6
137.9	102.6	172.1	137.9	102.7	211.0	18.4
137.9	137.5	174.3	137.9	137.7	243.6	28.5
137.9	210.4	147.8	137.9	277.4	239.0	38.2

Note: *percent difference is relative to vibratory compaction sample Mr

Table I. 7. Summary of resilient modulus test and quick shear test results on shelby tube samples

Sample	Confining Stress (kPa)	Deviator Stress (kPa)	Mr (MPa)	Witczak and Uzan (1988) Model Coefficients				Shear Strength τ_{max} (kPa)	Shear Strength at 1% strain $\tau_{1\%}$ (kPa)	Strain at failure (%)
				k_1	k_2	k_3	R^2			
	41.4	13.3	75.7							
	41.4	24.4	189.5							
	41.4	40.3	194.8							
	41.4	54.8	141.0							
	41.4	66.9	148.2							
	27.6	11.5	117.9							
	27.6	24.4	159.9							
27 # 1B	27.6	41.0	163.2	1487.40	0.03	0.08	0.21	290.6	290.6	1.0%
	27.6	50.7	154.2							
	27.6	69.4	139.2							
	13.8	12.8	194.8							
	13.8	24.8	111.3							
	13.8	39.7	105.5							
	13.8	55.0	124.5							
	13.8	67.3	132.4							

27 # 2	41.4	12.4	143.8	892.93	0.43	-0.08	0.61	332.5	280.0	1.6%
	41.4	26.4	141.4							
	41.4	38.3	110.1							
	41.4	54.5	109.9							
	41.4	67.2	151.5							
	27.6	13.2	83.8							
	27.6	27.4	80.9							
	27.6	38.8	85.7							
	27.6	52.8	110.7							
	27.6	67.5	130.9							
	13.8	13.2	95.5							
	13.8	27.5	112.0							
	13.8	40.3	78.6							
	13.8	53.9	83.2							
	13.8	68.4	101.3							

Sample	Confining Stress (kPa)	Deviator Stress (kPa)	Mr (MPa)	Witczak and Uzan (1988) Model Coefficients				Shear Strength τ_{max} (kPa)	Shear Strength at 1% strain $\tau_{1\%}$ (kPa)	Strain at failure (%)
				k_1	k_2	k_3	R^2			
28 # 2	41.4	12.8	70.9	701.34	0.16	-0.06	0.31	84.2	80.0	1.3%
	41.4	26.7	99.2							
	41.4	38.8	92.9							
	41.4	54.7	82.2							
	41.4	67.2	88.0							
	27.6	12.8	63.6							
	27.6	27.5	77.6							
	27.6	38.4	67.9							
	27.6	53.9	79.7							
	27.6	67.8	82.4							
	13.8	12.9	101.9							
	13.8	27.2	70.2							
	13.8	38.3	65.5							
	13.8	53.3	65.4							
	13.8	67.5	65.7							

28 # 3	41.4	13.0	96.6	495.18	0.40	-0.29	0.92	135.2	80.0	3.0%
	41.4	26.4	102.4							
	41.4	38.5	74.5							
	41.4	53.0	78.6							
	41.4	66.7	71.2							
	27.6	12.9	88.6							
	27.6	27.1	88.3							
	27.6	38.5	69.5							
	27.6	52.4	65.9							
	27.6	66.0	66.6							
	13.8	13.3	70.2							
	13.8	27.1	65.6							
	13.8	38.8	58.4							
	13.8	52.8	57.7							
	13.8	66.5	60.4							

Sample	Confining Stress (kPa)	Deviator Stress (kPa)	Mr (MPa)	Witczak and Uzan (1988) Model Coefficients				Shear Strength τ_{max} (kPa)	Shear Strength at 1% strain $\tau_{1\%}$ (kPa)	Strain at failure (%)
				k_1	k_2	k_3	R^2			
28 # 4	41.4	13.1	89.2	286.32	0.42	-0.44	0.91	104.2	55.0	4.0%
	41.4	27.4	67.0							
	41.4	38.4	51.4							
	41.4	53.2	48.7							
	41.4	65.6	48.0							
	27.6	13.1	56.6							
	27.6	27.3	48.1							
	27.6	38.6	43.8							
	27.6	53.7	42.3							
	27.6	64.2	42.9							
	13.8	13.8	62.6							
	13.8	27.1	46.8							
	13.8	38.5	34.3							
	13.8	53.5	37.5							
	13.8	66.6	38.1							

I-11

	41.4	13.3	-*							
	41.4	26.4	74.7							
	41.4	38.6	60.5							
	41.4	51.9	53.9							
	41.4	66.6	55.2							
	27.6	13.2	74.3							
	27.6	27.0	54.4							
28 # 5	27.6	39.5	-*	295.20	0.58	-0.47	0.91	142.6	45.0	5%**
	27.6	39.5	-*							
	27.6	39.5	-*							
	13.8	14.2	59.1							
	13.8	26.0	38.8							
	13.8	39.0	40.7							
	13.8	53.0	32.7							
	13.8	64.4	42.6							

| Sample | Confining Stress (kPa) | Deviator Stress (kPa) | Mr (MPa) | Witczak and Uzan (1988) Model Coefficients | | | | Shear Strength τ_{max} (kPa) | Shear Strength at 1% strain $\tau_{1\%}$ (kPa) | Strain at failure (%) |
				k_1	k_2	k_3	R^2			
28 # 6	41.4	13.1	95.8	572.77	0.37	-0.22	0.94	128.9	85.0	2.6%
	41.4	26.2	88.5							
	41.4	38.2	91.1							
	41.4	53.6	78.2							
	41.4	66.2	81.8							
	27.6	13.2	84.3							
	27.6	27.3	85.7							
	27.6	38.8	76.2							
	27.6	52.8	75.8							
	27.6	66.0	73.1							
	13.8	13.3	77.7							
	13.8	27.5	64.2							
	13.8	38.4	59.6							
	13.8	53.2	63.1							
	13.8	66.4	64.4							

Notes: * Data Not Available; ** Test stopped at 5% strain. Sample did not fail